CHEMICALLY STIMULATED EXO-ELECTRON EMISSION

Thesis

submitted for the degree of

Doctor of Philosophy

of the

University of Glasgow

by

Maureen E. Cooper, B.Sc.

May 1978.

Acknowledgements

I should like to take this opportunity to express my gratitude to the many people who helped me in the course of my research.

In particular I should like to thank Mr. J. Connolly for his patience and help in constructing various detectors and Mr. J. Hardy and Mr. A. Anderson for their invaluable help with problems of an electronic nature. My thanks are due to Dr. T. Baird of the Chemistry Department and Mr. S. Orr of the Engineering Department for their assistance. I will also take this opportunity to thank Dr. W. Jack and Mr. J. Lloyd of the Physics Department for their help and advice and Dr. J. Cairns for lending us the detector developed by him at Harwell (133). My thanks also go to Dr. G. Webb for the help he gave me throughout my Ph.D.

I should like to express my appreciation to Miss E. Forbes for the high standard of the typing throughout my thesis.

In particular my thanks are due to Professor S.J. Thomson for suggesting this research topic, for his help and encouragement throughout the period of my research and for the many discussions I had with him.

I take this opportunity to acknowledge the financial support of the Science Research Council which provided me with a grant.

Finally, I should like to express my gratitude to Professor S.J. Thomson, Dr. D.D. MacNicol and to my husband for the help and encouragement they gave me while I wrote my thesis.

Summary

This thesis begins with a review of exo-electron emission i.e. the release of slow (<10eV) electrons from solid surfaces when they are altered by abrasion, plastic deformation, oxidation or chemisorption. Exo-electron emission is also observed during magnetic and non-magnetic phase changes and after irradiation of solids with ionising radiation i.e. α, β, γ rays or neutrons.

In the next part of the thesis there are described the problems associated with detection of exo-electrons: either they have been recorded in gas counters, where the surface has to be exposed to a counting-gas mixture, or they have been recorded under ultra high vacuum conditions. The first aim of the research therefore was to develop a detector which could be used for in-situ studies of gas-solid interactions, that is without the need to switch to counting gases or ultra high vacuum. This was accomplished by the evolution of such a counter through five designs.

The successful counter was unusual in that a wire filament, which could be heated electrically, was placed inside a proportional counter. Gas-solid interactions could be studied on this filament. The electronic characteristics of the system were established by calculation, calibration and field plotting. It was shown that the field gradient at the filament surface was 13×10^3 V cm^{-1} i.e. the filament was not operating under field emission conditions.

The third section of the thesis is concerned with the

exploitation of the counter. It was discovered that exposure of a heated platinum filament to Q gas (90% Argon, 10% methane) gave an excellent exo-emission source. This type of carbided filament was heated to 900°C in flows of a variety of gases; among them oxygen, nitrogen, argon, argon/10% ethylene, argon/10% acetylene. When the platinum filament was heated in each of these gases to 900°C and then allowed to cool in the same gas, the electron emission fell typically from a few thousand counts per second to fewer than 100 counts per second over a period of five minutes. Such behaviour was also observed with hydrogen and helium although here the initial temperature of the filament was below 550°C (i.e. red heat). What was unexpected was the observation that some of the gases gave counting curves versus time with a definite structure. Thus it was observed that when platinum was cooled in argon/10% methane the count rate fell from 10,000 counts per second to 1500 as the temperature fell from 900°C to 110°C, but then rose sharply to a level of 4000 counts per second followed by further decay. This maximum occurred at 110°C. This kind of behaviour occurred with Ar/10% CH_4 Ar/10% ethylene, Ar/10% acetylene, Ar/10% ethane, hydrogen, argon, nitrogen, ~~hydrogen~~.

The electron emission which was measured during the cooling process was known to arise from multiple electron detection, for the counter multiplication factor was such that single electrons could not be detected. The cooling curve emissions are interpreted in terms of a basic tenet which arose from the literature survey, namely:- when bonds are made or broken at a surface exo-electrons are emitted.

Contents

CHAPTER 1

Chapter 1

INTRODUCTION

1·0 Definition

As this is an unusual field of research, it was decided to review the literature at some length. Exo-electron emission is the emission of very low energy electrons (E~0 to 10 eV) from defects and traps at or near the surface of a solid. This emission may be brought about in several ways e.g. by mechanical working of a piece of metal, abrasion of a metal surface or irradiation of a solid with ionising radiation i.e. α, β, γ or X-rays. Exo-electron emission also accompanies phase changes and many chemical reactions.

In general it is found that there are two distinct types of emission. One occurs at ambient temperature immediately after excitation. This type of emission decays to zero usually within a few hours, rarely persisting longer than a few days and it generally requires illumination of the sample. The other occurs when a previously excited sample is heated from room temperature after decay of the first type. A plot of emission rate versus temperature can give several distinct maxima which are characteristic of the sample being investigated. This plot is known as a glow curve by analogy with luminescence glow curves. This emission may proceed in the dark.

As well as thermally stimulated emission, exo-electrons may also be released after irradiation of surfaces with light from the near U-V or visible range of the spectrum. This phenomenon is distinct from the photo-electric effect per se since the wavelengths used are far longer than the photoelectric threshold of

the material being investigated. Exo-electrons have also been observed after stimulation of samples with ultrasonic frequencies.

1·1 Historical Background

Kramer (1) was the first to carry out a systematic investigation of this phenomenon. Working in Germany during the last war, he discovered that if a piece of abraded or deformed metal was brought near the anode of a point counter a very high count-rate was observed. This subsequently decayed with time.

Some of the many experiments Kramer carried out in an effort to explain this effect dealt with the heating and cooling of a metal alloy. He found that when a sample of Wood's metal was melted and then allowed to cool beneath a point counter a massive surge of counts was observed when solidification commenced. The high count-rate continued until a temperature below the freezing point was reached when the number of pulses quickly fell away to background level. No such emission was observed during melting.

Because solidification is an exothermal process, and there was no enhanced emission during melting, Kramer concluded that the electrons emitted were thermal electrons with the energy being provided by the latent heat of fusion of the metal. On this basis Kramer proposed that when electron emission occurred an exothermal process must be taking place. Thus he called the phenomenon exo-electron emission.

To explain his observations with worked metals Kramer suggested that mechanical treatment caused the formation of an unstable, non-metallic phase which released energy on spontaneously reverting to the stable, crystalline, metallic phase. Energy was thus available to give rise to exo-electron emission.

Kramer finally published his results in book form in 1950 (1) and this stimulated much work on investigation of the phenomenon.

Although Kramer was the first to study this effect systematically, it had been reported on several occasions before. Often earlier workers had not realised what they were dealing with. For example, in 1899 Curie (2) noted that if materials were brought near a sample of radium for a time, they exhibited what he described as a decaying radioactivity, while Rutherford observed the same effect with thorium in 1900 (3). He found the half-life of the decay was around eleven hours. In 1897 Russel (4) found that a piece of mechanically treated or irradiated zinc foil could darken a photographic plate. If only part of the zinc had been treated then only part of the emulsion was darkened. He also found that the effect was more pronounced at higher temperatures. In 1900 Villard (5) obtained the same effect using cathode rays to excite samples of bismuth.

In a very interesting investigation carried out in 1902 McLennan (6) irradiated many different sulphates, chlorides and sulphides with spark discharge from an induction coil, or cathode rays from a discharge tube. He measured the subsequent emission with a gold-leaf electroscope both at room temperature and while heating the specimens with a bunsen burner. He was able to record the glow curves in this way. He found there was no pressure dependence of total emission or emission rate between 1-480 mm Hg [sic]. McLennan was the first to realise the negative charge and low energy of the emitted particles.

Various reports appeared of an emission of charged particles accompanying chemical reaction taking place at solid surfaces. For example, in 1914 Hartley (7) reported an emission of electrons

from gold while H_2/O_2 reacted in its presence or while $2CO/O_2$ reacted. Finch (8) found that changes in the rate of emission followed changes in catalytic activity while Denisoff and Richardson (9) measured the energy distribution of the electrons released as various gases reacted with a potassium-sodium alloy, K_2Na.

However, no real advance was made in trying to explain this phenomenon until 1936 when Lewis and Burcham (10) found that if samples of abraded or scratched metals such as aluminium, copper, brass or nickel were introduced into a Geiger counter then a large number of counts were recorded. They suggested that these pulses might be due to ionization phenomena accompanying the reaction of oxygen with the deformed metal surface and that this would thus provide a very sensitive means of following the progress of a surface reaction. This helped to explain why freshly manufactured Geiger-Mueller counters often gave rise to an abnormally high background count which decreased as the counter aged.

In 1935 Tanaka found that metal surfaces which had been bombarded by electrons showed a cold emission which decayed with time to zero. In 1940 he published a summary of his results (11). He found that the effect depended on the presence of an oxide layer on the metal surface and that the intensity of the emission depended on the thickness of the oxide layer. The emission intensity went through a maximum and the corresponding oxide thickness varied with different metals. This work provided a substantial contribution to the elucidation of the role that surface layers play in the delayed emission from irradiated metals.

Unfortunately, these results went unnoticed and it was not

until Kramer drew attention to the fact that this phenomenon afforded a means of investigating metal surfaces and processes occurring on them that interest became more widespread. Although it is now known that it is not an exo-thermal process, as was proposed by Kramer, which is involved in this phenomenon, for historical reasons the term exo-electron emission has been retained.

1·2 Abrasion

Although earlier workers showed that freshly abraded metals gave rise to an emission of charged particles (e.g. (10)), it was Kramer (1) who realised during his work that this phenomenon provided the means of studying surface changes and surface processes.

Haxel, Houtermans and Seeger (12), following the ideas of Kramer (1), proposed that abrasion exposed fresh metal to the atmosphere and that the heat of chemisorption of oxygen on the clean metal would provide sufficient energy for the emission to take place. They also heated abraded specimens inside a gas-quenched Geiger-Mueller tube and found several emission maxima at well defined temperatures. These were attributed to adsorption centres with different activation energies for oxygen adsorption. Roubinek and Seidl (13) confirmed that oxygen was essential for initiating the emission process. While they did not agree with Haxel's theory that exo-electron emission was stimulated by oxygen chemisorption, they believed that oxide growth might be responsible for the decay in the emission. In fact Haxel and co-workers' theory was subsequently criticised on the following grounds. Even at 10^{-5} torr, monolayer formation of oxide takes place in a few seconds while at this pressure exo-electron emission from the abraded metal increased for a few minutes

before starting to decay. The implication was that exo-emission was more likely to be due to oxidation.

Kramer (14) and later Grunberg and Wright (15) showed that surfaces which emit exo-electrons also emit photo-electrons at wavelengths far beyond the photo-electric threshold of the metal. Grunberg and Wright further demonstrated that a freshly cleaved zinc crystal surface gave no such emission when irradiated with visible light, unless it had also been abraded. They went on to investigate the exo-electron emission at different wavelengths from a number of freshly abraded metals (16). They found that all the metals investigated emitted in the range 3,000-3,700 Å while aluminium, magnesium and zinc gave emission in the visible with a strong peak at 4,700 Å. They also noted that the emission rate varied with the intensity of the illumination.

From further studies of the decay of the peak at 4,700 Å, Grunberg and Wright proposed that this emission maximum was due to the decay of F'-centres, oxygen ion vacancies associated with two electrons. By etching the surface of the metals with 4% hydrofluoric acid, these workers showed that there was a region of high activity extending from 5 - 10 μ below the surface, with very little activity actually at the surface. Okamoto, Sato and Ohashi (17) confirmed this for iron in 1964. They found that exo-electron sources extended as deep as 60 μ with a maximum at 2 - 6 μ below the surface. They also obtained glow curves for specimens which had been annealed in vacuum (10^{-2} mm Hg) or hydrogen (1 atm) before abrasion. To compare these methods of pretreatment Ohashi and co-workers plotted the total electron emission up to the threshold of the Richardson emission versus the depth of the dissolved surface layer (μ) for several specimens. They found that the

distribution of the thermo-exoelectron traps differed appreciably (see fig 1, page 7a), thus demonstrating the importance of the method of pretreatment on the exo-electron emission characteristics.

Meanwhile Seidl (18) had suggested, on the basis of work on the oxidation of copper and iron films, that the electron traps responsible for exo-emission were created by adsorbed oxygen. Bohun (19) (20) and others had noticed the similarities between exo-electron emission and luminescence in insulating crystals and this led Bohun, Karpiskova and Duskova (21) to suggest that there might be a connection between the electron emission and the dissociation by photo-excitation of colour centres in the oxide layer.

Müller and Weinberger (22) proposed that abrasion, deformation or evaporation all led to the exposure of clean metal on which oxygen adsorption could take place. They proposed yet another explanation of the observed results. They argued that adsorption would lower the photoelectric work function of the metal while oxidation increased it and that this would account for the initial rise in emission rate followed by its decay.

Lohff (23) worked in high vacuum with abraded, deformed and evaporated metals, particularly aluminium and zinc. He showed that the shape of the emission curve, the time taken to reach the peak maximum and its intensity all depended on the residual gas pressure of the apparatus. If the pressure was lowered during an experiment the count rate decreased, if raised, the emission increased. Ramsey (24) confirmed these results (see fig 2 and 3, page 7b) although he found that illumination of the sample was necessary, whereas Lohff made no mention of this. Both of these workers found that if the residual pressure in the system was less than 10^{-8} torr no emission was observed. Wüstenhagen (25)(26)

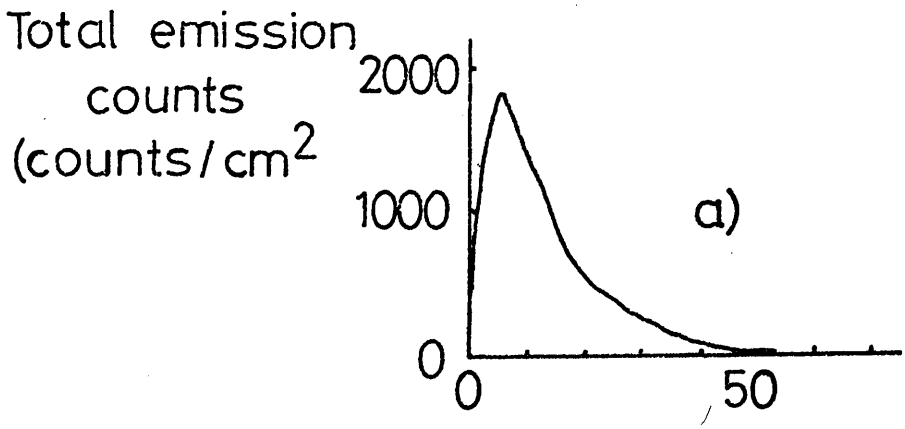

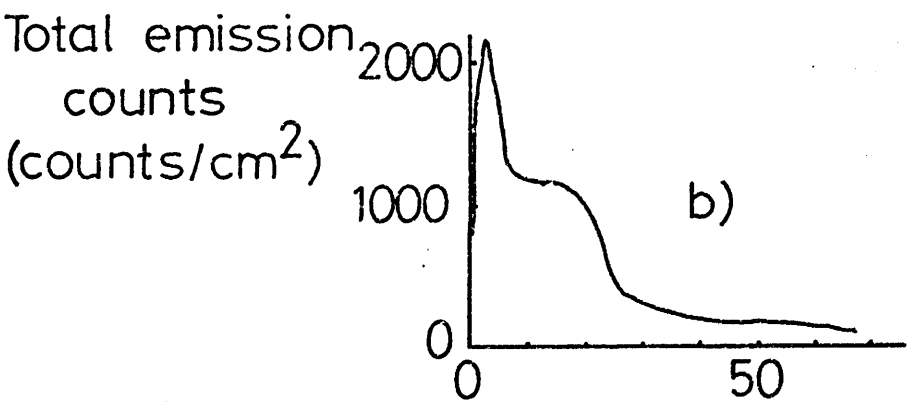

a):- vacuum-annealed iron.
b):- hydrogen-annealed iron.

Variation of thermo-exoelectron emission activity (integrated counts of the exoelectrons emitted) with depth of dissolved layer from abraded iron surface.

figure 2.

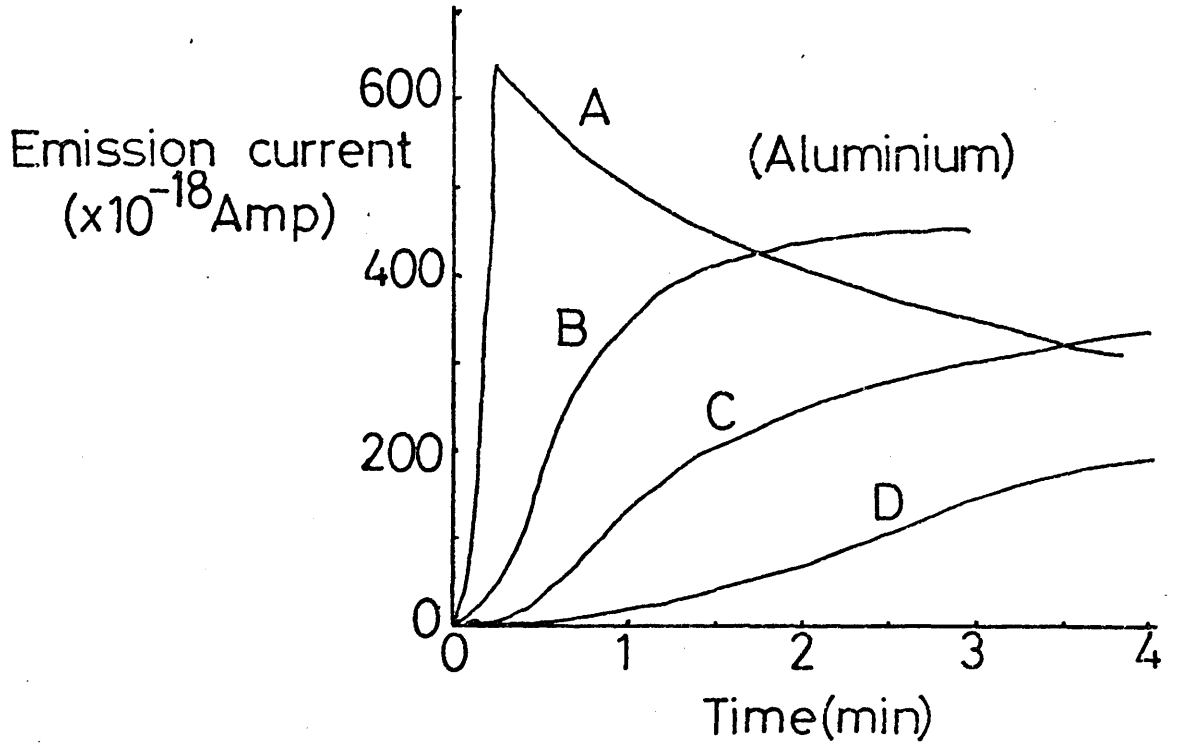

Electron emission current versus time after abrasion at various pressures of air and at 20°C. A):-10^{-5} torr, B):-2×10^{-6} torr, C):-10^{-6} torr, D):-4×10^{-7} torr.

figure 3.

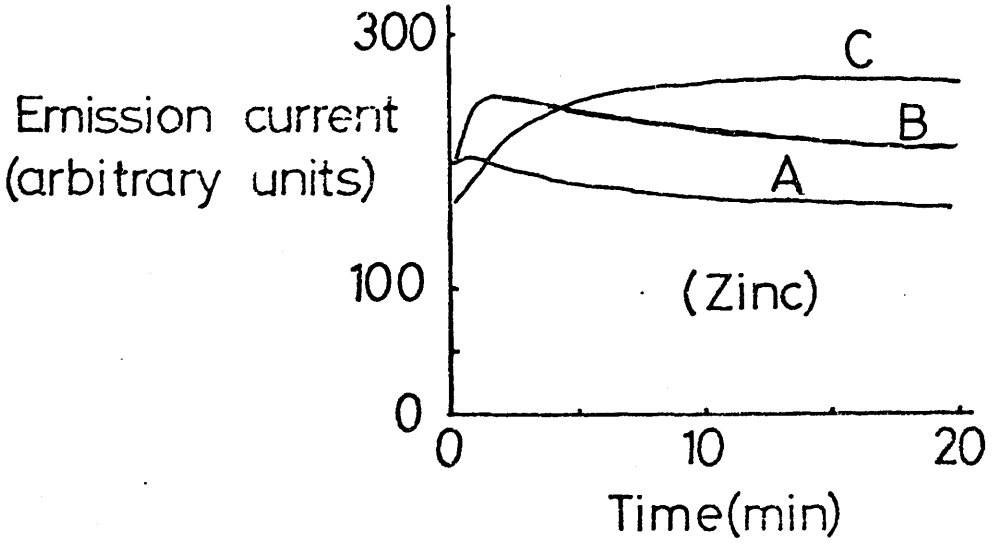

Electron emission current versus time after abrasion at various pressures of air and at 20°C. A):- 6×10^{-4} torr, B):-$2{\cdot}8\times10^{-4}$ torr, C):-10^{-5} torr.

obtained the same results with evaporated aluminium. Ramsey (27) put an upper limit of $2{\cdot}5 \times 10^{-18}$ Amp on the emission current at a pressure of 10 ntorr until air was introduced, when the current increased.

In 1964 Ramsey and Garlick (28) had investigated the exo-electron emission from aluminium and zinc abraded in atmospheres of air or oxygen over a range of temperatures and pressures. They found no emission could be observed in the dark during or after abrasion unless the temperature was very high.

They also observed that if, during emission, the specimen was suddenly cooled the emission fell rapidly to zero or a very small value. Emission was restored when the sample regained its original temperature. The decay of the emission could also be halted by cooling, thereby demonstrating that the processes involved had thermal activation energies.

These workers also found that if illumination was not provided until a lapse of time after abrasion, the emission had reached the stage it would have if light had been falling on the specimen all the time.

As temperature was increased from room temperature, Ramsey and Garlick found that the initial stage of exo-electron emission was prolonged and that the exo-electron activity of the surface persisted much longer (see (28 and 29) and fig 4 and 5, page 8a).

These workers made a tentative attempt to explain their results in terms of oxidation of the metal. To prove that oxygen was the gas responsible for exo-electron emission, Ramsey later carried out a series of most significant experiments where aluminium was abraded in atmospheres of dried air and dried, spectroscopically pure oxygen and nitrogen (24). He found that at very low pressures there was an 'incubation' period before emission commenced, which

figure 4.

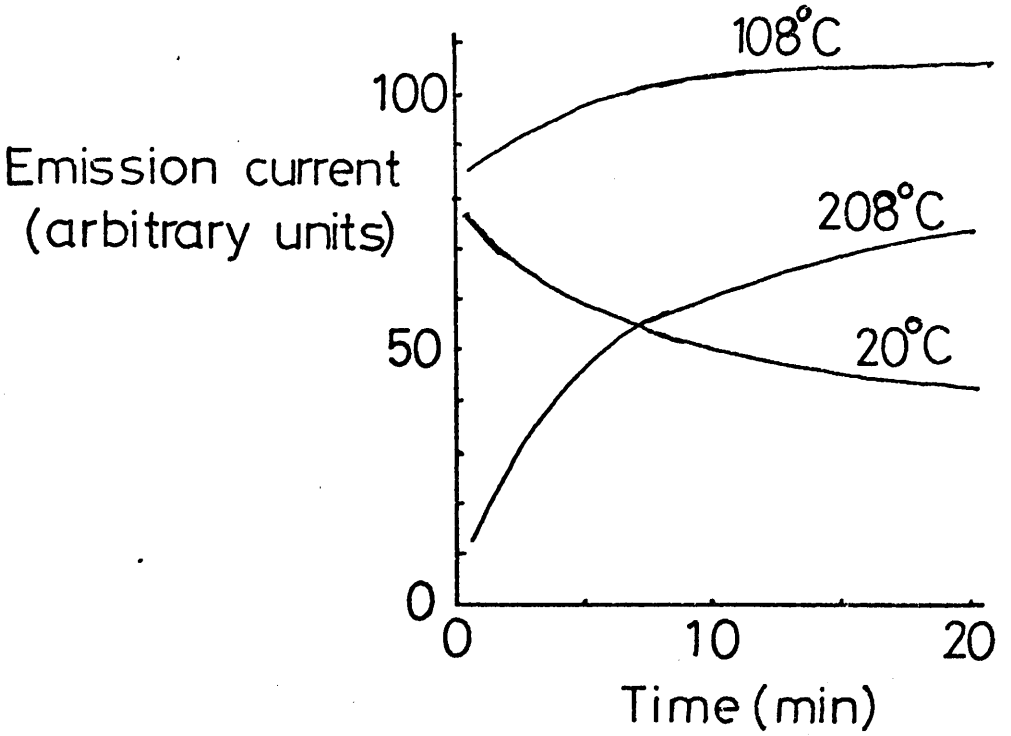

Exo-emission from abraded aluminium at 10^{-5} torr to illustrate the effect of temperature.

figure 5.

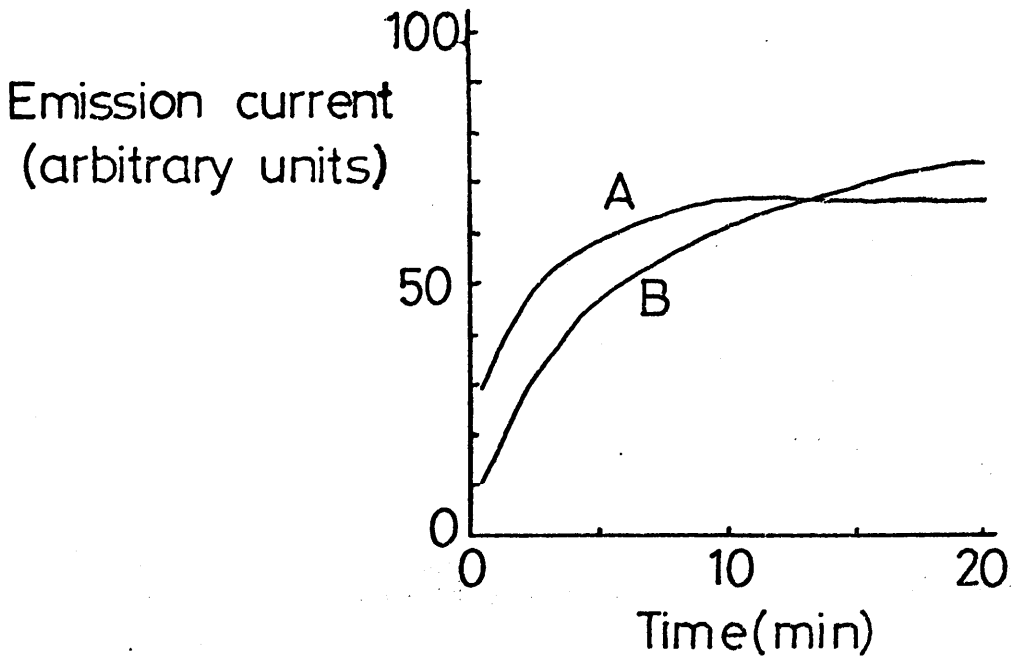

Exo-emission from abraded aluminium at 208°C to illustrate the effect of pressure.
A):- $2{\cdot}8 \times 10^{-4}$ torr, B): 10^{-5} torr.

was the same in oxygen and air. Although the peak maximum was reached sooner for oxygen, it was less intense than for air. Unlike the situation in air, the peak was relatively pressure independent in pure oxygen. There was a small amount of emission from specimens abraded in nitrogen but this was attributed to impurities, such as traces of oxygen in the nitrogen rather than to any interaction of nitrogen itself with the surface.

Ramsey explained the incubation time as being due to formation of a monolayer which was necessary before emission could start. The time would be long at low pressures due to the small amount of gas present.

Since these results indicated that oxygen was not solely responsible for exo-electron emission, Ramsey (30) examined aluminium surfaces abraded in atmospheres containing water vapour and found that there was a rapid rise in exo-emission, which remained steady over about 200 seconds in pure water vapour but which decayed in a water vapour/oxygen atmosphere (see fig 6, page 9a). This implied that oxidation is responsible for the decay in exo-electron emission.

Most studies of the interaction of oxygen with aluminium (see (31) for references) indicate that the work function of aluminium, ϕ_{Al}, decreases by $\frac{1}{2}$ - 1 eV due to the presence of chemisorbed oxygen or to a thin oxide layer. In direct contradiction, however, Huber and Kirk (31) have shown in a thorough investigation carried out at pressures in excess of 10^{-7} torr that the work function of the aluminium surface only changed by 0·05 eV when absolutely dry, spectroscopically pure oxygen was used. When water vapour was introduced ϕ decreased by 1 eV.

If the aluminium had been exposed to sufficient oxygen to give

figure 6.

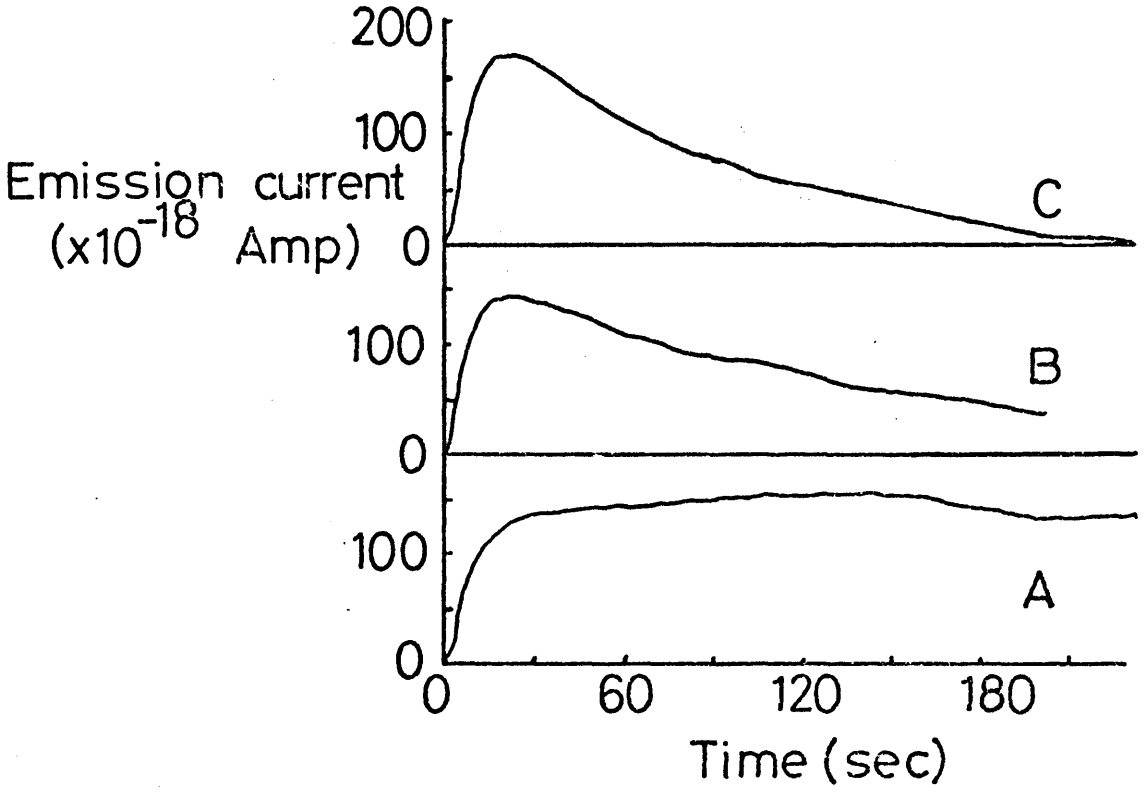

Electron emission current versus time after abrasion in water vapour and oxygen;

A):- water vapour 6×10^{-6} torr,

B):- water vapour 6×10^{-6} torr, oxygen 10^{-5} torr,

C):- water vapour 6×10^{-6} torr, oxygen $2{\cdot}5 \times 10^{-5}$ torr.

monolayer cover then ϕ decreased by 1 eV immediately water vapour was introduced. If, however, water vapour was introduced to a clean aluminium surface, ϕ remained almost constant for some time before it started to decrease.

Huber and Kirk proposed that water interacted with clean aluminium to give a monolayer of oxide on which more water could adsorb to produce the 1 eV reduction in ϕ_{Al}.

To explain the surprisingly small decrease in ϕ brought about by adsorption of pure O_2, Huber and Kirk invoked a place exchange model similar to one proposed originally by Lanyon and Trapnell (see (31)). This may be represented schematically as

This exchange of place of an oxygen atom with a metal atom after oxygen adsorption on a dual adsorption site will lead to an alternating dipole arrangement, whose resultant would be close to zero.

Ramsey cited these results to explain the incubation time he had observed in the work he carried out in ultra high vacuum. This was the time required to prepare the aluminium surface for the adsorption of the traces of water to be found in a glass vacuum system which he had used.

The photoelectric threshold of aluminium is 2,900 Å. Ramsey used light of wavelength 3,400 Å in his investigations. This corresponds to a work function decrease of 0·5 eV.

Ramsey also cited the work of Doherty and Davis (32) who showed that an aluminium oxide film formed below 500°C is amorphous. This invalidated the concept of a geometrically well-defined trapping centre and so Bohun's use of an analogy with colour centres and Grunberg and Wright's theory of emission from F' centres had to be discarded. Grunberg and Wright's theory was suspect in any case since no other workers, including Ramsey and Garlick (28) had been able to find an emission peak at 4,700 Å.

Pimbley and Francis (33) suggested that abrasion created vacancies which diffused to the surface. During their subsequent annihilation these could give rise to electron emission. Emission decay was due to exhaustion of the supply of these vacancies. Later work by Mueller and Pontinen (34) with abraded and etched aluminium before and after ageing disproved this theory.

Scharmann and Seibert (35) found with abraded aluminium that the ability to emit photo-electrons decreased with time when the abraded specimens were stored in vacuum, presence or absence of light having virtually no effect on this loss of emitting ability, which would seem to the present author to be due to slow oxidation by adsorption of the residual gas in the system. They also heated abraded specimens in the dark at various pressures and found that they could only obtain glow curves if the pressure was 10^{-5} torr or greater. No emission was observed at 10^{-8} torr, thus proving that an oxide layer is essential to thermo-stimulated emission from metals.

Gesell, Arakawa and Callcott (36) investigated bulk magnesium abraded in water vapour or oxygen in the range from 5×10^{-10} to 1×10^{-6} torr partial pressure in total darkness at room temperature. They obtained emission currents as high as 2×10^{-11} Amp/cm^2

from the specimens and found similar results with vacuum evaporated films.

The emission characteristics varied with pressure as shown in fig 7, page 12a. The two maxima were taken to indicate that the process was not simple, unlike the case with aluminium where only one maximum is ever obtained. The possibility that the second maximum was due to adsorption of residual water vapour in the system was considered, however.

When magnesium samples were exposed to water vapour only one maximum was obtained. For the corresponding pressure it took longer to reach this maximum than in oxygen and the high emission rate persisted longer. They also found a small emission when magnesium was exposed to methanol.

Gesell and his co-workers examined aluminium under the same conditions and found no emission. In a further series of experiments Gesell and Arakawa and Callcott showed (37) that the work function of a freshly abraded magnesium specimen varied between 3·3 and 1·8 eV and that in oxygen it went through two minima which corresponded to photoemission maxima and which were closely related to the two maxima of exo-emission from the surface.

Gesell, Arakawa and Callcott (36) concluded that the energy given to the excited electrons was almost certainly derived from the reaction of oxygen or water with a freshly exposed magnesium surface and that an emission current could be obtained in the dark when highly energetic reactions take place on a surface with a very low work function, for example at approximately monolayer coverages of oxygen or perhaps OH or H_2O on magnesium.

In a most significant study Gel'man and Roikh (38) carried out simultaneous measurements of the exo-electron emission,

figure 7.

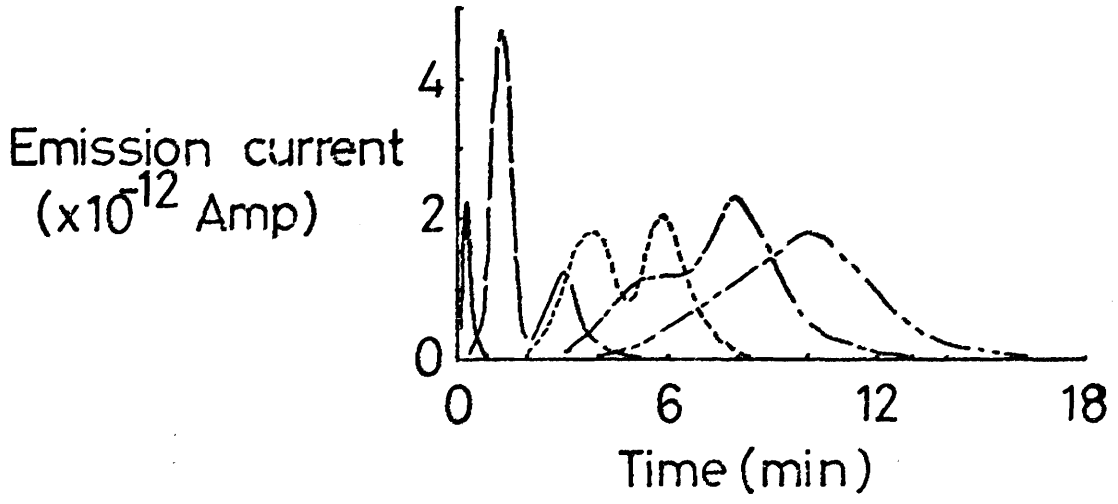

Electron emission current versus time after abrasion of magnesium in oxygen at various pressures.

——————— :- 9×10^{-8} torr,
— — — :- 2×10^{-8} torr,
---------- :- 6×10^{-9} torr,
— - — - — · :- 3×10^{-9} torr,
— - - - — - - — ·· :- $1{\cdot}5 \times 10^{-9}$ torr.

surface potential and oxide thickness of deformed and undeformed magnesium samples. With vacuum-deposited metal they found that the initial count-rate was high but that it fell away quickly and then remained almost constant (see fig 8, page 13a). With bulk samples they found that the emission characteristics followed the change in surface potential for about an hour and then the emission decayed despite continued lowering of the surface potential. They realised that while the oxide layer was thin the emission followed changes in the surface potential but as the oxide thickness increased the effect of the oxide became more pronounced.

Gel'man and Fainshtein (39) continued this investigation of the two stages of oxidation of a metal. At first emission kinetics followed changes in surface potential until a critical oxide thickness, L, was reached. Then they were affected by the thickness of the oxide layer. Gel'man and Fainshtein tried to correlate this effect with the wavelength of the electron, λ_{el}, and film thickness L. They proposed that the first stage corresponded to $L < \lambda_{el}$ so that exo-emission was an oxidation-stimulated photo-effect. In the case of $L > \lambda_{el}$ scattering and capture of electrons by film defects became important and electrons released from local levels associated with oxide defects and adsorbed molecules subsequently participated in the emission. They carried out parallel studies of exo-emission, surface potential and oxide growth on magnesium samples irradiated with monochromatic light of different energies.

Change in light energy did not affect surface potential or oxide growth but it was found that as photon energy increased, i.e. λ became shorter, the correspondence between time dependence of emission and surface potential was disrupted at lower oxide thick-

figure 8.

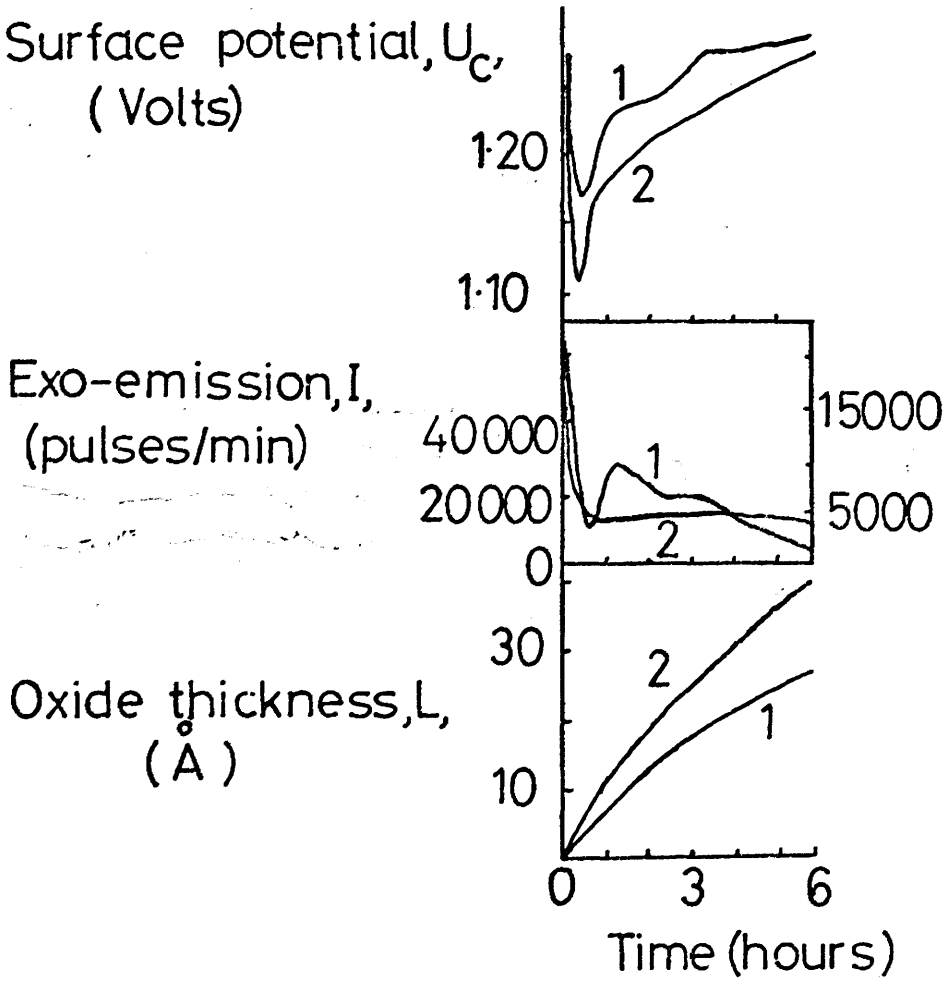

Kinetic curves for the contact potential difference U_c, the exo-emission I, and the oxide increase on cast magnesium (1) and vacuum condensates (2) after mechanical cleaning. The scale on the right is for the exo-emission of cast magnesium.

nesses as predicted (see fig 9, page 14a).

In fact it seems apparent to the present author that these key results tend to reconcile the two main conflicting theories of exo-electron emission from abraded metals. The first is that exo-electron emission is a pressure-dependent photostimulated emission where the emission threshold is shifted to longer wavelength (except where the work function of the metal is sufficiently low that chemically-stimulated emission may take place in the dark: see for example (36) (37)). Gel'man and Fainshtein suggested that these results have always been found in vacuum conditions over comparatively short times so that the condition $L < \lambda_{el}$ is satisfied at all times.

The other, earlier, view suggesting that emission was from well-defined defects analogous to colour centres, or from surface adsorption sites may also be accepted since these results have generally been obtained in the atmosphere or under much poorer vacuum conditions so that $L > \lambda_{el}$ and emission <u>is</u> from the oxide. This theory of well-defined sites would therefore be applicable to electron release from thick oxide films on metals where the oxide is regular or ~~for~~ to emission from pure oxides. Thus Krylova (40) showed that thermally-stimulated emission centres are also the centres of activated desorption while Euler, Kriegseis and Scharmann (41) again demonstrated the importance of adsorption and desorption centres. These results will be dealt with in greater detail later.

From fig 9, page 14a it may be seen that a 0·12 V ~~in~~de crease in surface potential reduced the exo-emission intensity by a factor of 5. Thus Gel'man and Fainshtein concluded that 80% of the electrons detected had energies below 0·12 eV at the metal-oxide interface.

figure 9.

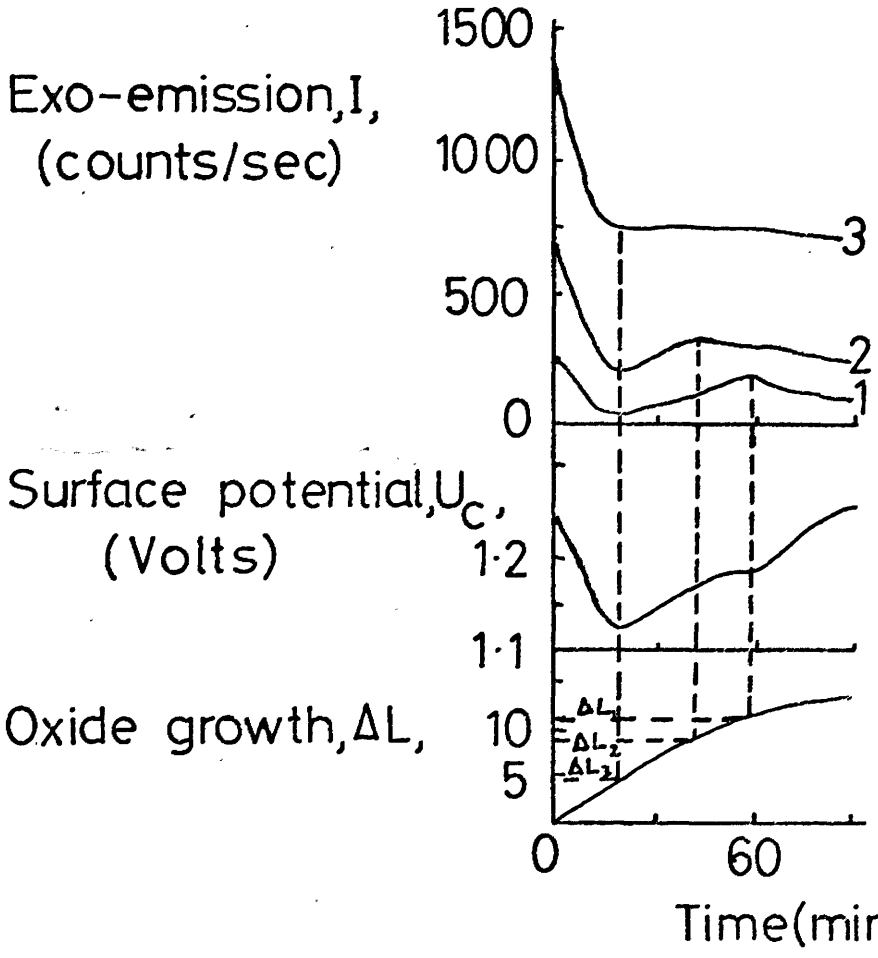

Kinetic curves for the exo-electron emission I, the contact potential difference U_c, and the oxide growth ΔL on magnesium samples oxidised in air after mechanical treatment to show the effect of illumination by light with various photon energies, hν, eV:-

1):- 3·55, 2):- 3·78, 3):- 4·27 eV.

1·3 Deformation

Studies of abraded and plastically deformed metals are both important in attempting to elucidate the processes involved during mechanical working or fatiguing of a metal.

Exo-electron emission studies after abrasion give a very sensitive means of studying oxidation and other gas adsorption processes on a clean metal surface. Their main disadvantage, however, is that the degree of deformation of the surface can not be accurately estimated. This is why studies of plastic deformation are important since the extent and degree of deformation may be easily controlled and measured: emission during deformation may also be studied. Furthermore a fairly clear picture of the mechanism of plastic deformation has evolved through more conventional studies; thus the results from exo-emission studies may be related to this.

As the methods of stimulation are very different, abrasion immediately laying bare clean metal, plastic deformation initially straining the oxide until its eventual fracture exposes clean metal, it seems unlikely that the respective emission mechanisms will be the same.

1·3·1 Plastic Deformation at Constant Strain Rate

Meleka and Barr (42) applied a highly radiation-sensitive stripping emulsion to single zinc crystals which were subsequently strained. Black lines appeared in the emulsion (cf (4)) which exactly corresponded to the sliplines on the crystal surface. They proposed that areas of slip, where the underlying metal comes through the oxide layer, act as emission sites for electrons. The blackening of the photographic emulsion is due to the presence of hydrogen peroxide which Grunberg, see (15), has shown is formed

by the interaction of a low energy electron, emitted from the metal surface, with oxygen in the presence of moisture.

In a review of exo-electron emission from metallic materials Brotzen (43) refers to a review by Hempel, Kochendörfer and Tietze (44) where they mentioned some of their own results from mechanical working of aluminium and carbon steel. They found it necessary to irradiate samples with light of $\lambda < 5{,}000$ Å to obtain emission. Etching increased emission while heating lessened it. They found a strain of at least 1% was necessary to initiate emission and they did not observe any emission in the dark. They suggested emission was from defects in the oxide layer.

Brotzen himself (45) (46), tried to correlate quantitatively the mechanically induced changes in polycrystalline aluminium with exo-electron emission. He and his co-workers found that the emission rate during and after straining depended strongly on the strain history of the specimen, indicating the structure-sensitivity of the process. He and von Voss (45) postulated a model to explain their findings similar to that of Pimbley and Francis (33) for abrasion. They proposed that vacancies formed during mechanical working diffused to the surface where they could form centres for photo and thermionic emission in an unspecified manner. The work done by Mueller and Pontinen (34) similarly disproved this theory.

Sujak and his co-workers have carried out many investigations of exo-electron emission phenomena, e.g. (47)-(56), including emission from deformed aluminium. Most importantly, Gieroszynski, Mader and Sujak (47) found that if oxides of different thicknesses were deposited electrolytically on aluminium, a definite amount of tensile strain, ε_0, had to be applied before emission could be

detected. ε_o increased with increasing oxide thickness to a maximum around 1μm and then as oxide thickness continued to increase, ε_o decreased again, see fig 10, page 17a. They measured crack width, B, and oxide thickness, D, and found the ratio B/D decreased monotonically with increasing oxide thickness. They later found (48) that in the presence of moisture the increase in ε_o was less pronounced.

Sujak, Gieroszynski and Mader (49) found that as the intensity of the light used to stimulate emission was increased, the exo-electron emission rate also increased. An open-window air-filled point counter was used for this investigation.

Sujak, Gieroszynski and Pega (50) studied the emission from plastically deformed aluminium at a pressure of 10^{-5} torr. They found that emission increased with deformation until the sample fractured, when emission started to decay. They also noted that, as was the situation with samples examined in air atmospheres, there was a critical oxide thickness beyond which emission only commenced when the sample had been fractured. This limiting thickness increased with the frequency and intensity of the stimulating radiation, and also with the applied field (50), (51). These workers also found (50) that the amount of strain, ε_o, required to initiate emission depended on several factors. Apart from a dependence on oxide thickness, D, ε_o decreased exponentially with increasing field strength. An increase in the intensity of the stimulating light caused a decrease in ε_o while pretreatments such as annealing also had an effect.

A later study by Gieroszynski and Sujak (52) showed that, as the wavelength of the stimulating light increased, the value of the strain required to initiate emission also increased.

figure 10.

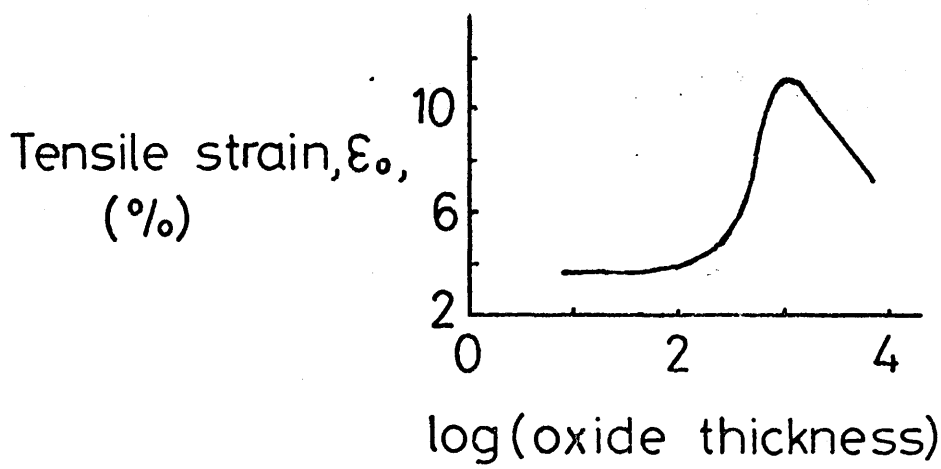

Plot of tensile strain, ε_o, required to effect exo-electron emission from anodically oxidised aluminium as a function of the oxide thickness.

Gieroszynski, Mader and Sujak (48) had proposed that emission was due to cracks formed in the oxide layer. Fissures gave rise to a charge separation, opposite faces having opposite sign, and hence an electric field was set up. Electrons were released from the transitional metal-oxide layer at the bottom of the cracks (50), (53), (54), (55) but this transverse field hindered their escape from the fissures so that a space charge was set up which varied with time, thereby varying the emission rate. Presence of water molecules or an applied field distorted the transverse field, thus making emission easier.

Although the basic results obtained seem valid, the present author found the theory proposed to explain these results to be unacceptable. Several gross assumptions were made for which there were no clear proofs. The most fundamental of these was that cracks formed in the oxide layer would give rise to a charge separation (see fig. 11, page 18a). This must be discounted since as Doherty and Davis (32) have shown (see Ramsey (30)) a film of aluminium oxide formed below 500°C is amorphous. In this situation charge separation would seem to be most unlikely.

For oxide thicknesses in excess of 50 nm Gieroszynski and Sujak (56) found a dark emission, though there was no electron release on fracture of the specimen unless it was illuminated. As strain increased at a constant strain rate, two maxima were obtained at low deformation values, with or without illumination when under vacuum, but only in the presence of light in air. The strains at which these maxima occurred decreased as the oxide thickened.

Arnott and Ramsey (57) corroborated the main findings of Sujak's group in a study of the electron emission from anodically

figure 11.

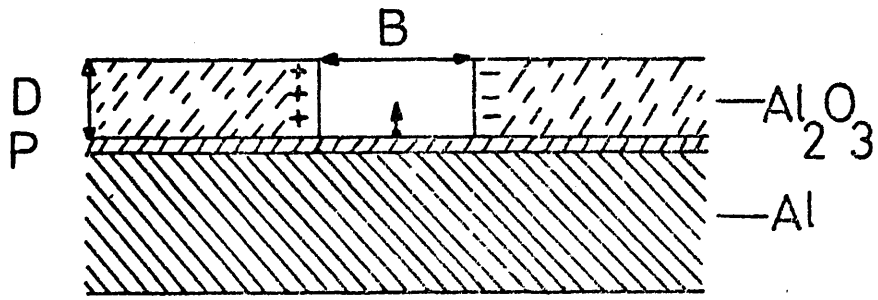

Diagram of a chink: B:- width of the chink,
E_o :- electric field strength within the fissure,
D:- thickness of the oxide layer,
P:- transitional metal-oxide layer.

oxidised aluminium. That is, they found a pressure-dependent photostimulated emission similar to that from abraded metals but here the clean metal was exposed by two distinct mechanisms (a) slip penetrating the oxide film: this occurred for thicknesses less that 45 nm, (b) specimen breakage.

Above 45 nm they found a dark emission. Microscopically there was no sign of slip but formation and propagation of cracks in the oxide layer were observed. Arnott and Ramsey interpreted their results differently, however. They did not believe that aluminium oxide would crack in a way that would cause charge separation (see (30)). They postulated that the photostimulated emission was due to oxygen adsorption on the metal surface that had been freshly exposed by the slip mechanism. In contradistinction, Thomas (58) proposed that clean metal itself would not be revealed. He believed a thin transitional oxide or water vapour adsorption layer would remain over the clean metal at the slip plane. Oxidation, with accompanying emission, would still proceed faster giving enhanced emission. Arnott and Ramsey proposed that ε_o increased due to inhibition of slip as the oxide became thicker. They further suggested that emission in the dark was due to cracking of the oxide film and was relatively pressure independent. Dark emission commenced at 2 - 3% strain and required a non-zero strain rate for emission to continue. This occurred with or without photostimulation. Dark emission might be expected at all oxide thicknesses but it probably only becomes appreciable above 40 - 50 nm.

It is the present author's belief that these results could well be explained in terms of Gel'man and Fainshtein's theory (39) of the two stages of exo-electron emission depending on the

thickness of the oxide film with respect to the wavelength of the emitted electrons. Thus it would seem there are greater similarities between these two methods of stimulation than might have been expected.

Finally it should be noted that Yoshiro (59) and Tanaka (60) have both shown that the surface potentials of aluminium, magnesium and titanium changed during tensile deformation. After straining ceased the surface potential gradually returned to its original value in a manner strongly reminiscent of exo-electron emission after deformation.

1·3·2 Cyclic Stress

As well as deformation at a constant strain rate, exo-electron emission from samples undergoing cyclic stress has also been investigated. For example, Mints, Kortov, Aleksandrov and Kryuk (61) studied austenitic steels of different compositions under a cyclic stress of 50 c.p.s. As well as measuring the resultant exo-electron emission, they monitored the strengthening of the samples by measuring the changes in the microhardness of the surface, and measured the changes in their cross-sections. During stress cycles the impedance of the specimens was also measured and the internal dissipation of the strain energy was determined from the changes in the amplitude-dependent internal friction.

It was found that exo-emission increased fastest during the initial stages of stress ($\sim 10^5$ cycles) and then emission increased more slowly before it levelled off or even decreased.

As a metal undergoes cyclic stress it strengthens. Mints and his co-workers found that the degree of strengthening varied with the alloy composition. In chromium-manganese based austenitic steels mechanical energy may be dissipated internally to a much

greater extent than in chromium-nickel based alloys. Thus the strengthening of chromium-manganese based alloys is greater and it was found that exo-emission was far lower from these samples. Mints suggested that this was because less energy was stored in defects able to be used for the release of electrons.

In fact, chromium-manganese based austenitic steels are less stable and the dissipated mechanical energy goes towards the disintegration of the metastable austenite.

Mints and his co-workers proved that energy dissipation was important by examining a steel alloy in the brittle and ductile states. After temper-embrittlement of a ductile steel the only physical property which changes appreciably is the internal friction. The same degree of strengthening was obtained during stressing of the two alloy states but energy dissipation was lower for the temper-embrittled case and exo-emission was correspondingly lower also.

Thus it was demonstrated in this work how sensitive a technique exo-electron emission is for studying deformation processes in metals.

By scanning samples of aluminium undergoing fatigue cycling with a small spot of ultraviolet light at 10^{-8} torr, Baxter (62), (63) was able to measure the localised electron emission rather than the integrated count. He recorded emission after 0·1– 1% of the fatigue life and was able to show that, as cpm were plotted against distance along the sample in mm, localised emission peaks built up as cycling proceeded. Each of these peaks occurred where a crack eventually formed in the oxide. Cracks cannot be observed until at least 5% of the fatigue life (64), and then only on electron micrographs of carefully polished surfaces. More usually

cracks are observed between 10 - 50% of the fatigue life.

Baxter has always found that fracture takes place in the region of most intense emission, although that crack may not always be one of those formed initially.

More recently Rabinowicz (65) published results of an investigation into the way in which ball and roller bearings fail. It was known that surface-fatigue wear was the main cause of failure with these items and that it made a very important contribution to wear in gears and in wheels rolling on rails. It was also known that with ball-bearings surface fatigue developed when a crack formed in a ball and grew until a sizeable chip spalled off. Rabinowicz was able to show that as the level of stress experienced by a ball-bearing increased then peaks of exo-electron emission increased and spalling eventually took place at the site responsible for one of these peaks.

More importantly, however, he confirmed conclusively that when a crack started to form in a ball which had always rotated in the same direction, then it was propagated from the leading edge to the trailing edge. In other words the crack grew in a direction opposite to the direction of rotation. Previously only indirect evidence had been available to support this view.

As detection techniques improve then the applications of this method of detecting incipient metal fatigue must surely increase.

1·4 Phase Changes

Kramer (1) noticed that when Wood's metal was solidified from its melt what he called exo-electron emission was observed. Futschik (66) confirmed this in 1955 and demonstrated the same effect for solidification of mercury. Then Futschik, Lintner

and Schmid (67) carried out a series of experiments on lead-tin alloys using a hydrogen-ethanol filled Geiger-Mueller counter. They found a perfect correlation between the phase diagram and temperatures at which emission maxima occurred during the cooling cycles.

Bathow and Gobrecht (68) showed that if the specimen surfaces were really clean and they were held in a vacuum better than 10^{-6} torr then no electrons were observed during phase change. Thereby they proved that it was not an exothermic process that was involved. They kept their samples in a specially designed vacuum system and used an electron-optics device to focus the emission current into their counter, thus avoiding gas interactions with the specimen surfaces.

Kahlert and Kralik (69) studied tin, lead and bismuth during melting and freezing. Unlike most other workers they found emission during melting as well as freezing of tin and lead but only during melting of bismuth. They observed an optimum oxide thickness for which emission peaks were most pronounced and also that reduced surfaces gave no emission at all. They proposed that the volume changes in the metal during melting and freezing caused strain in the oxide layer. Kahlert and Kralik then suggested that dislocations would be formed to ease the strain and dislocations of opposite sign could annihilate each other. The energy thus produced would be sufficient to release electrons from defects in the oxide. This view rationalises the observation of an optimum oxide thickness by assuming that the defect density in the oxide layer was greatest near the metal-oxide interface.

In view of the findings of Bathow and Gobrecht (68) that no emission was observed from clean surfaces at pressures below

10^{-6} torr it would seem to the present author that emission is from defects and cracks in the oxide layer. The defects and cracks would be formed by the volume changes of the underlying metal in a manner akin to plastic deformation. Thus these results may be interpreted according to the model proposed by Arnott and Ramsey (57) to explain exo-emission from strained aluminium.

Sujak and his group have found exo-electron emission accompanying both magnetic and non-magnetic phase changes of metals and alloys ((70)-(74)). They found (70) that photo-stimulation was necessary and also that during recrystallisation cracks formed in the oxide layer. Peaks have been observed at the Néel point of NiO and the Curie point of Ni (71),(72), and also at the Néel point of Cr_2O_3 and the Curie point of the underlying pure Cr (72). These peaks were more pronounced on heating specimens and less pronounced during cooling.

A peak corresponding to exclusion of excess Mg_2Si from super-saturated solution was observed by Sujak, Biernacki, Tokarski and Gorecki (73) during ageing of an Al-Mg-Si alloy. This always occurred about 60 minutes after ageing commenced.

During heating of a sample of magnetic pyrites, FeS, two polymorphic phase changes occur, one a low temperature α-phase transformation and the other at the high temperature β point. The α transformation temperature depends on S-content and so the peak corresponding to this may give an accurate estimate of the % S. Pyrrhotite also undergoes several magnetic transitions. Heating samples of the mineral gives rise to five emission maxima which may be assigned to the magnetic and non-magnetic transitions (74).

These workers have clearly shown what a sensitive method

exo-emission is for studying both magnetic and non-magnetic phase changes and this must have important technological applications. Indeed, in (74) Sujak et al showed that the temperature of the emission peak corresponding to the α phase transformation could be used to determine the amount of sulphur present.

In general exo-electron emission is only observed when the surface-structure of the sample under investigation is altered, by abrasion, plastic deformation, irradiation. It must be stressed that Sujak's group have made no mention of any other physical changes accompanying magnetic phase transformations, which certainly should not give rise to volume changes in the metal. Thus it becomes difficult to understand how electron emission can occur when the distribution of defects in the surface layer remains constant and no chemical reaction is occurring at the surface.

However, since the numbers of electrons available at the surface controls the amount of adsorption and desorption of gases that can take place, it seems reasonable to the present author to suggest that magnetic changes within a sample could alter the electron-distribution at the surface; this would change the 'adsorbability' of the surface and hence its emission characteristics. The nett adsorption or desorption would give rise to an emission of exo-electrons.

To test this theory it would be necessary to monitor magnetic phase changes in high vacuum where any accompanying pressure change might be observed.

Some support is given to this idea by the findings of Kedavichus, Yuodvirshis and Belyatskas (74a) who observed electron emission during the ferro-electric phase transition of semiconductor SbSI which occurs at room temperature.

These workers found that if the sample was irradiated with an X-ray dose of 1200R the emission accompanying the phase transformation was increased by a factor of 10. They proposed that since X-irradiation increased the electron emission then emission must be from structural defects.

At the phase transition they found that the pyroelectric current is severely modulated and both the permittivity, ,ε, and the loss-angle tangent, tan δ, increase rapidly (see fig 12, page 26a).

The pronounced change in the pyroelectric current could certainly alter the electron distribution at the surface.

Kania, Pirog and Sujak (75) have even shown that there is a photostimulated exo-electron emission during freezing of dilute aqueous solutions of NH_4OH.

1·5 Alloying

Hoenig and Pope (76) carried out a study of the electron emission from metal filaments used to evaporate other metals for deposition of thin films. They found that if the metal being evaporated could alloy with the filament then a significant number of high-energy electrons (E = 5 eV) were emitted during the alloying-evaporation. If, however, the metal could not alloy with or wet the filament then the electron current was the same as with the bare filament.

Thus Hoenig and Pope suggested that this method could be used for investigation of dilute alloy systems where X-ray techniques lack sensitivity.

1·6 Ionising Radiation

In general ionising radiation, α, β, γ or X-rays, has been

figure 12.

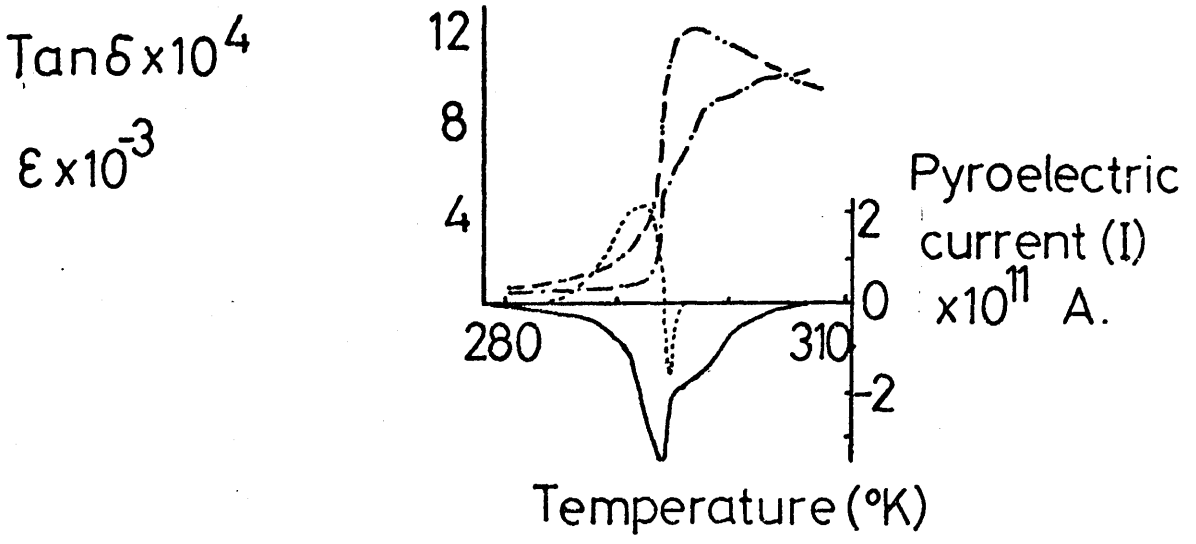

Temperature dependence of the pyroelectric current I, permittivity ε, and loss-angle tangent tan δ, of SbSI single crystals, determined parallel to the (001) crystallographic axis.

..... :-pyroelectric current, temp increasing,
——— :-pyroelectric current, temp decreasing,
- - - - - - - - :-permittivity, temp increasing,
-·-·-·-·-·- :-loss-angle tangent, temp increasing.

employed to study non-metals to try to find analogies between exo-electron emission and luminescence and to ascertain if exo-electron emission from radiation-damaged solids could have applications in dosimetry. A very few studies have been carried out on pure metals.

1·6·1 Exo-Emission from Metals after Exposure to Ionising Radiation

Work was done in the fifties in Vienna on the emission from oxidised and X-irradiated metals during heating cycles. The emission curves were very similar to luminescence 'glow curves' and this accounted for the popularity of the theory proposed by Bohun (19) and other workers that exo-electron emission was from colour centres in the oxide layers. Hieslmair and Müller (77) showed that, regardless of the temperature at which they had been oxidised, metals which were subsequently X-irradiated and heated at a constant heating rate all gave two glow peaks, one at 160° and the other around 260°C. Peak heights and the relative intensities of the two peaks varied. These results were taken to indicate that electrons came mainly from the surface layer which must be virtually identical for all oxide surfaces and that the metal substrate was relatively unimportant. They also found that the average temperature for an emission peak from a metal sulphide was 140°C.

Vogel (78) confirmed this using electron-bombarded metals. He monitored the emission with an electron-multiplier instead of a Geiger counter. Meanwhile Birgfellner (79) showed that X-irradiation with 30 kV X-rays gave rise to a surface layer capable of emission 20 μm thick with copper, zinc, iron and an iron-nickel alloy.

There has been controversy about whether results are valid if they have been obtained in a counter with an atmosphere instead of under vacuum conditions. Kralik (80) examined the emission from X-irradiated metals using an electron-multiplier and a Geiger-Mueller tube to see if the method of detection was important. He found no difference in the results obtained by these two methods for metals but there was a significant difference for non-metals. Kralik attributed this behaviour to the tighter binding of the oxide layer to a metal than a non-metal. It is obvious, however, that if oxidation or any other chemical process were being investigated then the nature of the counting atmosphere would be of the utmost importance.

In a most interesting study Scharmann and Seibert (35) investigated the position of the glow peaks of aluminium as a function of the method of stimulation. They obtained two peaks, one around 115°C and the other around 250°C. β-irradiation enhanced the peak at 250°C while mechanical working caused an increase in the peak at 115°C. Exposure of aluminium to 4 keV electrons gave rise to glow peaks at the same temperatures as before. The intensity of the peaks was much greater, presumably since much more damage was done to the aluminium surface by this bombardment.

Drost (81) reviewed exo-electron emission from metals subjected to glow discharges. He showed that plots of the decay in electron emission with time at constant temperature were similar to those obtained after other forms of irradiation or after abrasion.

Glow discharge gives rise to a much more intense emission than other forms of stimulation and Brotzen reported in his review

of exo-emission from metals (43) that Sinelnikov (82),(83) found that electrons were emitted with energies up to 150 eV. This should be compared with the value of 0·1 - 0·2 eV for electrons emitted during oxidation of abraded magnesium (39).

1·6·2 Exo-Electron Emission from Irradiated Non-Metals

It has been clearly shown by many investigators that the presence of a non-metallic layer was necessary before exo-electron emission was possible from metals. Thus it was a logical step to proceed to a study of non-metals.

For example, Kramer (1) reported that after mechanical disintegration of minerals such as fluorspar, corundum, pyrites and orthoclase a definite count rate was obtained. He further demonstrated that the constant-temperature decay curve for a non-metal was very similar to that of a metal. He later showed that a sample of X-irradiated pyrites gave a decay curve very similar to that of mechanically deformed pyrites (84) while X-irradiated gypsum heated gradually underneath a point counter gave rise to several emission maxima (14).

Bohun (85) realised that heating the sample meant that definite electronic energy levels could be studied. Accordingly, he proposed that emission from non-metals was from colour centres or other crystal imperfections. He carried out extensive studies of alkali halides, for example assigning glow curve peaks from rock salt to various types of colour centres found in it (86),(19).

There have been many other investigations of exo-electron emission from alkali halides, with much of the work in this field being executed by Kramer and Bohun. In 1955 Lepper (87) reported that when a crystal gave rise to both exo-electron emission and phosphorescence then the same decay law was obeyed. This

parallelism was also shown to exist for exo-electron and luminescence glow curves when they were observed simultaneously. This was discovered independently by Bohun (19),(88).

By investigating pure and Mn-doped $CaSO_4$ Lepper also demonstrated that while thermo-luminescence requires the presence of both donor and activator levels, pure $CaSO_4$ is not a phosphor, the exo-electron glow curves from the pure and doped salts were identical. Thus he concluded that exo-emission requires only donor levels. This meant that exo-electron emission could be used to study a much wider range of materials.

Exo-emission may also be detected below room-temperature with both metals and non-metals (46),(89). Gourge and Hanle (89) were among the first to suggest the possibility of using calcium sulphate as a radiation dosimeter since there is a linear relation between radiation dose and exo-electron emission.

Since 1957 many materials have been investigated with a view to their use as dosimeters for radiation by measuring their exo-electron emission. Although many were very sensitive, for example, Mn-activated $CaSO_4$ gave a response to a dose as low as 0·1 mR, signals tended to fade rapidly and results were often not reproducible. There were often sensitivity changes due to alterations in the surface and there was a response saturation often as low as 100 R. These disadvantages far outweighed the advantages over photographic film of low cost, lack of sensitivity to light prior to exposure, no need for complicated processing, re-usability and wide dynamic range as well as greater sensitivity to low energy radiation.

No progress was made until 1963 when Kramer (90) showed that by addition of a non-emitting, thermal and electrical conductor,

such as graphite, to a material that exhibits thermally stimulated exo-electron emission, such as BeO, thus making the electron-emitting layer an electrical conductor, the radiation response became linear over a wide dose range, at least six orders of magnitude. BeO is suitable as a dosimeter because of its relatively high sensitivity, its chemical and physical stability, its insolubility in water and its low atomic number. Furthermore its main thermal emission peak is conveniently located at a temperature of just over 300°C.

Becker, Cheka and Gammage (91) continued investigating BeO, impregnating it with several high-melting metals, notably platinum, palladium and gold. They found that incorporation of platinum and palladium increased the sensitivity of BeO. Unfortunately the response to dose level was not linear although this was outweighed by the fact that it was possible to detect doses in the μR region.

Some materials suitable for use as thermo-electron dosimeters emit only a sharp, single peak in the temperature range, 100 - 300°C, generally used. Examples of these are LiF and BeO. Various others, for example $CaSO_4$, $SrSO_4$ and $BaSO_4$ give rise to several peaks in this range.

Becker and Chantanakom (92) have shown that materials with a complex surface trap distribution, and hence thermally-stimulated emission spectrum, exhibit considerable differences in their responses to α and γ radiation (see fig 13, page 31a). Materials which give rise to only one emission peak, however, show only a slight shift to lower peak temperature on exposure to α-radiation (see fig 14, page 31b).

Becker and Chantanakom proposed that the high-LET (Linear

figure 13.

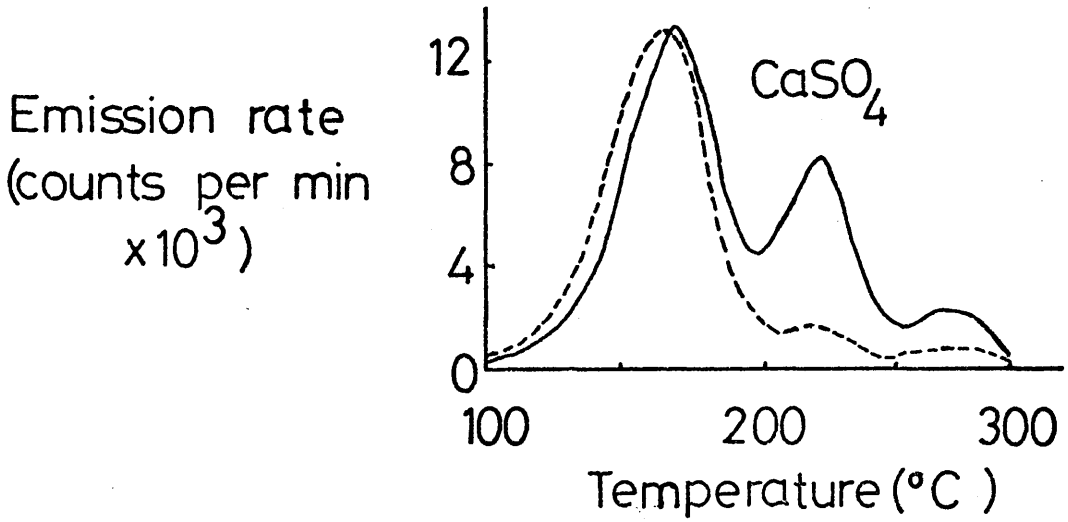

Thermally stimulated exo-emission curves of $CaSO_4$ (nonlinear heating-rate, 400°C/min to 200°C/min, maximum temperature 300°C) after exposure to α or to γ radiation.

———— :- γ radiation,

---------- :- α radiation.

figure 14.

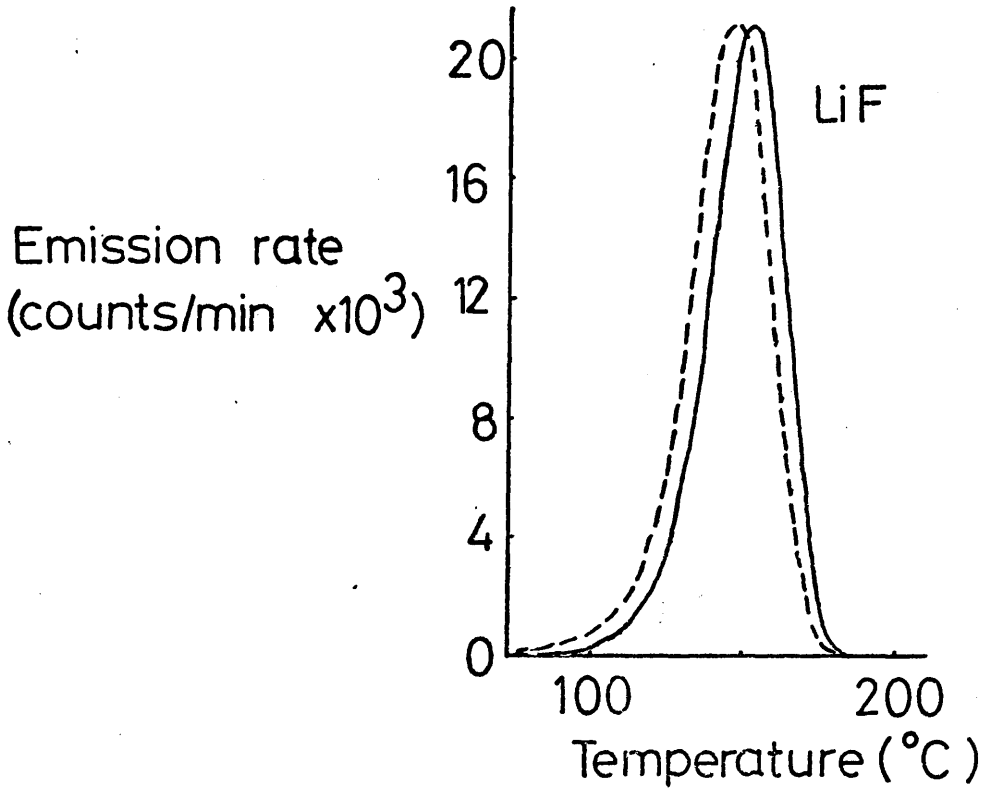

Thermally stimulated exo-emission rate as a function of temperature in LiF (E. Merck "suprapur", $<5\times10^{-5}$% heavy ions) after exposure to 5 MeV alpha and 1·25 MeV gamma radiation, heating rate approximately 200°C/min.

——— :- γ radiation,

---------:- α radiation.

Energy Transfer) alpha irradiation tended to fill the shallow traps corresponding to low-temperature peaks more than the deeper, high-temperature traps. Thus it should be possible to obtain information on the effective LET of the radiation, or, by measuring the low-temperature response only, to discriminate against γ radiation.

More recently Becker, Cheka, Crase and Gammage (93) have shown that instead of impregnating a BeO detector with a noble metal, heat treatment at 1400°C prior to use gave rise to even better behaviour.

Since then Gammage, Crase and Becker (94) have found that the presence of silicon as an impurity in BeO led to a greatly increased sensitivity. They found that the silicon present tended to concentrate in the surface region of the BeO disc.

They have subsequently shown (95) that while β and γ radiation had no permanent effect on the emission properties of the detectors even up to 10^7 rad, as low an exposure as 3×10^3 rad of α particles gave rise to semi-permanent changes. This was attributed to lattice damage, giving rise to interstitials and vacancies, caused by the α radiation.

1·7 Chemisorption and Catalysis

Since exo-electron emission is a surface process, and a surface-sensitive phenomenon, it was not long before its applications to the study of chemisorption processes other than oxygen adsorption were realised.

Nassenstein and Menold (96) investigated the electron emission from a series of silver catalysts of the same chemical composition prepared by different methods, which had been used in the catalysed reaction between ethylene and oxygen to give

ethylene oxide. Differences in yield, which ranged between 0 - 90%, could be related to the different electron glow curves from the catalysts.

Meanwhile Lohff (97),(23), had shown that exo-electron emission accompanied oxidation of zinc and Seidl (18) had observed emission during the oxidation of copper.

Menold (98) also investigated zinc oxide. He compared exo-electron and conductivity glow curves of single crystals and doped powders after stimulation by X-rays in the temperature range 20 - 280°C. He found maxima of electron emission at 135°, 192° and 260°C but no maximum for conductivity in this temperature range. He concluded on this basis that the exo-electron emission maxima were due to centres in the sorption layers.

Gibson (99) carried out a study of the effects of γ radiation on iron oxide catalysts used for the Fischer-Tropsch synthesis. He concluded that the centres for exo-electron emission consisted of oxygen ion vacancies containing trapped electrons and that the role of the irradiation was to fill these vacancies with electrons.

In each of these studies catalytic activity and exo-emission were measured separately.

Ohashi, Kano, Sato and Okamoto (100) confirmed the findings of Nassenstein and Menold for silver catalysts and further demonstrated that emission activity was proportional to catalytic activity. Ohashi et al also observed electron emission peaks at several temperatures below 200°C after irradiation of silver catalysts with X-rays. This activity bore no relation to catalytic activity however. After pretreatment with a mixture of ethylene and air the same catalysts emitted exo-electrons in the range 400 - 90°C and it was this emission which was proportional

to catalytic activity.

Sato and Seo (101) monitored catalyst samples inside a Geiger-Mueller tube while a mixture of argon, ethylene and oxygen was passed through the counter. They found that electron emission occurred during chemical reaction and that the emission rate was proportional to the rate of formation of ethylene oxide. They postulated (102) that exo-electron emission was a thermionic emission from a thin, n-type, semiconducting oxide layer formed by the adsorption of oxygen on the surface of the silver. The work function of this layer was lowered sufficiently by the adsorption of ethylene in the form of ethylene oxide to make thermal emission possible. Emission was at a constant rate because oxygen adsorption was occurring continuously, thereby regenerating emission sites all the time.

In 1955 Hauffe (103) had stated that a change in defectiveness of the surface layer must lead to a change in the adsorbability or desorbability of the surface. Krylova (40) and Rakhmatullina and Krylova (104) have shown the parallel that exists between the phenomena of gas adsorption and desorption and exo-electron emission in a study of thermal desorption and electron emission from MgO (104) and other oxides (40).

In the work by Sujak and his group on exo-electron emission accompanying phase changes ((70) - (75)) an ethanol-quenched, air-filled counter was used. It was suggested by Sujak (72) that the emission effect might be enhanced by the interaction of the ethanol with the specimen surface.

On the basis of this and the work by Hauffe (103) and Krylova and Rakhmatullina (40),(104), Sujak, Gorecki and Biernacki (105) postulated the following argument. Any process which led to a

change in the concentration of crystal lattice defects, particularly in the surface layer, would bring about a change in the adsorbability and hence in the catalytic activity of a material. Furthermore, any change in surface defect concentration would alter the exo-electron flux. Thus it should be possible to use the kinetics of exo-electron emission to study the catalytic properties of a material. It is therefore to be expected that when reaction conditions give rise to a peak in catalytic activity there should be a maximum of exo-electron emission and vice versa.

To test this theory Sujak et al investigated a Zn - ZnO system produced by oxidising metallic zinc in atmospheric air. They compared their exo-electron emission measurements made with an ethanol-quenched open point counter with literature data on the temperature dependence of the catalytic activity of Zn - ZnO for methanol oxidation, which is at a maximum around 570 K. There was good agreement between the two sets of results (see fig 15, page 35a). Sujak cited Cabrera (106) who suggested that as temperature rises from room temperature the resulting thermal stresses in the oxide layer cause an increase in the concentration of lattice defects in the oxide. This leads to an increase in catalytic activity and in the electron flux. As temperature rises further, the rate of diffusion of zinc into the zinc oxide layer increases. This leads to an annihilation of defects, with the maximum number of defects being observed at a temperature of 570 K.

Sujak also referred to work carried out by Stone (107) which showed that below 570 K oxygen is adsorbed on ZnO as O^-_{ads} while above 570 K it is found as O^{2-}_{ads}. Oxygen adsorbability is at a

figure 15.

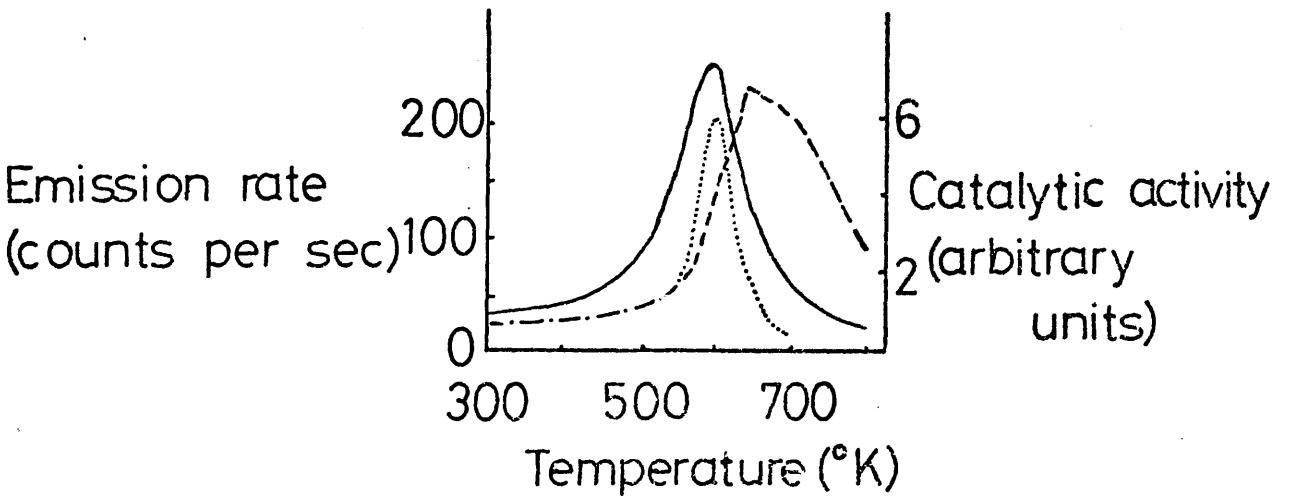

Temperature dependence of catalytic activity and exo-emission from zinc oxide:-

.....:- temperature dependence of intensity of exo-electron emission from ZnO on Zn system,

————:- catalytic activity of ZnO in methanol decomposition reaction versus catalyst annealing temperature,

--------:- catalytic activity of chromium oxide (Cr_2O_3) promoted ZnO in methanol dehydrogenation versus catalyst working temperature.

maximum near 570 K.

This significant work by Sujak's group has shown how useful exo-electron emission could be for quickly finding the optimum working temperature and conditions for a particular catalyst.

In 1968 Hoenig and Lane (108) investigated the effect of a D.C. electric field on the chemisorption of oxygen on zinc oxide. As already stated oxygen is adsorbed on zinc oxide in the form of O^-, and O_2^-, at room temperature. The electrons to form these species come from the ZnO conduction band. Oxygen adsorption thus gives rise to a negatively charged surface layer. Irradiation of ZnO with U-V light causes electrons and holes to form. The holes migrate to the negatively charged surface layer where the oxygen ions may be discharged and desorbed into the gas phase. On the basis of this hole theory of desorption it is to be expected that the application of external electric fields would affect adsorption and desorption processes taking place on the surface of ZnO. Volkenshtein (109) has discussed this in detail, proposing that electric field effects might be used to control chemisorption on semiconductors; a field bringing electrons to the exposed surface would enhance oxygen adsorption on ZnO while the opposite field would not only limit chemisorption but also tend to cause desorption of any oxygen species already present by bringing holes to the surface.

Hoenig and Lane (108) found that application of an electric field had the predicted effect.

Since Volkenshtein predicted this field effect it has been demonstrated many times. For example, Stadnik and Fentsik (110) showed in 1961 that a negative bias on a silver catalyst increased the yields from oxidation of methyl, ethyl, isopropyl and butyl

alcohols while a positive charge decreased the yield. Effectively the catalyst would be silver oxide which is an n-type semiconductor. They found that the effect became noticeable for an applied potential of 5 - 10V while there was no further enhancement of the effect for V > 50 volts. In contrast Hoenig and Lane worked over a voltage range from -800 to +800 V.

Another example has been afforded by Vladov, Dyakovitch and Dinkov (111). They showed that application of a negative bias increased the rate of decomposition of NH_3 from a Pt-Rh-Pd catalyst. The accompanying ion current also increased.

Hoenig decided to determine whether chemically-stimulated exo-electron emission was merely incidental to the reaction or whether it was a necessary step in the process. He and Tamjidi (112) observed the effect of an external potential on the exo-electron current from a platinum wire during oxidation of CO, NH_3 and H_2. They found exo-emission was proportional to the reaction rate. They also noted that if the catalyst was biased during an experiment the electron current changed although the reaction rate, k, remained constant. It was only if a negative bias was applied before the catalyst was heated that both electron emission and k increased. Similarly a positive bias was only effective if it was applied before a reaction commenced. Although exo-electron emission continued to decrease almost to zero as the bias potential was increased to +80 V, no effect was observed on k above +30 V. The reaction rate continued to increase under the influence of a negative bias up to -100 V. Hoenig and Tamjidi also observed that if the catalyst had been positively biased for a run and was then biased in a negative way for the next experiment, k and the electron current both increased. They did not, however, increase to the

level they would have reached solely under the influence of a negative bias. If the catalyst was annealed in vacuum at 950°C for one hour both k and the exo-emission rate were restored. Hoenig and Tamjidi concluded that application of a positive field 'structured' the surface in some unspecified way which hindered reaction and electron emission. Finally they plotted electron current, I, against V for increasingly positive V, up to +33 V, and found that I decreased 'smoothly', thereby indicating that no reaction intermediates are involved in exo-electron emission.

Momose and Tamai (113) observed the exo-electron emission during reduction of copper oxide by ethanol vapour. They examined sheets of copper oxide activated by discharge from a Tesla coil. As a standard for comparison they also investigated untreated sheets.

They found that the activated sheets gave two exo-electron glow peaks, at 94° and 240°C while the unactivated sheets only gave an emission peak at 240°C. They proposed that the peak at 94°C was due to electrons trapped in surface defects caused by the discharge from the Tesla coil. The peak at 240°C was attributed to the reduction reaction itself.

In 1974 Kasemo and Walldén (114) observed emission of both photons and electrons during chemisorption of chlorine on a sodium surface prepared by vacuum evaporation. They found a photon yield of $10^{-6} - 10^{-7}$/molecule reacting and an electron yield of 10^{-5}.

Much earlier than this, in 1961, Sujak and Wawrzyniak (115) reported that a photo-stimulated exo-electron emission occurred from the surface layer of abraded amphoteric metals, Al, Zn, Sn,

Pb, during reaction with sodium or potassium hydroxide. No such emission was observed during reaction with acids. Emission was not found with any other metals during reaction with either acid or alkali. Sujak and Wawrzyniak found that the energy of the stimulating light required to excite emission increased from Al-Pb in accordance with the fact that hydroxide affinity decreases in the same sequence. As the affinity of the metal for hydroxide decreases the reaction will become less vigorous.

In 1964 Sujak and Bójko (116) investigated the influence of halogens, present in the counting gas of their Geiger-Mueller tube, on the observed exo-electron emission. In 1955 Grunberg and Wright (16) investigated the time-dependence of the decay of electron emission from a surface with different counting gases. Sujak and Bójko, however, were interested in how the counting yield varied. They found that with many halogen-containing compounds, e.g. C_2H_5I, CH_2BrCH_2Br, all of which are strongly electronegative, no exo-electrons were recorded from an illuminated, freshly-abraded aluminium surface. If such an atmosphere were pumped away and replaced by an Ar/EtOH mixture electrons were recorded immediately. This effect was explained by the proposal that such electronegative compounds captured the released electrons so tightly that they could not be released again at the anode.

In 1968 Tamai and Momose (117) investigated the glow-curve characteristics of exo-electron emission from sand blasted metals and concluded, like earlier researchers, that the emission was mainly from the particles of sand embedded in the metal.

Kralik (80) has shown that there was no detectable difference in exo-electron emission from a metal whether it was examined using an electron-multiplier in a vacuum or whether a gas-filled

counter was used. Lewowski (118) meanwhile demonstrated that the rate of decay of electron emission from an abraded metal varied with the relative humidity of the counting gas, in this case air. Because of the apparent contradiction of these results Momose (119) decided to investigate the interaction between counting atmospheres, composed of organic vapours, and freshly deformed metal surfaces by measuring the exo-electron emission from these surfaces.

He studied sand-blasted mild steel under the influence of several organic vapours and found that the intensity of the glow peak, whose position varied between 51 and 66°C, depended on the proton attracting power of the compounds examined. He found that intensity increased in the following sequence:-
n-butyl chloride $<<$ acetonitrile $<$ benzene $<$ methanol $\simeq$ toluene $\simeq$ acetone $\simeq$ ethanol $\simeq$ isopropyl alcohol $<$ ethyl acetate $<<$ propylamines.

He interpreted this to mean that electron emission could be enhanced by the formation of hydrogen bonds between the functional groups and the deformed surface of the sand embedded in the steel, since it was the sand which was responsible for this emission peak.

Baazov, Kolbanovskii and Polak (120) have shown how sensitive a phenomenon exo-electron emission is. They obtained the electron glow-curve from $\gamma - Al_2O_3$ after irradiation of the oxide with X-rays with a dose of 1000R and found the main peak, which lay between 70 - 100°C with a maximum around 85° $\pm$ 3°. They took this peak to be typical of exo-electron emission from irradiated $\gamma - Al_2O_3$. In fact $\gamma - Al_2O_3$ does not emit exo-electrons. Emission is from the small amount of the α form of Al_2O_3 which is present at room temperature (121).

Baazov et al (122) then investigated the exo-electron emission from irradiated $\gamma - Al_2O_3$ with a surface coverage of hydrogen, $\theta = 10^{-3}$, and then deuterium, $\theta = 10^{-3}$, (see fig 16, page 41a for glow curves obtained).

They found that the total number of electrons emitted increased in the series:- pure $\gamma - Al_2O_3$, $\gamma - Al_2O_3$ + deuterium, $\gamma - Al_2O_3$ + hydrogen. Since Dolidze, Kolbanovskii and Polak had earlier shown (123) that hydrogen adsorbs dissociatively on $\gamma - Al_2O_3$ to form shallow donor levels in the forbidden zone, these results were taken to prove that H and D have different donor capacities during chemisorption. Thus they give rise to the formation of impurity levels at different depths.

In a further study (124) Baazov et al compared the glow curves of irradiated $\gamma - Al_2O_3$ with a surface coverage of H_2 or CO_2, $\theta = 10^{-3}$ again (see fig 17, page 41b). H_2 is a donor gas so the total electron emission increased and emission also occurred from new donor levels. CO_2, in contradistinction, is an acceptor gas. Thus its chemisorption leads to an overall reduction of electron emission and to the destruction of the shallow, low temperature donor levels.

A peak corresponding to the acceptor level formed by adsorbed CO_2 is clearly evident (see fig 17) and by making use of the relation $E = 25\ kT_{max}$, Baazov et al assigned an energy of $0{\cdot}9 \pm 0{\cdot}015$ eV to this level. The corresponding depth for adsorbed H_2 is $0{\cdot}7 \pm 0{\cdot}005$ eV.

It may be seen therefore, that exo-electron emission provides a very sensitive method for determining the donor or acceptor nature of an adsorbed gas, particularly where the surface coverage is too low to permit the use of more conventional methods.

figure 16.

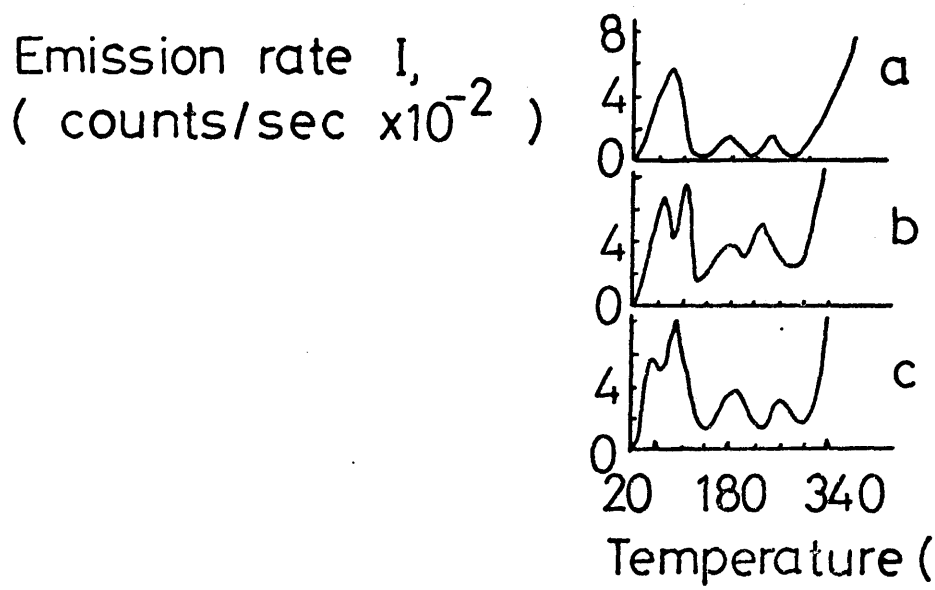

Exo-electron emission, I, versus temperature in the range 20-300°C,

a):- γ-aluminium oxide,

b):- γ-aluminium oxide with adsorbed hydrogen, degree of coverage $\theta \sim 10^{-3}$.

c):- γ-aluminium oxide with adsorbed deuterium, degree of coverage $\theta \sim 10^{-3}$.

figure 17.

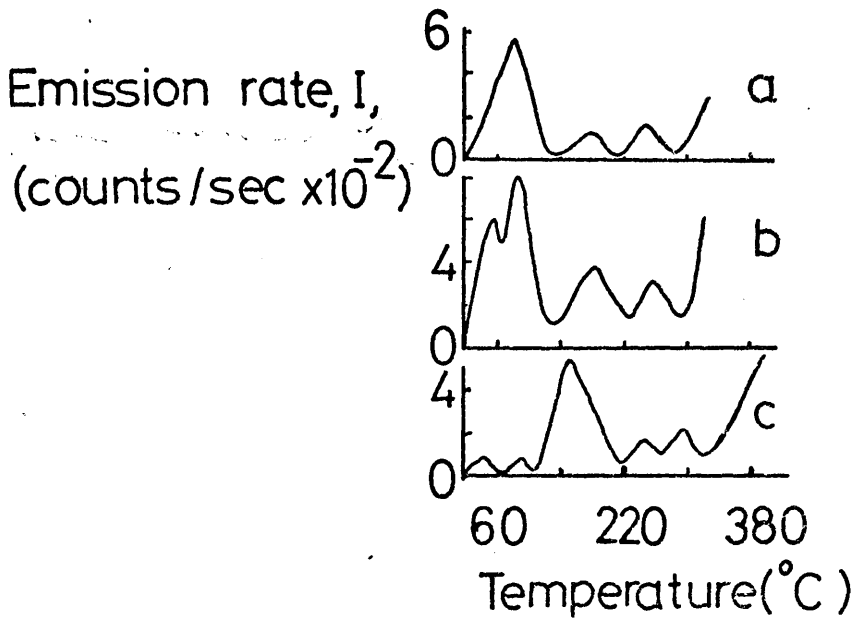

Thermally stimulated exo-electron emission spectrum for γ-Al_2O_3 excited with x-rays at a dose of 1000R and a dose rate of 34R/min,

a):- γ-Al_2O_3 after evacuating to a residual pressure of 10^{-7} torr at 220°C over a period of 10 hours,

b):- H_2/γ-Al_2O_3 ($\theta \sim 10^{-3}$),

c):- CO_2/γ-Al_2O_3 ($\theta \sim 10^{-3}$).

Clearly exo-electron emission is most sensitive to the state of the emitting surface and many investigations have been carried out both on metals and non-metals to try to elucidate the role of adsorbents. With metals electron emission does not depend on volume defects. Rather it comes predominantly from a layer about 20μ thick. Emission is from a thin oxide layer or from sorption layers of gases. In other words it is exclusively an extrinsic effect.

The situation is much more complex for non-metals where surface and volume effects can both be important. With some ionic crystals adsorbed gases play an important role while with others emission continues even in very high vacuum.

For example, in 1959 Wüstenhagen (26) examined the electron emission from NaCl exposed to O_2 and water vapour. The emission characteristics did not change while the pressure was lowered to 2×10^{-5} torr. Bohun (125) confirmed this for rocksalt and potassium chloride crystals excited by X-rays but he found that below 10^{-5} torr there was a marked decrease in emission which disappeared completely below 10^{-6} torr. He attributed this to a strong desorption of O_2 and H_2O between 10^{-5} and 10^{-6} torr. Such a desorption would be followed by a considerable increase in electron affinity with a resulting decrease in electron emission from the surface. Unfortunately he did not make it precisely clear what he meant by 'electron affinity'.

This correlation between sorption and electron affinity was also noted by Scharmann, Kriegseis and Seibert (126) who studied the induced photo-electric effect of KCl crystals cleaved in ultra-high vacuum. This is in direct contrast to the situation which exists with LiF where there is only a very slight dependence of its glow curves on pressure even at pressures as low as 10^{-9} torr

(see Gordon and Scharmann (127)).

Kralik (80) found a marked difference in the decay period of electron emission with CaF_2:Sm depending on whether it was counted in a Geiger-Mueller tube or with an electron-multiplier in a vacuum system. The decay rate was much faster when counting took place in vacuum. Kralik attributed this to the desorption of O_2 and H_2O in high vacuum which would give rise to a marked increase in electron affinity.

In 1969 Kriegseis and Scharmann (128) investigated $BaSO_4$ powder. After irradiation with electrons of energy 2·5 keV in high vacuum two maxima in the thermal glow curve from the salt were found at 115° and 160°C. These workers found that if samples were heated to 300°C in high vacuum before irradiation then the high temperature peak almost disappeared while the peak at 115°C became more pronounced.

These results were attributed to the presence of adsorbed water giving rise to surface states capable of emitting electrons at 160°C. Heating the salt to 300°C would cause this adsorbed water to leave the surface. It was found that exposure to water vapour after irradiation of the thermally-treated samples regenerated the peak at 160°C. A new peak appeared around 190°C. A similar treatment with oxygen generated the peak around 190°C but there was no enhancement of the peak at 160°C. Kriegseis and Scharmann suggested that this was due to a change in the electron distribution of the surface. It was found that nitrogen had no effect.

ZnO has also been characterised and it has been agreed that its emission comes from sorption states of oxygen acting as traps (see for example Holzapfel and Nink (129)).

Krylova (40) investigated the thermally-stimulated exo-electron emission from the powdered oxides Al_2O_3, SiO_2, zeolite, MgO, ZnO, TiO_2, ZrO_2, Cu_2O and NiO, after they had been excited by bombardment with a current of 10μA of 1·5 keV electrons. For this study he used a secondary electron multiplier. Most of the oxides examined gave a thermally stimulated emission without prior excitation and Krylova showed that electrons and negative ions were emitted. MgO emitted only negative ions.

After excitation emission maxima occurred at the same temperature although the electron bombardment itself often caused some desorption.

It was found that the species desorbed were for the most part water with some CO_2, CO and O_2.

A comparison of exo-electron glow peaks and the temperatures corresponding to the maximum rates of desorption showed a close agreement between the two, proving that for most oxides the centres of activated desorption are also the centres for thermally stimulated exo-electron emission. Krylova showed that for silica gel it was only hydroxyls paired by hydrogen-bonding which were the centres for electron emission.

With the exception of ZrO_2 each oxide gave rise to a glow peak in the range 140 - 160°C.

Krylova found that chemisorption of CO_2 neither increased electron emission from the oxides at room temperature immediately after electron bombardment, nor during the subsequent heating cycle (cf. Baazov et al (124)). Water adsorption intensified both types of emission enhancing thermally-stimulated emission over the whole temperature range investigated. Oxygen was found to increase the intensity of the peaks in the range 140 - 160°C (cf.

Kriegeis and Scharmann (128) who found that oxygen gave no enhancement of the peak at 160°C (from $BaSO_4$). Krylova argued that H_2 would have the same effect as water since it would give rise to the formation of surface OH groups. From this he concluded that the peak at 140 - 160°C was due to chemisorption of H_2O or O_2 while any other peaks obtained were due to the presence of surface water, existing either as discrete water molecules or as differently coordinated hydroxyl groupings.

Different activators were introduced both to the bulk oxides and to their surfaces. It was found that they did not affect the number or the positions of maxima in the basic temperature curves. They only varied the intensity of these peaks, by varying the amount of gases adsorbed on the surface.

Euler, Kriegseis and Scharmann (41) investigated BeO because of its applications for radiation dosimetry. They confirmed that oxygen adsorption centres were active, both for thermally and optically stimulated electron emission from BeO.

Styrov and Kharlamov (130) exposed various phosphors to atomic hydrogen and atomic oxygen. With oxygen, ions were emitted, i.e. O_2^-, giving a thermal desorption maximum whose position depended on whether the sample was an oxide or a sulphate. With hydrogen, electrons were emitted. Again the position of the maximum depended on the nature of the sample. The maxima corresponded to maxima in the rates of radical recombination.

Emission from ionic crystals and semiconductors may be from surface states created by sorption but such states do not necessarily occur. Then sorption will only change the electron affinity, as is the case with rock salt and potassium chloride.

Sometimes emission may occur from surface states which are

not caused by sorption. This has only been proved unambiguously for LiF (see (126)) which gives glow peaks at 120 and 310°C after X-irradiation. The latter peak is due to F and M centres. Etching the surface removes the peak at 120°C since the new surface traps are empty. The high temperature peak is due to colouration of the crystal volume and thus is scarcely influenced. The surface traps have been attributed to dislocations.

CHAPTER 2

Chapter 2

2·0

As this was the first attempt undertaken in this Department to study exo-electron emission, it was decided to try, in the first instance, to duplicate experiments already carried out. To this end, an investigation by Sato and Seo (102) into the exo-electron emission accompanying the partial oxidation of ethylene to ethylene oxide by a powdered silver catalyst was chosen.

2·1·0 Apparatus

A preliminary investigation was carried out as a B.Sc. project by the present author. A block diagram of the apparatus used is shown in Diagram 1 page 47a.

A pressure-reducing head was used so that each cylinder of gas, Ar, C_2H_4, O_2, gave a pressure of 15 psi. Thus the composition of any gas mixture was proportional to the flow rates of its constituents. The gases were mixed and allowed to pass through a trap, T_1, surrounded by solid CO_2 to dry them before they entered the counter. After passing through the counter the gas mixture flowed through another trap, T_2, again surrounded by solid CO_2, to trap out any ethylene oxide formed.

2·1·1 Counter/Reaction Vessel

The reaction was carried out inside a windowless 2π Geiger-Mueller tube whose walls were made of stainless steel, which is chemically inert to ethylene oxidation (see Diagram 2 page 47b). The anode wire was 0·001" tungsten threaded under tension

Diagram 1.

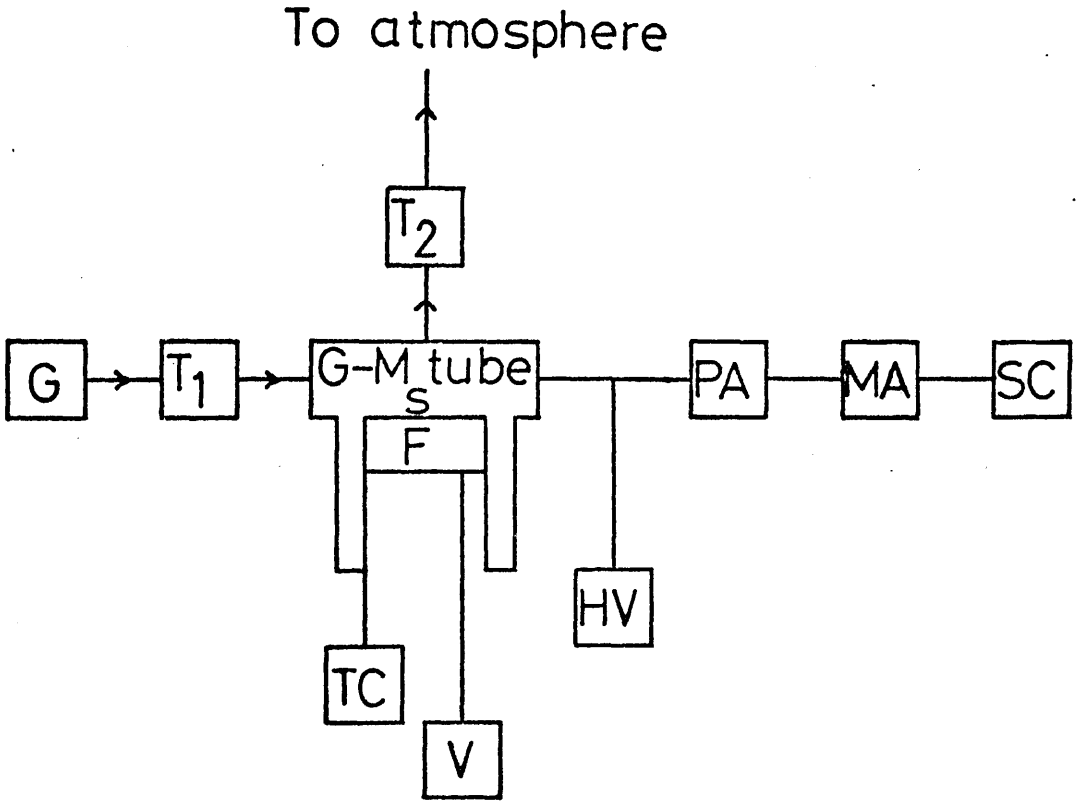

Block diagram of apparatus: exo-electron emission from silver catalysts during partial oxidation of ethylene to ethylene oxide.

G=gas, T=trap, S=catalyst sample, F=furnace, TC=thermocouple, V=low voltage supply, HV=high voltage supply (3 kV Ekco power supply N570B), PA=preamplifier, MA=main-amplifier, SC=scaler (Ekco N529D).

Diagram 2.

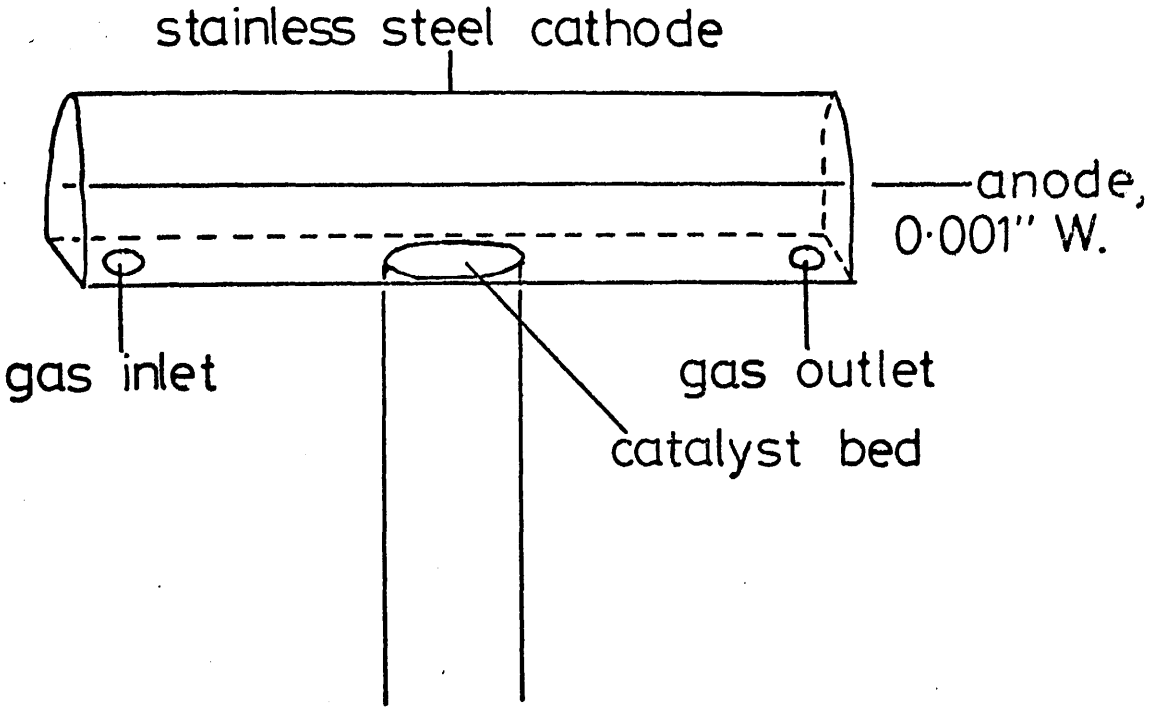

Geiger-Müller counter / Reaction vessel.

approximately 0·5" above the wall which comprised the diameter of the semi-cylindrical counter. There was an aperture in the centre of this wall into which a glass socket fitted to give an airtight seal. At the top of the socket there was a platform which could hold about 0·5 g catalyst (see Diagram 3, page 48a). A thin, hollow glass rod ran up the centre of the socket and a Chromel-Alumel thermocouple passed through this tube to a dimple in the middle of the platform so that catalyst temperature could be measured. The furnace winding was of 22·2 ohm/m resistance wire coiled round asbestos string. This was taped with asbestos paper to insulate it and then wound round the glass rod.

The anode voltage was supplied by a 3 kV Ekco power supply (N570B) and the signal was picked up, amplified and shown on an Ekco scaler unit (N529D).

2·1·2 Gas Composition

When catalyst samples were tested for exo-electron emission the gas mixture was composed mainly of Argon with a flow of 2 ml/sec. Ethylene flowed into the system at a rate of 0·08 ml/sec and oxygen 0·1 ml/sec. This gave compositions of Ar - 96·2% and C_2H_4 - 3·8% in an Ar/C_2H_4 mixture and Ar - 91·7%, C_2H_4 - 3·7% and O_2 - 4·6% in an $Ar/C_2H_4/O_2$ mixture. These compositions were those used by Sato and Seo. Unfortunately, however, these workers did not specify their flow-rates.

Two catalysts were prepared, precipitated silver and silver precipitated onto an α-alumina support. Before investigating their exo-electron emission, these catalysts were tested for catalytic activity by flowing an O_2/C_2H_4 mixture over a large sample of each. Oxygen was metered in at a rate of 1 ml/sec and ethylene at 0·5 ml/sec. See Diagram 4, page 48b.

Diagram 3.

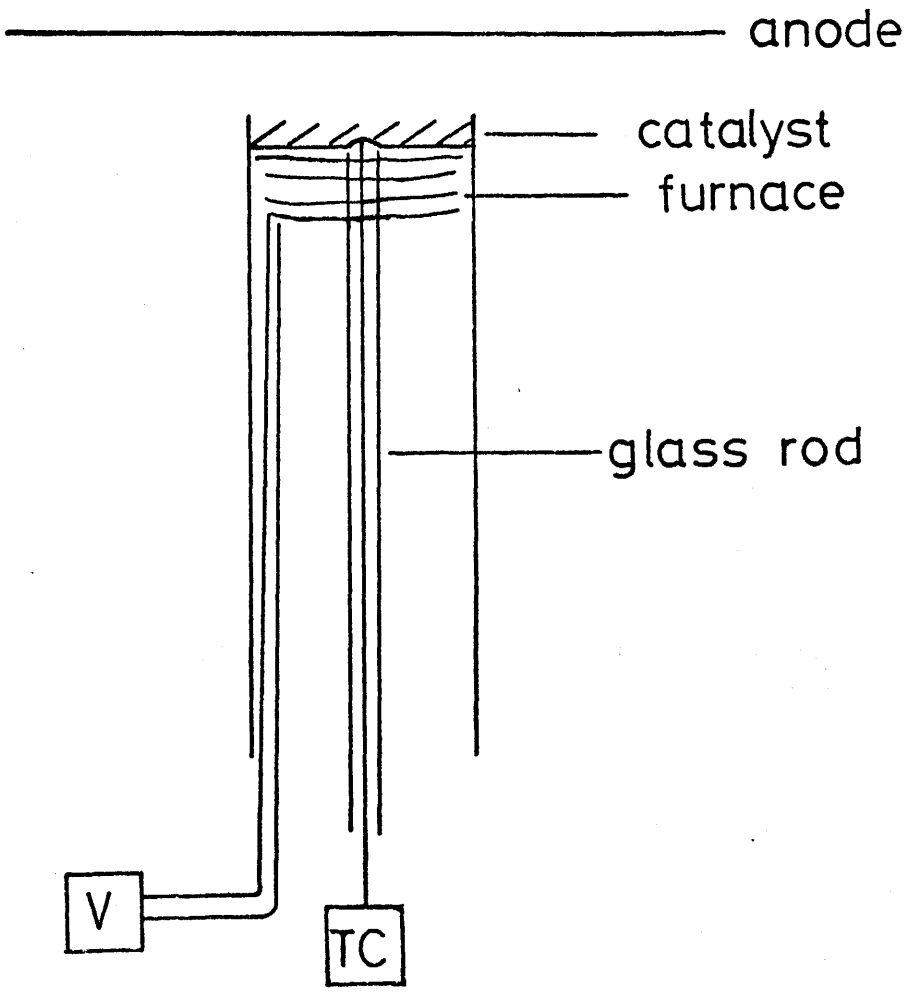

To show the position of the furnace and the thermocouple with respect to the catalyst.

V = Variac power supply,
TC=Chromel-Alumel thermocouple connected to a Comark electronic thermometer.

Diagram 4.

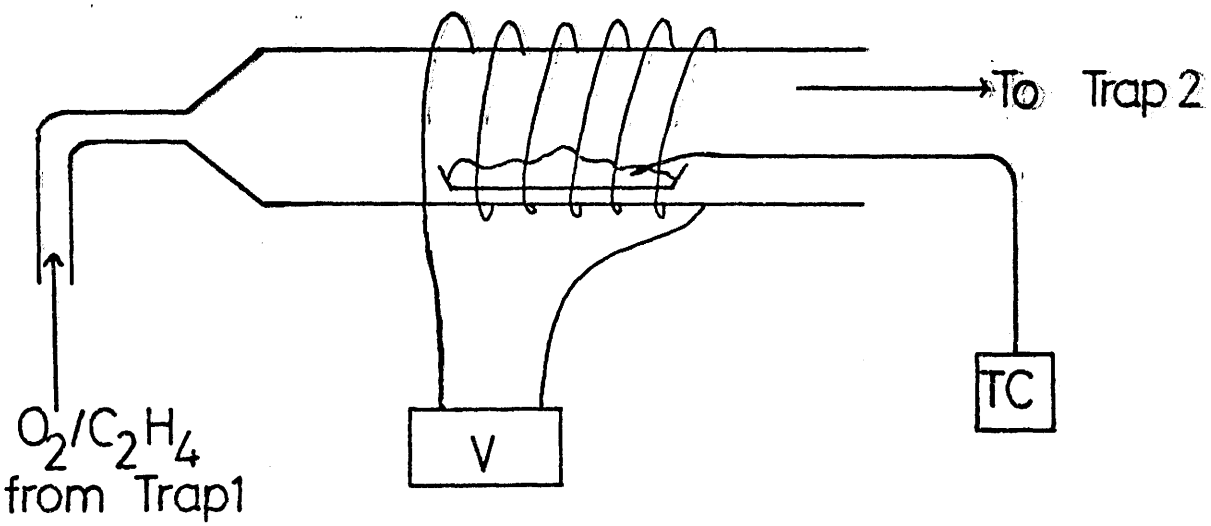

Apparatus used for large-scale testing of catalysts.

V = Variac power supply,
TC = Chromel-Alumel thermocouple connected to a Comark electronic thermometer.

Trap1 dries reactant gases,
Trap2 collects any ethylene oxide produced.

The precipitated catalyst, Catalyst A, was prepared according to the recipe given by Sato and Seo (102). See Appendix 1.1 for details. About 7 g catalyst A was heated to around 250°C for three hours - Sato and Seo operated at 210°C.

The supported silver catalyst, Catalyst B, was prepared according to McBee, Hass and Wiseman (131), except that powdered α-alumina was used instead of ~~γ~~-mesh pellets. See Appendix 1.2 for details. A sample of catalyst B (again approximately 7 g) was heated to around 280°C for about three and a half hours. 280°C was the recommended temperature for optimum activity.

2·1·3 Product Analysis

There was no column packing readily available suitable for separation of ethylene oxide, so the contents of the trap T_2 were hydrolysed each time by addition of a few drops of mineral acid dissolved in 99·9% ethanol, dried over magnesium sulphate to remove any water and finally filtered. If ethylene oxide were present, it would now be in the form of ethylene glycol, so samples of the products of reaction from catalysts A and B were tested for the presence of ethylene glycol using a Perkin-Elmer F11 gas chromatograph with a hot wire detector. The column was a 4' tube of 0·25" o.d. stainless steel packed with Chromosorb 101, a packing suitable for separating polar molecules. The column temperature was 190°C and the carrier gas was nitrogen which flowed through the column at a rate of 400 ml/min. The detector temperature was 200°C.

4 μl samples were injected each time. Those from catalyst A showed no ethylene glycol while those corresponding to catalyst B did. See Appendix 1.3 for the chromatograph charts. It was

concluded that catalyst A was inactive so only catalyst B was examined for exo-electron emission.

2·2·0 Characterisation of the Counter

^{14}C-doped polymethylmethacrylate was used to establish the characteristics of the counter. The specimen was placed in the catalyst bed of the Geiger counter and an Ar/C_2H_4 mixture passed over it. At first argon was metered in at a rate of 4 ml/sec and ethylene at 0·16 ml/sec i.e. twice the flow-rate given previously.

2·2·1 Effect of Flow on Count Rate

Initial experiments were carried out with a flow-rate of just over 4 ml/sec but it was decided this was too fast. When the flow rate was halved it was discovered that the appearance potential (i.e. the voltage at which the Geiger counter just starts to count) for any gas mixture was lowered.

2·2·2 Determination of Plateau Region

Counts/minute with the ^{14}C-β emitter present were plotted against voltage from 1-2 kV at 0·05 kV intervals (see Graph 1, Appendix 2). The source was then removed and a background count taken at a voltage in the plateau region. The count rate at 1·75 kV was 976 cpm with the source and 273 cpm with the source removed. Having shown that the detector was sensitive to low energy β particles, a ^{137}Cs-γ source was used for the rest of the calibrations since it could activate the counter from outside. Furthermore, the number of counts, N, per unit time increased so that the associated error $\pm\sqrt{N}$ became less significant.

Having shown that the Geiger counter was operational, it was then necessary to find plateaux for the different gas mixtures.

The appropriate gas mixture was allowed to flow through the Geiger-Mueller tube for at least ten minutes to allow the mixture to stabilise. Then counts with the γ source present were measured at 0·05 kV intervals and plotted against voltage to obtain the plateau, if any, for that gas mixture.

It was found that only Ar/C_2H_4 gave a stable plateau. Graphs of cpm vs voltage for Ar/C_2H_4 (1 - 2), $Ar/C_2H_4/O_2$ (3), and Ar (4) are contained in Appendix 2. A comparison of Graphs 1 and 2 shows the effect of flow rate on appearance potential and plateau range for Ar/C_2H_4.

As samples of the catalyst were to be heated inside the Geiger tube, the effect of temperature on count rate was determined for Ar/C_2H_4. The effects of heating and cooling are shown in Graphs 5 - 6 (Appendix 2) respectively. In both cases it was found that count rate was virtually independent of temperature between 20°C and 250°C.

The effect of varying the proportion of ethylene was also investigated. It was found that the appearance potential increased as ethylene concentration increased and also that the plateau was at a lower count rate and was less well-defined. (See Graph 7, Appendix 2).

2·3·0 Experimental Procedure

A typical experiment was as follows. An Ar/C_2H_4 mixture, flow rate around 2 ml/sec, was allowed to flow through the Geiger-Mueller tube at an operating voltage of 1·65 kV. Background counts were measured at room temperature and around 250°C. The counter was allowed to cool and then about 0·5 g catalyst was placed on the platform. The counting mixture was allowed to stabilise again and counts were taken at room temperature and

around 250°C. Oxygen was metered in at a flow rate of 0·1 ml/sec and the count rate obtained at room temperature and around 250°C. Finally the catalyst sample was removed, the gas mixture allowed to stabilise and counts obtained for $Ar/C_2H_4/O_2$ in the absence of catalyst. Usually a fresh sample of catalyst was used each time.

Because the counter was not cooled it was impossible to carry out counting at high temperatures for long since sometimes continuous discharge occurred, especially if the temperature was much in excess of 250°C. Four short counts were taken and averaged to try and reduce their statistical error so that comparison of the results could be made.

No attempt was made to test for the formation of ethylene oxide since it was believed that the amount formed in the course of an experiment, approximately fifteen minutes, would be undetectable.

The results of these experiments are given in Tables I, II and III, page 52a. The catalyst sample used in run 2 was the one used in run 1. Because these results appeared to contradict each other it was decided to use fresh catalyst for all subsequent runs.

With sample 1 in run 1 counts were measured in $Ar/C_2H_4/O_2$ first. In run 2 the same catalyst was used but no note was made of whether Ar/C_2H_4 or $Ar/C_2H_4/O_2$ was introduced first at high temperature in this run. In run 3 the catalyst was exposed to Ar/C_2H_4 first at high temperature while in run 4 $Ar/C_2H_4/O_2$ passed over the catalyst first.

When the catalyst was exposed to $Ar/C_2H_4/O_2$ first at high temperature the count rate at T = 250°C was very much higher than

Table I

Ar 2 ml/sec. C_2H_4 0·08 ml/sec. V = 1·65 KV

a. Without catalyst					b. Catalyst B present				
Run	T°C	cpm	T°C	cpm	Run	T°C	cpm	T°C	cpm
1	25	720	247	1440	1	-	-	258	1020
2	-	-	250	870	2	26	168	248	576
3	36	204	248	768	3	24	198	248	912
4	24	192	249	396	4	30	840	253	522

Table II

Ar 2 ml/sec. C_2H_4 0·08 ml/sec. O_2 0·1 ml/sec. V = 1·65 KV

a. Without catalyst					b. With catalyst				
Run	T°C	cpm	T°C	cpm	Run	T°C	cpm	T°C	cpm
1	28	156	250	840	1	28	900	248	6840
2	28	180	250	1209	2	28	72	250	318
3	33	150	248	1092	3	31	132	247	500
4	29	78	252	456	4	27	120	251	1836

Table III

All experiments with Catalyst B present

Ar 2 ml/sec. C_2H_4 0·08 ml/sec. O_2 0·1 ml/sec V = 1·65 KV

a. $Ar/C_2H_4/O_2$.				b. Ar/C_2H_4		c. $Ar/C_2H_4/O_2$	
Run	T°C	25°	248°	262°	250°	261°	251°	262°
5	cpm	312	2598	6756	1770	2814	744	1026

a. Ar/C_2H_4				b. $Ar/C_2H_4/O_2$	
6	T°C	31°	250°	261°	246°	264°
	cpm	450	612	1368	366	504.

background. In runs 2 and 3, however, the catalyst samples were heated in Ar/C_2H_4 before exposure to oxygen. In this case the count-rate at T = 250°C was around background level.

To test the significance of this, two further experiments were carried out - see Table III, page 52a for the results. In the first run, run 5, a fresh sample of catalyst was heated in $Ar/C_2H_4/O_2$ to T = 248°C and the count-rate measured. It was then heated to T = 262°C and the count-rate measured again. Then oxygen was removed from the flow and the catalyst heated again. Counts were measured at T = 251°C and 261°C. Finally oxygen was reintroduced and counts found at T = 251 and 262°C.

In run 6 another fresh sample of catalyst was used. It was heated first in an Ar/C_2H_4 mixture and then in $Ar/C_2H_4/O_2$.

By inspection of Table III it may be seen that the order of introduction of the gases to the catalyst is very important, exposure to ethylene before oxygen causing a reduction of exo-electron emission from the catalyst.

These results will be discussed more fully later.

2·4·0 Limitations

In the course of this repetitive work several severe limitations to the usefulness of this system as a tool for the study of chemisorption and catalysis were discovered. From this work, however, it became possible to specify the ideal requirements of an exo-electron emission detector suitable for studying catalytic processes.

2·4·1 Counter Atmosphere

It was found that only Ar/C_2H_4 mixtures gave counting plateaux. $Ar/C_2H_4/O_2$ gave very poor counting characteristics, but

it could be used if background was measured each time before a count was taken of a catalyst sample. With the present detector design this necessitated frequent removal of the catalyst samples. While this was permissible for the qualitative work under discussion, where a fresh catalyst sample was used each time, it would present a severe handicap to work of a more quantitative nature, especially if the effects of different pre-treatments were under investigation.

2·4·2 Temperature

The counter did not count reliably at temperatures above 260°C, which offers a very narrow temperature range for studying chemisorption and catalysis. Cooling the counter might have alleviated this problem. However, lowering the temperature to around 250°C usually restored the normal counting behaviour, implying that this problem might be due more to convection currents which would remain even if the tube walls were cooled.

2·4·3 Counter Design

In this detector catalyst was exposed directly to the accelerating field (see Diagram 2, page 47b), which brought about the possibility of field emission. Since the catalyst was uncovered there was also the possibility that particles might be blown into the body of the counter. In fact when this counter was later dismantled some catalyst particles were found adhering to the walls of the vessel, and one was even attached to the anode wire.

2·5 Improvements Required

As a result of the preliminary work it was decided that to

study exo-electron emission in the context of chemisorption and catalysis the catalytic process must be broken down into its basic steps, the first of which is adsorption. Thus, to further this work a counter was required which could be used to follow simple adsorption-desorption processes. This meant that a detector in which a much wider variety of gas fillings could be used for adsorption and for counting was necessary. As soon as a different gas, e.g. Q gas, has to be introduced to permit G-M or proportional counting, the process under investigation is completely changed. There would also be the problem of catalyst contact with a counting gas, which often has a carbon-containing compound as the quenching agent, contaminating the catalyst.

1. Ideally, therefore, an exo-electron detector should be capable of counting in any gas so that any reaction might be studied.

2. A great deal of exo-electron work has been carried out in high and ultra-high vacuum conditions, but an exo-electron detector would be far more versatile if it was capable of counting low energy electrons at atmospheric pressure: thus it was decided to make this another of the requirements of our ideal detector.

3. It would also be desirable to design a counter which could operate successfully over a wide range of temperatures so that exo-electron 'glow-curves' might be investigated.

4. Another feature required was that the catalyst should be shielded from the electric field, both to eliminate the possibility of field emission and, when a powdered catalyst was being investigated, to prevent particles from being blown through the active volume of the counter. It was decided to introduce in

one of the designs a wire mesh grid at earth potential between catalyst and anode to achieve this.

2·6·0 Counters

Several attempts were made to design a detector incorporating these desirable features and the evolution of a good, working model will be traced in the following pages, with a discussion of the merits and failings of those designs which were rejected. Any results obtained with them will also be presented.

As well as improving counter design, several modifications were made to the experimental set-up. Negretti-Zambra pressure regulators were introduced after the gas cylinders to ensure a steady back-up pressure and hence a steady flow. The bubble flow-meters were replaced by GEC-Elliot rotameters so that flow could be monitored visually at all times and any fluctuations quickly corrected. A glass tube packed with anhydrous sodium carbonate was used to remove any moisture from the gas flow. After passing through the reaction vessel the gases were vented to atmosphere via a Perkin-Elmer gas sampling valve, by means of which samples could be introduced into a Perkin-Elmer F11 gas chromatograph with a flame ionisation detector, (see Diagram 5, page 56a for new experimental set-up). The column was 6' of 0·25" o.d. stainless steel tube packed with Porapak R. More sophisticated electronics were obtained, comprising a Nuclear Enterprises SR5 scaler-ratemeter with a 0-4 kV high voltage power supply, a linear pulse analyser, a ratemeter and a scaler/timer. This was used in conjunction with a Nuclear Enterprises solid state preamplifier serial number 5287 SC, a low noise, charge-sensitive preamplifier with an FET input stage, serial number 5287 AC.

Diagram 5.

Modified apparatus for work on exo-emission from supported silver catalyst during the partial oxidation of ethylene to ethylene oxide.

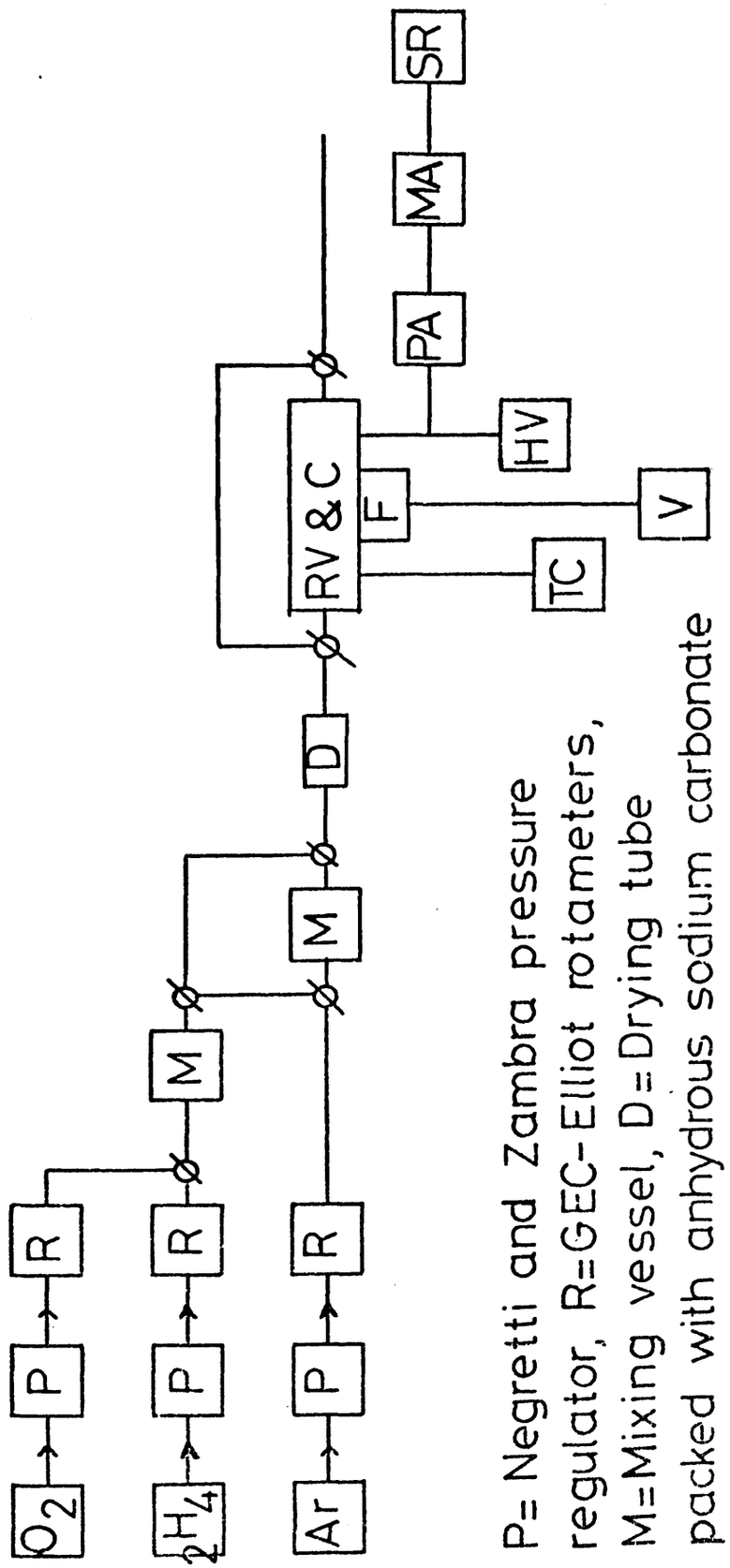

P= Negretti and Zambra pressure regulator, R=GEC-Elliot rotameters, M=Mixing vessel, D=Drying tube packed with anhydrous sodium carbonate crystals, F=Furnace, TC=Cr/Al thermocouple connected to a Comark electronic thermometer, V=Voltage supply to furnace.

RV&C=Reaction vessel in which window proportional counter was mounted.
HV=0-4kV power supply, part of SR.

PA=Nuclear Enterprises 5287SC preamplifier unit used with a 5287AC input stage,
MA=Nuclear Enterprises main amplifier,
SR=Nuclear Enterprises SR5 scaler-ratemeter with built in energy discriminator.

2·6·1 Counter 1

Attix, see (132), and several other workers e.g. Baazov et al (120), (122-124) and Gel'man et al (38), (39) have successfully used loops of wire as anodes, generally in hemispherical detectors.

Because of these successes it was decided to investigate the counting characteristics of a cylindrical open-window counter with a loop anode. To facilitate this study a small bench counter was made comprising a polished copper cathode 0·8" in internal diameter with an anode loop made of platinum wire 0·002" in diameter (see Diagram 6, page 57a). The loop was made by threading both ends of the wire through the shaft of a syringe needle whose point had been sawn away and then rounded off to remove any high points. Q gas, 90% Argon, 10% methane, was used as the counting gas and ^{14}C-doped polymethylmethacrylate and tritiated sodium formate were used as β^- sources.

Using the ^{14}C source counting plateaux were found for various Q gas flow rates to see whether there was any effect on the voltage range of the plateau. No definite effect was found. Counting started around 1·1 kV. The plateau extended from around 1·9 - 2·1 kV then counts fell away again. Above about 2·4 kV count-rate increased again. The general shape of the curve was always as shown in fig 18 (see Appendix 3 for examples).

fig 18 shown overleaf.....

Diagram 6.

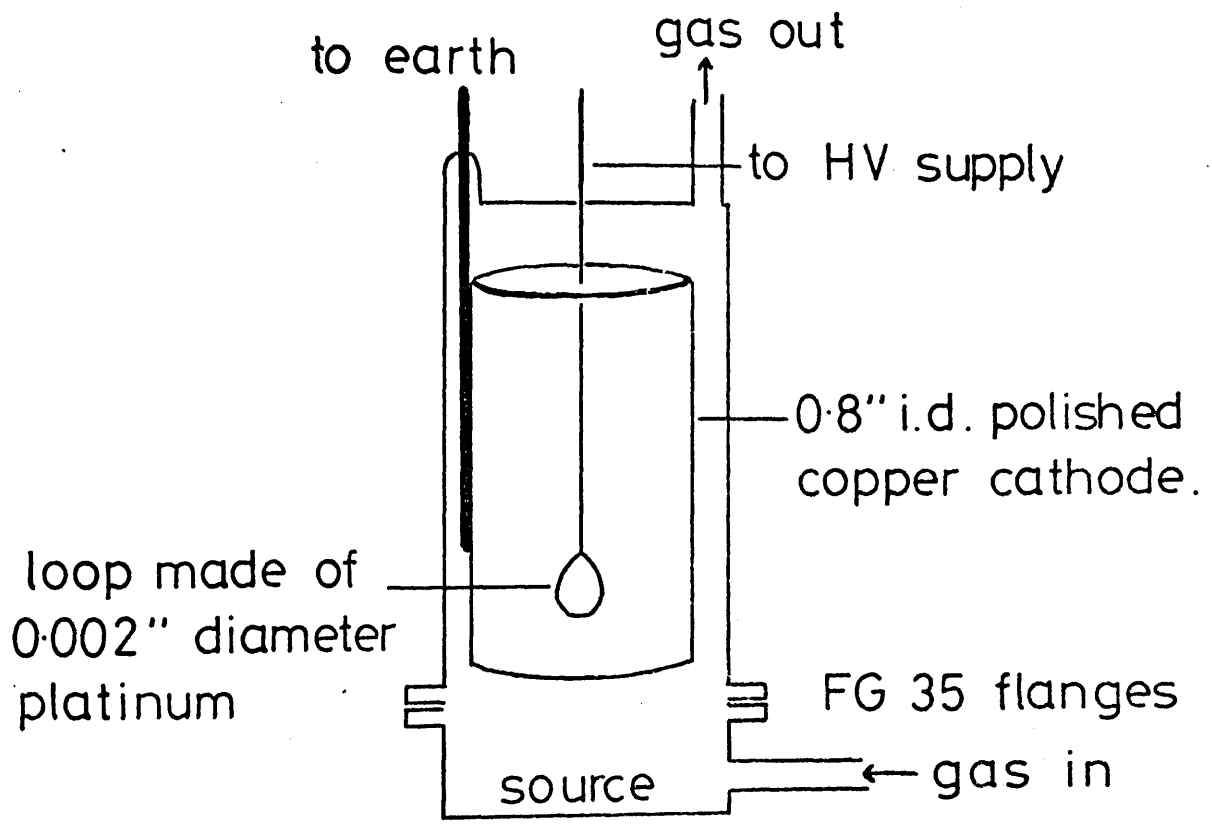

Bench counter used to investigate loop geometry.

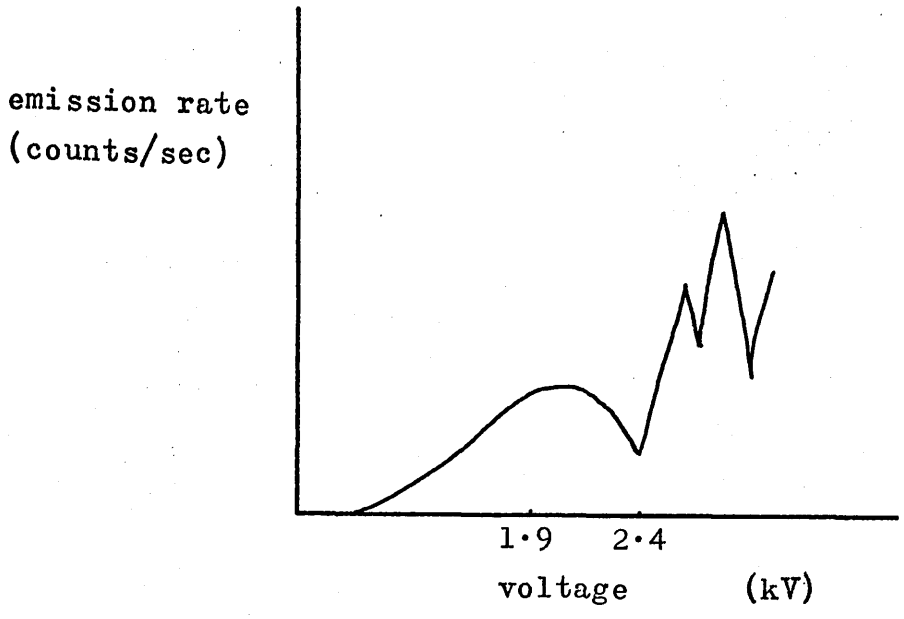

figure 18

At the time this effect could not be explained although it now seems likely that it is due to saturation of the head amplifier.

Platinum was chosen for the anode because it would be chemically inert: however it was found to be too soft to be of practical use since it was too easily distorted. The syringe needle in the bench counter was about 2" long and a platinum loop could be threaded with ease. The length of needle required in the actual reaction vessel was about 5" and the platinum was too soft to be pushed through this length of tube without kinking and eventually breaking.

Because of these limitations it was decided to replace the platinum wire with 0·002" tungsten, a more robust wire. It had already been shown by use of the bench counter that a loop behaved well as an anode, although not every loop mounted was successful, so that a tungsten loop was introduced straight into the reaction vessel/counter.

2·6·2 Counter 2

See Diagram 7, page 59a. Catalyst was held in a stainless steel basket with a wire mesh base which allowed gas to flow (see Diagram 8, page 59b). Beaten, polished stainless steel mesh (size 15) was placed on top of this to act as a shield between catalyst and anode. The basket was supported by three steel rods which were joined to tungsten rods with barrel connectors to facilitate dismantling the counter. A polished copper cylinder, 1" i.d., at earth potential rested on the stainless mesh on top of the basket to increase the active counting volume and to shield the steel rods and the thermocouple from the anode field. Because of this contact the mesh and the catalyst were at earth potential also.

Although it was easy to thread the 0·002" W wire through the long syringe needle it proved almost impossible to obtain a loop whose plane was vertical. Perhaps for that reason a tungsten loop did not give good counting characteristics, giving only a very narrow, steep plateau: see Graph 11, Appendix 3 for a typical curve.

After discussions with Dr. J.A. Cairns from Harwell it was decided to abandon this geometry of anode, which gives rise to a non-uniform field distribution, in favour of an anode unit developed by him at Harwell (133) (see Diagram 9, page 59c).

The unit comprised two hollow stainless steel tubes 0·005" i.d. mounted in bakelite supports. A brass skirt helped to protect the anode itself. The anode wire was threaded under tension and held in place by the screws in the stainless steel platform. A ~~hollow~~ tube passed through the platform so that counting gas could flow into the system. The ~~hollow rod~~ tube was

Diagram 7.

Apparatus used for testing catalyst samples for simultaneous exo-electron emission and catalytic activity.

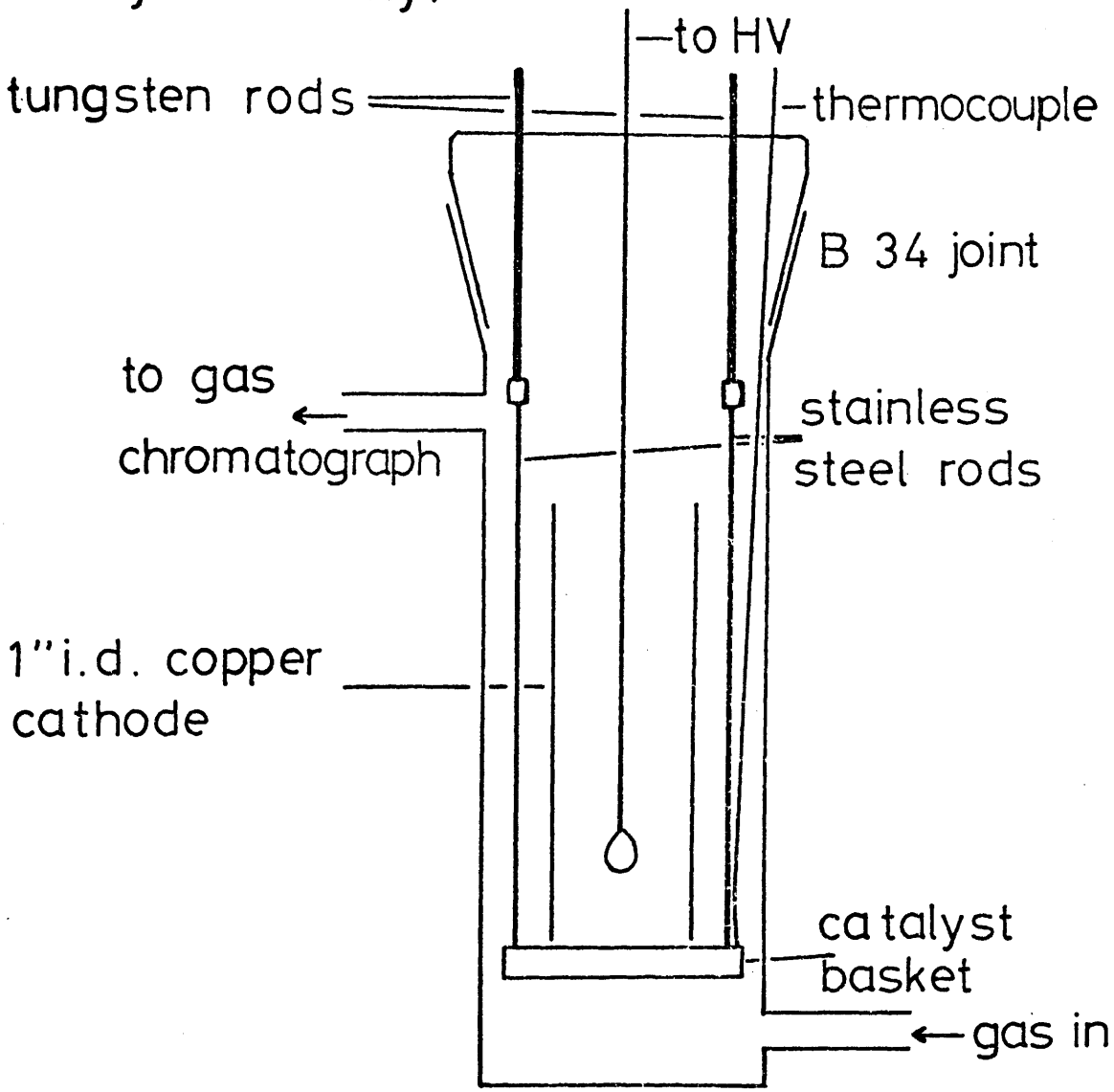

The loop was made of 0·002" diameter tungsten wire.
3 ground tungsten rods supported the catalyst basket. One was connected to earth to maintain catalyst and cathode at earth potential. The catalyst was heated by passing current through resistance wire wound round the outside of the glass vessel.

Diagram 8.

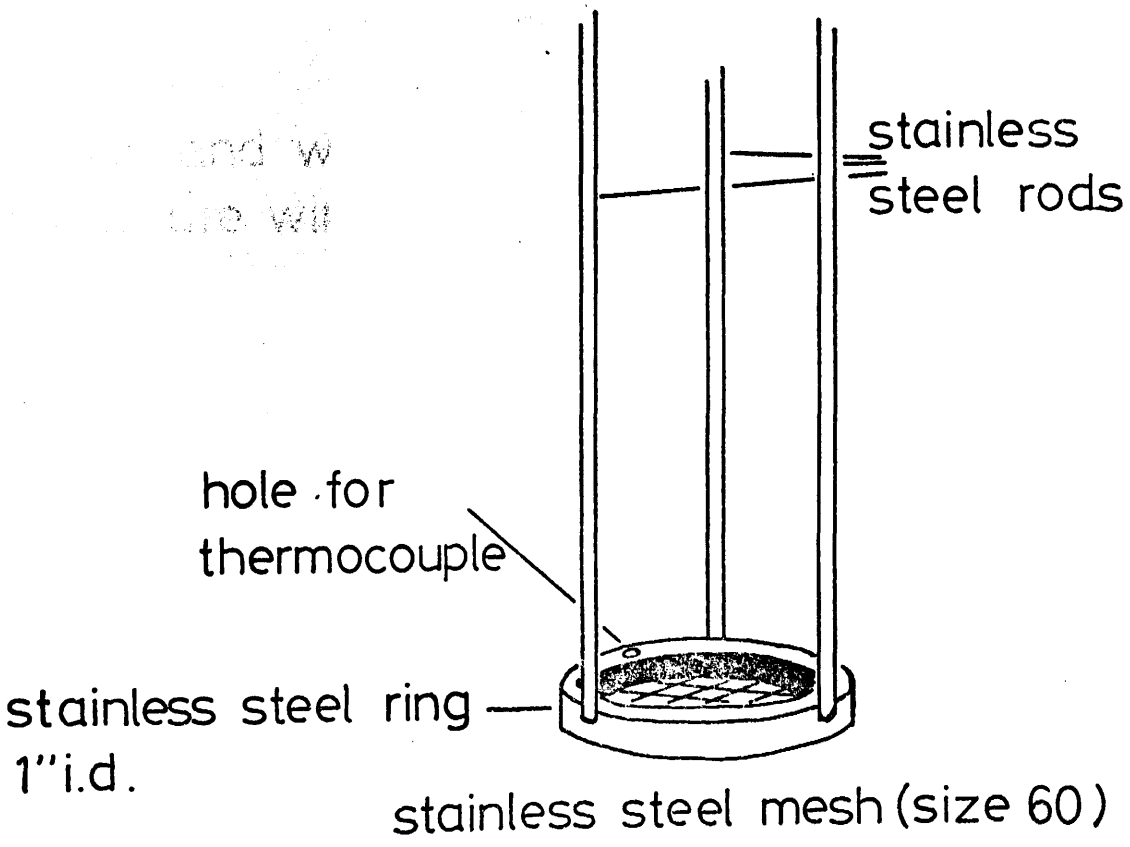

Stainless steel catalyst basket with wire mesh base.

The stainless steel rods were brazed to the stainless steel ring at 120° to each other.

Diagram 9.

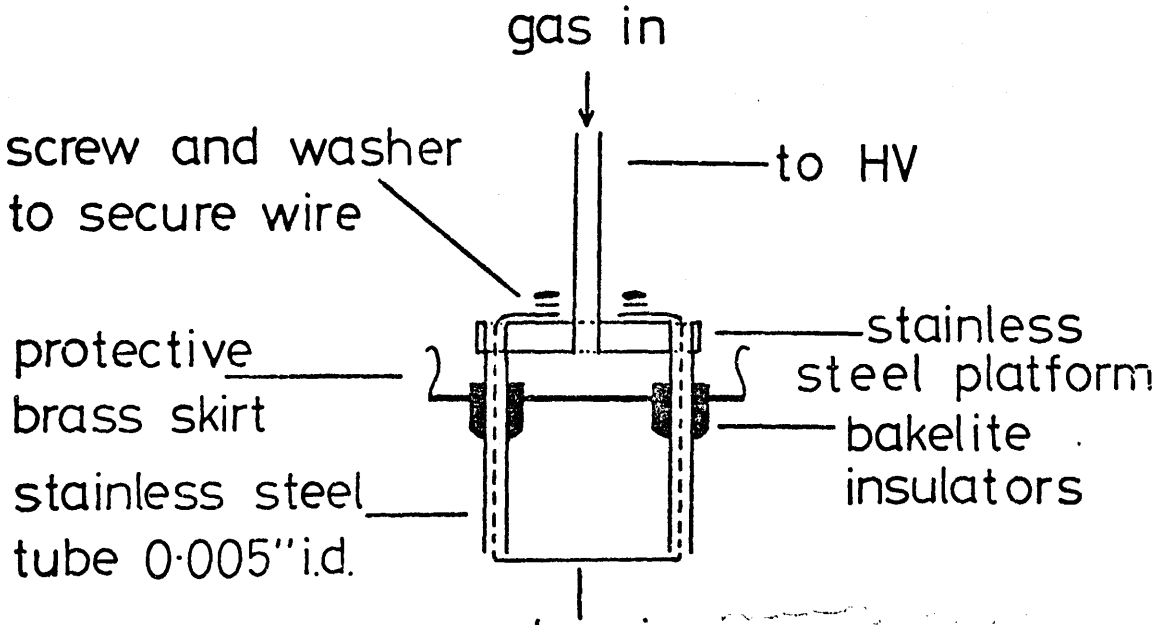

Section through anode unit devised by Dr Cairns

o o holes to allow counting gas to reach anode

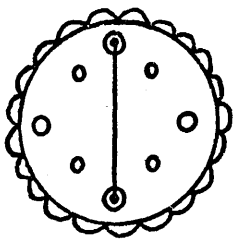

Anode unit from below

mounted in a chuck so that the distance between the anode and the sample could be varied.

Since the anode wire was straight the field between it and the sample under investigation would be uniform, neglecting end effects, so that much better counting characteristics could be expected.

At first 0·002" tungsten wire was used for the anode. The counter did not start to detect emission until about 3 kV, so the anode was replaced by flame-annealed 0·001" tungsten wire which brought the appearance potential down to about 2·1 kV with a plateau around 2·5 - 2·6 kV (see Graph 12, Appendix 3).

A Telequipment Oscilloscope Type S51E was introduced into the system so that peak shape could be monitored in addition to actual measurement of the count-rate. Thus it was possible to observe when background or electrical interference was being counted.

Since it had been shown that this anode unit gave good counting characteristics in Q gas it was decided to attempt to count exo-electrons in an argon, ethylene, oxygen mixture.

A sample of freshly prepared supported silver catalyst was used. The recipe and method were as before except that the 30-60 mesh portion of the α-alumina was sieved out and the silver precipitated onto it. Then the 30-60 mesh portion was separated out again to remove any dust. A micro-reactor was used to show that the catalyst was active for ethylene oxide formation (see Diagram 10, page 60a).

of counter I

0·42 g catalyst was place in the catalyst bed. The $Ar/C_2H_4/O_2$ mixture was arbitrarily set at a ratio of 95:25:50 giving a total flow of around 170 ml/min. $C_2H_4:O_2$ was in the

Diagram 10.

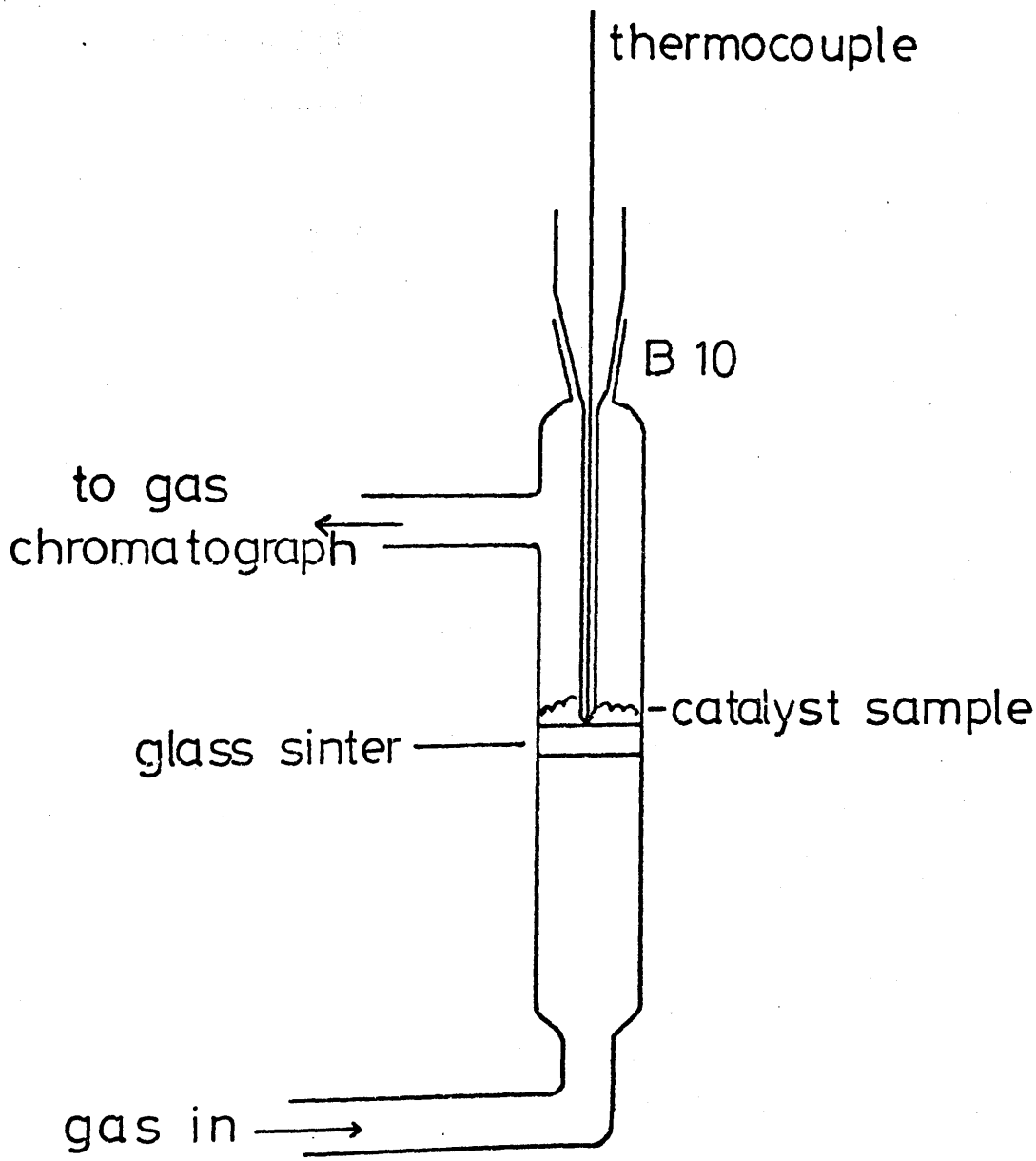

Microreactor used to test catalysts for catalytic activity.

Catalyst samples were heated by placing the microreactor inside a furnace.

ratio 1:2 to give good conversion to ethylene oxide and this mixture was well diluted with argon to lessen the risk of explosions. It was also hoped that if the percentage of ethylene was sufficiently high counting would be possible.

The catalyst was heated to around 250°C and gas chromatography showed ethylene oxide was being formed. C.p.s. were measured with a ^{137}Cs-γ source positioned outside the reaction vessel. Well-shaped peaks corresponding to pulses produced by passage of γ rays showed on the oscilloscope screen. Although background was high, 340 cps at 2·9 kV, peaks started to appear on the oscilloscope screen around 2·6 kV and at 2·9 kV for a discriminator setting of 1·27 x 0·2 (Integrate), the count rate with the γ source present was 358 cps i.e. 18 cps above background.

A typical set of results obtained when counting took place during a heating cycle is shown in Table IV, Appendix 4. Results were obtained for two discriminator settings, 0·1 x 0·2 (Integrate) and 1·27 x 0·2 (Integrate). At a discriminator setting of 0·1 x 0·2 (Integrate) every pulse sufficiently energetic to cross the minimum energy threshold is counted, while at a setting of 1·27 x 0·2 (Integrate) the threshold energy was raised sufficiently to cut out many low energy pulses, mainly due to electrical pick-up.

When counts were measured in the presence of the heated catalyst it was rather surprisingly found that, at both discriminator settings, the count rate was higher in the absence of the γ source than in its presence. This effect was only observed for voltages in excess of 3·3 kV. This was taken to mean that exo-electron emission was occurring and that this detector was

sufficiently sensitive to count these low energy particles at voltages greater than 3·3 kV, while presence of the γ-source must mask counting of these particles in some way.

It was found that in this gas mixture, as in Q gas, counts reached a maximum and fell away again when plots of cps vs V were prepared for the γ and β sources used. See for example Graph 13, Appendix 4.

After these preliminary results had been obtained some attempts were made to calibrate this counter, to find the effect of distance between the anode and the sample on the position of the plateau and to determine if there was any effect of discriminator setting on plateau position. It was also decided to investigate the effect of temperature on the plateau. It had been decided to investigate the effect of distance to see if this could explain why count-rate fell away at the end of the plateau, although, as previously stated, it is now believed that this was due to saturation of the head amplifier.

^{14}C-polymethylmethacrylate was used for this work.

For the effect of temperature see Graph 14, Appendix 4. It was found that as temperature increased the voltage range of the plateau shifted to lower voltage, which may be due to an increase in gas gain with temperature giving saturation of the amplifier at lower temperature.

The effect of varying anode distance at room temperature is shown in Graph 15, Appendix 4.

The position of the counting plateau was also dependent on flow rate. Halving the flow rate shifted the plateau 0·2 kV lower. Changing the discriminator setting had little effect on the position of the plateau.

Despite these favourable preliminary results, this counter design was discarded because voltages in excess of 3 kV were required to count exo-electrons and it was found that at such high fields sparking and arcing occurred. Each time this happened the Field Effect Transistor in the input stage of the preamplifier had to be replaced.

2·6·3 Detector 3

An attempt was made to measure the current flow from exo-electrons instead of using particle counting methods. A Keithley 602 Solid State Picoammeter which could detect currents as low as 10^{-14} amps was used.

The reaction vessel constructed for this work is shown in Diagram 11, page 63a and the circuit in Diagram 12, page 63b. The reaction vessel comprised two glass flanges 5·5 cm diameter which could be clamped together. Catalysts were supported on the lower aluminium disc while the upper was used as an electron collector. Both discs were supported by aluminium rods. A small positive bias was applied to the upper plate for collection of electrons. A furnace was coiled round the outside of the lower glass flange so that the catalyst could be heated.

This design was favoured because, if it was successful, it would have very wide applications since it would not require a counting gas, could be used to study any reaction and should be operable at any temperature. Furthermore, field emission would be impossible with the small ion collecting voltage used.

Although ethylene oxide was produced in this system when an $Ar/C_2H_4/O_2$ mixture in the ratio 40/15/30 was flowed over the supported silver catalyst, no electrons were collected for a collector bias of + 8·3 V with a catalyst bias of - 15·9 V.

Diagram 11.

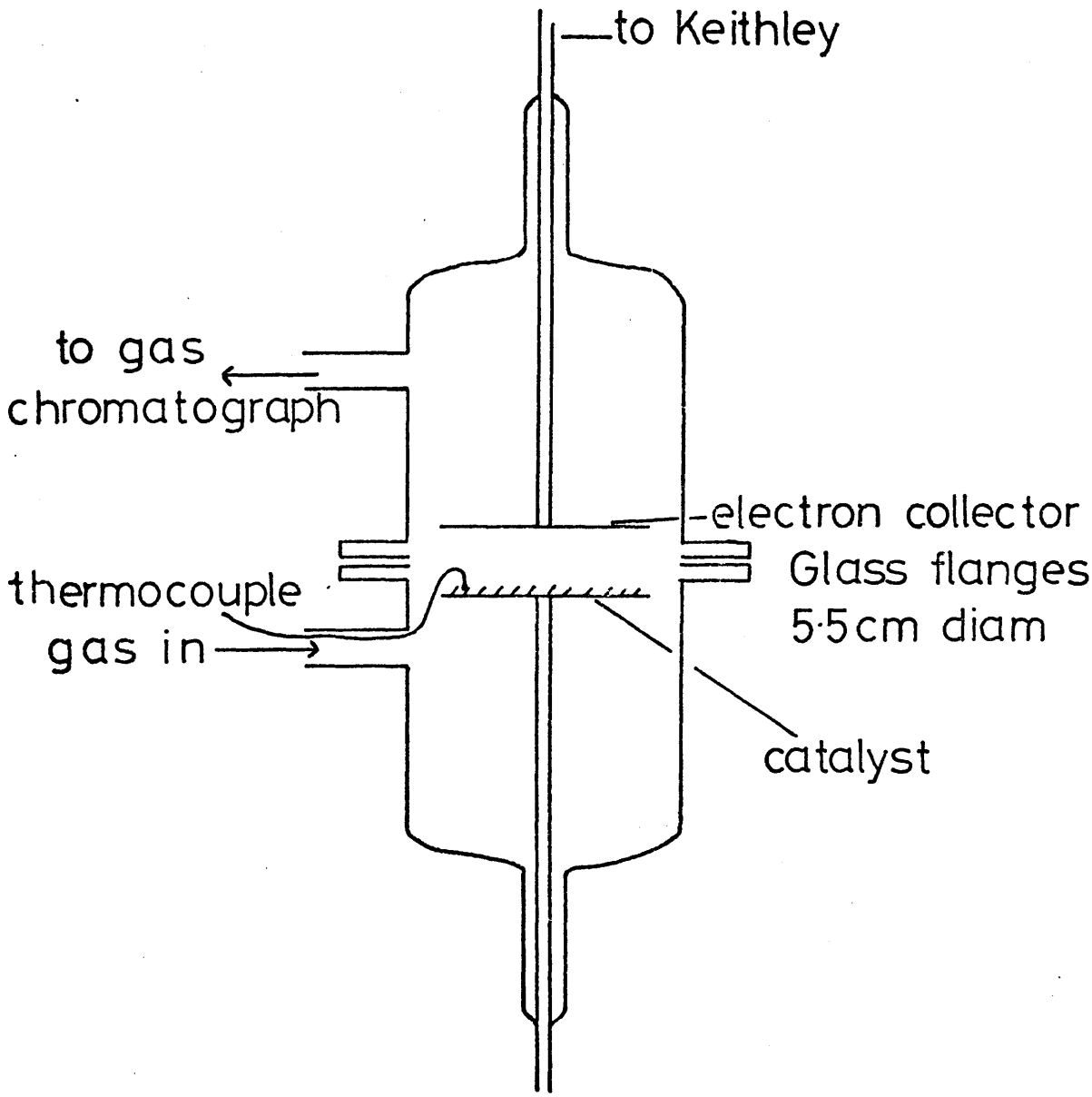

Detector used to try to measure exo- electron current from a supported silver catalyst during the partial oxidation of ethylene to ethylene oxide.

Diagram 12.

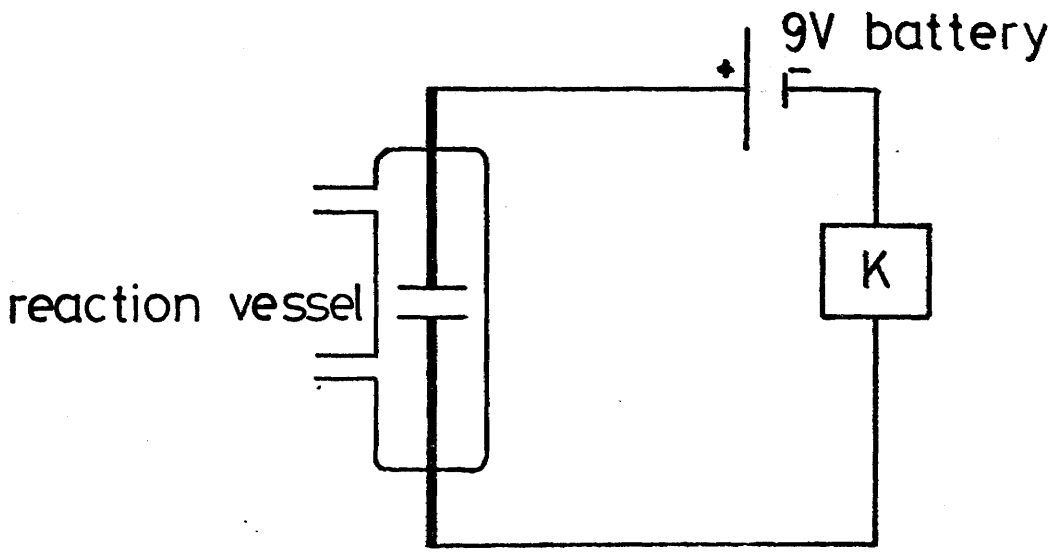

Circuit diagram for the measurement of the current flow of exo-electrons.

K:-Keithley 602 solid state picoammeter

Despite this failure to measure any current, an attempt was made to determine whether biasing the catalyst had any effect on reaction yield. No conclusive results were obtained and this was attributed to the fact that supported silver catalyst was being used and it possibly did not 'charge up' properly (see for example, Hoenig's work (112) for the inspiration for this).

Although a fresh precipitated silver catalyst could have been prepared to further this interesting investigation, it was decided to abandon this design of detector since no exo-electron current could be detected at atmospheric pressure with the Keithley picoammeter.

2·6·4 Detector 4

At this time some discussions took place with Dr. J. McNamee of the Engineering Department at Glasgow University who had made a preliminary study of electron emission from abraded aluminium using an open window Geiger-Mueller tube. Counting gas flowed through the counter and out onto the aluminium sample which was in air in front of the window.

Dr. McNamee had found that when a sample of aluminium was abraded and brought up to the detector the count rate was high but that counts decreased with time, emission often continuing for up to two days. He had also confirmed that the rate of emission was proportional to the intensity of illumination of the sample. Finally he also demonstrated to us that if the sample was earthed after counting had commenced, the count-rate was much higher and continued for much longer than if the sample was not earthed. Indeed, if the sample was not earthed positive charge built up on it so that eventually no more electrons could escape. If the sample was then discharged counting recommenced.

When Dr. Cairns lent us the anode unit described earlier, he also provided a complete detector comprising a stainless steel cylindrical cathode 1" i.d. and an anode unit sealed into a hollow rod so that counting gas could flow (see Diagram 13, page 65a). This detector had a detachable window so that it could operate as a windowless proportional counter. It was decided to investigate its counting characteristics to determine how well it satisfied the requirements for a counter specified earlier.

It had been found with Detector 2 that exo-electrons could be counted at voltages corresponding to the end of the plateau region and beyond. Thus a plot of cps vs voltage was prepared for Detector 4 to determine where the plateau region was (see Graph 16, Appendix 5). Q gas was used for counting and the collimated $^{137}Cs-\gamma$ source was placed in front of the window.

The appearance potential was around 1·4 kV and the plateau extended from around 2·0 - 2·2 kV. 2·5 kV was chosen as the operating voltage for investigating electron emission from abraded aluminium specimens in the hope that a high counting yield might be obtained.

A polished aluminium disc was abraded with emery paper and wiped to remove dust particles. The specimen was then brought up to the counter window and cps averaged over ten second periods were recorded. The results obtained are shown in Table V, Appendix 5. The specimen was not earthed so it was held periodically by the author to see what effect this had on count rate.

It was found that while the specimen was being held by the author the count rate was appreciably higher than when the disc

Diagram 13.

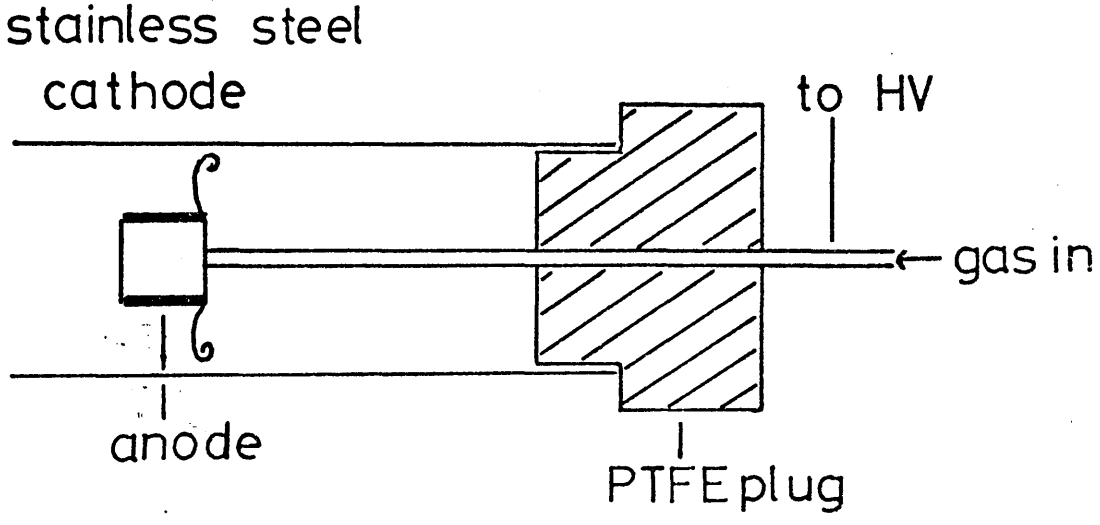

Windowless proportional counter incorporating anode unit devised by Dr Cairns.

was free, despite the poor earthing this contact provided.

Background was 143 cps averaged over 10 secs. When the scratched disc was brought up to the detector the count rate was always lower than background. If the aluminium plate was then removed the count rate increased to background level again.

A polished aluminium disc was introduced in front of the open window to determine whether the difference in count rate was due to interference with the gas flow. It was found that counting continued at background level. It was thus proposed that a component of the background was due to photo-emission, probably from the cathode walls which had been scratched by the protective brass skirt when the anode was being positioned. The polished disc could reflect light (daylight or the overhead lights) into the proportional counter, thereby permitting photo-emission to continue, while the abraded aluminium would not reflect light efficiently. Here emission would be mainly due to chemically (oxidation) stimulated exo-electron emission.

When an attempt was made to clarify this, sparking took place and it was found to be impossible to eliminate its source. It was finally concluded that tracking was occurring across the bakelite supports. Thus this anode unit was not suitable for use at such high voltages so this detector had to be abandoned.

Because of the problems of arcing and tracking encountered with this design, and also the fact that counting gas had to be used, it was decided that its applications were too limited to be useful for studies of chemisorption and catalysis. It was thus decided to find a more suitable geometry of counter, one which could detect exo-electrons at much lower fields and in which a much wider variety of gas fillings could be used.

2·6·5 Detector 5

It was decided to investigate the possibilities of a cylindrical gas flow proportional counter with a central anode wire, a design used successfully in the Surface Chemistry group for ^{14}C counting.

The counter design is shown in Diagram 14, page 67a. Several modifications were made to the basic design. These are shown in Diagram 15, page 67b. The experimental set-up is shown in Diagram 16, page 67c.

The basic design consisted of a central tungsten wire 0·001" in diameter threaded under tension and a polished, cylindrical copper cathode.

The modified design was made of glass in three sections. A polished, cylindrical copper cathode 1" i.d. was sealed into the bottom section which also had a gas inlet. The middle and bottom pieces were joined together with a B40 cone and socket joint held together with springs to give an airtight seal. The gas outlet was contained in the middle section which was introduced to facilitate dismantling the reaction vessel. At the top of the middle section there was a B24 cone and socket joint which was turned back in on the middle section so that the weight of the top section would hold itself in place and give an airtight seal.

The top section had two tungsten rods, sealed into the glass at 180° to each other, to provide electrical contacts for the wire catalyst which was joined to them with stainless steel barrel connectors (see Diagram 17, page 67d). In between the two rods there was a size 10 Kovar seal into which a small piece of fine bore glass tubing was sealed to centralise the anode wire.

Diagram 14.

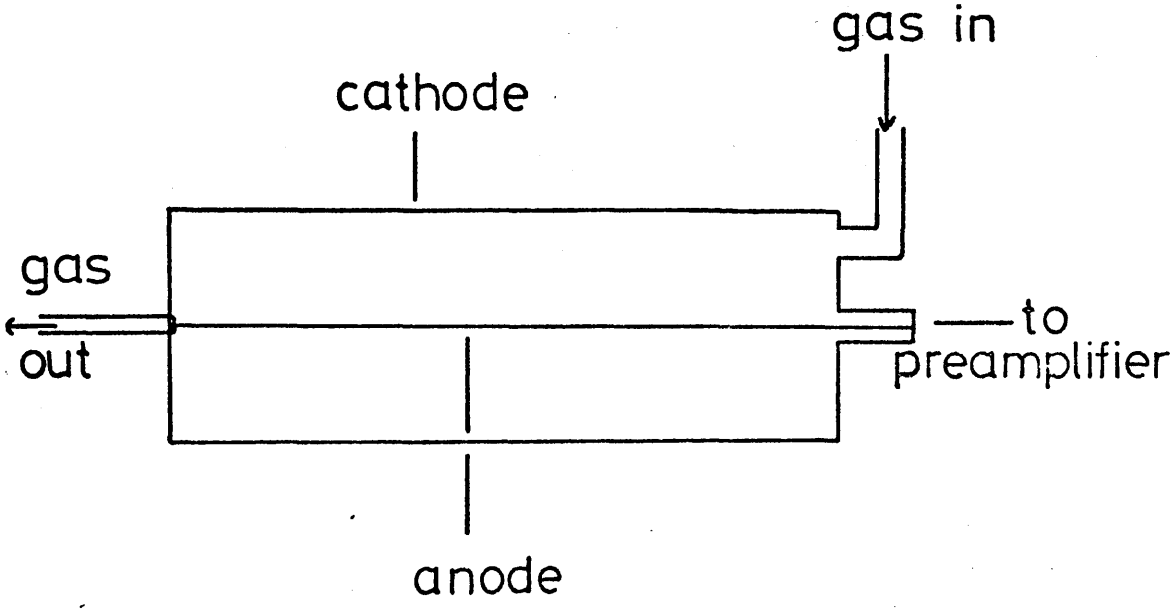

Cylindrical gas flow proportional counter before modification.

Diagram 15.

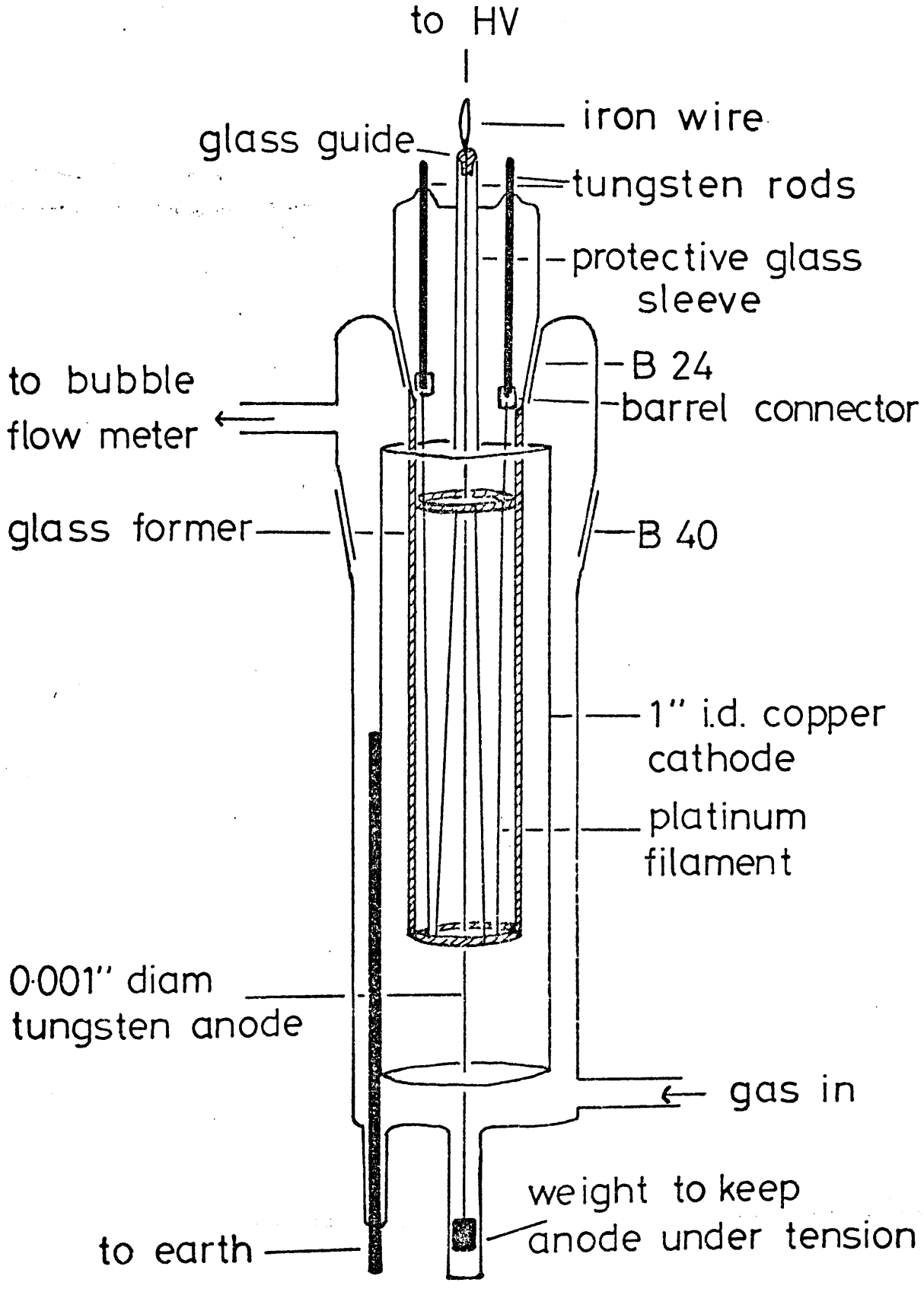

Modified gas flow proportional counter.

Diagram 16.

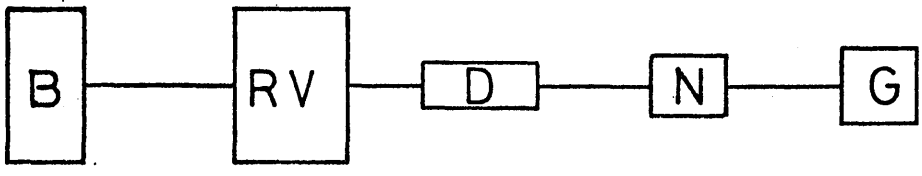

Experimental set-up

B:- Bubble flow meter,
RV:- Reaction vessel / exo-electron detector,
D:- Drying tube filled with anhydrous sodium carbonate,
N:- Needle valve to regulate gas flow,
G:- Gas cylinder.

Diagram 17.

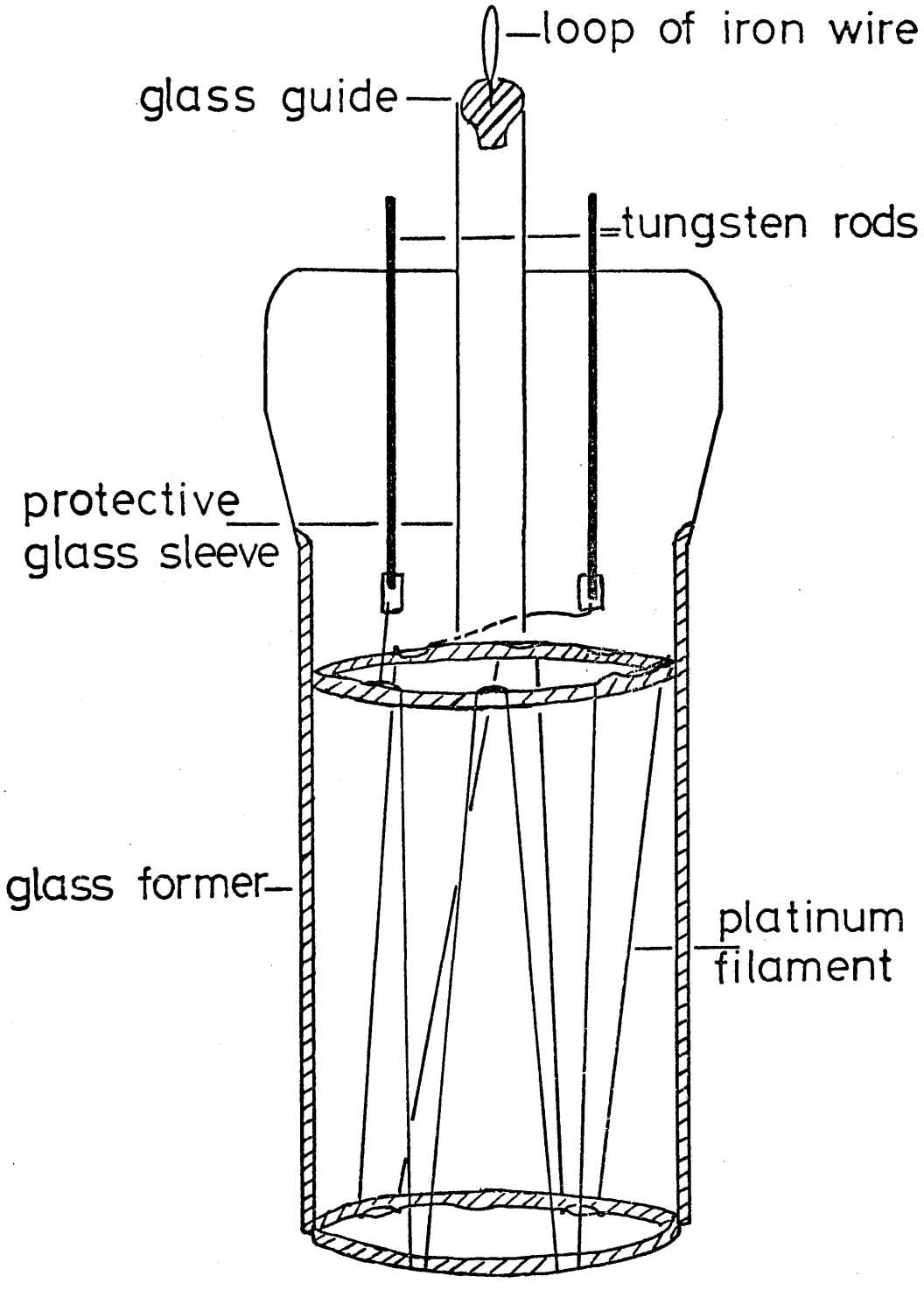

Detail of catalyst assembly.

A few inches of iron wire was doubled over and twisted round on itself and inserted into the top of the glass tube to provide a more robust connection for the HV supply.

A glass tube came down inside the socket to protect and insulate the anode and thereby prevent sparking to the tungsten rods.

Two glass rods were joined onto the bottom of the B24 cone to support the former on which the catalyst wire was mounted. These were offset from the tungsten rods by 90°. The former consisted of two circles of glass about 0·5" diameter with six hooks placed symmetrically round them, held about 6" apart by the glass rods. The wire was wound round alternate hooks and when threaded it formed a double- W placed as symmetrically as possible round the anode.

The bottom glass section was drawn in beneath the copper cathode to give a narrow, central, glass tube. The bottom of the anode wire was tied to a small spring which was almost flush with the walls of the tube. A small bolt was screwed into the spring to provide added weight. These were suspended from the anode wire so that their weight kept it under tension.

The anode was flame-annealed 0·001" tungsten wire which was then polished with Brasso to remove any carbon deposited by the flame, and finally cleaned with Analar acetone to remove any grease.

The reason for designing a counter with the facility for mounting a wire between the anode and the cathode was so that the catalyst wire could be heated in situ, thereby providing a source of thermal electrons. It would then be possible to determine whether the counter was sensitive to such low energy particles

(E ~0·0025 eV). A D.C. power supply was used to heat the wire since, when current was flowing, the wire picked up mains interference and this could only be earthed out with a D.C. supply. In the early work a car battery was used but this was later replaced by a 24 V D.C. transformer which provided a more reliable current.

The first wire investigated was platinum which was chosen for a variety of reasons. The first was that platinum is catalytically active and, as it has been the subject of many investigations, its reactions are well documented. Thus it was hoped that the existing body of literature might be employed to help to explain any results obtained with this reaction vessel.

Another reason for choosing platinum was that it has a comparatively low electrical resistance so that with a 24 V D.C. supply a reasonable length, say 1m, could be investigated and yet sufficient current pass to allow the wire to be heated to red or orange heat. The highest temperature to which the wire was heated was about 900°C. Platinum has the advantage of remaining 'stable' at this temperature, unlike for example gold, whose surface atoms become mobile, which can lead to a gold wire fusing. Furthermore a platinum surface can be cleaned by heating alternately in oxygen and hydrogen. It was hoped this would provide a means of regenerating the surface when necessary.

In all five platinum wires were investigated. Each sample was taken from a length of platinum wire supplied by Johnson Matthey. The platinum was 0·3 mm diameter bright drawn pure platinum.

98 cm of 0·3 mm diameter platinum wire was wound round the former. A Pt - 13% Rh wire was attached to the platinum wire

about 1" below one of the barrel connectors to make the hot junction of a Pt/Pt,Rh/Pt thermocouple.

The counting characteristics of the detector were investigated with the platinum in place to determine whether its presence would have an adverse effect on counting.

Plots of cps vs. voltage for two different flow rates were prepared using ^{137}Cs as an external source and Q gas as the counting gas (see Graphs 17, 18, Appendix 6). It was found that the detector gave a counting plateau in Q gas from about 1·6 - 2 kV regardless of flow rate. Thus it was concluded that the presence of the platinum wire did not affect counting in this voltage range.

Having shown that the detector could count, its behaviour as temperature varied was then investigated.

The current passing through the wire was increased gradually to 1·6 amp by varying an 8 ohm rheostat, capable of carrying 10 amp direct current, over a period of about ten minutes. At room temperature the count rate without a source was 160 cps. After 1·6 amp had been passed through the wire for about three minutes the count rate had reached 1900 cps. The current was then switched off and the decay curve obtained is shown in Graph 19, Appendix 6. A car battery was used to provide current at this time and when the negative terminal was disconnected the count rate fell away very quickly.

This was repeated with a current of 3 amp which caused the wire to glow cherry red (i.e. $T \sim 550 - 600°C$), thereby providing a good source of thermal electrons. These were recorded by the SR5 scaler-ratemeter, a typical count-rate being in the range $0·9 - 1 \times 10^5$ cps for the minimum discriminator setting of

0·1 x 0·2 (Integrate).

To determine whether the counter had gone into continuous discharge because of the high temperature or high count rates involved, or whether it was in fact counting properly, the current was switched off. The count rate immediately started to decay (see Graph 20, page 71a for a typical decay curve of the electron emission from platinum wire 1 cooling in Q gas).

This decay curve was of the utmost significance and several important points emerged from it.

1. Counts started to decrease as soon as the heating current was switched off. This meant that the detector was counting properly while current was passing through the wire and that it was not in continuous discharge. This in turn implied that the counter is sensitive to low energy electrons: E thermal electrons ~0·025 eV.

2. The fact that the initial part of the decay curve, (a), was smooth proved that the counter operates well at high temperatures.

3. Thermal emission rate is governed by an exponential expression. Thus as a source of thermal electrons cools the number of electrons emitted will decrease exponentially with temperature. A plot of cps vs time when such a process is monitored should yield a smooth curve.

Portion (b) of the decay curve clearly was not smooth.

This section of the graph was interpreted to indicate that chemical reaction or phase change was occurring on the platinum surface with an accompanying release of exo-electrons. That the graph was fairly reproducible implied that this was not an artefact.

The reproducibility of the graph confirmed that, despite

Graph 20.

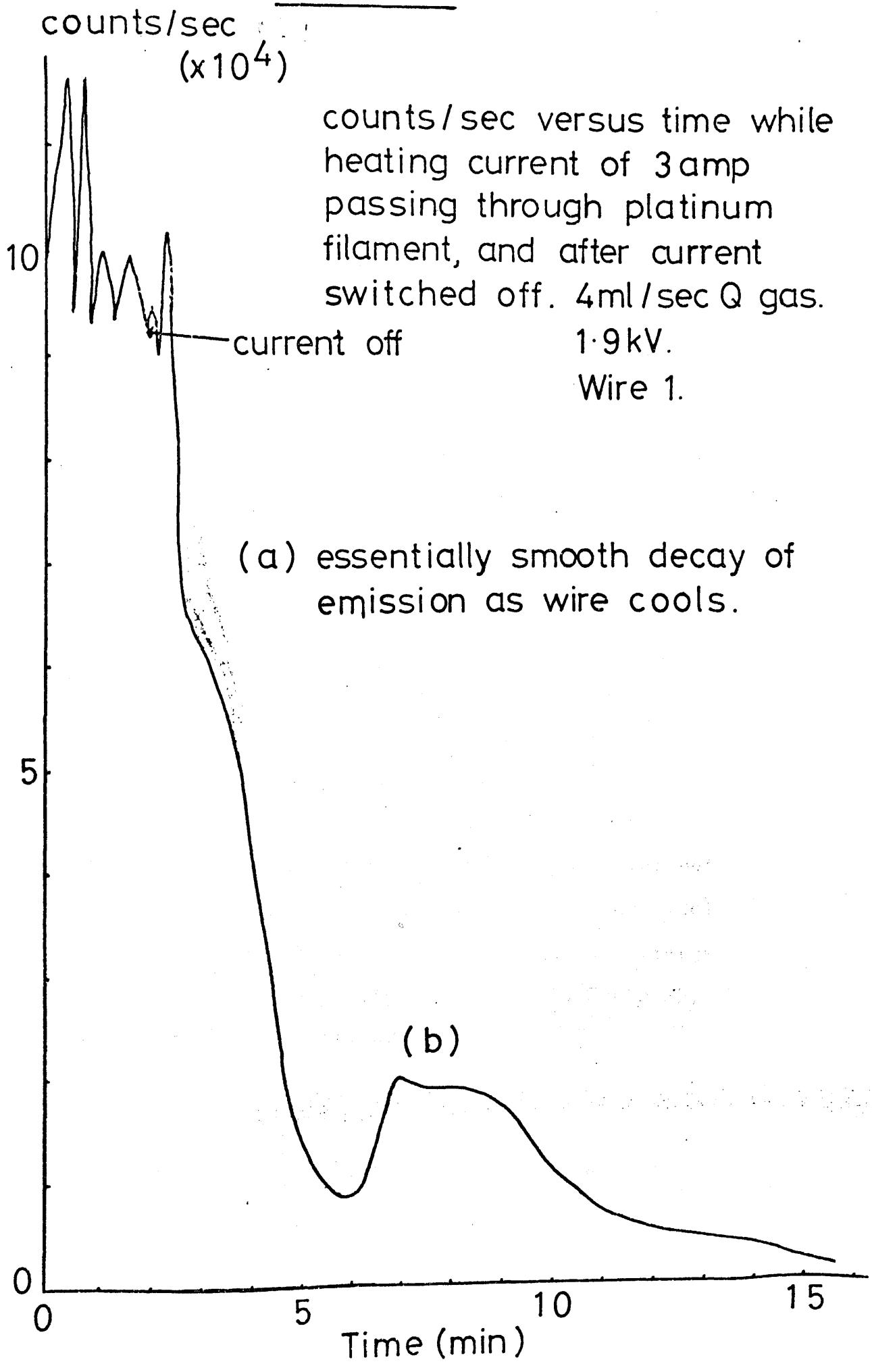
counts/sec
(x10⁴)
counts/sec versus time while heating current of 3 amp passing through platinum filament, and after current switched off. 4ml/sec Q gas.
1·9kV.
Wire 1.
current off
(a) essentially smooth decay of emission as wire cools.
(b)
10
5
0
0
5
10
15
Time (min)

the exceptionally high count-rates, of the order of 10^5 cps, encountered while current was passing through the wire, the detector was not in continuous discharge.

Continuous discharge occurs if the following reactions take place:-

$$Ar^+ + \text{wall} \rightarrow e^- \qquad (1)$$

$$Ar^+ + e^- \rightarrow Ar^* \rightarrow Ar + UV \qquad (2)$$

Both of these reactions could give rise to an avalanche of electrons at the anode.

Thus the detector was sensitive to thermal electrons. Portion (b) of the cooling curve further demonstrated that the detector was sensitive to chemically-stimulated electrons.

To prove that this portion of the graph represented a genuine effect, the wire was heated in hydrogen.

H_2 gave a counting plateau (see Graph 21, Appendix 6) and a background count-rate of around 90 cps at 1900 V. When the platinum wire was allowed to cool in hydrogen a smooth decay curve was obtained for a plot of cps vs time (see Graph 22, page 72a).

Plots of log (cps) vs time were prepared for both of these sets of results (see Graphs 23, 24, page 72b and 72c). The hydrogen curve (Graph 24) yielded a series of straight lines. The deviation from linearity is obvious in Graph 23, providing added confirmation of the effect.

These preliminary results showed that the counter was sensitive to low energy electrons, both thermal and chemically stimulated exo-electrons, and also that it was capable of:

1. operating at atmospheric pressure,
2. operating in O_2 gas and H_2 - other gases, N_2, O_2 Ar, He,

Graph 22.

Counts/sec versus time as platinum filament cooled in hydrogen. Heating current was 3·4 amp. 4 ml/sec hydrogen. 1·9 kV. Wire 1.

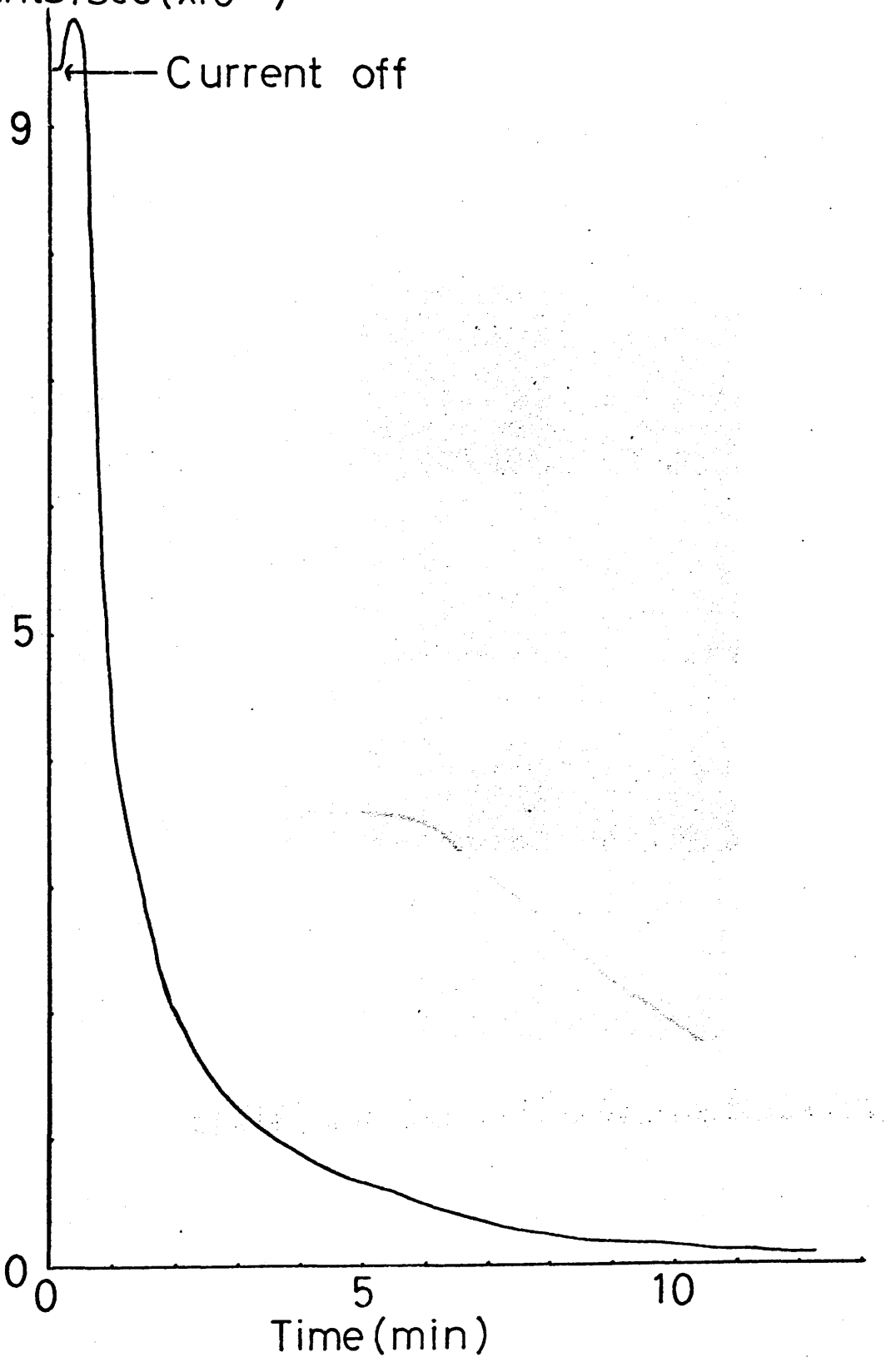

Graph 23.

log(counts/sec) versus time for platinum cooling in Q gas.

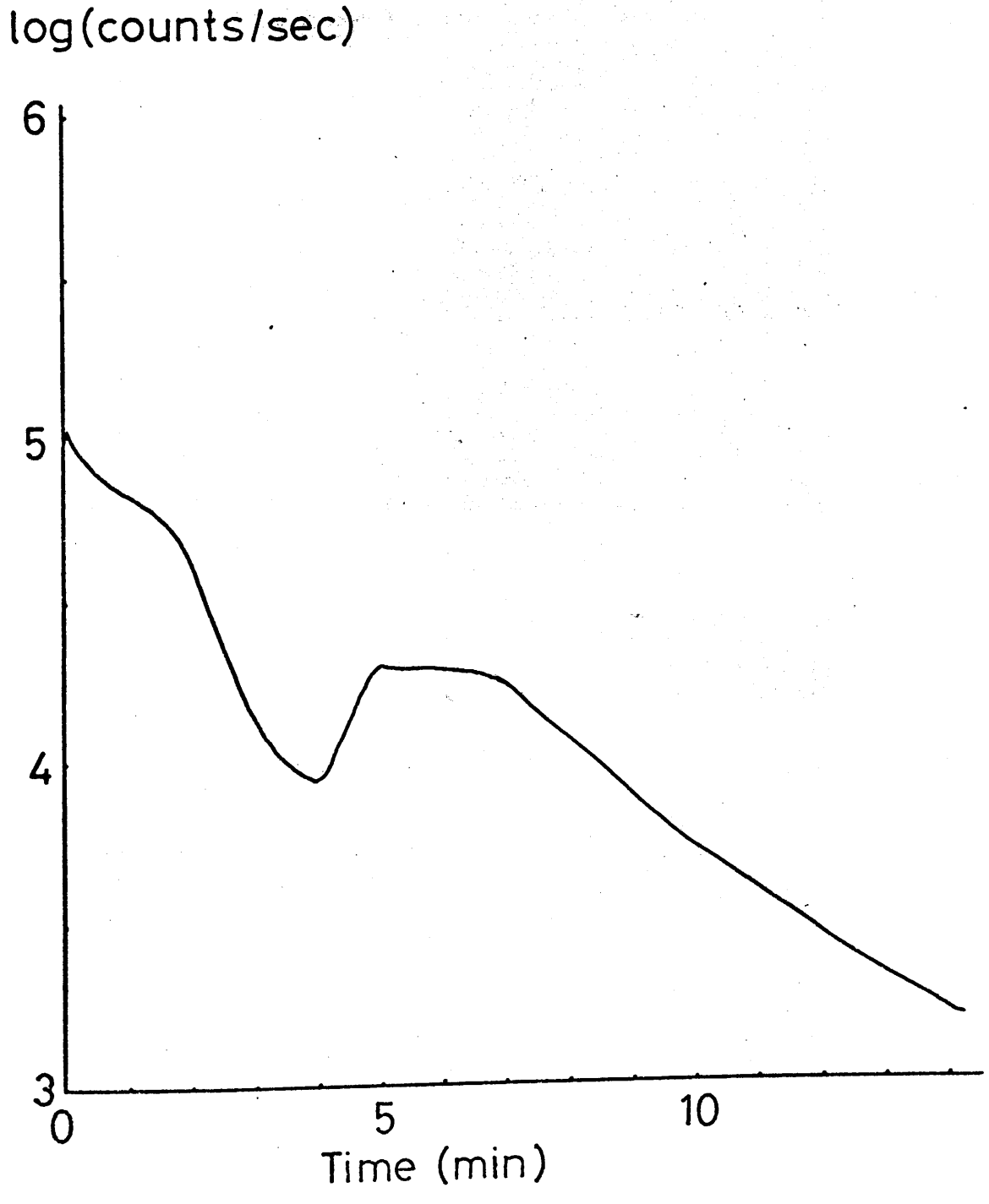

Graph 24.

log (counts/sec) versus time for platinum cooling in hydrogen.

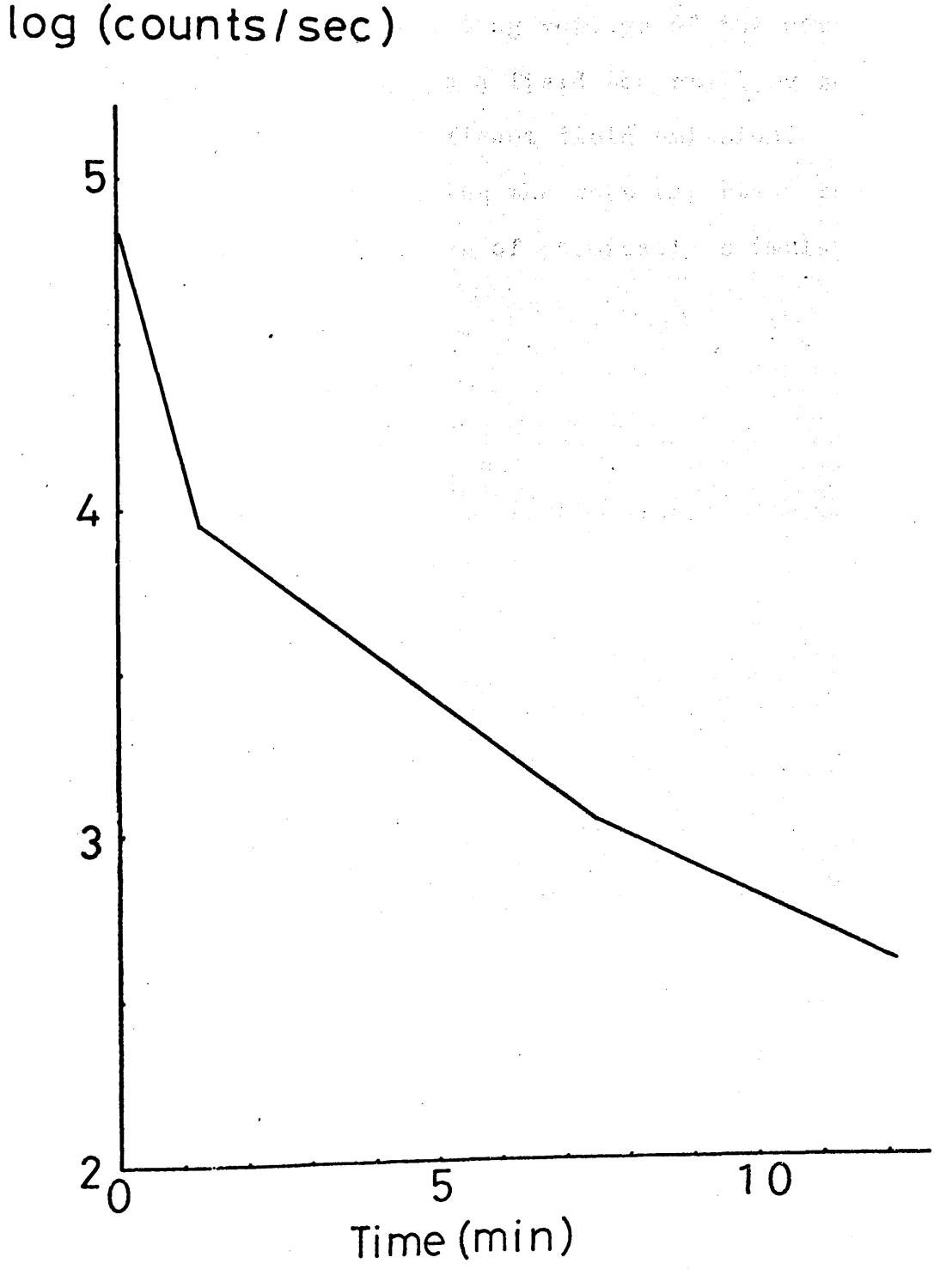

Ar/C_2H_2, Ar/C_2H_4, were tested later and also found to be suitable for use as counting atmospheres: thus this detector fulfilled the requirement of variety of counting and adsorption atmospheres,

3. operating over a wide range of temperatures.

It did not meet the requirement of having the catalyst shielded from the anode. However, calculations to be shown later indicate that the operating voltage of the counter, generally 2 kV, gives rise to a field too small by some orders of magnitude to permit significant field emission.

Thus this design satisfies the most important requirements laid down by us for a detector of chemically stimulated exoelectrons.

CHAPTER 3

Chapter 3

3·1 Apparatus

Diagram 16 page 67c and Diagram 18 page 74a, show the apparatus and electronics used in ~~this~~ the work described in this chapter. The thermocouple arrangement is shown in Diagram 19 page 74c. A curious and unexpected effect was observed with the thermocouple system. It is described in Appendix 7.

3·2 Characterisation of Detector 5

A Laben 400-channel energy analyser, Spectrascope, MOD 400, was introduced into the system to try to assign absolute energies to the emitted electrons. Americium ($^{95}_{241}$Am-γ emitter, 36% with E = 59·57 keV) was used as a source of low energy γ-rays to calibrate the Laben. When, during initial trials, pulses from the detector and preamplifier passed straight into the Laben, their 'rise time' was too slow to permit analysis. Thus no peak was obtained. A Nuclear Enterprises amplifier, type NE5259, and a Nuclear Enterprises biased amplifier, NE5261A, part of the 'Edinburgh' series, were introduced between the preamplifier and the Laben to shape the pulses. Direct connection was still maintained between counter, scaler and chart recorder.

It was found that at the operating voltage of 2kV the pre-amplifier saturated for the dynamic range 6·5V so that nothing was recorded above channel 274 for a Laben amplification of x25 and a channel width of 40 mV. The dynamic range of the preamplifier was therefore increased from 6·5V to 12V. Under certain conditions peaks could still appear above channel 190 but in general they appeared below channel 200 so the channel width was changed to 20 mV/channel so that the region of interest could be

Diagram 18.

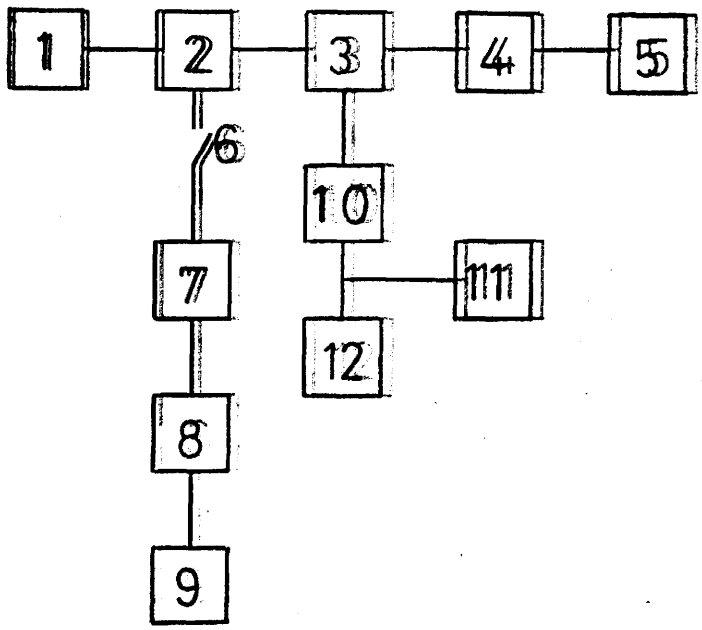

Electronic circuits.

1) Thermocouple potentiometer; see Diagram 19 for thermocouple arrangement.
2) Reaction vessel/exo-electron detector. The detector and the preamplifier were screened by copper mesh cages to eliminate electrical noise, often as high as 10^4 cps.
3) Nuclear Enterprises 5287 AC-SC solid state preamplifier.
4) Nuclear Enterprises SR5 Scaler-Ratemeter. Typical settings:-HV- 2kV, Time constant- 4 sec, Range- $x10^4$, Energy discriminator 0·1x1, 2% window or 0·1x0·2, Integrate. Counts were averaged over 3 or 6 sec for scaler.

5) Pen recorder. Settings - Range 100 mV, Chart speed 600 mm/hour, Full scale deflection 10^4 cps.
6) Switch.
7) 0-10 amp D. C. ammeter.
8) 0-8 ohm rheostat capable of carrying 10 amp.
9) Transformer capable of producing a 24V, 10 amp D.C. supply.
10) Pulse shaping equipment - Nuclear Enterprises Amplifier, NE5259, and Nuclear Enterprises Biased Amplifier, NE5261A. Typical settings- Amplifier- Coarse gain x500, Fine gain x0·9, Time constant, Int-0·5, Diff-max, both on switch position 2, Output negative; Biased Amplifier- Polarity positive, Gain x5, Bias level 1·2V.
11) Laben Spectrascope, MOD 400, multi-channel analyser. Signal from biased amplifier output to low input. Input positive. Typical settings- Gain x25, Channel width 20 mV, 0 back bias, Maximum upper threshold.
12) Telequipment Oscilloscope S51E.

The signal from the biased amplifier was passed through a T-connector to the Laben Spectrascope and the oscilloscope so they received the same signal.

Diagram 19.

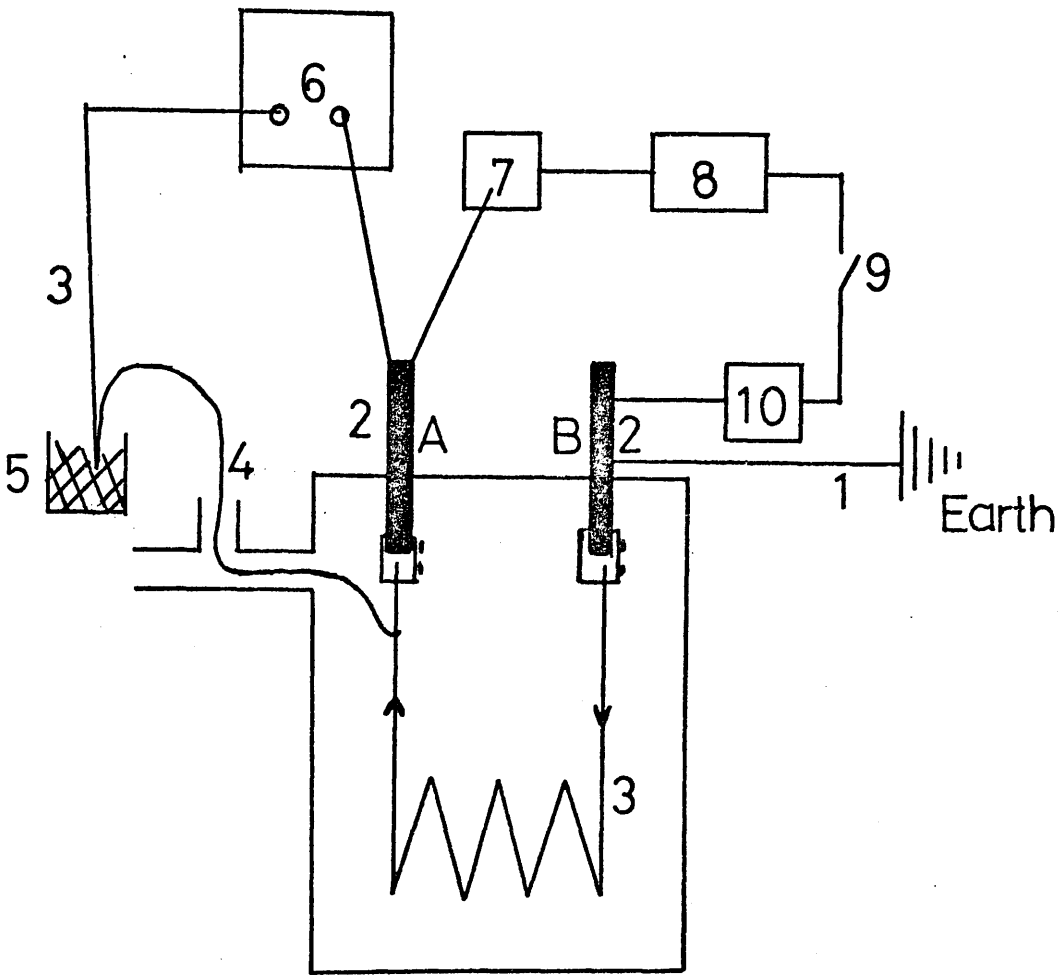

1) Earth lead.
2) Tungsten rods.
3) Platinum wire.
4) Platinum, 13% Rhodium wire.
5) Melting ice to provide reference cold junction.
6) Derritron thermocouple potentiometer.
7) 8 ohm rheostat.
8) D.C. power supply.
9) Switch.
10) 10 amp D.C. ammeter.

expanded to fill the screen. This effect will be discussed later.

When these modifications to the system had been effected, it was found that americium gave a maximum energy edge at channel 328. The anode voltage was 2kV and the Q gas flow rate was 4 ml/sec. The biased amplifier had a gain of x5 and a back bias of 1·2V. This work was later repeated for a biased amplifier gain of x2 with zero bias, and a photograph was taken of the resulting spectrum (see Appendix 8). The anode voltage was 1·9kV.

In a separate experiment the signal from the preamplifier was passed straight into the oscilloscope. Americium gave peaks which ranged in height from 0·2 - 0·4 mV as measured on the oscilloscope screen. The preamplifier was operating in the 12V dynamic range.

It was found, as expected, that the position of the americium edge varied with anode voltage. The peak shifted from channel 328 to channel 323 when the voltage was decreased from 2 - 1·6 kV. When this trial was repeated the corresponding channel numbers were 330 and 326. This behaviour was satisfactory since in meant that any drift in anode voltage would have little effect on results.

Since the americium edge appeared at channel 328 it was expected that if exo-electrons could register on the Laben, which has an energy threshold of 0·1V, they would accumulate in the first few channels.

The platinum wire was heated and allowed to cool in several gases in turn; a typical experiment will be described later. A plot of cps vs time was traced on the chart recorder for each experiment. Such plots will in future be referred to as cooling curves. Photographs were taken of the corresponding Laben

spectra. Examples are shown for nitrogen and hydrogen in Appendix 9. From inspection of these spectra it is obvious that, surprisingly, peaks appeared at much higher channel numbers than predicted. For example, spectrum 3 showed peaks in channels 40, 64 and 109 when counts were accumulated during the first three minutes of the cooling cycle. This will be explained later.

3·3 Plateau Region

It has already been shown in Chapter 2 that this detector gave a counting 'plateau' with Q gas between 1·7 - 2·0kV (see Graph 17 Appendix 6). An external ^{137}caesium source was used in establishing the plateau.

The effect of gas flow rate on the position of the plateau was also investigated. Comparison of Graph 18 Appendix 6 and Graph 17 Appendix 6 where the flow rates were 4 ml/sec and 1·6 ml/sec respectively showed that the flow-rate had little effect on the position or width of the plateau.

3·4 Gas Flow

A pressure reducing head was used so that each cylinder of gas gave a pressure of 10 psi. The flow was regulated by means of needle valves. The gases were dried by passing them through a tube packed with anhydrous sodium carbonate before they entered the reaction vessel. The flow-rate was measured by means of a bubble flow meter and a stop clock and it was generally 4 ml/sec.

3·5·0 Experimental Procedure

The experiments carried out fell into two categories.

In the first of these the wire was heated for 30 sec in the gas under investigation and then allowed to cool in the same gas.

A different gas was introduced while the wire was cold. In the second the wire underwent prolonged heating in several gases in sequence so that introduction effects could be observed at high temperature. Thus the effect of pretreatments on the shape of a cooling curve could also be investigated.

A standard procedure will be described for an experiment in each category and some typical results presented. These results will be discussed in Chapter 6.

Some experiments were conducted with a gold filament instead of a platinum filament and the results obtained will also be presented. Gold was chosen because it is generally considered to be chemically inert, and it was expected that no structure would be observed in the cooling curves obtained.

3·5·1 Type 1 Experiment:- Short Heating Time

To keep electronic drift to a minimum, the scaler-ratemeter, preamplifier and Laben were left switched on continuously since their performance may take a long time to stabilise after they have been off.

Before an experiment was begun the gas cylinders were turned on and left to allow the gas flows to be stabilised. The gas to be investigated first flushed out the detector. The HV was increased gradually to 2kV and also left to become stable. The oscilloscope, the chart recorder, the D.C. transformer and the pulse shaping equipment were then switched on and left to warm up. Here electronic drift was less likely to be important.

An ice and water mixture was prepared in a Dewar flask to be the cold junction of the thermocouple and the thermocouple potentiometer was switched on.

After about half an hour a series of experiments would be started.

The thermocouple potentiometer was centred. The gas flow rate was checked, and if necessary adjusted to 4 ml/sec. The pen recorder was set in motion and the current to heat the platinum wire was switched on. The stop clock was started immediately and the position marked on the chart. After about twenty seconds, when the current had steadied, it and the colour of the wire were recorded on the chart. After thirty seconds the current was switched off, a 'live' count started on the Laben and the point corresponding to the current being switched off marked on the chart recorder.

Taking the time when the current was switched off as $t = 0$, thermocouple readings were taken every 30 sec for the first five minutes and thereafter each minute. The Laben count was stopped usually after three or five minutes and the channel number of any peaks noted.

If required, a photograph of the display on the Laben was then taken with a Telford Type P oscilloscope camera using Polaroid Land film type 20C.

Two or three heating cycles were monitored for each gas under investigation and then the next gas was introduced and allowed to flow for several minutes to flush out the reaction vessel. The flow rate was checked and a new sequence of experiments started.

Some typical cooling curves are shown in Appendix 10. These experiments were carried out with the preamplifier range switch at the 12V position.

3·5·2 Type 2 Experiment:- Long Heating Time

These experiments were carried out with the low range preamplifier setting of 6·5V.

The experimental procedure was identical to that for a Type 1 experiment until the current was switched on. The switch-on point was marked on the chart of the pen recorder. The current and the colour of the wire were noted periodically. The wire was heated in a particular gas until the emission, as traced on the pen-recorder, was steady. Then the next gas in the sequence was introduced while current still flowed in the circuit. The times when one gas was disconnected and the next introduced were marked on the chart and any changes in current or the colour of the wire were noted. The flow rate of the new gas was checked and adjusted if necessary.

This procedure was carried out for each gas in the desired sequence.

Each time a new gas was introduced there was a change in the emission characteristics of the wire. Standard 'Introduction Curves' became recognisable. These were characteristic of the gas which had just been introduced but they had a fine structure dependent on the nature of the precursor. Some typical introduction curves are shown in Appendix 11 while Appendix 12 shows some typical cooling curves. In general a peak or peaks were obtained in the cooling curves indicating that some chemical process was occurring.

Within this category of experiments there were two sub-categories. The first was when the wire was heated in a sequence of three or four gases to determine the effect pre-

treatment had on the shape of a cooling curve.

The second was when gases were introduced in sequence to find the effect of precursors on the shapes of the introduction curves.

Introduction curves were also obtained at room-temperature in the absence and presence of the platinum wire to establish the behaviour of the system. Some examples are shown in Appendix 13.

A gold wire was also briefly investigated and the results obtained are shown in Appendix 14. Because the wire under investigation frequently fused, a large body of results could not be collected.

It must be stressed that if there were peaks in the electron emission curves recorded when a wire cooled in a particular gas, then peaks were also observed when the wire was heated from room temperature in the same gas; see Appendix 15 for examples.

3·6 Carbiding of the Wire

It must also be emphasised that none of these effects were observed when experiments were carried out with a clean platinum wire; see Appendix 16. With the exception of nitrogen and hydrogen, a prerequisite for the observation of structure in a cooling or heating curve obtained with a platinum wire was that the wire had been heated in Q gas.

Appendix 16(a) shows the changes in the introduction curves before and after exposure to Q gas and later to air. Appendix 16(b) shows the changes in the cooling curves. There was little structure in the cooling curves from the clean wire. Exposure of the wire to methane increased the emission from the wire but

it was not until the wire had them been exposed to air that the introduction and cooling curves became similar to those for Wire 1.

The obvious explanation of this effect was that exposure of the wire to methane caused the formation of a carbide or carbidic layer on the surface of the platinum and that adsorption, desorption and possibly catalysis occurred on this layer. It may also be partly due to the fact that the 'clean' wire was cooler. This idea was tested however when cooling curves were obtained from the red hot wire before it had been exposed to methane. The counting curves showed no structure.

There is no doubt that methane interacted in some way with the wire. Prior to exposure of Wire 3 to methane, introduction of hydrogen caused a drop in current for a constant applied voltage, from 3·0 to 2·6 A or from 4·4 to 3·6 A. After exposure to methane and air, hydrogen introduction caused an increase in current from 3·2 to 4·2 A.

With a clean wire of resistance 1·5Ω at room temperature a current of 4·2 A was required to heat the wire to red heat in nitrogen or oxygen. After Q gas (Ar 90%, CH_4 10%) was introduced the current fell to 3·85 A for the same rheostat setting and the wire glowed cherry red. A Q gas cooling curve was obtained but it was not the same as those obtained with Wire 1. After exposure of the wire to air it was heated in Q gas to determine whether this treatment had had any effect on the shape of the cooling curve. The same rheostat setting gave a current of 3A and the wire glowed red. When the wire was cooled it yielded a typical Q gas cooling curve. The effective resistance of the

circuit increased from about 5·7 ohms to 8 ohms at high temperature.

A few prolonged-heating experiments were made on a platinum wire in hydrogen and nitrogen after it had been carbided by heating it in a flow of acetylene. The wire had already been exposed to Q gas. The structures of the cooling curves, introduction curves and Laben spectra were different from those obtained for a Q gas-treated wire subsequently heated in nitrogen and hydrogen (see Appendix 17).

3·7 Effect of Applied Voltage on Emission Peaks

The effect of anode voltage on the cooling curve was also investigated to see if the shape depended on the applied anode voltage. The results are shown in Appendix 18. The peak size diminished as applied voltage decreased.

3·8 Contribution to the Observed Emission by the Copper Cathode

In prolonged heating experiments there was a possibility that the copper cathode might contribute to the emission. A chromel-alumel thermocouple was bound by a copper wire to the outside of the cathode. Current was passed through the platinum wire for about ten minutes. Once the current was switched off the temperatures of the platinum wire and the cathode were measured every 30 sec and a plot of temperature against time prepared with the two sets of results; see Appendix 19 where an example for a run in Q gas is shown. For this work a Pt/Pt, 10% Rh/Pt thermocouple was used while for the rest of the experiments Pt, 13% Rh was used. The calibration curves to convert mV into °C are also given in Appendix 19.

CHAPTER 4

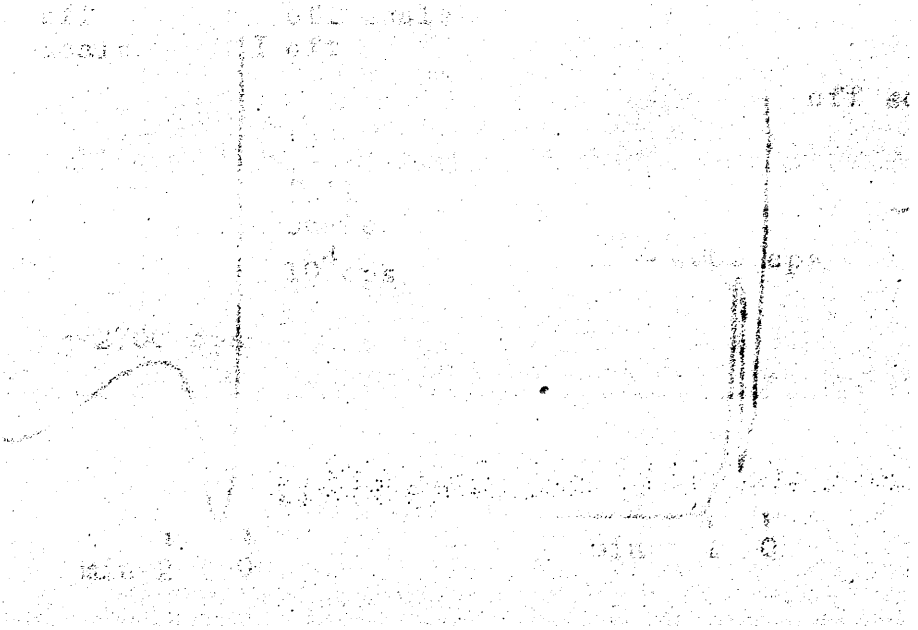

Chapter 4

4·0 Results

In this chapter the results of the different experiments will be presented. Sketches of typical results will be included where appropriate. Traces of actual curves obtained will be found in the Appendices.

4:1 Short Heating Experiments

See Appendix 10. All the short heating experiments were carried out on platinum wire 5. When these commenced Q gas yielded a cooling curve of the type shown in fig 20. This structure was reproducible but gradually disappeared as the wire received further treatment until eventually a typical Q gas curve looked like the one shown in fig 21.

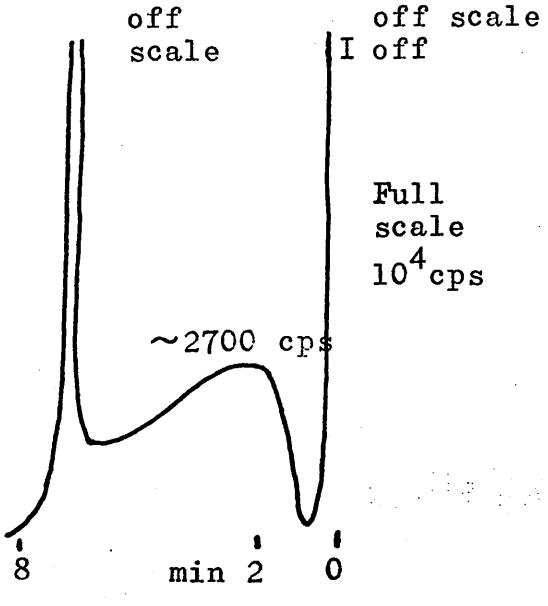

fig 20

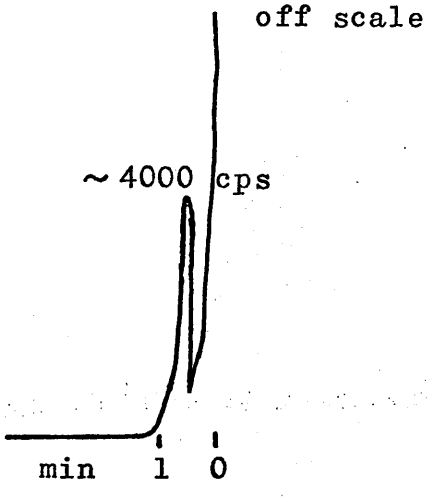

fig 21

Sketches of the differently shaped peaks will be presented below. The different pretreatments will be given underneath the curves. It should be noted that full scale on the chart recorder corresponds to 10^4 cps. These sketches are not to scale.

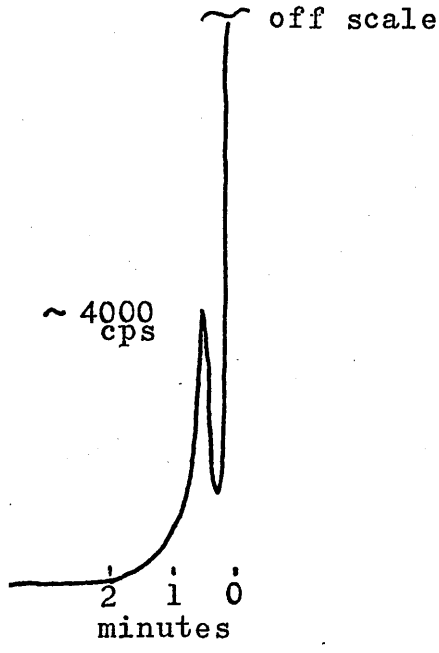

Typical Q gas curve.
Q gas after N_2, H_2, Ar, Q gas, or O_2 (preceded by N_2 flush).

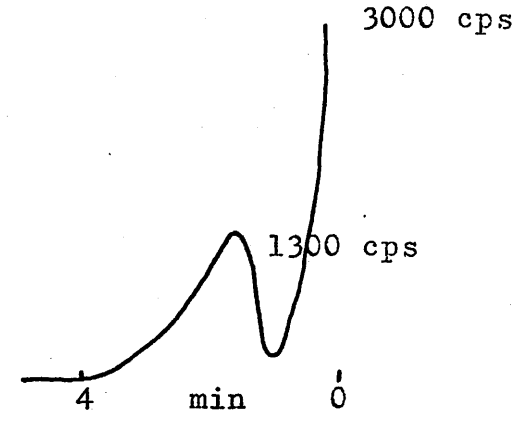

Q gas after Ar/C_2H_2

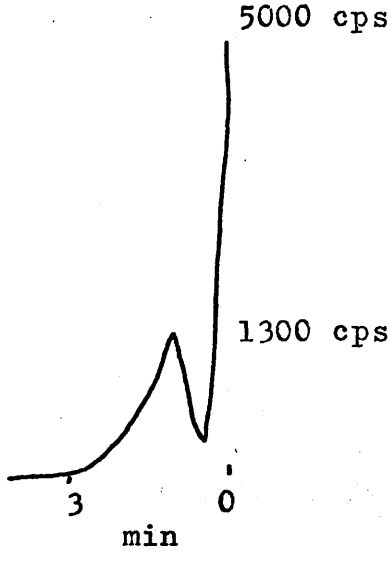

Q gas after Ar/C_2H_4

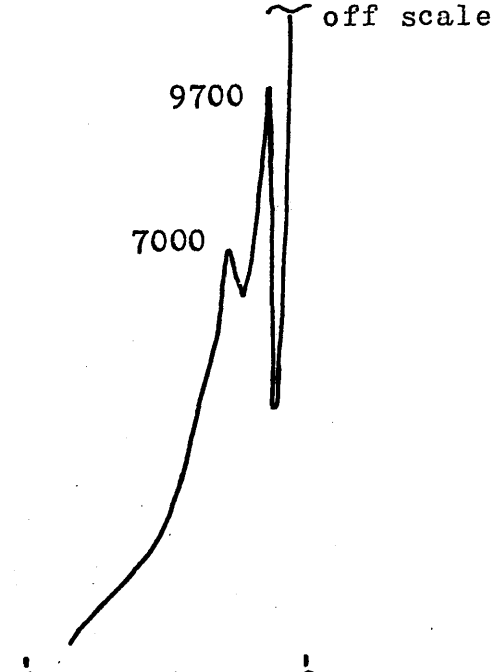

Q gas after Ar/C_2H_6

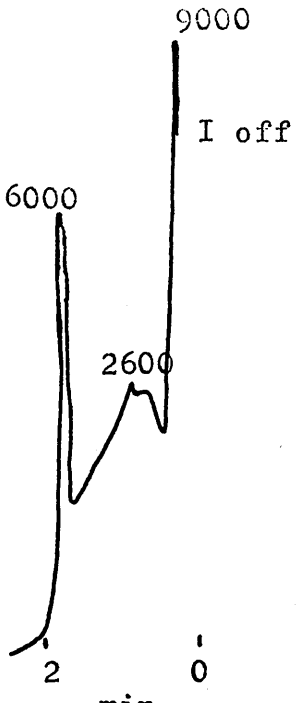

Ar/C_2H_4 after Ar/CH_4

Ar/C_2H_4 after Ar/C_2H_4 or after Ar/C_2H_2 preceded by Ar/CH_4.

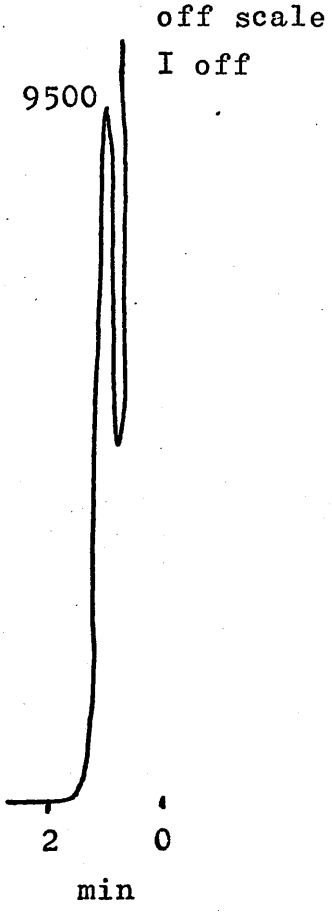

Ar/C_2H_4 after Ar/C_2H_2.

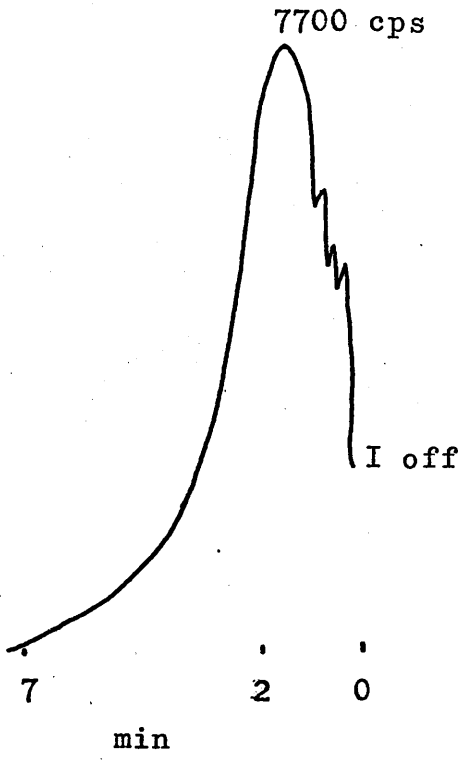

Ar/C_2H_4 after lying overnight in N_2 (Prior exposure to CH_4 and C_2H_4).

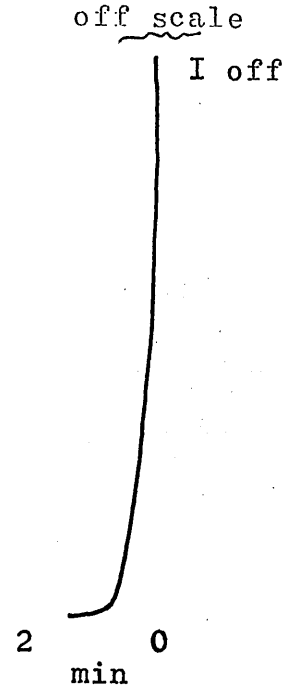

Ar/C_2H_2 after wire lay in N_2 overnight

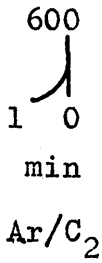

Ar/C_2H_2 after Ar/C_2H_2

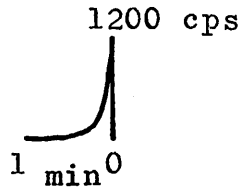

Ar/C_2H_2 after Ar/C_2H_4

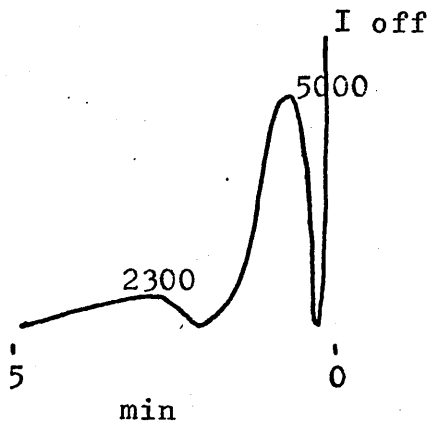

Ar/C_2H_2 after Q gas.

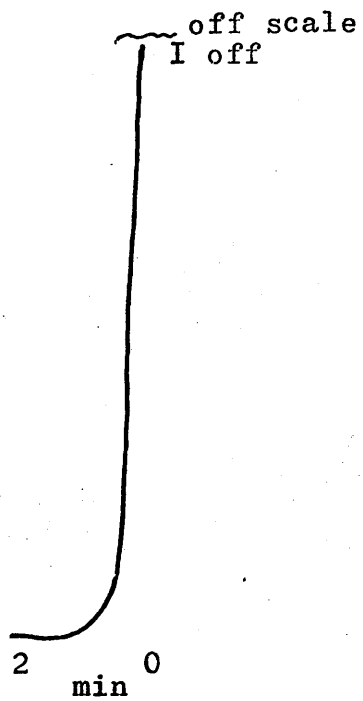

Ar/butadiene after wire lay in N_2 overnight.

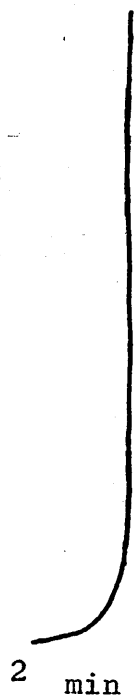

Also Ar/butadiene after Ar/butadiene i.e. effect reproducible.

The peak obtained when the wire cooled in Ar/C_2H_6 increased from zero intensity as the number of heating cycles increased (see Appendix 10). A typical ethane curve after several exposures was as shown.

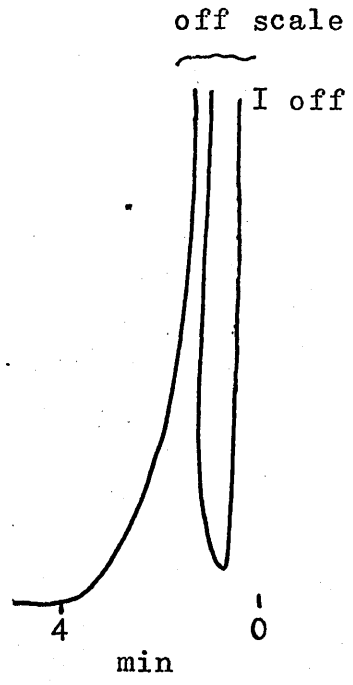

Ar/C_2H_6

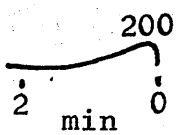

H_2 after N_2.

Disc 0·1 x 1, 2%

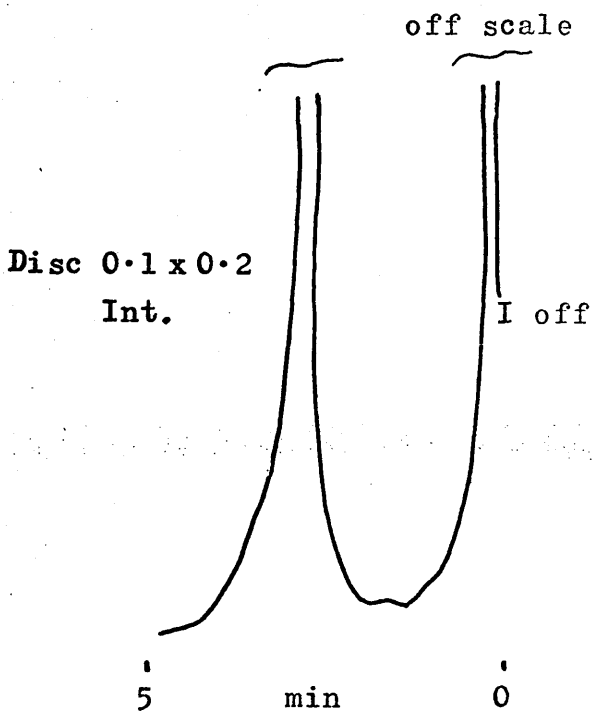

H_2 after Q gas.

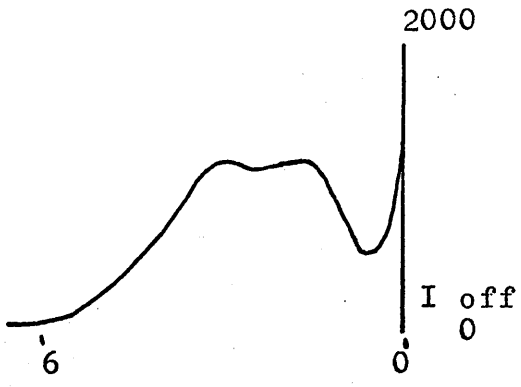

Ar after Q gas

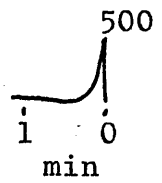

Ar after Ar/C_2H_4.

or Ar after Q gas after Ar/C_2H_2.

or Ar after Ar/Bu.

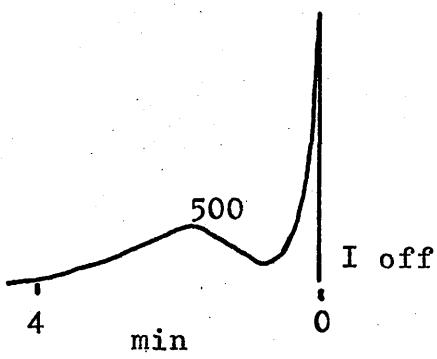

Ar after Ar/C_2H_2.

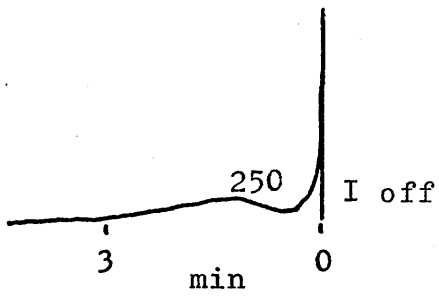

Ar after Ar/C_2H_6

or Ar after Ar/Bu after wire aged for a while.

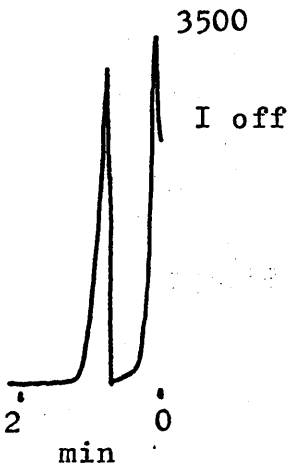

N_2 after Q gas
N_2 after Ar/C_2H_4
N_2 after Ar/C_2H_2
} after wire aged overnight in N_2.

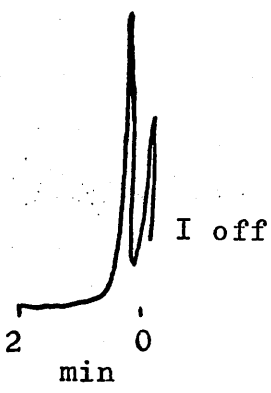

N_2 after H_2.

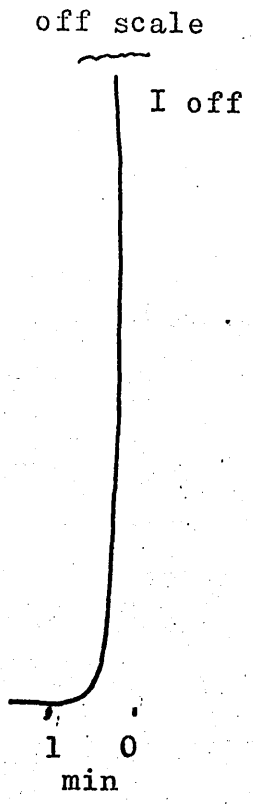

N_2 after O_2

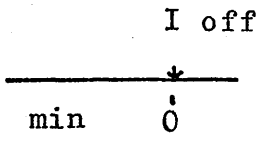

N_2 after Ar/C_2H_4

N_2 after Ar/C_2H_2.

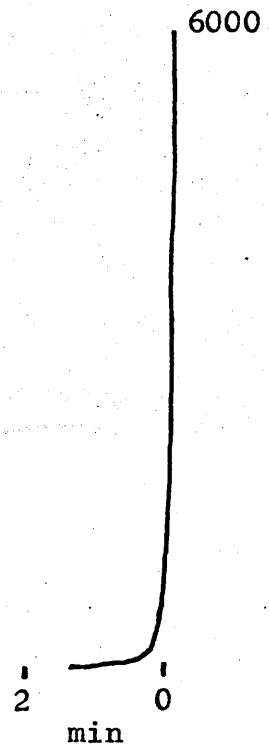

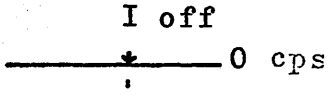

O_2 after O_2

O_2 after N_2

or O_2 after Q gas (N_2 flush)

O_2 after C_2H_4.

O_2 after Ar/C_2H_2 gave this curve several times;
2nd heating cycle yielded highest emission rate.

4·2 Long Heating Experiments

4·2·1 Introduction Curves

See Appendix 11. Sketches of some typical Introduction Curves are shown below for Wire 3.

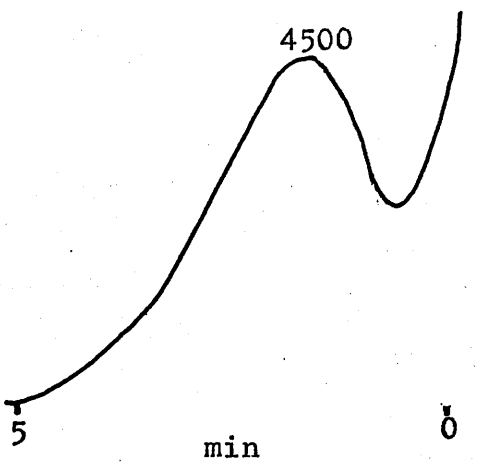

N_2

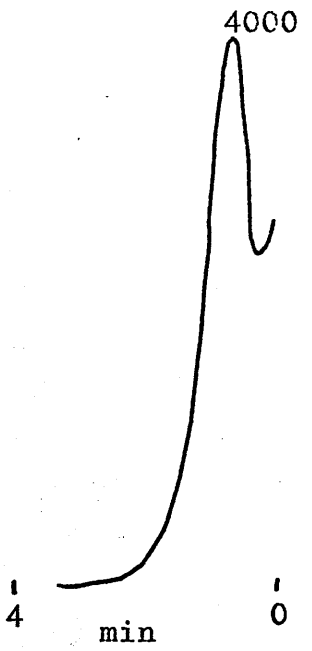

H_2 (varies)

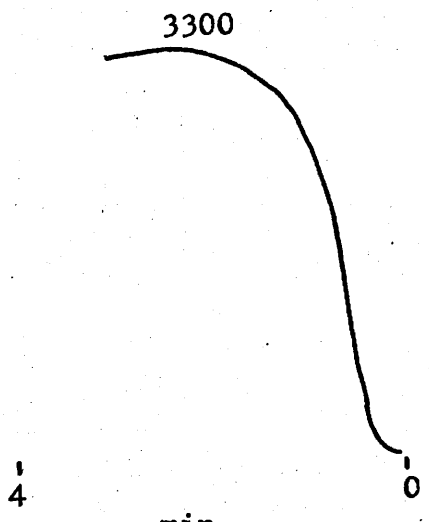

O_2

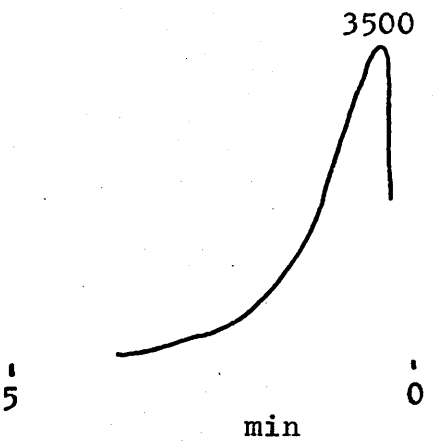

Q gas (after N_2).

Q gas varies greatly.

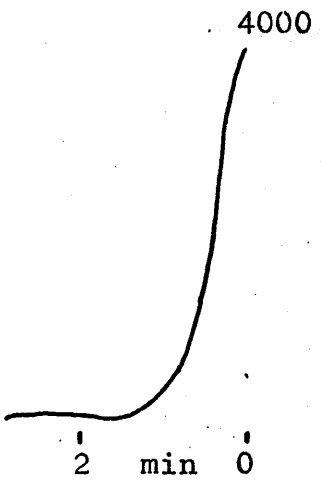

Ar.

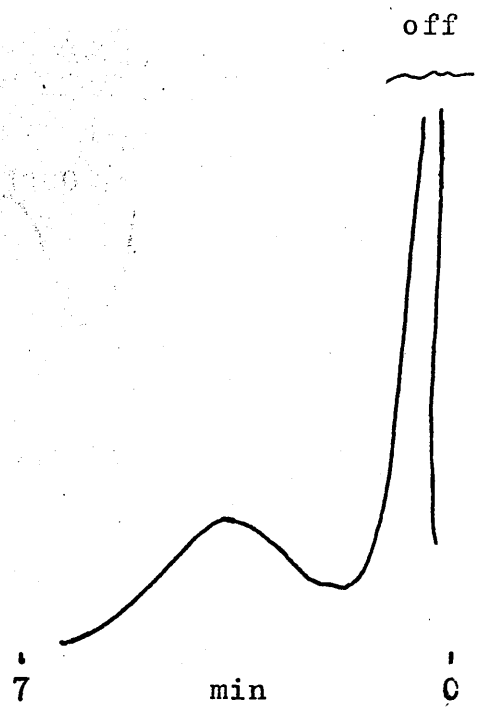

He (after Q gas)

He varies greatly.

Similar results were obtained with Wire 1 (See Appendix 11b)

4·2·2 Cooling Curves

See Appendix 12. Sketches of some typical cooling curves are given below for Wire 3. The detailed cooling curves and sketches of the corresponding Laben photographs are given in Appendix 12a.

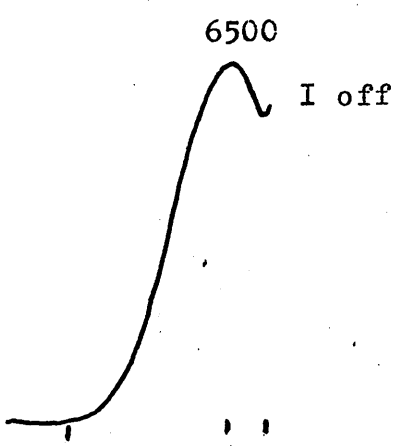

N_2 after O_2.

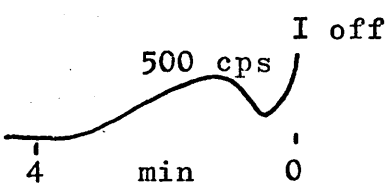

N_2 after H_2, or N_2 after Ar
or N_2 after He (after Q gas)

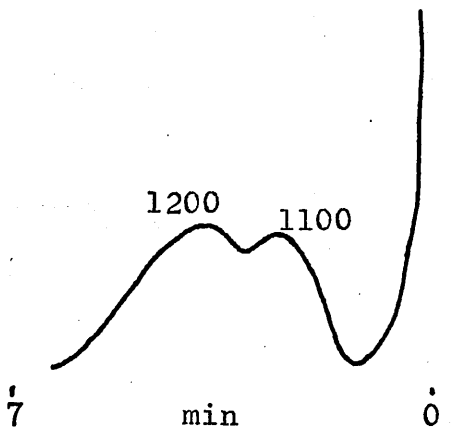

N_2 after Q gas

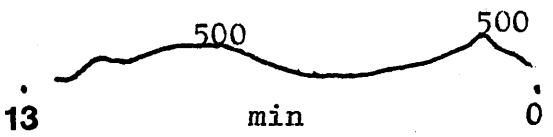

H_2 after N_2.

H_2 after Ar (after N_2) similar.

H_2 after He (after N_2) similar.

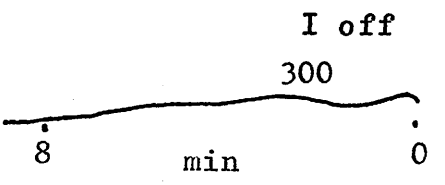

H_2 after Q gas

H_2 after O_2 (N_2 flush) similar.

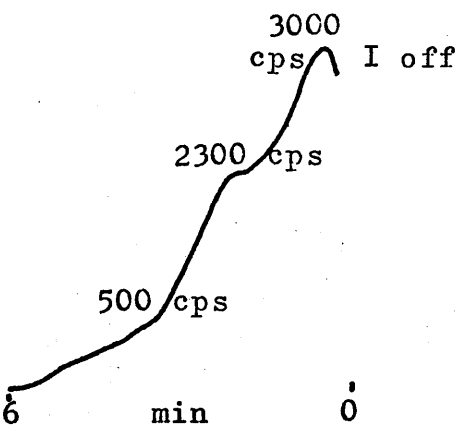

O_2 after N_2.

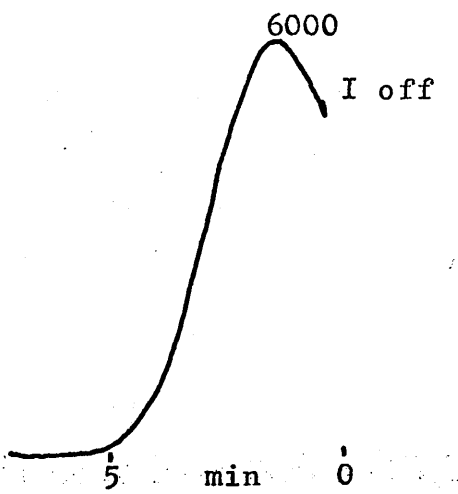

O_2 after Q gas (N_2 flush)

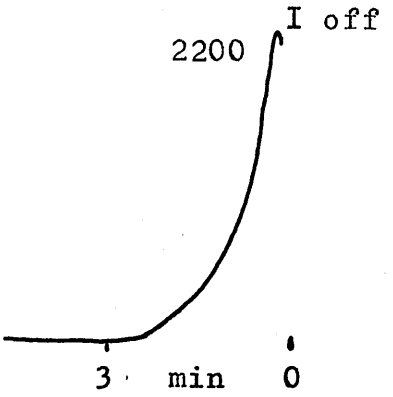

O_2 after H_2 (N_2 flush)

O_2 after Ar , O_2 after He (started at 4000 cps)

Full scale ≡ 10^4 cps.

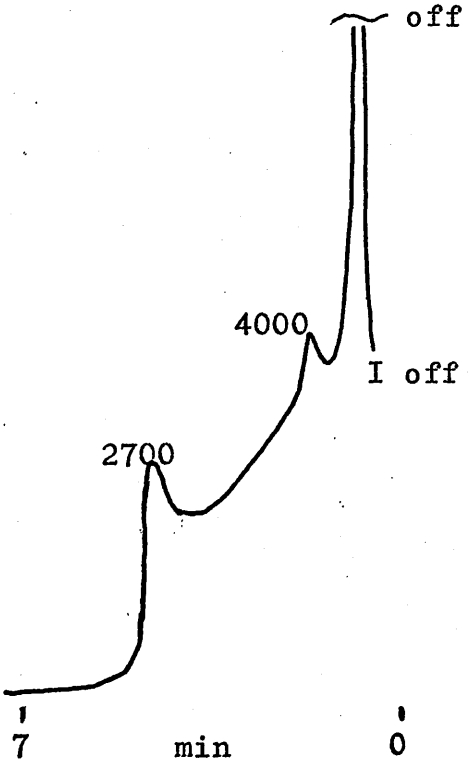

Q gas after N_2

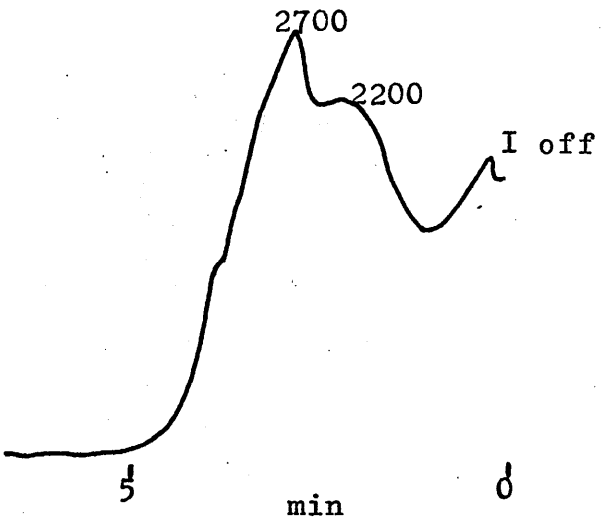

Q gas after H_2

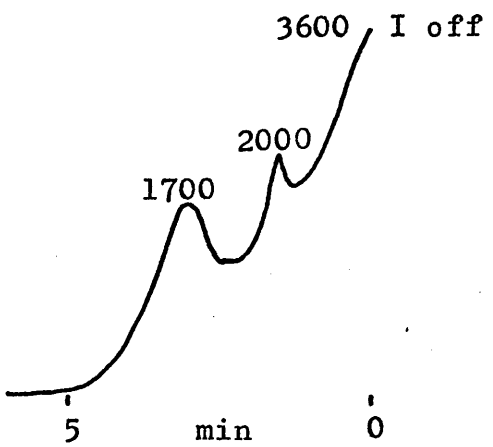

Q gas after O_2 (N_2 flush)

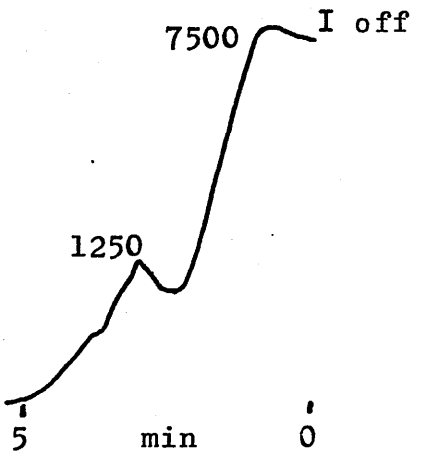

Q gas after Ar: Q gas after He similar.

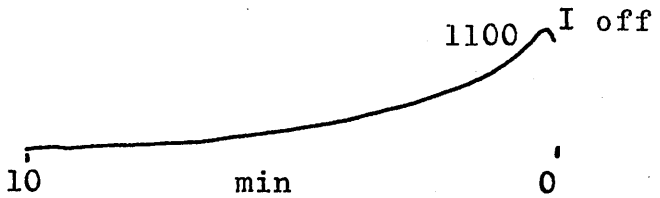

He after O_2

He after Ar (after N_2)

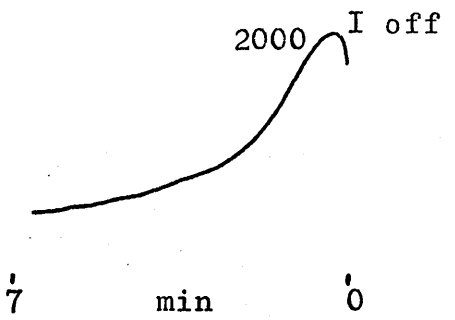

He after N_2

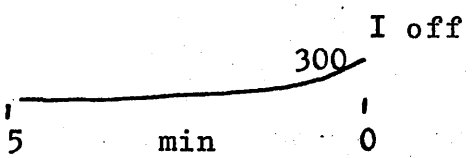

He after H_2

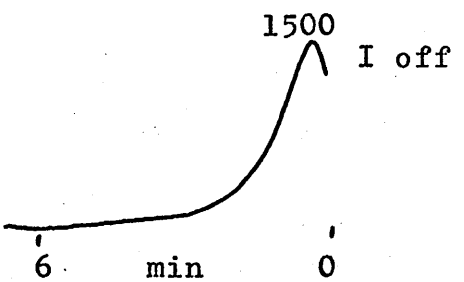

He after Q gas

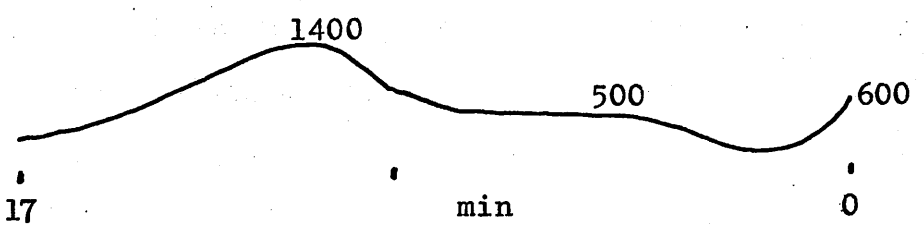

Ar after N_2

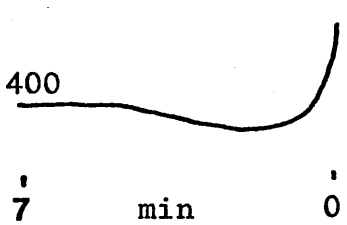

Ar after H_2

Ar after He (after H_2)
similar.

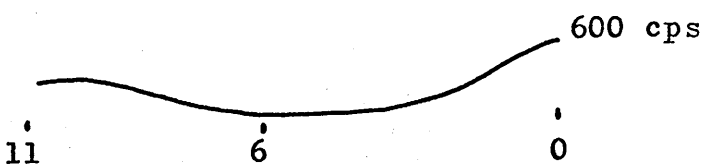

Ar after O_2.

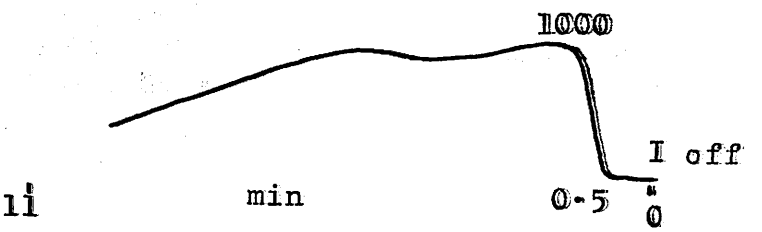

Ar after Q gas.

Essentially similar results were obtained with Wire 1. These may be seen in Appendix 12b.

4·3 Room Temperature Introduction Curves

Intruduction curves were obtained at room temperature for several gases in the absence and presence of a platinum filament to determine whether or not structured introduction and cooling curves were due to the presence of the platinum wire disturbing the electric field. Sketches of some of the curves obtained will be presented below. Curves obtained with the catalyst mounted in the detector will be shown on the right and those obtained with no platinum wire present on the left.

A full set of curves may be seen in Appendix 13.

Without platinum wire.

Platinum wire present

N_2 after O_2

Without Pt

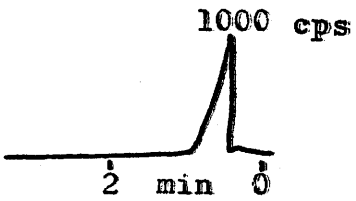

Pt present

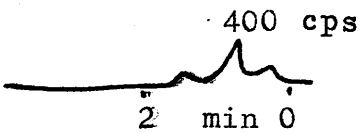

N_2 after H_2

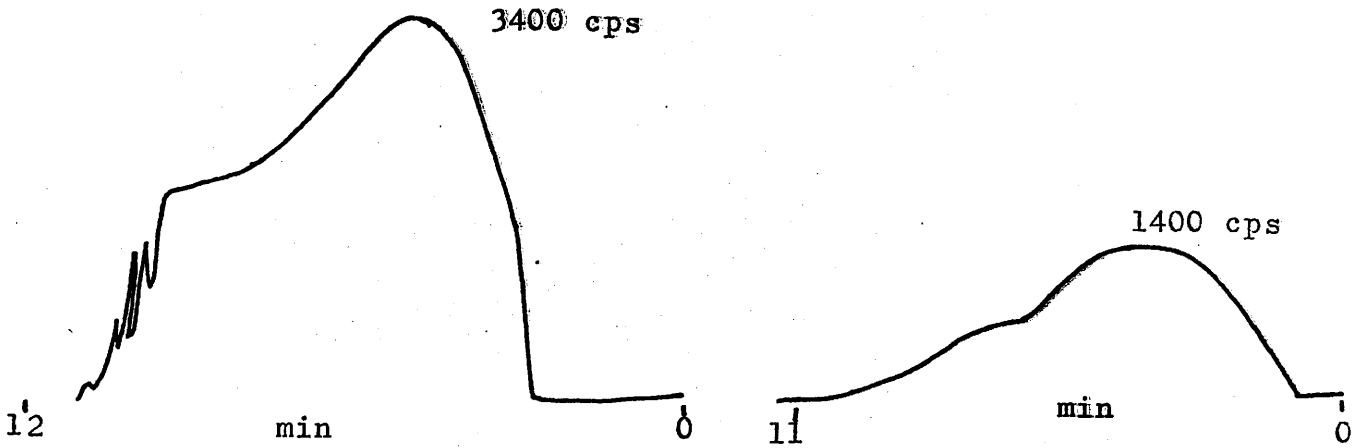

H_2 after N_2

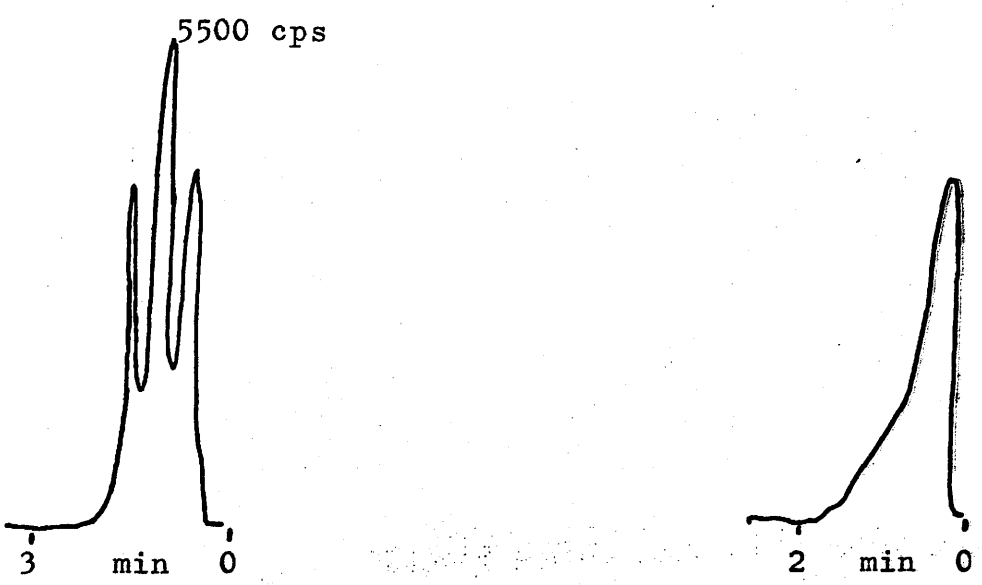

H_2 after He

Without Pt

Pt present

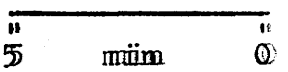

0 cps

O_2 following N_2

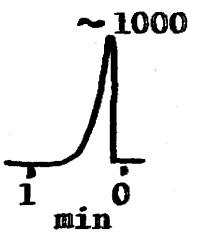

O_2 following He

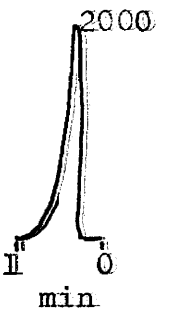

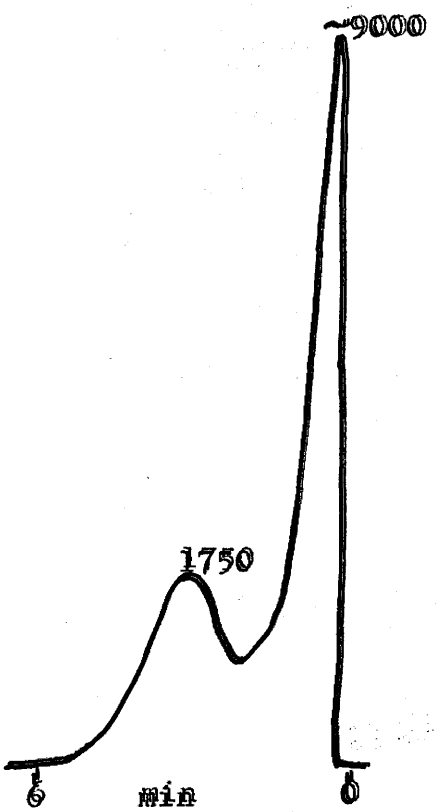

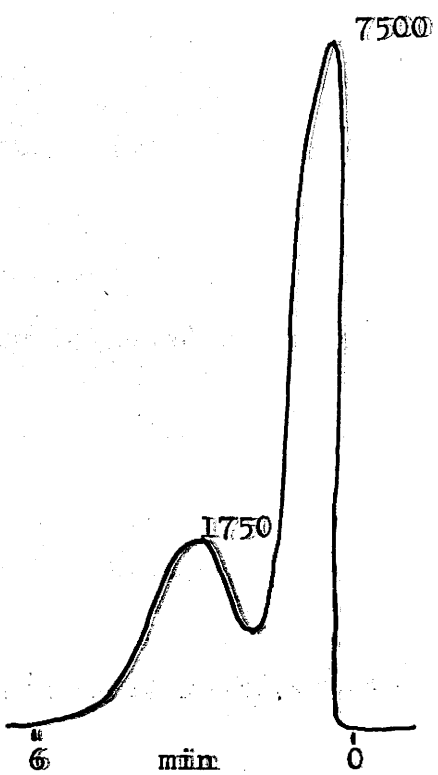

He following H_2

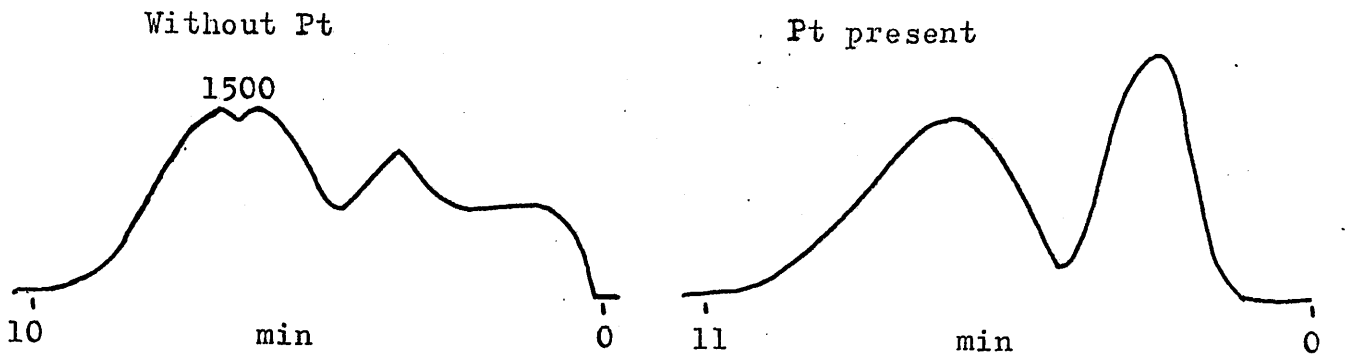

He following N_2

These results were obtained with Wire 3 before it had been exposed to Q gas.

4·4 Heating Curves

A few examples of heating curves are given in Appendix 15 to demonstrate that if peaks were obtained when the platinum wire cooled down in a gas then structure was also observed when the wire was heated in that gas. With these particular examples heating the wire in the gas immediately followed cooling the wire in the same gas. Examples are shown for Q gas, nitrogen and hydrogen.

4·5·0 To Show the Effect of Carbiding the Wire

Some sketches will be presented of the changes in the introduction and cooling curves obtained with Wire 3 after it was heated in Q gas and then exposed to air at room temperature. Finally it was heated in Q gas again. The results are given in more detail in Appendix 16.

4·5·1 Introduction Curves See Appendix 16a

These sketches are not to scale

Clean wire

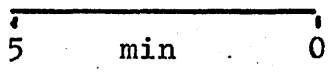

After exposure to Q gas

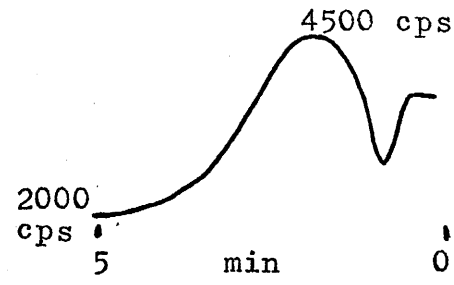

After exposure to Q gas and air.

N_2 following O_2

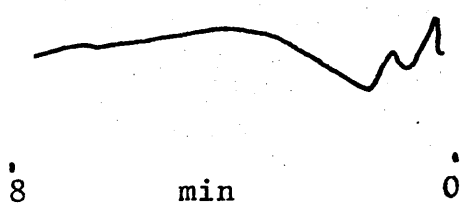

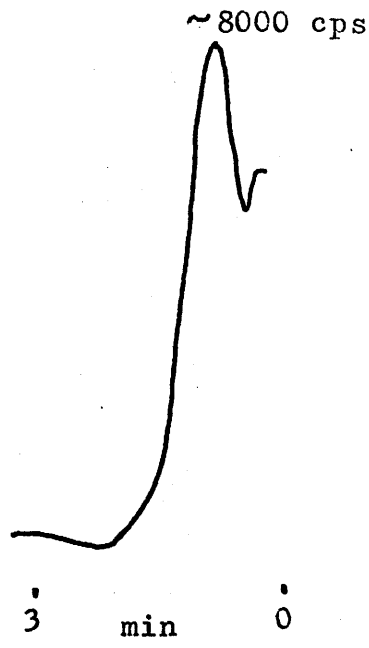

H_2 following N_2

Clean wire

After exposure to Q gas

After exposure to Q gas and air.

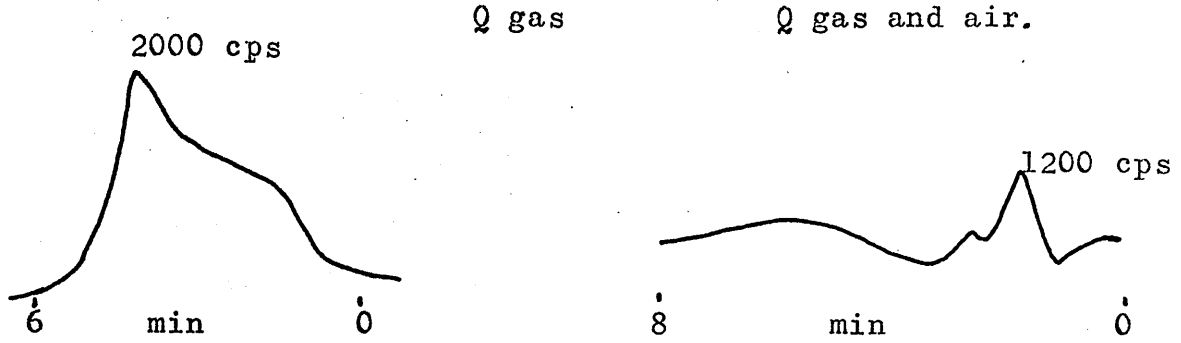

N_2 following H_2

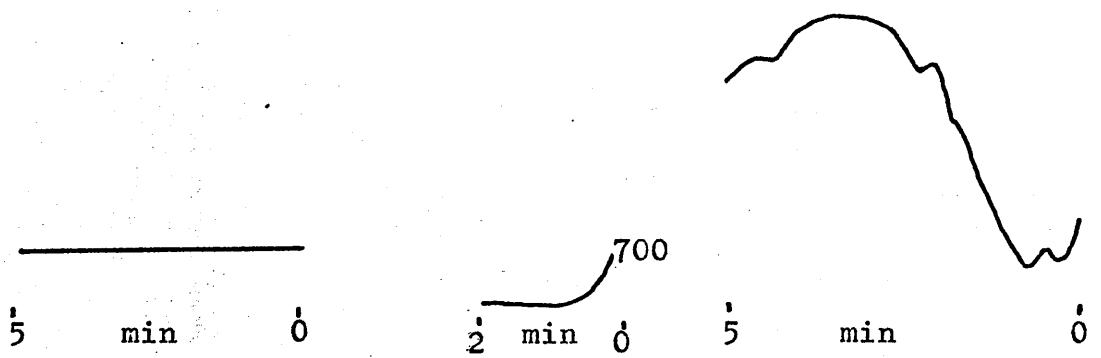

O_2 following N_2

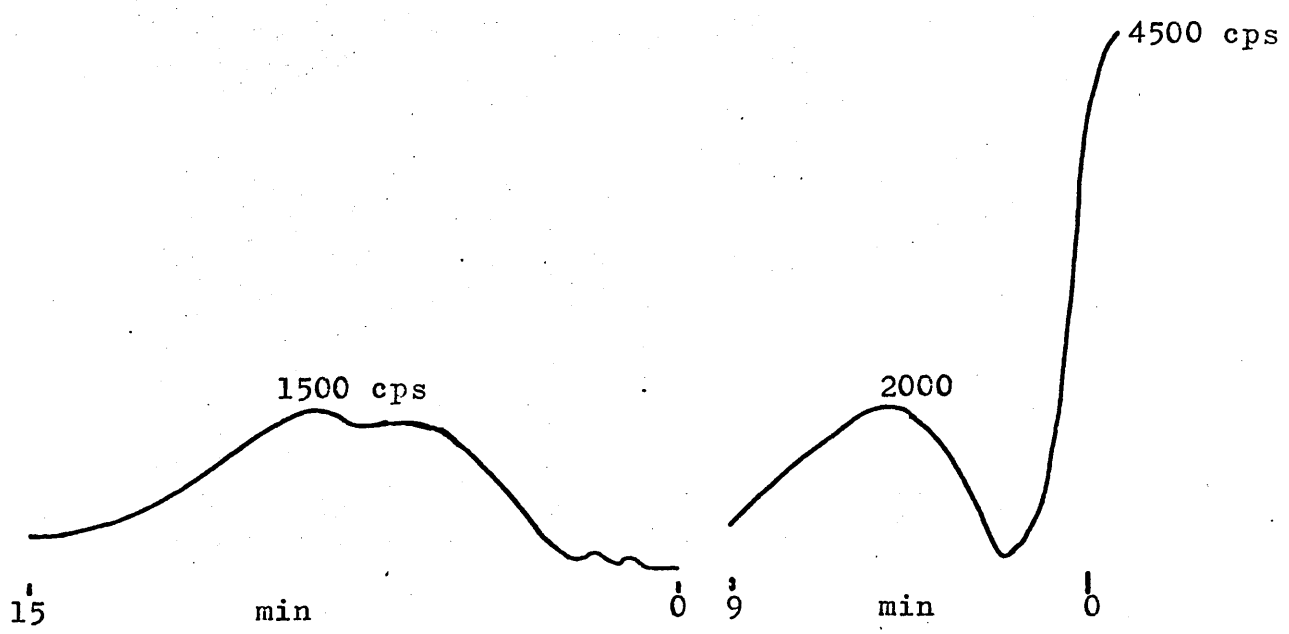

He following O_2

Clean wire

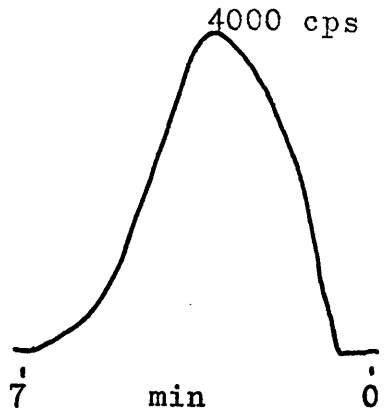

Wire after exposure to Q gas

After exposure to Q gas and air.

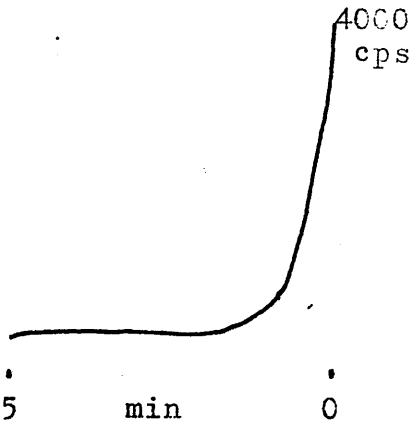

Ar after N_2

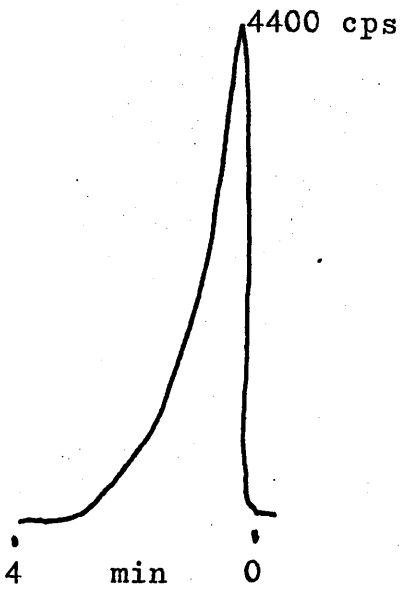

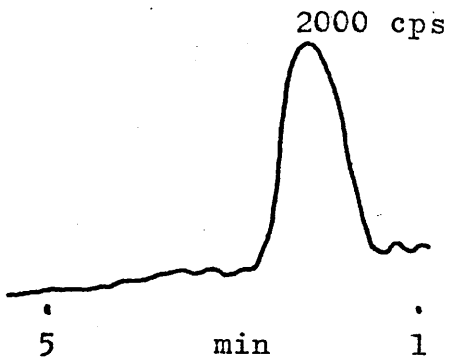

H_2 after Ar (after N_2)

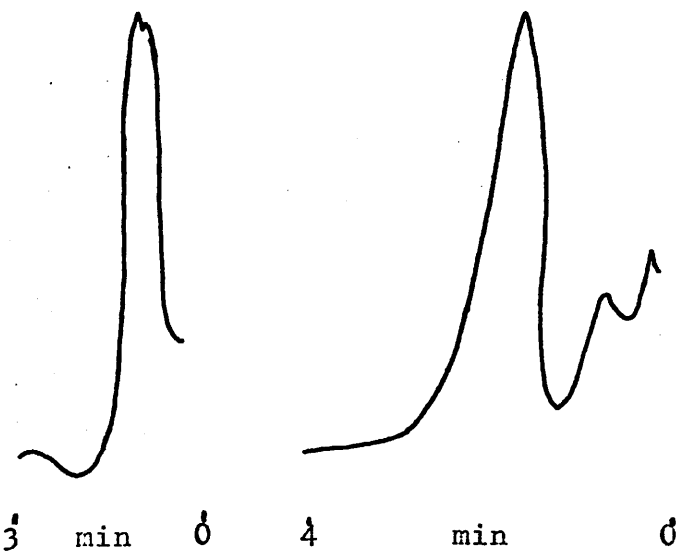

H_2 after Q gas

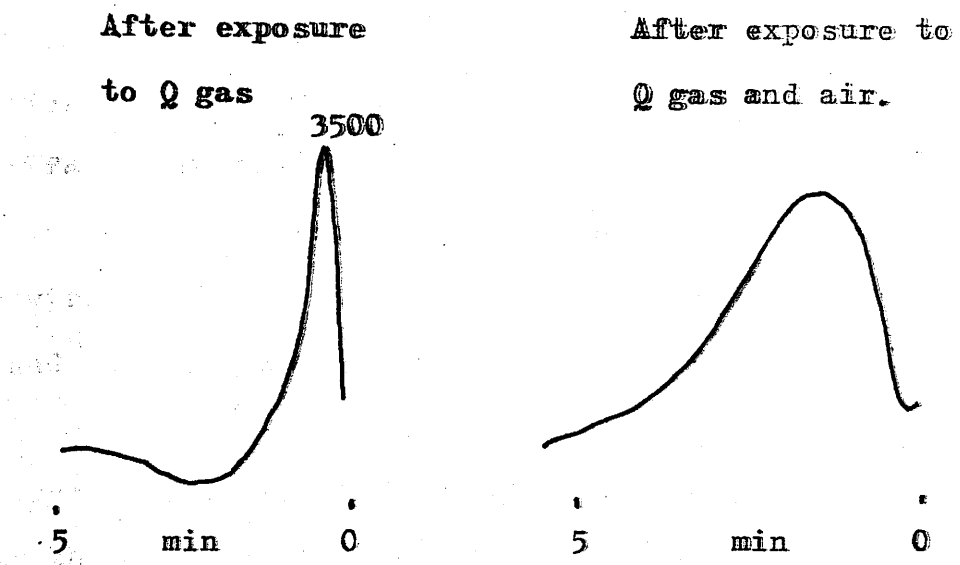

N_2 after Q gas

It may be seen by inspection of the preceding curves that H_2 and N_2 both give introduction curves with the clean wire as do the 'inert' gases He and Ar. O_2 gives no emission while N_2 gives no emission when it follows O_2. These results will be explained later. In most cases the emission characteristics were very different in the two cases of the clean wire and the wire after exposure to methane and air. The differences between the wire after exposure to methane and after exposure to methane and air are more apparent with the cooling curves; see later.

A 'memory' effect was observed in these Introduction curves in the sense that the shape of a curve depended not only on the gas whose flow had just ceased but on the gas before that also. Some examples are given below. More examples are to be found in Appendix 11.

[H = heating
C = cooling]

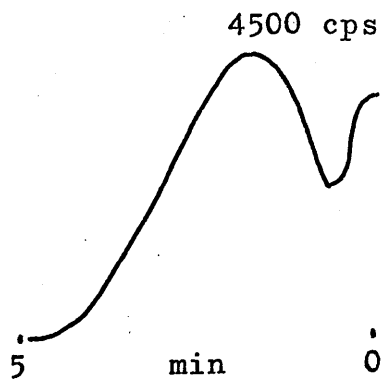

N_2, O_2, Ar, O_2.

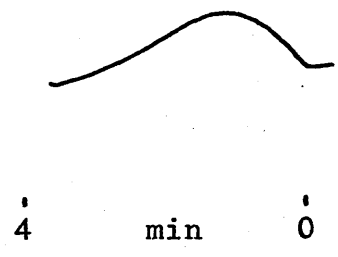

N_2, O_{2H}, He, Q gas_C.

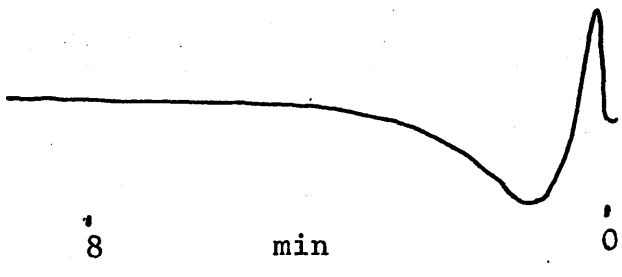

N_2, Ar, He, H_2

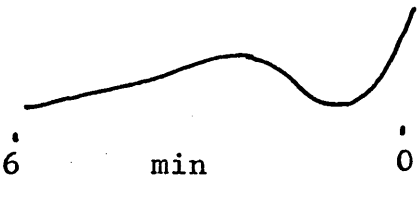

N_2, Ar_H, H_{2C}, Ar_H.

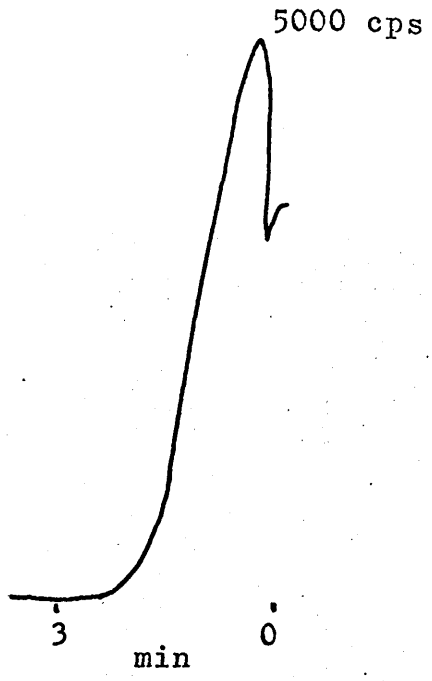

H_2, N_2, O_{2_H} (He).

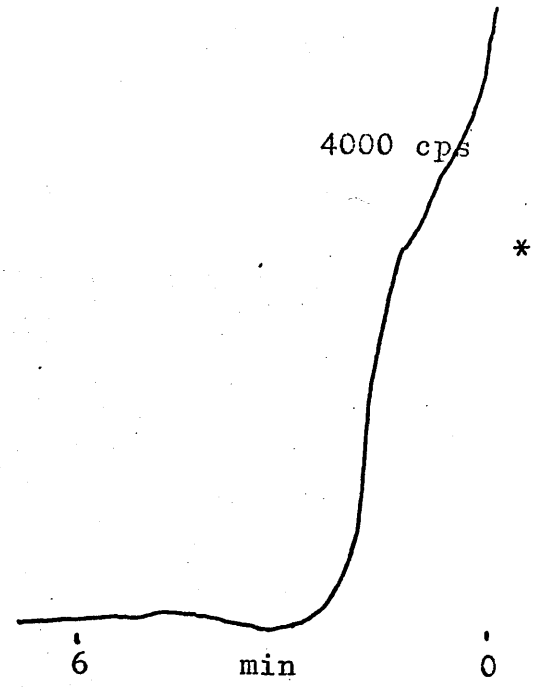

H_2, N_{2_H}, Q gas_C, N_{2_H}.

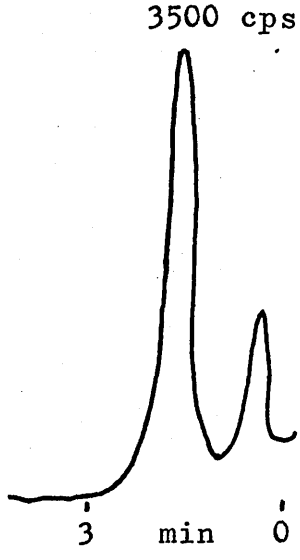

H_2, Q gas, He, Q gas.

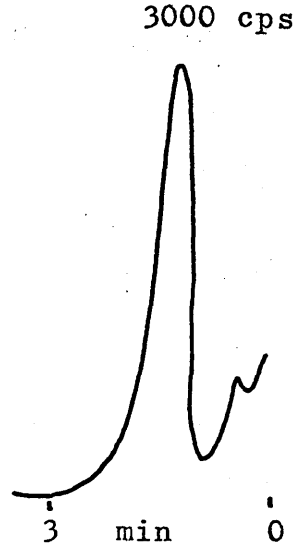

H_2, Q gas_H, Q gas_C, Q gas_H.

H_2, Q gas_H, N_{2_C}, Q gas_H.

The gas on the extreme left is the one to which the platinum filament was exposed last. Thus for the introduction curve marked * the platinum filament was exposed to hydrogen after being heated in nitrogen. Prior to that the wire was cooled in Q gas after being heated in nitrogen.

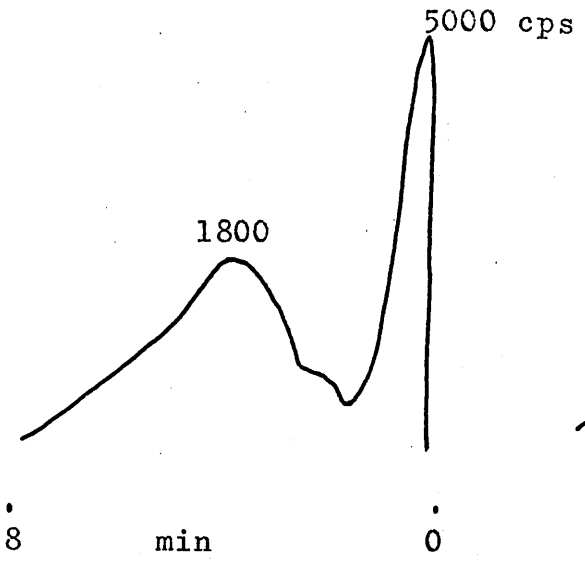

He, H_2, Ar, N_2.

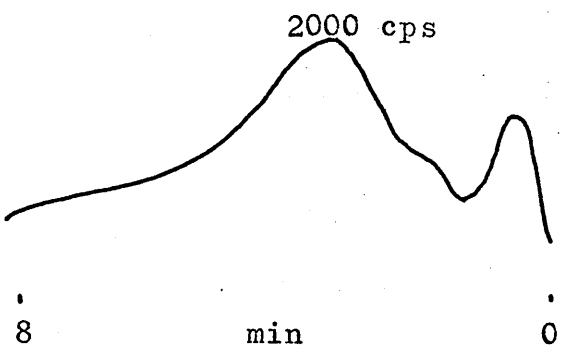

He, H_2, N_2, O_{2_C}.

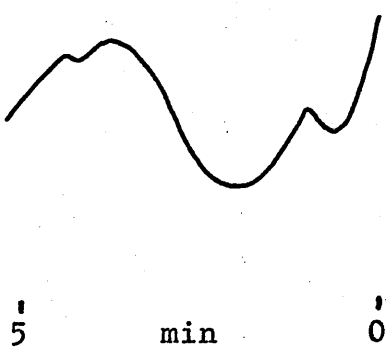

He, N_2, Ar, He.

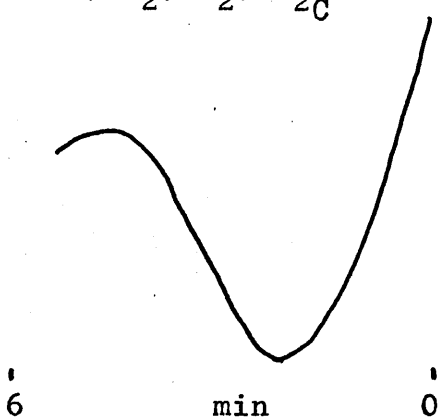

He, N_{2_H}, O_{2_C}, N_{2_H}.

4·5·2 Cooling Curves

See Appendix 16b. The following curves clearly show the differences between the clean and the carbided wire. It should be remembered that before the wire was exposed to methane introduction of hydrogen caused a drop in current for a constant applied voltage while after exposure to methane and air, hydrogen introduction caused an increase in current (see 3·6 page 80). In addition a current of 4·2A was required to heat the wire to red heat in N_2 or O_2. The applied voltage and rheostat setting were left unchanged yet after exposure to Q gas the current fell to 3·85A and the wire glowed cherry red. After exposure to air the wire was heated in Q gas and these same settings produced a current of only 3A. Again the wire was red hot. It is clearly seen that the presence of a carbonaceous layer on the platinum wire is essential before structure may be observed in the cooling curves.

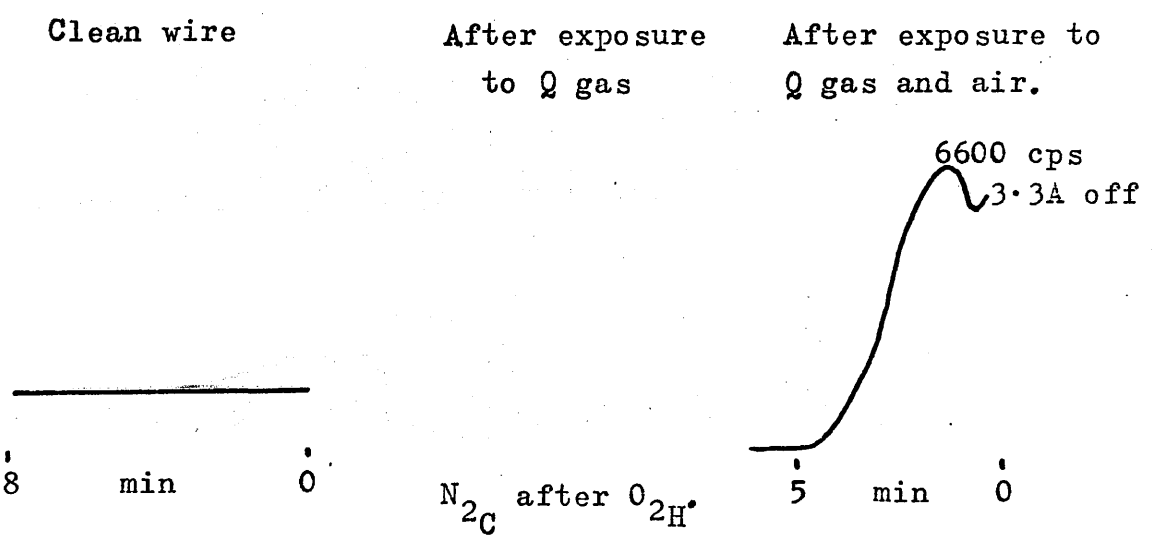

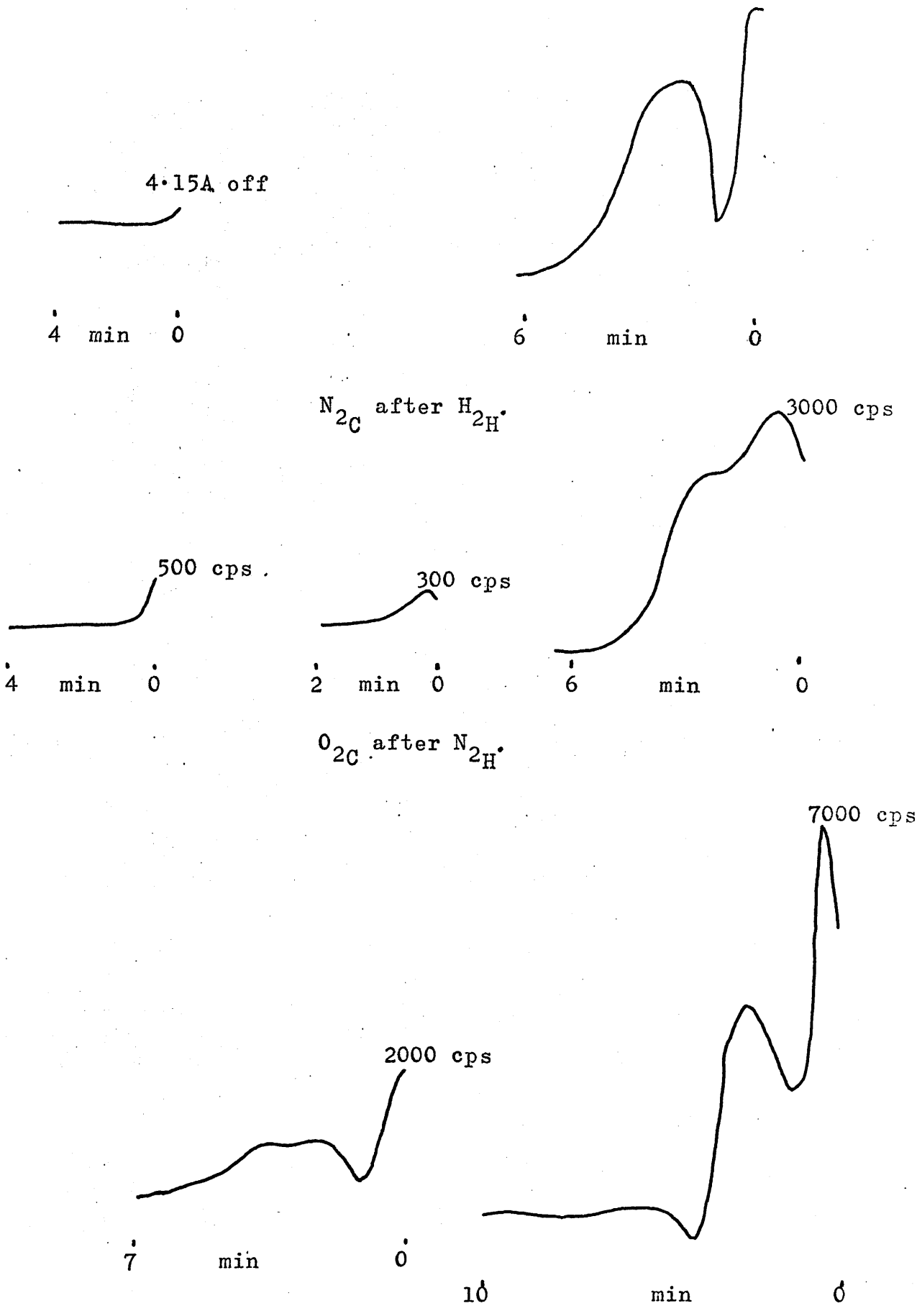

Typical Q gas_C after Q gas_H. 1st Q gas cooling curve after exposure to air.

Clean wire

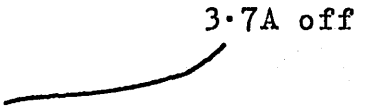

4 min 0

After exposure to Q gas and air.

5 min 0

H_{2C} after N_{2H}.

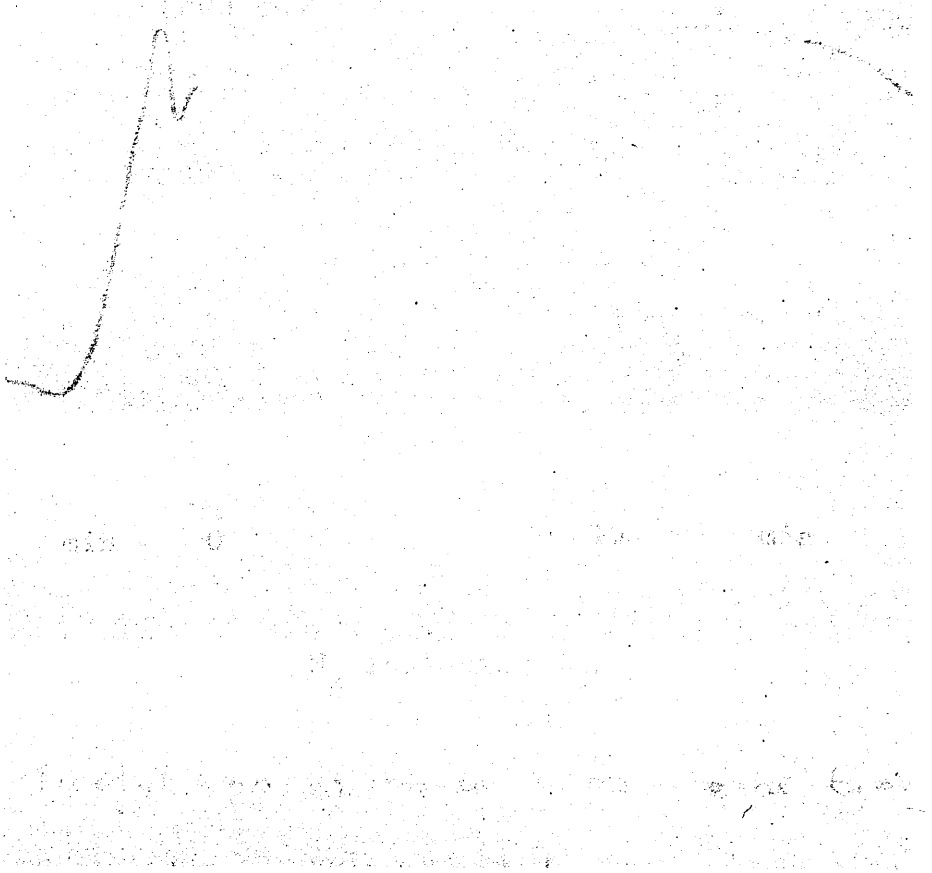

4·6 Introduction and Cooling Curves after Acetylation* of Wire 3

See Appendix 17. The following sketches show the differences found in the Introduction and Cooling Curves of N_2 after H_2 and H_2 after N_2 obtained after exposing a platinum filament to Q gas and subsequently to acetylene.

4·6·1 Introduction Curves

The following sketches are not to scale. See Appendix 17a for accurate results.

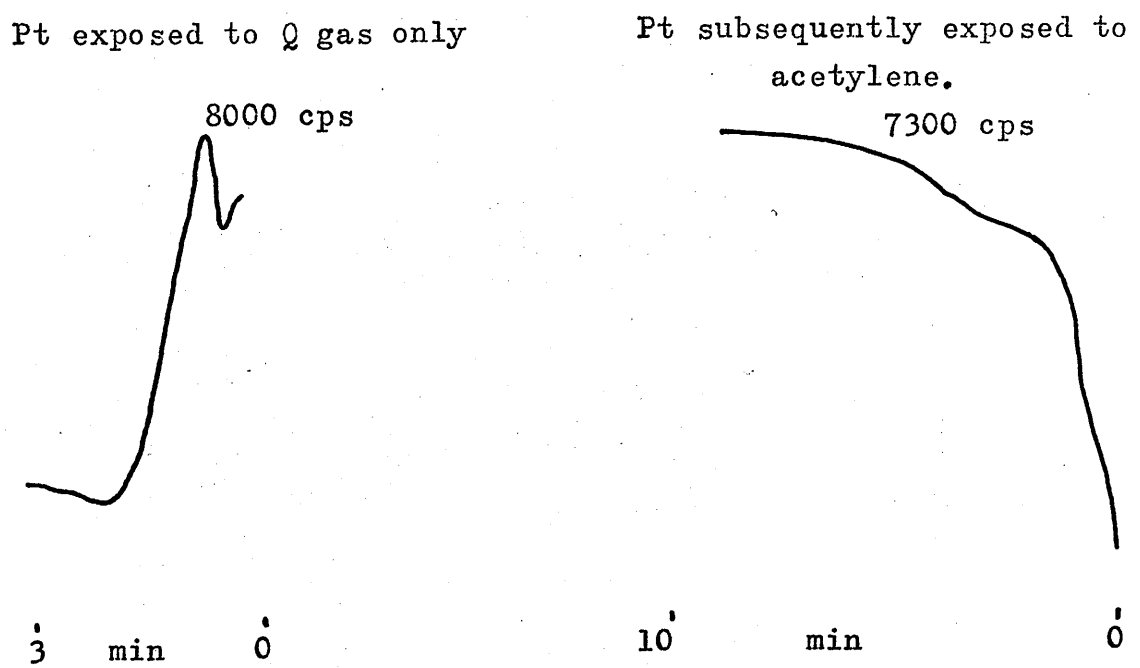

H_2 following N_2.

* N.B. Acetylation in these terms means treatment of the wire with acetylene.

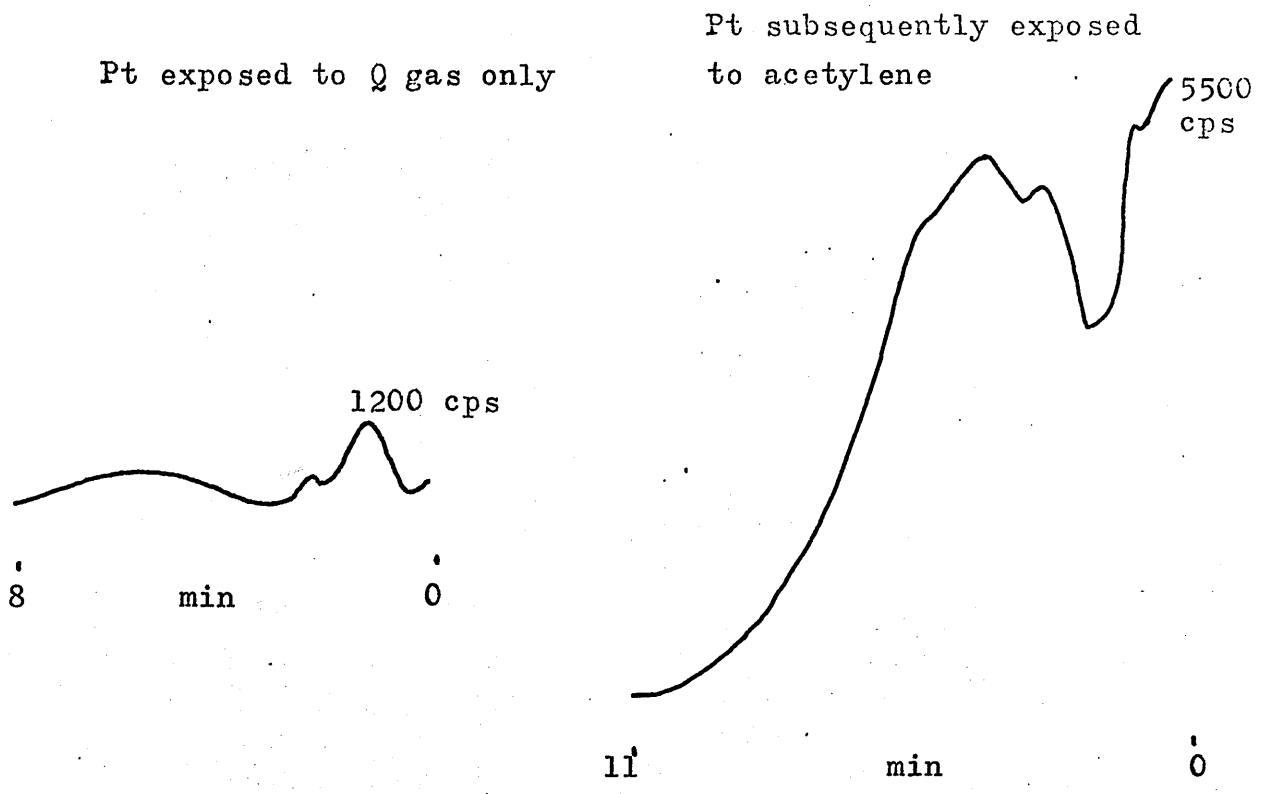

N_2 following H_2.

4·6·2 Cooling Curves See Appendix 17b for more accurate results.

Pt exposed to Q gas only

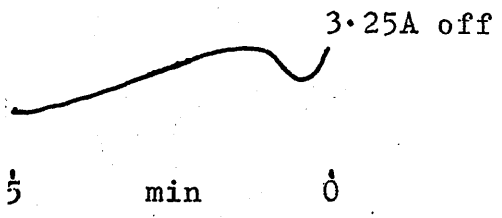

Pt subsequently exposed to acetylene

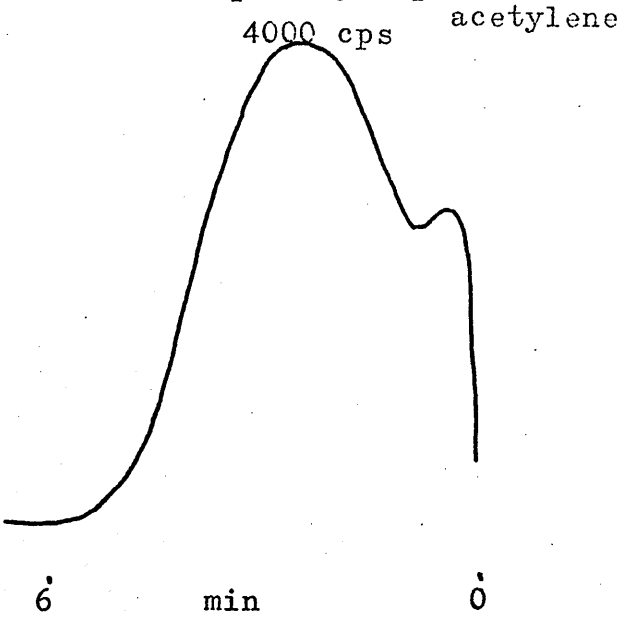

N_{2C} after H_{2H}.

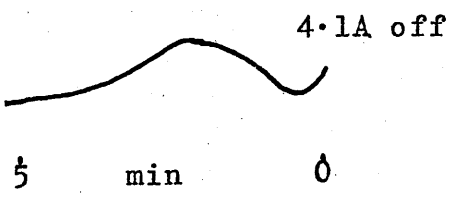

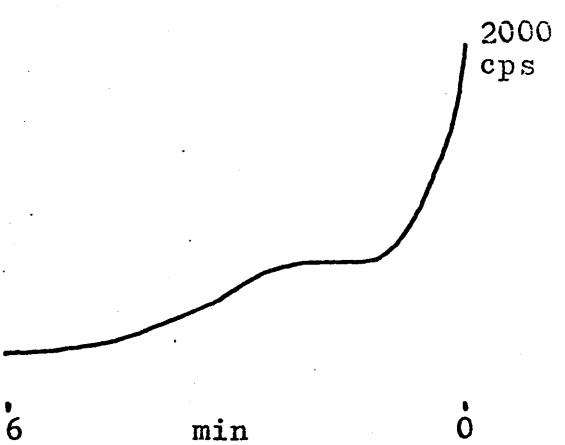

H_{2C} after N_{2H}.

Pt subsequently exposed to acetylene.

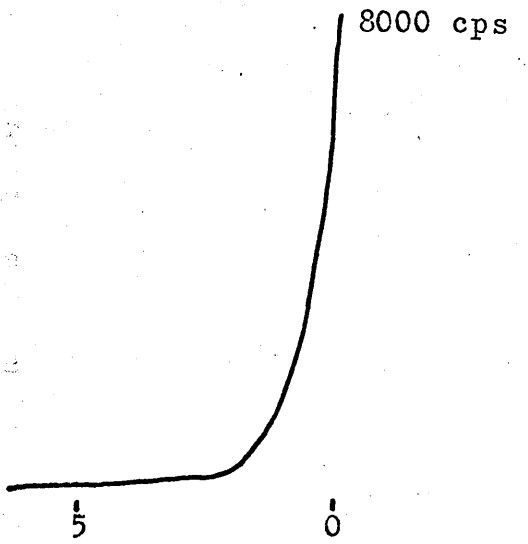

H_{2C} after prolonged heating in H_2.

After several cycles of heating in H_2 and cooling in N_2, the cooling curve resolved into two peaks whose relative intensities varied; the hotter the wire to start with, the more intense the high temperature peak (a).

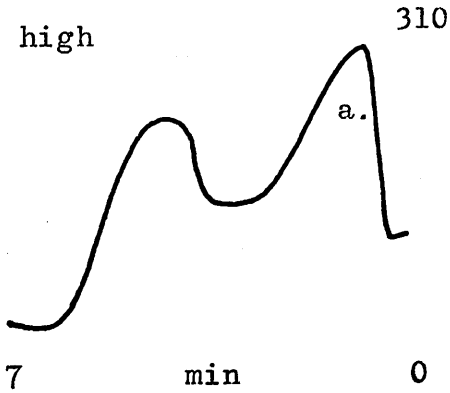

4·7 Effect of Anode Voltage

The effect of anode voltage on the cooling curve was investigated to determine whether the shape depended on the applied voltage (see Appendix 18). It was found that the level of emission decreased as voltage decreased, as was expected for a drop in counter multiplication factor, but that the actual structure remained the same.

4·8 Introduction and Cooling Curves from Gold

Approximately 1m of gold wire 0·16 mm diam. was used each time. Because of its extreme ductility it was found that gold filament fused readily if it underwent prolonged heating at around 900°C: gold melts at around 1000°C. It also broke easily when being handled.

To try to counteract this two gold wires were twisted round each other. A few results were obtained from the doubled wire before it fused. Sketches are drawn below. The results are shown in greater detail in Appendix 14.

4·8·1 Cooling Curves Some Q gas curves are shown below.

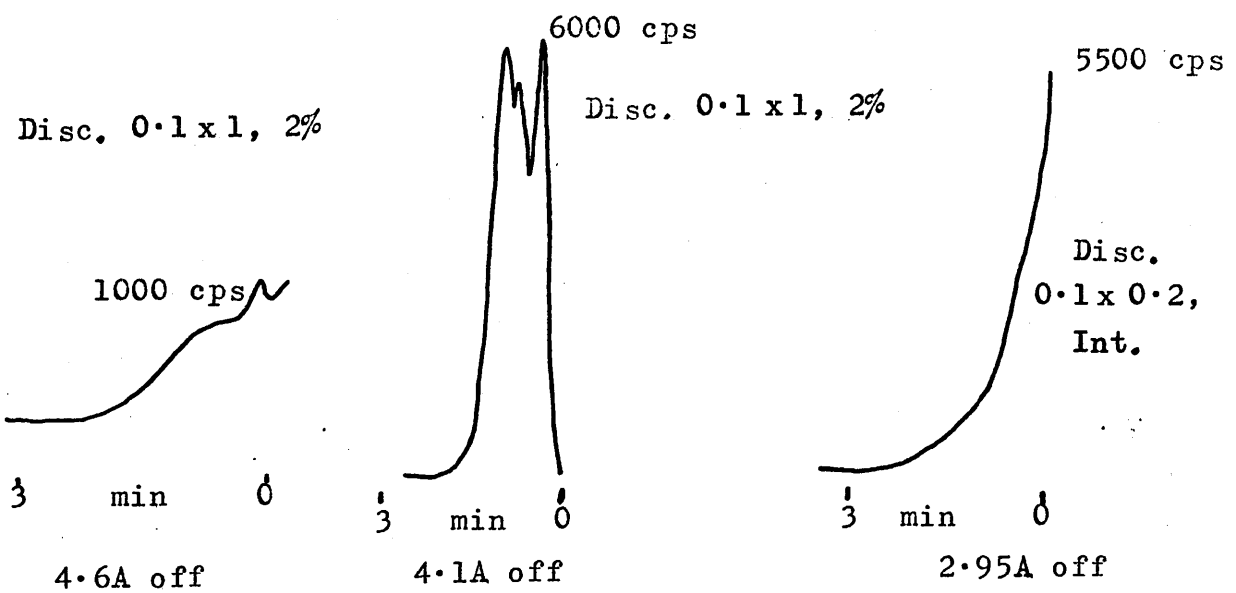

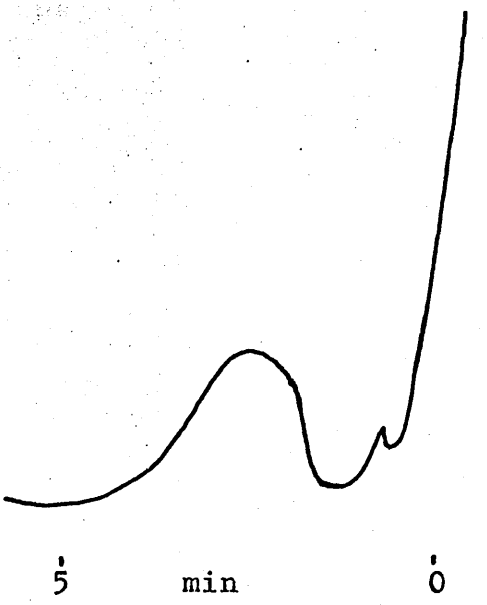

5·3A off wire red hot

Q gas cooling curve

Some hydrogen and nitrogen results are given in Appendix 14.

4·8·2 Introduction Curves

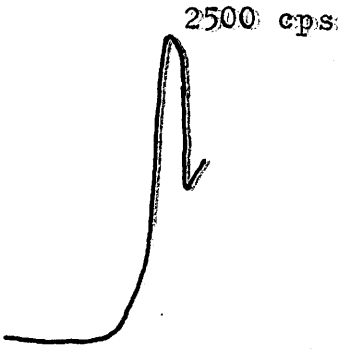

2 min 0

N_2 after H_2 (1·9 kV).

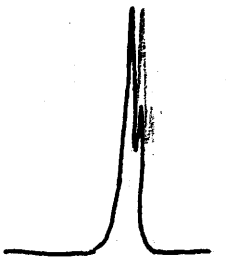

1 min 0

H_2 after N_2.

Too few results were obtained to be able to explain what was happening at the surface of the Gold filament. All of these experiments were prolonged heating ones.

4·9 Contribution from Cathode

The possibility that the cathode might contribute to the observed emission was investigated. Graphs were prepared of temperature against time for the copper cathode and the platinum wire cooling to determine how probable a contribution was from the cathode (see Graph 27 Appendix 19).

It may be seen from Graph 27 that there was a strong possibility that the copper cathode contributed to the effect. Thus results from prolonged heating experiments may only be interpreted qualitatively and doubt must be cast on the validity of the results obtained with the gold filament.

CHAPTER 5

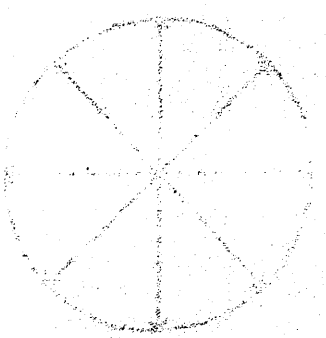

Chapter 5

Discussion I. The Counting System

5·0 Introduction

Detector 5 was designed to operate as a gas flow proportional counter. In order to interpret the results obtained with this detector it was therefore necessary to examine in detail the whole operational process starting from a mechanism for the release of electrons from the surface to an explanation of how they were counted.

The presence of the platinum wire, held at earth potential, between the anode and the cathode meant that the electric field distribution within the counting volume would not be the regular radial distribution normally encountered within a cylindrical counter. In such a design the lines of force would be as shown in fig 22. Furthermore, if points of equipotential were joined up a section across the counter would show a series of concentric

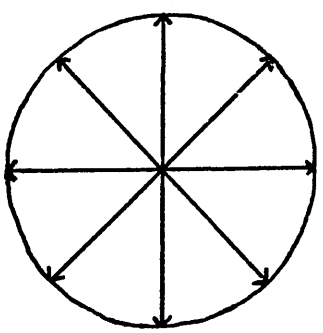

fig 22

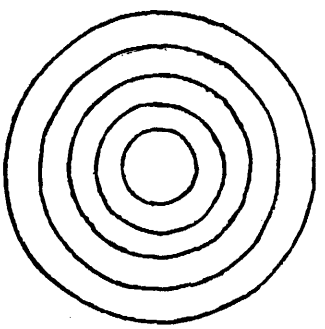

fig 23

circles about the anode (see fig 23).

Thus it was essential to examine the electric field near the platinum wire for several reasons. The first was to find the perturbation caused by the platinum to the field around the

anode. If the field close to the anode, say within ~0·01 cm was disturbed then the counting characteristics of the proportional counter would not be predictable.

If, however, the electric field was not disturbed near the anode it was then essential to discover (1) whether electron multiplication occurred immediately an electron left the platinum surface since this would affect the multiplication process in the tube; (2) whether the field strength was sufficient to lower the work function significantly perhaps even to the extent that field emission might occur.

Examination of an equation governing thermionic emission, such as the Richardson equation which is in the form

$$I = AT^2 e^{-(e\phi/kT)}$$

shows that at temperatures below 500°C no significant thermionic emission in terms of electric current will occur. It is clear from our results that significant levels of 'pulsed' emission were often encountered well below such a temperature. Thus the examination of the whole release-counting mechanism became of the utmost importance to establish the validity of the present results.

In addition to the investigations already outlined, it was necessary to find whether the gas multiplication factor was reasonable, to determine whether or not single electrons were being counted and to explain the integration effect which seemed to be occurring in the Laben pulse-height analyser.

Thus in Chapter 5 will be presented the results of the calculations and experiments carried out to determine the mode

Diagram 24.

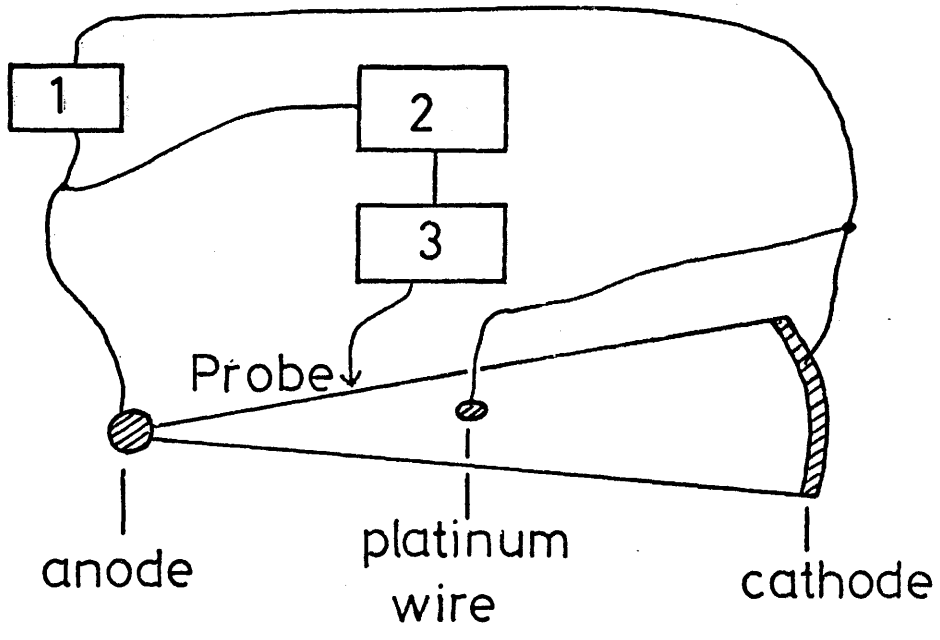

Circuit used to obtain the field plot shown in figure 24, page 99a.

1):- 9V PP7 battery,
2):- 1Kohm multipot,
3):- 400 ohm galvanometer.
/// Silver paint.

of operation of the detector. This will be used as a basis for the explanation of the emission results which will be dealt with in Chapter 6.

5·1 Electric Field Gradients within the Proportional Counter

To determine if field emission or electron multiplication near the platinum wire or the central anode was likely, it was necessary to find the electric field gradients within the proportional counter. Two methods were employed. The first involved making potential plots on Teledeltos paper which is electrically conductive, while in the second the field gradient at the platinum wire was calculated directly.

5·1·1 Field-Plotting Method

By this method it was possible to estimate the field strength at various points within the counter. This was measured by making potential plots on conducting paper on which the anode, cathode and platinum wire had been represented by properly scaled lines and areas painted in silver paint (see Diagram 24, page 98a).

The representation was made on the scale 1·27 cm in the counter ≡ 27·5 cm on the Teledeltos paper. Only one eighth of the counter, which is symmetrical, was represented. The representations were as follows:

a) centre wire radius 0·00127 cm → 0·0274 cm.

b) distance from anode to Pt wire, 0·6 cm → 12·99 cm.

c) diameter of Pt wire, 0·030 cm → 0·65 cm.

d) anode to cathode distance, 1·27 cm → 27·5 cm.

The circuit is shown in Diagram 24, page 98a.

By means of the multipot, 1KΩ in 10^3 steps, the potential of the probe could be set at any value between 0 and 9V. Thus the Cambridge Spot Galvanometer could be used as a null instrument to find points of zero current flow. The potential at those points could be read off on the multipot.

The potentiometer scale was then extended by inserting an 18KΩ resistor in series with the variable potentiometer as shown:-

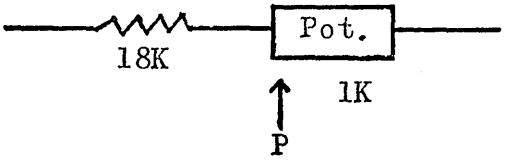

Then the potential at one end of the potentiometer, say the point P, for 1000V across the system would be $^{18}/_{19}$ x 1000V.

If the tap P were moved x divisions, where x is the reading on the 0 to 1000 scale of the multipot, the potential at the new point would be $\left(^{18}/_{19}\right)$ x 1000 + $\left(\frac{x}{1000}\right)$ x $\frac{1000}{19}$.

Fig 24, page 99a, shows the potential gradient as it was explored close to the platinum wire. Graph 28, page 99b, shows the variation in voltage with distance from the platinum wire. The field gradient at points close to the wire was found by calculating the gradient of the corresponding point on the graph.

For example, a point at a distance of 10^{-4} cm from the platinum wire corresponds to the point at 0·07 cm on Graph 24. Thus the gradient at 10^{-4} cm from the wire

$$= \frac{999{\cdot}85 - 982{\cdot}0}{2{\cdot}55} = \frac{17{\cdot}85}{2{\cdot}55} \quad \text{for 1000V.}$$

For 2000V on the centre wire, the gradient = 2 x $\frac{17{\cdot}85}{2{\cdot}55}$

figure 24.

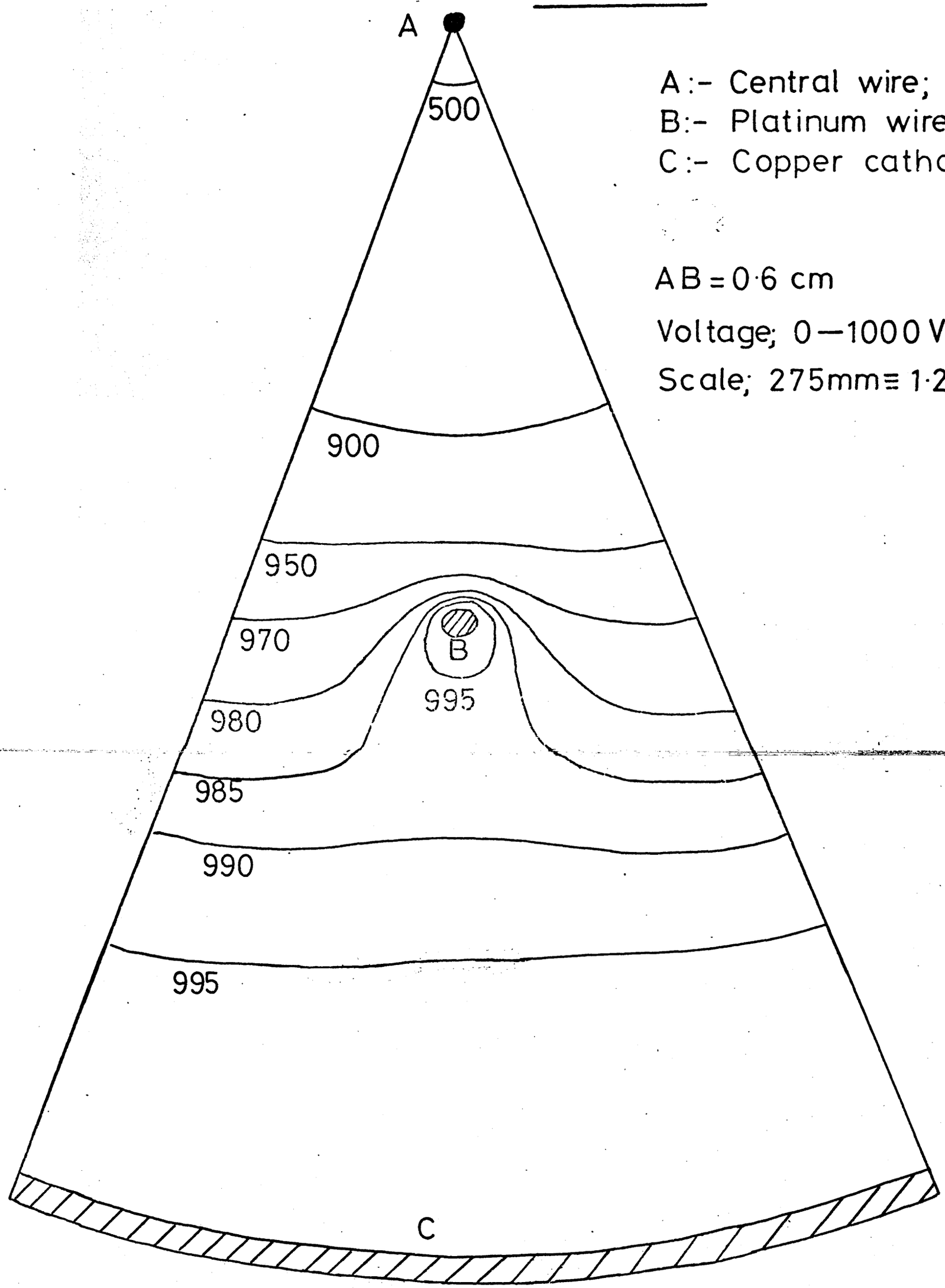

A :- Central wire; r=0·00127 cm.
B:- Platinum wire ; r = 0·015 cm
C :- Copper cathode ; r = 1·27cm

AB = 0·6 cm

Voltage; 0—1000 V

Scale; 275mm ≡ 1·27cm

P66

Graph 28.

Volts versus distance from the platinum wire.

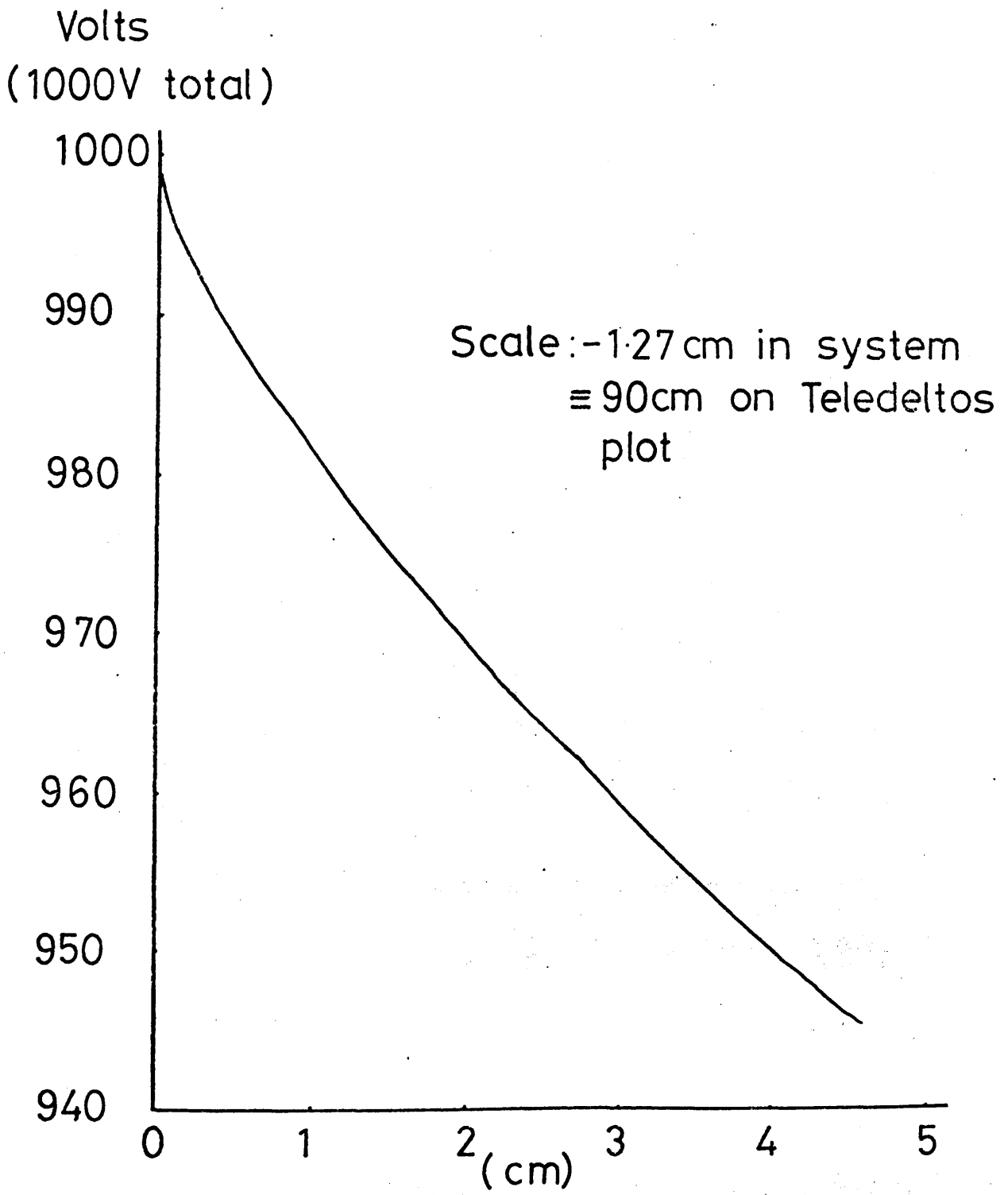

Distance from the platinum filament as represented on Teledeltos paper.

This is eqivalent to 9921 volts cm^{-1} i.e. 10^4 volts cm^{-1}. Similarly a point at 10^{-3} from the platinum wire, is equivalent to a point at 0·7 cm on Graph 24.

$$\text{Thus gradient} = \frac{998{\cdot}83 - 982{\cdot}00}{6{\cdot}2} = \frac{16{\cdot}83}{6{\cdot}2} \text{ for 1000V.}$$

Thus for 2000V on the centre wire in the real proportional counter the gradient is $\frac{63{\cdot}66}{6{\cdot}2}$ which is equivalent to 2586 volts - cm^{-1} i.e. $2{\cdot}5 \times 10^3$ volts cm^{-1}.

5·1·2 Gradient at the Platinum Wire by Direct Calculation

Let charge/unit length on the central wire be +Q coulomb $metre^{-1}$. Let charge/unit length on Pt wire be -Q coulomb $metre^{-1}$. At a general point on the common axis distant x from the central wire, see Diagram 25, the electric flux density, D_x, is

$$D_x = \frac{Q}{2\pi x} + \frac{Q}{2\pi(D-x)}$$

Hence the electric field at x is

$$E_x = \frac{D_x}{\varepsilon_o} = \frac{Q}{2\pi\varepsilon_o}\left[\frac{1}{x} + \frac{1}{D-x}\right] \quad \ldots\ldots\ldots\ldots\ldots\ldots (1)$$

The potential difference between the wires then is

$$V = -\int_{D-r_2}^{r_1} E_x dx = \frac{Q}{2\pi\varepsilon_o}\left[\log_e x - \log_e(D-x)\right]_{r_1}^{D-r_2}$$

$$= \frac{Q}{2\pi\varepsilon_o}\left[\log_e \frac{D-r_2}{r_1} - \log_e \frac{r_2}{D-r_1}\right]$$

$$= \frac{Q}{2\pi\varepsilon_o}\left[\log_e \frac{(D-r_1)(D-r_2)}{r_1 r_2}\right]$$

Diagram 25.

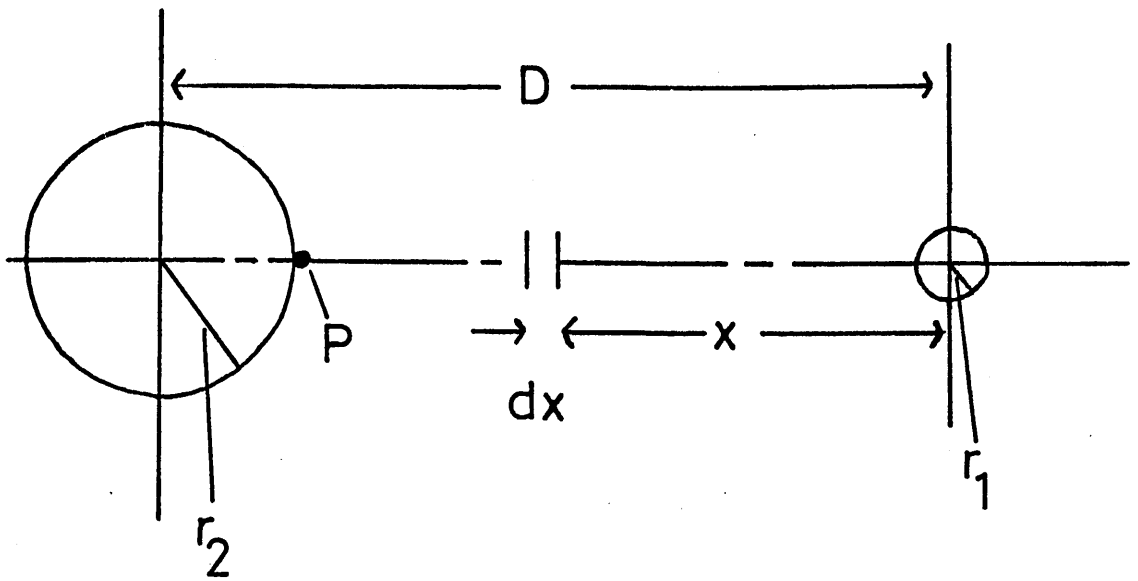

r_1 :- radius of anode wire,
r_2 :- radius of platinum wire,

P is the point on the surface of the platinum wire which lies on the common axis between the two wires.

D:- distance between the centres of the two wires.

$$\text{i.e.} \quad Q = \frac{2\pi\varepsilon_o V}{\left[\log_e \frac{(D-r_1)(D-r_2)}{r_1 r_2}\right]} \qquad \ldots\ldots\ldots\ldots (2)$$

Substituting (2) in (1) gives

$$E_x = \frac{V}{\left[\log_e \frac{(D-r_1)(D-r_2)}{r_1 r_2}\right]} \left[\frac{1}{x} + \frac{1}{D-x} \right].$$

When $x = D-r_2$ this becomes

$$E_{D-r_2} = \frac{V}{\left[\log_e \frac{(D-r_1)(D-r_2)}{r_1 r_2}\right]} \left[\frac{1}{D-r_2} + \frac{1}{r_2} \right].$$

When $D = 0{\cdot}6$ cm, $r_1 = 0{\cdot}00127$ cm, $r_2 = 0{\cdot}015$ cm then for $V = 2$kV

$E \sim 14 \times 10^3$ V cm^{-1} at zero distance from the wire. (This is for the ideal case of a smooth wire).

Thus it may be seen that the results for the experimental method and the calculation method are in accord since they show that the field gradient rises steeply as the platinum wire is approached. The sequence of potentials in volts cm^{-1} are as follows:-

Distance from Pt wire	10^{-3} cm	10^{-4} cm	0 cm (ideal)
Field gradient (volts cm^{-1})	$2{\cdot}5 \times 10^{-3}$	10×10^3	14×10^3.

What must be deduced from this is whether an electron released from the platinum wire will cause secondary ionisation and gas multiplication.

If the path length of an electron were say 10^{-3} cm then near

the platinum wire its energy would be only around 14 eV at the most.

This is only half the average energy to create an ion pair in air, N_2, H_2, Ar (see Appendix 20 for values). At 10^{-4} cm from the platinum wire the energy gained by an electron in moving through 10^{-3} cm would be $(10^{-3} \times 10 \times 10^3)$ eV = 10 eV. This is around $\frac{1}{3}$ of the energy necessary to produce an ion pair.

Thus multiplication of electrons at the platinum wire would seem to be most unlikely.

It is also clear from fig 24, page 99a, that the platinum wire causes no disturbance of the electric field near the anode.

When the counter was later dismantled and the dimensions checked it was found that the distance between the anode and the Pt wire was $^{11}/_{32}$" ($\equiv$ 0·87 cm) instead of the value of $\frac{1}{4}$" ($\equiv$ 0·6 cm) used in the calculation. However, this would serve only to reduce the field strength at the surface of the wire.

The direct calculation was repeated with the corrected values which yielded

Field strength at surface of Pt wire = 12,800 V cm^{-1}

$\sim 13 \times 10^3$ V cm^{-1}.

5·2 The Potential Barrier to Removal of an Electron from a Metal

(See Handbuche der Physiche 21, page 183 (134)). Since electron multiplication at the platinum wire seems unlikely, it would be of interest to examine the effect of the 13 kV cm^{-1} field gradient on the electron emission process itself. If the electric field lowered the work function of the metal sufficiently then even field emission might become possible in this way.

If an electric field F volts cm^{-1} is applied to a metal, then at a point x outside the metal the electron is subjected to (1) an image force and (2) the force of the electric field.

Thus the electron potential at x, V(x) is given by

$$V(x) = -eFx - \frac{e^2}{4x} \quad \text{for } x > 0 \quad \ldots\ldots\ldots\ldots\ldots\ldots \text{(a).}$$

The maximum value of the potential V(x) is at

$$\frac{dV(x)}{dx} = -eF + \frac{e^2}{4x_o^2} \ .$$

Thus $$eF = \frac{e^2}{4x_o^2} \quad \text{and} \quad x_o = \tfrac{1}{2}\sqrt{\frac{e}{F}}$$

Substitution in (a) gives

$$V_{max} = -eF \times \tfrac{1}{2}\sqrt{\frac{e}{F}} - \frac{e^2}{4.\tfrac{1}{2}\sqrt{\frac{e}{F}}}$$

$$= -e\sqrt{Fe}.$$

A field strength of around 4×10^7 V cm^{-1} is necessary for field emission to occur at room temperature.

Changing to absolute units of volts gives

$$F = \frac{4 \times 10^7}{300} \quad \text{absolute volts } cm^{-1}.$$

$$V_{max} = -e\sqrt{Fe} = -4{\cdot}8 \times 10^{-10}\left[\frac{4{\cdot}8 \times 10^{-10} \times 4 \times 10^7}{300}\right]^{\frac{1}{2}}$$

where $e = 4{\cdot}8 \times 10^{-10}$ esu.

Conversion to eV gives

$$e\sqrt{Fe} = \frac{4{\cdot}8 \times 10^{-10}}{1{\cdot}6 \times 10^{-12}}\left[\frac{4{\cdot}8 \times 10^{-10} \times 4 \times 10^7}{300}\right]^{\frac{1}{2}}$$

$$= 2{\cdot}4 \text{ eV.}$$

In this case a work function of say 4·5 becomes

$$4{\cdot}5 - 2{\cdot}4 \quad = 2{\cdot}1 \text{ eV.}$$

$$\text{i.e.} \quad \phi' \quad = 2{\cdot}1 \text{ eV.}$$

The lowering of ϕ for a field of 13000 volts cm^{-1}

$$= 0{\cdot}04 \text{ eV.}$$

Thus it may be seen that the work function is lowered only slightly (0·04 eV) by the applied field in the detector. The effect of this change in work function would be small.

Although it is clear that field emission is impossible when an ideal metal surface is considered, it must be remembered that in the present situation metal or carbon asperities may be present on the wire. Their presence could greatly increase the field at those points, and hence the electron emission.

5·3 Operation of the Proportional Counter

For a counter of the dimensions shown, the field strength at any point distant r cm from the centre is

$$E = \frac{V}{r} \ln\left(\frac{b}{a}\right).$$

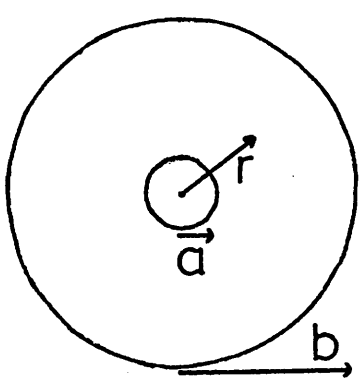

For a counter with a cathode of diameter 1" and an anode wire of diameter 0·001", a = 0·0005" = 0·00127 cm and b = 0·5" = 1·27 cm.

Thus for an applied voltage of V = 2 kV

$$E = \frac{2000}{r} \quad \ln\left(\frac{1{\cdot}27}{1{\cdot}27 \times 10^{-3}}\right) = \frac{6{\cdot}9 \times 2000}{r}$$

and at 0·01 cm from the central wire

$$E = \frac{6{\cdot}9 \times 2000}{0{\cdot}01} = 1380000 \text{ V cm}^{-1}.$$

According to Rossi and Staub (135) the mean free path of an electron in argon at atmospheric pressure is $0{\cdot}9 \times 10^{-4}$ cm. Thus at 0·01 cm from the anode if an electron moves through $0{\cdot}9 \times 10^{-4}$ cm it will acquire energy.

$$\begin{aligned} \text{K.E.} &= 1{\cdot}38 \times 10^{6} \times 0{\cdot}9 \times 10^{-4} \text{ eV} \\ &= 1{\cdot}242 \times 10^{2} \text{ eV} \\ &\sim 1{\cdot}2 \times 10^{2} \text{ eV} \\ &= 120 \text{ eV}. \end{aligned}$$

According to Rossi and Staub the mean free path of an electron in gases at 1 atm is as follows:-

H_2, $0{\cdot}3 \times 10^{-4}$ cm; Ar, $0{\cdot}9 \times 10^{-4}$ cm; N_2, $0{\cdot}3 \times 10^{-4}$ cm.

The average energies required to produce an ion pair are w(eV) = 36·0 for H_2, 28·2 for Ar, 37·1 for N_2. (see The Nuclear Handbook (136)). Thus it is clear that at 0·01 cm from the centre of the counter the field strength is already in excess of the value required for electron multiplication.

5·4 Gas-Multiplication Factor

5·4·0 Americium Calibrations

In order to establish the multiplication factor for the

counter experiments were conducted with ^{241}Am as a source of 60 KeV γ-rays (36% + other γ-rays). The electrons produced by these γ-rays would have a maximum energy of 60 keV. In Ar at N.T.P. electrons of this energy produce around 150 electron-ion pairs per 1·00 mg cm^{-2} of Ar (137).

At N.T.P. $22{\cdot}4 \times 10^3$ cm^3 Ar ≡ 40g Ar

$$\therefore \quad \frac{22{\cdot}4 \times 10^3}{4 \times 10^4} \text{ cm}^3 \text{ Ar} \equiv 1\text{mg Ar}$$

i.e. $0{\cdot}56$ cm^3 Ar ≡ 1mg Ar.

Thus in a path length of 0·56 cm there are created 150 electrons.

If a γ-ray had a path length of 3cm in the counter then $\frac{3}{0{\cdot}56}$ x 150 ion pairs would be formed.

i.e. ~804 ion pairs.

In order to work out the multiplication factor for the counter it was necessary next to determine the sensitivity of the pre-amplifier.

5·4·1 Preamplifier Output Signal

The preamplifier comprises two stages, a charge sensitive stage NE5287AC and a voltage gain stage, NE5287SC.

The charge sensitive stage employs a field effect transistor and the charge sensitivity of this stage is determined by the value of the feedback capacitance. The output is independent of the detector capacity, C, giving this system a considerable

advantage over a voltage sensitive system. The circuit for the charge sensitive stage is shown in Diagram 26, page 107a.

The voltage developed in the charge sensitive stage will be

$$V = q/c \text{ volts}$$

$$q = 1{\cdot}6 \times 10^{-19} \text{ coulombs for an ion pair}$$

$$c = 1\text{pF} = 10^{-12} \text{ Farads}$$

$$\therefore V = \frac{1{\cdot}6 \times 10^{-19}}{10^{-12}} \times 10^{6} \ \mu V$$

$$= 0{\cdot}16 \ \mu V/\text{ion pair.}$$

The present preamplifier was modified however, to prevent surges of current from damaging the FET. This modification is shown in Diagram 27, page 107b.

5·4·2 Modified Preamplifier Output Signal

Whereas the resistance R in the original circuit was 1KMΩ and the leakage was negligible, in the modified circuit leakage may take place through a 22 KΩ resistor: thus the sensitivity of the circuit is reduced.

The sensitivity of the modified amplifier, which may be defined as the mV output per charge input in coulombs, was determined experimentally as follows. A Lyon's pulse generator, type PG 73N, was used to provide a signal on a double-beam oscilloscope; the other signal was produced by the pre-amplifier output. Thus the two mV signals could be compared directly. The result was:-

Input 400 mV, Output 12 mV.

The input was fed into the 1 pF test input capacitor; thus

Diagram 26.

Original preamplifier circuit.

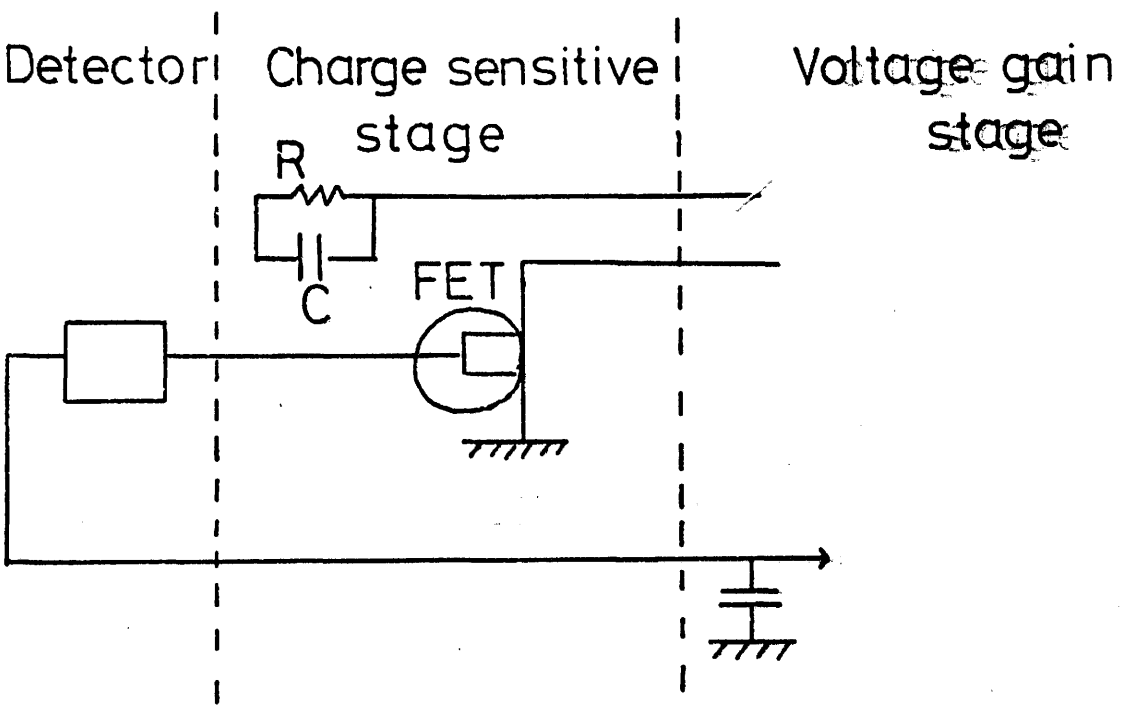

R:- Resistor,
C:- Capacitor,
FET:- Field effect transistor.
:- Earth

Diagram 27.

Modification to preamplifier.

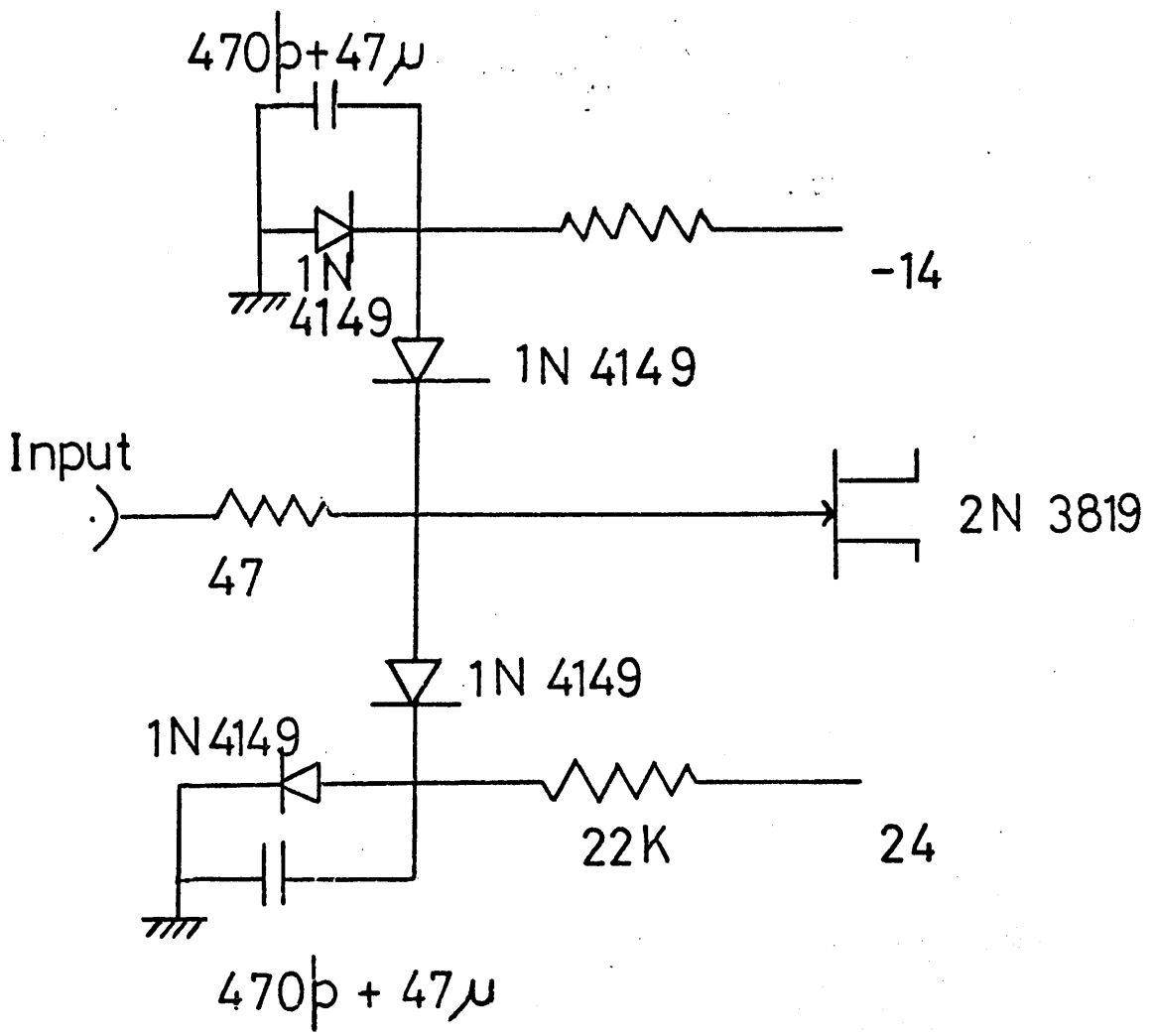

FET protection circuit.

the charge input was $q = 0{\cdot}4 \times 10^{12}$ coulombs.

The sensitivity = 12 mV per $0{\cdot}4 \times 10^{-12}$ coulombs

$\equiv 0{\cdot}0048$ μV per ion pair.

The original value was 0·16 μV per ion pair. Thus it may be seen that there was a considerable loss of sensitivity when the FET protection circuit was introduced.

5·4·3 Gas-Multiplication Factor from Calibration Experiments

The gas multiplication factor for the counter could now be calculated as follows.

Ion pairs produced by ^{241}Am γ-ray ~ 804.

$\therefore$ Charge released = $804 \times 1{\cdot}6 \times 10^{-19}$ coulombs

The output pulse was measured. It was found to be about 0·24 mV.

$$\therefore \text{ Multiplication factor} = \frac{0{\cdot}4 \times 10^{-12} \times 0{\cdot}24}{12 \times 804 \times 1{\cdot}6 \times 10^{-19}} \sim 60.$$

This is in the expected region for a multiplication factor for a counter of the given dimensions operating at atmospheric pressure.

5·4·4 Gas-Multiplication Factor by Calculation

An alternative approach to determination of a multiplication factor is as follows.

If it was assumed that a 60 keV γ-ray gave all of its energy to the gas filling in the counter and if 30 eV was taken as the energy required to produce an ion pair then 60,000/30 = 2000 ion pairs would be created.

Thus the amount of charge collected would be

$$2000 \times 1{\cdot}6 \times 10^{-19}\text{C}$$
$$= 3{\cdot}2 \times 10^{-16}\text{C}.$$

By calibration the output pulse is known to be about 0·24 mV. This is equivalent to a charge input of

$$\frac{0{\cdot}4 \times 10^{-12}}{12} \times 0{\cdot}24 = 8 \times 10^{-15}\text{C}.$$

Thus the multiplication factor $= \frac{8 \times 10^{-15}}{3{\cdot}2 \times 10^{-16}} = 25.$

5·4·5 Conclusion

The two multiplication factors, 60 and 25, indicate without doubt that a single electron emitted in an exo-electron process, even if it was gas-multiplied 60 times, would not give an output from the preamplifier which could be recorded.

The actual output (using x60) would be 0·0048 x 60 = 0·0288 μV. It is not clear whether this important point has been ignored in other papers on exo-electron counting.

5·5 Energy Spectra

Since, on the basis of the foregoing calculations, it was evident that single electrons were not being counted, it was then necessary to find an explanation for the appearance of peaks in the spectra obtained with the Laben pulse-height analyser when exo-electrons were being counted.

The basic proposal which had to be examined was whether or not during a fast emission of exo-electrons the amplifier-detector system in some way integrated electron-produced signals

to give a pulsed output of apparently higher energy.

It will be shown in the next section that the scaler and chart recorder systems showed a true pulse record whereas the 'spectra' obtained with the Laben Spectrascope arose from other causes.

5·5·1 Energy Spectra

Whereas the spectrum obtained from ^{241}Am on the Laben Spectrascope showed an expected maximum energy in say channel 328, it was possible to find exo-electron spectra with maxima beyond this channel number. For example, counts were accumulated over periods of 0·5 min at several stages while Pt wire 5 cooled in hydrogen after being heated in nitrogen. Between 4·0-4·5 min and 9·0-9·5 min after the current was switched off, peaks appeared in channels 356 and 372 respectively. The corresponding anode voltages were 1·8 and 2·1 kV (see Appendix 21).

No reasonable process effecting chemically stimulated emission from platinum could produce electrons of energy greater than 60 keV: in fact energies of around 0·025 - 1 eV would have been expected for exo-electrons.

It was therefore decided to inject low energy white noise pulses into the preamplifier to find out how the output behaved.

Initially noise was generated in a forward biased diode system. After amplification the signal was fed directly into the

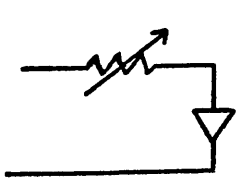

Forward biased diode system

Laben pulse height analyser and a spectrum of the form shown in Laben Spectrum 9, page 111a was obtained as would be expected from such a source.

White noise was then fed into the preamplifier, through the pulse shaping equipment and into the Laben Spectrascope. Spectra were obtained of the form shown in Laben Spectrum 10, page 111a. These spectra showed a high energy peak.

Next pulses from a Lyon's pulse generator, type PG 73N, having adjustable pulse height and width were injected into the overall system. It was found that pulses whose width fell within the range 7 to 10 μs gave spurious spectra as shown in Laben Spectrum 11, page 111b. Further analysis showed that these spurious peaks arose in the back biased amplifier. It may be seen from fig 25, page 111b that the width of pulses which do not have an infinitely fast rise time is affected by the back biasing.

Thus if a number of low energy pulses have a pulse width which falls between 7 - 10 μs after back biasing they can form an apparent high energy peak.

Pulses were fed into the preamplifier and through to the digital ratemeter of the SR5 and the pen recorder which records what appears on the ratemeter, see Table VI, page 111c. There was found to be good agreement between the input rate to the preamplifier and what appeared on the digital ratemeter. The signal from this output of the preamplifier did not pass through the Nuclear Enterprises pulse shaping equipment. Thus the chart recorder and the scaler-ratemeter systems provided a true pulse record and these results could be used to indicate

Laben Spectrum 9.

Spectrum which resulted when white noise was fed directly into the Laben pulse-height analyser.

Counts / channel.

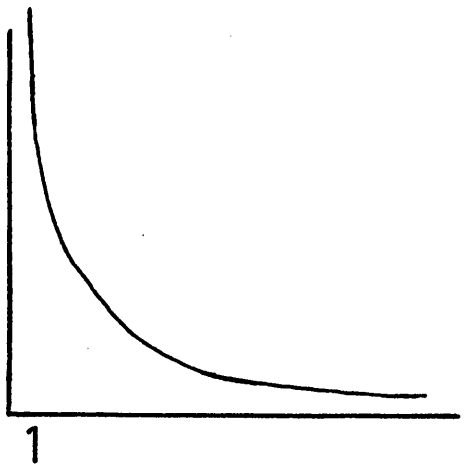

Channel number (400 channels)

Laben Spectrum 10.

Spectrum which resulted when white noise was fed into the preamplifier, through the pulse shaping equipment and into the Laben Spectrascope.

Counts / channel.

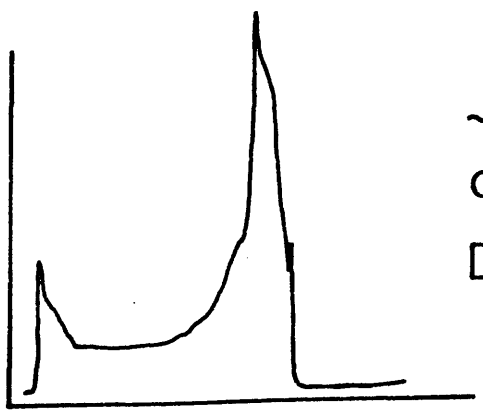

~1,100,000 counts accumulated.

Dead time 80%.

Channel number (400 channels)

Laben Spectrum 11.

Spectrum obtained when pulses whose width fell in the range 7–10μs were injected into the overall system.

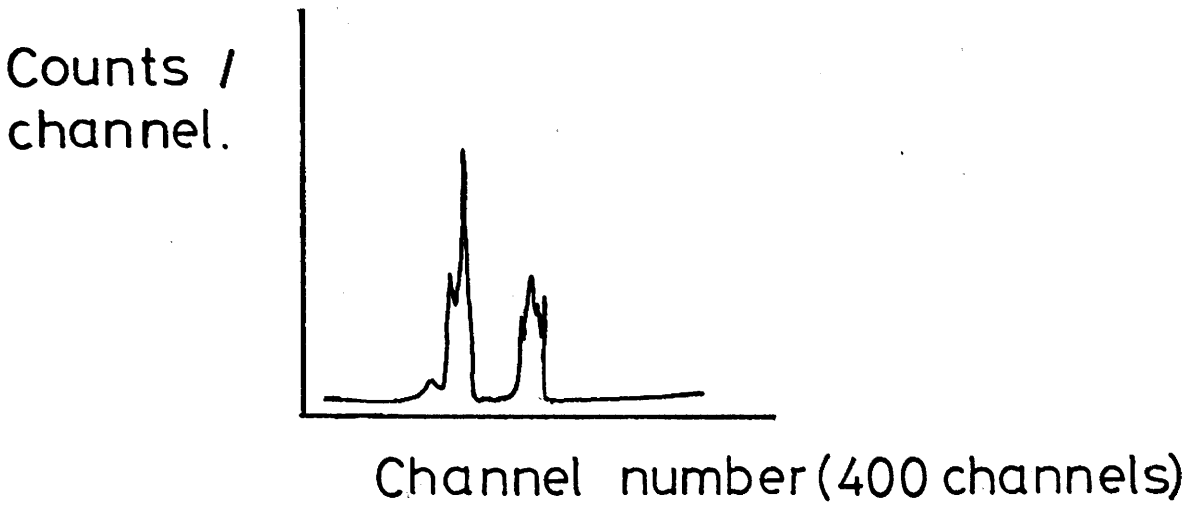

figure 25.

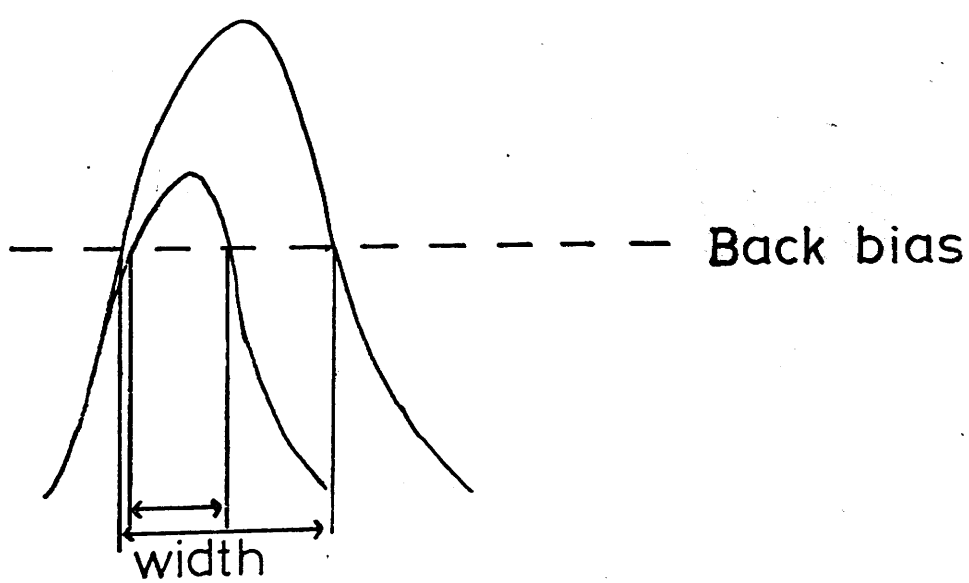

To show that the width of a pulse which does not have an infinitely fast rise time is affected by the back biasing.

Table VI

Pulse rate from pulse generator (pps)	count-rate on Digital Ratemeter (cps)
100	93
1000	956
10000	14600

The pen recorder records what appears on the ratemeter.

reliably increased emission from the platinum filament.

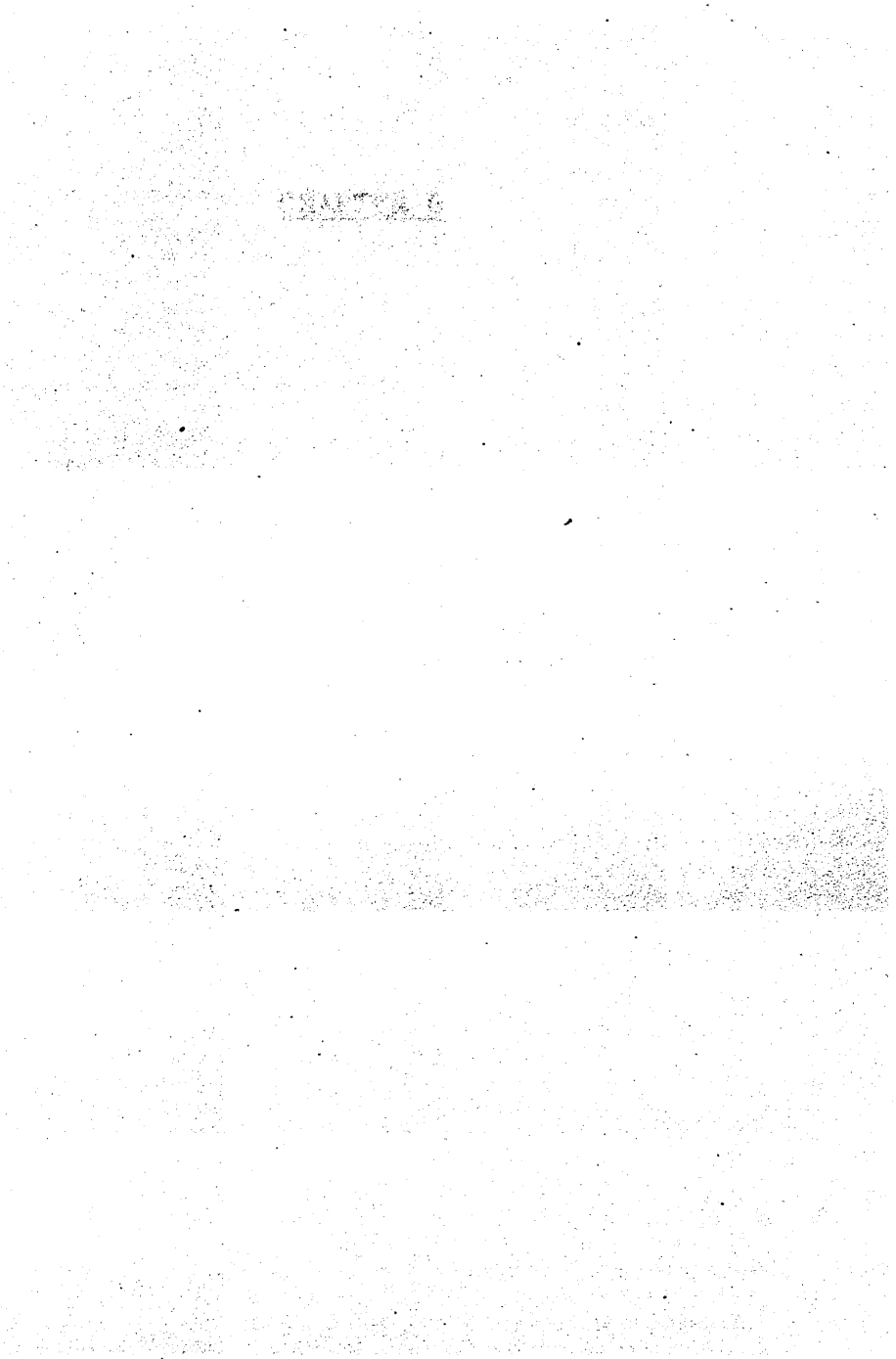

CHAPTER 6

Chapter 6

DISCUSSION II RESULTS

6·0 INTRODUCTION

In Chapter 5 the mode of operation of the exo-electron detector developed by us was investigated. Several important points emerged.

1. The presence of the platinum wire within the active counting volume of the detector did not perturb the electric field close to the anode, see fig 24, page 99a. This meant that the multiplication behaviour of the counter was predictable for electrons near the central wire.

2. The field gradient at an infinitely small distance from the platinum wire was found by calculation to be about 13×10^3 V cm^{-1} for the ideal case of a smooth wire. This was too low to cause significant field emission from the wire, for which a field of the order of 10^7 V cm^{-1} would have been required to effect electron release at room temperature. The field gradient was also too low to bring about gas multiplication of an electron in the region of the platinum wire. All gas multiplication occurred in the region of the anode. At most a slight enhancement of electron emission might be obtained due to the small lowering of the work function of the platinum surface ($\sim 0{\cdot}05$ eV) or to the presence of asperities at the surface of the wire.

Below 500°C no significant thermal electron emission current was predicted, yet the results presented in Chapter 4 clearly indicate high levels of pulsed emission well below normal

thermionic emission temperatures.

3. The gas multiplication factor lay in the range 25-60, which is that expected for a cylindrical gas flow proportional counter of the given dimensions operating at one atmosphere.

The value for the gas multiplication factor signified that electrons emitted from the platinum wire could not be counted singly. Nevertheless, since an emission rate was being measured, it was shown that all the results which were recorded by the pen recorder were valid. 'Packets' of low energy electrons were being counted and an emission peak in a cooling curve reliably indicated an increase in emission rate from the platinum wire.

Thus it was demonstrated in Chapter 5 that the configuration of the counting system was satisfactory. With this detector it was possible to study the electron emission from a platinum wire as it was heated or cooled in a variety of gases. It was not necessary to evacuate the system and then introduce a special counting gas.

It was possible to study emission over a wide temperature range since the detector counted 'properly' even when the platinum was heated to 900°C. It was shown that prolonged heating e.g. 45 min, of the platinum wire at such a temperature only raised the temperature of the cathode to about 300°C; see Chapter 3.8.

Since the characteristics of detector 5 were 'established' satisfactorily in Chapter 5, it then became possible in Chapter 6 to consider the emission results obtained with this system. Explanations are required therefore of electron emission and of

the growth and decay of these emissions.

6·1 Previous Observations

6·1·0 Principal Features of Emission

The main features of the experiments which require interpretation are the following.

(a) Emission peaks were observed, for example, at 20, 45, 56°C which correspond to 293, 318 and 329K. For a temperature of 329K, the Richardson equation would have predicted an emission current $I \sim 6 \times 10^{-80}$ Amp.

(b) Platinum wires, after certain pretreatments, yielded cooling curves in various gases.

Whereas a smooth decay of electron emission might have been expected as temperature fell, there was observed first a fall in emission then a succession of growths and decays in electron emission.

6·1·1 Literature Survey

First the literature dealing with exo-electron emission phenomena was evaluated to determine whether any common factor existed. From this reading the following proposition may be offered.

Exo-electron emission always accompanied the making or breaking of bonds at a surface.

This proposition emerges because the following features became evident.

(a) Chemisorption upon a clean surface produced exo-electrons. For example Kasemo and Walldén (114) observed electron emission during the chemisorption of chlorine on sodium films prepared by evaporation in ultra high vacuum conditions, and later (138), during the chemisorption of chlorine, bromine or iodine on sodium films. Lohff (23) and Wüstenhagen (25), (26) found an emission of exo-electrons from metal films prepared by vacuum evaporation. The emission kinetics depended on the residual gas pressure of the apparatus.

(b) Exposure of fresh metal through abrasion may lead to the creation of chemisorption sites. Ramsey (24), (27-30) demonstrated that adsorption of water vapour and oxygen on freshly abraded aluminium effected exo-electron emission. Gesell and co-workers (36), (37) observed electron emission in the dark from abraded magnesium during exposure to oxygen and water vapour. Gel'man et al (38), (39) also recorded exo-electron emission during the air oxidation of abraded magnesium while Okamoto, Sato and Ohashi (17) investigated the differing exo-emission characteristics of abraded iron which had previously been annealed in vacuum or in an atmosphere of hydrogen.

Kramer (139) has shown that after mechanical disintegration several minerals, for example fluorspar, corundum, pyrites or potassium orthoclase, gave rise to exo-electron emission at room temperature which decayed in a manner similar to the emission observed from metals abraded at room temperature in air.

(c) Fresh sites on a surface can be created by the production of defects and boundaries.

One method by which such an effect may be produced is the plastic deformation of metals.

For example, Sujak and his group (47-56) and Arnott and Ramsey (57) investigated the electron emission from anodically oxidised aluminium subjected to plastic deformation.

Where oxide thickness was less than about 45 nm, both groups found a pressure-dependent photostimulated emission, similar to that from abraded metals, but in this case fresh metal was exposed by slip penetrating the oxide film or by specimen breakage.

When oxide thickness was greater than 45 nm (57) - 60 nm (56) emission occurred in the dark. Microscopically there was no sign of slip but the formation and propagation of cracks in the oxide was observed. Arnott and Ramsey (57) proposed that this was responsible for the dark emission.

Meleka and Barr (42) confirmed that exo-electron emission from strained, single zinc crystals originated from areas of slip. Large slip displacements produced continuous black lines on a photographic emulsion in contact with the metal. It was also noted that with decreasing displacement due to slip the lines became discontinuous and finally resolvable into rows of individual spots. These spots resembled the dislocation etch pits found along the slip lines of zinc single crystals.

Thus emission may originate from points where dislocations terminate at the surface of the crystal.

Baxter (62), (63) confirmed that exo-electron emission originated in cracks in the surface oxide of aluminium subjected to cyclic stress while Rabinowicz (65) has observed electron

emission from steel ball-bearings as fatigue cracks developed.

Mints and Kortov (61) showed that for the same level of applied cyclic stress the resultant exo-emission from austenitic steels of various compositions depended on the composition. In each case some of the mechanical energy went to the formation of defects at the surface and the more defects generated, as indicated by the ~~increase~~ change in surface microhardness and the internal friction, the greater the observed emission.

Ionising radiation may also damage crystal structure (140), with α-radiation producing the greatest effect. In general holes and interstitials may be formed. For example, much work has been done on the applications for dosimetry of exo-emitters such as beryllium oxide (94), (95) which, after suitable pre-treatment shows a linear response to α, β, γ and neutron irradiation.

After irradiation the sample is generally heated to produce thermally-stimulated exo-electron glow curves from which information may be obtained about the nature of the incident radiation (93), (95); see also (41).

(d) Exo-electron emission may also accompany desorption of species from a surface. For example, Krylova (40) and Rakhmatullina and Krylova (104) observed maxima of electron emission during the heating of several oxides. Each emission maximum corresponded to a maximum of thermal desorption. In general the species desorbed were oxygen and water. Euler, Kriegseis and Scharmann (41) found that oxygen adsorption centres were active for exo-electron emission from beryllium oxide.

Thus exo-electron emission accompanying thermal desorption

of adsorbed species is well established.

Desorption of species adsorbed on the surface as a sample is heated is an accepted phenomenon and it forms the basis of flash and thermal desorption studies of catalysts. For example, McCabe and Schmidt (141) studied the adsorption of hydrogen and carbon monoxide on clean and oxidised platinum by the flash desorption method, while Wilf and Dawson (142) investigated the adsorption and desorption of nitrogen on a platinum film by thermal desorption studies.

Although these investigations were carried out at low pressure, Wilf and Dawson worked at a maximum exposure of 2×10^{-4} torr sec, it seems reasonable to propose that when a platinum wire is heated in a gas at a pressure of one atmosphere thermal desorption will occur, and it should be accompanied by exo-electron emission. The heating curves obtained in the present work, see Appendix 15 for examples, confirm this.

(e) Exo-electron emission may also be observed during catalysed chemical reactions, where adsorption and desorption proceed continuously at the catalyst surface so that new adsorption sites are generated constantly.

For example, Sato and Seo (102) found that the rate of emission of exo-electrons from a silver catalyst was proportional to the rate of formation of ethylene oxide.

Sujak, Gorecki and Biernacki (105) observed a maximum emission intensity from a zinc oxide catalyst at a temperature of 570K. Catalytic activity also reached a maximum in this temperature range. Hoenig and Tamjidi (112) observed exo-emission during

the catalytic oxidation of carbon monoxide, hydrogen or ammonia on hot platinum. They found that the exo-electron current was related to the rate of reaction and that suppressing or enhancing the exo-electron emission decreased or increased the rate of reaction.

(f) Finally it was noted that exo-electron emission did not occur under UHV conditions, where the residual pressure of the vacuum apparatus was less than 10^{-9} torr. The only exception was found for lithium fluoride whose electron emission after X-irradiation was relatively independent of pressure. In this case the surface states responsible for emission were not sorption states.

If heating a platinum wire leads to desorption of adsorbed species from the surface (141), (142) then allowing it to cool from high temperatures in a gas should lead to adsorption.

Thus the exo-electron emission results presented in Chapter 4 will be interpreted in terms of chemisorption. In this study it appeared that adsorption of the gases in which the platinum wires were cooled provided the common factor which emerged from the literature and from the system presented in Chapters 3, 4 and 5 i.e. the necessity for the making and breaking of bonds.

Evidence will also have to be considered for the creation of fresh sites on platinum surfaces.

6·2 Interpretation of the Results

6·2·0 Before it is possible to explain the exo-electron

results obtained by the present author in terms of chemisorption processes it was necessary to show that no other effect contributed to the observed emission.

Other factors which might have contributed to the observed effect were field emission and emission due to the presence of carbon asperities or other high points on the wire.

6·2·1 Field Emission

It was demonstrated in Chapter 5 both by field plotting methods and by direct calculation that the field at an infinitely small distance from the platinum wire was two orders of magnitude too small to permit significant field emission.

6·2·2 Carbiding of the Platinum Wire

It has already been pointed out in Chapters 3 and 4 that, with the exception of nitrogen and hydrogen, no structure was observed in a cooling or heating curve unless the platinum wire had been heated in Q gas (90% Ar, 10% CH_4); see Appendix 16. Introduction curves obtained before and after exposure of wire 3 to methane are also shown. The differences here are less pronounced. However, these results are not so reliable since they may only be a reflection of the differing electronegativities of the gases.

After wire 3 was heated in methane the same applied voltage produced a smaller current and the wire glowed red. The electron emission from the wire increased since its temperature had increased. However, it was only after this platinum filament was subsequently exposed to air at room temperature that cooling

curves became structured and introduction and cooling curves started to resemble those obtained with wire 1. Heating wire 3 in pure, dried oxygen after the initial exposure to methane was not sufficient to generate structured cooling curves. The exposure to air was essential. This raises the question of whether traces of moisture in the air were responsible for the effect.

After the wire had been exposed to air, the current which passed through it decreased again for a constant applied voltage. In other words the resistance of the wire increased again.

Heating a platinum wire in the presence of methane is a process likely to produce carbon deposition on platinum. For example Tesner and Rafal'kes (143) demonstrated that if platinum was heated in a flow of CH_4/N_2 to temperatures in the range 700-1000° [sic] then carbon was deposited on the surface. They also showed that as the amount of carbon on the surface increased the rate of deposition became faster. As well as increasing the resistance of the wire, see 4·5·2, the presence of carbon on the surface would decrease the work function of the metal; see later.

In addition to the lowering of the work function, the possibility that exposure of the platinum wire to hydrocarbons could give rise to the formation of carbon asperities was considered, since this could lead to field emission from these high points. Growth of carbon 'whiskers' has been observed by Rostrup-Nielsen (144) during the decomposition of methane and carbon monoxide on supported nickel catalysts, while Baker, Harris, Thomas and Waite (145) investigated the formation of

filamentous carbon from iron, cobalt or chromium-catalysed decomposition of acetylene.

Nickel, iron and cobalt are the most effective catalysts for production of carbon near 700°C while platinum and other metals have also catalysed carbon deposition at higher temperatures; see (146) for references. In general no carbon formation has been reported on platinum below 600°C. However, Fryer and Paal (146) demonstrated that carbon fibres were produced on platinum black at temperatures not exceeding 360°C after exposure of the catalyst to 1-hexene and cyclohexene.

In order to examine the possibility of production of carbon in say a filamentous, form Mr S. Orr of the Engineering Department of Glasgow University examined a section of wire 5 in a Philips P.S.E.M.500 scanning electron microscope after completion of all the experiments. By the time the platinum sample was investigated it had been heated in ethylene and also in acetylene. These gases decompose more readily than methane to yield surface carbon of a filamentous nature; see for example (145) or (158).

There was no evidence for the presence of large deposits of carbon on the surface. Thus it was concluded that the exo-electron emission observed from the platinum wires was more likely to be the result of the lowering of the work function of the platinum due to the presence of carbon: chemically stimulated exo-electron emission might then occur through the making and breaking of chemical bonds.

In recent years the Low Energy Electron Diffraction (LEED) technique has been used to study adsorption phenomena.

For example, Somorjai (147) has studied the adsorption of

hydrocarbons on platinum. In every case he observed a decrease in work function when adsorption occurred. Some examples are given in Table VIII, page 124a. Values are also listed of the change in work function, $\Delta\phi$, of a platinum surface after adsorption of other species. It should be noted that the presence of a graphite overlayer on platinum lowers the work function of the Pt(100) surface by 1·0eV and that of the Pt(111) surface by 1·1eV (147).

If the observation of chemically stimulated exo-electron emission has been made possible by the initial lowering of the platinum work function due to the deposition of carbon on the surface then whether or not emission is observed should depend on the electronegativity of an adsorbed gas and its effect on work function. Emission may be enhanced or diminished.

6·3 Electronegativity

6·3·0 The proposal that changes in work function provide a reason for emission can be tested by examining the present results.

6·3·1 Oxygen

Early adsorption work indicated that oxygen chemisorbed readily on platinum. For example, Trapnell (148) found that the strength of adsorption of some common gases, chemisorbed on evaporated films of platinum at room temperature and 30 torr pressure, decreased in the following sequence

$$O_2 > C_2H_2 > C_2H_4 > CO > H_2 > CO_2 \sim N_2 .$$

CO_2 and N_2 did not adsorb.

Since then, however, contradictory results have been

Table VIII

Adsorbate	$\Delta\phi$ (eV)	Temperature	Pt surface	Reference
Acetylene (C_2H_2)	-1·5	20°C	(111)	
	-1·65	20°C	(111)	
	-1·8	150°C	(111)	
	-1·65	20°C	(100)	
	-1·7	150°C	(100)	(147)
Ethylene (C_2H_4)	-1·5	20°C	(111)	
	-1·7	250°C	(111)	
	-1·2	20°C	(100)	
	-1·5		(100)	(147)
Graphitic overlayer from heating Pt in ethylene	-1·1	950°C	(111)	
	-1·0		(100)	(147)
Hydrogen	-0·3	77 K	(111) smooth	
	-0·23	150 K	(111) smooth	
increased to +0·25 then fell to		150 K	(111) stepped	(162)
	-0·30	250 K		(160)
Sulphur	-0·7		(100)	(178)
Methane (CH_4)	0— -1·0 (estimated)	20°C		see (147)
Ethane (C_2H_6)	0— -1·0 (estimated)	20°C		see (147)
Butadiene	-1·3— -2·0 (estimated)	20°C		see (147)
Oxygen	+1·04	300 K		(155)
	+1·0	400 K	polycryst.	(156)
Carbon Monoxide (CO)	+0·68		field emission tip	(157)
	+0·23		evaporated film	see (149)
	+0·68		evaporated film	see (149)
	0			see (149)
	-0·45	RT	(100)	(149)
Argon	$\leq$ -0·03	-196°C	Ni filament	(176)

obtained. For example, Morgan and Somorjai (149) found that oxygen did not adsorb on the (100) face of platinum at pressures $P \leqslant 10^{-7}$ torr in the temperature range 25 - 1400°C while Weinberg, Lambert, Comrie and Linnett (150) found an extremely low sticking probability of 7×10^{-7} for oxygen chemisorption on a platinum (111) surface. In contradistinction Weber, Fusy and Cassuto (151) and Procop and Völter (152) found a high sticking probability for oxygen of 0·14 on polycrystalline platinum.

Weinberg et al (150) proposed that high sticking probabilities were caused by the presence of carbon contamination on the surface. However, Völter, Procop and Berndt (153) showed that significant oxygen adsorption would only proceed on clean platinum foil, otherwise carbon monoxide was formed on the surface. They also demonstrated that to prepare a clean platinum surface it was not sufficient to heat the platinum in vacuum, as surface carbon is not removed by this treatment. Völter et al cleaned the samples of platinum foil under investigation by heating them to temperatures in the region of 1270 K for about four hours in an atmosphere of 10^{-6} torr oxygen.

Recent work by Lang, Joyner and Somorjai (154) indicated that although oxygen chemisorption was slight on smooth Pt(111) and (100) crystal faces, it chemisorbed readily on high Miller index platinum surfaces at relatively low temperatures and pressures. The adsorption generated disordered surface species and evidence for dissociation of the molecule was also obtained.

This recent work rationalises the discrepancies found in earlier results.

Adsorption of oxygen on platinum leads to an increase of the work function ϕ with respect to the clean metal because of the electronegativity of oxygen. For example, Heyne and Tompkins (155) found $\Delta\phi$ = +1·04eV at 300 K while Lewis and Gomer (156) found an increase in $\Delta\phi$ of about +1·0eV at 400 K.

Due to the large increase in $\Delta\phi$ when oxygen is adsorbed on platinum, little or no exo-electron emission would be predicted when a platinum filament is heated and cooled in oxygen.

If there was carbon, or carbonaceous species, on the surface, then heating the platinum wire in oxygen would form carbon monoxide on the surface (153) which would desorb in the temperature range 150 - 220°C (157). If carbon still remained on the surface then cooling the platinum filament in oxygen should generate surface CO at temperatures below 150°C.

According to Lewis and Gomer (157) chemisorbed CO increases ϕ_{Pt} by 0·68eV at monolayer coverage. Thus its presence should also diminish chemically stimulated exo-electron emission from a platinum surface. However, values for change in work function between 0 and +0·68eV have been reported, see (149), while more recently a decrease in the work function of platinum of -0·45eV was measured by Morgan and Somorjai themselves (149) when carbon monoxide had adsorbed to saturation on Pt(100). Since this value was obtained for a low Miller index surface it seems less reliable as a measure of work function change for a polycrystalline platinum wire.

The wide range of values reported makes it difficult to predict what effect carbon monoxide will have on exo-electron emission from a platinum wire.

In certain situations emission was observed from a platinum wire in oxygen during short heating experiments; see fig 52 Appendix 10. Any cooling curves obtained decayed smoothly, that is there were no peaks in them. During short heating experiments electron emission was observed from platinum in oxygen during the first heating/cooling cycle after oxygen introduction. Since adsorption of all the other gases investigated leads to a decrease in ϕ_{Pt}, see Table VIII, this result is reasonable. Emission can continue from the platinum filament until oxygen 'cleans' the surface, see (153). As oxygen itself starts to chemisorb onto the platinum surface ϕ will increase and the emission will diminish.

In second and subsequent heating/cooling cycles no emission was observed, except when oxygen was introduced after acetylene, when emission continued for several cycles.

This lack of emission must be interpreted with caution since two factors could contribute towards it. The first is the increase in ϕ by up to 1eV causing chemically stimulated exo-emission to cease. The second is the decreased sensitivity of the preamplifier due to the presence of the protection circuit described earlier; see 5·4·1. Because of this only 'packets' of pulses could register. Thus the fact that no emission was recorded does not mean that no electrons were released from the wire. However, when emission was observed from the wire in oxygen, the count rate just before the heating current was switched off was generally about $6-7 \times 10^3$ cps with a discriminator setting of 0·1 x 1, 2%. Thus it does imply a considerably reduced exo-emission from the filament if the

'packets' of pulses were not sufficiently energetic to register on the SR5 scaler-ratemeter. A combination of these factors seems likely.

It is generally accepted that acetylene is a good source of surface carbon and carbonaceous species (158). Thus it may be inferred from the continued electron emission from the acetylated platinum wire after the first heating cycle in oxygen that prolonged heating in oxygen would be necessary to remove all of the ϕ-lowering surface species generated by acetylene.

6·3·2 Hydrogen and Hydrocarbons

6·3·2·1 Hydrogen

Trapnell (143) has demonstrated that hydrogen chemisorbs at room temperature on films of platinum prepared by evaporation. Mignolet (159) has also shown that hydrogen adsorbs on evaporated films of platinum. He found that for hydrogen coverages $\theta_H \leq 0{\cdot}5$ hydrogen adsorption effected an increase of +0·15eV in the work function of the platinum surface. He interpreted this as evidence for adsorption of a tightly bound species. At higher surface coverages a weakly bound state was generated which gave a decrease in ϕ. The nett work function change was -0·23eV.

Lewis and Gomer (160) found that monolayer coverage of hydrogen on a platinum field emitter tip at low temperature led to a work function decrease of $\Delta\phi = -0{\cdot}3$eV. If the sample was heated the work function increased and reached a maximum, $\Delta\phi = +0{\cdot}15$eV at 250K. Desorption was complete at 320K.

In a LEED study of gas adsorption on the platinum (100)

single crystal surface Morgan and Somorjai (149) showed that hydrogen did not adsorb readily on Pt(100) unless the metal surface was clean, the temperature was in excess of 500°C, and the pressure greater than 2×10^{-5} torr.

Lang, Joyner and Somorjai (154) later showed that, like oxygen, hydrogen chemisorbed readily on stepped platinum surfaces although adsorption occurred with difficulty on the (111) and (100) crystal faces of platinum. Dissociation of the molecule occurred readily on stepped platinum surfaces as evidenced by a greatly enhanced rate of H_2/D_2 exchange.

Bernasek and Somorjai (161) confirmed this effect for hydrogen adsorption on smooth and stepped Pt(111). They found a difference in the rate of H_2/D_2 exchange of three orders of magnitude between smooth and stepped Pt(111). They also noted that the rate of exchange increased with increasing step density.

Christmann and Ertl (162) confirmed these results although they found that the differences between high and low index crystal planes were less than reported by Lang et al (154) and Bernasek and Somorjai (161). They also observed (162) that hydrogen adsorption on smooth Pt(111) faces led to a continuous decrease in work function, $\Delta\phi = -0{\cdot}23$eV at $\theta = 0{\cdot}8$. On a stepped Pt(111) surface, however, there was an initial increase in ϕ up to a maximum at $\theta \sim 0{\cdot}25$ followed by a decrease to a saturation value of $\Delta\phi = -0{\cdot}35$eV. The magnitude of the initial increase diminished as the adsorption temperature became higher. The increase in ϕ was attributed to adsorption of hydrogen on sites adjacent to the steps and the work function lowering to adsorption on the flat terraces.

Somorjai (147) later criticised Christmann and Ertl's work (162) on the grounds that near-monolayer surface coverages of hydrogen and deuterium were used so that the surface sensitivity of the reaction could be masked. Thus a less pronounced difference between high and low Miller index surfaces would be observed.

Although there is disagreement about the magnitude of the difference in rates of adsorption and dissociation of hydrogen on smooth and stepped platinum surfaces, it is generally agreed that at low surface coverages dissociation of hydrogen occurs most readily on high Miller index platinum surfaces (154), (161), (162). At higher pressures the difference between faces becomes less significant (162).

Christmann and Ertl's results (162) also explain the initial increase in ϕ observed by Mignolet (159) when hydrogen adsorption occurred on an evaporated platinum film, since here many high Miller index surfaces should be exposed.

Christmann and Ertl (162) showed that above room temperature hydrogen chemisorption no longer caused an increase in ϕ_{Pt}. They reported $\Delta\phi \sim 0$ up to $\theta \sim 0{\cdot}3$ and that it then started to decrease.

In general hydrogen adsorption is dissociative on platinum (154), (161), (162), so that chemisorption of hydrogen on a polycrystalline platinum filament should generate surface H. The work function should remain the same at low coverage (up to $\theta = 0{\cdot}3$) but as chemisorption proceeds ϕ will decrease.

Thus, if the hydrogen surface coverage is sufficiently extensive an enhancement of the exo-electron emission from the platinum wire should be observed. An examination of the

present results indicate that this is so. Some typical hydrogen results are shown in fig 43 and 44, Appendix 10. Copious exo-electron emission was observed from the platinum wire when the scaler-ratemeter was operating with the minimum energy discriminator setting of 0·1 x 0·2, Integrate; see fig 43. As the energy threshold was raised, however, emission decayed rapidly; see fig 44.

If the dissociative adsorption of hydrogen on platinum above room temperature leads to a lowering of the work function, and hence to enhanced exo-electron emission, then adsorption of any species which generates surface hydrogen should also increase exo-electron emission from the filament.

6·3·2·2 Hydrocarbons

The hydrocarbons investigated adsorb dissociatively on platinum to yield surface H and adsorbed carbonaceous species; see later for specific references. Adsorption of hydrocarbons on platinum leads to a lowering of the work function; see Table VIII page 124a.

Surface carbon may also be produced. For example, Lang (163) deposited carbon on several low and high index platinum surfaces by heating them in ethylene while Presland and Walker (158) generated a graphitic overlayer by heating platinum foil to 1000°C in the presence of acetylene at a pressure of about 1 torr.

The Pt-C system is characterised by the absence of carbide and also by a low solubility of carbon in platinum (163). Thus any carbon deposited stays at the surface. If the carbon-covered surface is heated to $T \geqslant 400$-500°C (163) or if the

carbon is deposited at high temperature (158) graphitisation occurs. Lang (163) found that a graphitic overlayer of limited thickness was formed.

Somorjai (147) has reported that the presence of a graphitic overlayer on platinum can lower the work function by leV for Pt(100) and by 1·1eV for Pt(111).

Thus adsorption of any hydrocarbon should lead to a lowering of ϕ and hence to the observation of chemically stimulated exo-electron emission.

Methane

Tesner and Rafal'kes (143) demonstrated that methane can generate carbon on platinum, which can effect a lowering of the work function (147).

Kemball (164) has shown that methane can chemisorb and undergo deuterium exchange on evaporated platinum films. Thus adsorption must be dissociative. However, in general methane is only adsorbed to a slight extent on most metals; see (165) for references.

No value for $\Delta\phi_{Pt}$ as a result of methane adsorption was found in the literature. However, Somorjai (147) reported that saturated hydrocarbons chemisorbed on platinum produce a lowering of the work function of 0·9 - 1·2eV with respect to the clean surface. Since methane adsorption is slight on platinum (165) then a work function decrease between 0 - 1eV might be predicted, depending on the surface coverage.

Since methane does not chemisorb to the extent of monolayer coverage of the platinum surface, continued heating and cooling of a platinum filament in Q gas, Ar/10% CH_4, should

lead to renewed methane adsorption during each cycle.

The presence of both surface carbon and carbonaceous species will lead to enhanced exo-electron emission from the platinum.

A typical Q gas cooling curve for a short heating experiment is shown in fig 28, Appendix 10. This structure was reproducible which indicates that methane adsorption on platinum is not extensive. It may be inferred that the surface does not become saturated.

Q gas gave differently shaped emission curves when the wire was pretreated with Ar/10% C_2H_2 or Ar/10% C_2H_4; see fig 30, 31, Appendix 10. The increased area under the peak indicates enhanced emission due to the presence of a greater number of ϕ-lowering species on the surface: both ethylene and acetylene adsorb readily on platinum (165).

The area under the Q gas cooling curve obtained after the wire was heated in argon/10% acetylene is greater. This accords with the fact that acetylene causes a greater lowering of the platinum work function; see Table VIII page 124a.

After the wire had been cycled in Ar/10% C_2H_6 several times it was then heated for 30 sec in Q gas and allowed to cool in it. The cooling curve obtained shows a different structure again; see fig 32, Appendix 10.

The sensitive dependence of the shape of the cooling curves on the nature of precursors suggests that valuable information will become available if further work is undertaken.

One conclusion which may be reached is that adsorption sites for methane differ from those for acetylene and ethylene since exo-emission is still observed from platinum cooling in

Ar/10% CH_4 when the surface is saturated with ethylene or acetylene.

Ethylene

Franken and Ponec (166) found that ethylene adsorbed readily on platinum films and that the work function decreased by 1·45eV when ethylene was introduced. When the system was evacuated ϕ increased to -1·2eV below that of clean platinum.

Morgan and Somorjai (149) found a maximum work function decrease of 0·76 $\pm$ 0·02eV when ethylene was allowed to chemisorb on a clean Pt(100) surface. The adsorbed species existed in an ordered array on the surface which could be represented by a centred c(2 x 2) mesh. It was found that surface carbon was deposited which inhibited the further adsorption of ethylene.

It has been reported by Baron, Blakely and Somorjai (167) that hydrocarbon chemisorption on low Miller index surfaces produced ordered surface structures and little or no chemical change in the adsorbed molecules in the pressure range investigated, $10^{-9} - 10^{-7}$ torr, and in the temperature range 300 - 500K. On high Miller index surfaces disordered adsorbate structure was found and carbonaceous deposits were generated since both C-H and C-C bonds are readily broken even at 300K and at pressures of $10^{-9} - 10^{-6}$ torr. Somorjai (147) reported a work function decrease of -1·5eV for ethylene adsorption on Pt(111) at 293K, and $\Delta\phi$ = -1·2eV for Pt(100) at 293K; see Table VIII page 124a.

On stepped platinum surfaces the nature of the carbonaceous deposits, which comprise carbon with an undetermined amount of hydrogen, depends on the hydrocarbon, surface temperature,

incident flux of the hydrocarbon and the orientation of the surface. With low Miller index surfaces ordered surface structures are formed. On heating, these give rise to a graphitic overlayer ~~regardless~~ independent of the orientation of the platinum substrate. Formation of a graphitic overlayer is favoured by a high incident flux of hydrocarbon at the surface.

Enhanced exo-electron emission should be observed when platinum is heated and cooled in Ar/10% C_2H_4. Typical ethylene results are shown in fig 33- 36, Appendix 10.

Allowing the platinum filament to cool in an Ar/C_2H_4 mixture produced cooling curves which depended for their shape on the past history of the wire. Fig 33 shows the cooling curve obtained when the platinum wire was heated in Ar/C_2H_4 after it had been heated in Ar/CH_4. A high level of emission is obtained, in keeping with the decrease in ϕ due to ethylene adsorption. A second heating and cooling cycle in Ar/C_2H_4 gave virtually no electron emission; see fig 36. Since ethylene adsorbs readily on platinum (149), (165) this result indicates that the platinum surface was saturated and the bond-breaking sites blocked. After the second ethylene cycle there was no emission when the wire was heated to 850 - 900°C in nitrogen. However, when the platinum wire was allowed to age overnight in nitrogen and was then heated and cooled in nitrogen several times, peaks were observed in the nitrogen cooling curves. This will be explained later.

Heating and cooling the platinum filament in Ar/10% C_2H_4 again gave a cooling curve whose shape differed from the first; see fig 35. This indicates the presence of different surface species, or at least changed proportions of the same ones.

Once again a second cycle gave no emission. Thus the surface had become saturated again, or at least emission was diminished so that the 'packets' of electrons were too low in energy to be counted.

Acetylene

Morgan and Somorjai (149) found that acetylene adsorbed on clean Pt(100) at room temperature to give a maximum work function change of $-1{\cdot}02 \pm 0{\cdot}02$eV. Again adsorption was ordered to yield a c(2 x 2) surface mesh. All features of the adsorption were more pronounced than for ethylene. More recently Somorjai (147) has reported a greater decrease in the work function of platinum after chemisorption of acetylene; see Table VIII page 124a.

Since the platinum work function decreases, enhanced exo-electron emission was predicted when platinum cooled in Ar/C_2H_2.

Ar/10% C_2H_2 was first introduced to the platinum wire after it had been exposed to Ar/C_2H_4. Surprisingly, virtually no emission was observed and there was no structure in the cooling curve; see fig 38, Appendix 10. However, ageing the wire overnight in nitrogen again regenerated the surface sites, and with the next exposure of platinum to Ar/C_2H_2 electron emission was observed although there was no peak in the cooling curve; see fig 37, Appendix 10. Subsequent heating and cooling in Ar/C_2H_2 gave no emission, see fig 39, which demonstrated that, like ethylene, acetylene quickly saturated the surface of the platinum filament.

The wire was heated and allowed to cool in Ar/C_2H_4 after

it had been saturated with acetylene. Electron emission was observed and there was a sharp peak in the cooling curve; see fig 34, Appendix 10. This shows that acetylene adsorption regenerates some of the ethylene adsorption sites, although ethylene does not have the same effect for acetylene adsorption on platinum.

A similar result has been reported by Yasumori, Shinohara and Inoue (168) who found that preadsorbing acetylene prevented poisoning or restored the activity of a palladium film for the hydrogenation of ethylene.

When acetylene was introduced to the platinum filament after it had been heated in Q gas, reproducible cooling curves were obtained, see fig 40, Appendix 10, whose structure was very different from previous acetylene cooling curves which were generally preceded by ethylene. The reproducibility of the curves implied that acetylene was not saturating the platinum surface.

Butadiene

Butadiene (169) is expected to behave in a manner similar to acetylene. No value for its effect on the platinum work function was found. However, Somorjai (147) has observed that unsaturated hydrocarbons generally effect a work function lowering of around 1·3 - 2·0eV when adsorption occurs on Pt(100) or Pt(111). Thus the work function decrease associated with adsorption of butadiene on platinum should fall in this range. The characteristic cooling curves, see fig 41, Appendix 10, were of the same shape as those for acetylene; see fig 37, Appendix 10.

The main difference, however, was that Ar/butadiene gave such a curve reproducibly during several heating-cooling cycles which implied that butadiene did not saturate the platinum surface as readily as acetylene.

Ethane

Like methane, ethane is only adsorbed to a slight extent on most metals; see (165) for references. However, ethane chemisorbs more readily (165) and also undergoes deuterium exchange more readily (170).

No value was obtained for the change in the platinum work function associated with ethane adsorption. However, a work function decrease in the range 0—-1·0eV would be expected depending on the surface coverage, and increased exo-electron emission would be predicted.

Dowie, Whan and Kemball (171) studied the hydrogenolysis of saturated hydrocarbons on evaporated platinum films with a deuterium:hydrocarbon ratio of 11.5:1 to minimise poisoning of the catalyst. It was observed that reactions of ethane were characterized by an induction period during which hydrogenolysis to methane occurred slowly. Subsequently the reaction followed zero order kinetics with respect to ethane at an increased rate. For a second experiment on the same platinum film the induction period was reduced to approximately half that of a first experiment and the hydrogenolysis quickly accelerated to a subsequent rate comparable to that for the first reaction.

These findings may be used to explain the results obtained in the present system when the platinum filament was exposed to

Ar/10% C_2H_6.

The cooling curves obtained are shown in fig 42, Appendix 10.

The lack of emission in the early cycles corresponds to the induction period observed by Dowie et al (171). Then the emission rate increased as the number of heating cycles in Ar/C_2H_6 increased. It may be inferred that the rate and extent of adsorption also increased.

6·3·3 Nitrogen

It has generally been reported that nitrogen does not chemisorb on platinum. For example, Trapnell (148) found no adsorption of nitrogen on polycrystalline platinum, while more recently in LEED studies of adsorption, e.g. (149), no evidence of nitrogen adsorption was found.

Wilf and Dawson (142) have demonstrated that nitrogen adsorbs dissociatively on platinum at room temperature, but only after any carbon contamination is removed from the surface by heating the platinum filament in oxygen. This study was carried out on a platinum filament, which will be polycrystalline, at pressures in the region 7×10^{-8} torr. It was observed that the carbon monoxide content of the background gas had to be substantially reduced otherwise carbon monoxide chemisorbed on the platinum in preference to nitrogen. Since the platinum filament underwent prolonged heating in oxygen, Wilf and Dawson suggested that irreversible incorporation of oxygen into the lattice might serve as active centres for dissociation of nitrogen molecules. As an alternative they suggested that dissociation might occur at surface defects or

grain boundaries. These workers also reported a low temperature weak adsorption of molecular nitrogen which had an activation energy for desorption of 12·6 kJ mol^{-1} when the low temperature state was fully occupied.

Shigeishi and King (172) have also reported weak molecular adsorption of nitrogen on platinum. They found the heat of adsorption was less than 50 kJ mol^{-1}, hence desorption will occur around room temperature. They investigated a Pt(111) oriented ribbon. Shigeishi and King only observed adsorption at 120K. It was also noted that adsorbed nitrogen was readily displaced by carbon monoxide, hydrogen and oxygen.

Weak reversible adsorption of molecular nitrogen on platinum has also been reported by, for example, Van Hardeveld and Van Montfoort (173), by Egerton and Sheppard (174) and by Niewenhuys and Sachtler (175). Egerton and Sheppard investigated silica-supported platinum. The ready displacement of nitrogen by carbon monoxide, hydrogen and oxygen was also confirmed.

It is apparent that nitrogen will only adsorb on platinum at or above room temperature if the metal surface is clean and the system is free of contaminants. The results obtained in the present study, see fig 49 - 51, Appendix 10, confirm this since emission was observed from a platinum wire cooling in nitrogen (or hydrogen) before the wire was heated in a hydrocarbon. After carbiding of the wire appreciable emission from platinum cooling in nitrogen was only observed if the wire had been heated in oxygen in the previous cycle.

Peaks in the nitrogen cooling curves were also observed after prior exposure of the wire to Q gas or hydrogen. When

the wire was saturated with ethylene or acetylene no emission was observed if it was heated in nitrogen. After allowing the wire to age for several hours, however, peaks were observed in the cooling curves. The level of emission was low however. This effect will be explained later.

6·3·4 Argon

Mignolet (176), (177) investigated the change in surface potential when non-polar particles were physically adsorbed on metals. He found that with xenon, methane, ethane or ethylene, for example, there was an increase in surface potential.

On the basis of this work an increase in surface potential might be predicted for argon; in other words exo-electron emission would be made easier.

In fact the argon results indicated that an appreciable level of emission was obtained. Since a continuous flow of gas passed through the detector, any hydrogen or hydrocarbons desorbed from the wire as it was heated in argon would be swept away so that cooling curve peaks could not be due to re-adsorption of such species. The shape of the peaks also depended on the precursors; see fig 45- 48, Appendix 10. When the wire was heated and cooled in argon after prior exposure to Ar/CH_4 or CH_4 a double peak was obtained. After Ar/C_2H_4 no structure was observed while after Ar/C_2H_2 a maximum of emission occurred at 50°C. Emission peaks were also recorded when platinum cooled in argon after pretreatment of the wire with butadiene or ethane. The fact that the peaks vary in shape proves that this effect is not due to any impurity in the argon.

Since neither chemisorption nor surface reaction would be

expected with argon, the possibility is suggested that the emission peaks might be the result of surface rearrangement of the platinum due to the presence of residual species on the surface. This idea has been suggested because surface rearrangement was one of the methods of producing exo-electron emission proposed earlier on the basis of the literature evaluation.

Such a mechanism might also be invoked to explain nitrogen cooling curve peaks from ethylene, acetylene or even methane pretreated platinum.

6·4 Temperatures of the Emission Maxima

By inspection of the cooling curves presented in Appendix 10, several common temperatures of the emission maxima became evident. Some values are given below; see Table IX page 142a.

By inspection of Table IX the following common features became apparent.

(1) An emission maximum was obtained in the temperature range 46 - 48°C after the wire was pretreated with Ar/CH_4, Ar/C_2H_6 or CH_4; that is after pretreatment of the wire with saturated hydrocarbons.

(2) The peak at 50 - 51°C was obtained after pretreatment of the wire with Ar/C_2H_2, Ar/C_2H_4 or Ar/butadiene; that is after pretreatment with unsaturated hydrocarbons. Ar/CH_4 also gave rise to an emission maximum in this temperature range early in the history of wire 5, or when it was followed by Ar/C_2H_2.

(3) An emission maximum was found at 54 - 56°C after pretreatment of the wire with Ar/CH_4 or Ar/C_2H_2.

Table IX

Gas in which cooling curve peak obtained	Peak temperature (°C)							Pretreatment
Argon			48		56			Ar/methane, methane
				50				Ar/acetylene
				51				Ar/butadiene
			46					Ar/ethane
Q gas							110	N_2,H_2,Ar,Q gas, O_2(N_2 flush)
							110	Acetylene
					66			Ar/ethylene
						77		Ar/acetylene
						76		Ar/ethane
		28						Early in history of wire 5.
Ar,10% ethylene			46		56			Ar/methane
					54			Ar/acetylene
				51				Ar/ethylene (aged in N_2)
Ar,10% acetylene				51		77		Ar/methane
Ar,10% ethane						78,79		Ar/ethane
Hydrogen	16	28	47					Ar/methane
Nitrogen							>100°C	

(4) A fourth common temperature for emission was found at 76 - 79°C after pretreatment of the wire with Ar/C_2H_2, Ar/CH_4 or Ar/C_2H_6.

(5) When the wire was pretreated with N_2, H_2, Ar, C_2H_2, Q gas or oxygen (with nitrogen flush), a Q gas cooling cycle yielded an emission maximum at 110°C.

(6) Early in the history of wire 5, when Q gas gave rise to an emission maximum at ~50°C, there was also a pronounced maximum at 28°C; see fig 28a, Appendix 10 for a typical cooling curve.

(7) At the same stage in the history of wire 5, hydrogen gave peaks in its cooling curve at 47 and 28°C. These peaks were obtained after pretreatment of the wire with Q gas. The hydrogen results are not reliable, however, and should only be taken as a guide.

(8) It was impossible to obtain an accurate temperature for nitrogen peaks since these often arose within the first 30 sec of the cooling cycle, when the temperature of the wire was still falling quickly. In general nitrogen emission temperatures were above 100°C.

The emergence of a series of common temperatures for emission maxima suggests the presence of common surface species. This is reinforced by the fact that some of the temperatures are found only after pretreatment of the wire with saturated hydrocarbons.

Other emission temperatures are common to both saturated and unsaturated hydrocarbons. This could indicate the formation of a surface species common to the hydrocarbons investigated, presumably after dissociative chemisorption onto the platinum surface.

6·5 Surface Rearrangement

6·5·0

If this idea of surface rearrangement is used in the interpretation of the results in this thesis, then the following schematic representation might be considered as a guide to the remainder of the thesis.

The sequence of events on a surface might be the following.

(1) Adsorption on a Clean Surface.

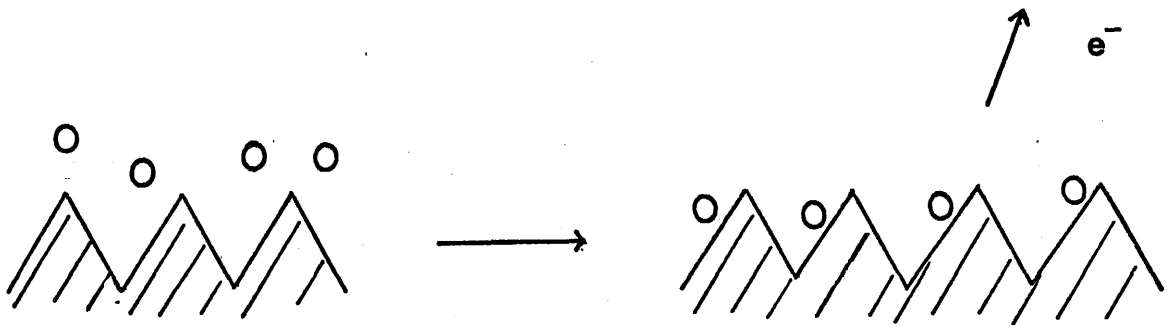

(2) Atomic Rearrangement of a Saturated Surface.

(3) Rearrangement of a Surface to give Faceting

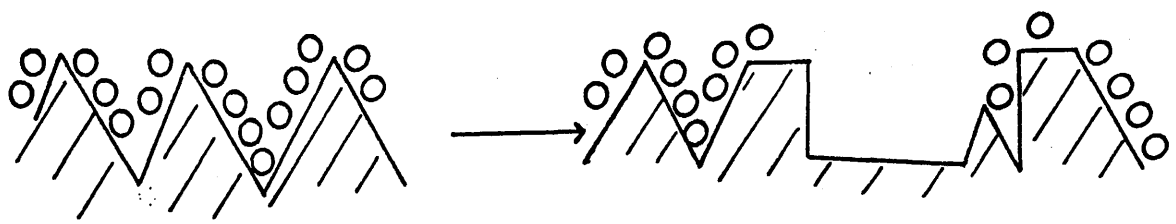

Faceting leads to exposure of fresh platinum. This may be followed by step 1.

Surface rearrangement will be discussed under two headings. The first is reconstruction which takes place on an atomic scale and which corresponds to event 2 in the scheme. The second is macroscopic surface rearrangement, or faceting, which corresponds to event 3 in the scheme.

6·5·1 Surface Reconstruction due to Gas Adsorption/Desorption

6·5·1·0

Many, well-documented examples of metal surface reconstructions are known from LEED studies of clean metal surfaces and the adsorption of gases on these clean, well-defined surfaces.

6·5·1·1 Definition

A clean surface is said to have undergone reconstruction if its LEED pattern indicates the presence of a surface unit mesh which is different from the (1 x 1) unit mesh that is expected from the projection of the bulk X-ray unit cell (179). Surface reconstruction is a means of lowering the surface free energy of a crystal face if the bulk-like (1 x 1) mesh does not represent the surface configuration of minimum energy.

6·5·1·2 Some Examples of Surfaces which undergo Reconstruction

In a review of the structure of solid surfaces Somorjai and Kesmodel (179) reported that several low Miller index surfaces undergo reconstruction. Some examples are the (111), (100) and (110) surfaces of silicon and germanium, the (111)

face of diamond and the (100) and (110) surfaces of platinum, gold and iridium.

If the surface is clean, such that no contamination shows up on an Auger Electron Spectrum, then a Pt (100) surface is found through LEED to have a (5 x 1) surface unit cell, where some of the diffraction spots are split into doublets or triplets (149). Clean gold (100) and iridium (100) are also characterised by a (5 x 1) surface structure (145) while for clean Pt (110) the surface unit cell is an apparent (1 x 2) mesh.

6·5·1·3 Unreconstructed Surfaces

For each of these metals the surface geometry in the (100) and (110) planes which gives rise to a (1 x 1) unit mesh is the metastable state. The clean (1 x 1) surface may, however, be prepared by indirect means. For example Bonzel, Helms and Kelemen (180) reported the preparation of Pt (100) - (1 x 1). They found that for the clean metal this arrangment was stable to 125°C but that above this temperature the surface reverted to a (5 x 20) arrangement. Because of the splitting of some of the diffraction spots Bonzel et al took the surface unit cell for Pt (100) to be (5 x 20) instead of (5 x 1) (149).

6·5·1·4 Stabilisation of the Unreconstructed Surface

The presence of adsorbed species stabilises the (1 x 1) surface. For example, Bonzel and co-workers (180) observed that the presence of small concentrations of surface carbon raised the (1 x 1) → (5 x 20) transformation temperature from 125°C for the clean metal to over 400°C.

6·5·1·5 Surface Reconstruction during Adsorption and Desorption on Platinum

C_3O_2

Lambert and co-workers studied the adsorption of various linear molecules on clean platinum surfaces; see for example (181). In a study of carbon suboxide, C_3O_2, adsorbed on Pt (110) to generate surface carbon Reed and Lambert (181) observed the following sequence.

$$C_3O_{2_{ads}} \xrightarrow{\text{fast}} 2CO_{(a)} + C_{(a)} \xrightarrow{\text{slow}} 2CO_{(g)} + C_{(a)}.$$

LEED investigation of the clean surface revealed a (1 x 2) pattern. The following sequence emerged from a LEED study of the adsorption process. Pt (1 x 2) $\xrightarrow{320K}$ Pt (1 x 1) occurred rapidly. Above 440K the (1 x 2) pattern started to reappear. Above this temperature desorption of CO became significant. The desorption rate reached a maximum at 513K. By then the (1 x 2) surface mesh was fully re-established.

C_2N_2

Netzer (182) exposed Pt (100) - (5 x 1) to C_2N_2 in the hope that CN species would be generated on the surface. He found that the initial adsorption at room temperature gave rise to a diffuse diffraction pattern corresponding to a (1 x 1) surface unit cell. At 200°C the diffuse (1 x 1) pattern became sharp. This corresponded to a desorption peak in the flash desorption spectrum at 190 $\pm$ 10°C. Between 600 and 650°C the (1 x 1) surface structure vanished and the (5 x 1) structure reappeared. At 500 $\pm$ 10°C and 600 $\pm$ 10°C a peak and a shoulder were observed in the flash desorption spectrum which corresponded to the

reappearance of the (5 x 1) pattern. There was also a desorption peak at 240 ± 10°C which was attributed to desorption of CN from the surface.

Similar changes in the surface structure were observed by Netzer with carbon monoxide. Thus it may be observed that the phenomena of surface reconstruction and adsorption and desorption are closely linked although desorption need not always accompany, or be due to surface reconstruction.

Bridge and Lambert (183) studied the adsorption of C_2N_2 on Pt (110) - (1 x 2). They observed reconstruction of the surface to a (1 x 1) mesh. If the sample was subsequently heated to 700K the (1 x 2) structure was restored.

NO

In a study by Comrie, Weinberg and Lambert (184), the adsorption of NO on Pt (111) and Pt (110) was monitored. With Pt (110) the (1 x 2) → (1 x 1) transformation was confirmed and it was shown that the surface reconstruction was complete at essentially monolayer coverage.

Clean Pt (111), however, gives a (1 x 1) LEED pattern and no significant change was observed as NO coverage increased.

6·5·1·6 Surface Reconstruction during Adsorption and Desorption on Iridium

Carbon

Reconstruction of Ir (111) has not been observed either (185). The surface rearrangements of Ir (100) are more complex than those for Pt (100) however, since more than one

rearrangement occurs. For example during adsorption of C, perhaps from C_2H_2, C_2H_4 or C_6H_6, Kanski and Rhodin (185) observed the following sequence:

Ir (100) - (5 x 1) $\xrightarrow[RT]{\text{adsorption}}$ (1 x 1) $\xrightarrow{400K}$ c(2 x 2) spot and fractional order (5 x 1) spots disappear

$\downarrow$ 700K, 1 min

(5 x 1) returns $\xleftarrow[30\ min]{1500K}$ (1 x 1) $\xleftarrow[1\ min]{1000K}$ max. intensity c(2 x 2)

due to diffusion of C into the bulk.

NO (185a)

Adsorption of NO on Ir (100) yielded a similar sequence although the transformation temperatures were different.

Ir (100) - (5 x 1) $\xrightarrow[RT]{NO}$ (1 x 1) $\xrightarrow{450K}$ (2 x 1)

$\downarrow$ 1200K

(5 x 1) $\xleftarrow{1500K}$ (1 x 1)

A flash desorption peak was recorded at 350K which corresponded to loss of weakly bound species. A second peak was observed at 500K which corresponded to loss of nitrogen. This was preceded by the Ir (1 x 1) → (2 x 1) transformation which occurred at 450K. A third flash desorption peak was observed at 1250K due to oxygen desorption. The (2 x 1)→(1 x 1) surface reconstruction took place at 1200K.

Again the close correlation between surface reconstruction and desorption may be noted.

The change in work function of the iridium surface was also monitored by Kanski and Rhodin (185a) as its exposure to NO increased; see fig 26.

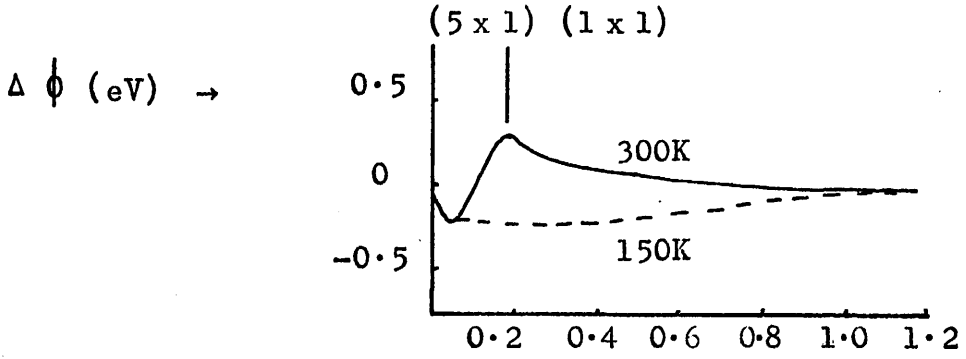

figure 26

Ir(100) - (5 x 1) + NO

Work function dependence on NO coverage at 150 K and at 300 K.

At an NO coverage of θ = 0·2 a remarkable work function change was observed which was attributed to the complete and sudden dissociation of NO when the hexagonal (5 x 1) Ir array superposed on the (100) surface transformed to a (1 x 1) array.

Although such drastic effects have not been found with Pt surfaces it is clear from these observations that a very strong correlation exists between the geometrical arrangement of the surface atoms and the capability of the surface for adsorption.

6·5·1·7 Dependence of Surface Electronic Structure on the Geometry of the Surface Atoms

It has been shown by Bonzel and coworkers (180) that the different surface arrangements lead to markedly different surface electronic structures, as determined by ultraviolet photoelectron spectroscopy, UPS. They examined clean Pt (100) - (5 x 20) and Pt (100) - (1 x 1). Fig 27 page151a, shows the UPS spectrum for a photon energy of $h\upsilon$ = 40·8eV.

A peak at 0·25eV below the Fermi level was evident for Pt (100) - (1 x 1). From this was inferred the presence of unsaturated surface bonds. This was confirmed since the chemisorption properties of the (1 x 1) and (5 x 20) surfaces are different. Neither O_2 nor H_2 chemisorb at room temperature and low pressure on Pt (100) - (5 x 20) while Bonzel et al have observed sticking coefficients ranging from 0·1 - 1·0 for both these gases on the clean (1 x 1) surface.

Bonzel et al compared UPS spectra for different degrees of exposure of Pt (1 x 1) to CO at 50°C. The 0·25eV peak disappeared after only a very low exposure which proved that it corresponded to the unsaturated surface bonds.

6·5·1·8 Possible Correlation between Surface Reconstruction and Exo-Electron Emission

Since surface reconstruction is so closely linked with adsorption and desorption on the (100) and (110) crystal faces of platinum, it is not unreasonable that this effect might contribute to exo-electron emission. Surface reconstruction may take place even at room temperature (182).

figure 27.

UPS energy distribution curves for a clean Pt(100) surface, $h\nu = 40{\cdot}8$ eV. Dashed curve, difference spectrum between (1x1) and (5x20) structure.

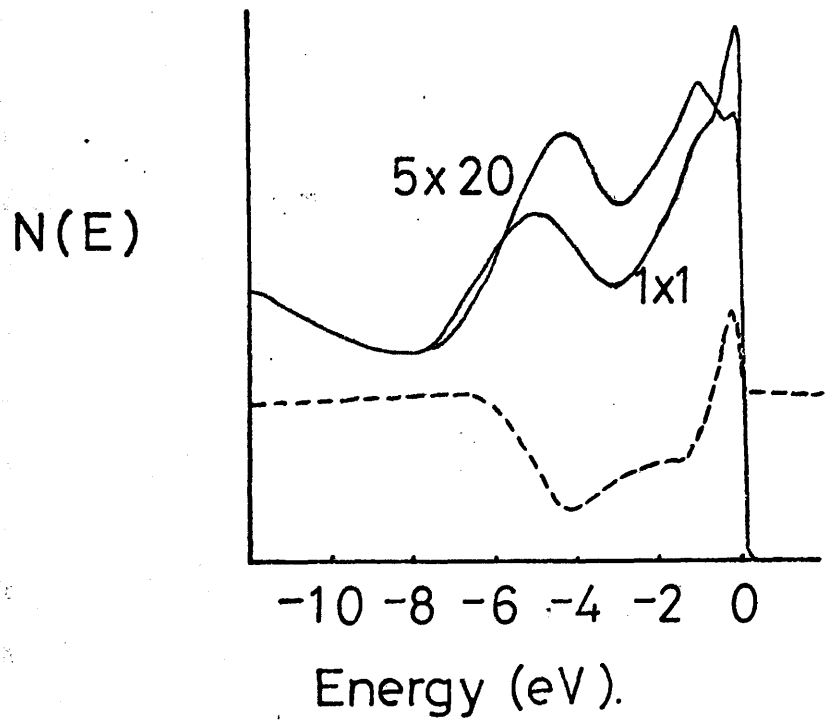

Although the changes in the surface unit cell dimensions have been recorded during flash desorption experiments, surface reconstruction should occur in the reverse sequence as a surface capable of reconstruction is allowed to cool. Thus surface reconstruction could lead to exo-electron emission when the platinum wire, on whose surface carbonaceous species are present, is allowed to cool in argon, or any of the other gases investigated, work function permitting.

Since maxima of exo-electron emission are observed when the wire cools in argon after prior exposure to hydrocarbons, the surface reconstruction would have to be due to interactions of the carbonaceous species on the surface.

However, surface reconstruction can not be invoked to explain the fact that after heating the wire more than once in ethylene or acetylene no more emission was observed, yet after ageing the platinum filament was capable of emitting again, and, by inference, capable of adsorption again.

Thus a mechanism for the production of fresh adsorption sites had to be found. To this end the possibility of gross surface rearrangement was considered.

6·5·2 Surface Rearrangement

6·5·2·0

As well as atomic reconstructions, surface rearrangements have been observed on a macroscopic scale.

6·5·2·1 Examples of Surface Rearrangement of Platinum in the Presence of Oxygen

It has been shown by many workers, for example Collins, Lee and Spicer (186), that prolonged heating of recrystallised platinum ribbons in oxygen at high temperature (T ~1120K) and under high vacuum (10^{-6} torr oxygen) leads to a preferentially (111) oriented surface.

Ducros and Merrill (187) studied the adsorption of oxygen on platinum. They considered adsorption to be more likely on a carbon-contaminated platinum surface. A stepped or severely etched Pt (111) surface was more active than a well oriented Pt (111) surface. Ducros and Merrill thus concluded that the presence of surface defects was important for oxygen chemisorption.

The (110) surface in the face-centred cubic system is composed of close-packed rows with a second series of close-packed rows below the surface plane. Ducros and Merrill pointed out that unreconstructed Pt (110) - (1 x 1) could be considered to comprise monatomic Pt (111) steps, while the reconstructed Pt (2 x 1) surface was made up of tilted micro-facets of (111) crystallography. In the face-centred cubic system the (111) face is expected to be most stable so that Ducros and Merrill viewed reconstruction as a growth of micro-facets of more favoured geometry.

If a perfect (110) surface faceted a (1x 3) array might be expected to evolve as large facets of (111) orientation developed. Ducros and Merrill believed that a (1 x 2) surface array was not unreasonable since no large facets of (111) orientation were observed.

They found that the Pt-O phase formed by oxygen

adsorption on Pt(110) was stable to temperatures in excess of 1000K. They further observed that if the crystal was heated for extended periods at 1300K, especially in oxygen, areas of (1 x 3) structure were in fact observed. Even then, however, no large facets were evident.

Pareja, Amariglio, Piquard and Amariglio (188) have demonstrated that considerable surface rearrangement may also occur at much lower temperatures. They heated a platinum ribbon for long periods at 260°C in the presence of traces of oxygen (H_2 + 2000 ppm O_2). The surface rearrangement which resulted could be easily observed with an optical or scanning electron microscope.

Surface rearrangements initiated by adsorption have been observed by methods other than LEED. For example, Pareja et al (188) employed optical and scanning electron microscopes to investigate surface change. Jech (189) studied gaseous adsorption on kryptonated platinum films by employing Kr as a radiotracer. He found that when oxygen was introduced no krypton was released. If, however, hydrogen was introduced to the oxygenated surface there was a considerable release of krypton. Water adsorption on the platinum surface also liberated krypton although Jech found that less krypton was released after water introduction.

Jech thus deduced that chemisorption of hydrogen or water caused surface rearrangement to occur.

6.5.2.2 Surface Rearrangement of Platinum Wire 5

It was shown earlier that it was necessary in the present

study to expose a platinum wire to air at room temperature after it was first heated in methane in order that reproducible cooling curves might be obtained. Since heating the platinum filament in pure, dried oxygen did not produce this effect, it is reasonable to conclude that the water vapour present in atmospheric air must have some effect on the platinum surface. Jech (189) showed that water adsorption caused a surface rearrangement. Thus water adsorption may enhance grain growth with a surface crystallography suitable for hydrocarbon chemisorption.

To determine whether surface rearrangement had occurred because of chemisorption processes occurring at the surface of the platinum wire under investigation, a sample of untreated wire was examined by Mr S. Orr in a Philips P.S.E.M.500 scanning electron microscope. The micrographs thus obtained, see Micrographs 1, 2 pages 155a,155b, were compared with those obtained from a sample taken from wire 5; see Micrographs 3, 4 pages 155c, 155d.

This provided clear evidence that extensive surface rearrangement had occurred. The micrographs of the untreated wire show the effects of cold working on the wire. The surface is rough and the grooves which run parallel to each other are caused by the extrusion process.

After chemical treatment all the surface damage in wire 5 had been removed. Treatment at high temperature will anneal out surface damage. Grain growth was pronounced. The white marker lines on the photographs are 10μ. Thus it may be seen that many of the grains are extremely large. The surfaces of some platinum crystals remained perfectly smooth while others showed evidence of considerable roughening, indicative of the

Micrograph 1

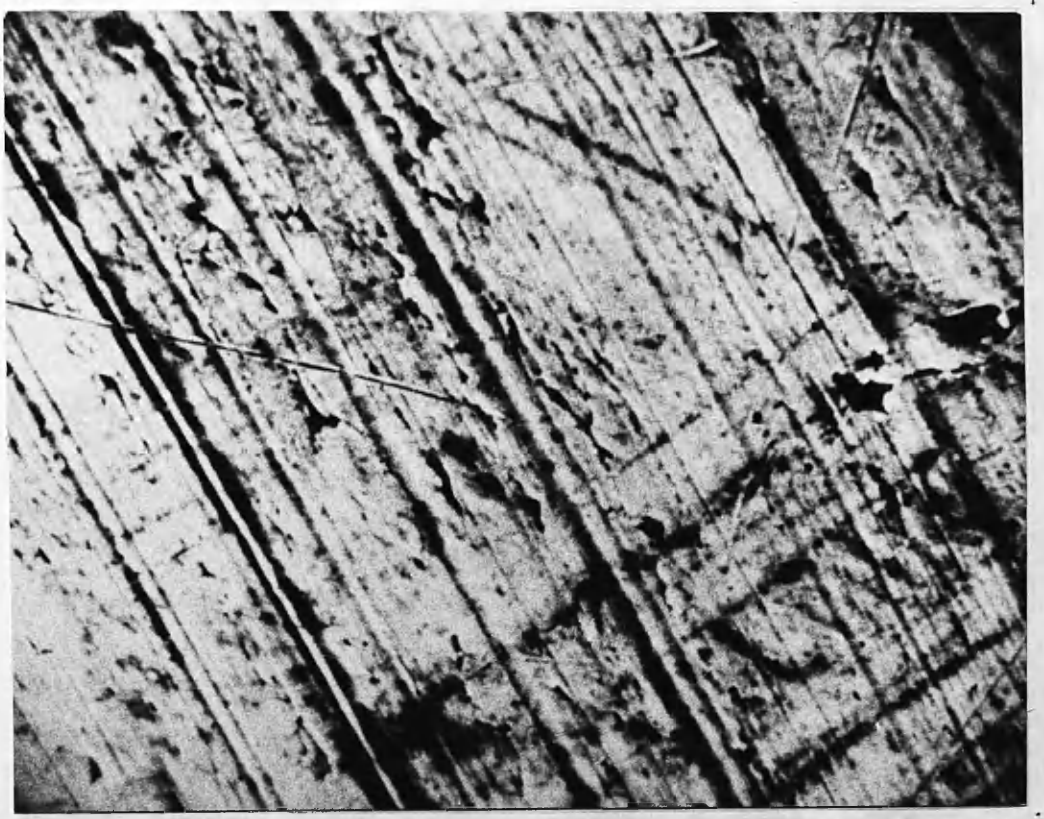

Micrograph 1 shows the state of the surface of the platinum wire when it was introduced into the counter.

Magnification x2,500

Micrograph 2

Micrograph 2 shows another typical area of 'virgin' platinum.

Magnification x2,500

Micrograph 3

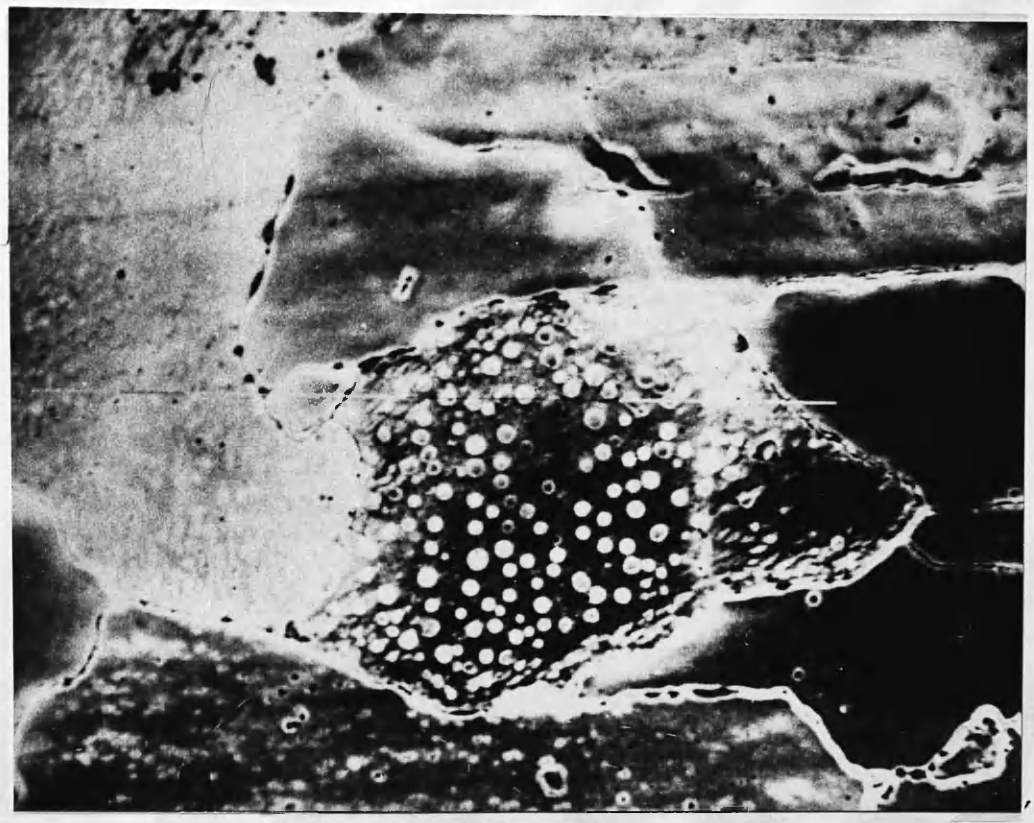

Micrograph 3 shows a typical area of platinum in a sample taken from wire 5 after all the experiments had been completed.

Magnification x2,500

Micrograph 4

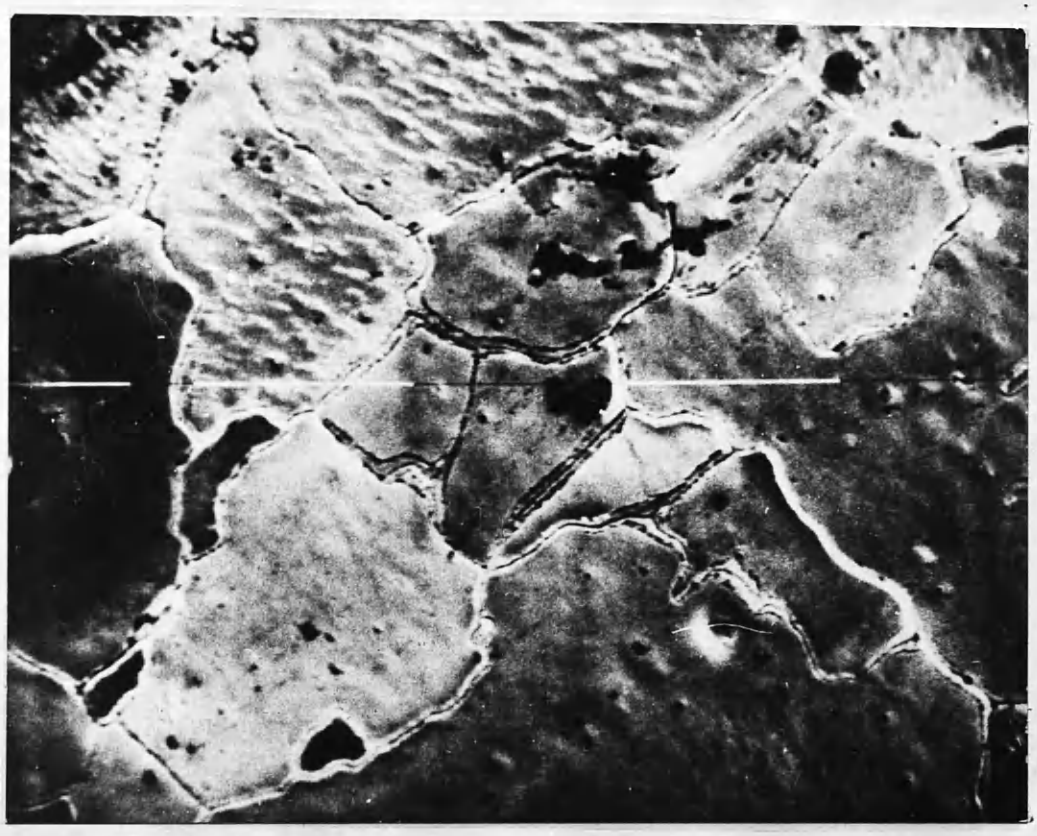

Micrograph 4 shows another typical area of the platinum surface after completion of the experiments carried out on wire 5.

Magnification x2500

early stages of faceting. Others showed circular structure on the surface which was believed to be structures on the surface rather than holes etched into the metal.

To determine the cause of the surface rearrangement, the grain growth and faceting, a sample of wire which had been heated to dull orange heat (T ~750 - 800°C) for 30 minutes in a flow of 4ml/sec of oxygen was also examined; see Micrograph 5 page 156a.

There was little change in the surface of the platinum wire. Platinum is reputed to have a strong tendency to facet when it is heated in oxygen ((186)-(188)) even at low pressures. However, these micrographs indicate that hydrocarbons must have a considerable influence on the stability of some platinum crystal surfaces while other surfaces remain relatively unchanged.

Since a polycrystalline platinum wire was used for this exo-electron emission investigation, many different platinum faces of high and low Miller index will be exposed. Thus a comparison of the properties of different crystallographic faces of platinum would be useful.

6·6 A Comparison of Low and High Miller Index Platinum Surfaces

6·6·0

Somorjai's group has investigated the stability of many low and high Miller index surfaces; see (147) for a review of the work.

It was shown by Lang, Joyner and Somorjai (190) that when a freshly prepared high Miller index platinum surface is heated it rearranges to give terraces of low index planes separated by steps often one atom in height. The appearance of such ordered

Micrograph 5

Micrograph 5 shows a typical area of a platinum surface after a length of 'virgin' platinum was annealed for 60 min at 750 - 800°C in a flow of 4ml/sec oxygen.

Magnification x2,500

structures is not confined to platinum. It has also been observed with, for example, germanium, gallium arsenide, copper and uranium dioxide; see (190) for references.

6·6·1 A Nomenclature for High Miller Index Surfaces

A nomenclature was devised (190) to describe high index surfaces to facilitate comparisons between them. Thus Pt (755) may be denoted Pt (S)-[6(111) x (100)] which indicates that this surface comprises terraces of (111) orientation six atoms wide separated by monatomic steps of (100) orientation. (S) denotes a stepped surface. Pt (911) may be represented as Pt (S)-[5(100) x (111)]. Thus Pt (911) is made up of terraces of (100) crystallography on average five atoms wide. The monatomic steps between the terraces have (111) orientation.

6·6·2 Thermal Stability of Platinum Surfaces in Vacuum

Lang, Joyner and Somorjai (190) investigated the thermal stability of three stepped platinum surfaces which may be designated Pt (S)-[9(111) x (111)], Pt (S)-[6(111) x (100)] and Pt (S)-[5(100) x (111)]. They found that each of the three ordered structures was stable in vacuum up to 1500K.

Lang et al observed that if Pt (S)-[9(111) x (111)] was heated in 10^{-5} torr oxygen to 950-1100K and then allowed to cool in oxygen, the surface became disordered with terrace widths greater and less than 9. However, vacuum annealing at 800K restored the surface to its original ordered state.

McLean and Mykura (191) demonstrated that surfaces close to the (111) orientation were stable with respect to faceting up to 1900K. This is because the (111) surface is the

configuration of lowest surface free energy for the crystal faces of a face-centred cubic solid. Surfaces close to the (100) face were found to be less stable: faceting commenced above 1500K.

This thermal stability is surprising since a rearrangement to unstepped (100) or (111) faces would be predicted from thermodynamic considerations and since platinum diffusion on the surface is rapid at temperatures as low as 900K. However, Lang, Joyner and Somorjai (190) suggested that there was no energetically feasible route by which these ordered, stepped surfaces could rearrange to thermodynamically more favoured structures.

Schwoebel (see (190)) has considered the problem theoretically. He examined the time-dependent change in terrace width as a function of the capture probability at a step of atoms arriving from different directions and of their detachment probability from a step.

His model indicated that for certain values of the capture and detachment probabilities a stepped surface can be stable, while for other values coalescence of steps could take place, leading to steps of multiple height, the first stage of faceting of a surface.

6·6·3 Thermal Stability of Platinum Surfaces in the Presence of Adsorbates.

6·6·3·1 Thermal Stability of Platinum Surfaces in the Presence of Hydrocarbons

The thermal stability in vacuum and in the presence of hydrocarbons, oxygen or hydrogen of various stepped surfaces of

platinum has been investigated by Somorjai's group.

For example, Baron, Blakely and Somorjai (167) compared and contrasted the behaviour of Pt (S)-[9(111) x (100)], Pt (S)-[6(111) x (100)], Pt (S)-[7(111) x (310)] and Pt (S)-[4(111) x (100)] during the chemisorption of n-heptane, toluene, benzene, ethylene and cyclohexane. Three of the four surfaces, the [9(111) x (100)], [6(111) x (100)] and [7(111) x (310)] could be heated above 1000°C in vacuum or in the presence of hydrocarbon without marked restructuring. In vacuum the [4(111) x (100)] surface faceted at temperatures above 900°C, while in the presence of hydrocarbon or hydrogen faceting occurred at temperatures as low as 300°C.

There were found to be four competing processes:

(1) nucleation and growth of ordered carbonaceous surface structures,

(2) dehydrogenation, i.e. breaking C-H bonds in the adsorbed organic molecules,

(3) decomposition of the organic molecules, i.e. breaking both C-H and C-C bonds at steps,

(4) rearrangement of the substrate by faceting.

Processes (1) and (2) were found to predominate on the [9(111) x (100)] and [6(111) x (100)] surfaces where the terraces between the steps are broad and the surface approximates more closely to a low Miller index surface. Process (3) was most important with Pt[7(111) x (310)] where there are kinks in the steps at frequent intervals. Process (4) predominated on [4(111) x (100)].

Thus it is obvious that different high Miller index

surfaces behave differently in the presence of hydrocarbons.

6·6·3·2 Thermal Stability of Platinum Surfaces in the Presence of Surface Carbon

Lang (163) showed that for low carbon doses ordered structures were formed on high index faces of platinum. However, as carbon dose increased the stability of the stepped surface decreased and faceting became more likely. Lang compared Pt (100), Pt (111), Pt (S)-[5(100) x (111)] and Pt (S)-[6(111) x (100)].

He found that a graphitic overlayer was formed on Pt (100) at temperatures $T \geq 400°C$ while some faceting occurred above 500°C. On the stepped (100) surface faceting commenced above 425°C. By contrast Pt (111) did not facet although the stepped Pt (111) surface underwent faceting above 600°C.

6·6·3·3 A Comparison of the Thermal Stability of Platinum Surfaces in the Presence of Chemisorbed Oxygen or Carbon

In a recent study Blakely and Somorjai (192) investigated the stability of twenty-two high Miller index surfaces of platinum in vacuum and in the presence of a monolayer of chemisorbed oxygen or carbon.

Unlike Lang (163) they found that the Pt (100) surface was stable under all their conditions. It was stable to 1600°C in vacuum, gave a stable graphitic overlayer and did not rearrange after carbon was deposited. Further, it was stable to temperatures $T \geq 1500°C$ in the presence of oxygen. However, there may have been a greater deposit of carbon on the surface in Lang's study. Alternatively, Blakely and Somorjai (192)

suggested that since only some of the (100) surface faceted, the rearrangement might have been due to the presence of surface contamination or defects. This demonstrates the sensitivity of a surface to the exact experimental conditions, and to the extent of surface contamination or surface carbon.

6·6·3·4 Interpretation of the Results using a Stereographic Projection

Crystal surfaces may be represented by making use of a stereographic triangle in which a low Miller index surface is found at each apex; see fig 53 page 161a.

Blakely and Somorjai (192) found that the three low Miller index surfaces, Pt (100), (110), (111) were stable in all conditions of their study. As well as the three low Miller index surfaces, the highly stepped surfaces midway between the low index planes on the zone lines were also found to be stable under all conditions. These surfaces are Pt [3(111) x (100)] and Pt [2(100) x (111)], Miller indices (112) and (113), which lie between the (111) and (001) planes and Pt [2-3(111) x (111)], Miller index (331)-(221), between the (111) and (011) planes. Between the (001) and (011) planes the Pt [2(100) x (100)] surface, Miller index (012), was found to be stable. The stable surfaces were characterised by the complete absence of steps, or else by a very high density of periodic steps one atom in height: none of the stable surfaces had a terrace width greater than three atoms.

Some of the other surfaces were found to be stable when clean or in oxygen, but not in the presence of a carbon overlayer. For example, kinked stepped surfaces vicinal to the

figure 53.

Stereographic projection showing the crystallographic orientation of some of the platinum single crystal faces studied by Blakely and Somorjai.

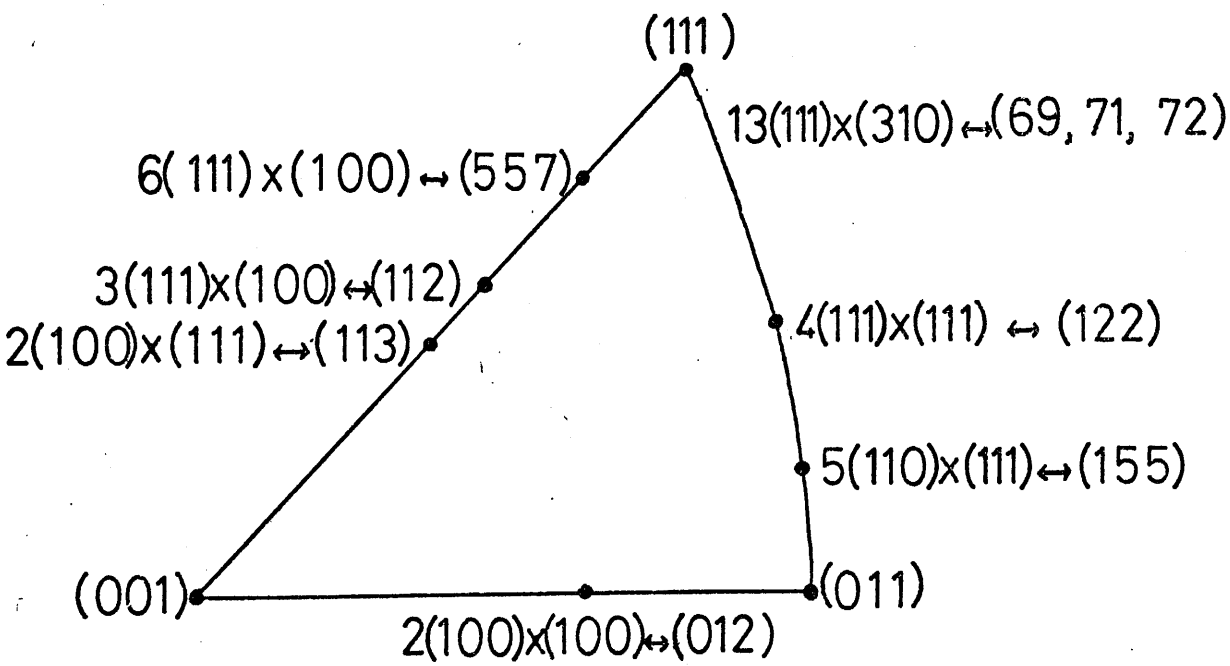

(111) crystallographic plane fell into this category. Other surfaces, for instance the (111) vicinal surfaces on the zone lines, were stable when clean or covered in carbon but they underwent faceting in the presence of oxygen. A few were stable in vacuum but underwent surface rearrangement in the presence of oxygen or carbon, while some surfaces faceted in vacuum or in the presence of oxygen or carbon.

Often faceting proceeded to give a mixture of low index faces and the appropriate stable, mid-zone surface. Chemisorption and catalysis of hydrocarbons, hydrogen, oxygen etc. can continue since the highly stable mid-zone surfaces all have a high density of steps and kinks which have been shown (147) to be responsible for bond breaking.

6·6·4 Catalysis by Stepped Platinum Surfaces

In addition to chemisorption studies on high Miller index surfaces, Somorjai's group has also investigated some reactions catalysed by platinum. For example, Somorjai (147) reported the findings of a study of the dehydrogenation and hydrogenolysis of cyclohexane on stepped and low Miller index surfaces.

6·6·4·1 Dehydrogenation & Hydrogenolysis of Cyclohexane on Platinum

Dehydrogenation of cyclohexane to benzene was found to be independent of step density, while the rate of hydrogenolysis to give hexane, propane, methane, ethylene, propylene and cyclohexene, varied in direct proportion to increases in step or kink density.

Cyclohexene is an intermediate in benzene formation from cyclohexane. It was shown that a structure-insensitive, slow step produced cyclohexene from cyclohexane and that this was followed by a structure-sensitive, fast reaction to give benzene; cyclohexene underwent fast dehydrogenation at steps on the surface. If the carbonaceous overlayer on the catalyst was disordered, as on a Pt (111) surface, benzene formation was inhibited, while cyclohexene production was enhanced. Alternatively, when the carbonaceous overlayer was ordered, benzene formation predominated.

Thus the presence of a disordered carbonaceous layer on the platinum surface poisons the dehydrogenation of cyclohexene to benzene.

The hydrogenolysis reaction was found to be surface-sensitive, depending on the presence of kinks for C-C bond breakage. However, this reaction was insensitive to the state of order of the overlayer.

Although it is not possible to use results obtained in LEED experiments directly to try to explain results obtained at higher pressures, the general principle of the structure-sensitivity of some reactions may be retained. Further, the presence of steps and kinks for C-H and C-C bond breakage, as well as H-H etc., is essential at all pressures.

6·6·4·2 Presence of Excess Hydrogen during Hydrocarbon Reactions on Platinum

In all hydrocarbon reactions, even dehydrogenation and hydrogenolysis experiments where hydrogen is being produced, a high hydrogen:hydrocarbon ratio in the region 20:1 was used.

If there was little or no excess hydrogen present the catalyst quickly became poisoned (147). Somorjai suggested that the role of the excess hydrogen appeared to be keeping the step and kink sites, and their vicinity, clean. He attributed this to the ease of dissociation and higher binding energy of hydrogen at steps compared with terrace sites.

To explain the role of steps in catalysis by platinum, Somorjai proposed that the species which formed as a result of bond scission at step sites might rearrange and then diffuse away onto the terrace which is covered with a carbonaceous overlayer. Desorption would occur from the terrace. Alternatively, he suggested that the rearrangement might equally take place on the ordered carbonaceous overlayer prior to desorption.

6·6·5 Implications for Exo-Electron Results

This explains why exo-emission from the platinum wire fell away so drastically during second and subsequent heating cycles in ethylene and acetylene. The lack of excess hydrogen means that step and kink adsorption sites will quickly become blocked so that no more dissociative adsorption can occur. This in turn implies that it is the dissociative chemisorption of molecules on platinum which is important for the observation of exo-electron emission, rather than adsorption on the terraces where chemical change only proceeds to a slight extent.

As a saturated wire is allowed to age, slow dehydrogenation of the ethylene or acetylene adsorbed on the terraces may proceed (147). The surface H thus produced may diffuse to step sites where hydrogenation of the carbonaceous species may occur. Heating cycles after ageing would permit thermal desorption of

these hydrogenated species and clean sites would be made available for adsorption.

Another possible mechanism for the generation of new adsorption sites is faceting which could occur at some crystal faces at high temperature in the presence of surface carbon. Certainly there is evidence of faceting in the micrographs obtained, see pages 155, 156. However, this mechanism would not easily explain the results obtained before and after a wire with a saturation coverage of ethylene or acetylene on its surface was aged.

6·7 Prolonged Heating Experiments

In general the results obtained from prolonged heating experiments, where the catalyst wire was heated for more than ten minutes, may be interpreted in the same way as those obtained from short heating experiments where the wire was heated for 30 sec.

6·7·1 Summary of the Results obtained from Prolonged Heating Experiments

The results obtained may be summarised as follows.

(1) No peaks were observed in cooling curves until after the wire had been heated in Q gas, Ar/10% methane. Reproducible results were not obtained until after the wire was subsequently exposed to air at room temperature; see Appendix 16.

Repetitive heating/cooling in Q gas gave variable structure. A fairly long period of treatment was required before results became reproducible for wire 3. This accords with the idea of optimum surface configuration for catalytic activity.

(2) Emission was observed when the wire underwent prolonged heating in oxygen. Since emission remained constant, often over periods of 60 min, it seems reasonable to suggest that structural rearrangement, to give for example enhanced grain growth and faceting, is responsible.

When the heating current to the wire was switched off emission decayed quickly and usually there were no peaks in the cooling curves. However, cooling curve peaks were observed in oxygen after nitrogen and Q gas pretreatment of the wire; see fig 69,71 Appendix 12.

(3) The level of emission from the wire was low in hydrogen, in keeping with its slight effect on the work function of platinum.

(4) Q gas gave cooling curves whose structure depended on which gas the wire was heated in before Q gas was introduced see fig 80-83 Appendix 12. Although the structural details varied, peaks or shoulders were generally observed at 202 - 204°C and 235 - 240°C.

(5) Nitrogen gave small cooling curve peaks (< 500 cps) after hydrogen, argon and helium; see fig 66 Appendix 12. Emission maxima after pretreatment of the wire with argon or helium suggests that some sort of surface rearrangement is being observed, possibly interaction of carbonaceous species on the surface.

When the platinum wire cooled in nitrogen after pretreatment with Q gas two emission maxima were observed in the cooling curves; see fig 65 Appendix 12. The cooling curve was similar to those obtained in argon after Q gas in short heating experiments.

After the wire was heated in oxygen, nitrogen gave a much higher emission rate, ~ 6000 cps. When the heating current was switched off emission increased to ~ 6500 cps then decayed

slowly; see fig 64 Appendix 12. This is in keeping with the idea proposed by Wilf and Dawson (142) that nitrogen chemisorption is enhanced on oxygenated platinum.

(6) Cooling curves obtained in helium gave no structure while argon gave a broad double peak after Q gas; see fig 79 Appendix 12.

With wire 1 and wire 3 cooling curves in oxygen were obtained after the wire had been heated in oxygen for at least five minutes. Perhaps here the peaks are due to surface reconstruction as oxygen chemisorbs. The same argument would apply to nitrogen cooling curves obtained after oxygen pretreatment.

6·7·2 Temperature of the Wire

The temperatures of the two emission maxima found in the Ar after Q gas cooling curve were 251 and 166°C in the first experiment and 295 and 154°C in the second.

Clearly the structure of this cooling curve corresponds to the double peak curve obtained in short heating experiments; see Appendix 10 fig 45. Here the peak temperatures were 56, 48°C.

Thus it is clear that all the peak temperatures measured in the course of long heating experiments were too high. This was because when the platinum wire was heated for long periods, often several hours, the whole reaction vessel became hot. When the heating current was switched off the platinum filament cooled quickly in the gas flow. However, the copper cathode and the glass vessel would have cooled much more slowly since their heat capacities were greater; see Appendix 19 for a comparison of the cooling rate of the wire and the cathode.

The thermocouple was attached to the platinum wire close to

the barrel connector, see Diagram 19 page 74c. Thus it gave the temperature of the glass reaction vessel when this was higher than the temperature of the catalyst.

In short heating experiments the glass vessel only heated up slightly so here temperatures were more accurate since the platinum wire would be above the temperature of the glass vessel.

6·8 Gold Results

Peaks in the cooling curves were observed for a gold wire cooling in hydrogen and in Q gas; see Appendix 14. One structured cooling curve was obtained when the filament was allowed to cool in nitrogen; however, this result must be regarded with scepticism since, in general, no emission was observed in nitrogen. Thus it would seem that nitrogen does not chemisorb on gold.

It was decided only to investigate the behaviour of nitrogen, hydrogen and Q gas on gold since structured cooling curves were obtained most consistently for these gases during long heating experiments with wire 3, and since there was considerable structure in the Laben spectrum obtained for H_{2C} , N_{2H}. Thus no attempt was made to obtain a cooling curve for gold cooling in oxygen.

From the results obtained in this study it would appear that hydrogen and methane both chemisorb on gold if a gold filament is allowed to cool from high temperatures in one of these gases.

6·9 Effect of Carbiding the Anode Wire

After the experiments with the gold wire a new platinum filament, wire 4, was introduced to the reaction vessel. The counting characteristics obtained with this wire were poor and cooling curves were not reproducible. Only rarely did nitrogen give any emission and eventually virtually no counts were obtained in any gas even at orange heat when emission should have been copious.

Wire 4 was replaced by wire 5 to determine whether this would improve the results. While wire 5 was being mounted the anode wire broke and had to be replaced. Once this had been done the counting characteristics were restored.

The anode which was used for the gold experiments and for the experiments carried out on wire 4 was the one in use when platinum wire 3 was heated in acetylene. The acetylene treatment produced a considerable amount of carbon inside the reaction vessel. Thus it is not unreasonable that some was deposited on the anode wire. If its diameter increased then gas multiplication would become less due to a decrease in the electric field and the appearance potential and counting plateau would be shifted to higher voltages; see Chapter 2·6·2.

At least for nitrogen as the flowing gas different results might be obtained for gold with a clean anode wire in the proportional counter.

6·10 Chemisorption of Oxygen, Water and Hydrocarbons on Gold

Chesters and Somorjai (193) investigated the chemisorption of oxygen, water and selected hydrocarbons on Au(111) and a

stepped gold surface. They found that oxygen chemisorbed on both gold surfaces at temperatures above 500°C to generate a stable oxide layer. Water also chemisorbed to give oxide while of the hydrocarbons investigated, ethylene, cyclohexene, n-heptane, benzene and napthalene, only napthalene chemisorbed under the experimental conditions employed, $T \leqslant 550°C$ and $P \sim 10^{-6}$ torr. On both surfaces napthalene adsorbed dissociatively to produce disordered surface species which were strongly bound.

Unlike the case with platinum, no difference in behaviour was observed between the low and high Miller index surfaces. Trapnell (148) demonstrated that reversible molecular adsorption was possible on gold with such gases as CO, C_2H_4 and C_2H_2 while Ford and Pritchard (194) have shown that atomic hydrogen and oxygen both chemisorb.

6·11 Summary of Results

The results presented and discussed in Chapters 3, 4 and 6 may be interpreted along the following lines.

(1) Methane probably causes deposition of carbon on platinum.

(2) Methane probably adsorbs to a slight extent on platinum so that reproducible exo-electron emission cooling curves may be obtained.

The surface does not become saturated under the influence of methane in the sense that surface sites responsible for exo-electron emission remain capable of releasing electrons.

(3) Ethylene chemisorbs extensively on platinum and quickly saturates the surface so that no more exo-electron emission is

possible. From this was inferred the poisoning of the surface for further adsorption of ethylene or acetylene.

(4) A similar effect is observed for acetylene except that acetylene regenerates some of the sites active for exo-emission in the presence of ethylene, and thus, by inference, active for ethylene adsorption.

(5) After methane treatment of platinum wires, acetylene gives a reproducible effect in exo-electron emission. This implies that acetylene was no longer saturating the platinum surface. However after methane treatment ethylene still poisons the catalyst for further olefin adsorption (at least for dissociative adsorption at steps and kinks; see 6·6·4·2).

(6) Cooling curves were still obtained from platinum in Ar/CH_4 after the wire had become saturated with acetylene or ethylene. This suggests that methane underwent adsorption on different sites.

(7) Butadiene gave emission cooling curves similar to those for acetylene but it could not have irreversibly poisoned the catalyst surface since the curves were reproducible when experiments were repeated.

(8) The intensity of the peaks in the cooling curves obtained in Ar/C_2H_6 increased with the number of heating/cooling cycles. This implies there was an induction period for ethane chemisorption of platinum after which the rate of emission/adsorption increased rapidly.

(9) Hydrogen cooling curves varied. The nature of a hydrogen cooling curve (i.e. emission measured from the platinum as it

cools in hydrogen) depended on the nature of the carbonaceous species on the surface.

(10) Nitrogen appeared to be chemisorbed on clean platinum, that is before exposure of the filament to methane, or after the wire had been heated in oxygen.

After the wire was saturated with ethylene or acetylene and left to 'age' overnight cooling curves were obtained in nitrogen. These have been attributed to surface rearrangement or to an interaction between residual species on the surface.

(11) Argon gave structured cooling curves. Again these have been attributed to interaction between residual species on the surface.

(12) Methane appears to interact or be chemisorbed on gold.

(13) Hydrogen was chemisorbed on gold.

6·12 Work Function

Throughout this discussion chapter values of work function change due to adsorption have been given with respect to the clean platinum surface.

Once the wire was heated in Ar/CH_4 some carbonaceous species would be likely to be present on the surface so that work function changes due to chemisorption of a gas would no longer be with respect to a clean surface. Thus the values cited for work function changes should only be taken as a guide. Composite work function changes will depend on many factors, the most obvious one being whether the two adsorbed species will react with each other.

For example, Franken and Ponec (166) studied the

chemisorption of ethylene on platinum at 293K by monitoring the change in work function of the platinum surface. When ethylene was first introduced ϕ decreased by -1·45 eV. When the system was evacuated ϕ increased to a value -1·21 eV below that of the clean surface, indicating that some irreversible adsorption had occurred. Hydrogen was introduced to a clean platinum surface to a pressure of 5×10^{-3} torr at room temperature. The change in work function, $\Delta\phi_{Pt}$ was -0·11 eV.

However, when hydrogen was introduced to a platinum surface with preadsorbed ethylene present, the work function increased from -1·21 eV to -0·56 eV below that of the clean surface.

6·13 Future Experiments

It is obvious that in the development of this work in the future an effort must be made to determine the nature of the surface species.

Mass spectrometry work would be most useful during heating cycles when thermal desorption is occurring. Thus temperature programmed desorption studies carried out in conjunction with mass spectrometry, or gas chromatography, would be of future interest.

Another area where improvements could be made is in the measurement of the temperature of the filament under investigation.

The thermocouple was kept clear of the anode wire by connecting it to the catalyst filament between the barrel connector and the top of the glass former; see Diagram 19 page 74c.

When the wire was heated, this point of attachment did not reach the same temperature as the section of wire wound round the former: the glass of the reaction vessel and the Pt/Rh wire acted as a heat sink. When the filament was allowed to cool, this point of attachment would cool more slowly, since heat probably flowed back from the glass vessel. Thus in prolonged-heating experiments the thermocouple readings would have been high.

Flash heating the wire for 30 sec circumvents this problem as much as possible since, in such a short time, the vessel did not warm appreciably. If flash heating cycles were kept far enough apart in time then only the catalyst wire itself was heated.

Another problem arose in measuring temperature in the present system. Decomposition of hydrocarbons on the platinum wire, and to a lesser extent on the Pt, 13% Rh wire, may well have changed the voltage response of the two wires to temperature. If this were so the standard calibration curve would no longer give an accurate conversion from milivolts to degrees celsius.

Again a programmed heating cycle, where allowance might more easily be made for the effect of carbide, might improve this aspect of the work.

Owing to the high thermal conductivities of hydrogen and helium, the temperature of the filament dropped below red heat ($\sim 550°C$) when either of these gases was introduced. If a mixture of 10 - 20% hydrogen in argon was used then the effect of hydrogen on platinum could be investigated at much higher temperatures without the necessity of continually changing rheostat settings.

6·14 Re-Evaluation of Selected Papers on Catalysis

From the results discussed in this chapter it may be seen that the observation of chemically stimulated exo-electron emission is made possible by the lowering of the work function of a surface to a value where emission may be observed at temperatures below the threshold for thermionic emission.

Sato and Seo (102) observed exo-electron emission during the partial oxidation of ethylene to ethylene oxide over silver catalyst and the emission rate was proportional to the rate of formation of ethylene oxide.

No emission was observed from catalysts over which complete oxidation of ethylene to carbon dioxide and water occurred.

Thus Sato and Seo concluded that exo-electron emission was a thermally stimulated emission from silver oxide, an n-type semiconductor, whose work function was lowered by the adsorption of ethylene as ethylene oxide.

The present author found that if ethylene was introduced to the catalyst first, emission was considerably reduced; see Table III page 52a. This implied that some at least of the ethylene chemisorbed irreversibly on the sites responsible for exo-electron emission and that no further emission would be possible from these sites until the adsorbed ethylene was removed. Thus it was concluded that oxygen had to be introduced before, or simultaneously with ethylene, to obtain optimum exo-electron emission from the catalyst.

Hoenig and Tamjidi (112) observed exo-electron emission during catalytic oxidation of carbon monoxide, hydrogen or ammonia on hot platinum. The exo-emission rate was

proportional to the rate of reaction. They found that suppressing or enhancing the exo-electron current by appropriate biasing of the wire decreased or increased the rate of reaction.

If a positive bias was applied to the wire the effective work function of the surface would be increased and it would be more difficult to remove an electron from the metal. Similarly if a negative bias is applied the effective work function of the surface would decrease and it would become easier to remove an electron from the surface.

Hoenig and Tamjidi found that applying a positive bias to the catalyst while a reaction was in progress decreased the exo-electron current. Similarly exo-electron emission increased if a negative bias was applied during a reaction. However, there was only an effect on the reaction rate if the bias potential was applied before the reaction started.

These workers suggested that application of a bias potential 'structured' the surface in some unspecified way, which either enhanced or diminished reaction and emission depending on the sign of the bias potential.

Thus it may be concluded that the relationship between exo-electron emission and reaction rate is not a simple one.

Sujak, Gorecki and Biernacki (105) compared the catalytic activity and exo-electron emission from surface-oxidised zinc.

Exo-emission from zinc oxidised in an air/ethanol vapour mixture reached a maximum in the vicinity of 570K. Zinc-oxide based catalysts generally exhibit optimum catalytic activity in the same temperature region i.e. 570K. Sujak et al (105) proposed that as temperature increased from room temperature,

thermal stress in the zinc oxide layer covering the bulk metal increased and that this led to an increase in the concentration of lattice defects at the surface. This increase in defect concentration was responsible for the increase in catalytic activity and exo-electron emission with temperature. As temperature increased further, the rate of diffusion of zinc from the bulk into the oxide became significant and this led to a decrease in the defect concentration.

Thomson and Wadsworth (64) and Kortov, Mints and Teplov (195) have noted that during cyclic stress of a metal defects become more numerous. This leads to a lowering of the work function. Thus any method by which defect concentration is increased should produce a lowering of the work function and should lead to an enhancement of exo-electron emission.

If one of the steps in a heterogeneous reaction involves donation of an electron from the metal to the adsorbate then any process which leads to a decrease in work function should make this reaction step easier.

Kasemo and Walldén (114), (138) observed emission of both electrons and photons during the interaction of chlorine, bromine and iodine with evaporated sodium films. The phenomenon of chemiluminescence is well known; see for example McCarroll (196) and Volkenshtein (197).

That the two occur simultaneously, with the photon yield $\sim 10^{-2}$ less than the electron yield suggests that some sort of chemical Auger mechanism is in operation.

6·15 Conclusions

The outcome of this research has been the development of

a versatile exo-electron detector.

These low energy particles may be counted at atmospheric pressure in the absence of a 'counting gas', over a wide range of temperatures, from room temperature up to 900°C. A large variety of gases was investigated and good counting characteristics were obtained in each.

Platinum and gold wires were examined. The ease of mounting filaments means that a wide range of catalysts, both pure metals and alloys, could easily be investigated and their behaviour compared with that of platinum.

Inspection of the cooling curves obtained with the platinum wire during short heating experiments showed that several common temperatures existed for peaks. This may imply the existence of common surface species.

It is in this area that the most important future development could occur.

The different temperature spikes are narrow and closely spaced. Thus if an exo-electron emission maximum indicates optimum catalytic activity of platinum for generating a particular species, it is clear that a very narrow range of temperature would give the best yield in a catalytic reaction. A variation of a few degrees in either direction could mean that the catalyst was now operating in the optimum temperature range for generation of a different, possibly competing, surface species. Conditions might easily no longer favour the desired reaction.

This will find a much greater application in the study of reaction mixtures. However, before work could proceed to an investigation of a gas mixture the behaviour of individual

components would need to be completely characterised to find temperatures of emission maxima and to characterise the different surface species present. Once this preliminary work had been completed progress could be made to a study of a reaction mixture under different experimental conditions.

Since, with this detector, surface processes are being monitored directly, it should be easy to determine which reactants in a catalysed reaction are chemisorbed. It should also be possible to obtain information about the extent of adsorption (cf methane/ethylene, acetylene) and the nature of surface species. Further, if intermediates are formed then the optimum temperature and pressure may be easily found to maximise the product yield.

Thus, it is obvious that the exo-electron detector developed by us has important and wide ranging future applications in the study of chemisorption on metals and in the elucidation of reaction mechanisms in heterogeneous catalysis.

Appendix 1

Appendix 1.

1·1

Method of preparation of precipitated silver catalyst used by Sato and Seo (102).

The silver catalyst, Catalyst A, was prepared as follows:- an alkaline solution (36·5g KOH in 30 ml water) was slowly added to a $AgNO_3$ solution (27·3g $AgNO_3$ in 300 ml water) at 10°C. After precipitation of silver (1) oxide, 12·5 ml 30% HCHO solution was added to the solution, which was then kept for 30 minutes then boiled for 1 hour. The precipitate was then filtered, washed with distilled water, treated with 2% HNO_3 solution for 2 or 3 minutes, and washed again with distilled water until no nitrate ions were detected. This precipitate was finally dried at 80°C before experiments.

$\frac{1}{10}$th quantities were used throughout.

1·2

Method of preparation of supported silver catalyst according to McBee, Hass and Wiseman (131).

The supported silver catalyst, Catalyst B, was prepared as follows:- an impregnation procedure is used. An α-alumina (8 mesh) carrier, 70g, 21·98g silver oxide and 2·24g of barium peroxide are dispersed in 100 ml water. The mixture is evaporated to dryness on a steam bath with vigorous stirring. After drying at 115°C the catalyst is ready for use. Again $\frac{1}{10}$th quantities were used throughout and powdered α-alumina was used.

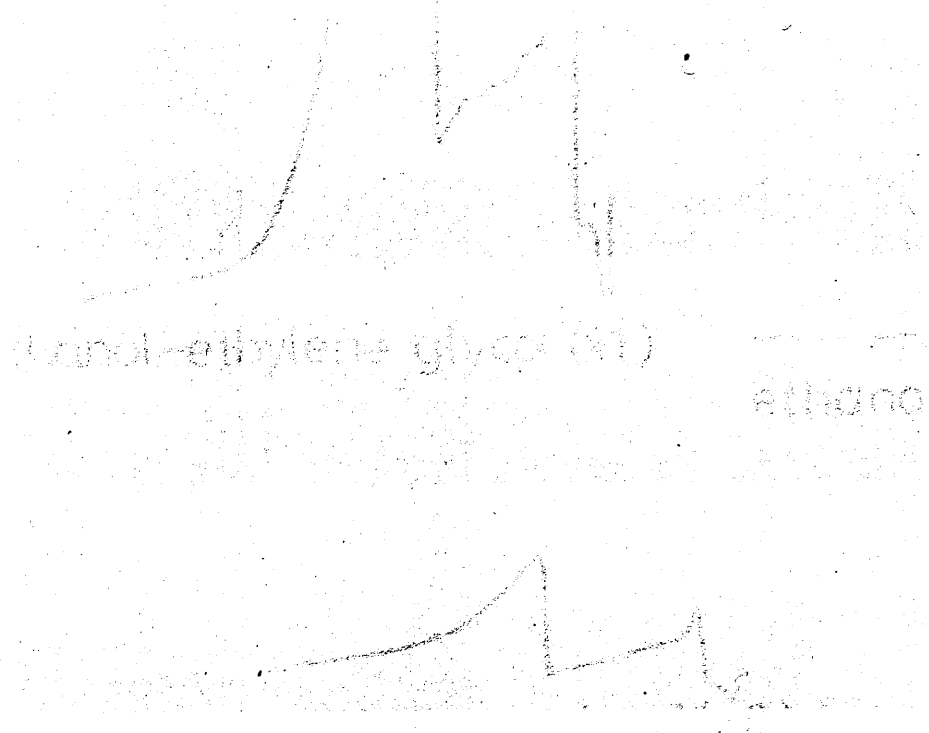

1·31 Gas chromatographs of ethanol, ethylene glycol and an ethanol-ethylene glycol mixture. 1 µl samples.

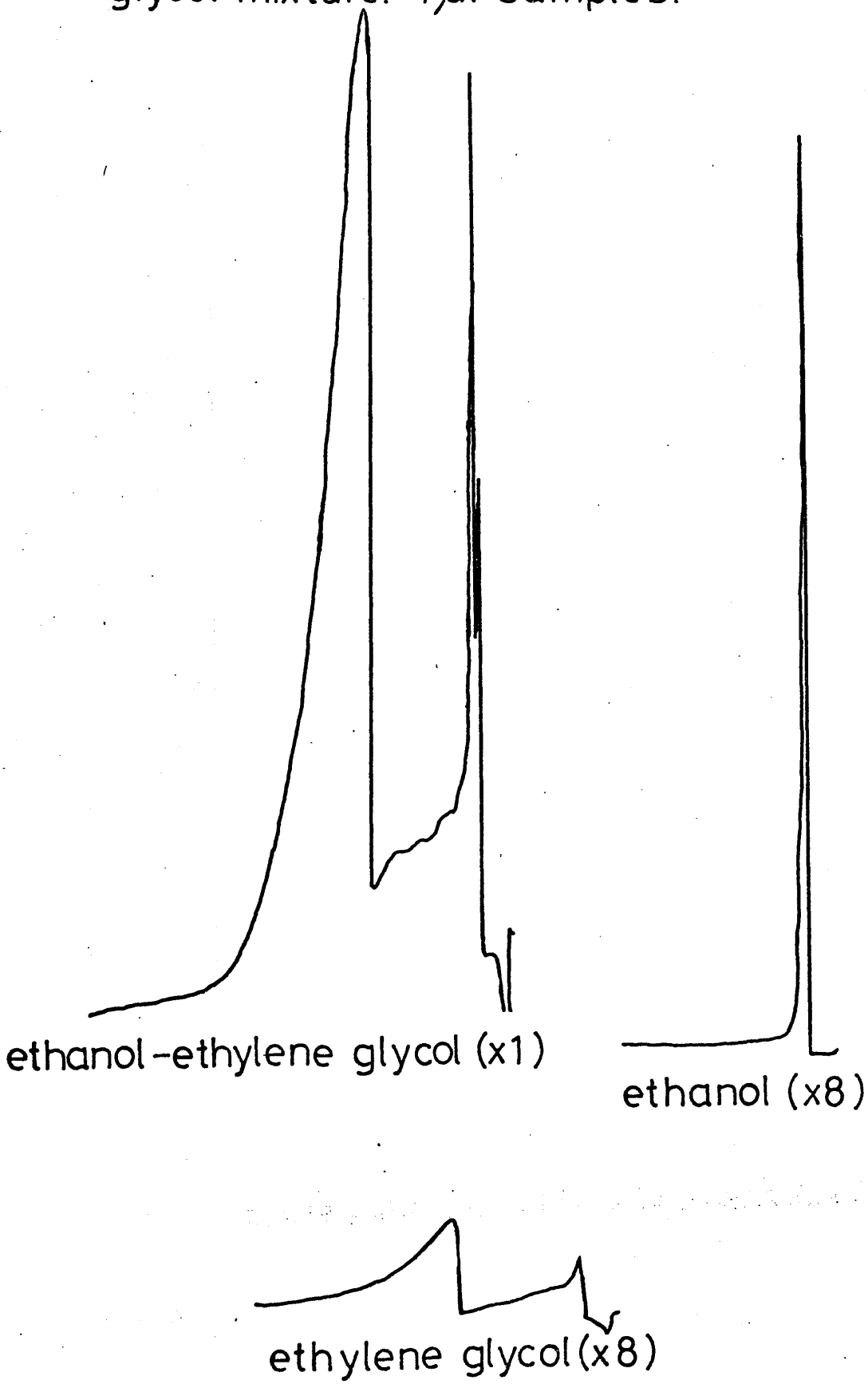

1·3·2 Gas chromatograph of product from large scale reaction with Catalyst A. 1 μl samples.

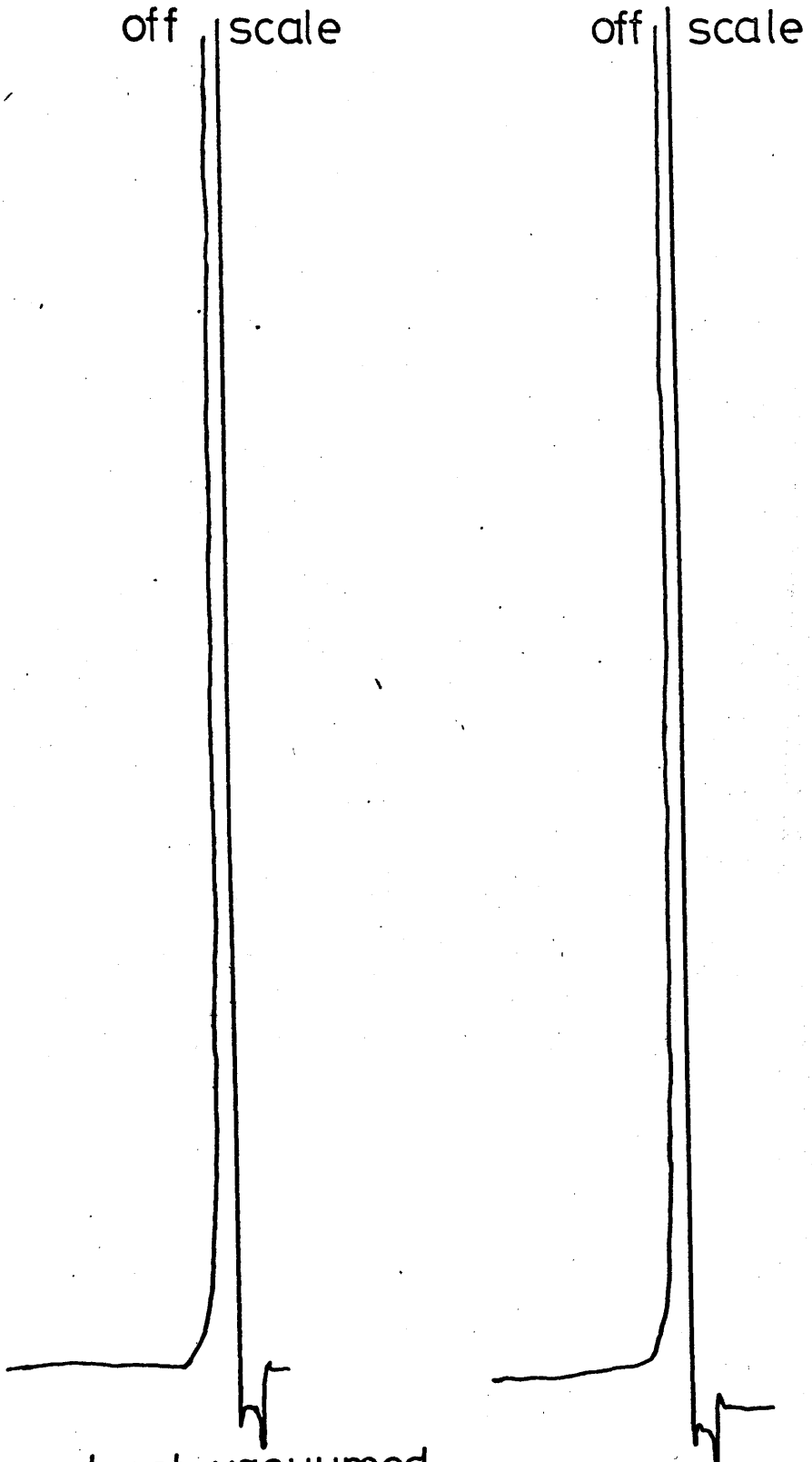

133 Gas chromatograph of product from large scale reaction with Catalyst B. 4 µl sample.

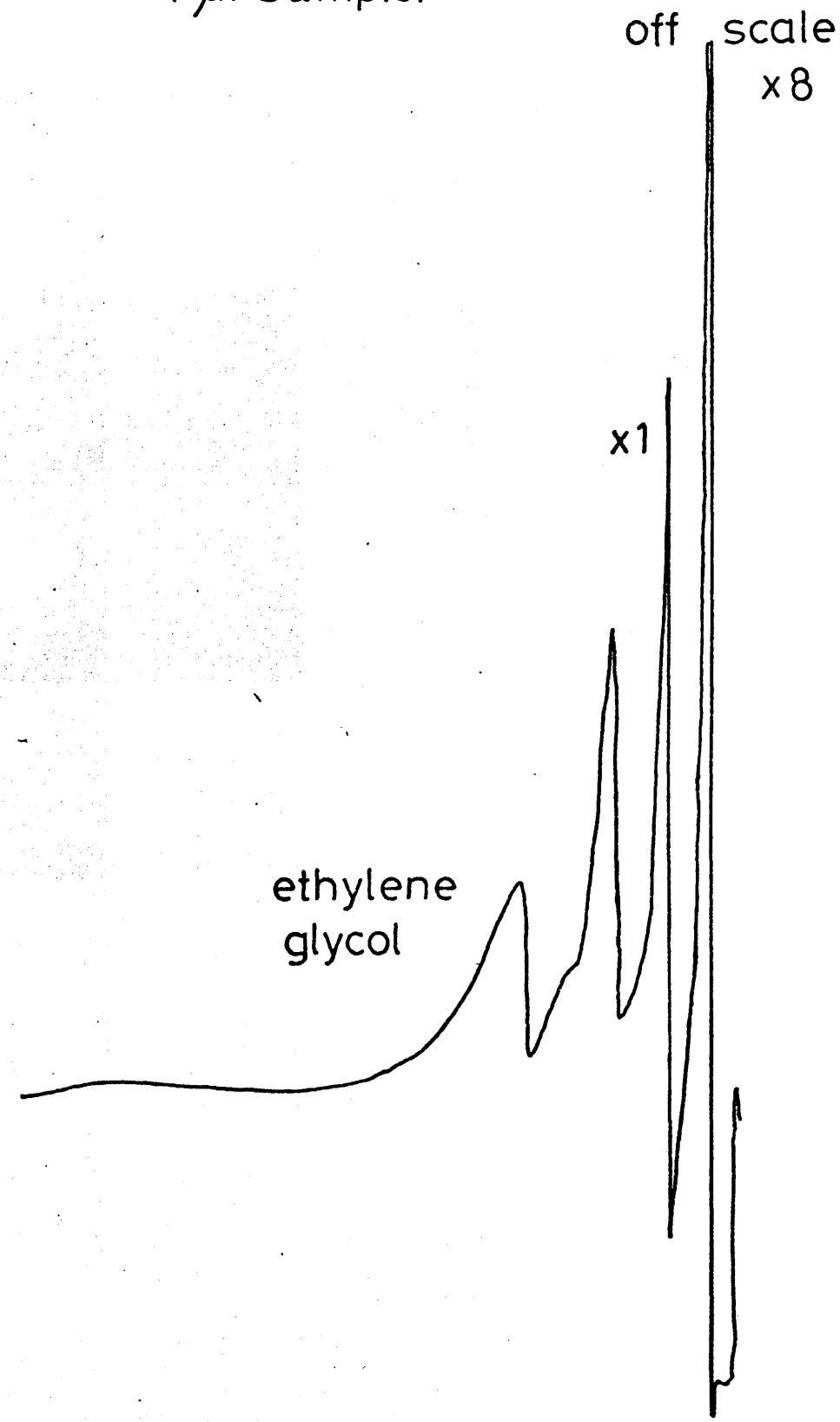

Appendix 2

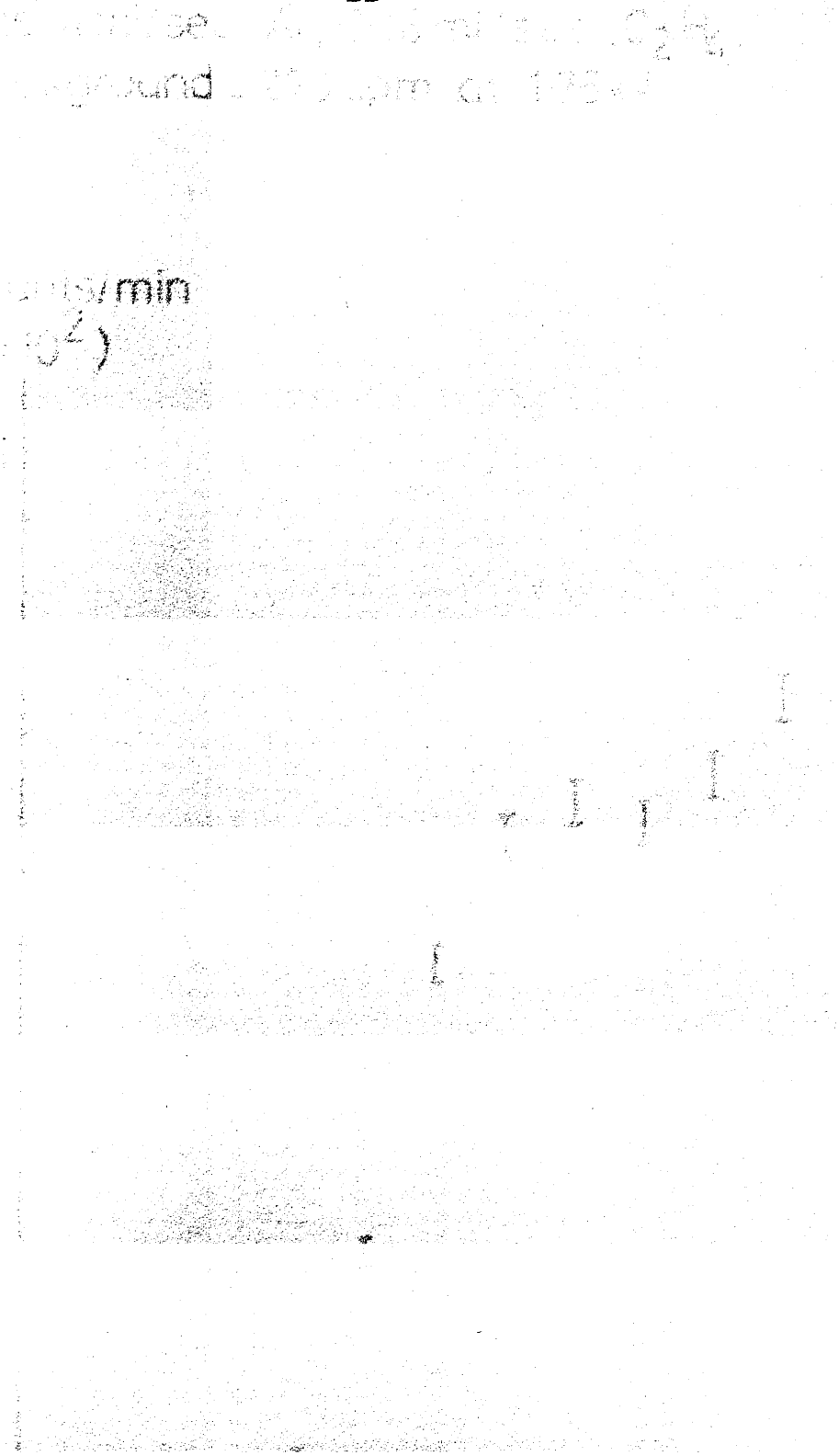

Graph 1.

Counts/min (uncorrected for background) versus voltage, internal ^{14}C source, counting gas 4 ml/sec Ar, 0·16 ml/sec C_2H_4.
Background = 273 cpm at 1·75 kV.

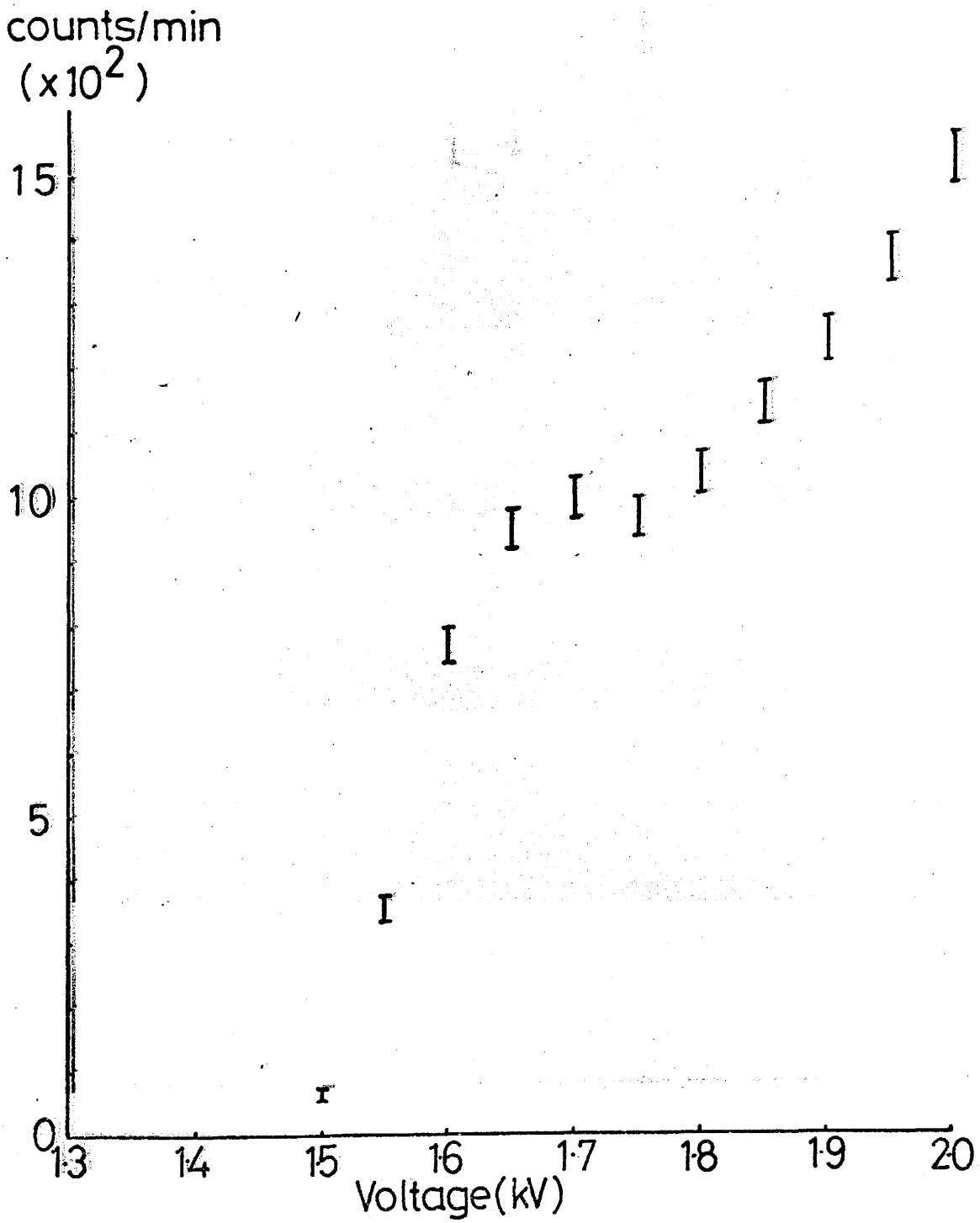

Graph 2.

Counts/min versus voltage to find plateau region with ^{137}Cs source, counting gas 2 ml/sec Ar, 0·08 ml/sec C_2H_4. Room temperature. No catalyst.

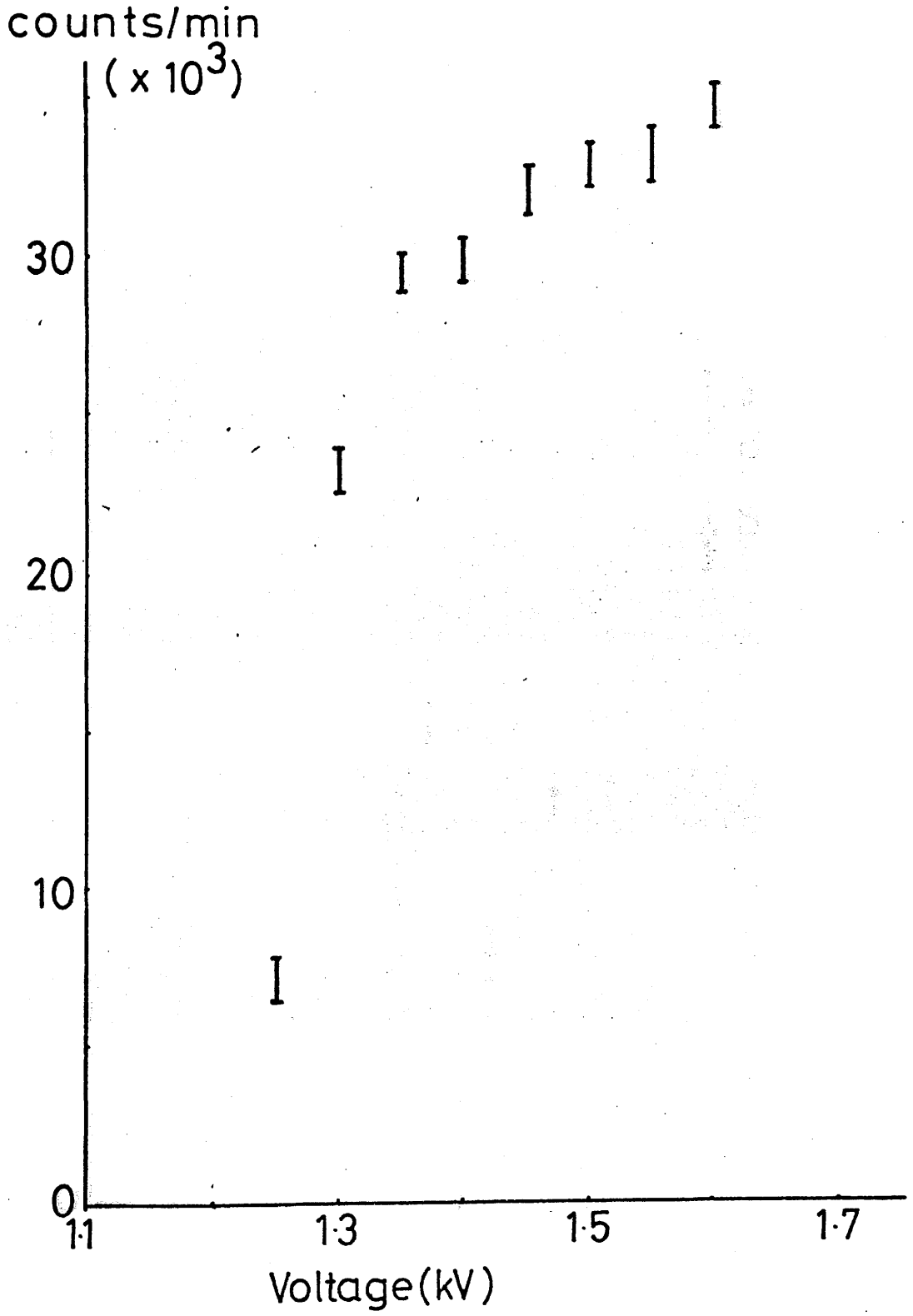

Graph 3.

Counts/min versus voltage to find plateau using a ^{137}Cs source. Counting gas Ar 2ml/sec, C_2H_4 0·08ml/sec, O_2 0·1ml/sec. No catalyst. Room temperature.

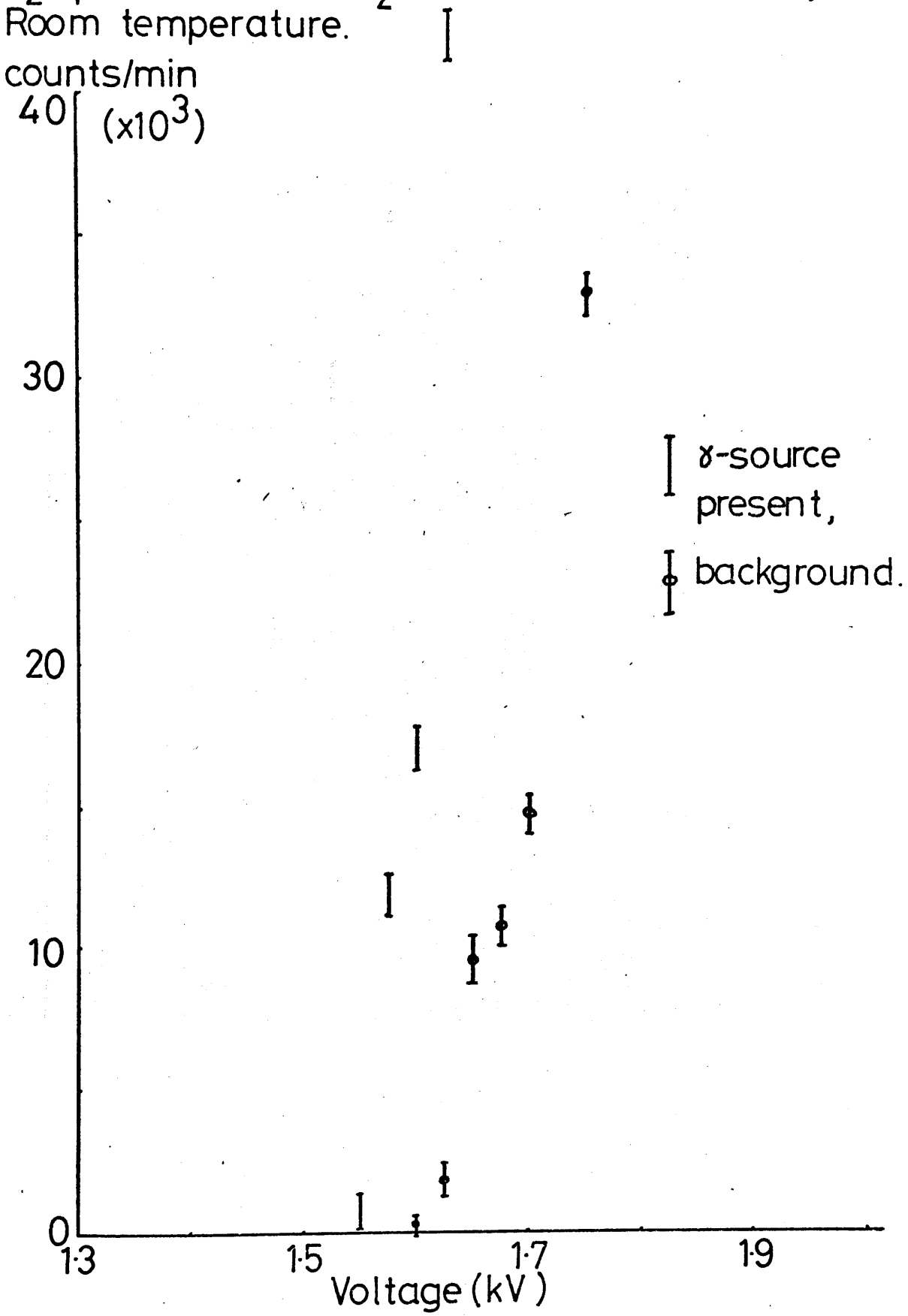

Graph 4.

Counts/min versus voltage to find plateau region using a ^{137}Cs source. Counting gas Ar 2ml/sec. No catalyst. Room temperature.

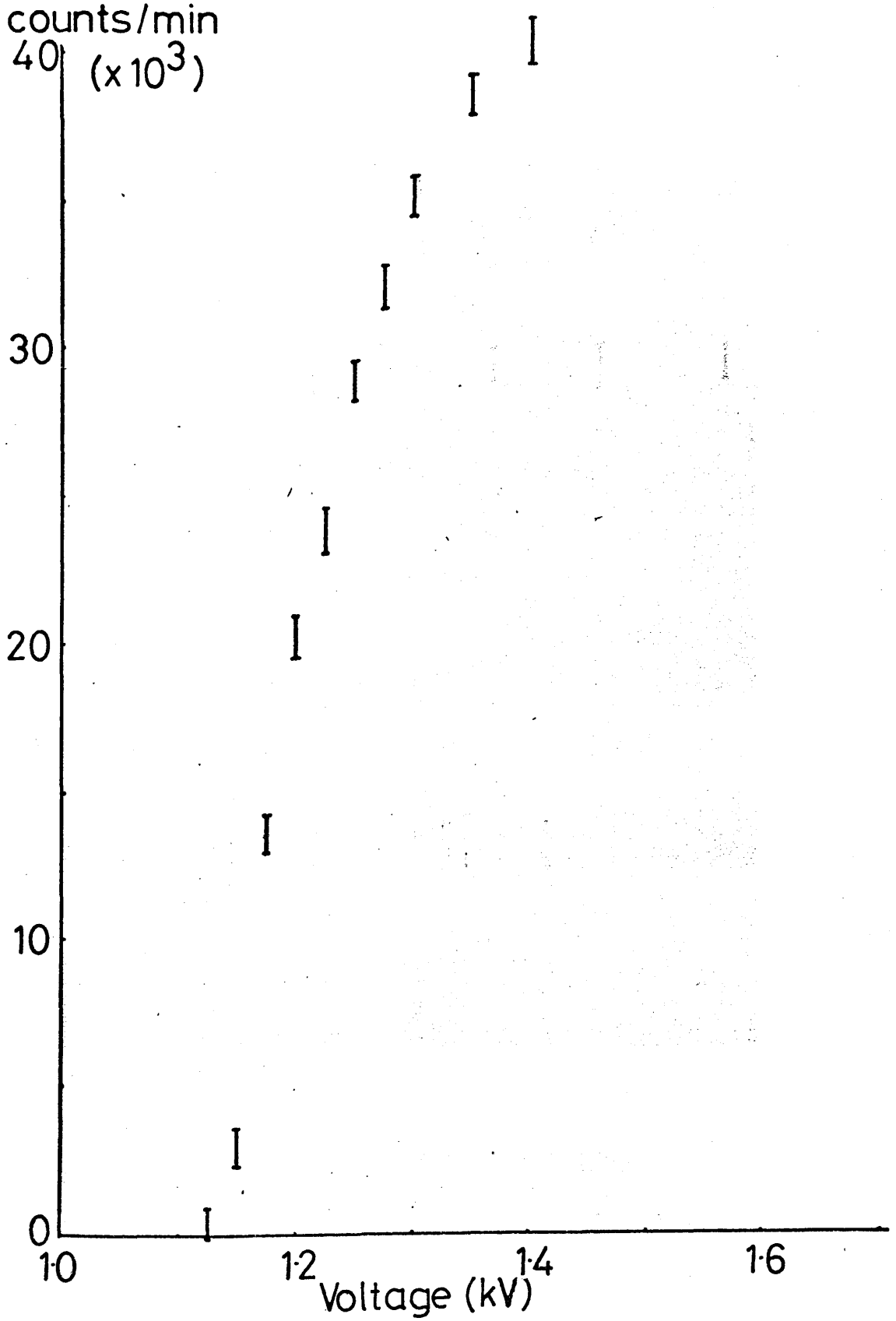

Graph 5.

Counts/min versus temperature to find the variation in the response of the Geiger-Müller tube. Counting gas Ar 2ml/sec, C_2H_4 0·08 ml//sec. No catalyst. Voltage constant, 1·525kV. Temperature increasing.

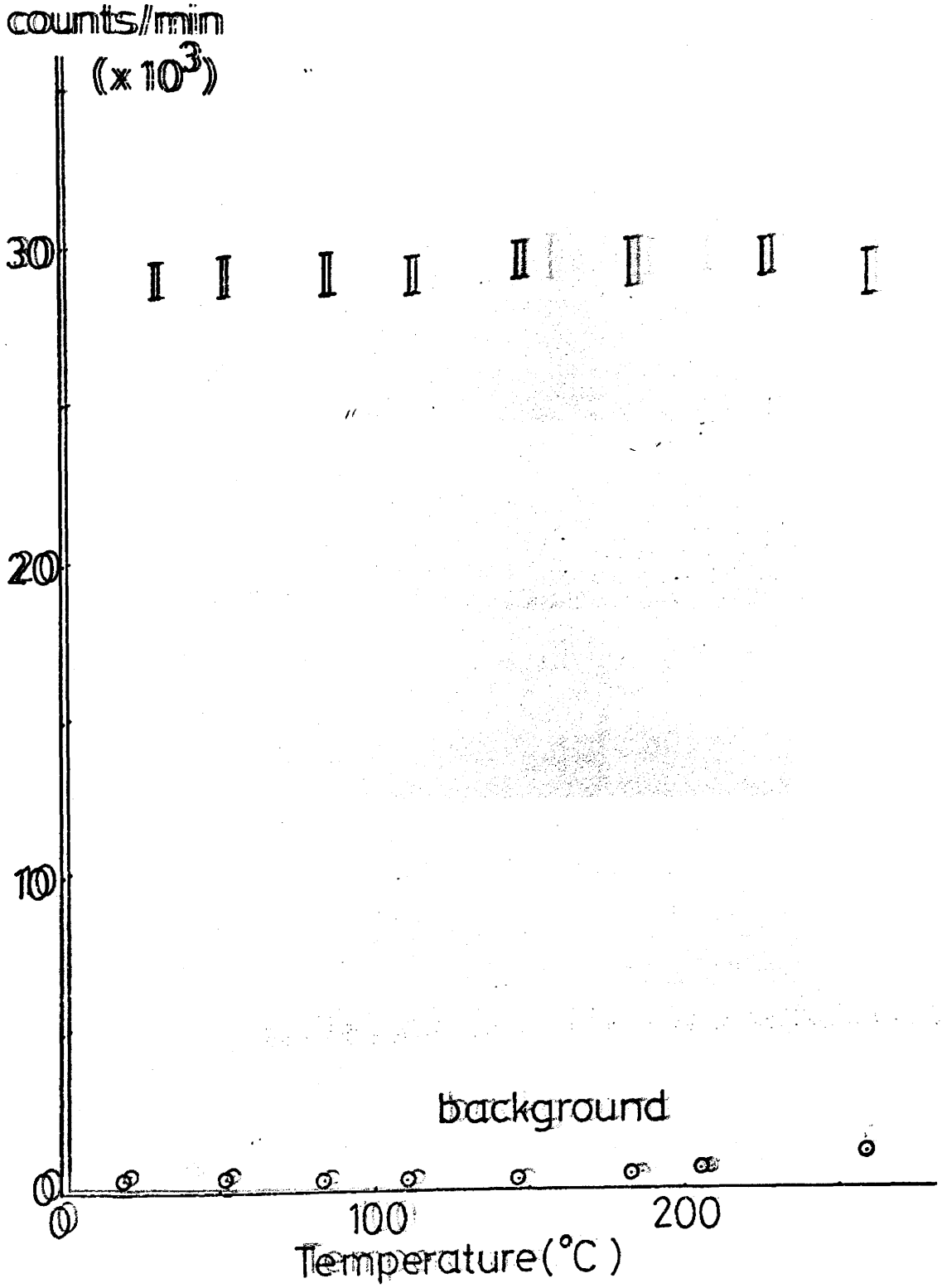

Graph 6.

Counts/min versus temperature to find the variation in the response of the Geiger-Müller tube. Counting gas Ar 2ml/sec, C_2H_4 0·08 ml/sec. No catalyst. Voltage constant, 1·525kV.

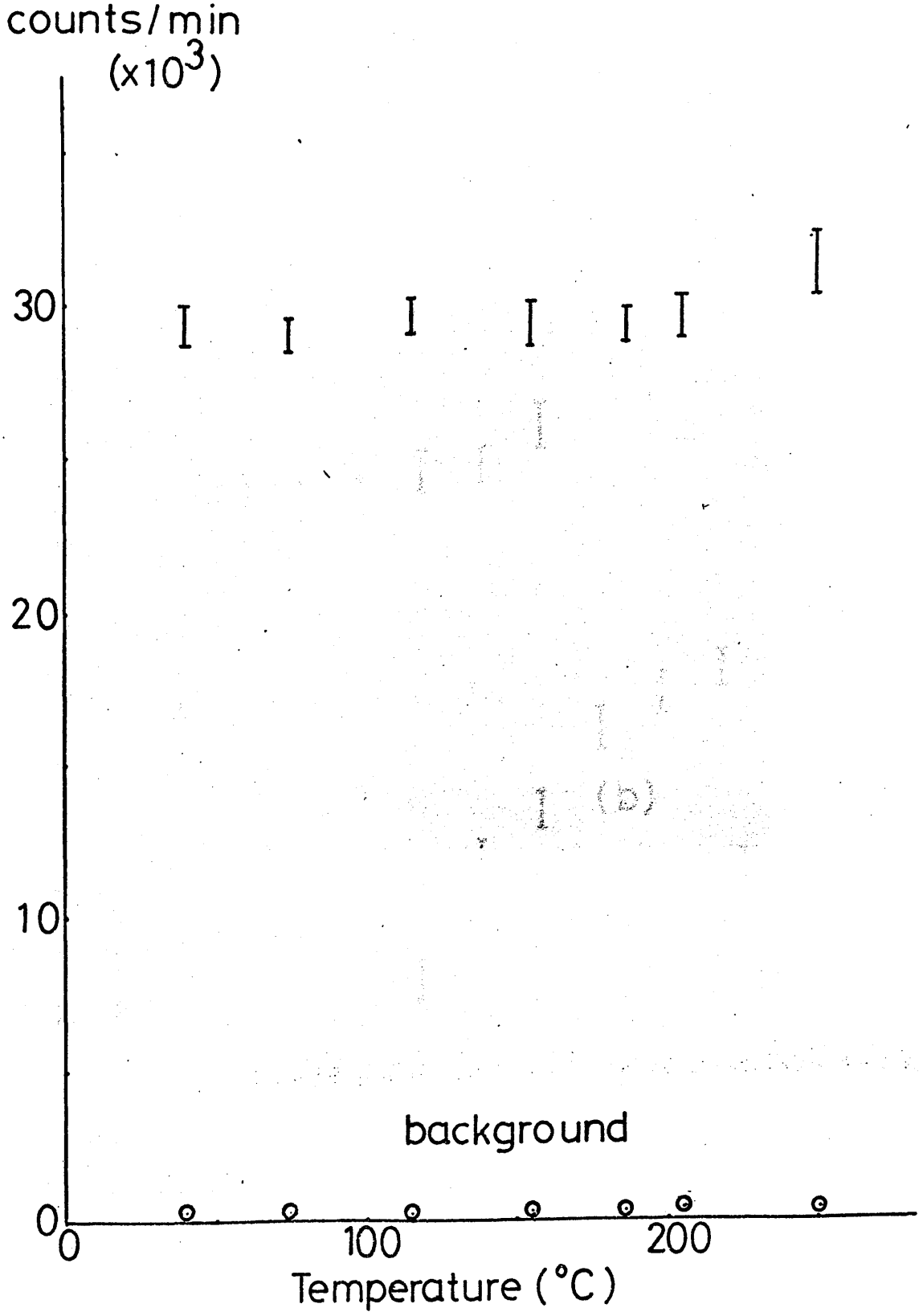

Graph 7.

Counts/min versus voltage to show the effect of varying the amount of ethylene.
Ar 2ml/sec, C_2H_4 0·08ml/sec, a),
Ar 2ml/sec, C_2H_4 0·16ml/sec, b).

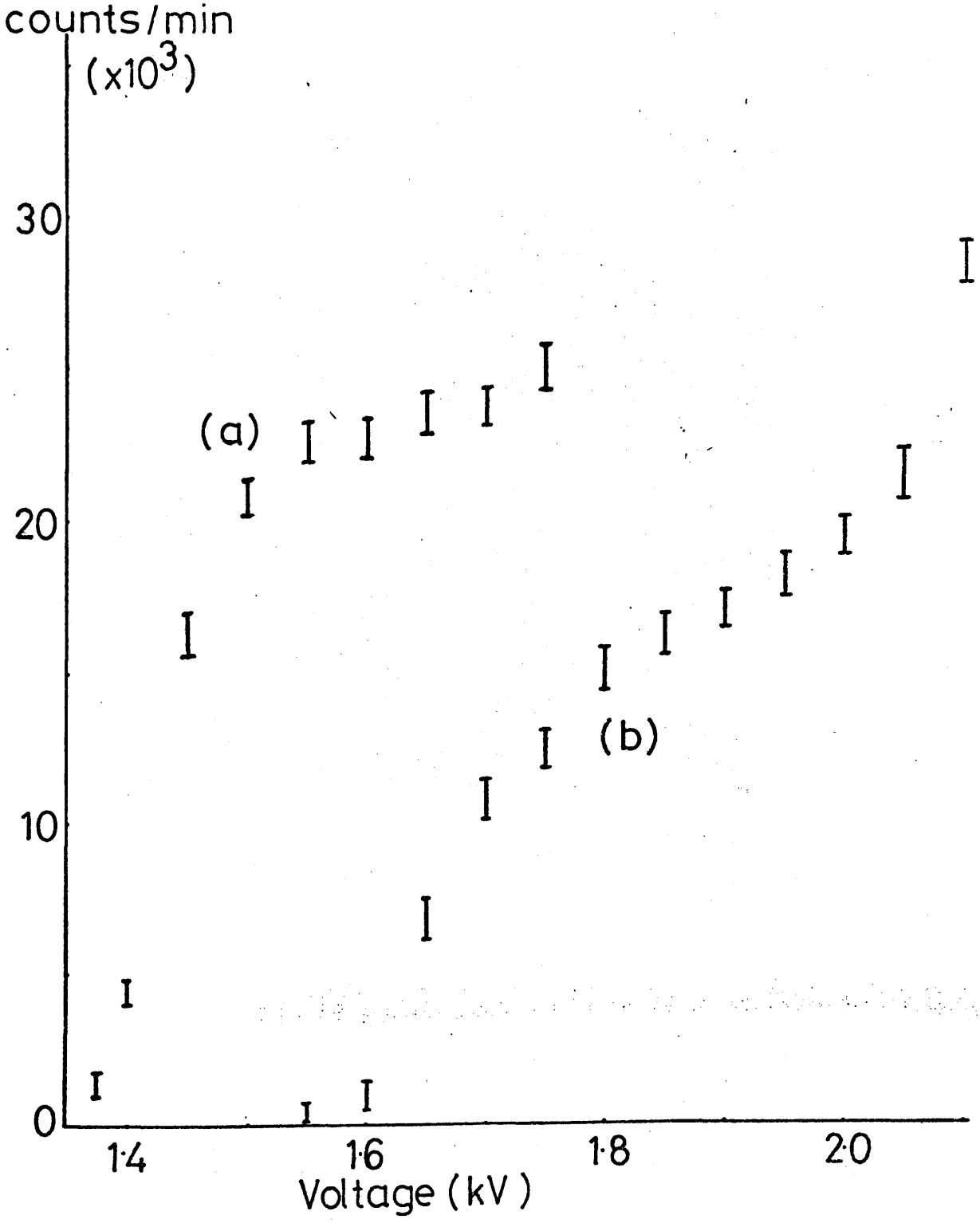

Appendix 3

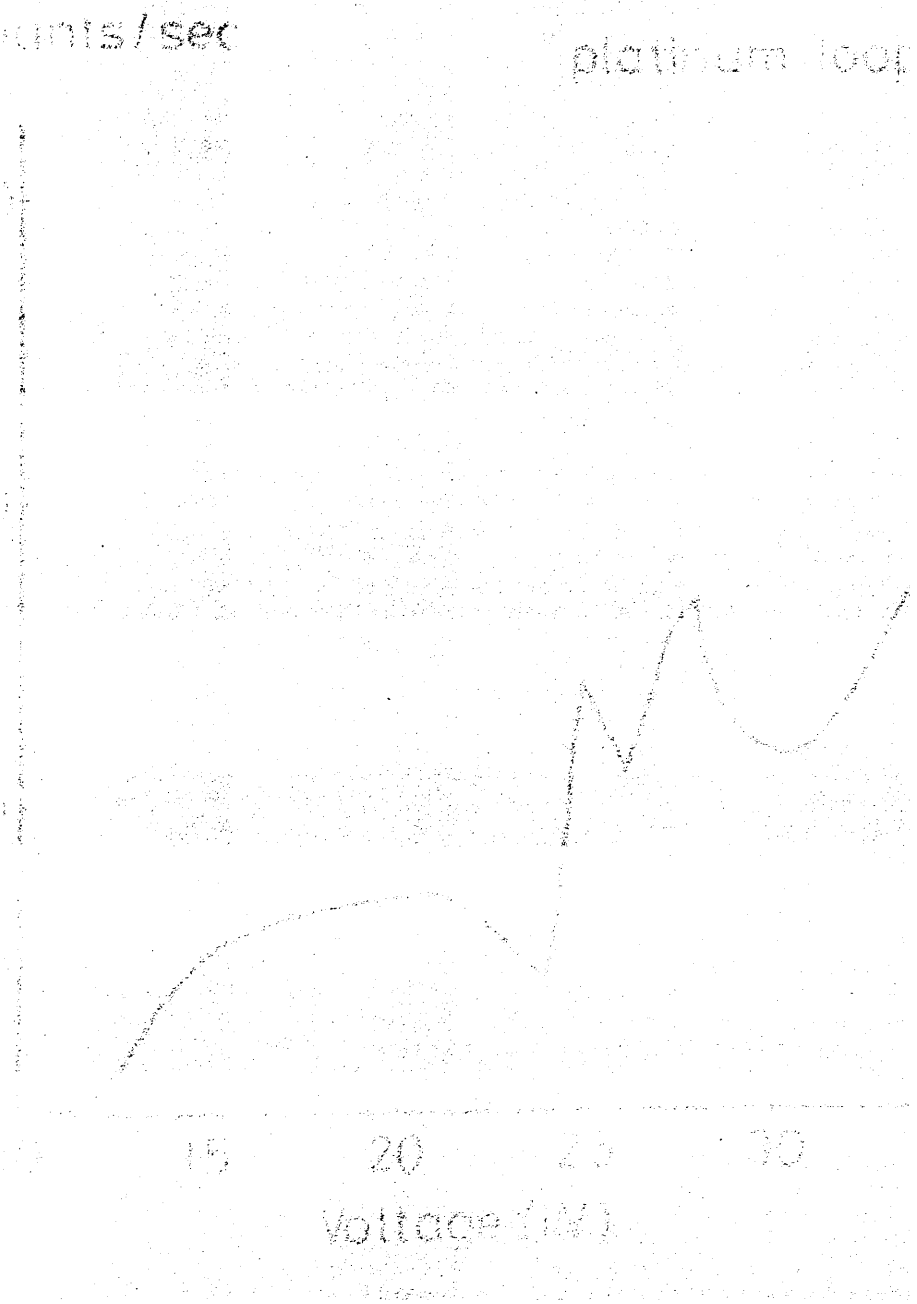

Graph 8.

Counts/sec versus voltage using internal ^{14}C source to determine plateau region.
Q gas flow rate 3ml/sec; room temperature.

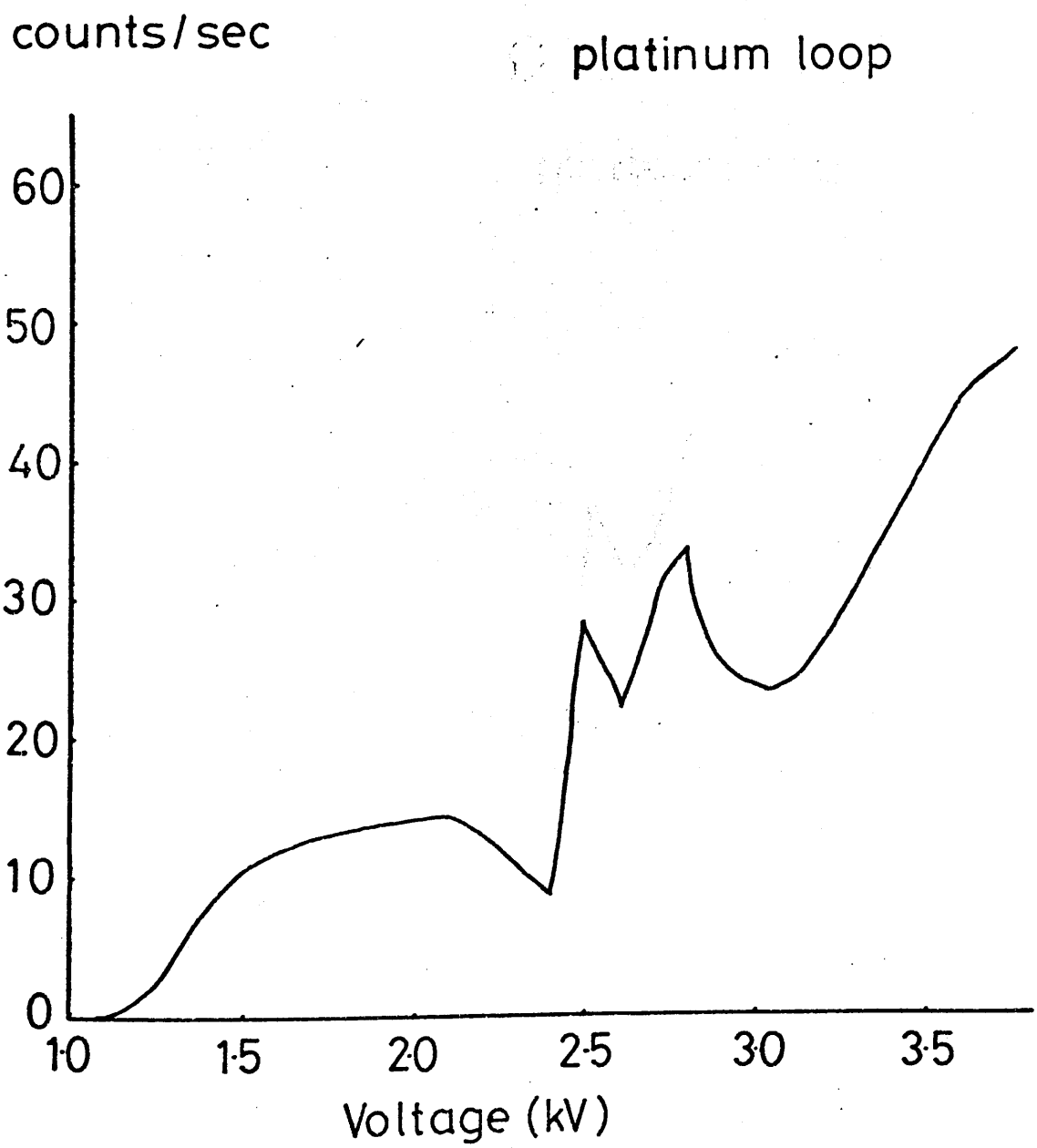

Graph 9.

Counts/sec versus voltage using internal ^{14}C source to determine plateau region.
Q gas flow rate 5 ml/sec; room temperature.

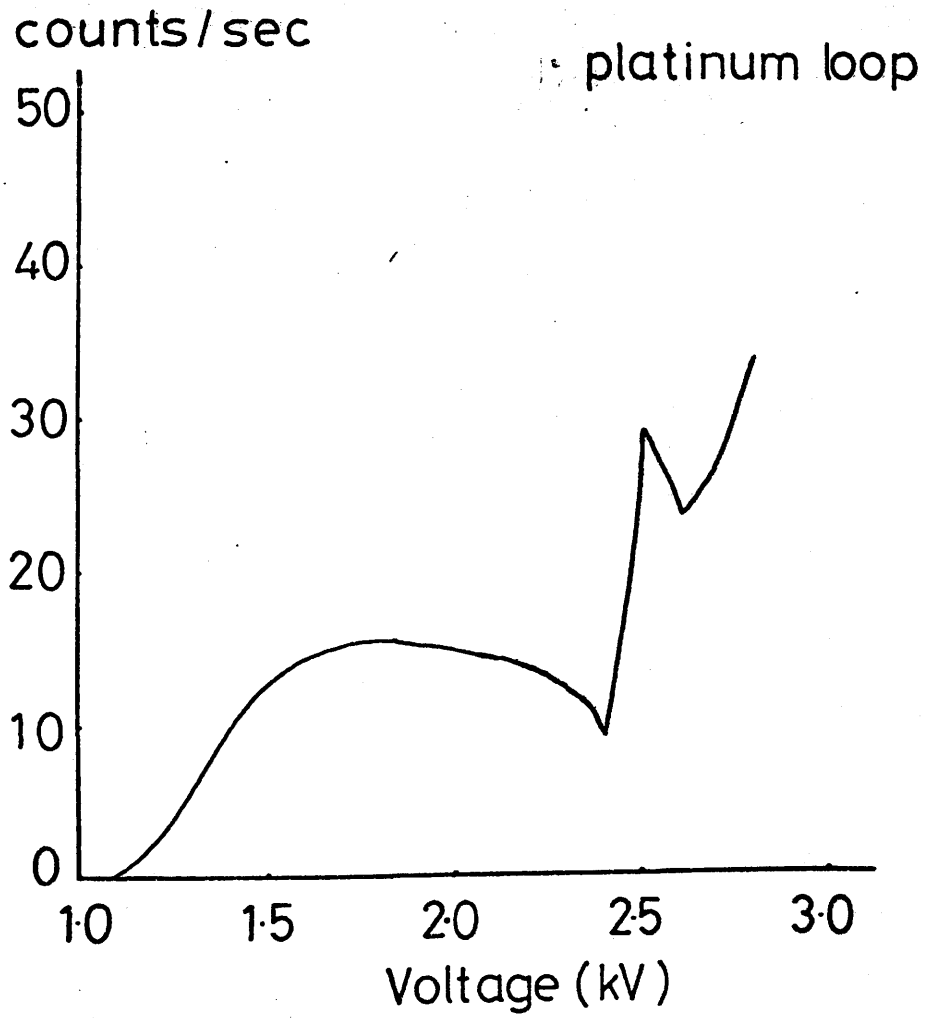

Graph 10.

Counts/sec versus voltage using internal ^{14}C source to determine plateau region.
Q gas flow rate 9ml/sec; room temperature.

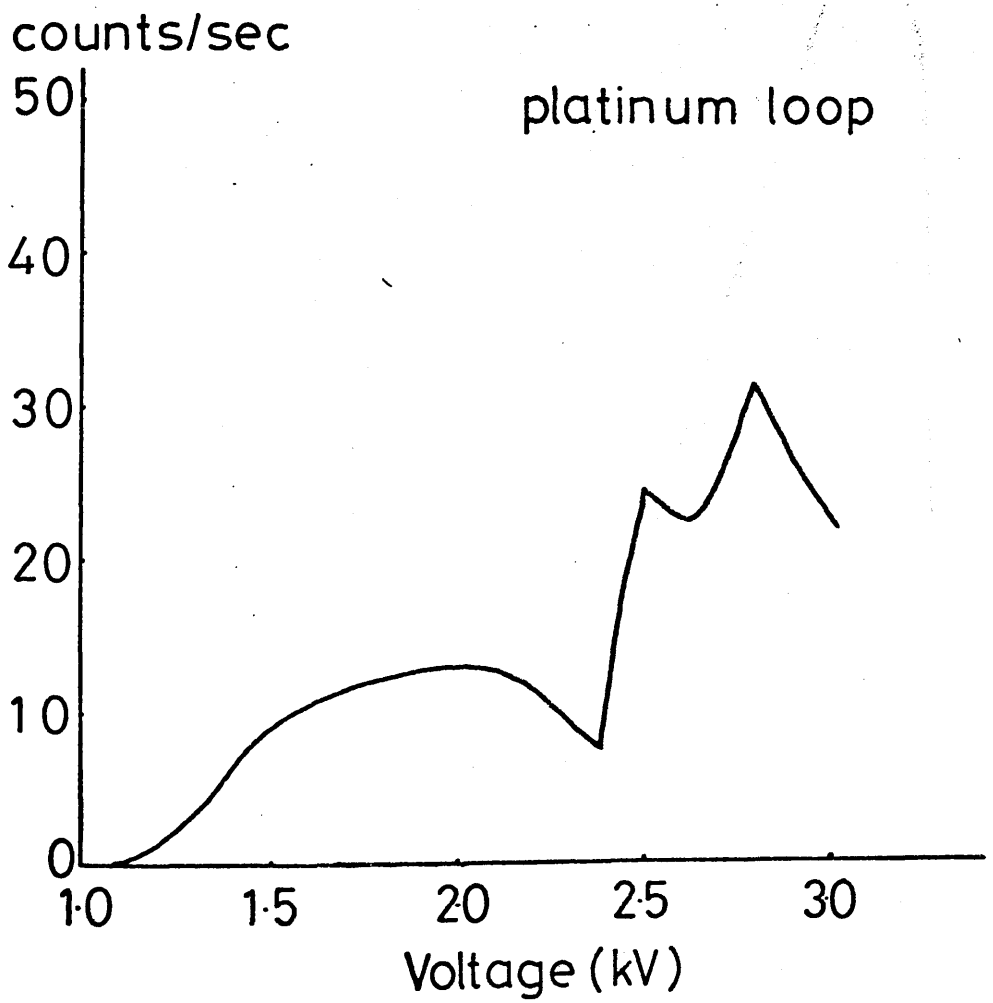

Graph 11.

Counts / sec versus voltage using external γ source to determine plateau region. Q gas flow rate 5ml/sec; room temperature.

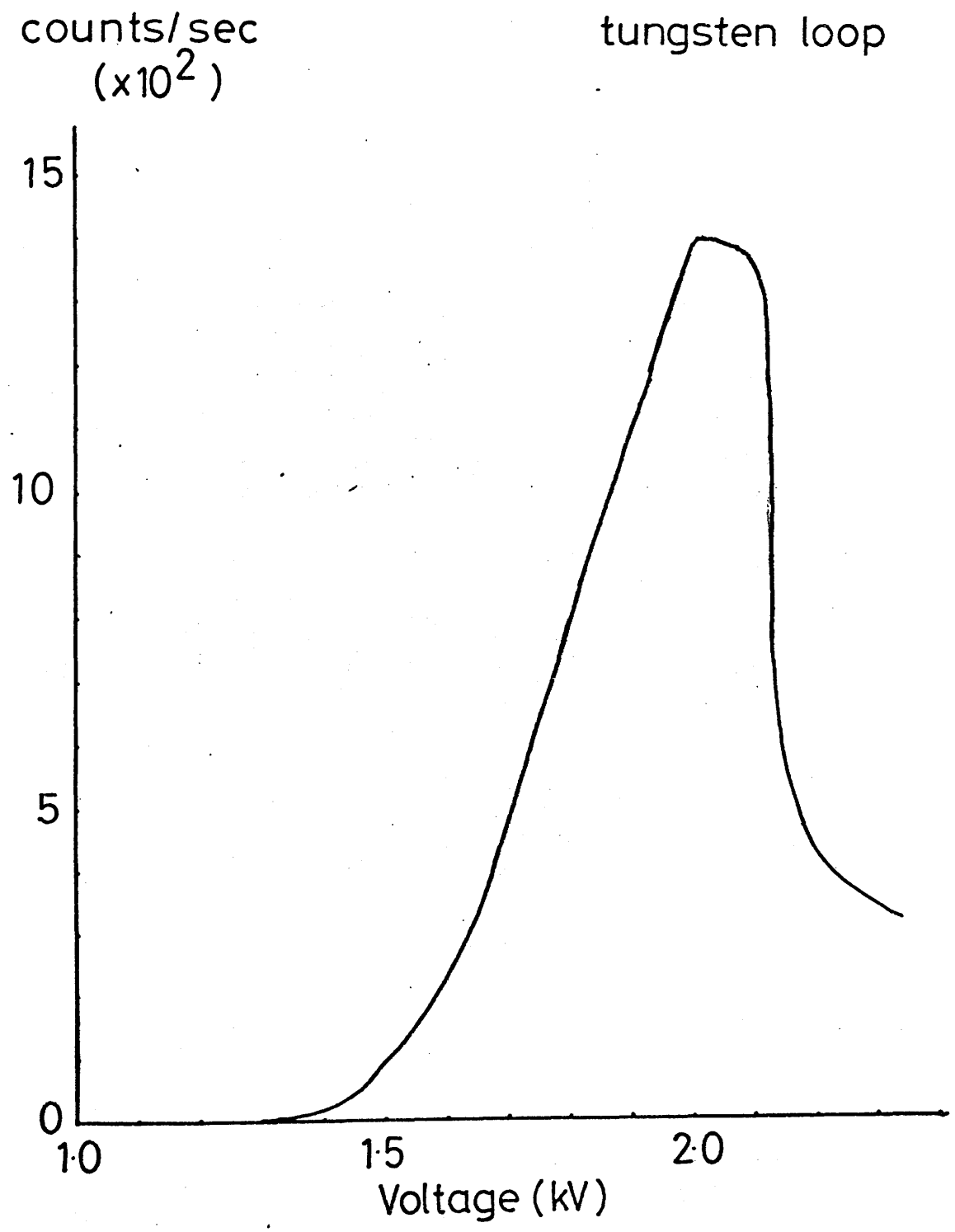

Graph 12.

Counts / sec versus voltage using internal ^{14}C source to determine plateau region. Anode shown in Diagram 9 page 59c.

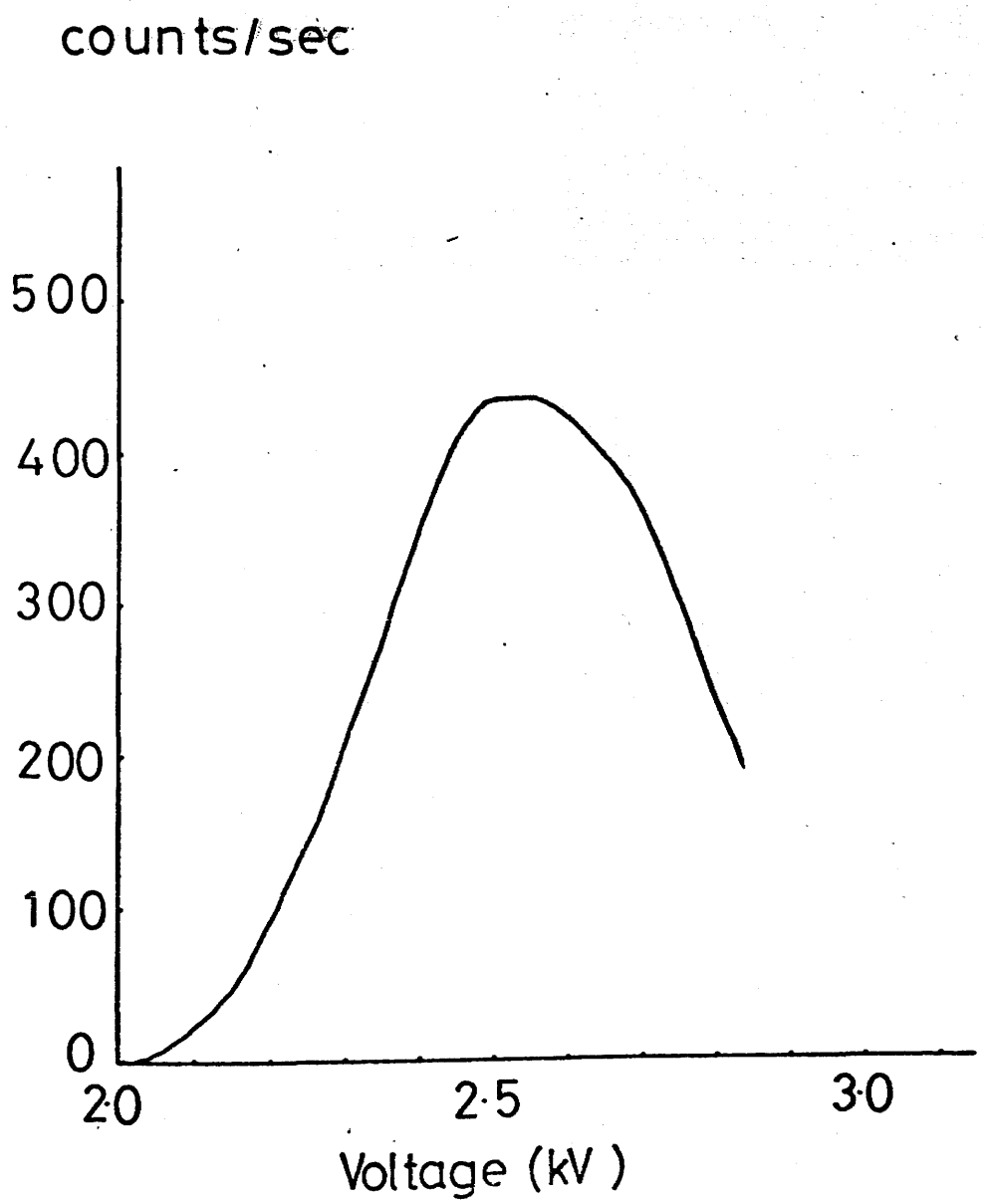

Appendix 4

Appendix 4

Table IV

Voltage (kV)	Discriminator setting 1·27 x 0·2 (Int) counts/sec		Discriminator setting 0·1 x 0·2 (Int) counts/sec		Δ(cps) cps(γ present) -cps(γ absent) 1·27 x 0·2 (Int)	Δ(cps) cps(γ present) -cps(γ absent) 0·1 x 0·2 (Int)
	γ present	γ absent	γ present	γ absent		
2·9	358	340			+18	-
3·0	420	345	2387	2342	+75	+45
3·1	453	339	2572	2372	+114	+200
3·2	433	340	1873	2721	+93	-848
3·3	263,312	329,429	628,1041	2670,2238	-92	-1620
3·4	148,132	315,311	249,228	1871,2226	-173	-1810
3·5	124,143	281,202	235,239	1782,1548	-108	-1428
3·6	131,138	238,264	209,200	1458,625	-117	-831
				989,1069		

If more than one value is presented, it is because there was a wide range of values. Only the average difference in emission rate is given in these cases.

Graph 13.

Counts/sec versus voltage using external γ source to investigate behaviour of an argon, ethylene, oxygen mixture as a counting gas. 0·42g supported silver catalyst present. Flow rate:- Ar 95ml/min, C_2H_4 25ml/min, O_2 50ml/min. T= 240°C.

Counts not corrected for background.

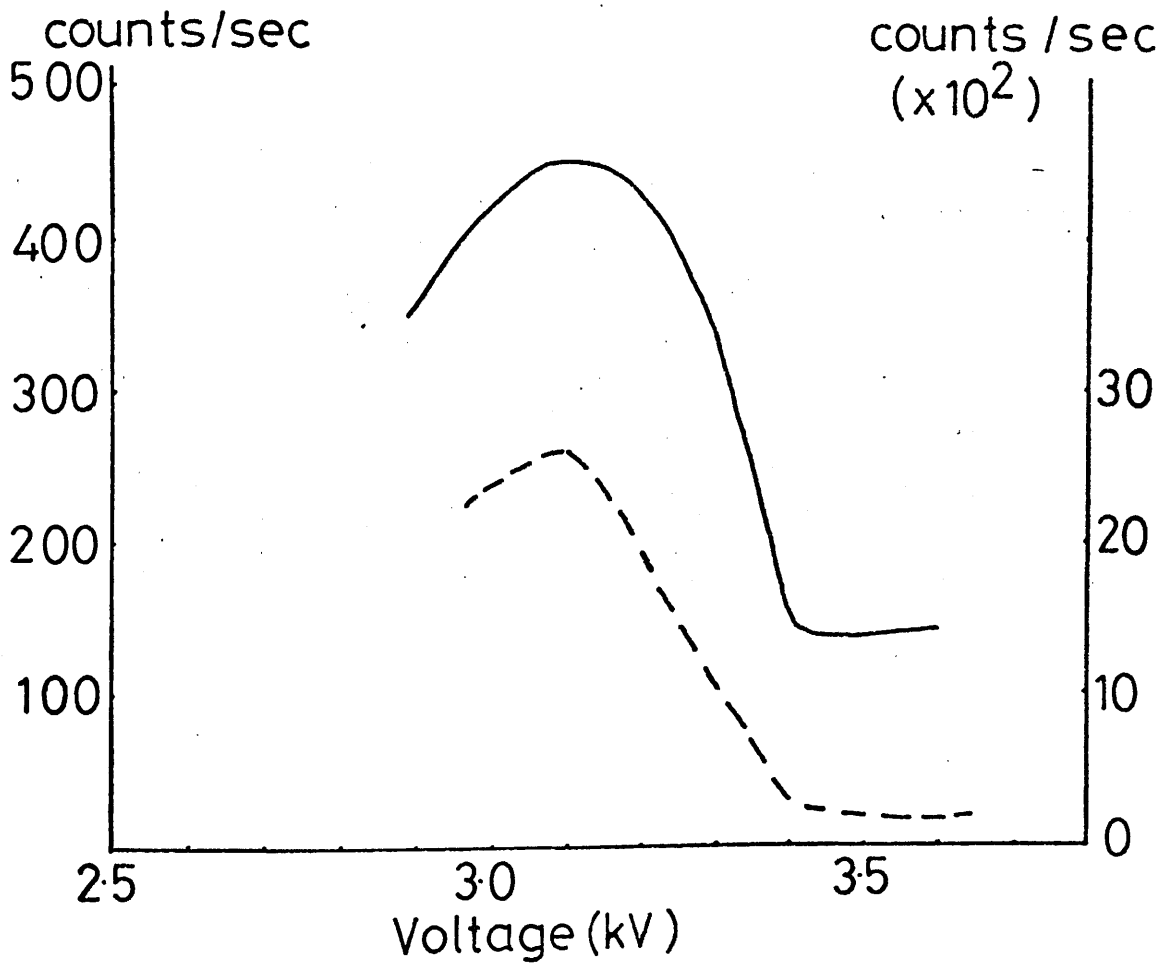

——— Discriminator setting 1·27x0·2 (Int)

- - - - - - - Discriminator setting 0·1x0·2 (Int)

(scale on the right).

Graph 14.

Counts/sec versus voltage at different temperatures to determine the effect on the counting characteristics. Internal ^{14}C source. Ar: C_2H_4 : O_2 95:25:50, flow rate 170ml/min. Anode 0·7cm from stainless steel mesh.

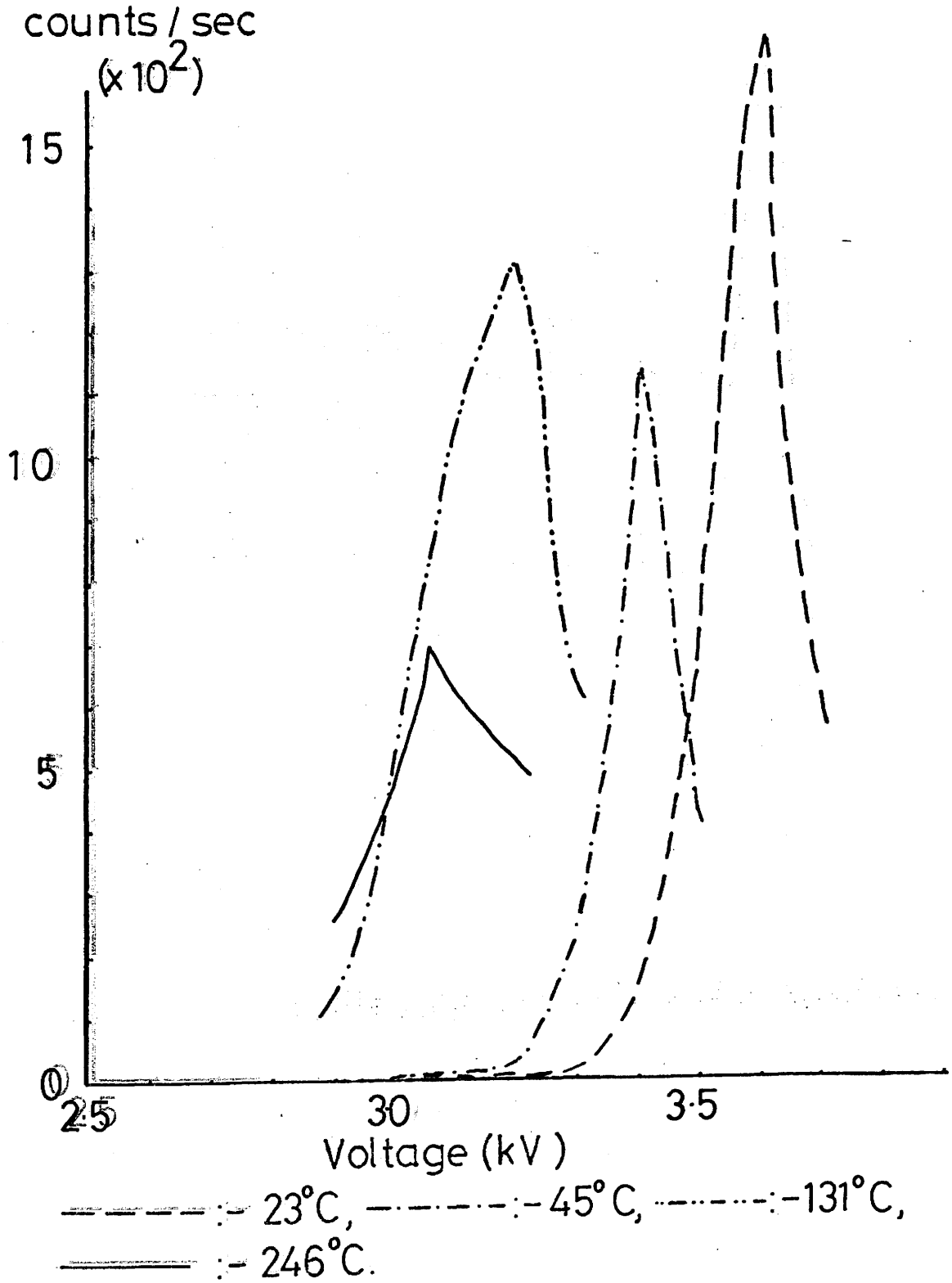

Graph 15.

Counts/sec versus voltage for different distances of the anode from the stainless steel mesh. ^{14}C source underneath mesh. Counting gas 170ml/min Ar, C_2H_4, O_2 in the ratio 95:25:50. Room temperature.

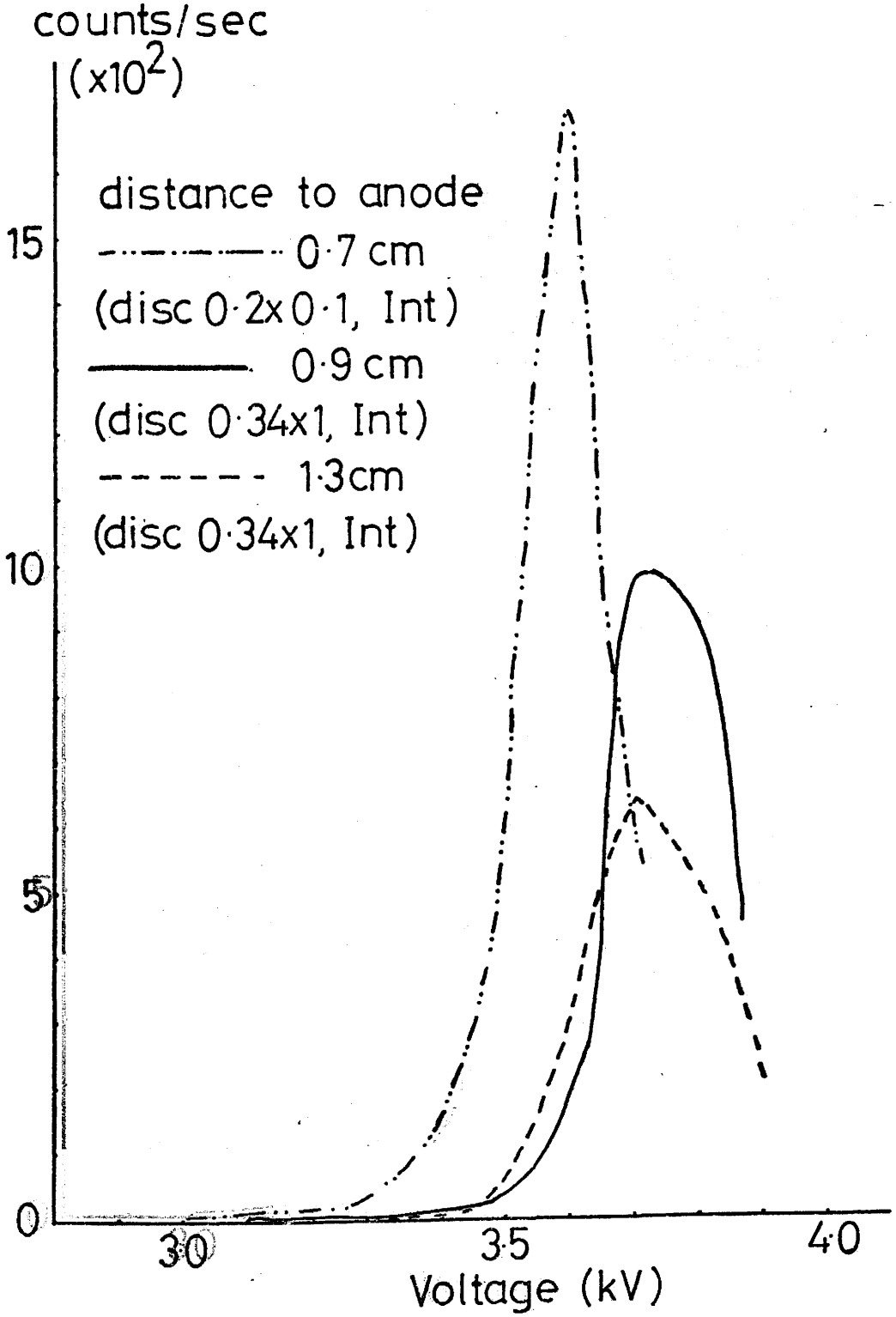

Appendix 5.

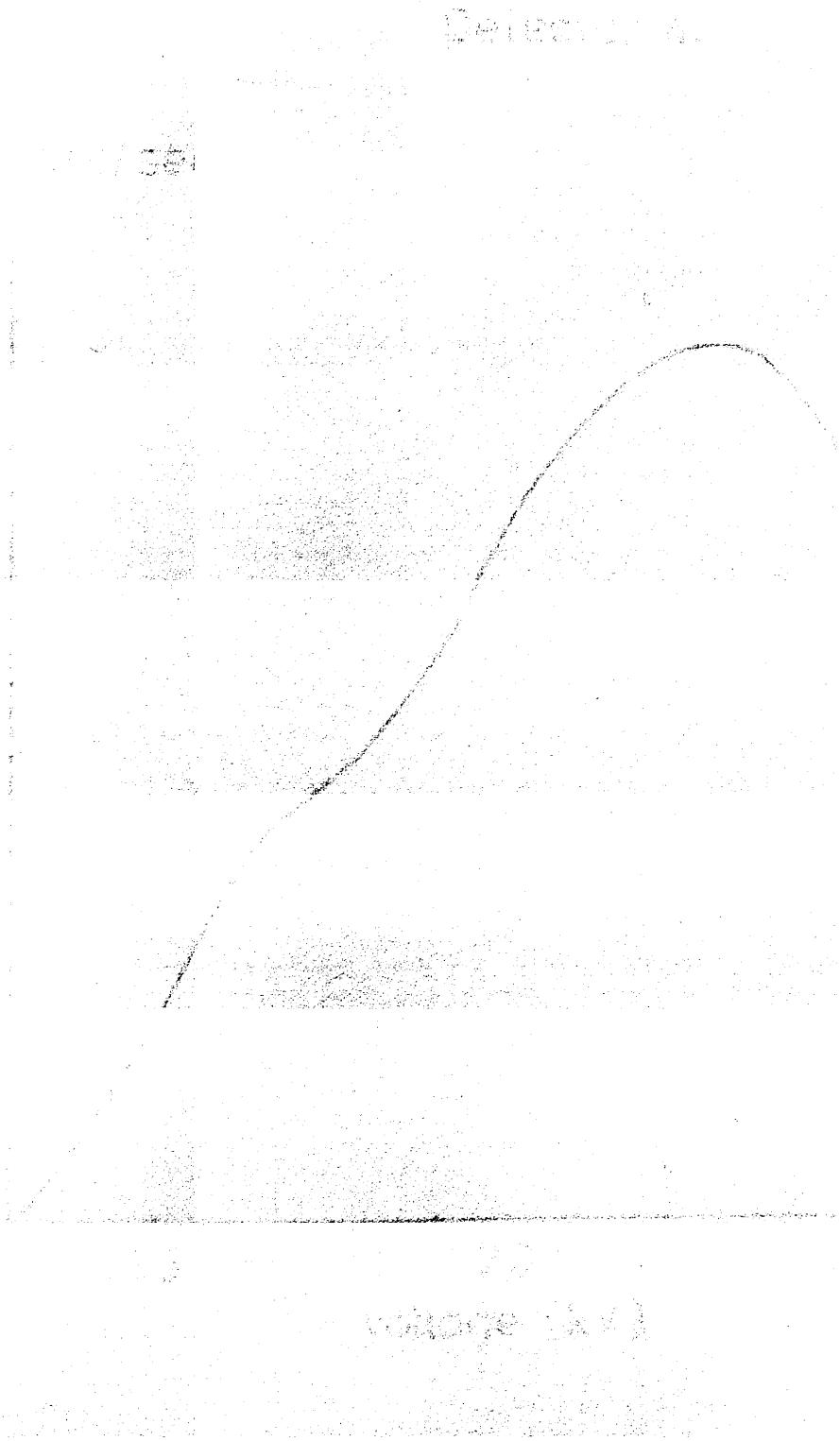

Graph 16.

Counts/sec versus voltage to determine plateau region using ^{137}Cs γ source.
Q gas the counting gas. Room temperature.

Detector 4.

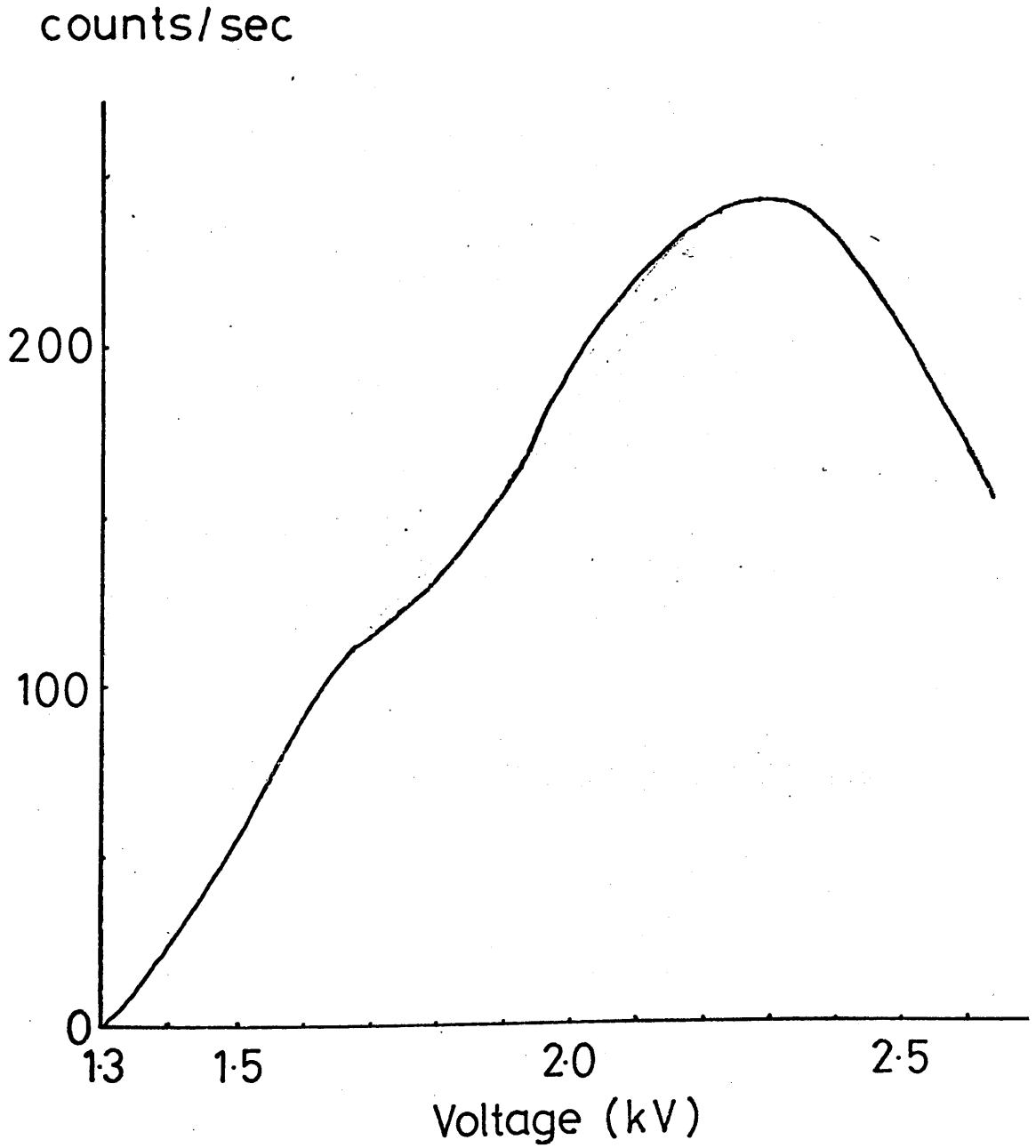

Table V

counts/sec after aluminium disc abraded.

counts/sec.	(averaged over 10 sec)
142·8	earthed
20·6	earthed (part of the time)
1·4	
55·1	earthed
2·3	
12·1	
11·1	
52·0	earthed
19·0	earthed (part of the time)
1·0	
3·2	
111·0	earthed
67·3	earthed
3·2	

The discriminator setting was 0·2 x 0·2 to bias out some of the background.

Appendix 6

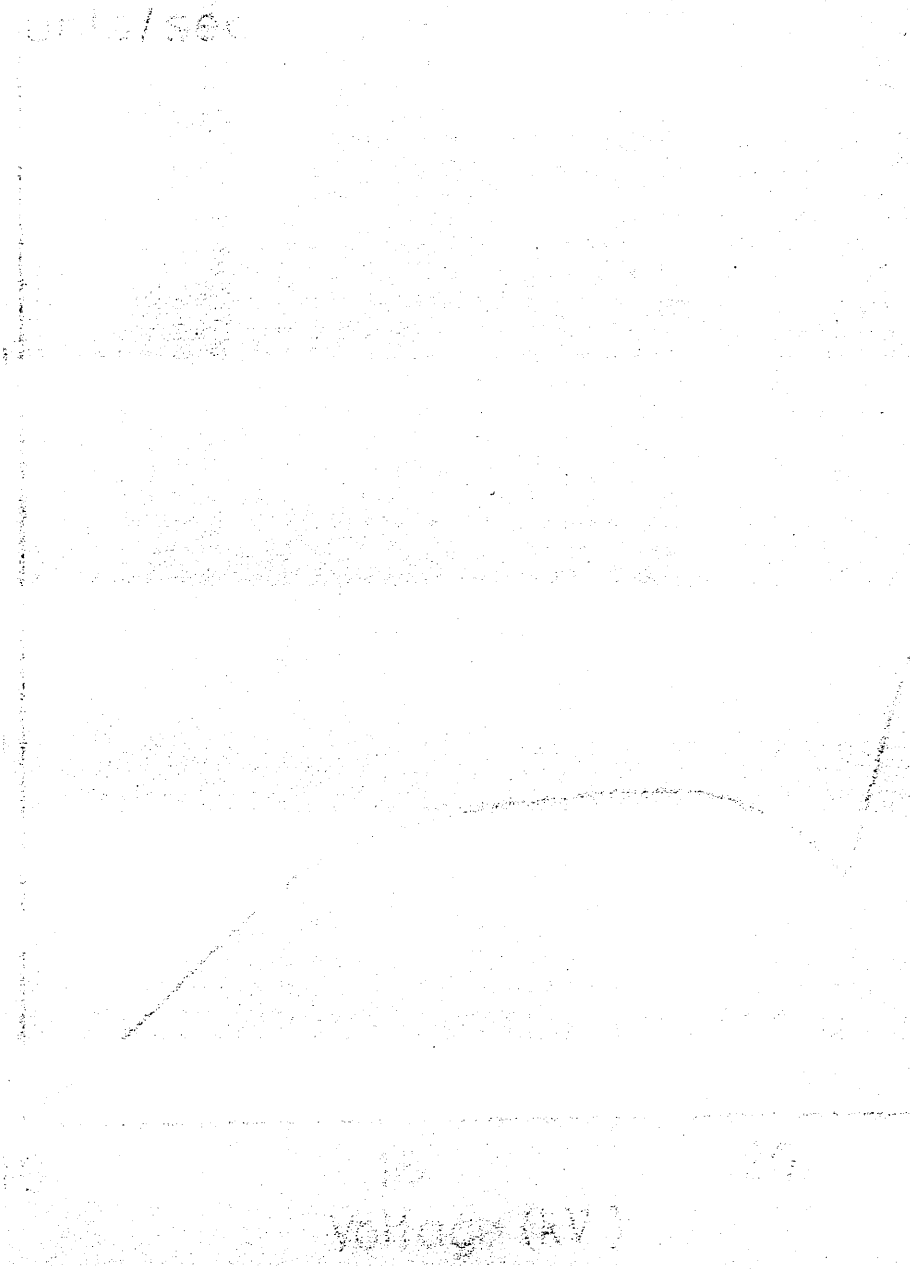

Graph 17.

Counts/sec, corrected for background, versus voltage to determine plateau region using ^{137}Cs as the source. Counting gas 1·6ml/sec Q gas. Room temperature.

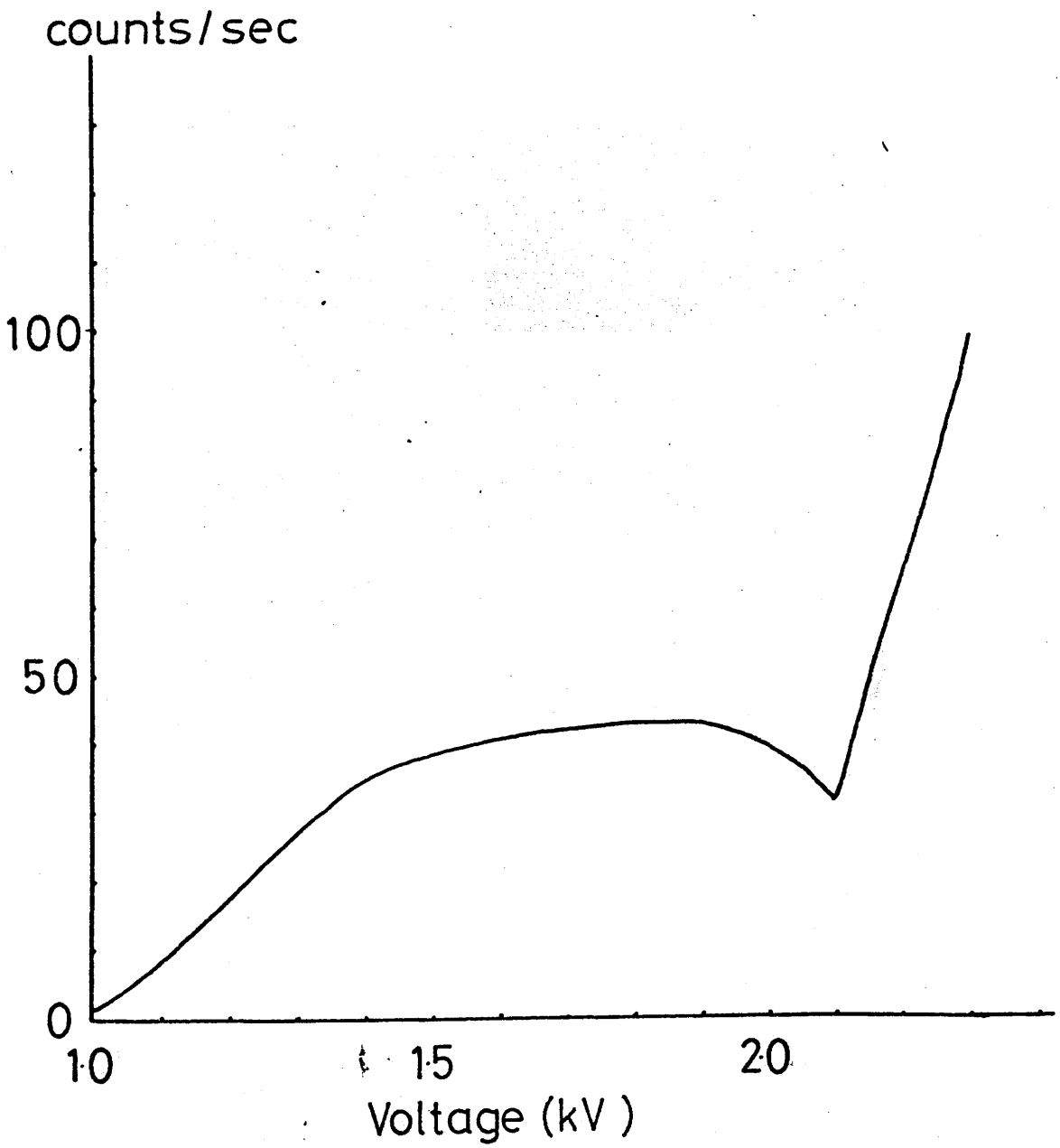

Graph 18.

Counts/sec versus voltage to determine plateau region using ^{137}Cs source. Counting gas 4ml/sec Q gas. Room temperature.

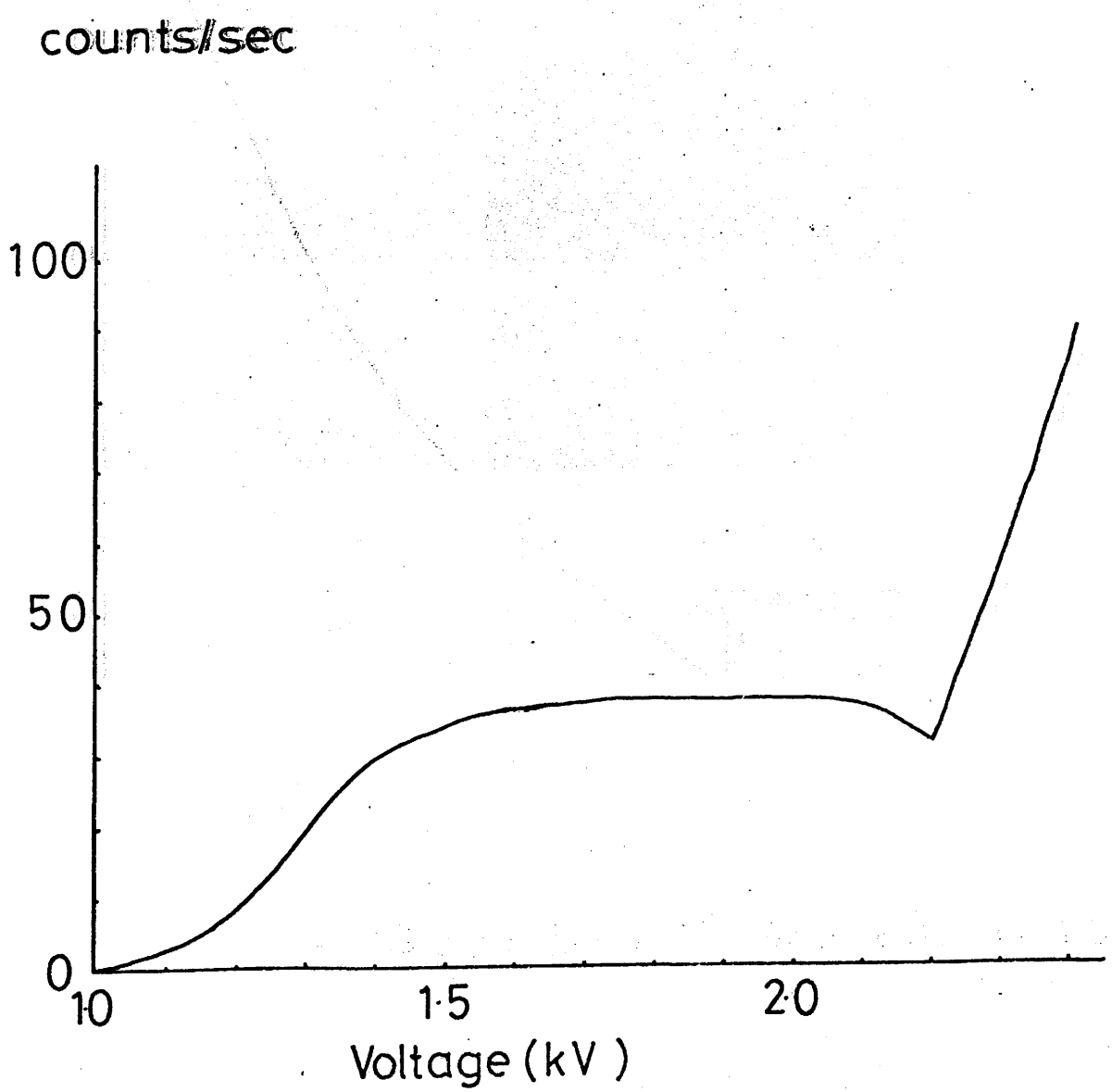

Graph 19.

Counts/sec versus time after 1·6A heating current switched off. Platinum filament.
Background ~~180~~ 160 cps.
Discriminator 0·1x0·2 Int.
Q gas

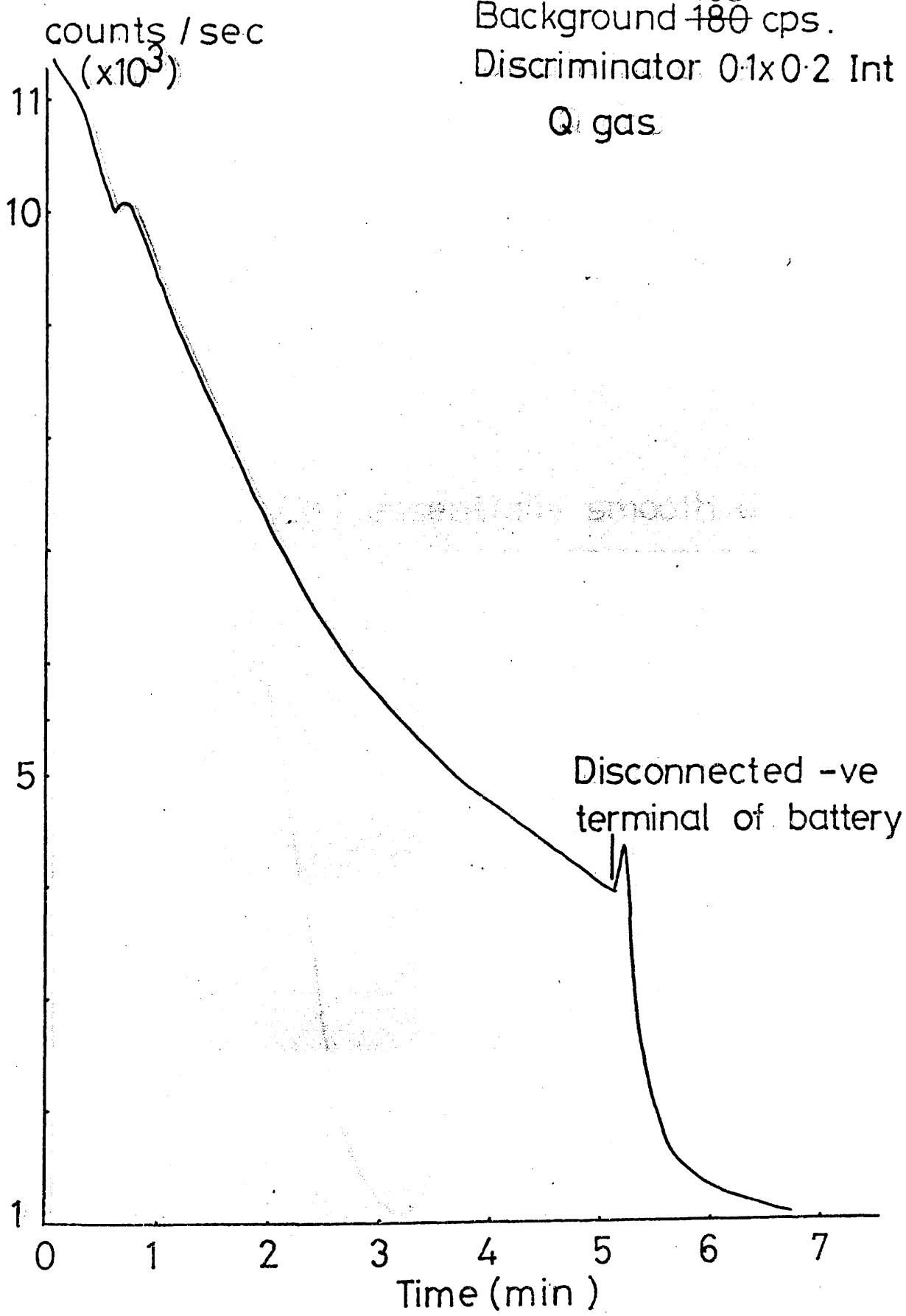

Graph 20.

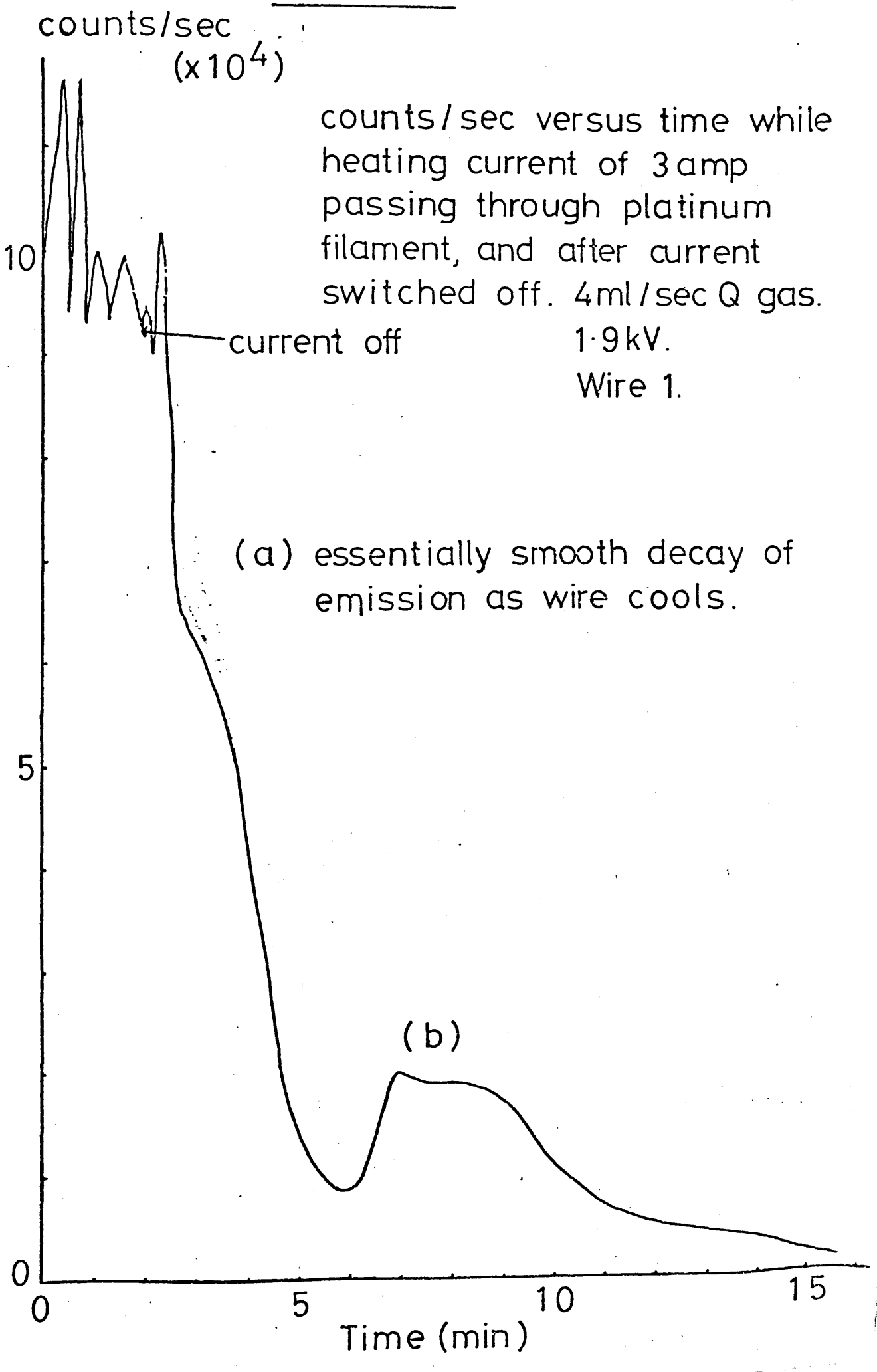
counts/sec
(x10^4)
10
5
0
0
5
10
15
Time (min)
current off
counts/sec versus time while heating current of 3 amp passing through platinum filament, and after current switched off. 4ml/sec Q gas.
1·9kV.
Wire 1.
(a) essentially smooth decay of emission as wire cools.
(b)

Graph 21.

Counts/sec versus voltage to determine plateau region using ^{137}Cs source. Counting gas 5ml/sec hydrogen. Room temperature.
1·9 kV.
Background ~ 90cps.

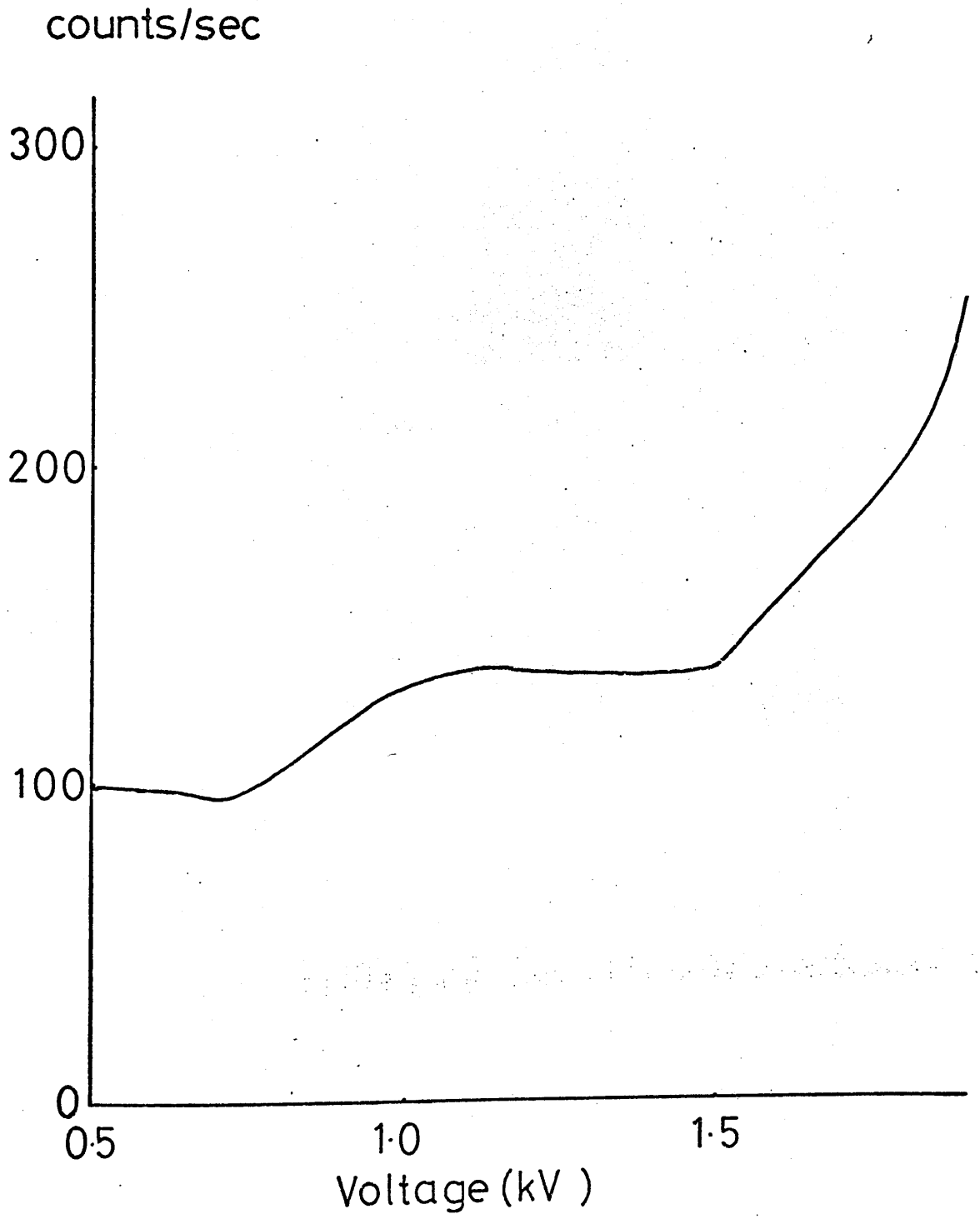

Appendix 7

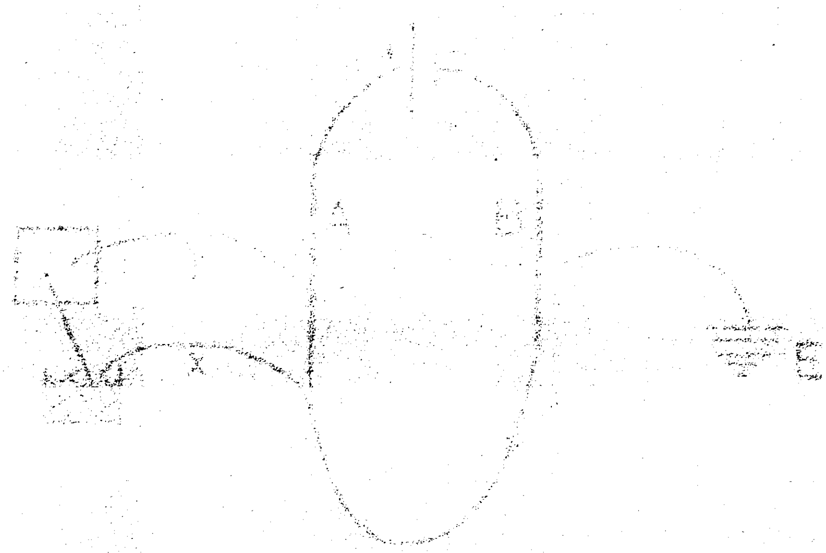

Appendix 7

Thermocouple Anomalies

An effect which can not be explained by us was observed with the thermocouple system. In general the arrangement of leads in the system was as shown in Diagram 19 page 74c. Both thermocouple leads, 'x' and 'y', came from the current output end of the wire with lead 'y' attached to tungsten rod A. Wire 'x', Pt,13% Rh, was twisted round the platinum wire to give a connection about one inch below the barrel connector used to connect the platinum wire and the tungsten rod, The earth lead was on the current inflow side attached to rod B. This is represented schematically in Diagram 20.

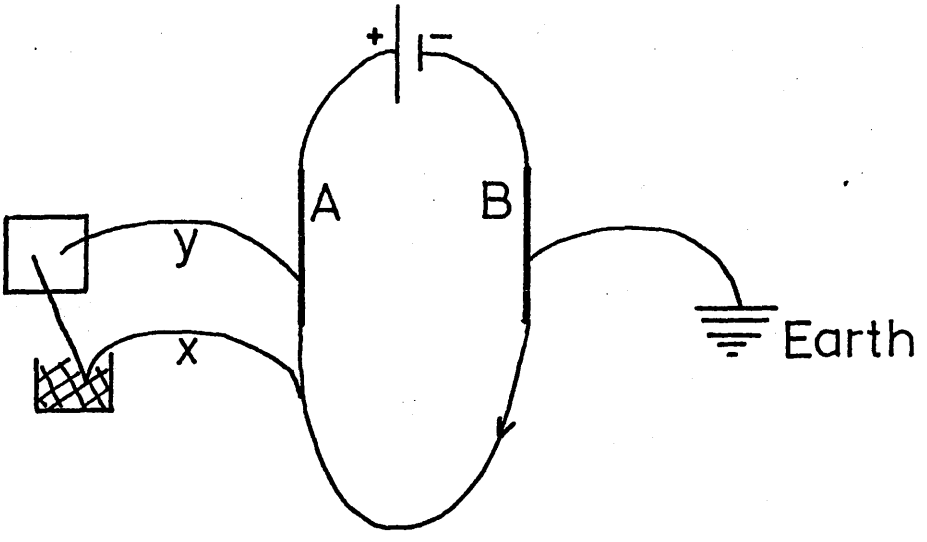

Diagram 20

With this arrangement if a current of say 4·1 A was passed through the circuit in the direction BA in an atmosphere of Q gas, the wire heated up evenly inside the cathode to a uniform bright orange. If the earth lead was disconnected the current became 3·5 A and the wire glowed orange.

If thermocouple lead 'y' and the earth lead were interchanged as shown in Diagram 21, but the current still flowed from B to A, then for the same rheostat setting the current registered on the ammeter increased to 4·8 A. The wire became bright orange almost up to the barrel connector on rod B. Because the wire outside the cathode was so bright, it was difficult to see inside the copper cylinder. However, it seemed that the wire was not uniformly orange, being much cooler near A. Some short-heating experiments were done with this

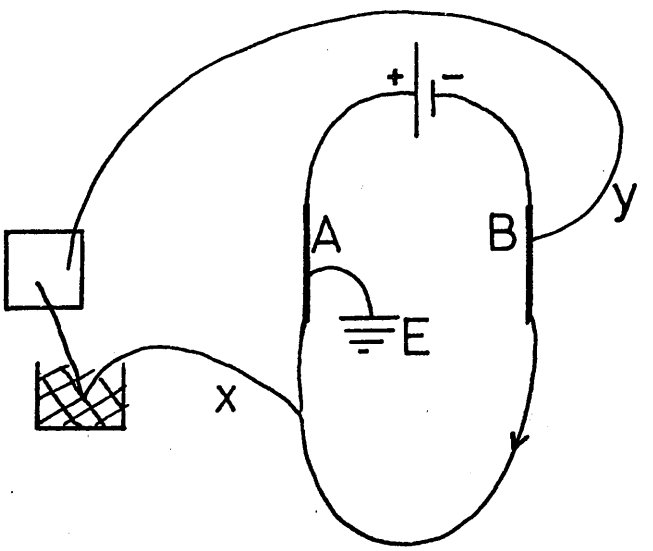

Diagram 21

arrangement and the thermocouple readings taken while the wire cooled were higher than in general; see Table VI page 210. Despite this, peaks were rarely obtained even with Q gas; see fig 19. Although the thermocouple readings may have been different because of the large distance separating 'x' and 'y', the few peaks obtained were taken to indicate that the wire was in fact much cooler than it seemed from its colour outside the cathode.

When current is flowing in the system some must go to earth and the difference in the magnitude of the current with the two arrangements may be accounted for by the fact that changing the position of the earth connection will change the effective resistance in the circuit.

These experiments were repeated with the direction of current flow reversed i.e. from A to B. Everything else was kept the same. When both thermocouple leads came from the current inflow side, as shown in Diagram 22, and the earth

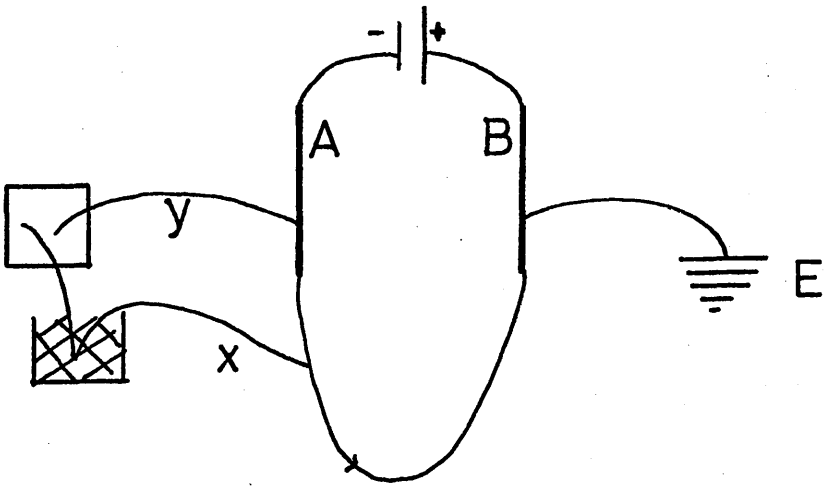

Diagram 22

Table VI

Dependence of Thermocouple Readings on Position of Thermocouple Leads. (a) - 'x' and 'y' both at A (b) - 'x' at A, 'y' at B.

Time after switch off	N_2		Q gas		H_2	
(min)	(a)	(b)(4·8A)	(a)(4·2A)	(b)(4·8A)	(a)(5·6A)	(b)(5·8A)
0·5		1·20	0·61	1·09	0·19	0·50
1·0		0·875	0·52	0·905	0·145	
1·5		0·70	0·43	0·715	0·115	0·19
2·0		0·565	0·37	0·63	0·095	0·15
2·5		0·485	0·32	0·57	0·085	0·13
3·0		0·42	0·28	0·515	0·08	0·12
3·5		0·365	0·235	0·465	0·0725	0·11
4·0		0·33	0·22	0·43	0·07	0·10
4·5		0·295		0·395	0·07	0·095
5·0			0·18	0·35		0·09

Time after switch off	N_2 (after H_2)		O_2		O_2	
(min)	(a)(4·3A)	(b)(4·9A)	(a)(4·4A)	(b)(5·0A)	(a)(4·4A)	(b)
0·5	0·54	0·755	0·75	1·20	0·635	
1·0	0·445	0·64	0·595	0·98	0·525	
1·5	0·365	0·55	0·49	0·785	0·4325	
2·0	0·305	0·475	0·405	0·69	0·36	
2·5	0·26	0·41	0·345	0·61		
3·0	0·22	0·40	0·295	0·56	0·28	
3·5	0·1725	0·375		0·52		
4·0		0·31	0·23	0·46	0·205	
4·5	0·14	0·285		0·41		
5·0		0·245	0·19	0·36	0·17	

figure 19.

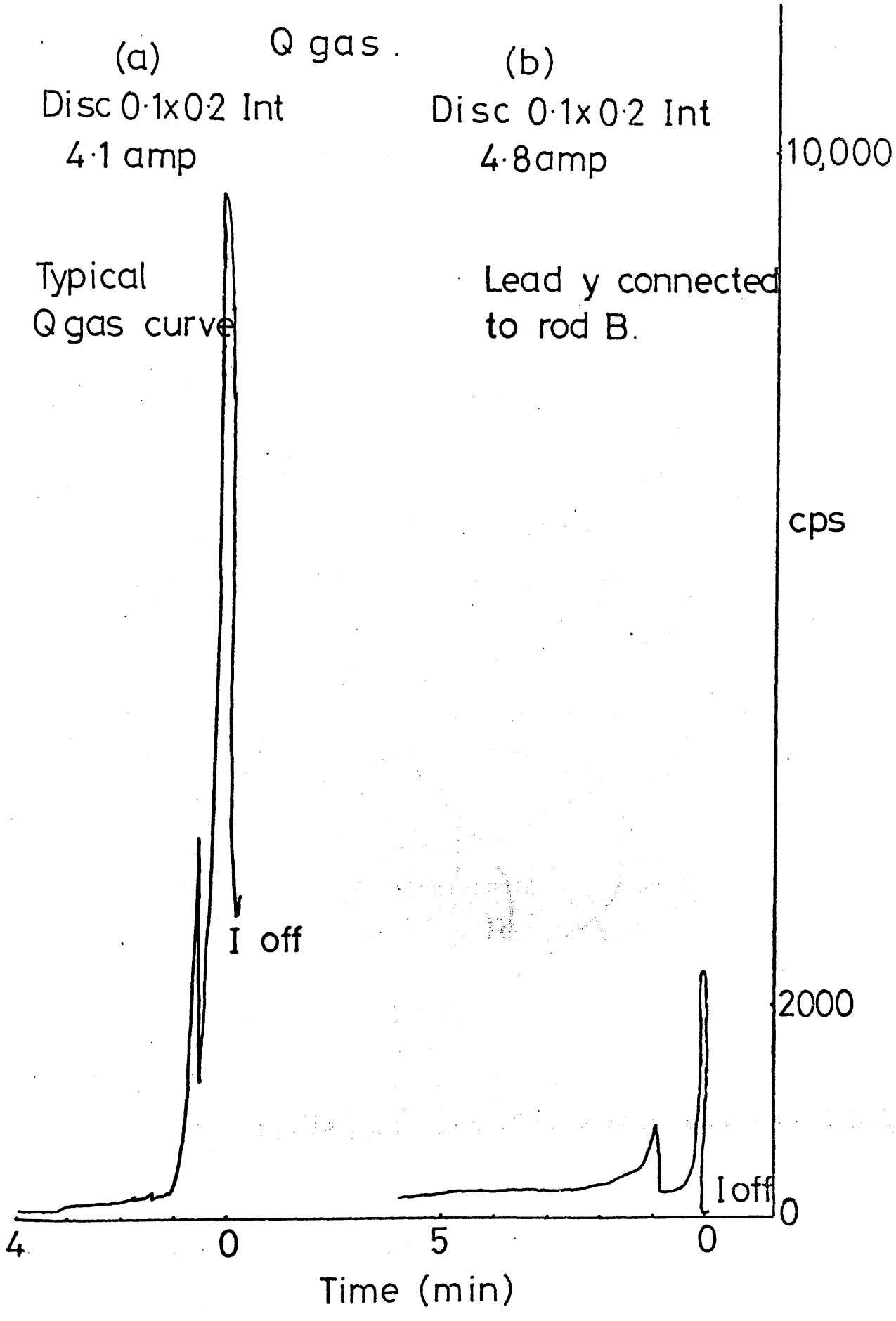
Q gas.
(a)
Disc 0·1x0·2 Int
4·1 amp
(b)
Disc 0·1x0·2 Int
4·8amp
10,000
Typical
Q gas curve
Lead y connected
to rod B.
cps
I off
2000
I off
0
4
0
5
0
Time (min)

lead was connected to B, the current was 4·1 A. The wire heated up evenly inside the cathode to a bright orange. It had been expected that the current would be 4·8 A since the earth connection was at the current outflow end of the wire.

When 'y' was connected to B and the earth lead to A as in Diagram 23, that is the earth at the current input end, the current measured was 4·7 A. The wire seemed to be bright orange outside and inside the cathode although it was difficult to see inside the copper cylinder. In this situation a current in the region of 4·1 A would have been predicted.

At present it is not possible to explain this effect. It should be noted that there was no potential difference across the wire when thermocouple readings were taken.

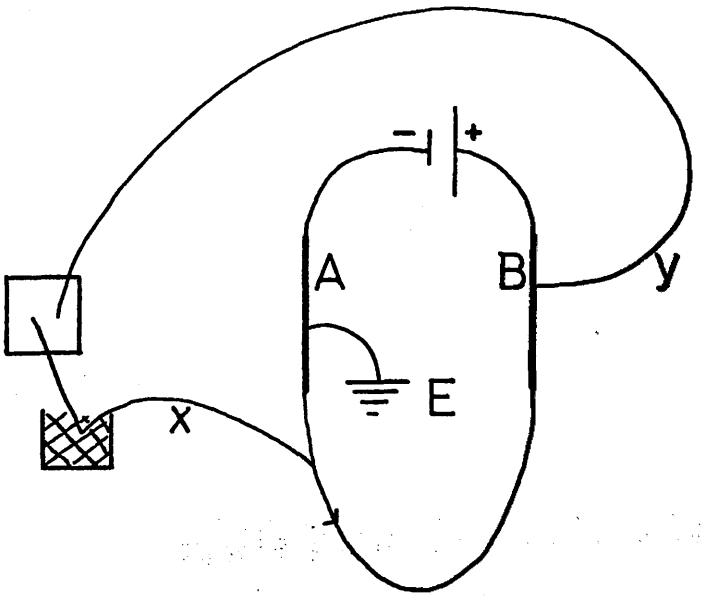

Diagram 23

Appendix 8

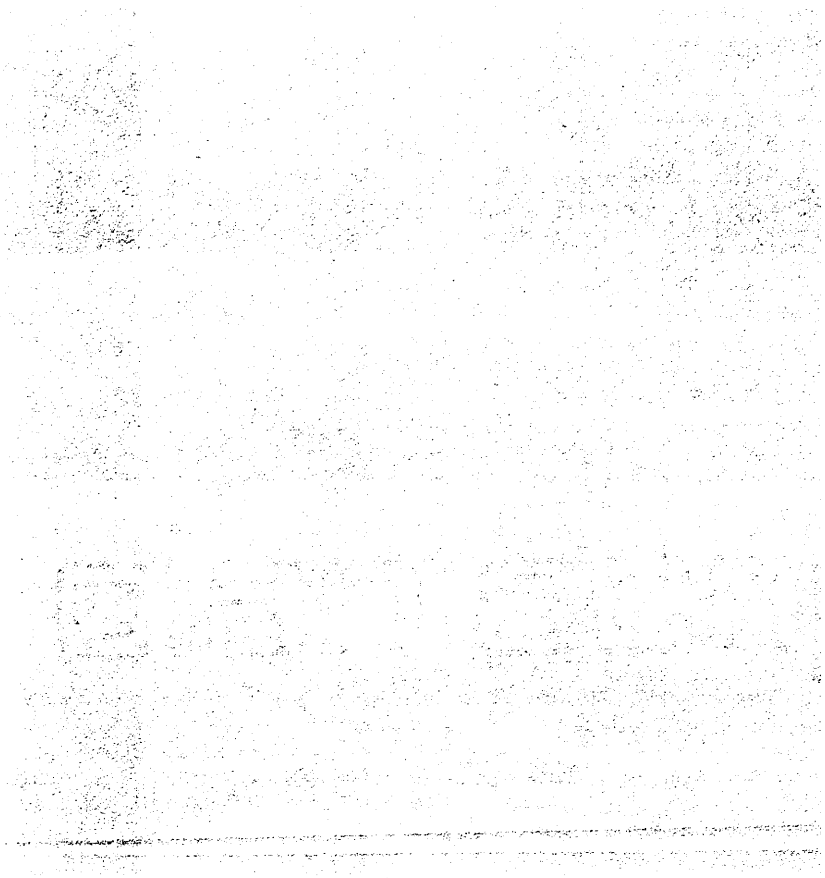

Laben spectrum 1

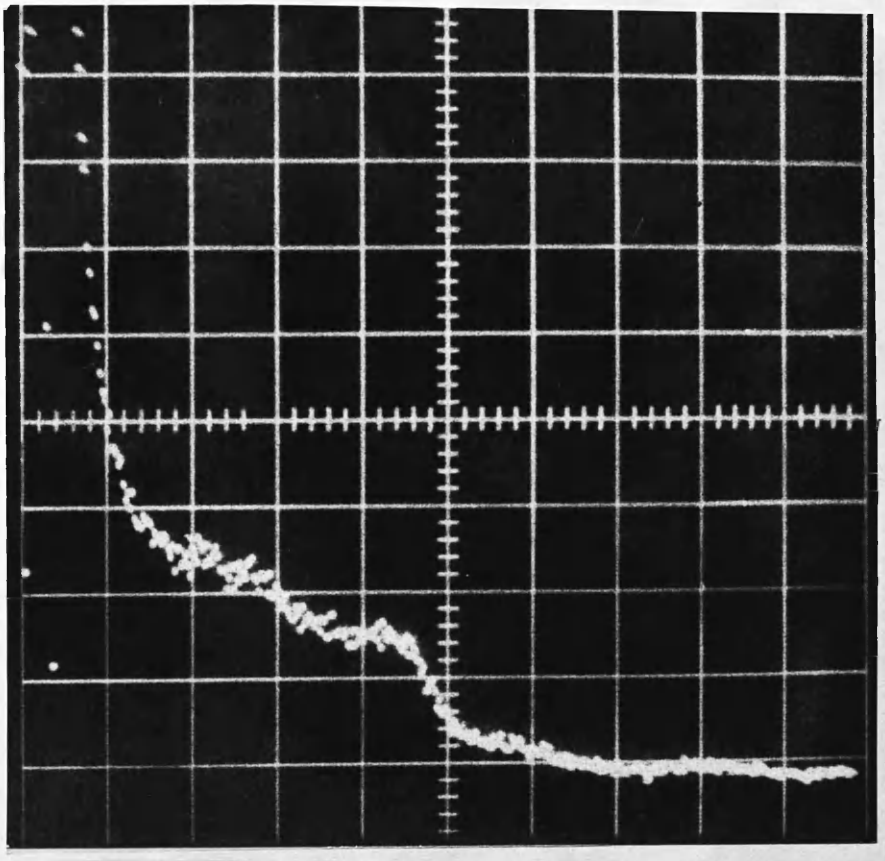

Counts accumulated for 120 min with $^{241}_{95}Am$ present.

Americium edge - channel 177.

(Laben gain x25 Range 5 x 10^3 Back bias 0

Channel width 20mV Biased amplifier gain x2 Bias 0.

Anode voltage 1·9kV.)

Laben spectrum 2

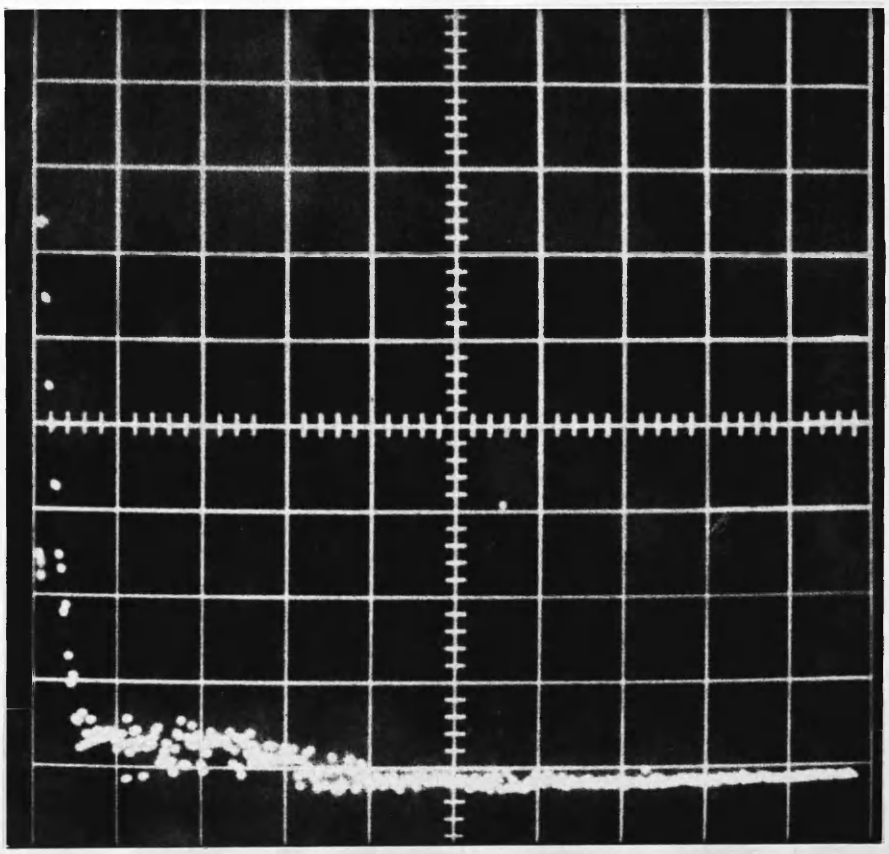

Counts accumulated for 30 min with no source present.

(Laben gain x25 Range x 10^3 Back bias 0
Channel width 20mV Biased amplifier gain x2 Bias 0.
Anode voltage 1·9kV.)

Appendix 9

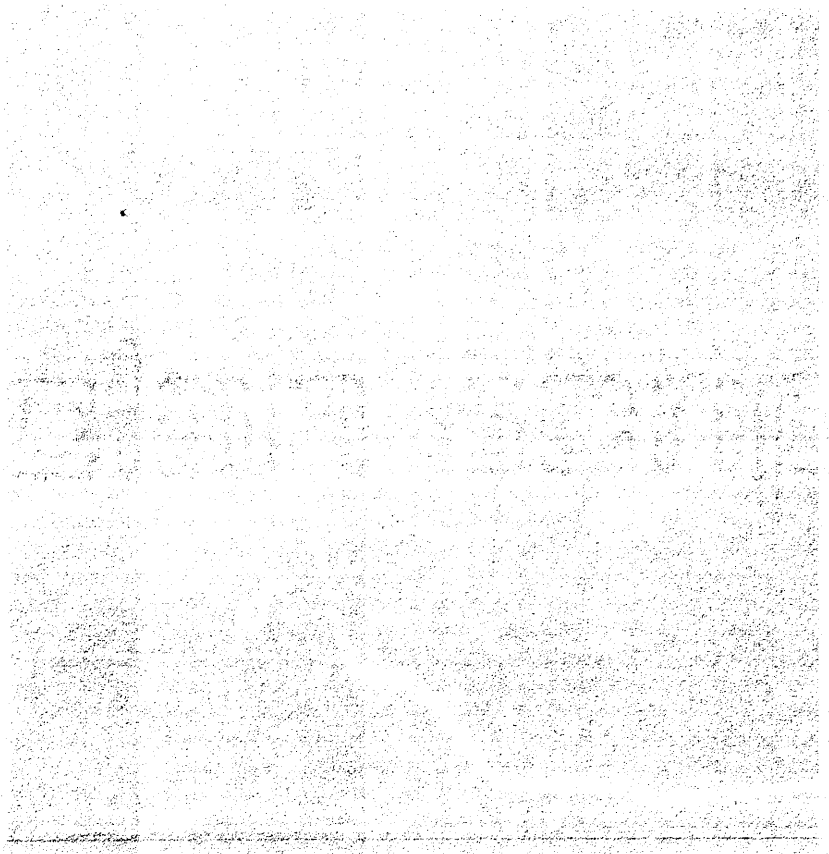

Laben spectrum 3

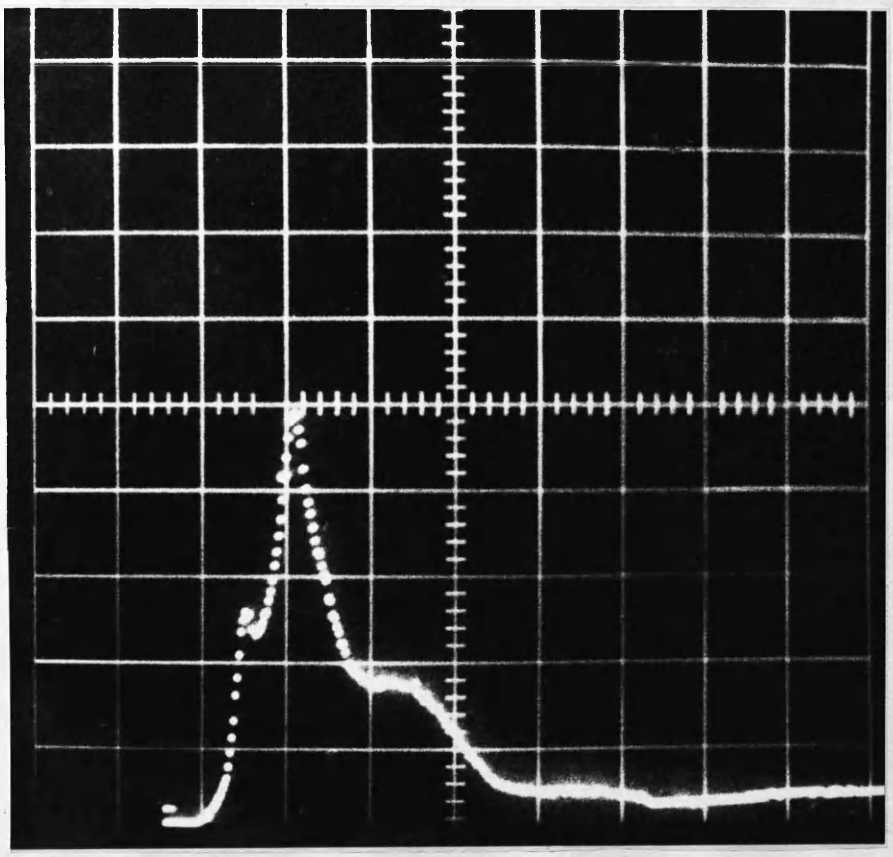

Range 5 x 10^4 channel width 20mV/channel

Peaks - channels 40, 64, 109.

Laben spectrum 4

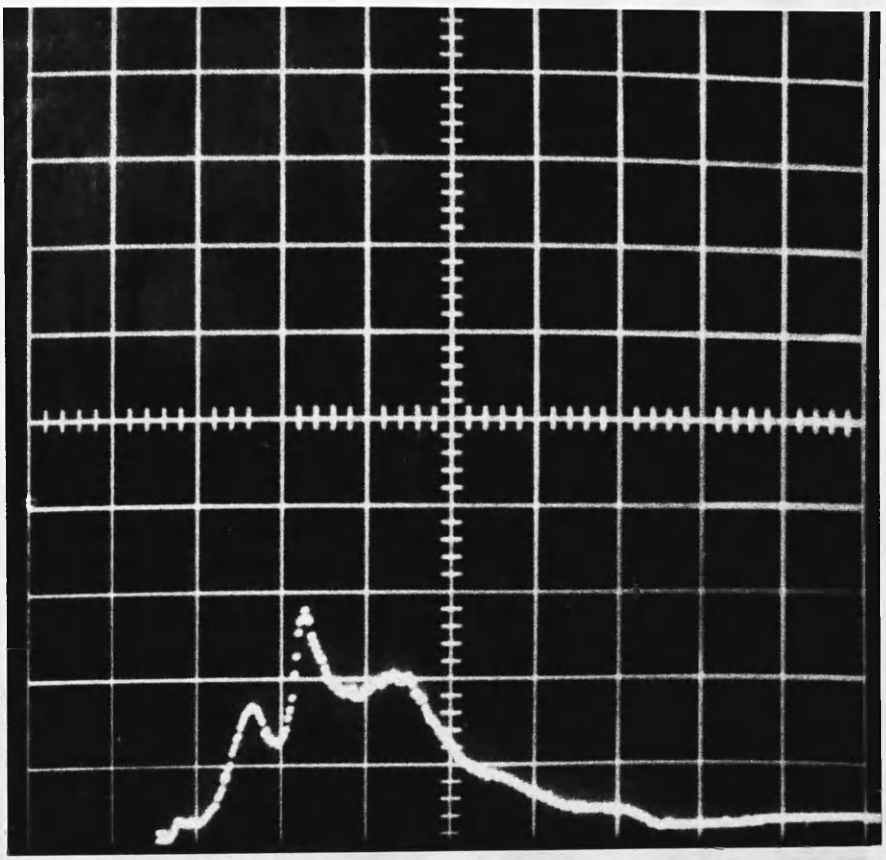

Range 5 x 10^4 Channel width 20mV/channel

Peaks 14, 45, 70, 112, shoulder 135 small peaks 160, 220.

Label spectra 3 and 4 each correspond to the first three minutes of the wire cooling in nitrogen after H_2, N_2, O_2 and N_2 passed over the hot wire in sequence.

Laben spectrum 5

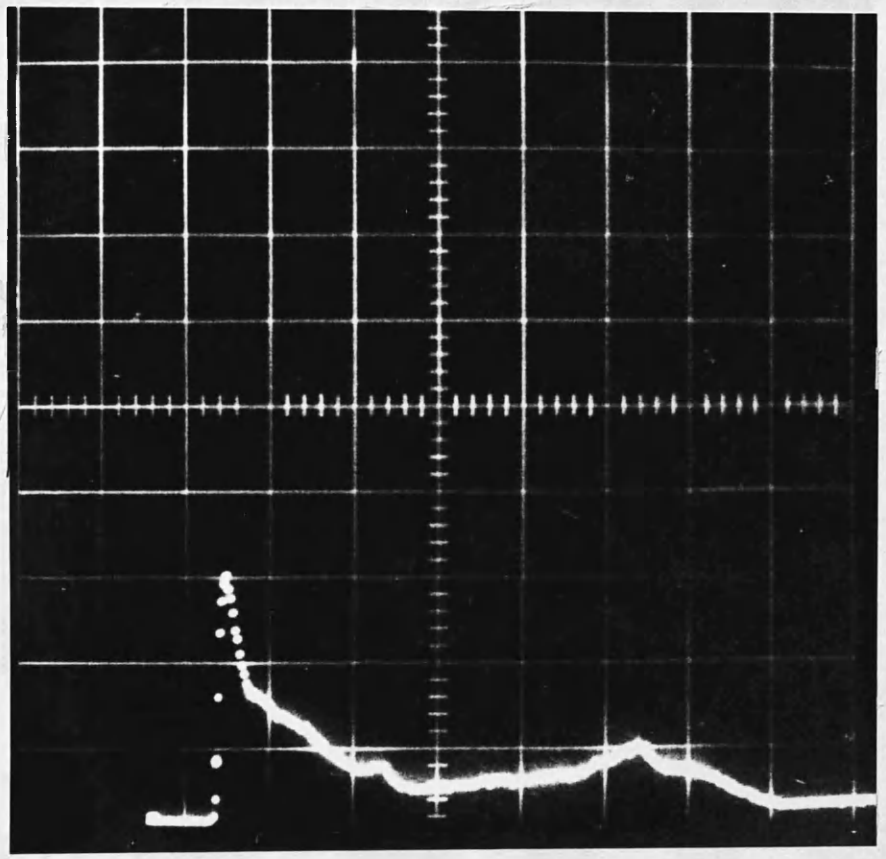

Range 5 x 10^4 Channel width 20mV/channel

Peaks 38, shoulder 53, shoulder 73, 109,

164, shoulder 212, 238, shoulder 258.

Laben spectrum 6

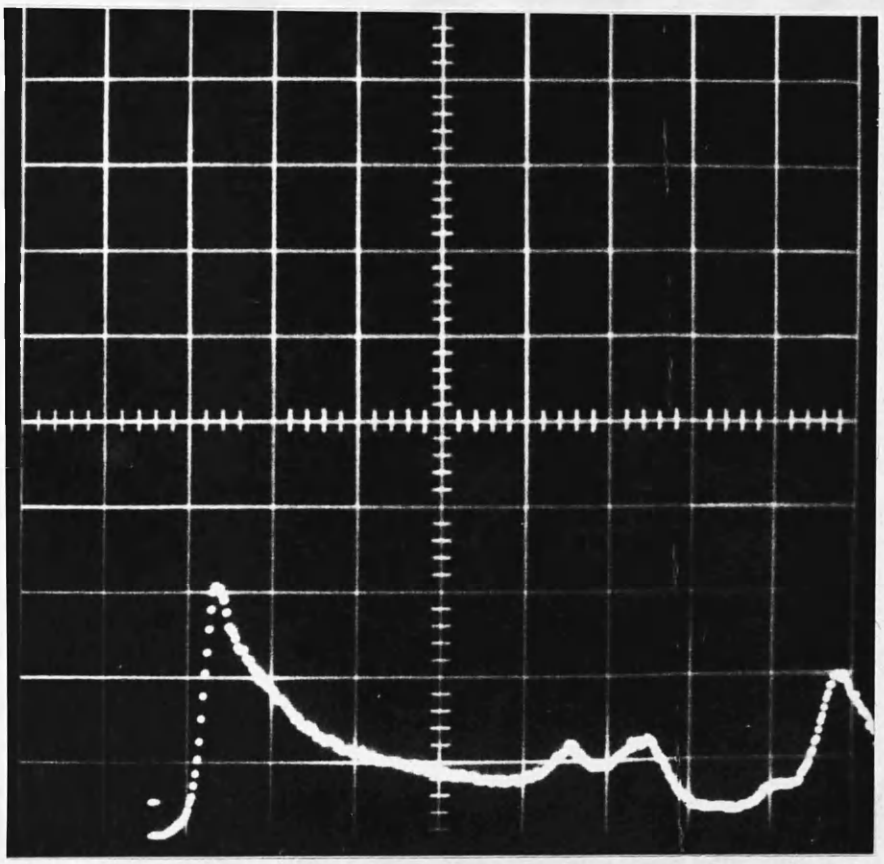

Range 5 x 10^4 Channel width 20mV/channel

Peaks 33, 200, shoulder 224, 237, 300, 336, shoulder 352.

Laben spectra 5 and 6 correspond to a cooling curve obtained in H_2 after the wire was heated in N_2. Laben spectrum 5 ≡ 0 - 3 min of curve. Laben spectrum 6 ≡ 5·5 - 7·5 min of cooling curve.

In future the Laben Spectra will be traced from the photographs and the traces presented.

Appendix 10

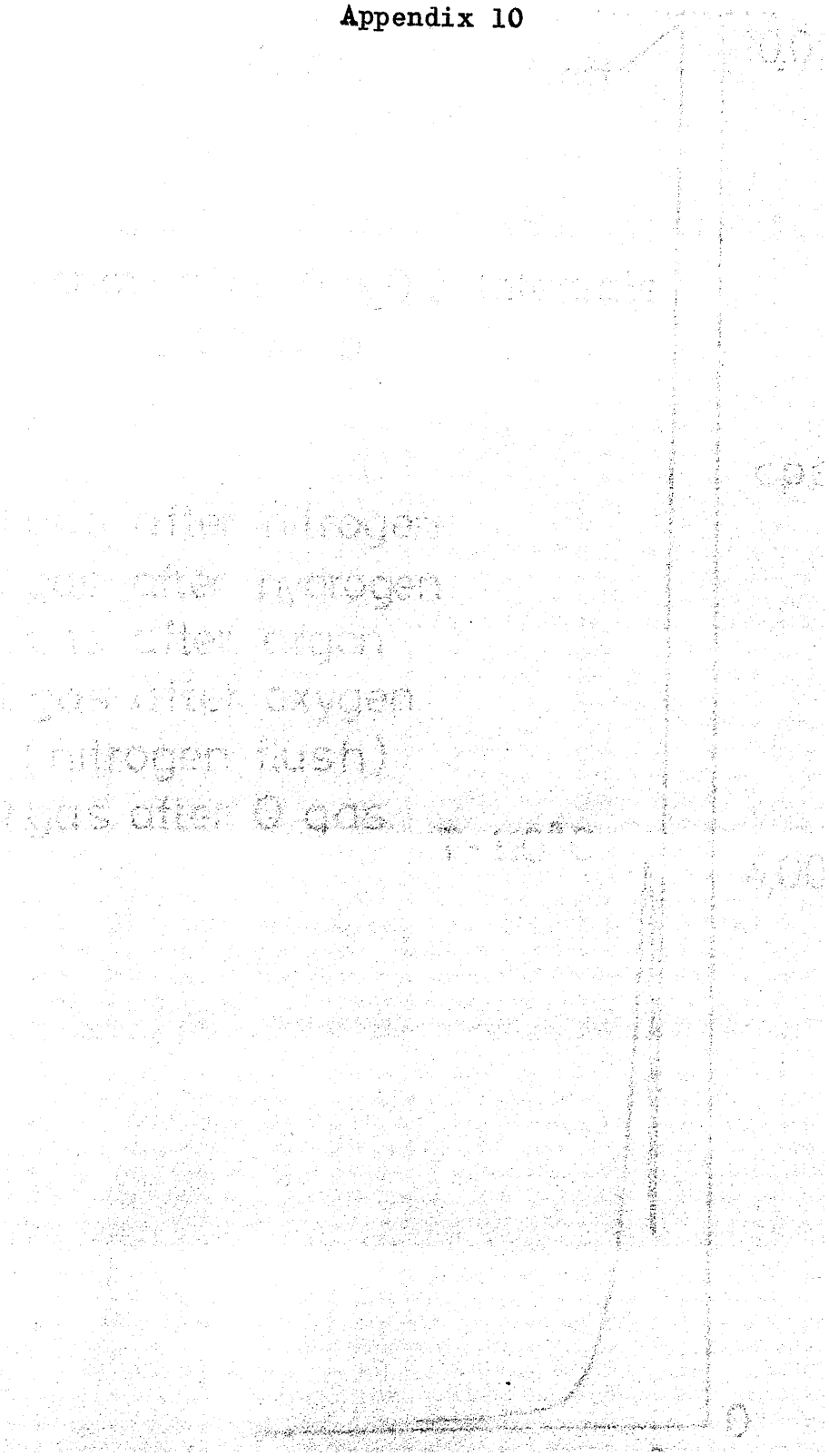

figure 28.

Typical Q gas cooling curve.

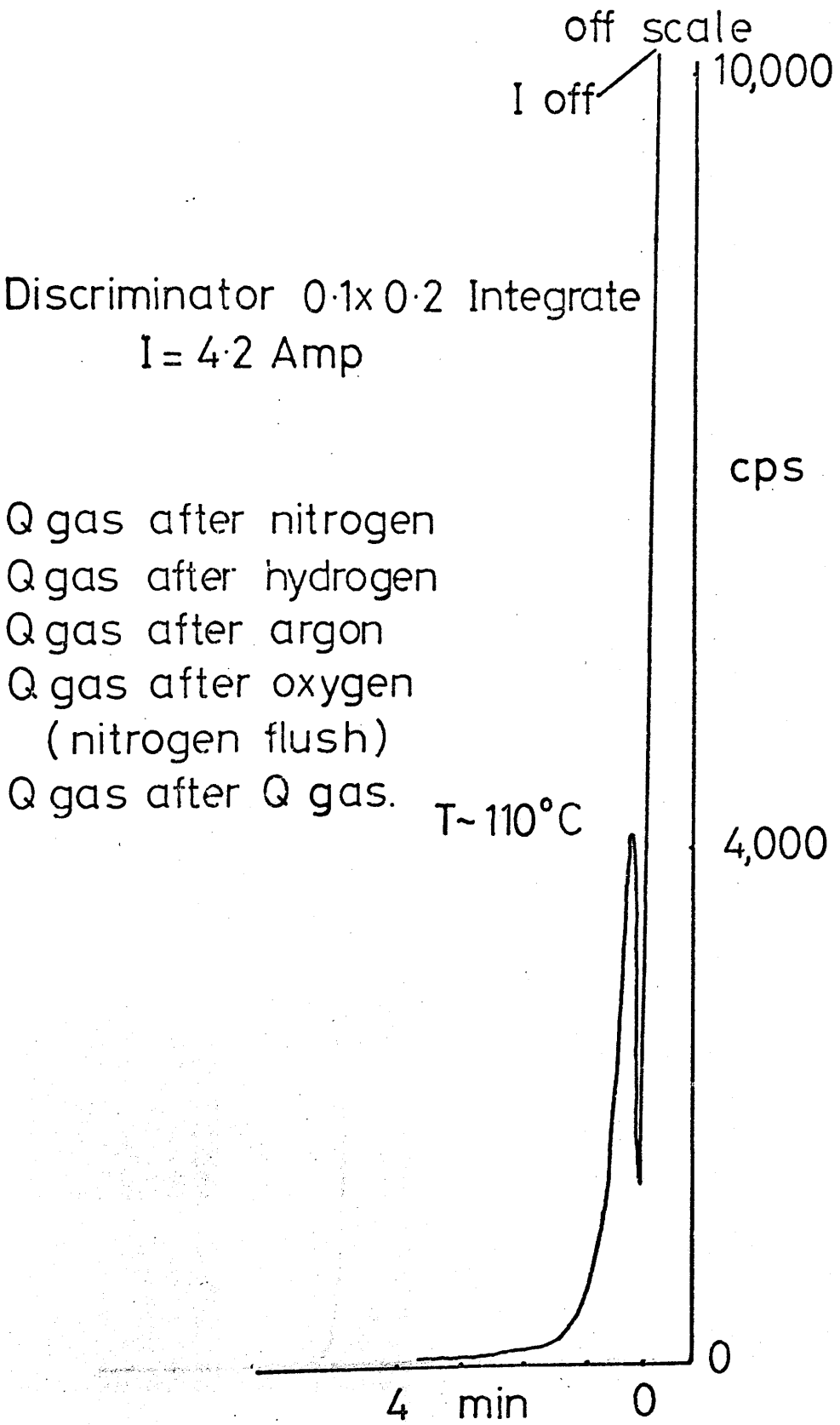

figure 28a.

Q gas cooling curve early in the history of wire 5.

Discriminator 0·1x1, Integrate.

I = 3·8 Amp

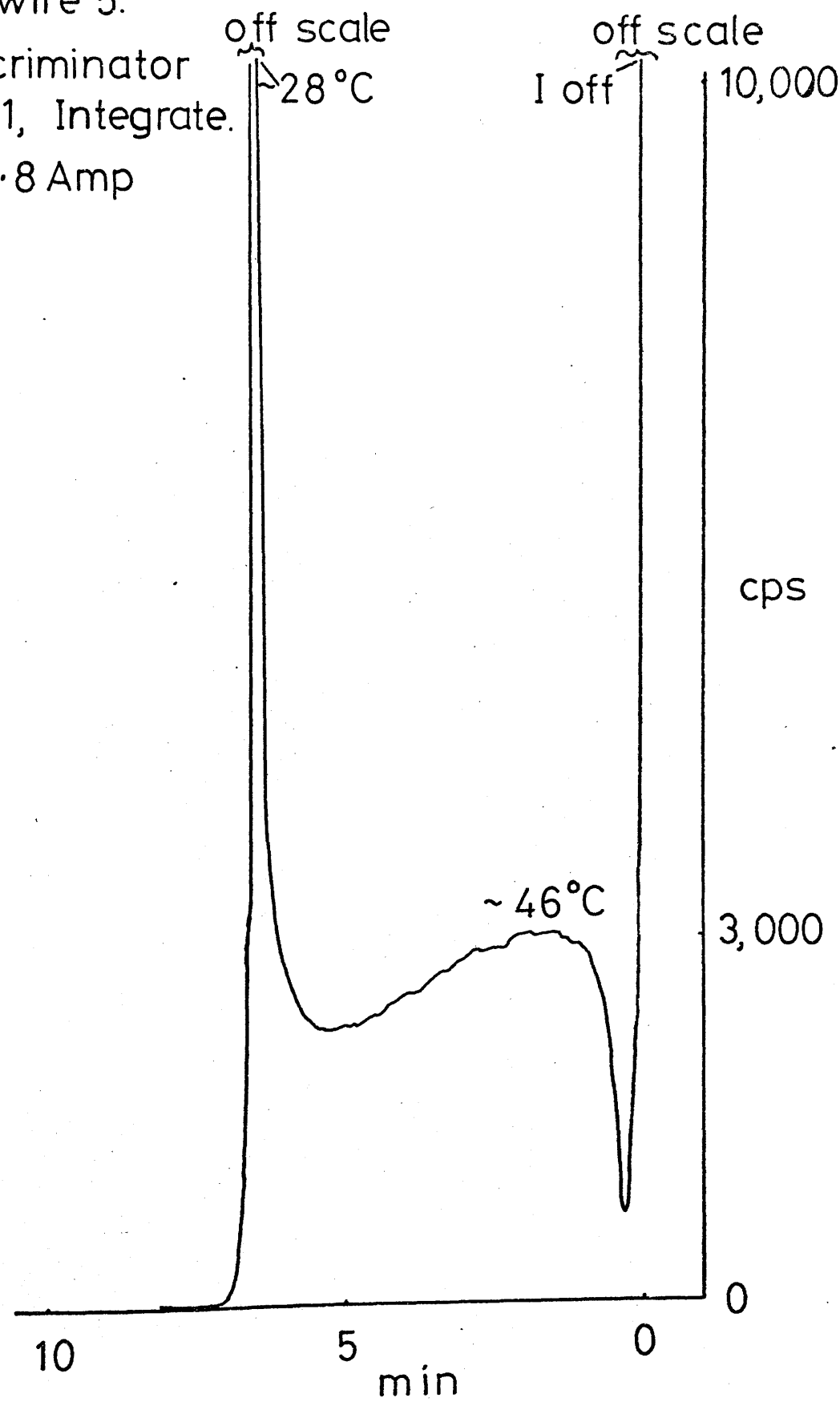

figure 29.

Q gas after acetylene.

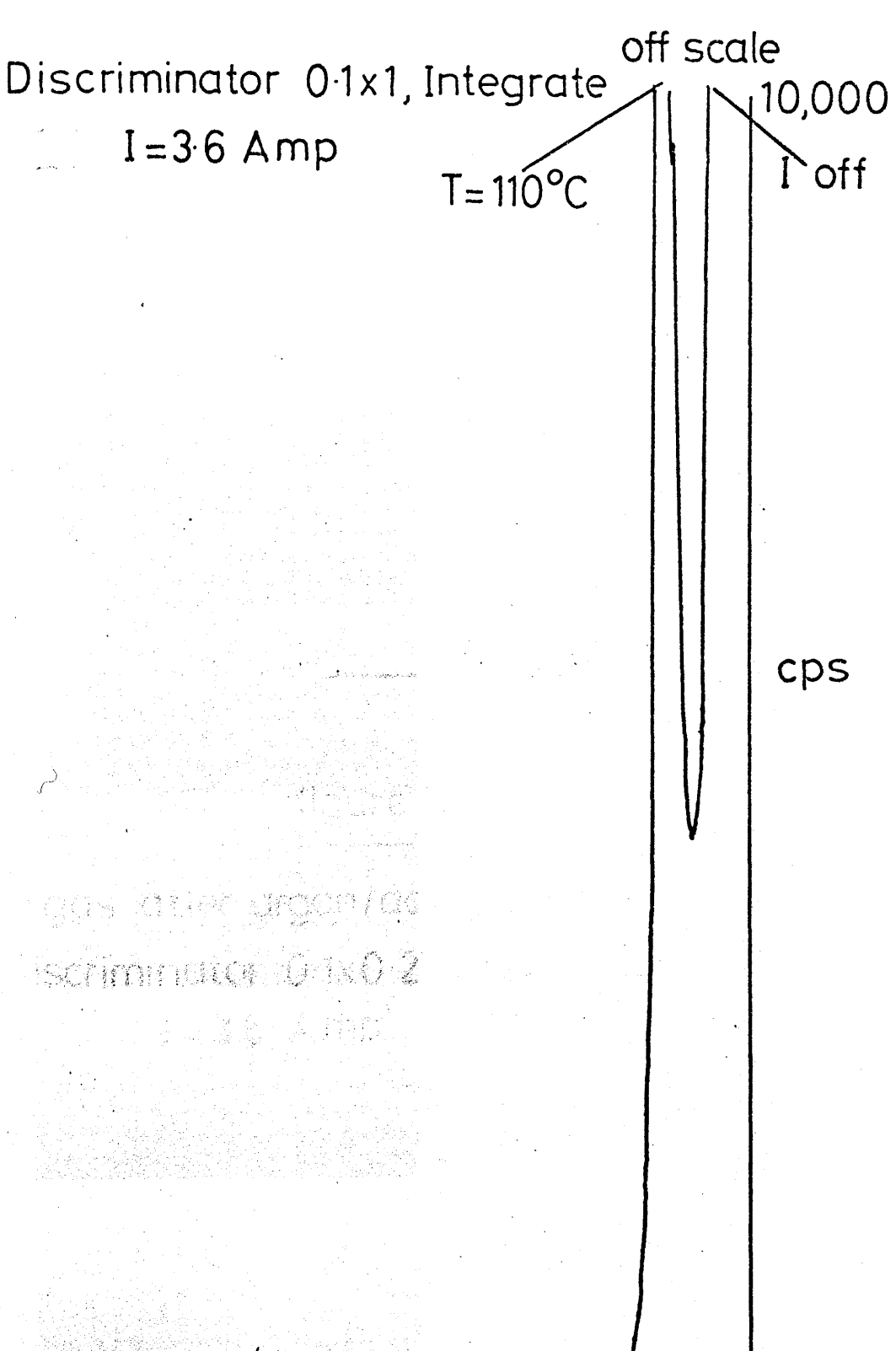

figure 30.

Q gas after argon/ethylene.

Discriminator 0·1x 1, Integrate.

I=3·6 Amp

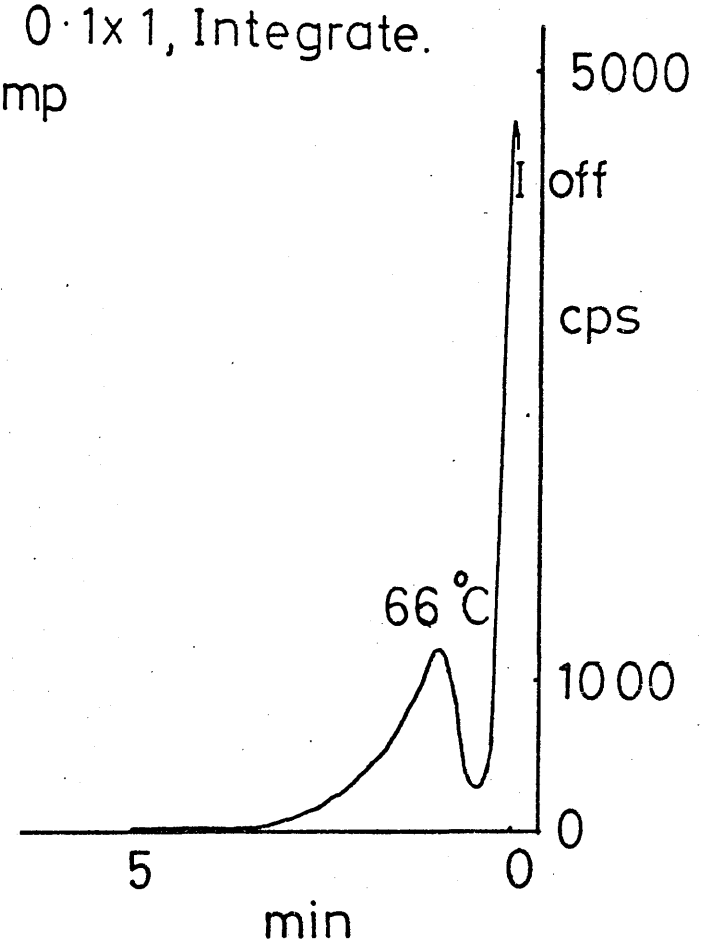

figure 31.

Q gas after argon/acetylene.

Discriminator 0·1x0·2, 2%window

I=3·6 Amp

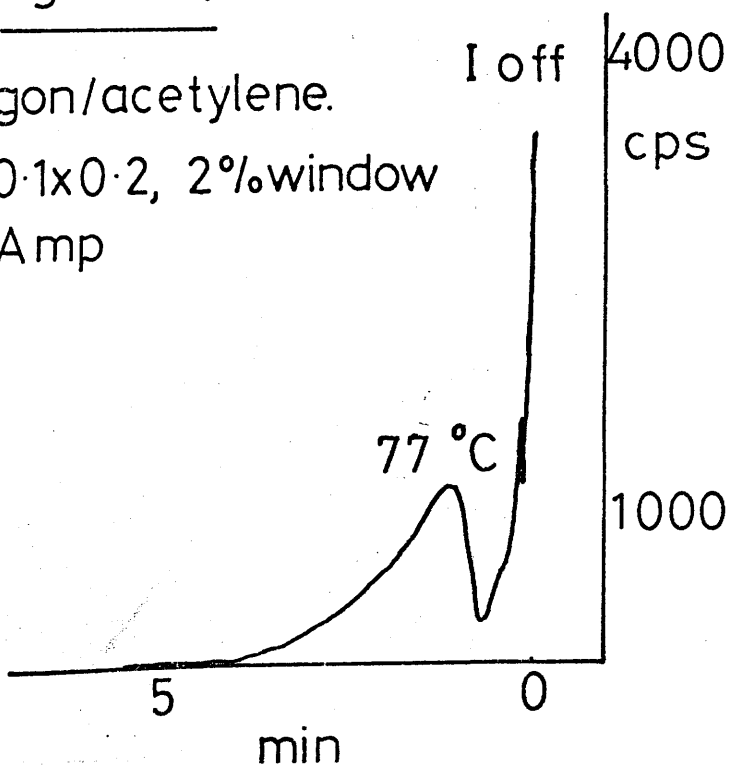

figure 32.

Q gas after argon/ethane.

Discriminator 0·1x1, Integrate

I = 3·7 Amp

V = 2 kV

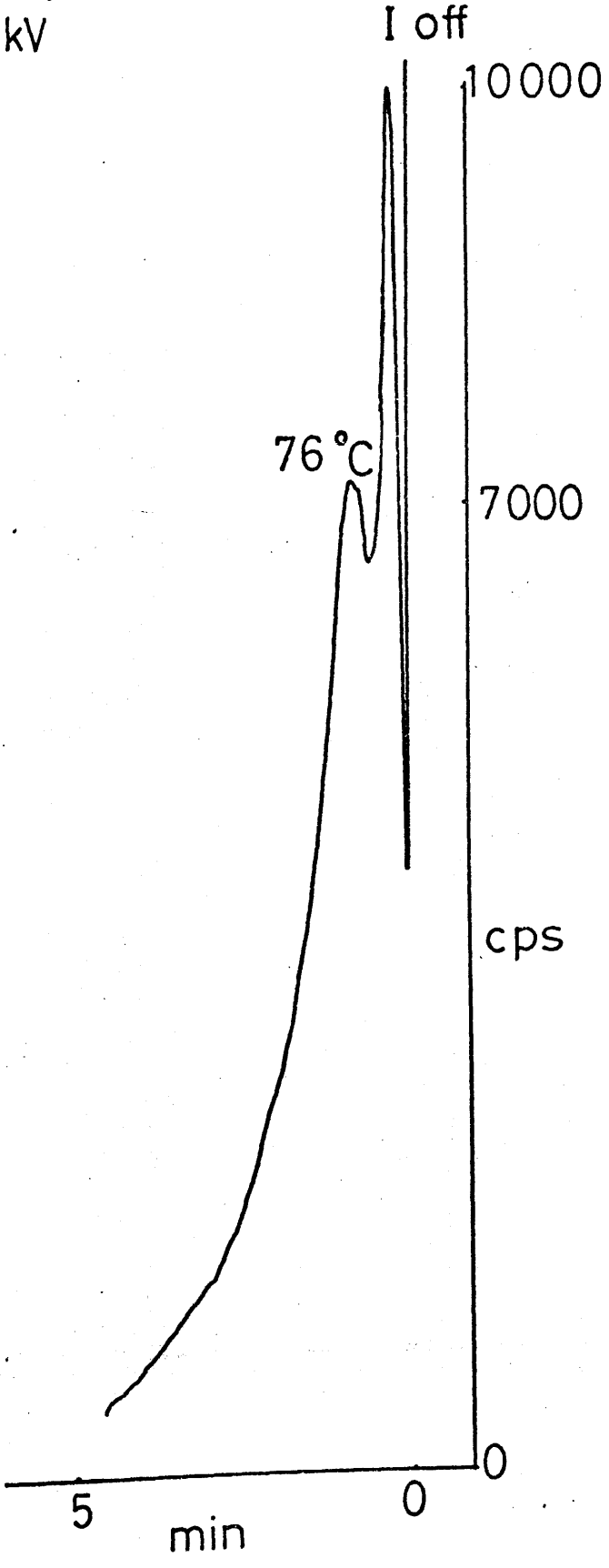

figure 33.

Argon/ethylene after argon/methane.

Discriminator 0·1x1, Integrate

I=3·5 Amp

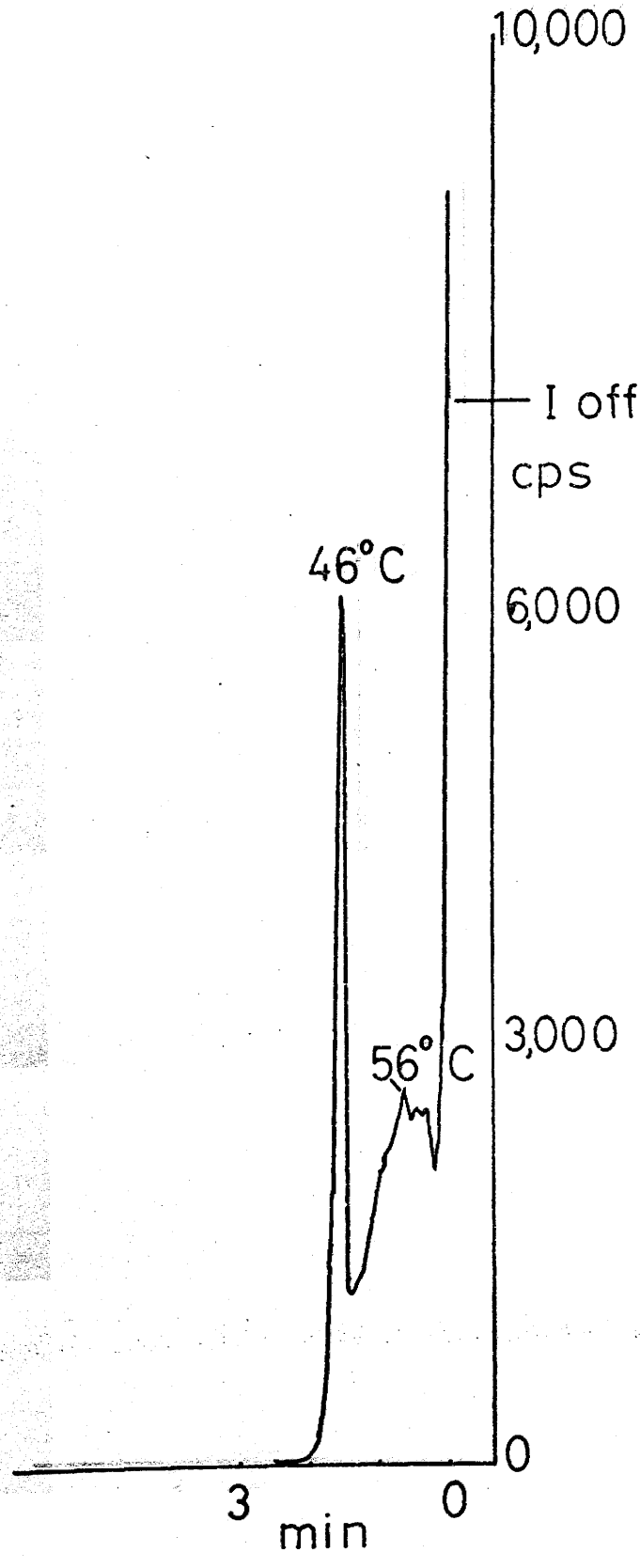

figure 34.

Argon/ethylene after argon/acetylene.

Discriminator 0·1x0·2, Integrate

I= 3·55 Amp

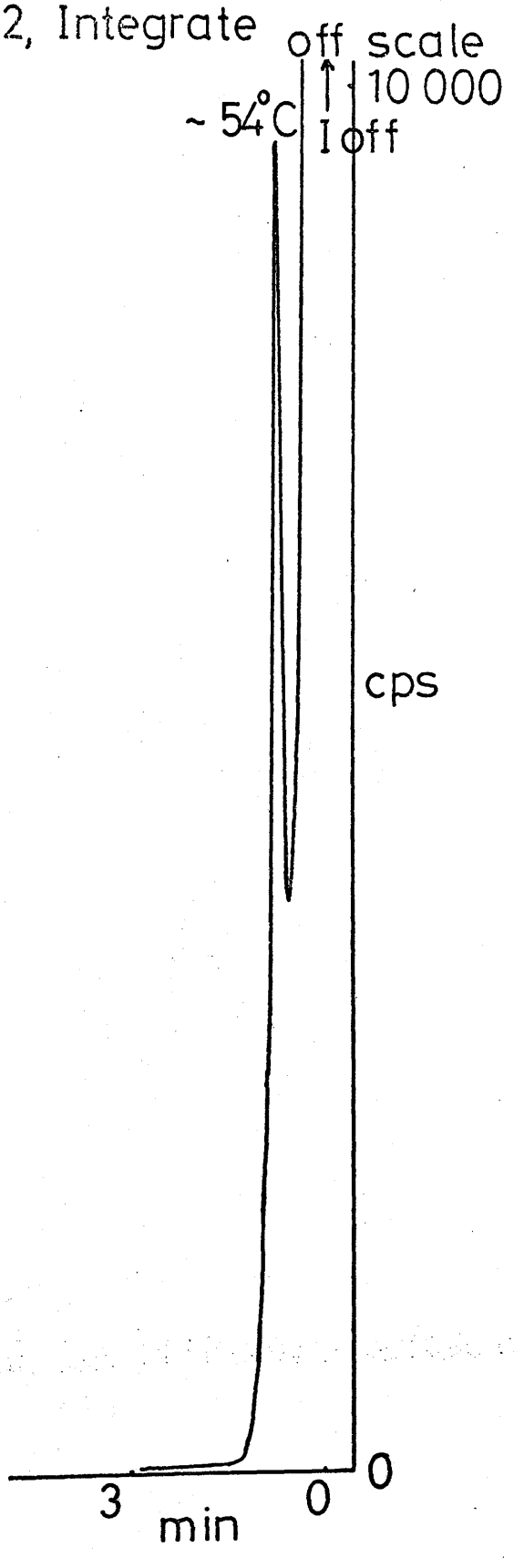

figure 35.

Argon/ethylene after wire aged in nitrogen; prior exposure to argon/ethylene.

Discriminator 0·1x 0·2, Integrate

I = 3·5 Amp

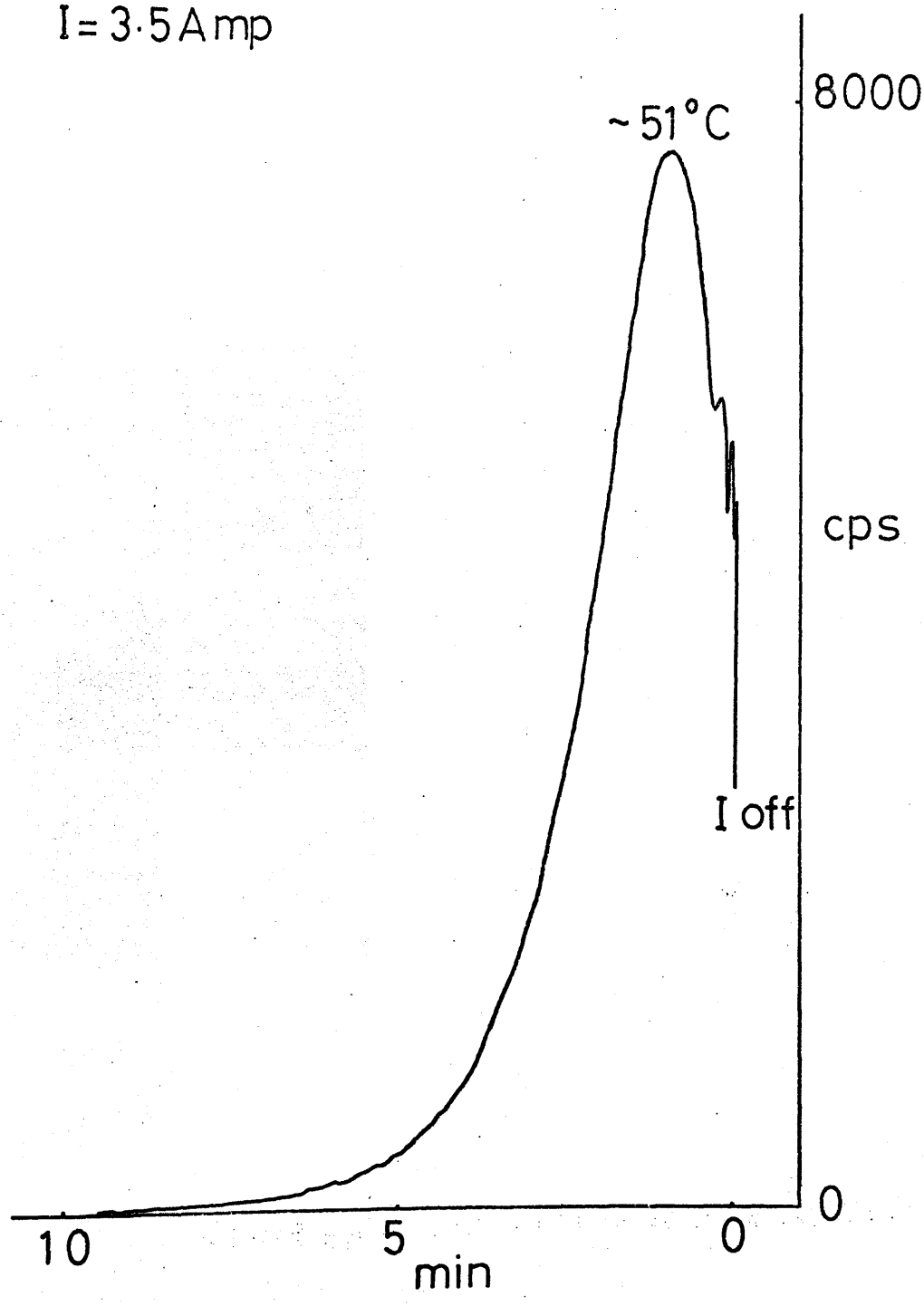

figure 36.

Argon/ethylene after argon/ethylene.

Discriminator 0·1x0·2, Integrate

I = 3·45 Amp

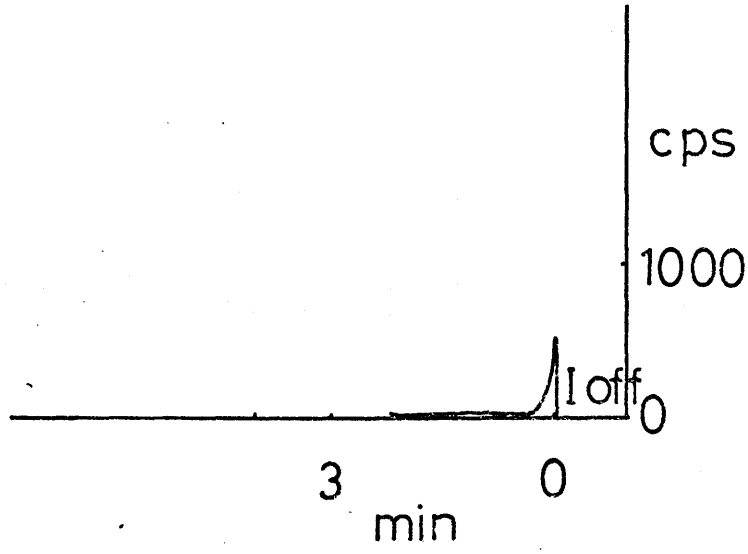

Also Argon/ethylene after argon/acetylene preceded by Q gas.

figure 37.

Argon/acetylene after wire aged in nitrogen; heating/cooling in argon/acetylene prior to ageing gave no emission, see fig 38.

Discriminator 0·1x0·2, Integrate

I= 3·55 Amp

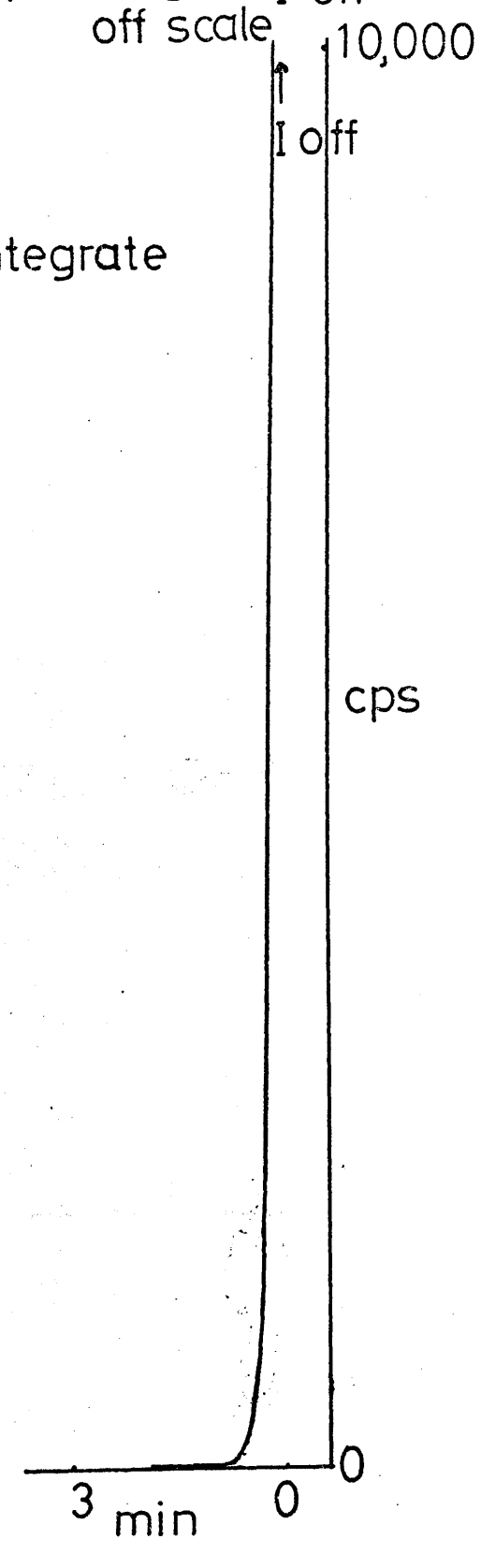

figure 38.

Argon/acetylene after argon/ethylene.

Discriminator 0·1x0·2, Integrate

I = 3·5 Amp

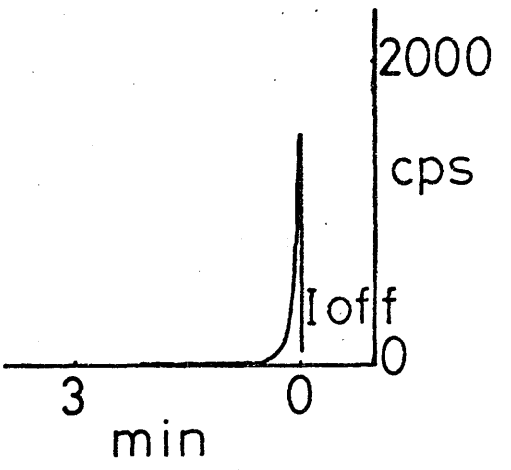

figure 39.

Argon/acetylene after argon/acetylene.

Discriminator 0·1x0·2, Integrate

I=3·45 Amp

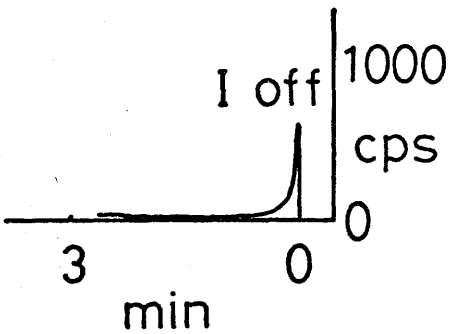

figure 40.

Argon/acetylene after Q gas.
Discriminator 0·1x0·2, Integrate
I=3·55 Amp

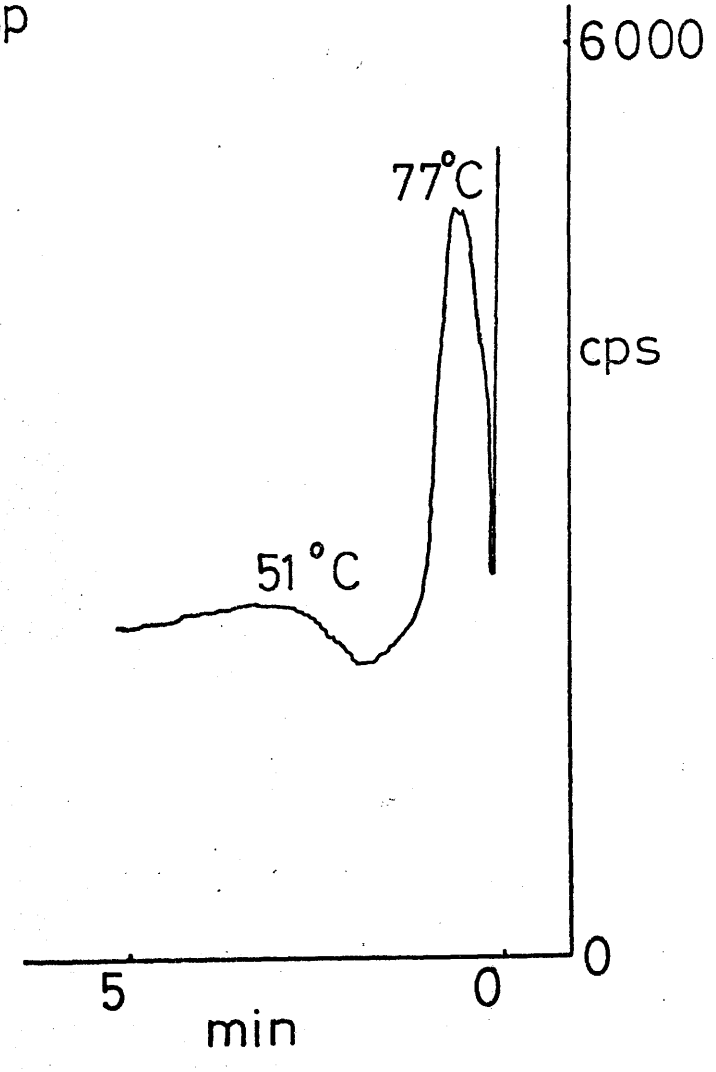

figure 41.

Argon / butadiene after Q gas.

Discriminator 0·1x0·2, Integrate

I = 3·7 Amp

V = 1·9 kV

Also Argon/butadiene after argon/butadiene, i.e. effect reproducible.

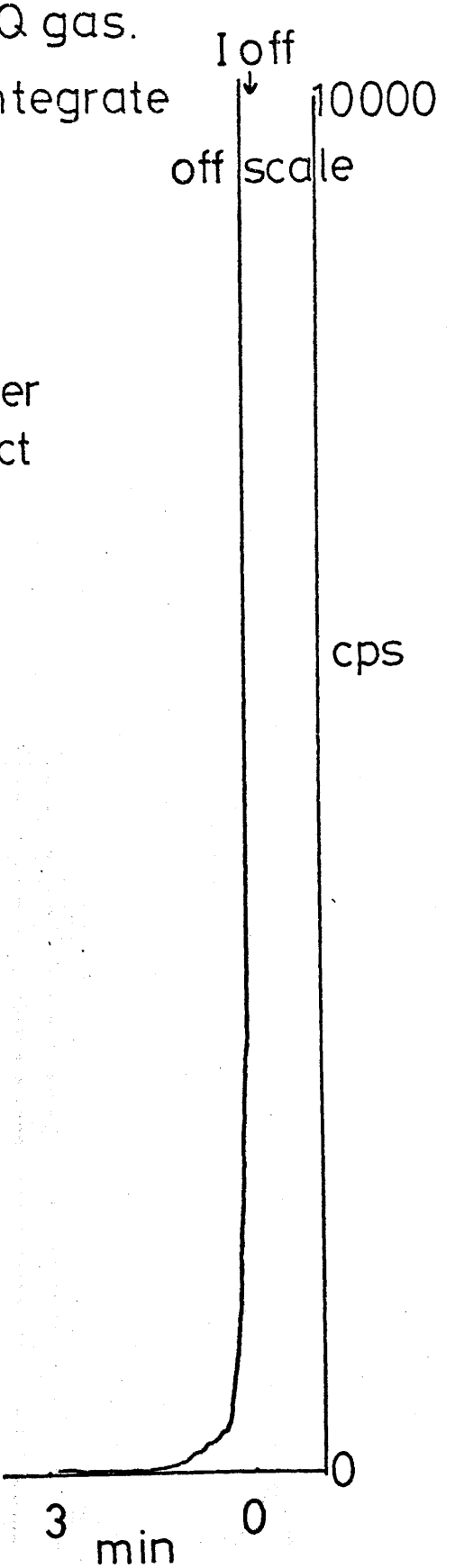

figure 42.

Argon/ethane cooling curves to show the increase in exo-electron emission.

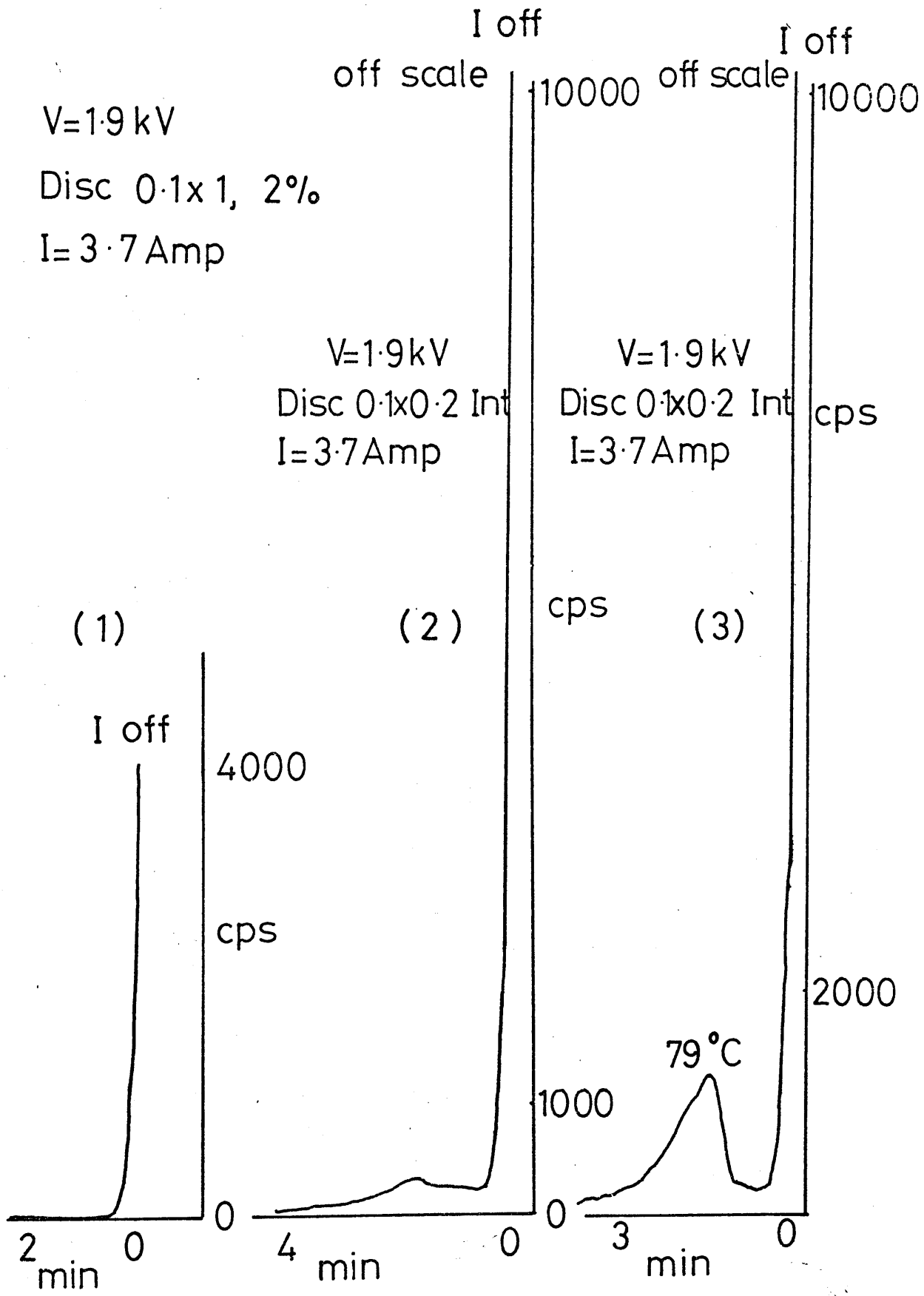

Argon/ethane cooling curves continued

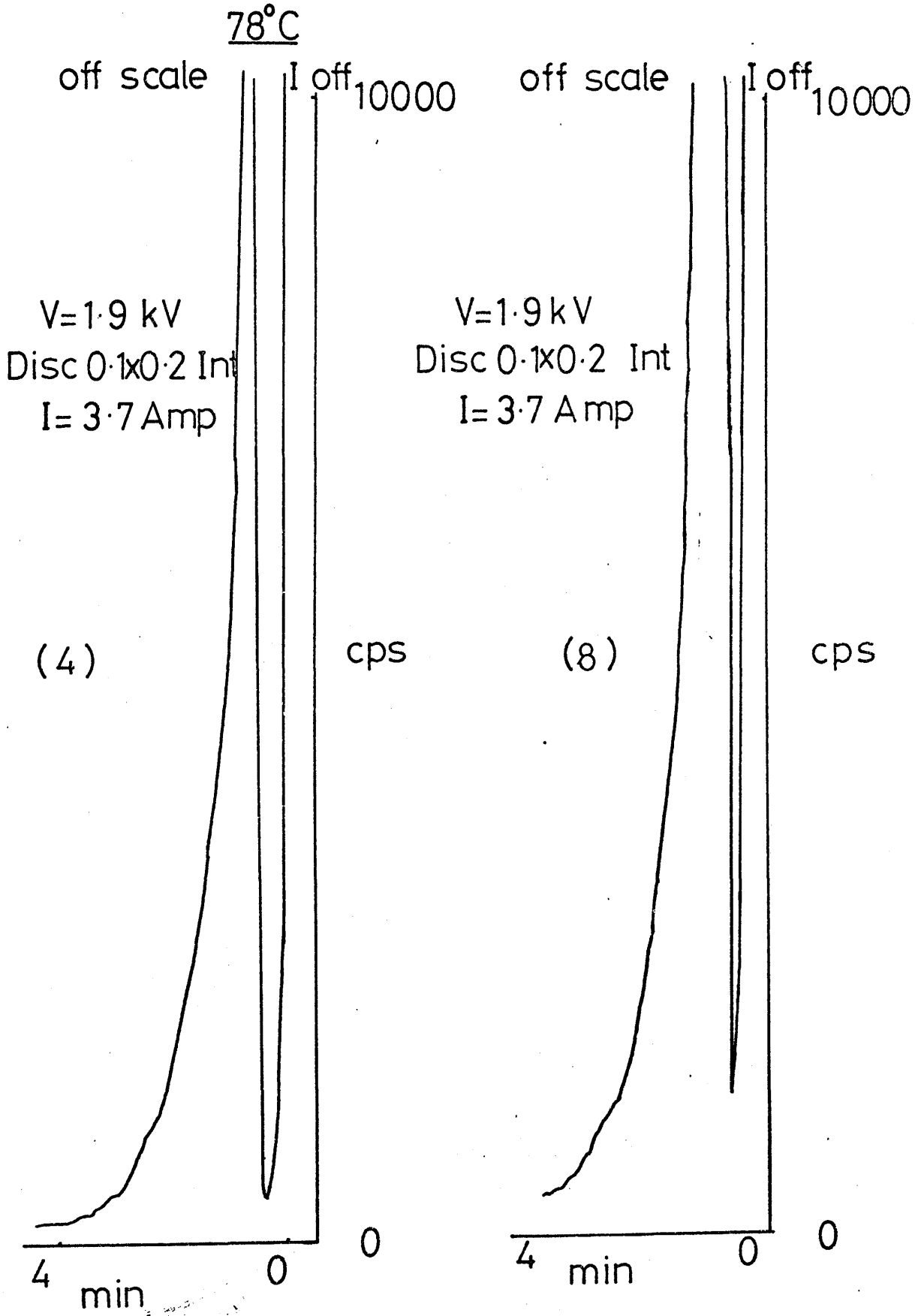

figure 43.

Hydrogen after Q gas

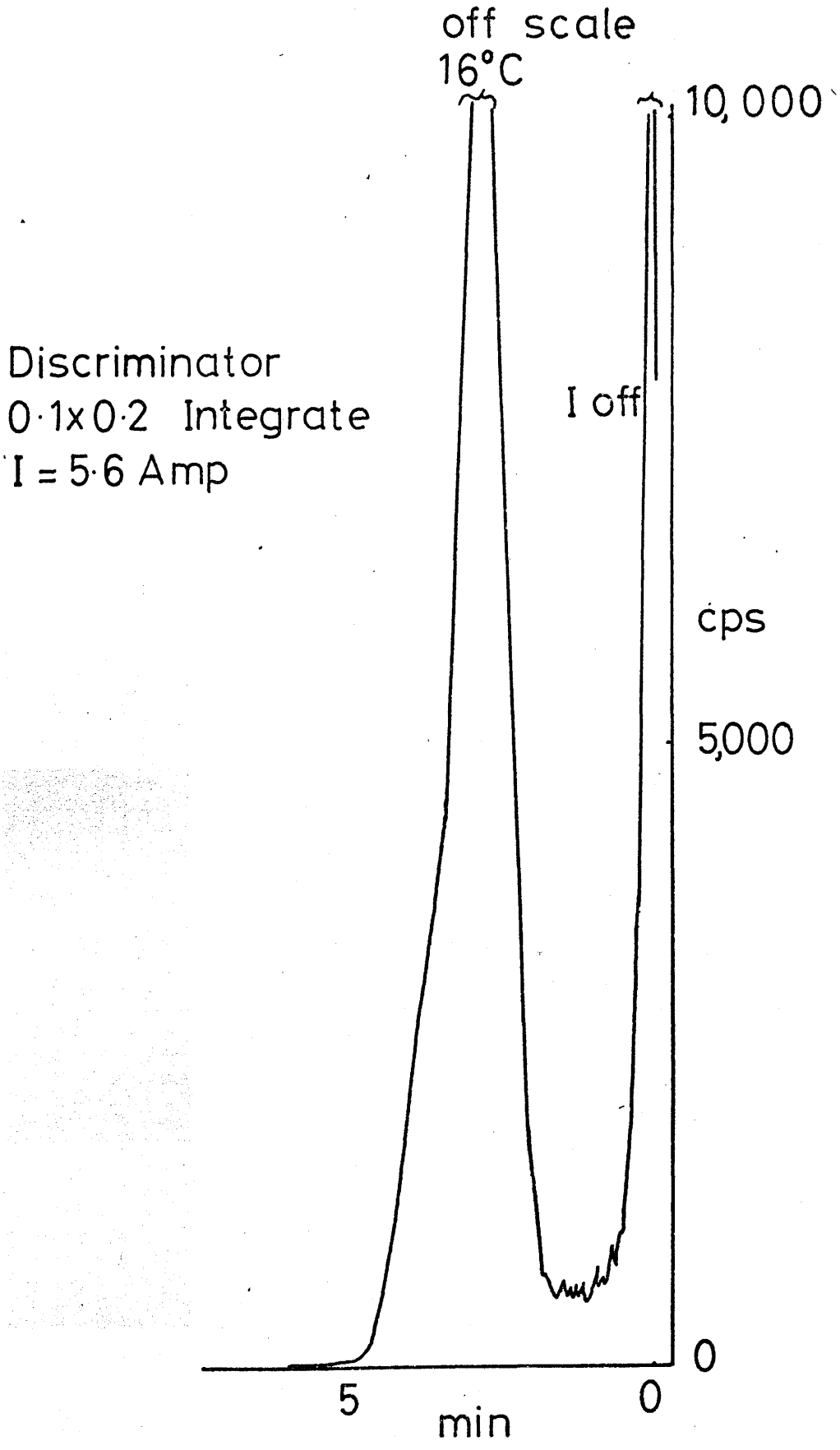

figure 44.

Hydrogen after nitrogen

Discriminator 0·1x1, 2% window

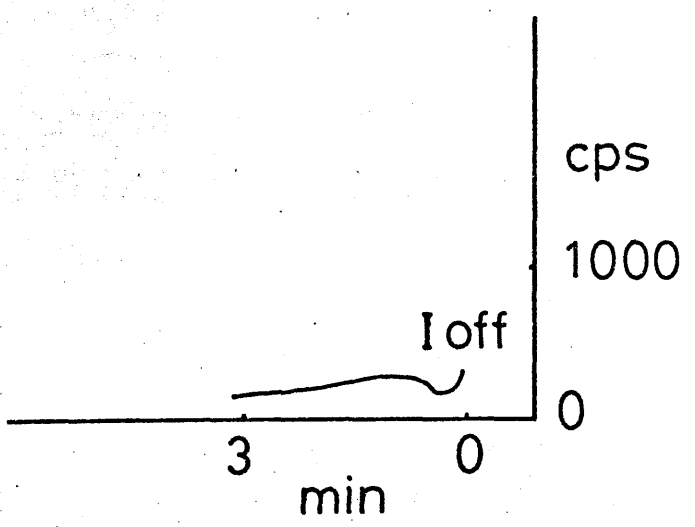

figure 45.

Argon after methane or argon/methane.
Discriminator 0·1x0·2, Integrate
I = 3·5 Amp

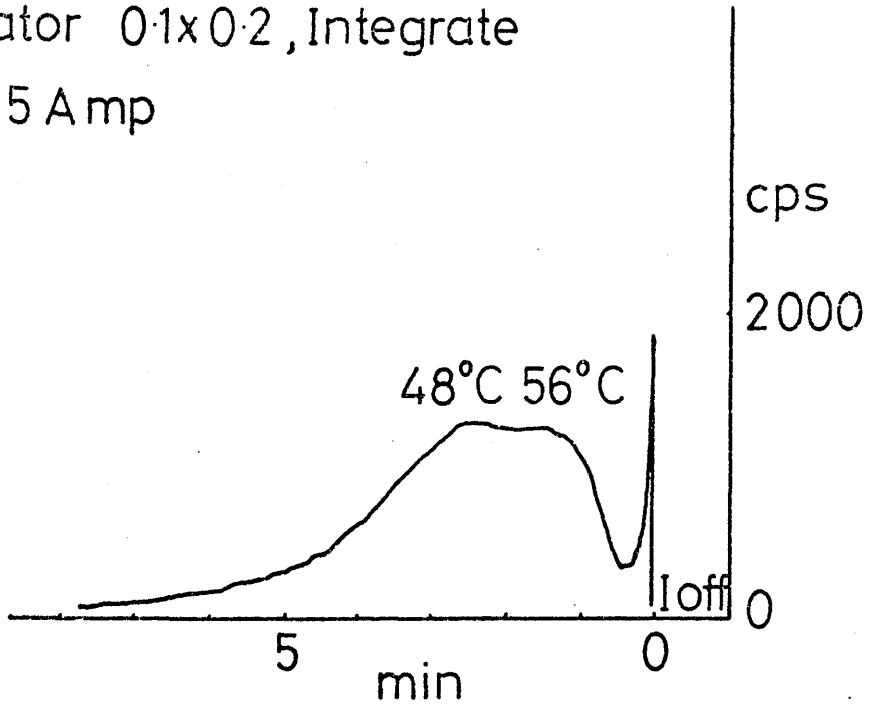

figure 46.

Argon after argon/ethylene.
Discriminator 0·1x0·2, Integrate
I=3·5 Amp

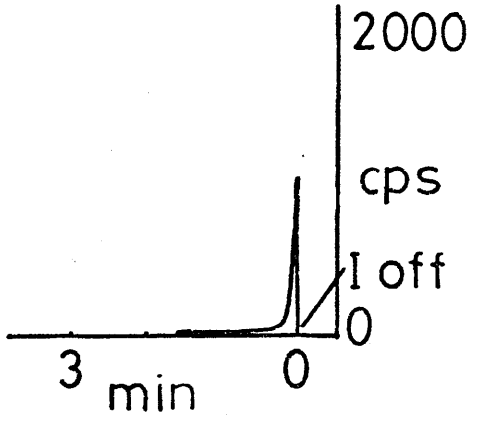

Also:- Argon after argon/butadiene and
argon after Q gas after argon/acetylene.

figure 47.

Argon after argon/acetylene.
Discriminator 0·1x0·2, Integrate
I = 3·45 Amp

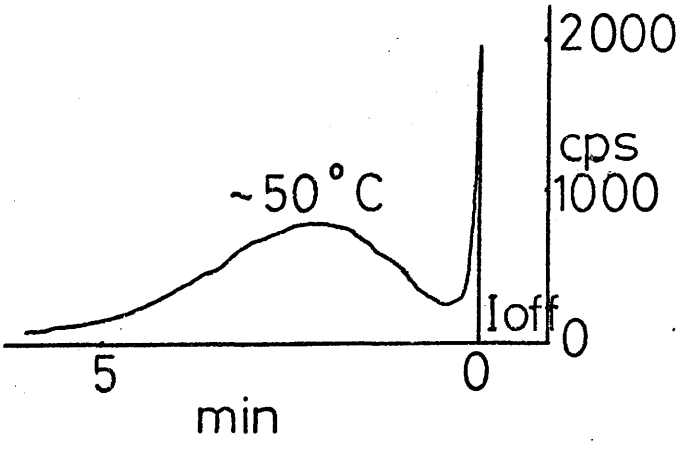

figure 48.

Argon after argon/butadiene afte wire aged in argon.
Discriminator 0·1x0·2, Integrate
I = 3·65 Amp
V = 1·9 kV

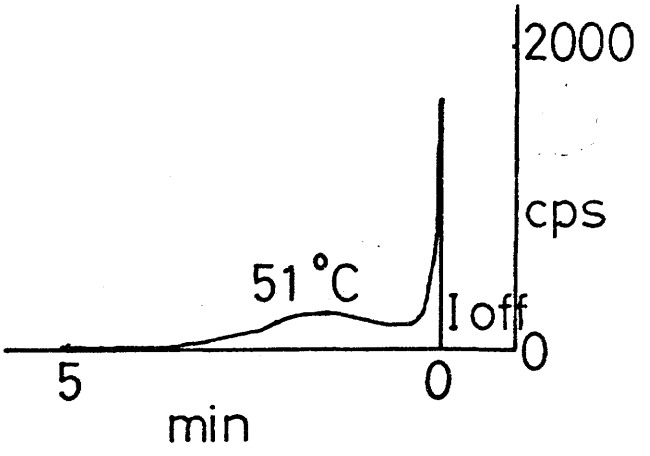

Also, Argon after argon/ethane; T = 46°C.

figure 49.

Nitrogen after argon/ethylene, after wire aged in nitrogen.
Discriminator 0·1x0·2, Integrate
I= 3·75 Amp

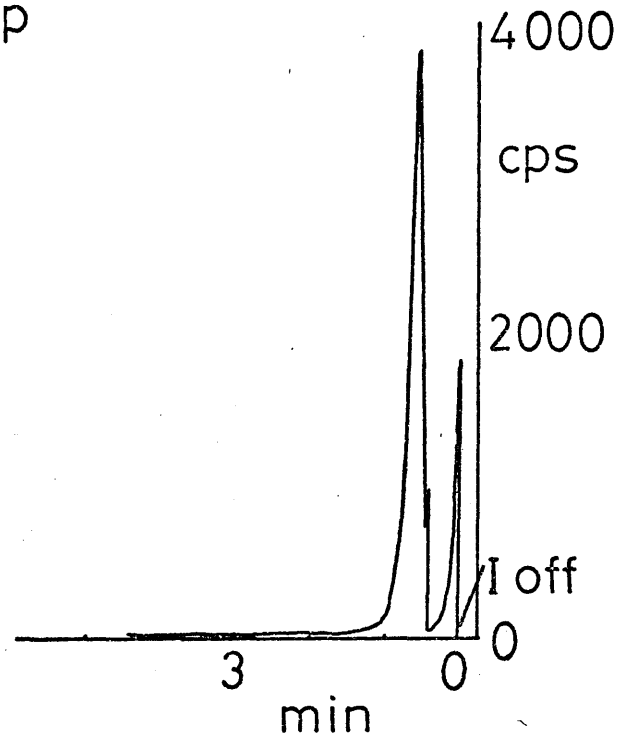

Also, Nitrogen after argon/acetylene, after wire aged in nitrogen.

Also, Nitrogen after Q gas.

Nitrogen after argon/ethylene or argon/acetylene, without ageing the wire, gave little or no emission.

figure 50.

Nitrogen after hydrogen.
Discriminator 0·1x0·2, Integrate
I ~ 3·8 Amp

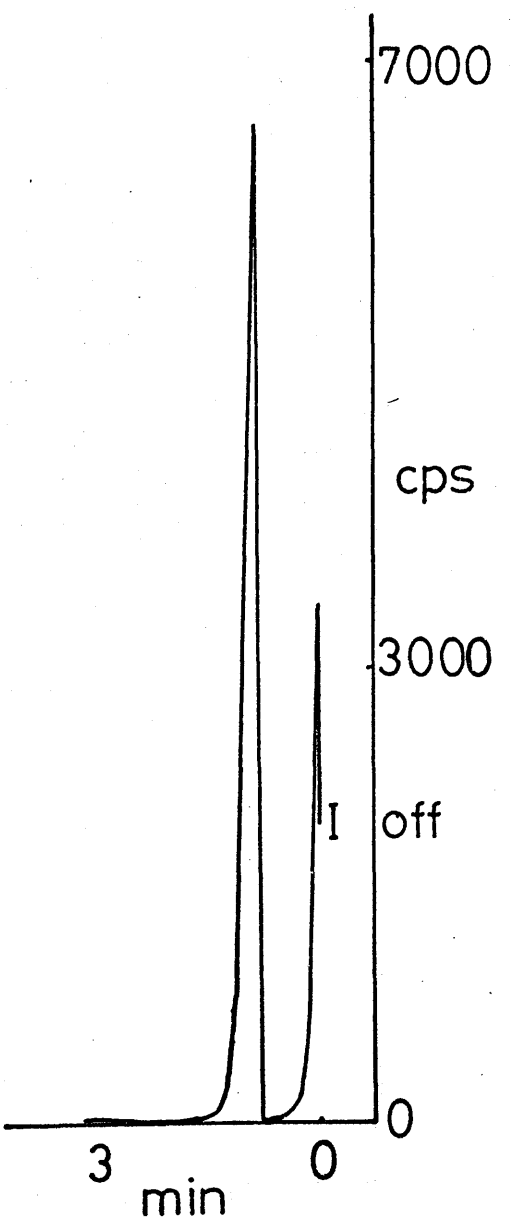

figure 51.

Nitrogen after oxygen.

Discriminator 0·1x 0·2, Integrate
I = 3·5 Amp

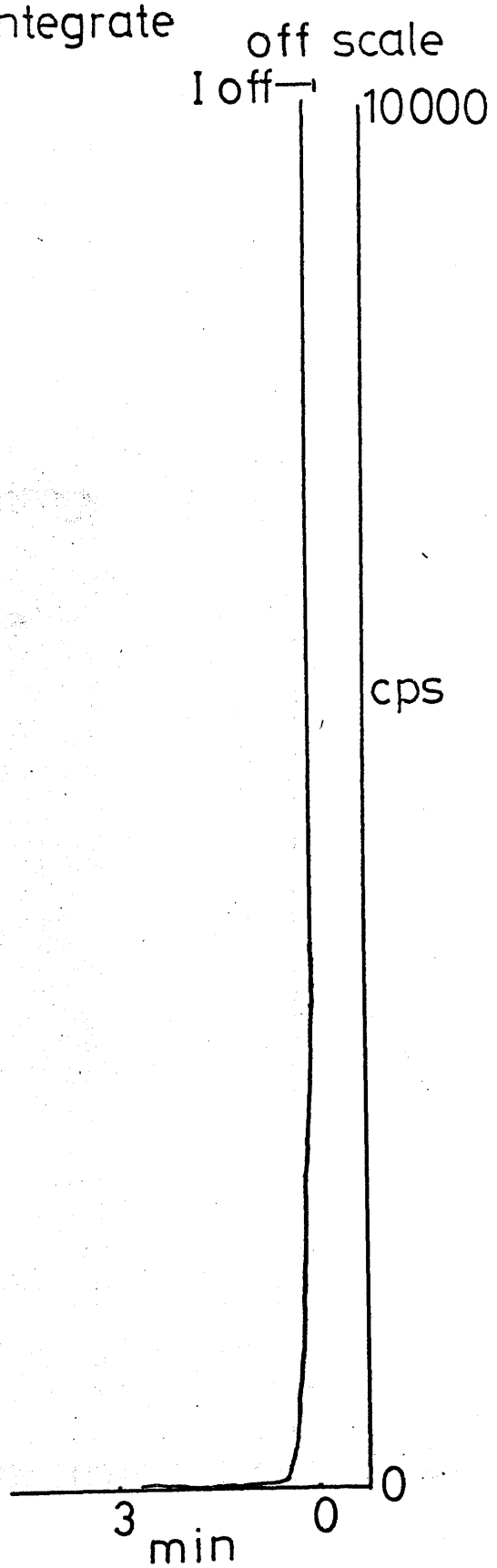

figure 53.

Stereographic projection showing the crystallographic orientation of some of the platinum single crystal faces studied by Blakely and Somorjai.

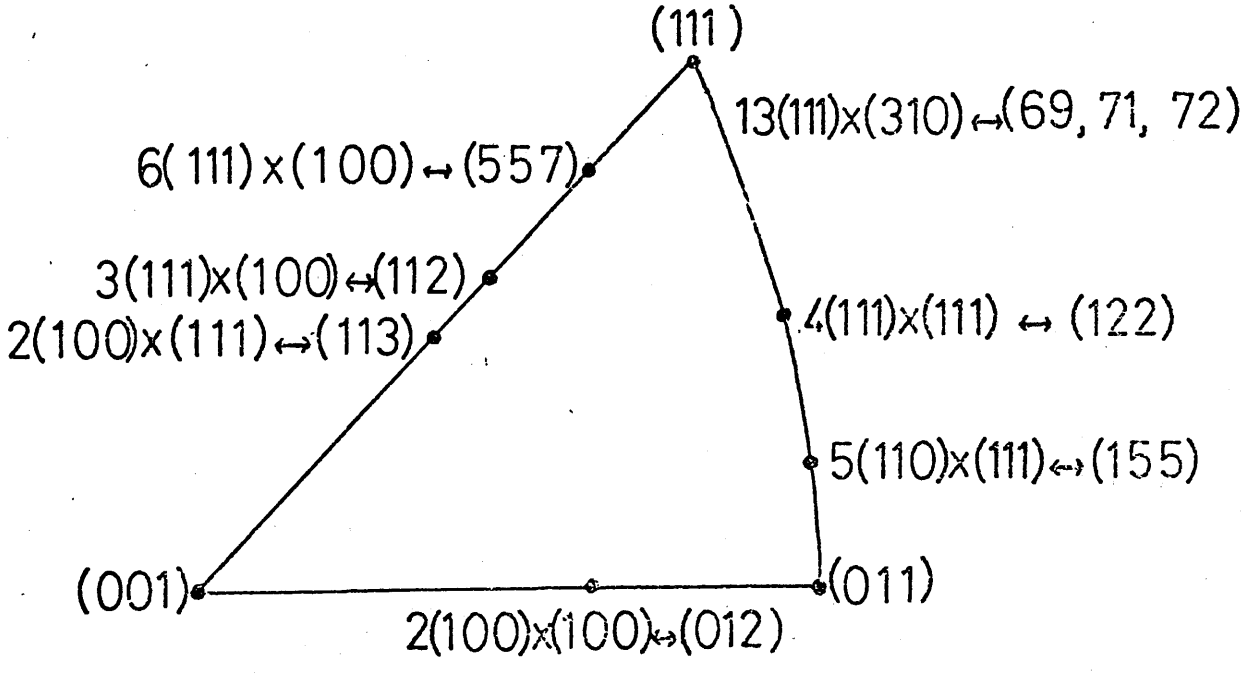

Appendix 11

Appendix 11a

Wire 3

Introduction curves after exposure to Q gas and air

$I \sim 3{\cdot}2A$

Discriminator 0·1 x 1, 2% window throughout.

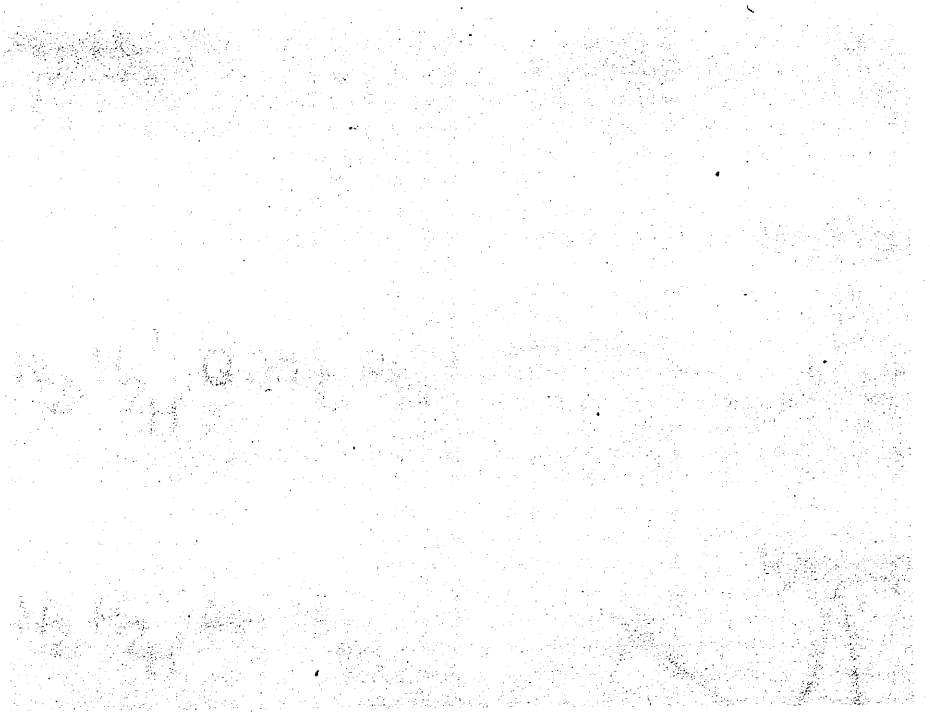

figure 54.

Nitrogen Introduction curves: Wire 3 after exposure to Q gas and air.

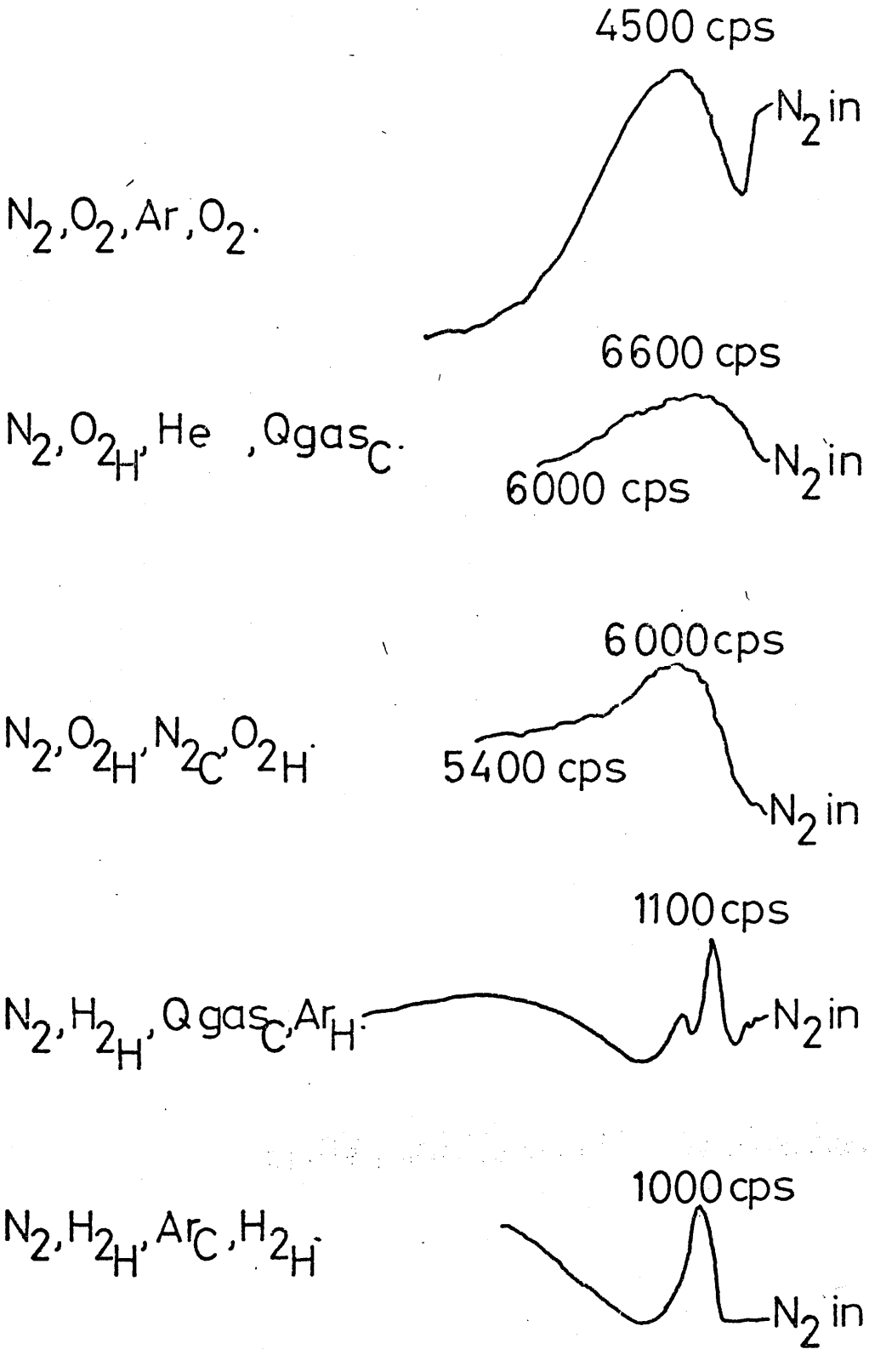

Nitrogen Introduction curves continued

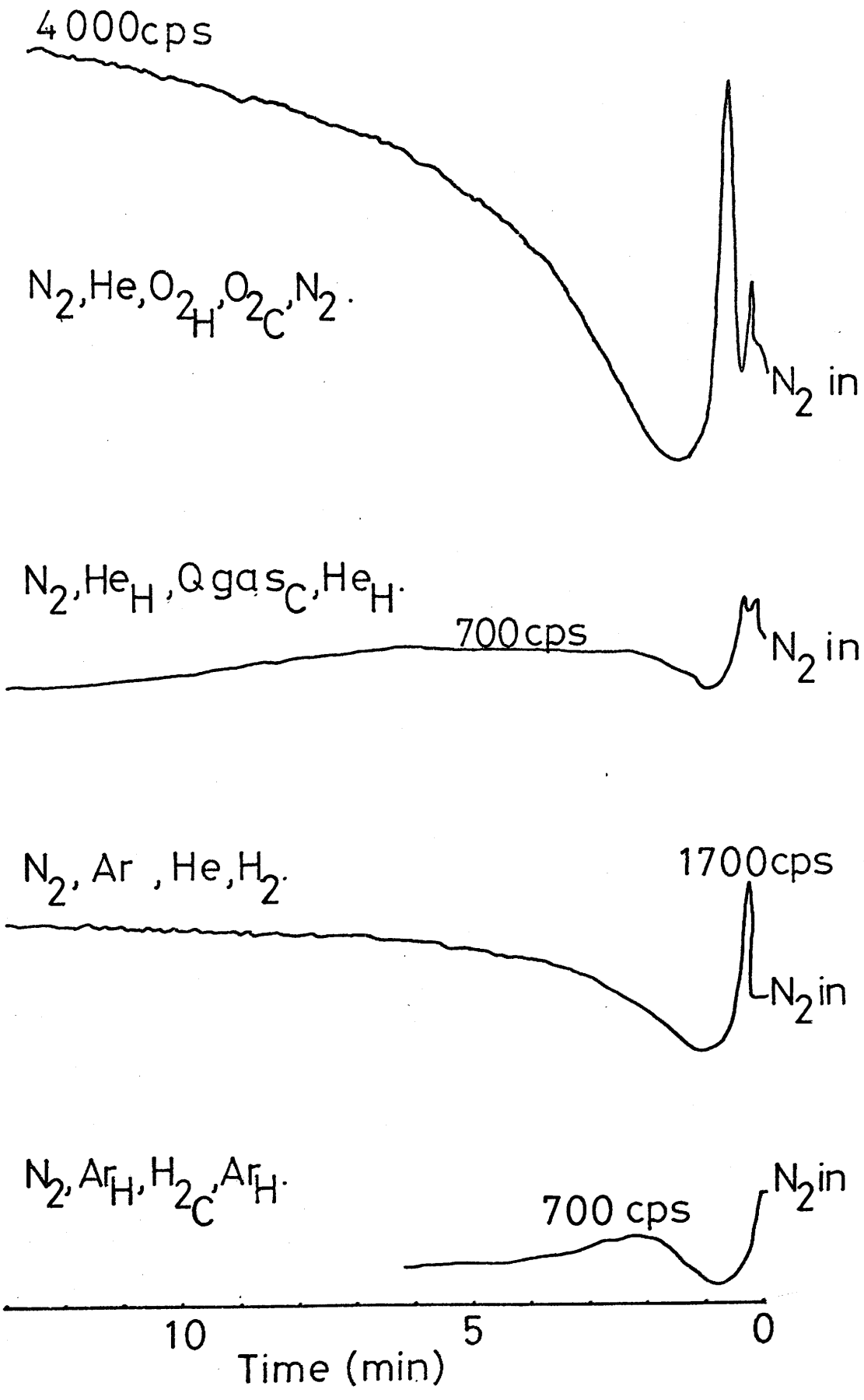

Nitrogen Introduction curves continued

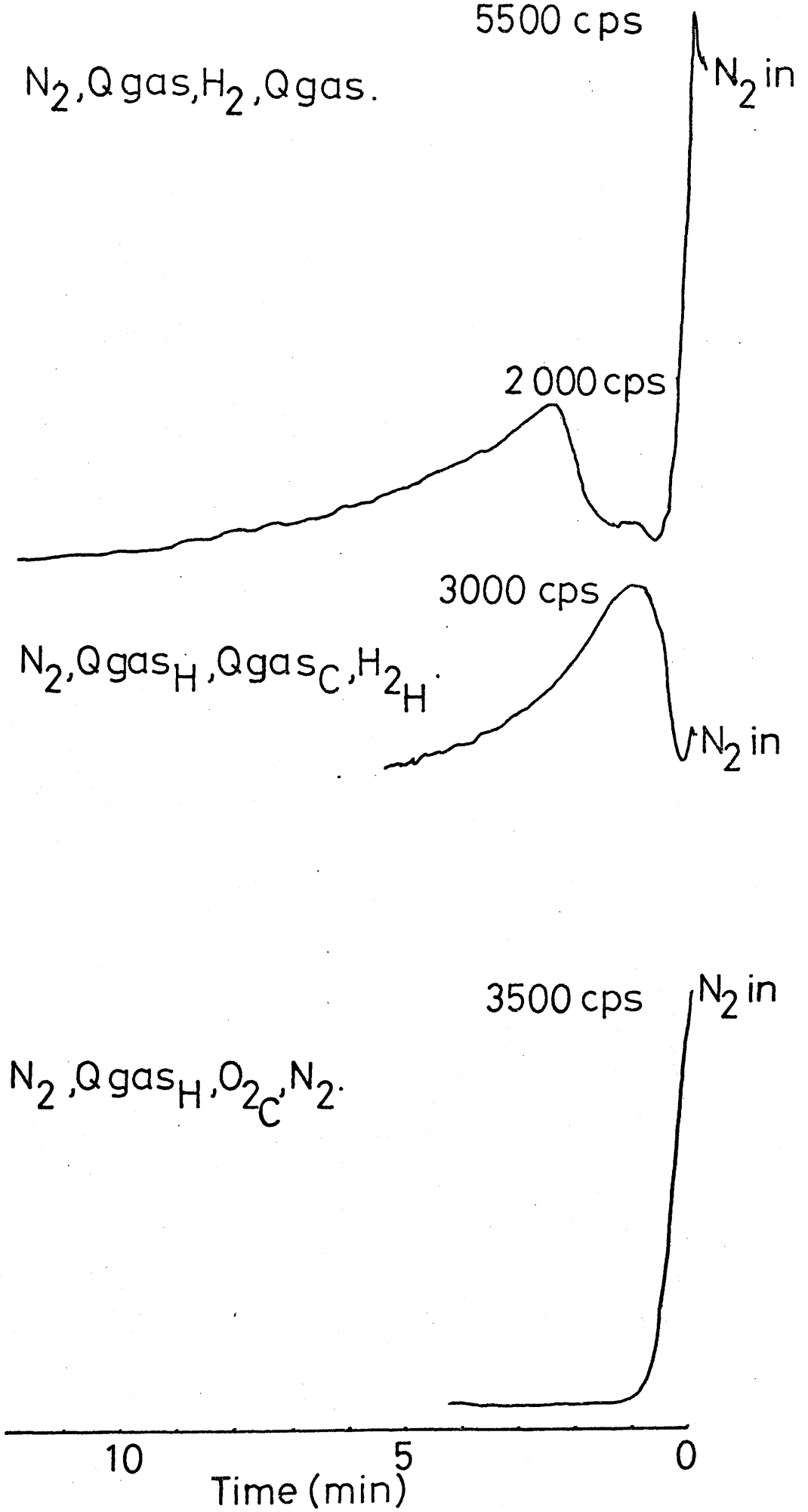

figure 55.

Oxygen Introduction curves: Wire3 after exposure to Q gas and air.

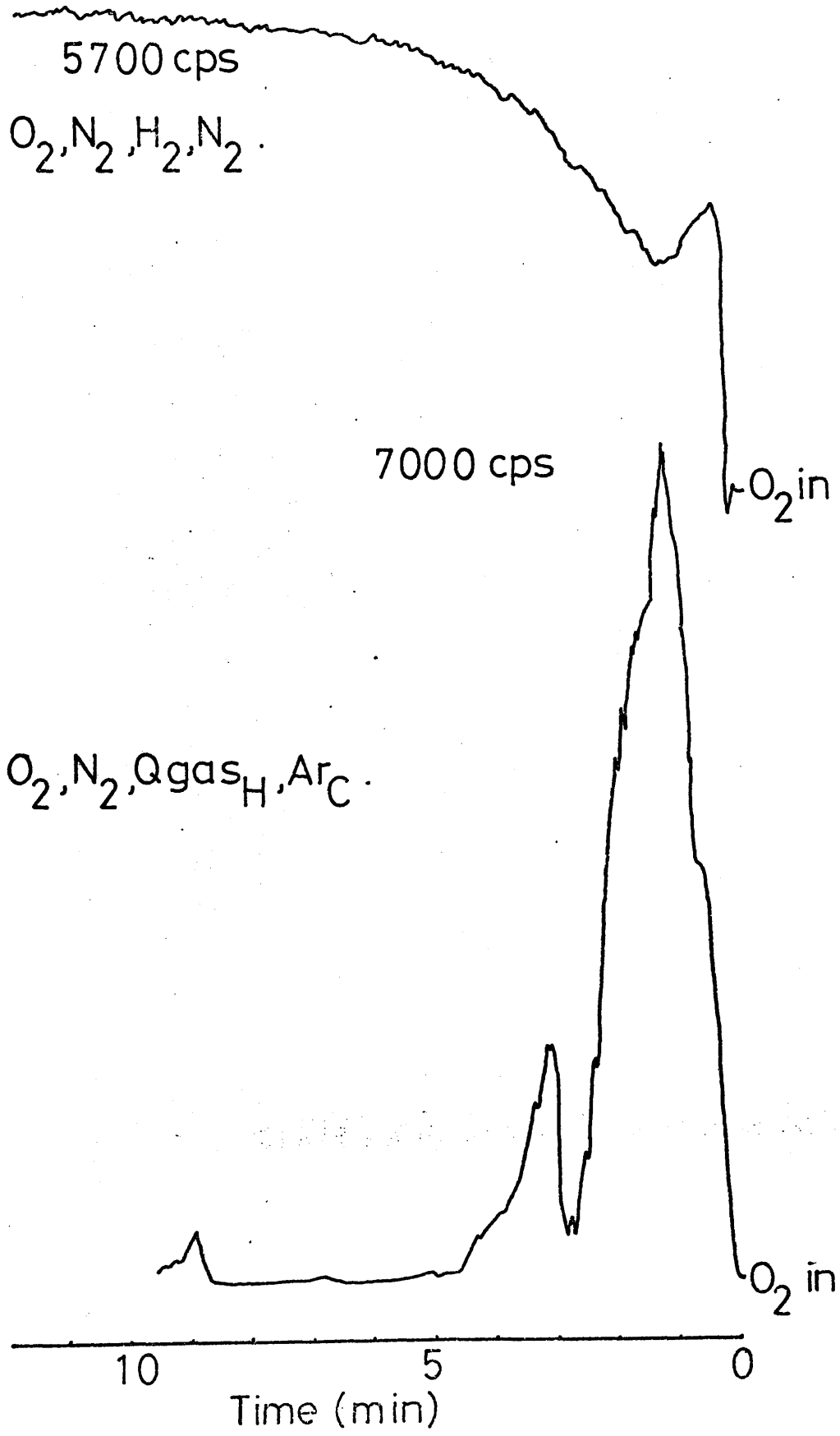

Oxygen Introduction curves continued

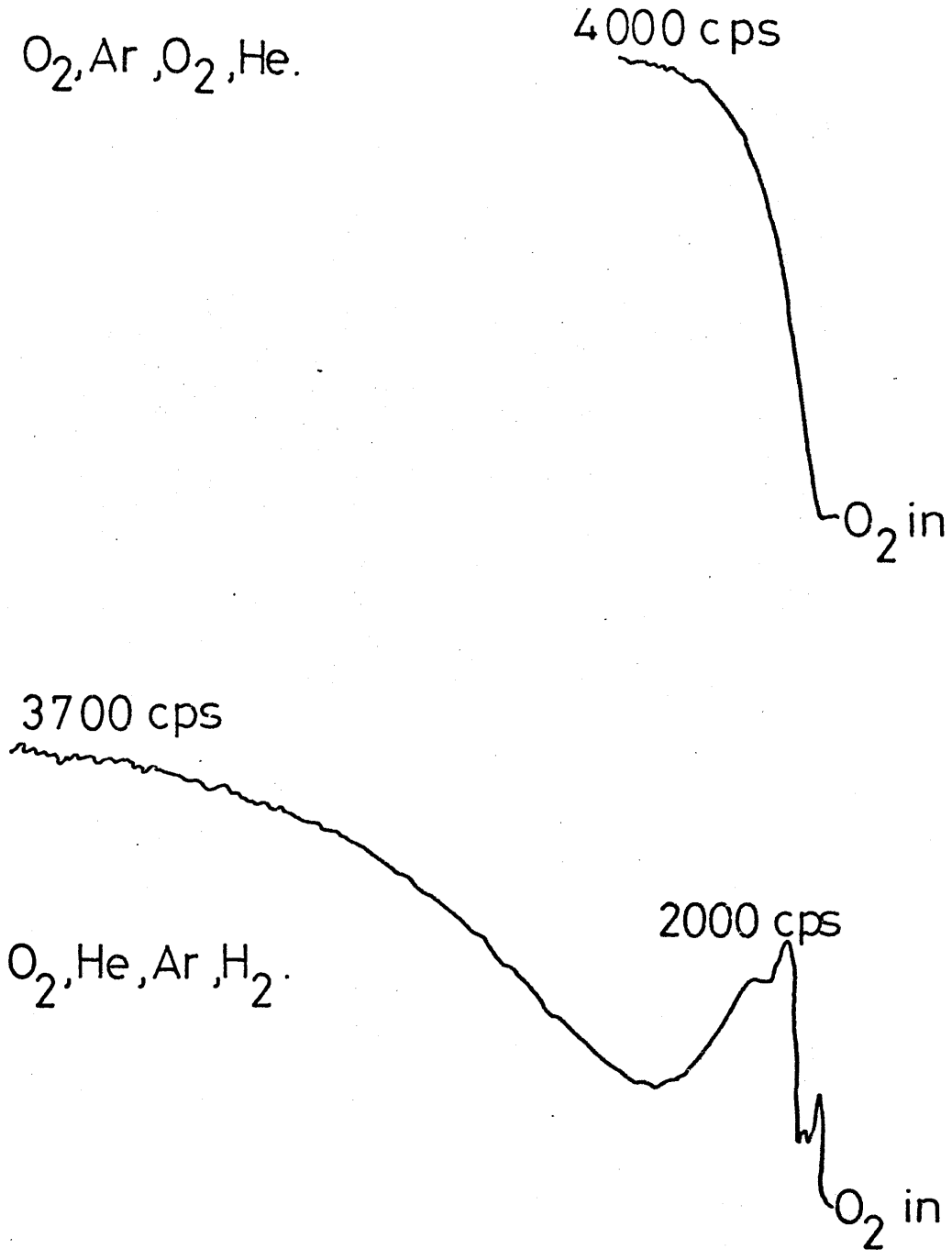

figure 56.

Hydrogen Introduction curves: Wire 3 after exposure to Q gas and air.

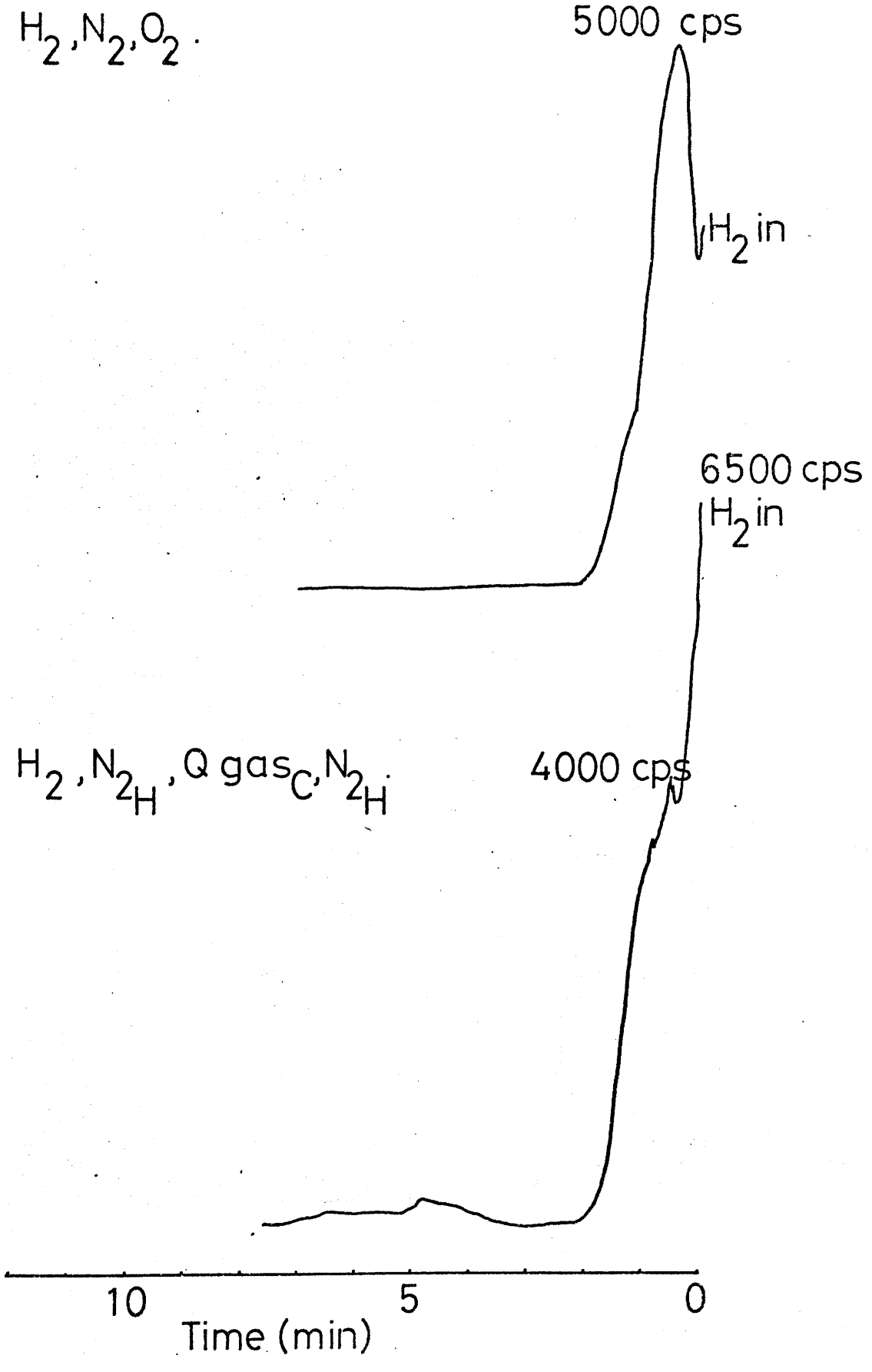

Hydrogen Introduction curves continued

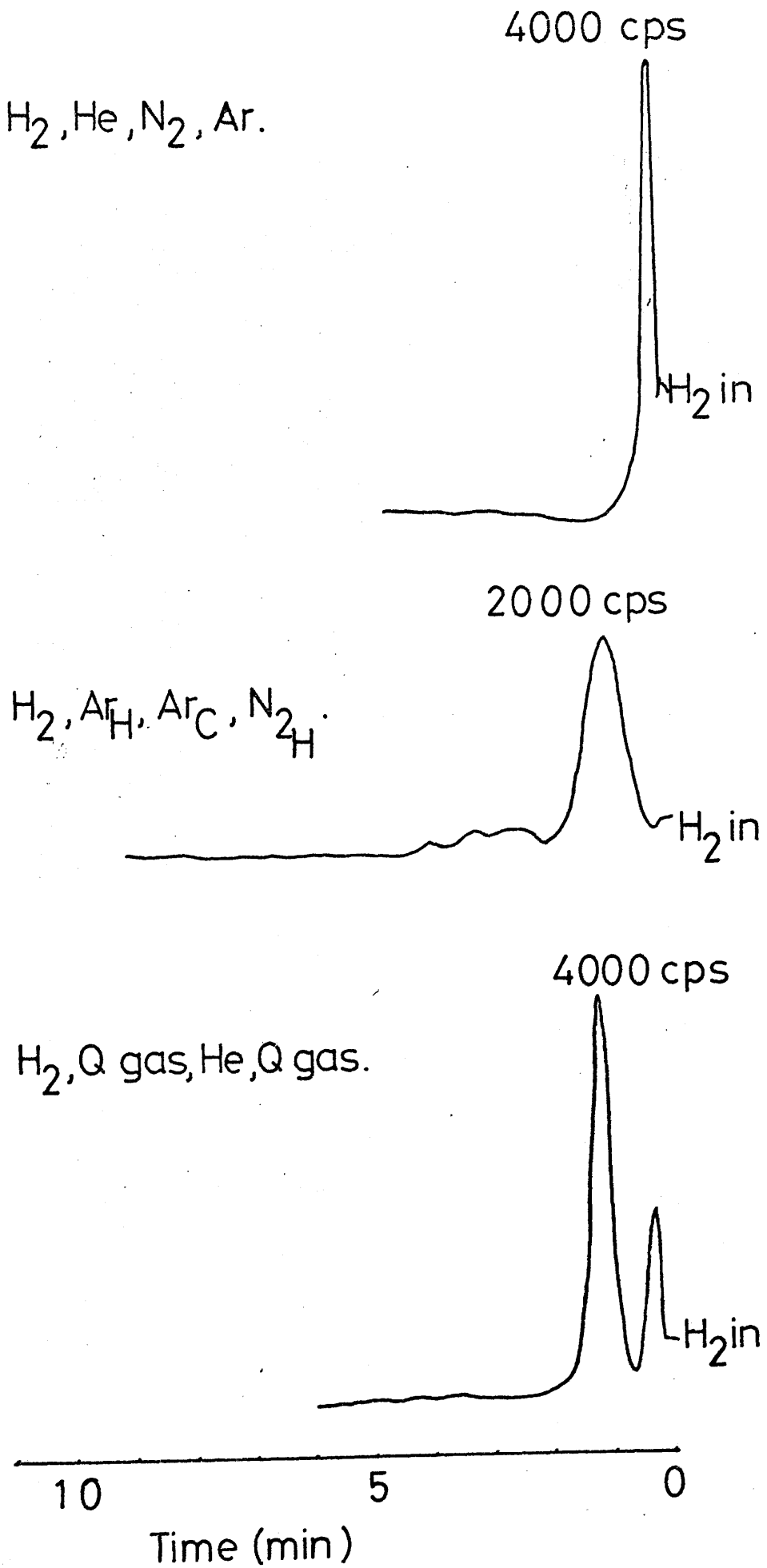

Hydrogen Introduction curves continued

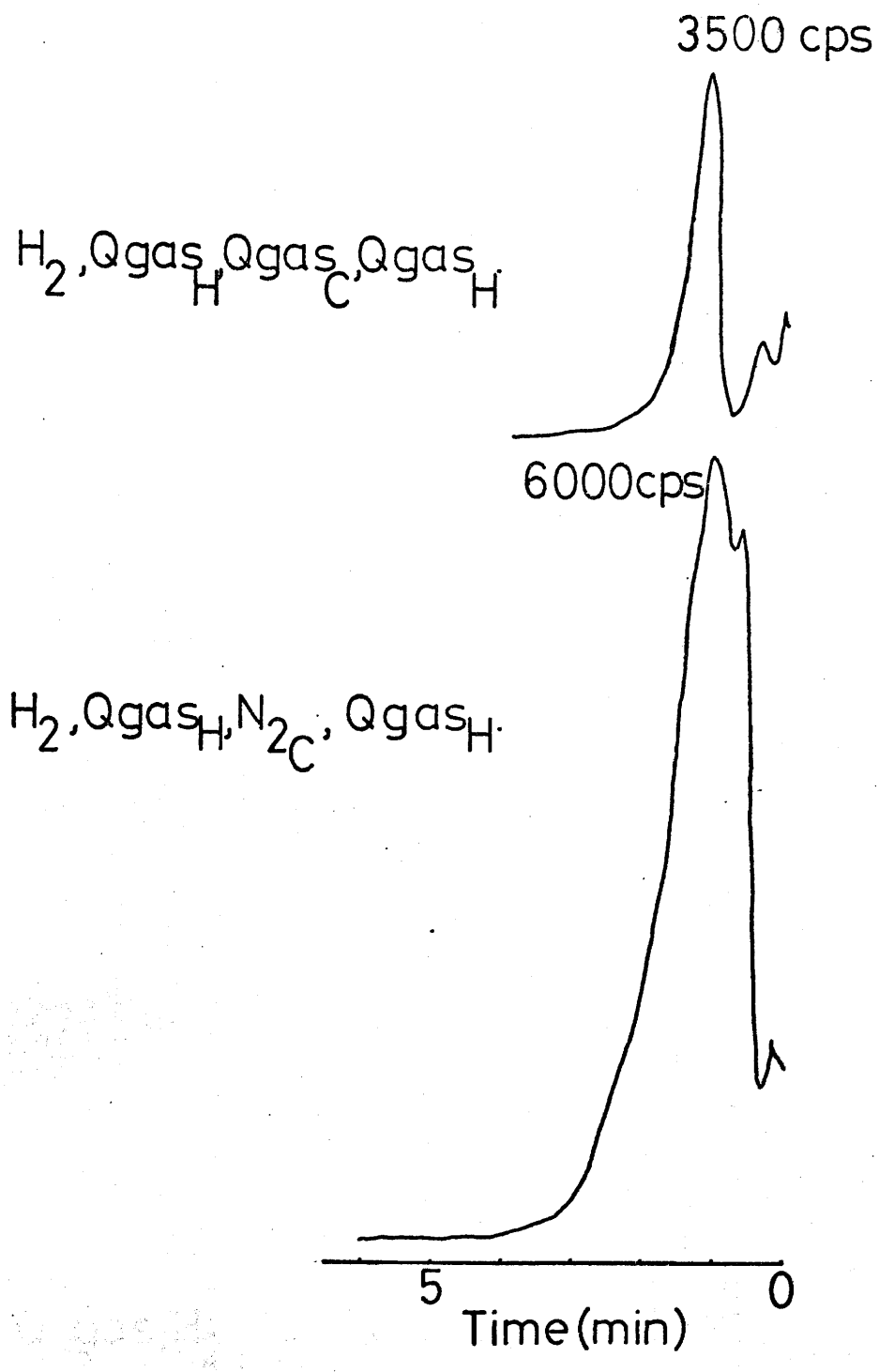

figure 57.

Q gas Introduction curves: Wire 3 after exposure to Q gas and air.

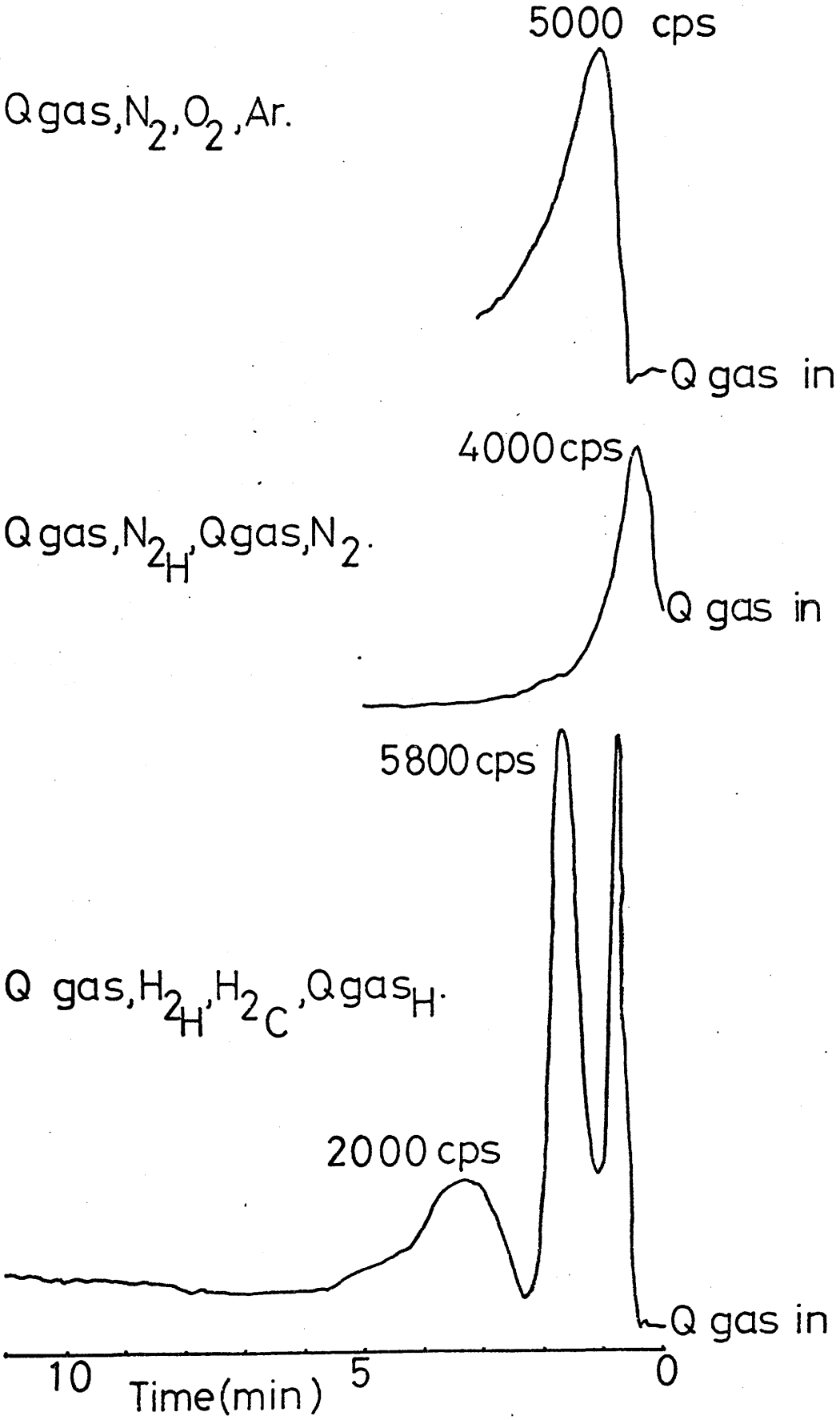

Q gas Introduction curves continued

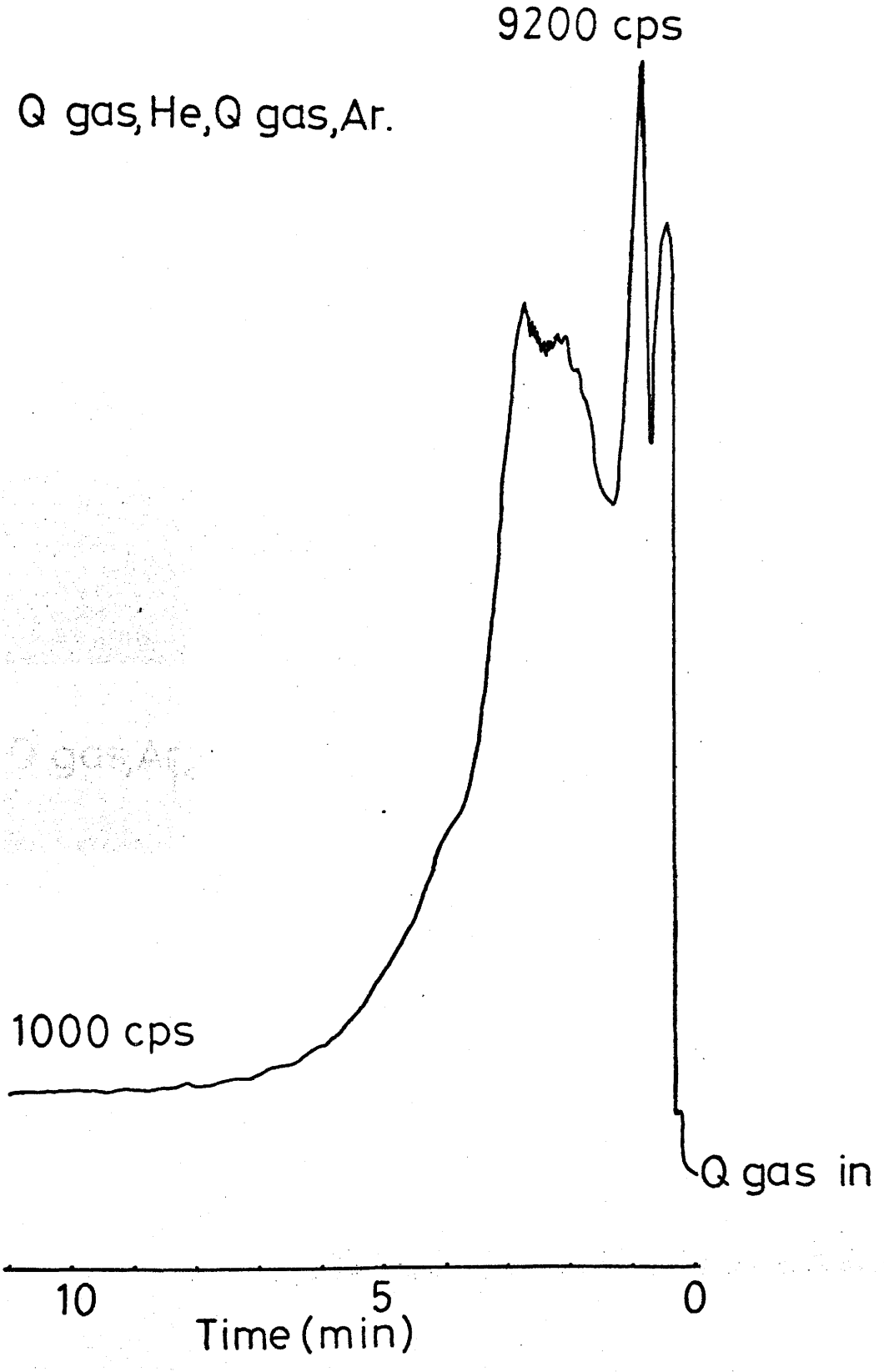

Q gas Introduction curves continued

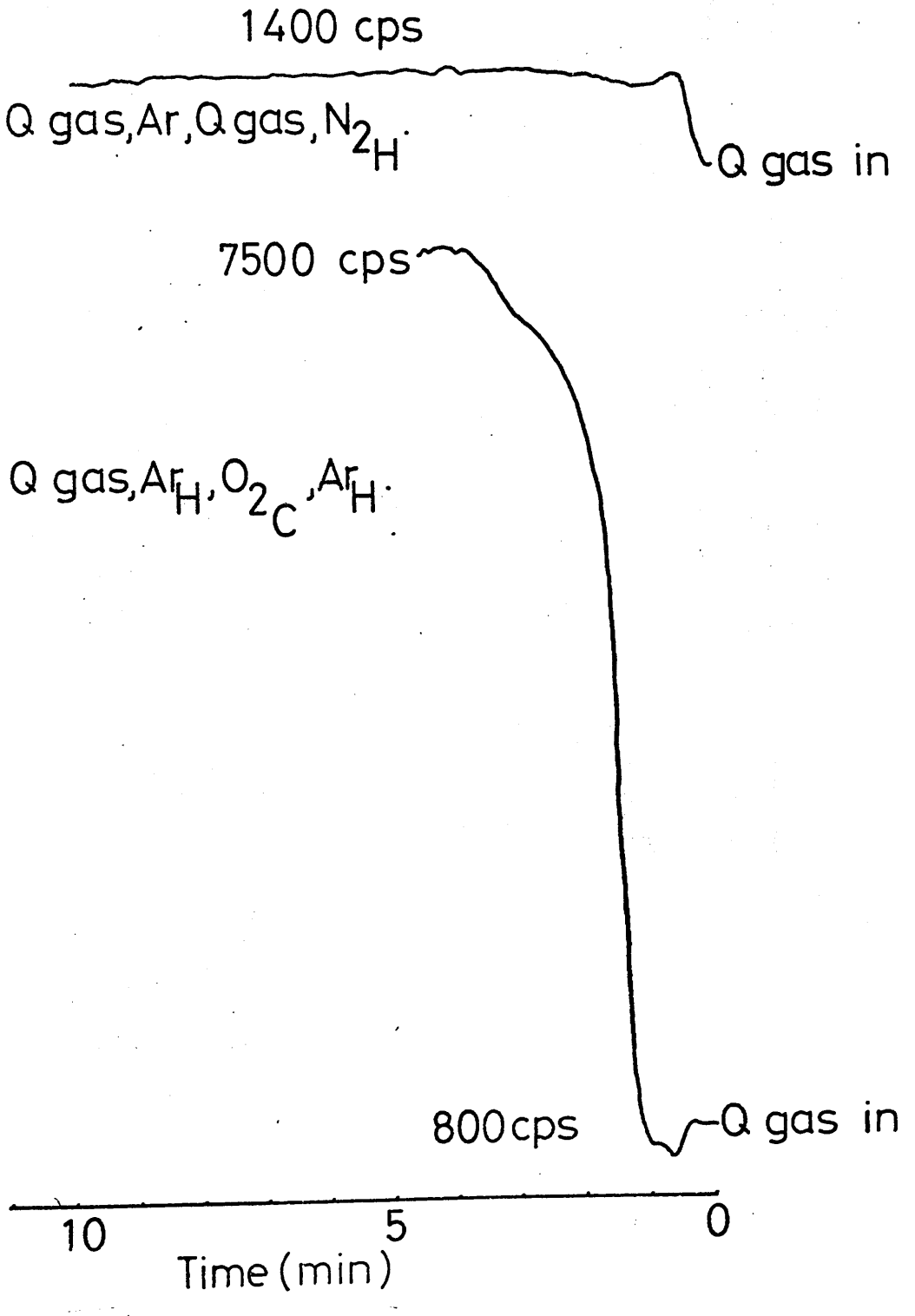

figure 58.

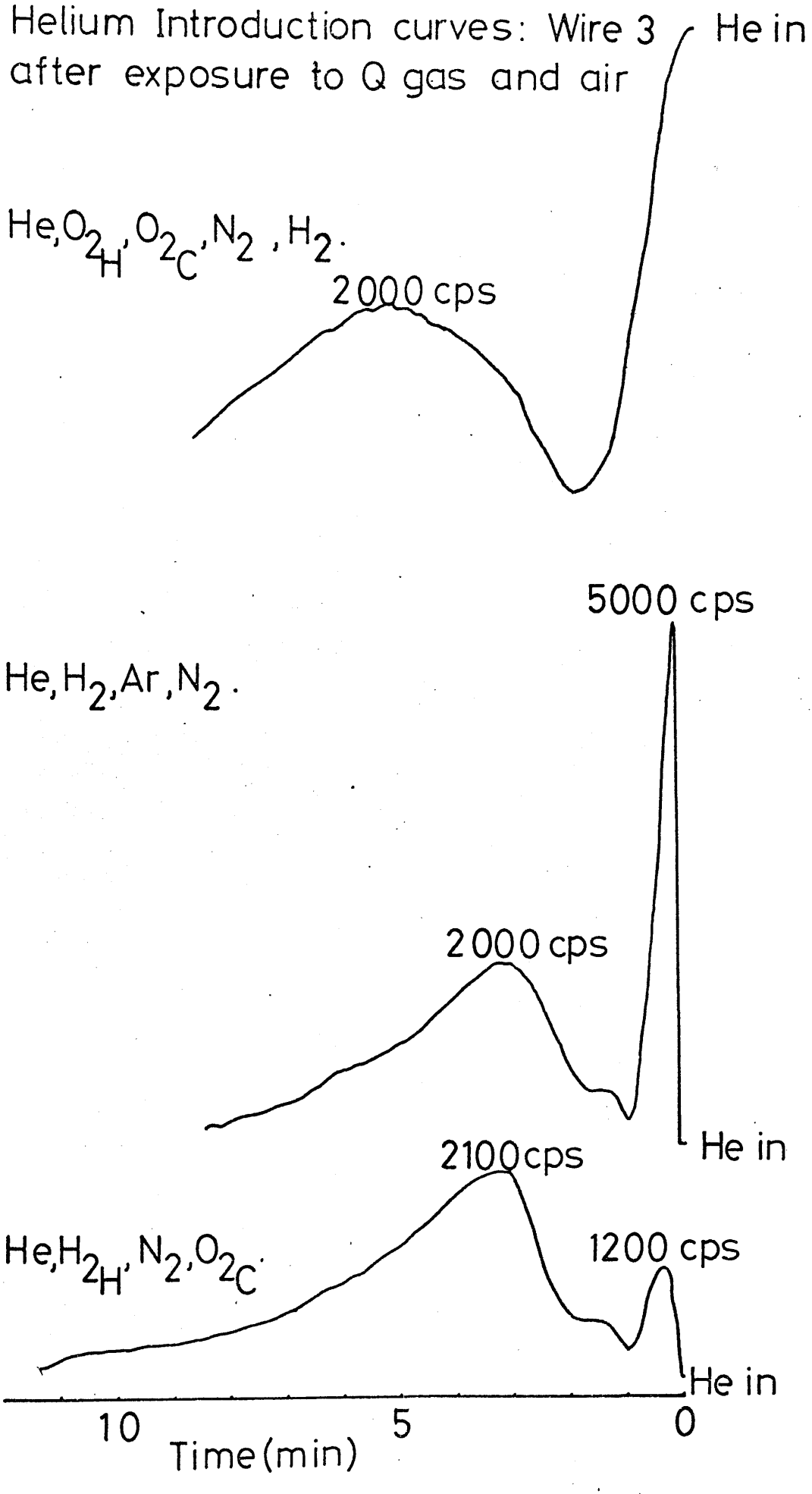
Helium Introduction curves: Wire 3
after exposure to Q gas and air
He in
He, O_{2_H}, O_{2_C}, N_2, H_2.
2000 cps
5000 cps
He, H_2, Ar, N_2.
2000 cps
He in
2100 cps
He, H_{2_H}, N_2, O_{2_C}.
1200 cps
He in
10
5
0
Time (min)

Helium Introduction curves continued

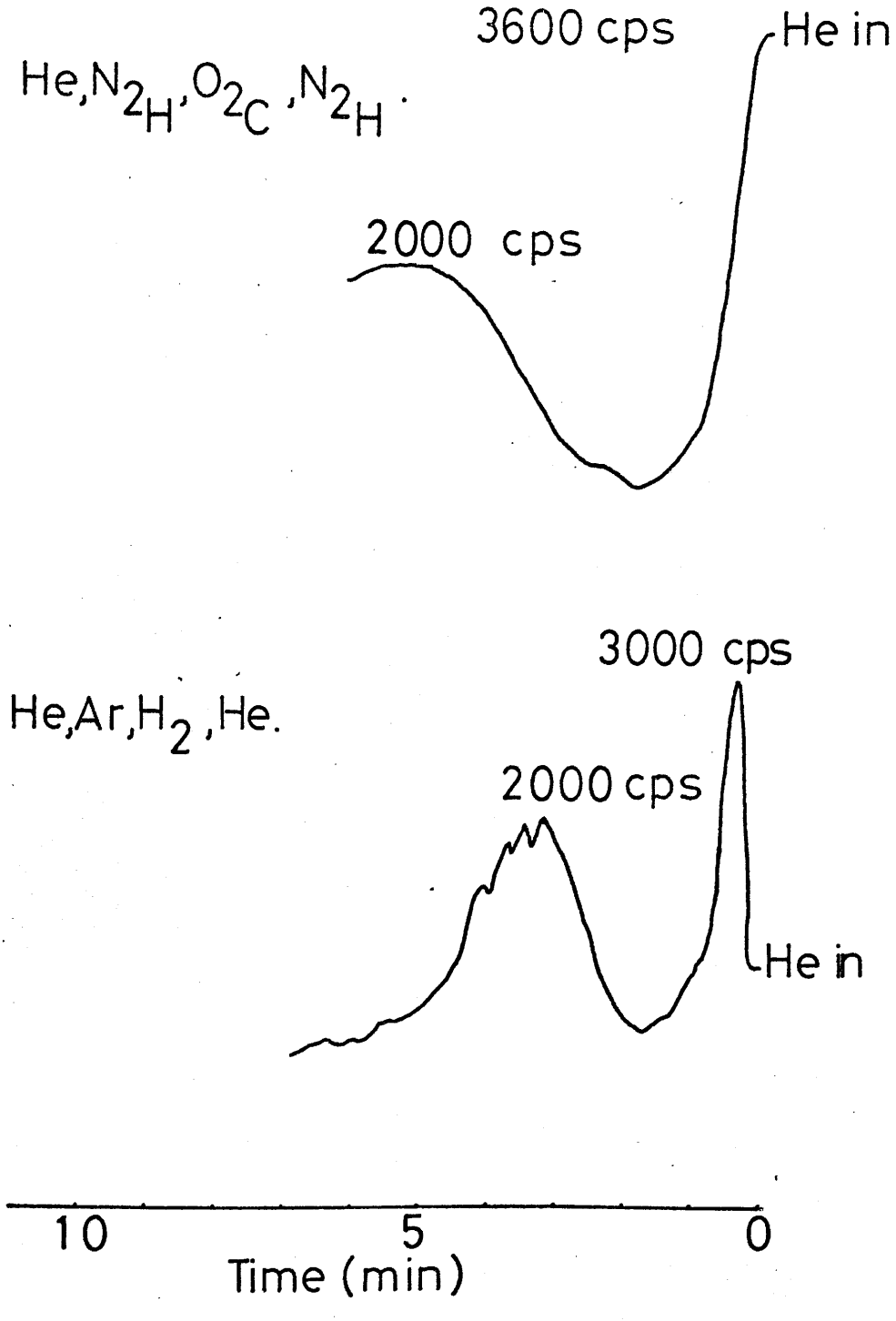

Helium Introduction curves continued

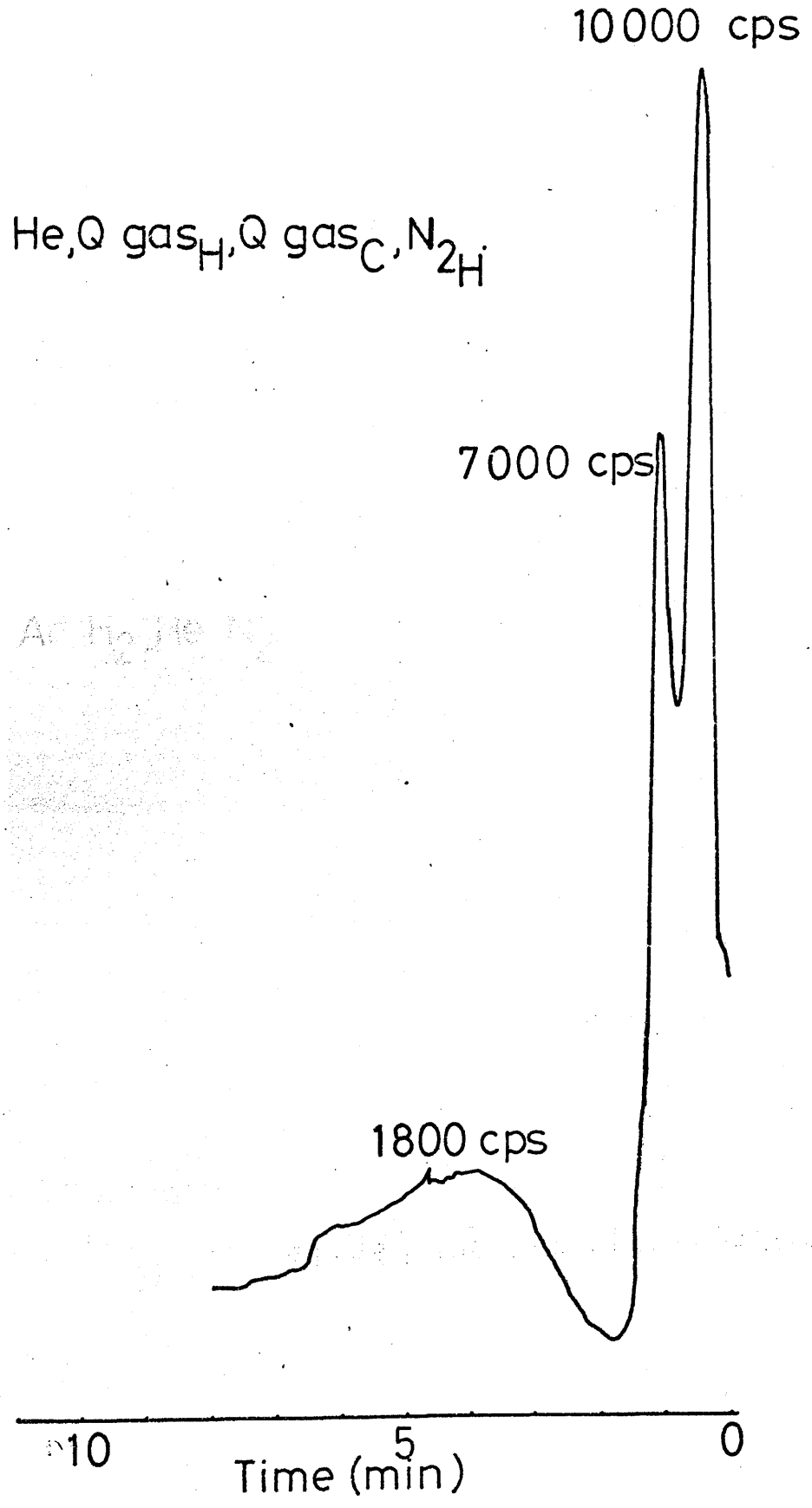

figure 59.

Argon Introduction curves: Wire 3 after exposure to Q gas and air.

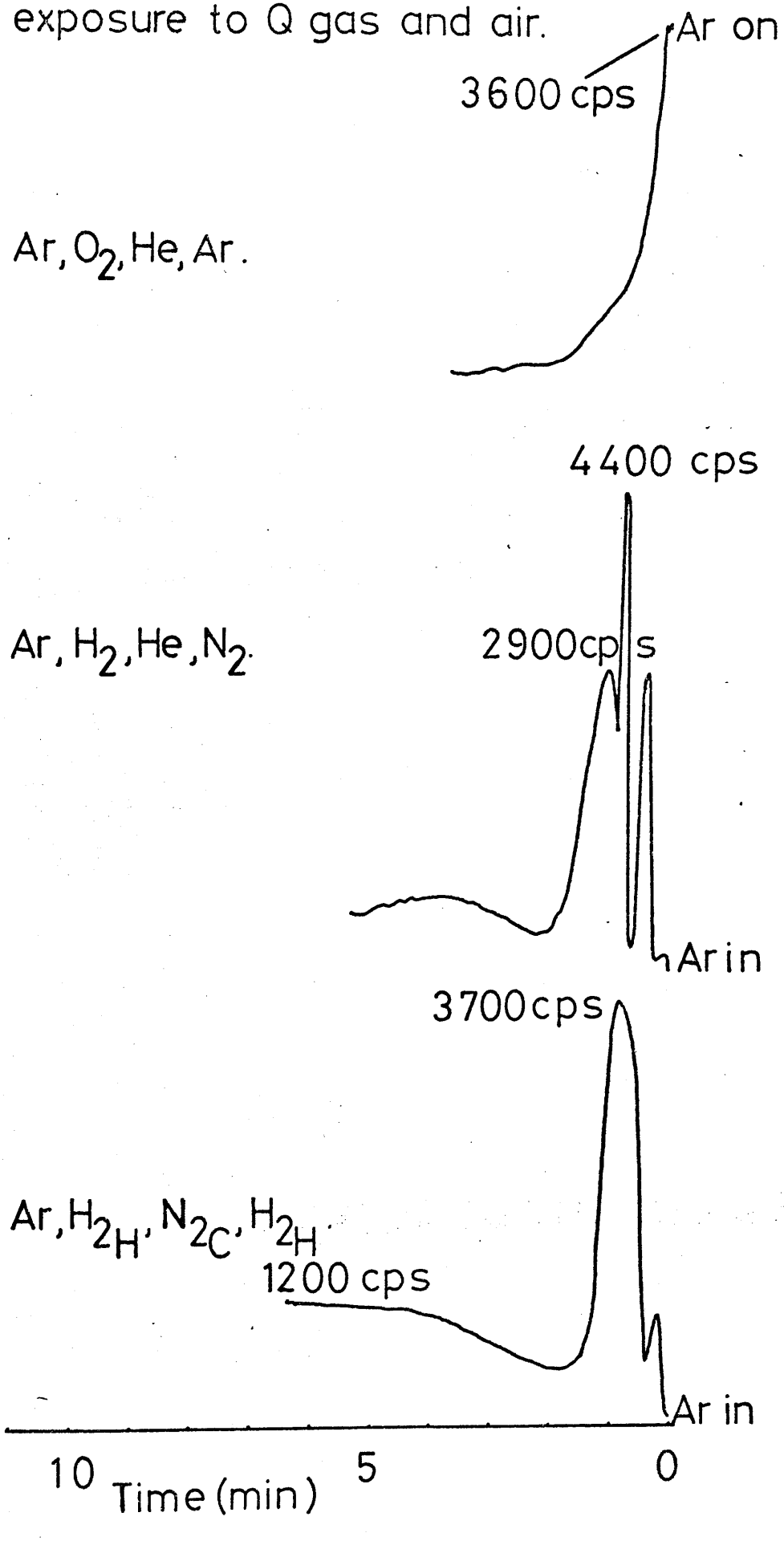

Argon Introduction curves continued

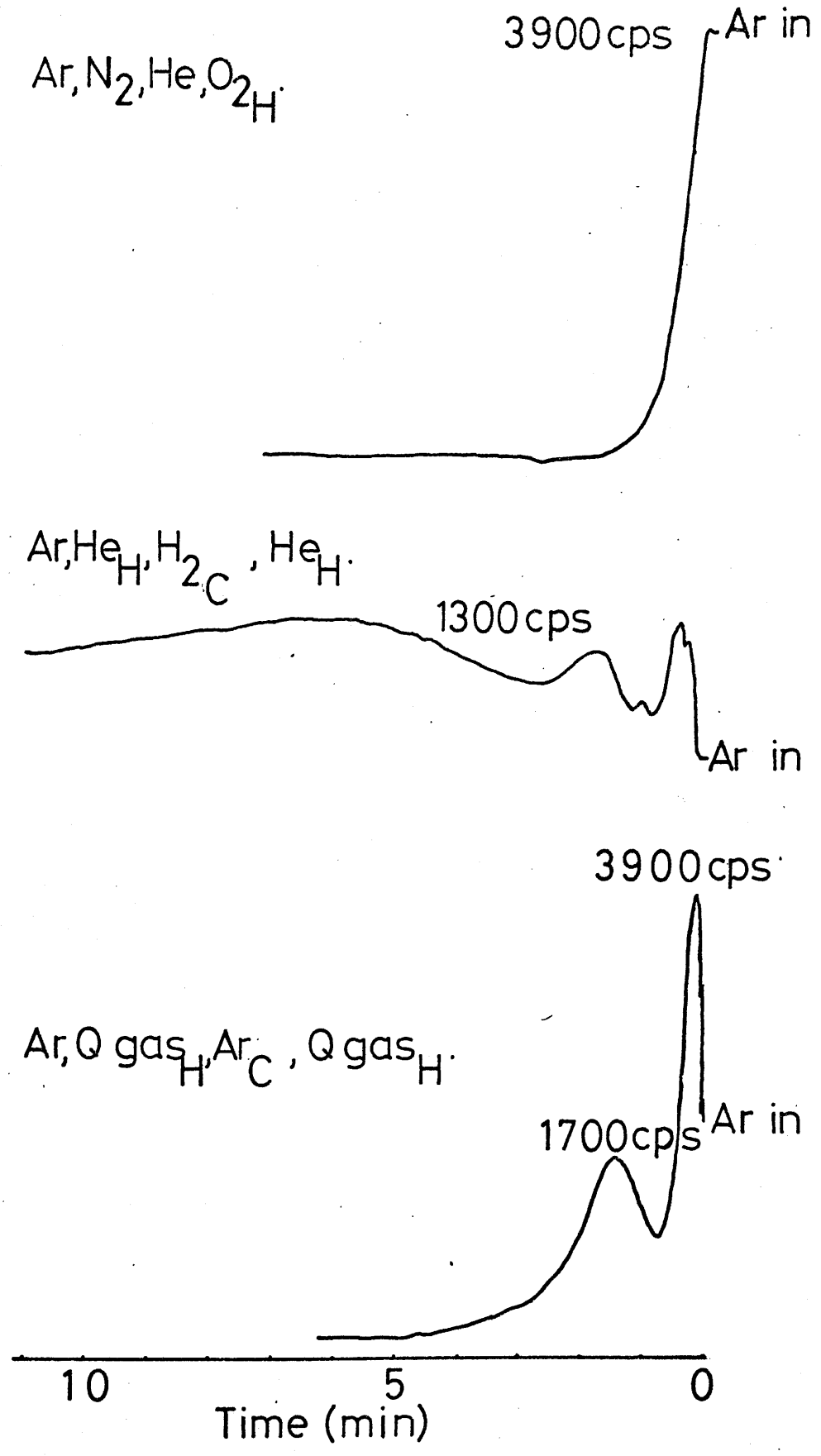

Appendix 11b

Wire 1

Introduction curves

I = 3A

Discriminator 0·1 x 1, 2% window throughout.

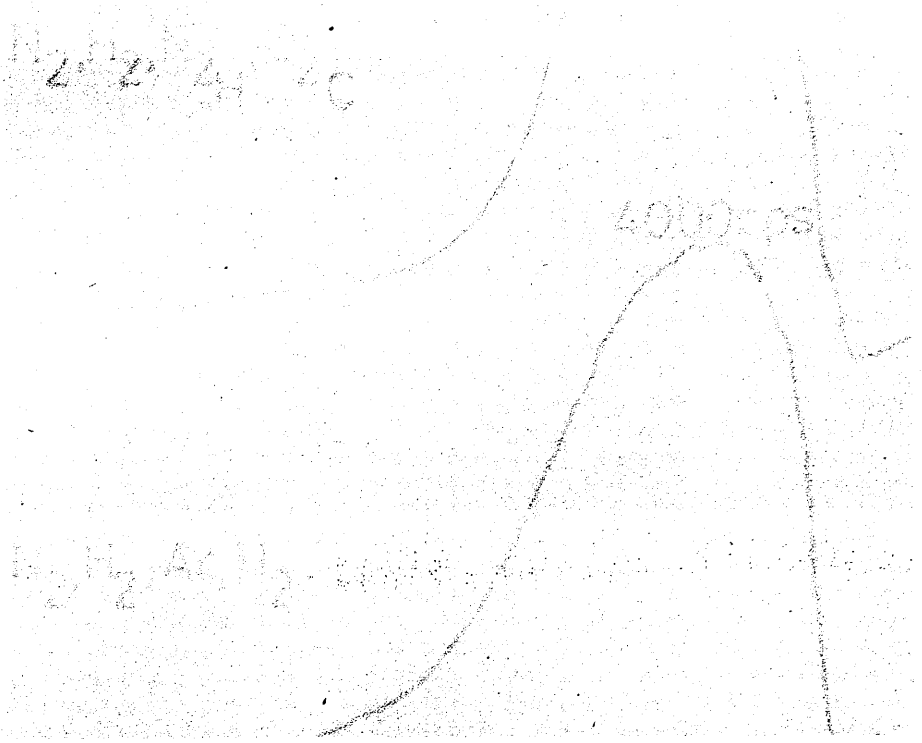

figure 60.

Nitrogen Introduction curves: Wire 1.

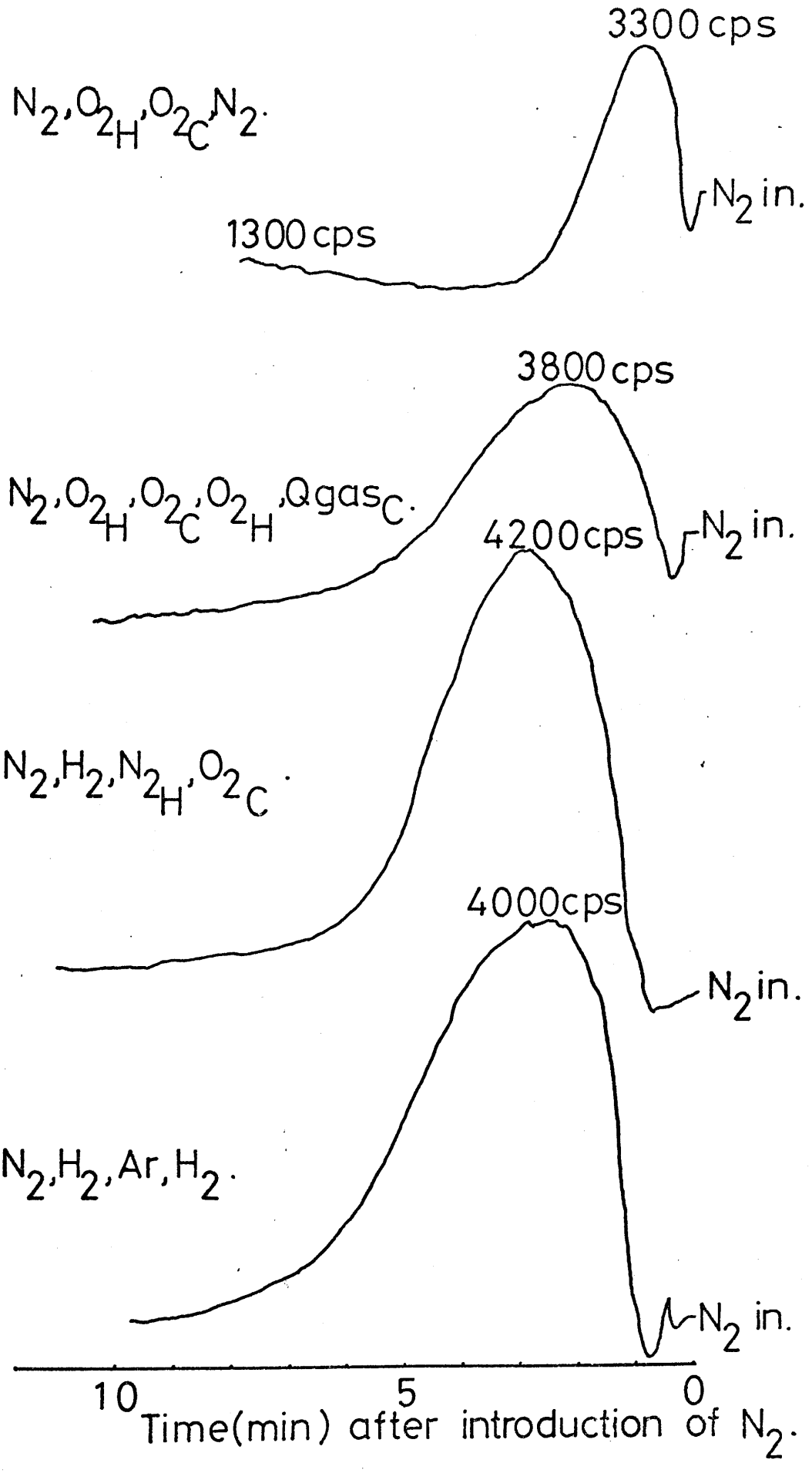

figure 61.

Oxygen Introduction curve : Wire 1.

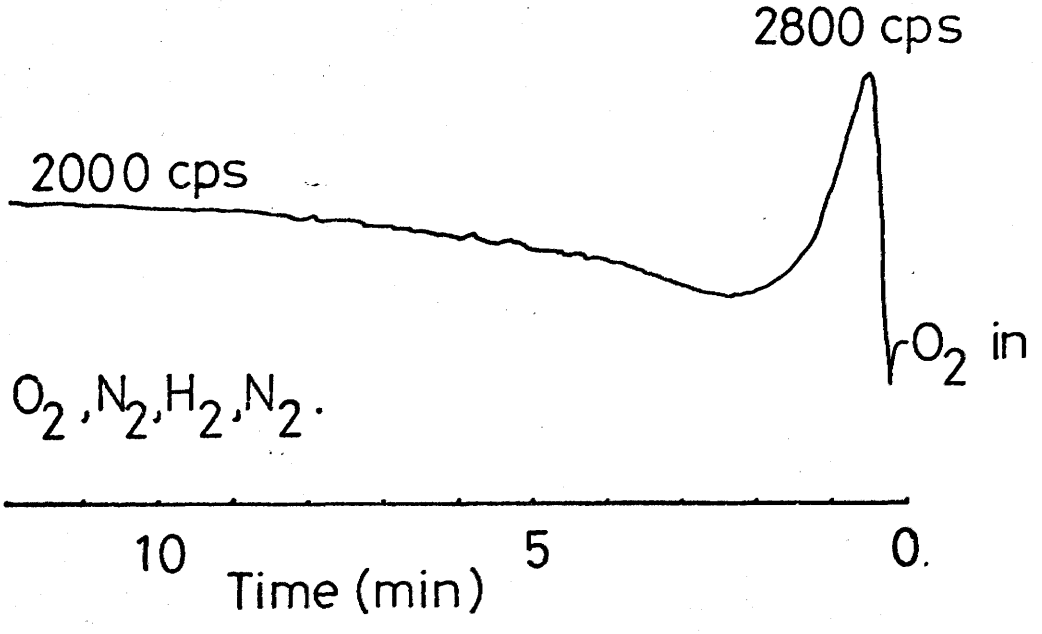

figure 62.

Hydrogen Introduction curves: Wire 1.

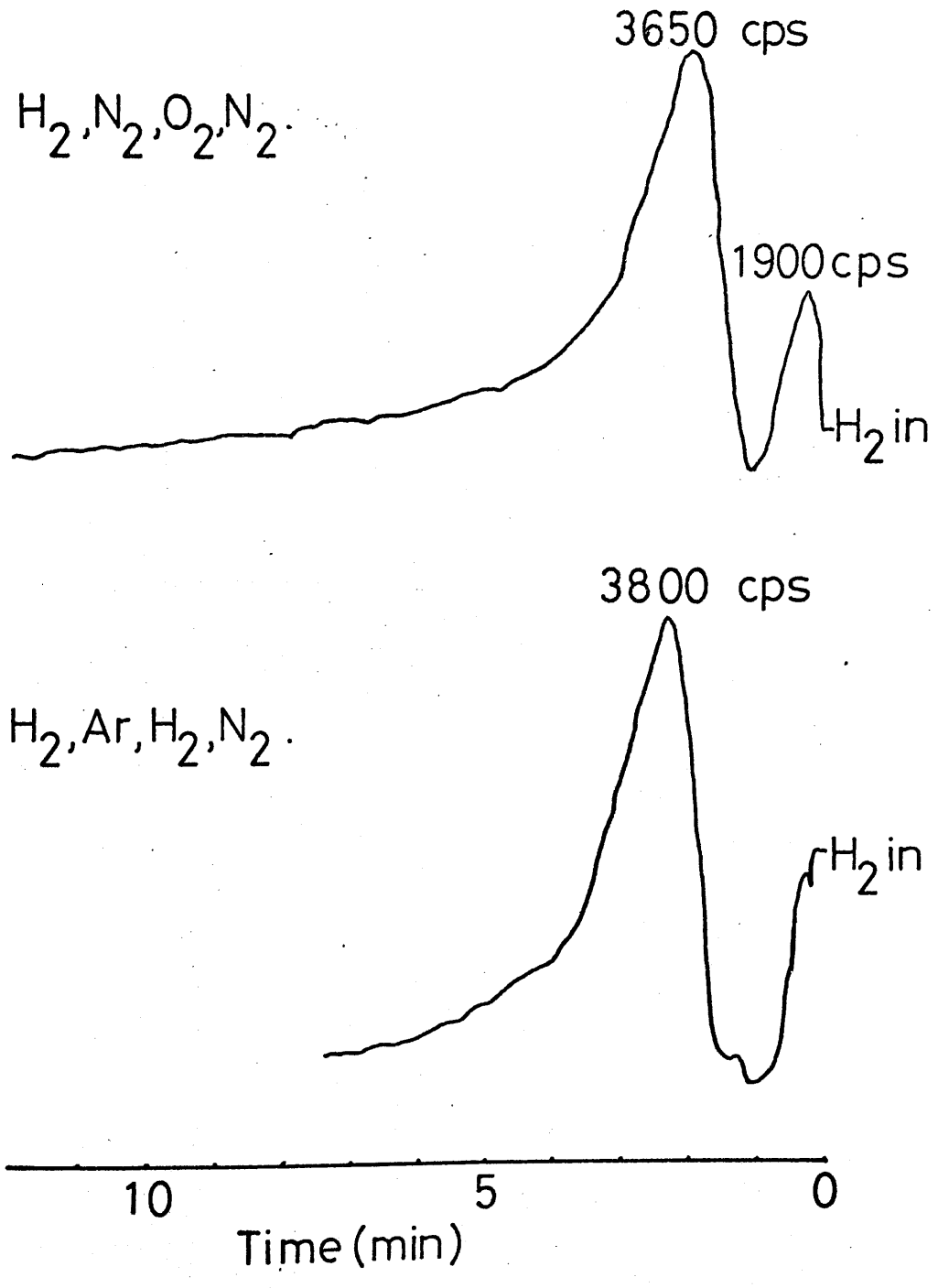

figure 63.

Q gas Introduction curve: Wire 1.

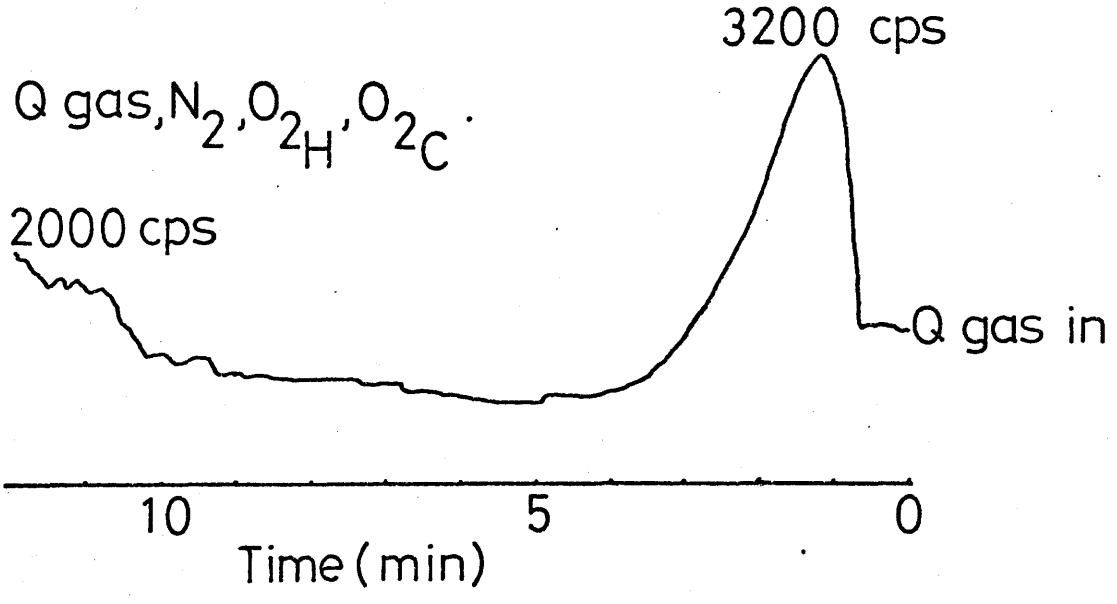

Appendix 12

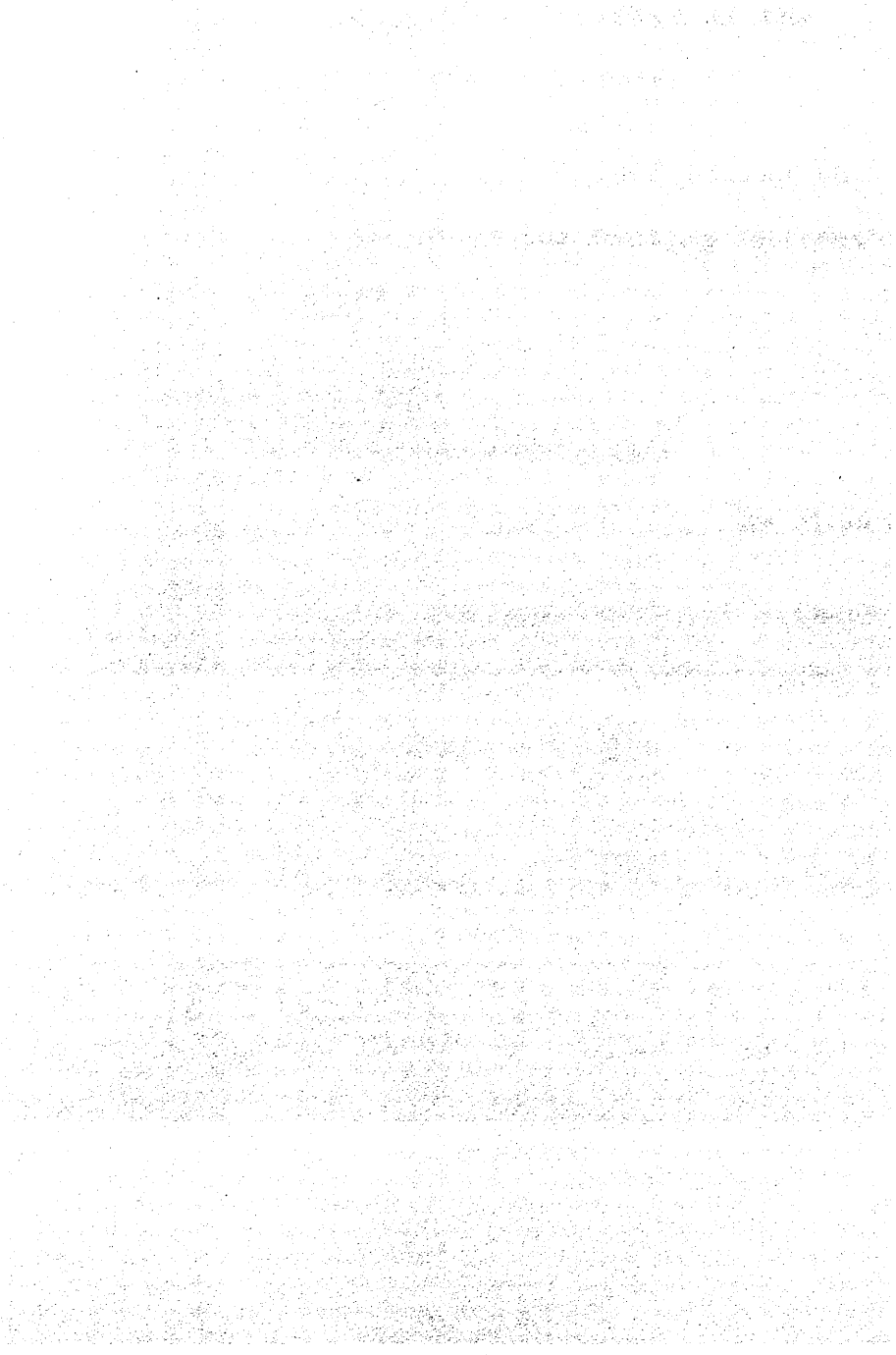

Appendix 12a

Wire 3

Cooling curves with sketches of the corresponding Laben Spectra.

Laben Spectra were recorded during the first five minutes after the heating current (I = 3A) switched off.

Laben Gain x25.
Channel width 40 mV/channel
Discriminator setting 0·1 x 1, 2% window throughout.

The Laben Spectra were obtained without pulse-shaping equipment and with the preamplifier at the 6·5V dynamic range setting.

figure 64.

Nitrogen Cooling curve; Wire 3
Nitrogen following oxygen heating.
V=2 kV
I=3·3 amp

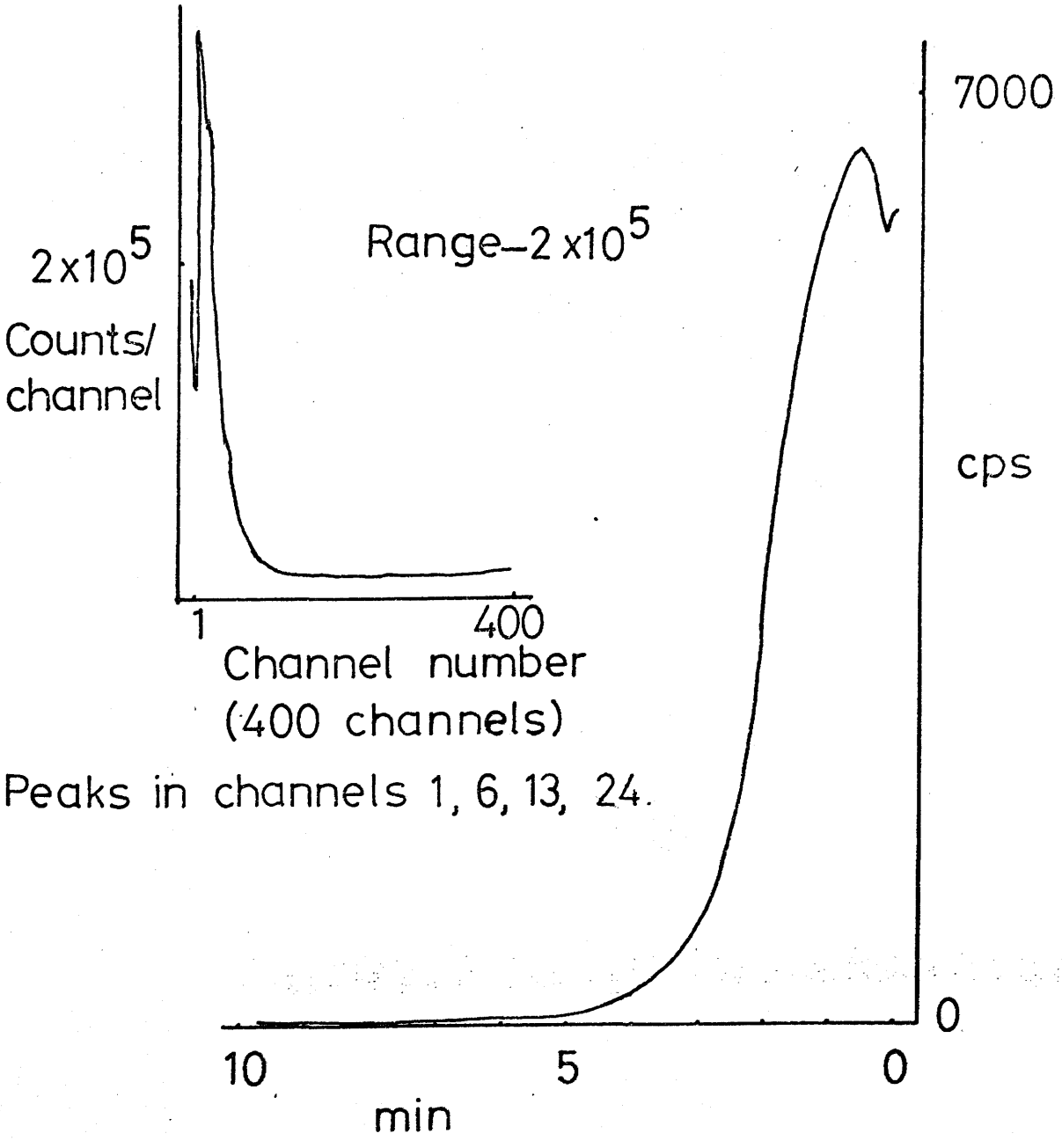

figure 65.

Nitrogen Cooling curve; Wire 3.
Nitrogen following Q gas heating.
V= 2 kV
I= 3·2 amp

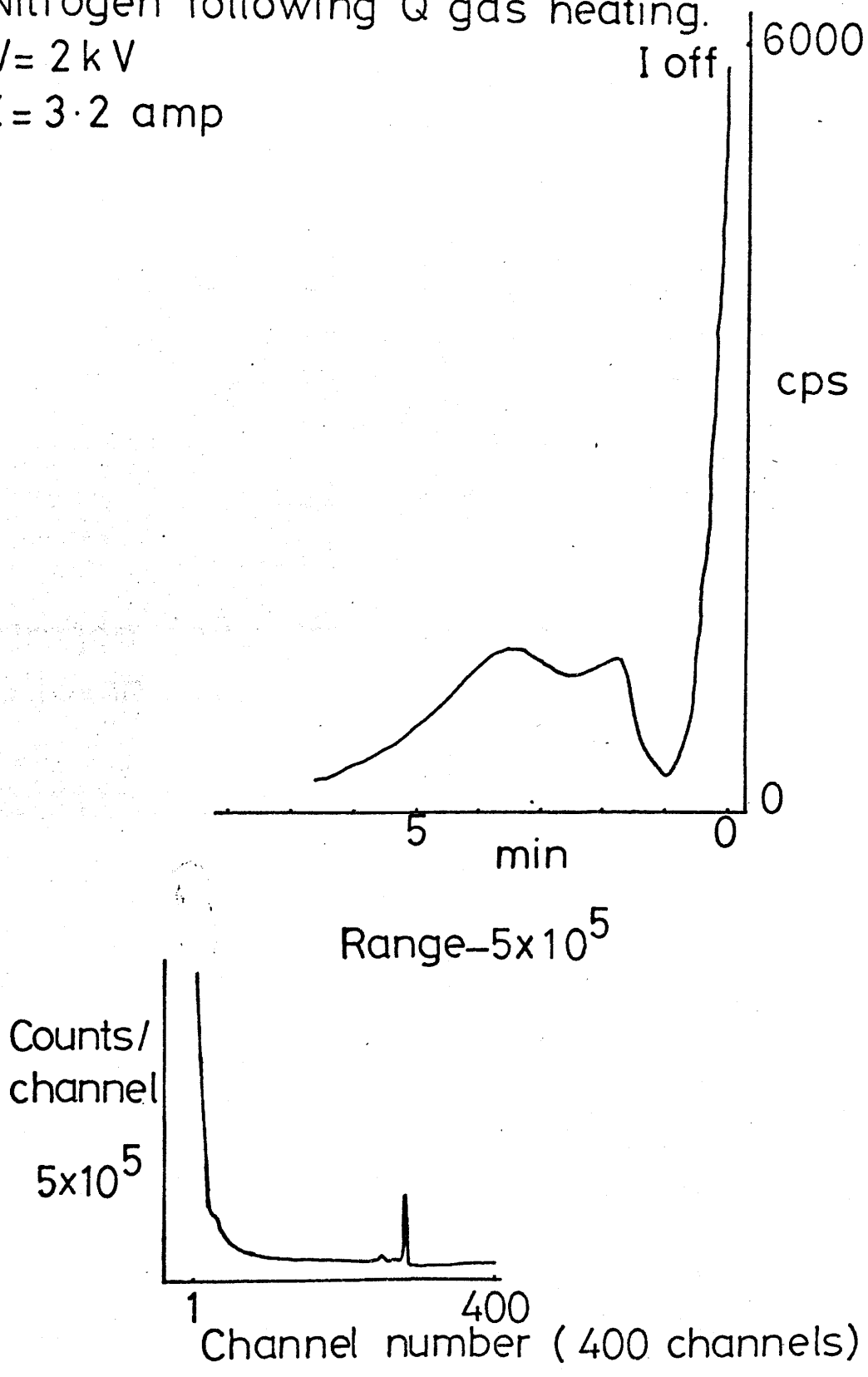

Peaks in channels 1, 25, 240, 272.
Peaks at 240 272 due to saturation of the preamplifier.

figure 66.

Nitrogen Cooling curve ; Wire 3.
Nitrogen following hydrogen heating.
V = 2 kV
I = 3·25amp

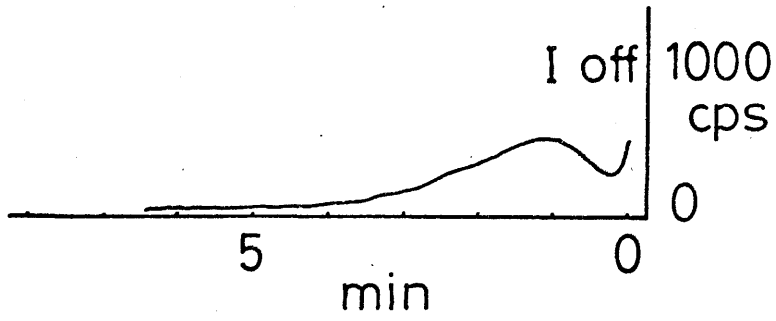

Nitrogen following argon heating and nitrogen following helium heating similar.

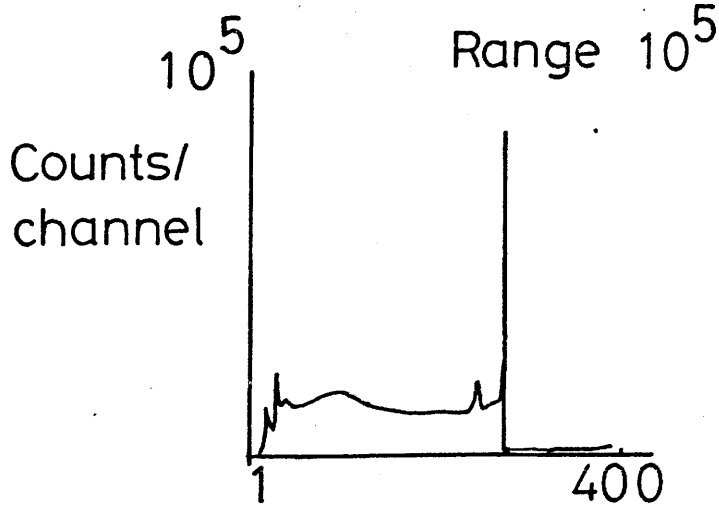

Channel number (400 channels).

Peaks in channels 6, 17, 27, 92, 240, 272.
Ar_H, N_{2C} :-Peaks at 5, 17, 27, 240, 272.
He_H, N_{2C} :-Peaks at 1, 18, 91, 241, 272.
Peaks at 240-1 and 272 due to saturation of the preamplifier.

figure 67.

Hydrogen Cooling curve; Wire 3.
Hydrogen following Q gas heating.
V= 2 kV
I = 4·1 amp

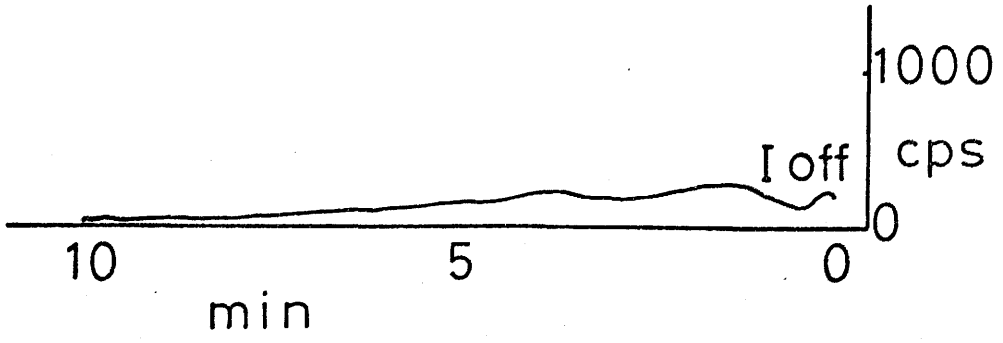

Hydrogen following oxygen heating (and nitrogen flush) similar.

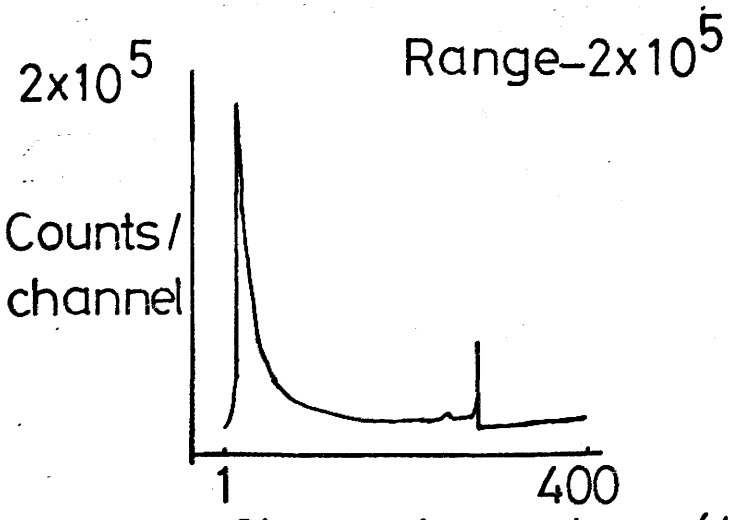

Peaks in channels 16, 92, 240, 272.
H_{2C}, O_{2H} Laben spectrum similar.
Peaks at 3, 16, 26, 240, 273. Peaks at 240, 272–3 due to saturation of the preamplifier.

figure 68.

Hydrogen Cooling curve; Wire 3.
Hydrogen following nitrogen heating.
V = 2 kV
I = 4·1 amp

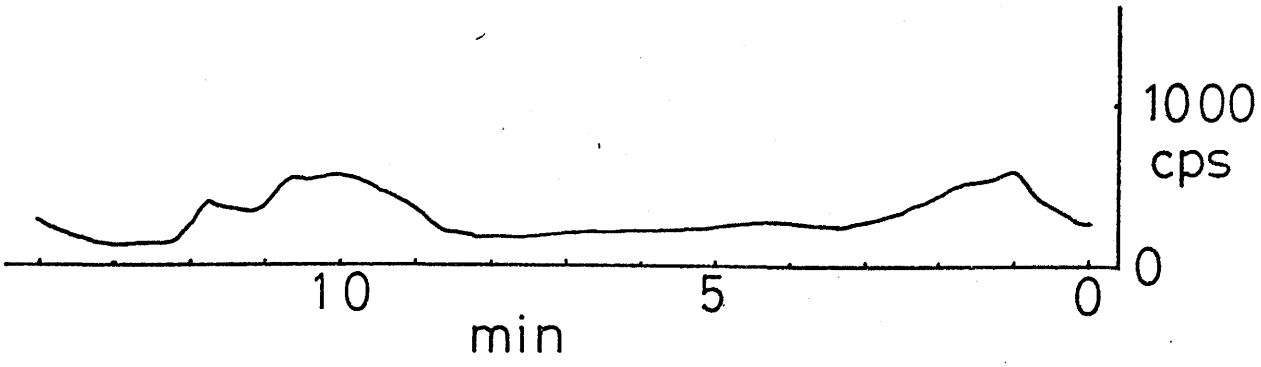

Hydrogen cooling after argon and after helium gives similar cooling curves.

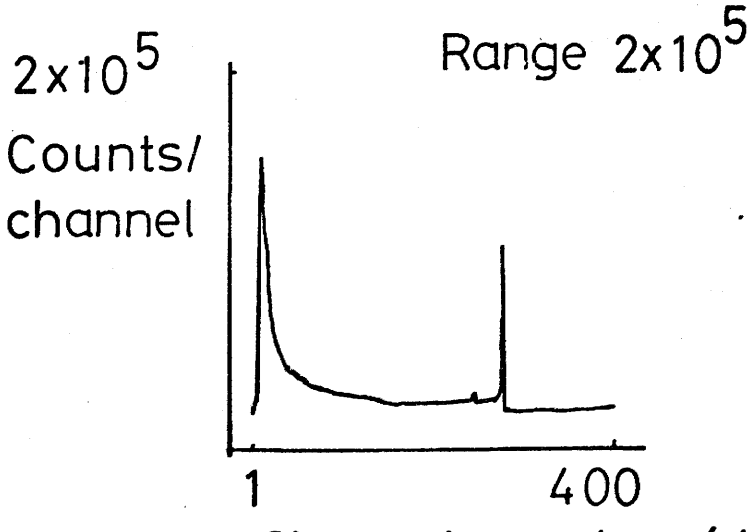

Peaks in channels 14, 118, 239, 273.
H_{2_C} , Ar_H; H_{2_C} , He_H both gave similar Laben spectra. with peaks at 12, 45, 240, 274 and 16 241 274 respectively.

Peaks around 240 and 273 due to saturation of the preamplifier.

figure 69.

Oxygen Cooling curve; Wire 3.
Oxygen after nitrogen heating.

V = 2 kV
I = 3·25 amp

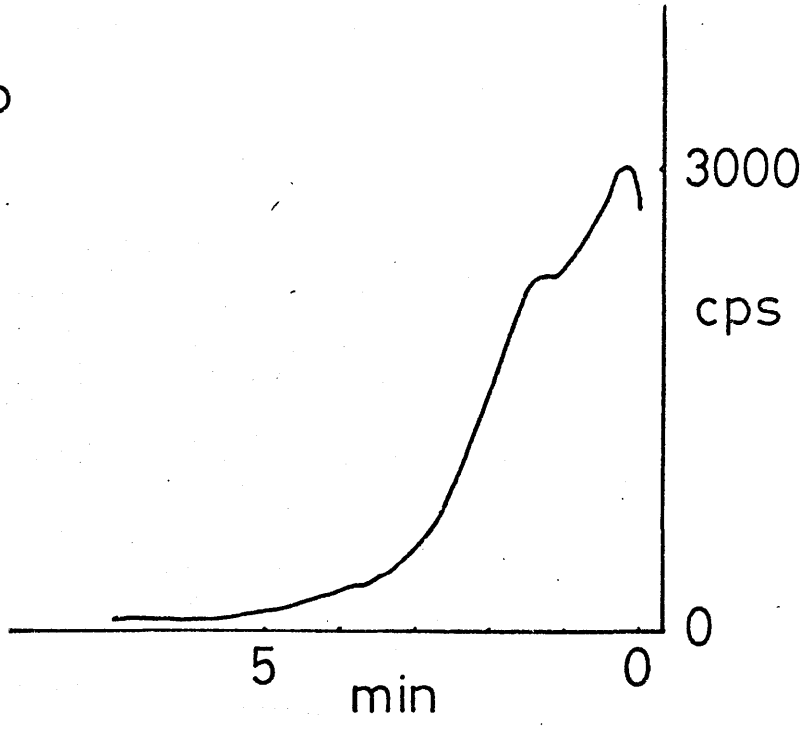

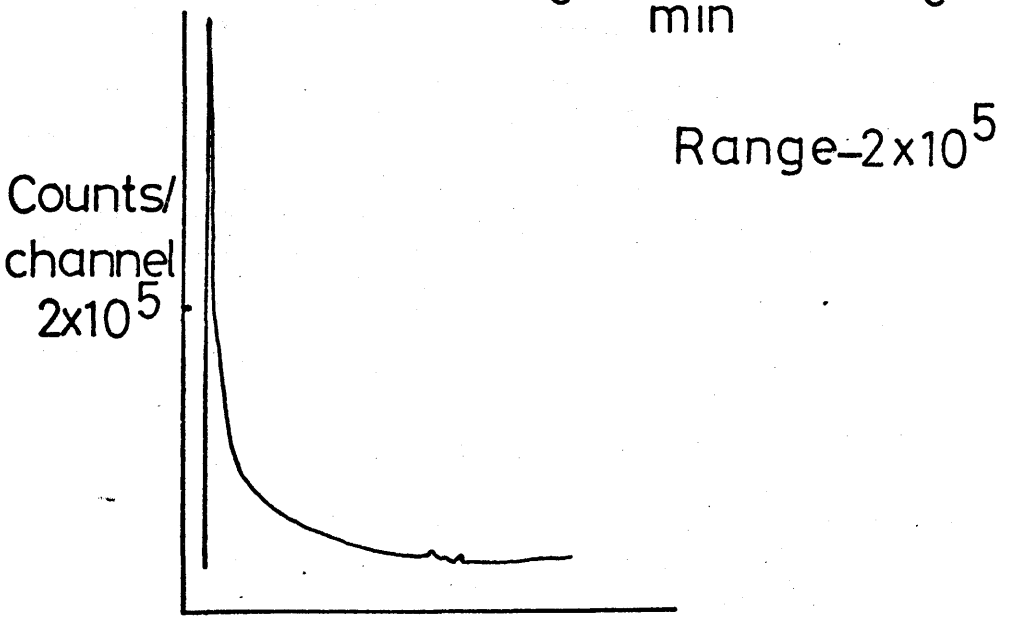

Channel number (400 channels)

Peaks in channels 4, 239, 272.

figure 70.

Oxygen Cooling curve; Wire 3
Oxygen following hydrogen heating and nitrogen flush.
V = 2 kV
I = 3·25 amp

O_{2_C}, He_H and O_{2_C}, Ar_H cooling curves and Laben spectra similar.

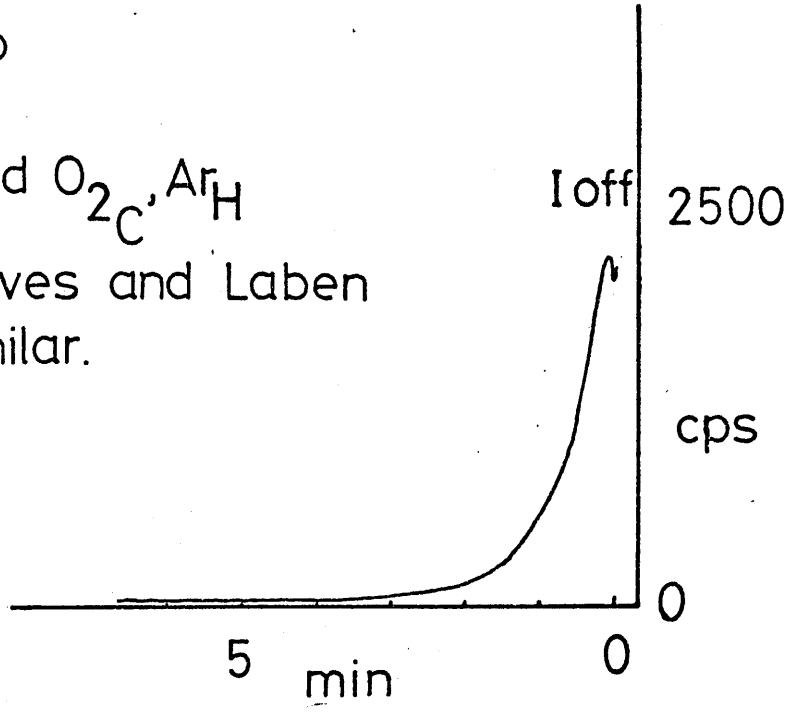

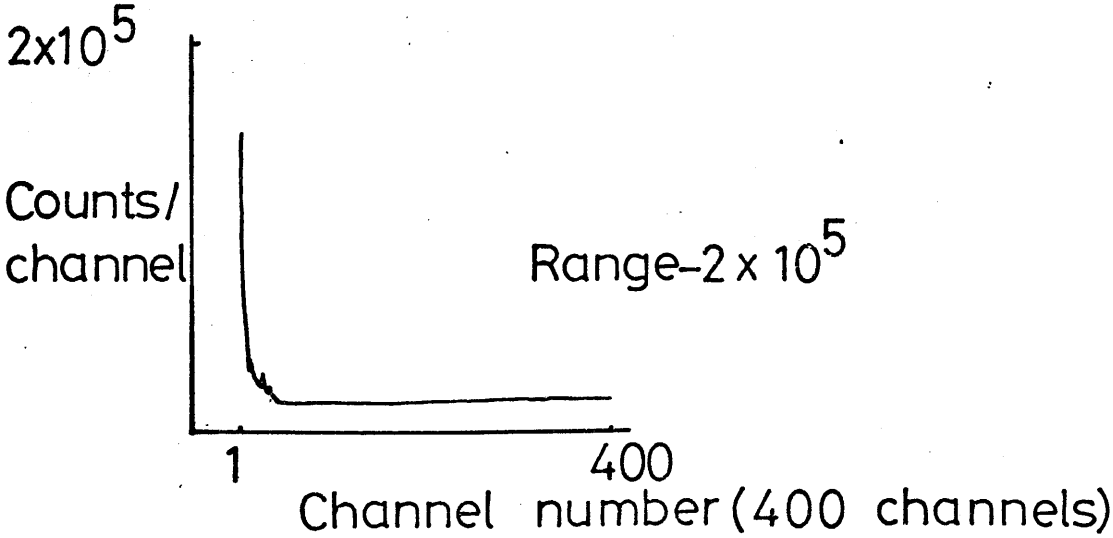

Peaks in channels 1, 8, 14, 23, 29.

O_{2_C}, He_H, Peaks – 1, 6 (off scale).

O_{2_C}, Ar_H, Peaks – 2, 22, 27.

figure 71.

Oxygen Cooling curve; Wire 3
Oxygen following Q gas heating and nitrogen flush.
V=2 kV
I=3·2 amp

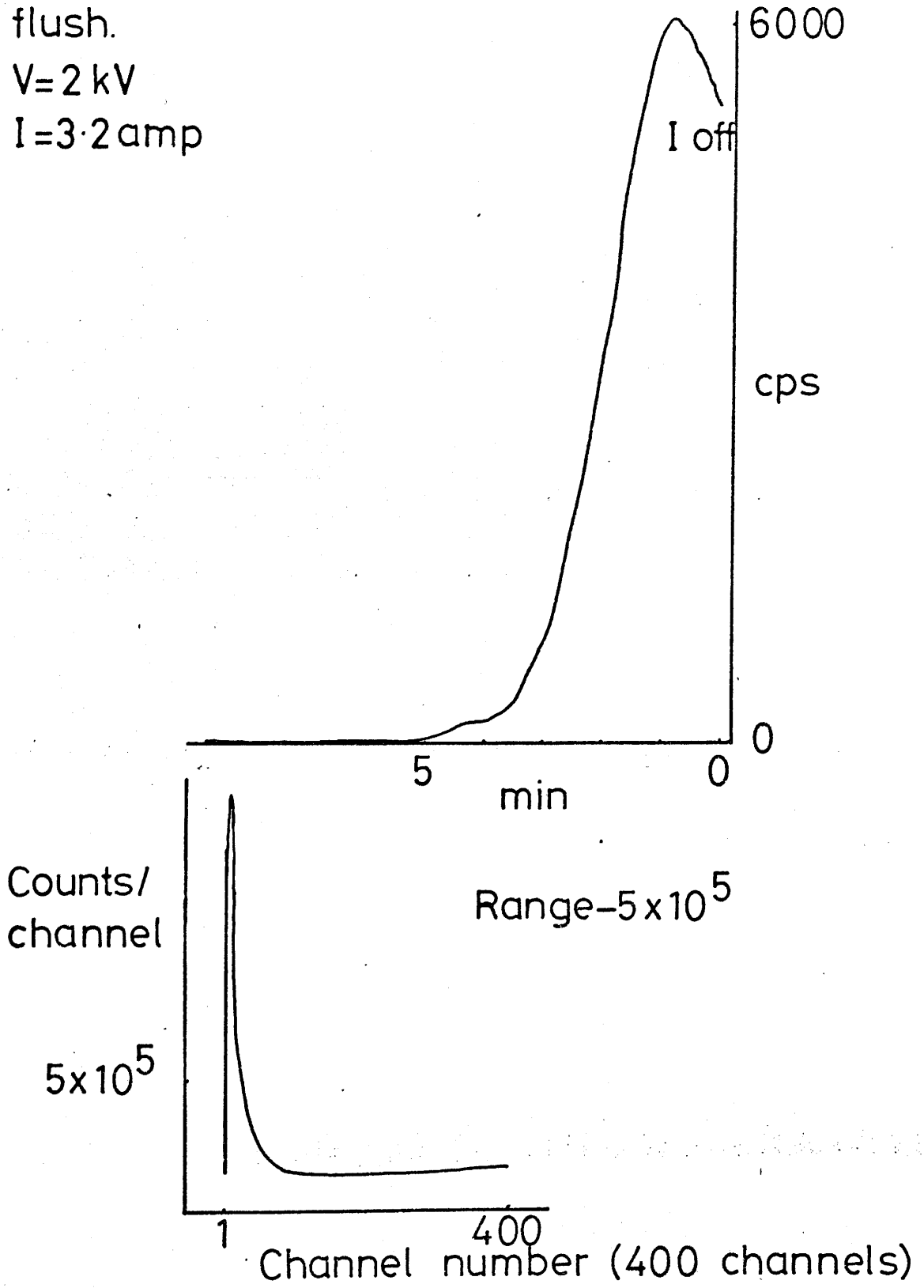

Peak in channel 4.

figure 72.

Helium Cooling curve; Wire 3.
Helium following oxygen heating.
V= 2kV
I = 3·95amp

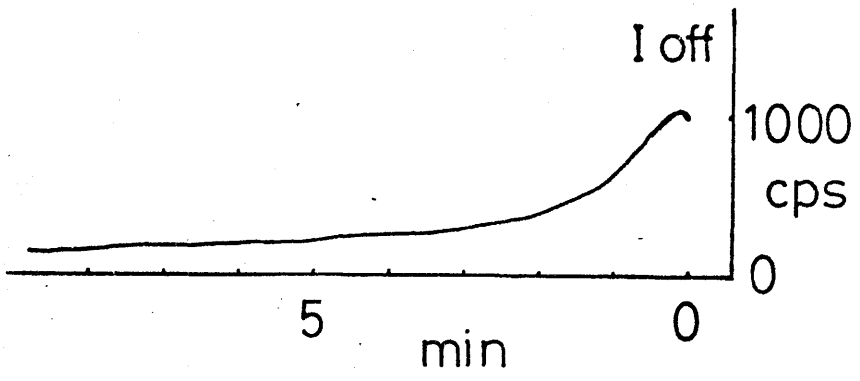

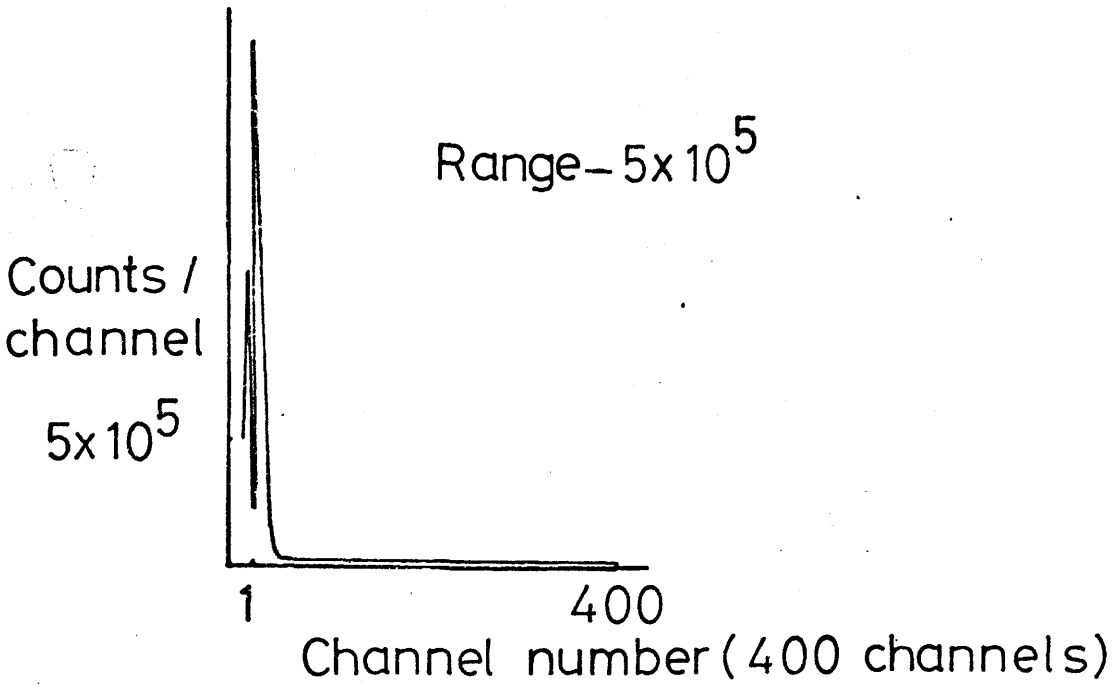

Peaks in channels 2, 8.
Helium cooling after argon heating similar.
Laben spectrum also similar.
Peaks at 2, 8.

figure 73.

Helium Cooling curve; Wire 3.
Helium following nitrogen heating.
V = 2 kV
I = 3·9amp

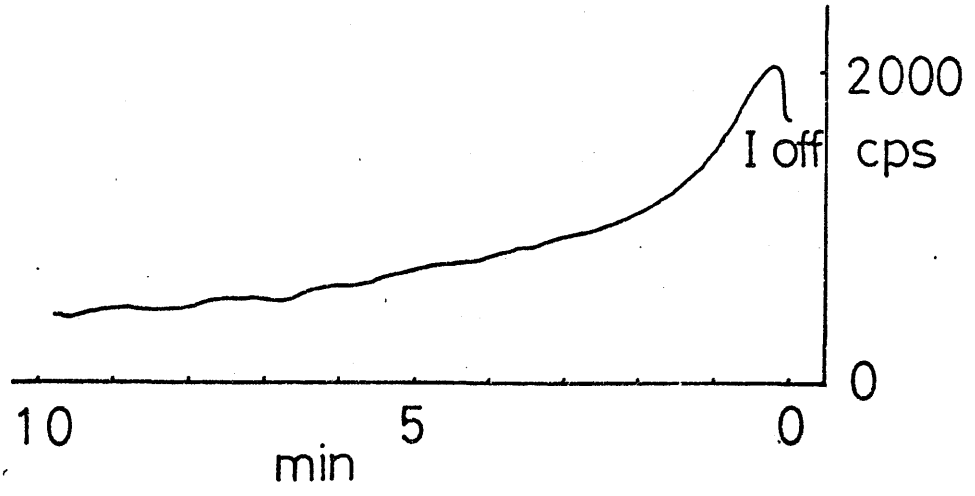

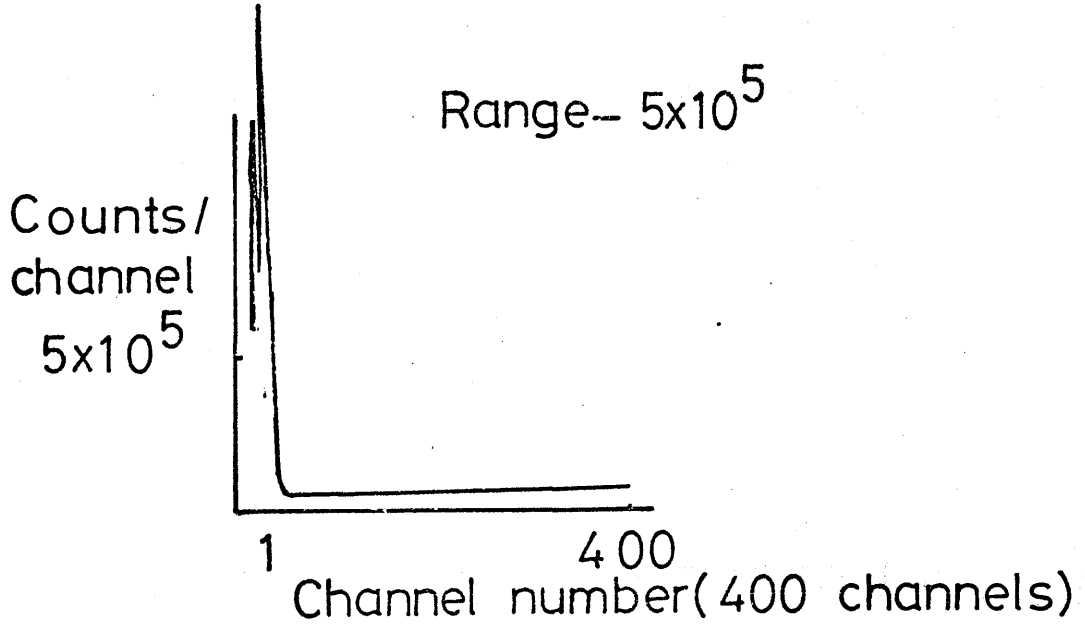

Peaks in channels 3, 9.

figure 74.

Helium Cooling curve; Wire 3.
Helium following hydrogen heating.
V= 2kV
I = 4·05amp

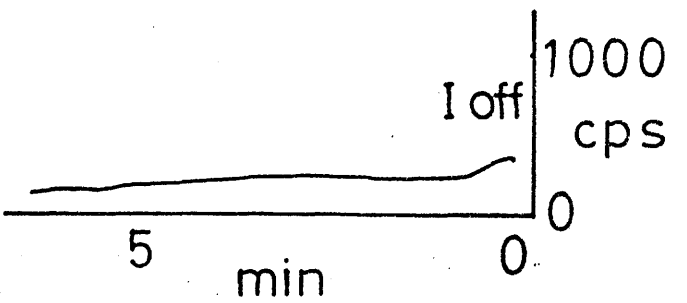

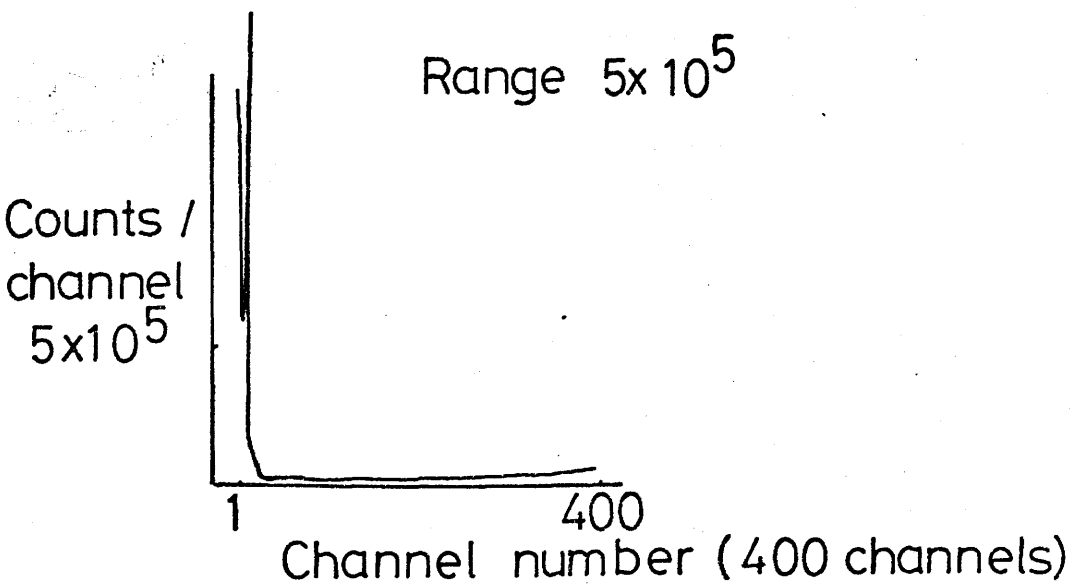

Peaks in channels 1, 7.

figure 75.

Helium Cooling curve; Wire 3.
Helium following Q gas heating.
V = 2kV
I = 3·9 amp

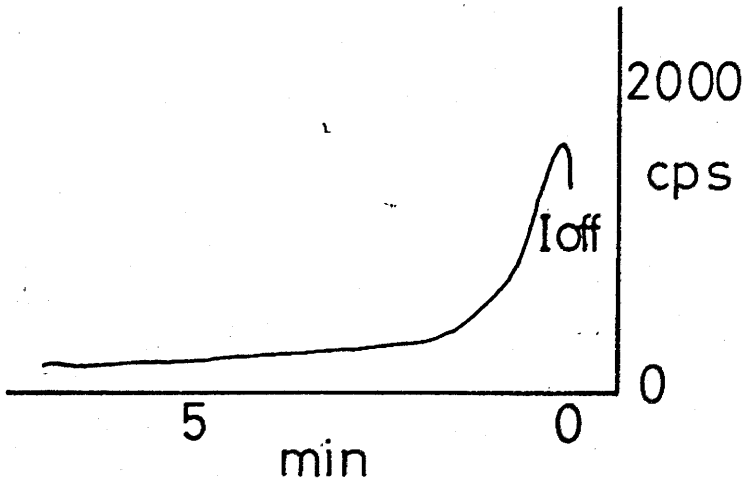

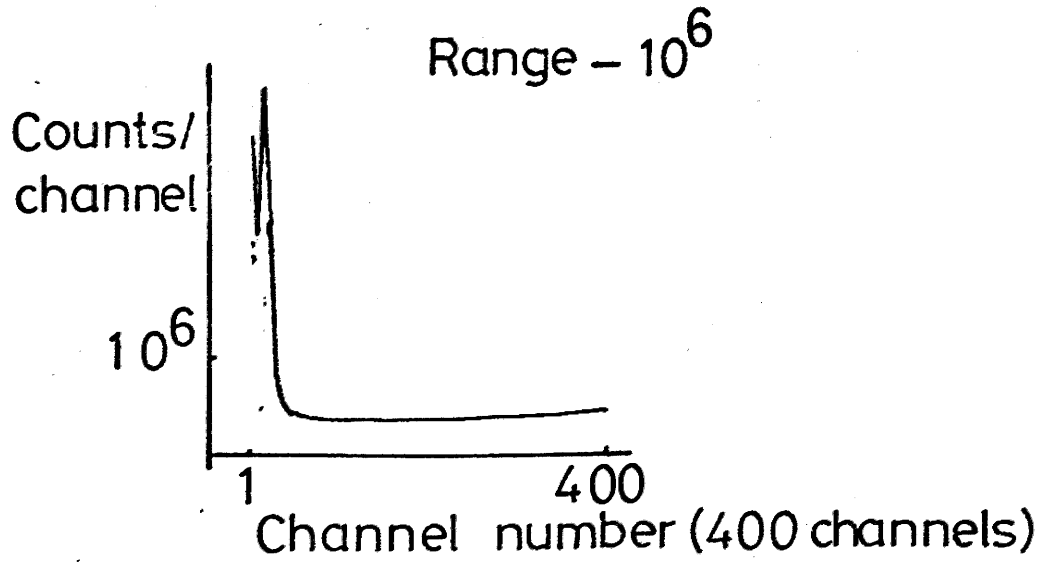

Peaks in channels 1, 8.

figure 76.

Argon Cooling curve; Wire 3.
Argon after oxygen heating.
V = 2 kV
I = 3·1amp

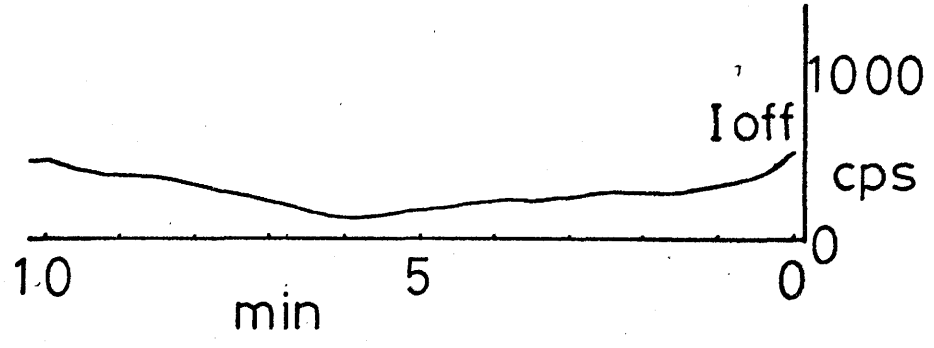

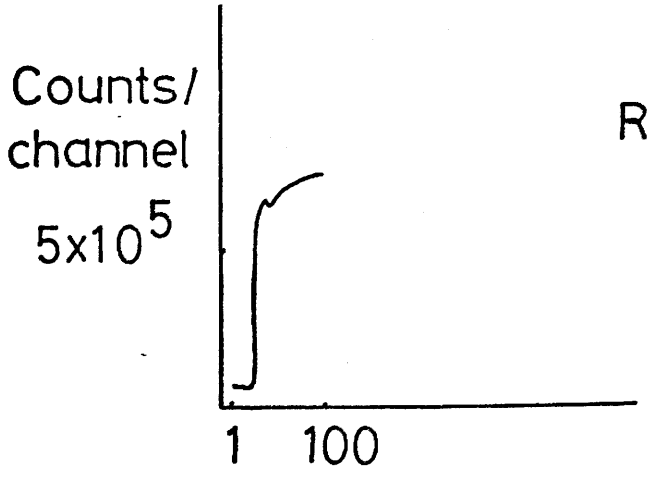

Channel number (only 100 channels recorded).

Peak in channel 39 then plateau.

figure 77.

Argon Cooling curve; Wire 3.
Argon following nitrogen heating.
V = 2 kV
I = 3·05 amp

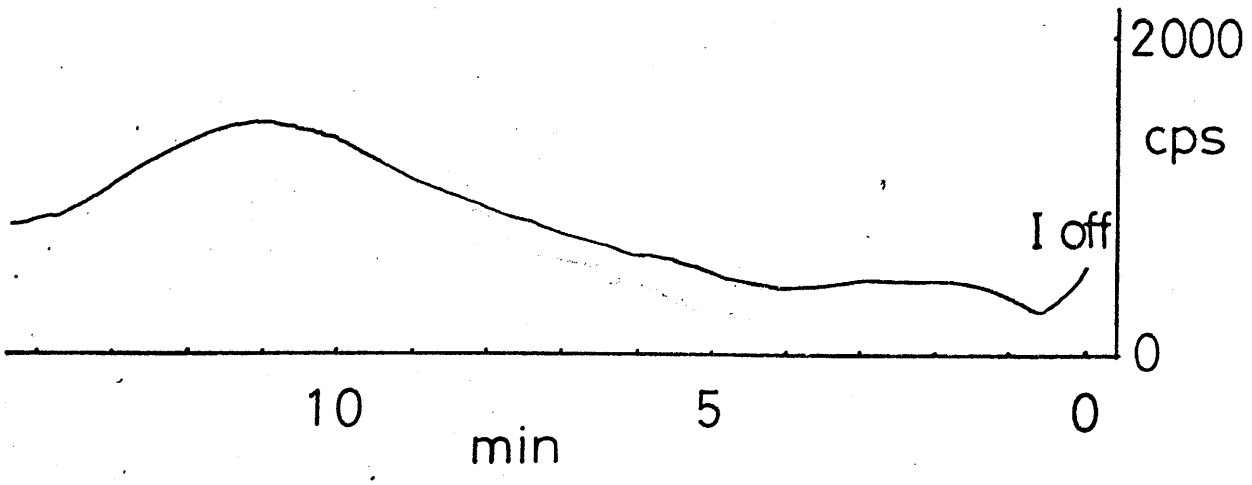

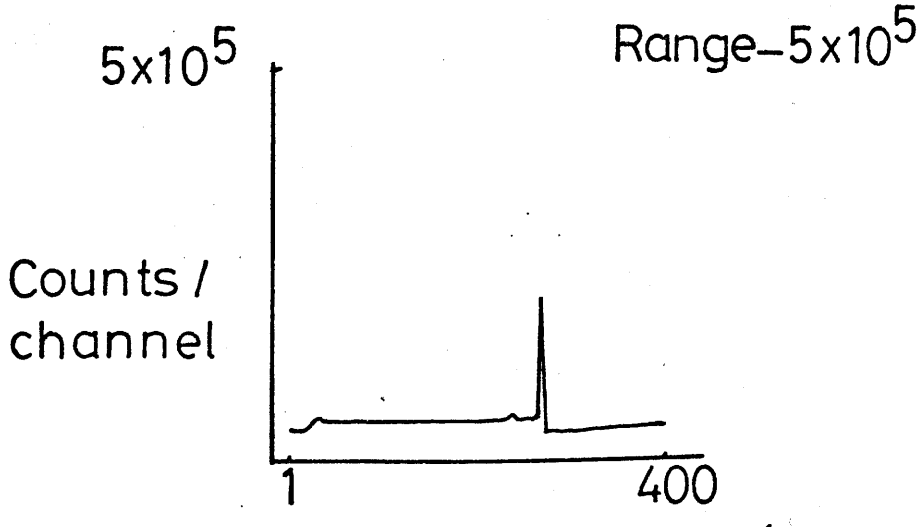

Peaks in channels 31, 239, 272.
Peaks at 239, 272 due to saturation of the preamplifier.

figure 78.

Argon Cooling curve; Wire 3
Argon after hydrogen heating.
V = 2 kV
I = 3·15 amp

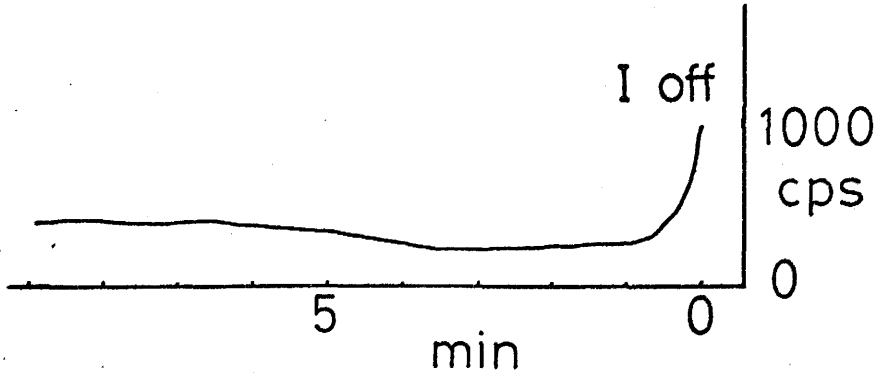

Argon cooling after helium heating similar.
Laben spectrum also similar.

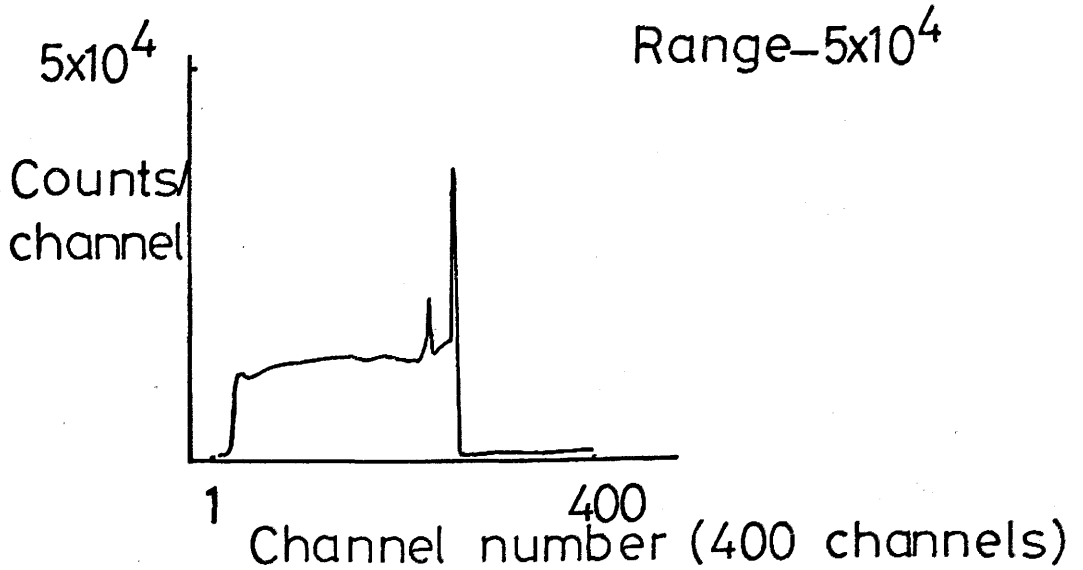

Peaks in channels 33, 241, 272.
Ar_C, He_H; Peaks – 32, 241, 272.
Peaks at 241, 272 due to saturation of the preamplifier.

figure 79.

Argon Cooling curve; Wire 3
Argon following Q gas heating.
V= 2 kV
I = 3·1 amp

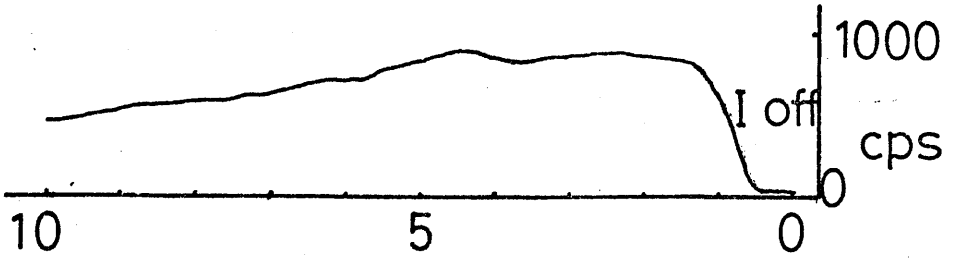

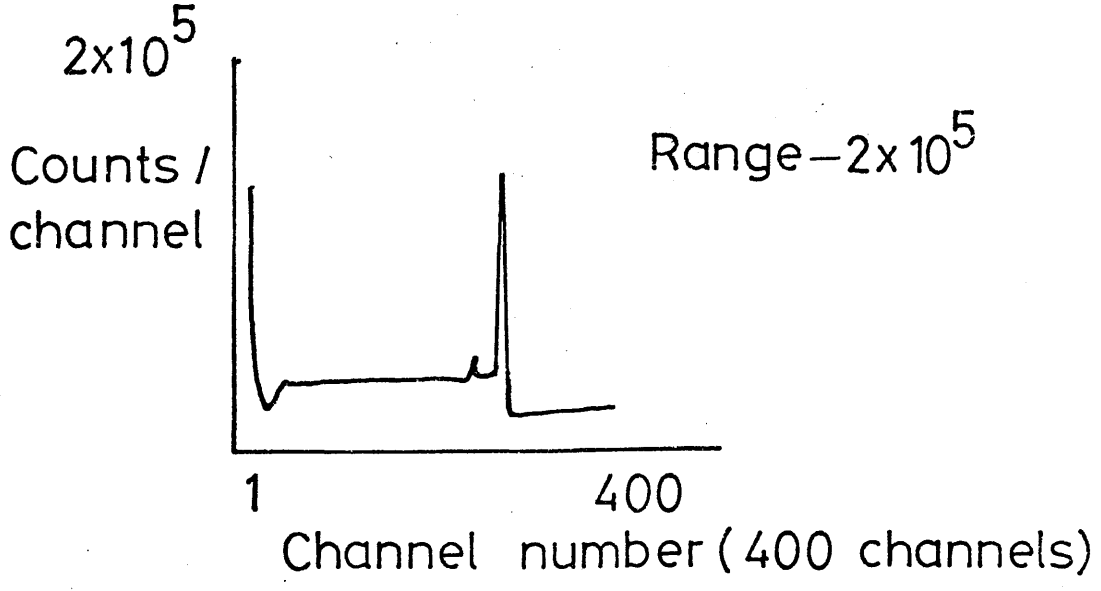

Peaks in channels 1, 33.
Peaks in channels 240, 271 due to saturation of the preamplifier.

figure 80.

Q gas Cooling curve ; Wire 3.
Q gas following oxygen heating and nitrogen flush.
V= 2 kV
I= 3·15 amp

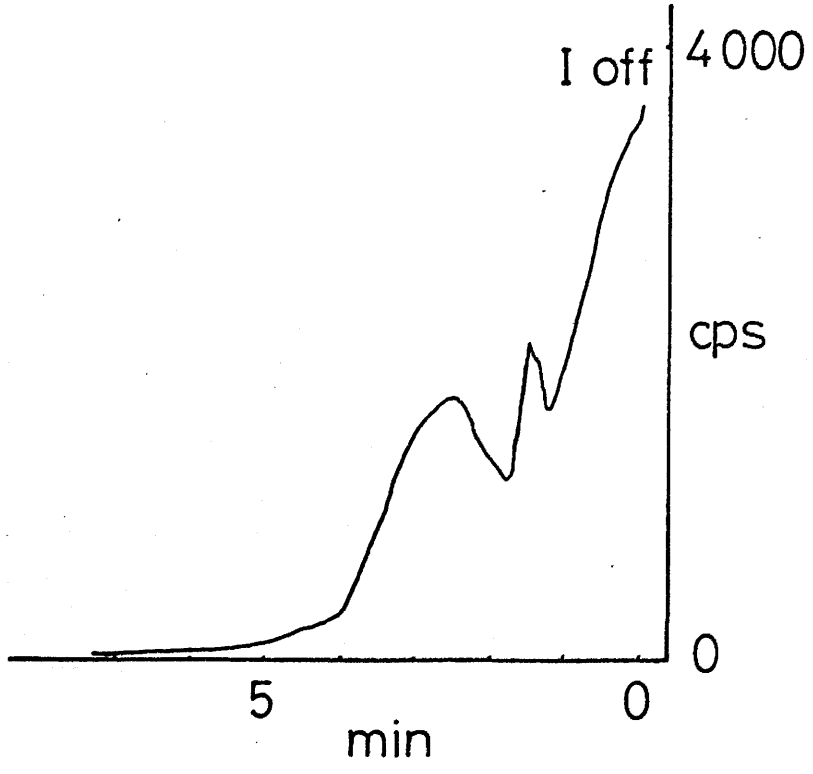

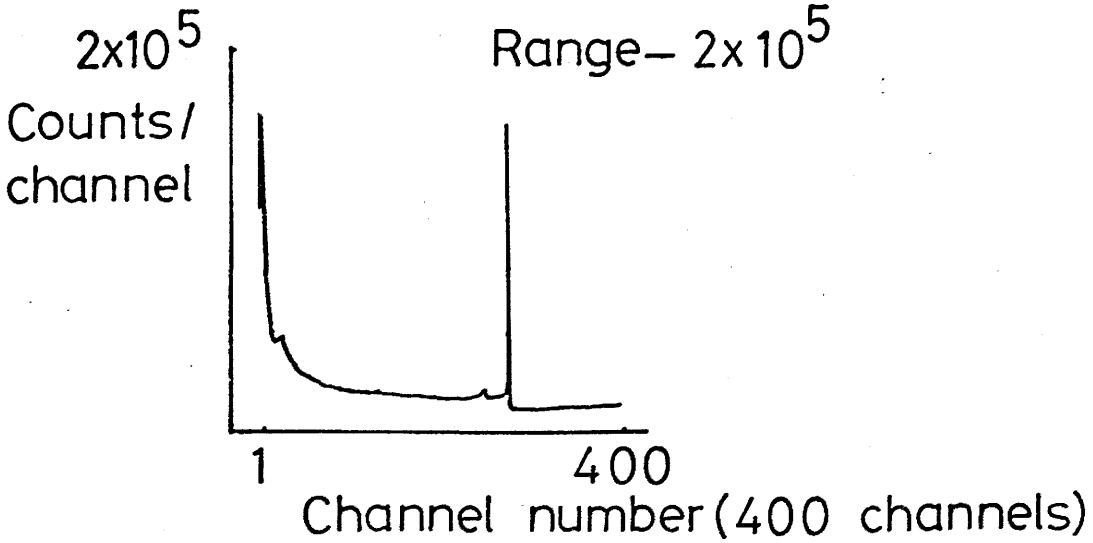

Peaks in channels 2, 20, 240, 273.
Peaks at 240, 273 due to saturation of the preamplifier.

figure 81.

Q gas Cooling curve; Wire 3.
Q gas after nitrogen heating
V = 2 kV
I = 3·15 amp

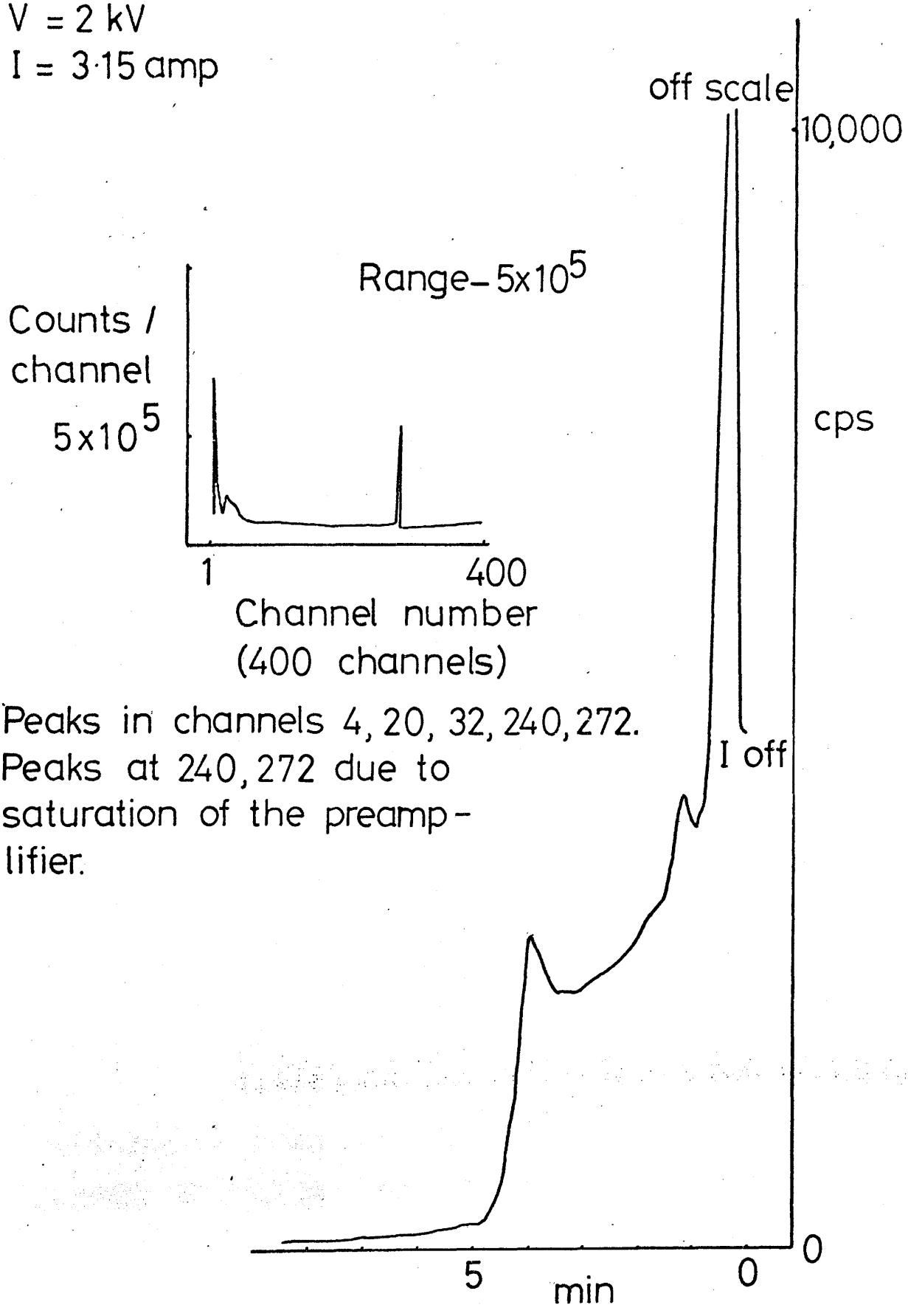

Peaks in channels 4, 20, 32, 240, 272.
Peaks at 240, 272 due to saturation of the preamplifier.

figure 82.

Q gas Cooling curve; Wire 3.
Q gas after hydrogen heating.
V= 2kV
I=3·2 amp

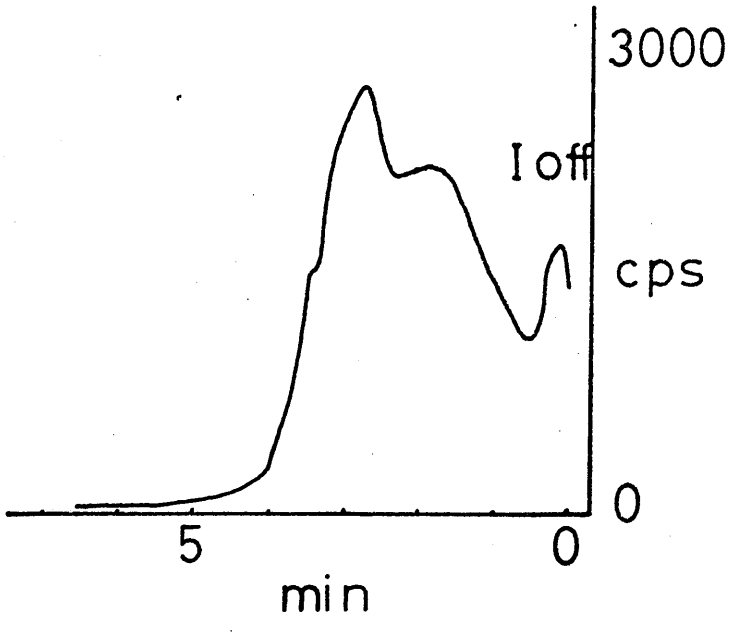

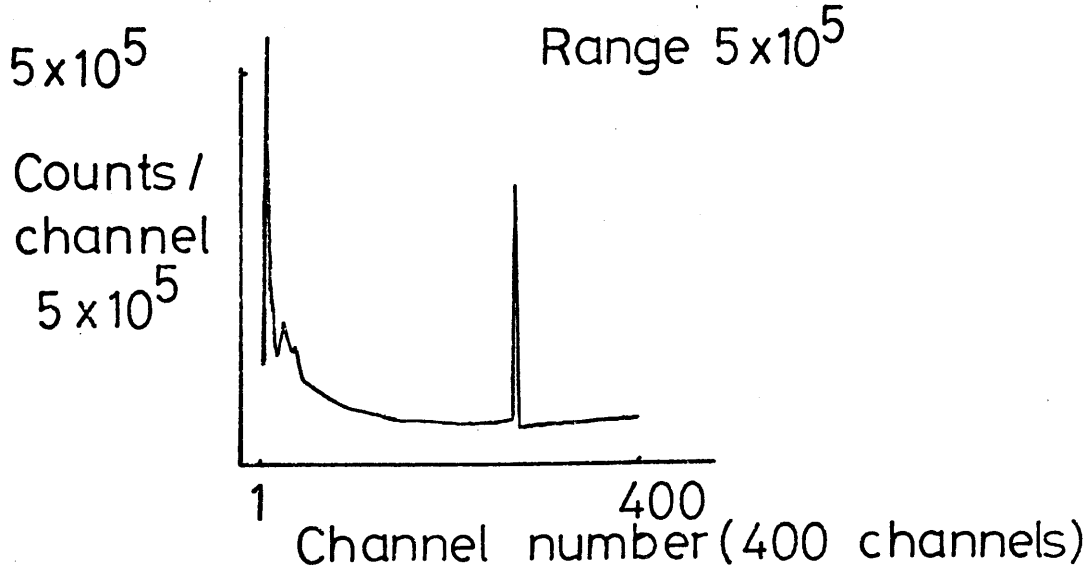

Peaks in channels 2, 18, 31, 272.
Peak at 272 due to saturation of the preamplifier.

figure 83.

Q gas Cooling curve ; Wire 3
Q gas following argon heating.
V = 2kV
I = 3·15amp

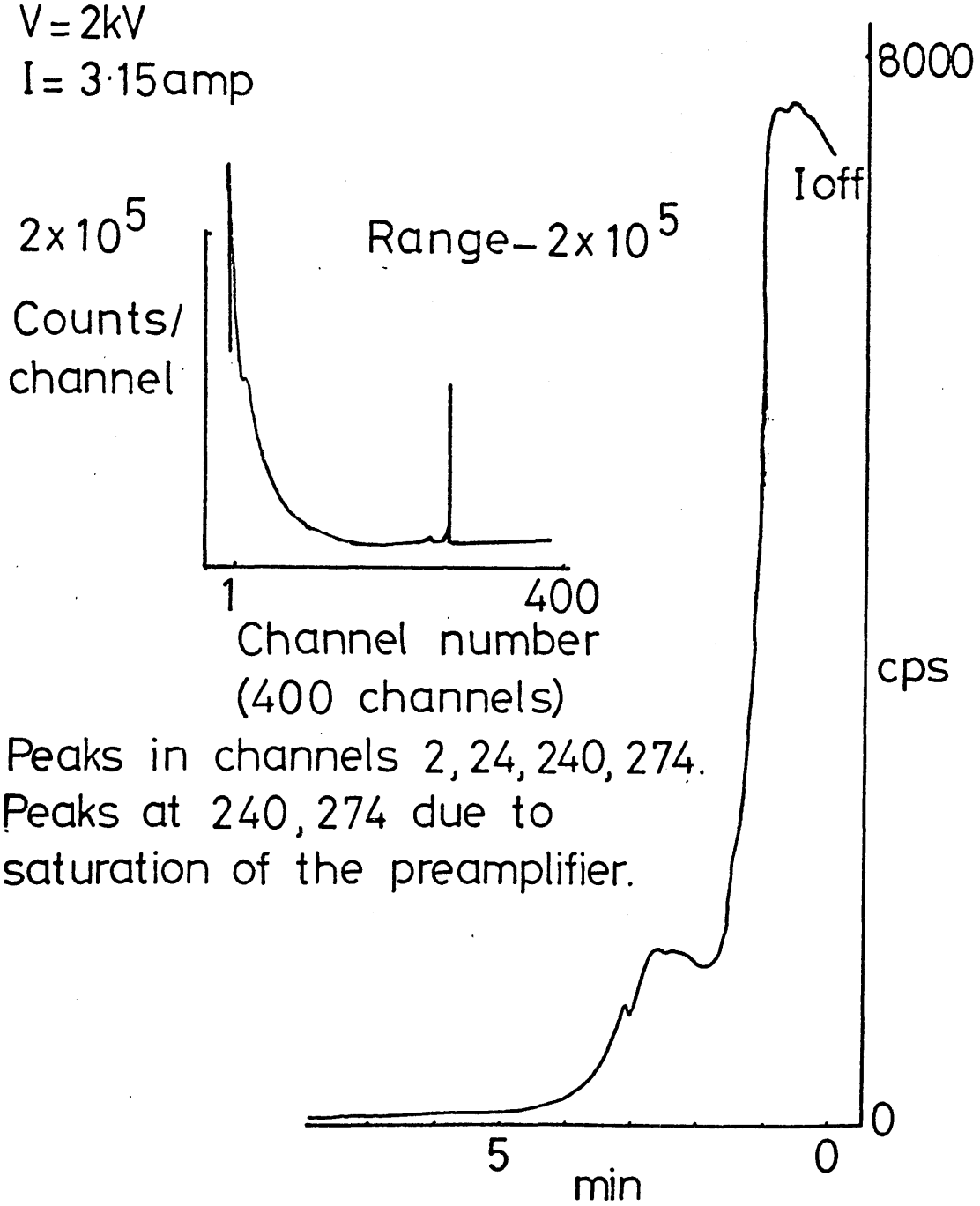

Peaks in channels 2, 24, 240, 274.
Peaks at 240, 274 due to saturation of the preamplifier.

Q gas cooling after helium heating similar.
Laben spectrum also similar.
Peaks in channels 3(off scale) 18, 240, 273.
Peaks at 240, 273 due to saturation of the preamplifier.

Appendix 12b

Wire 1

Cooling curves

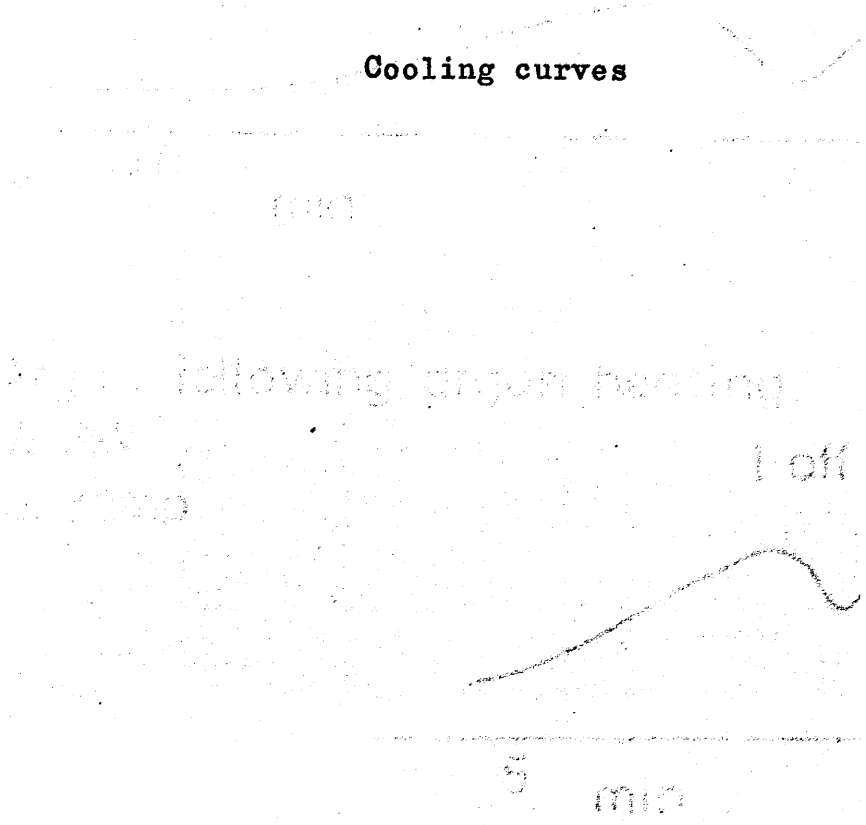

figure 84.

Argon Cooling curves; Wire 1.
Argon following hydrogen heating.
V = 2 kV
I = 3amp

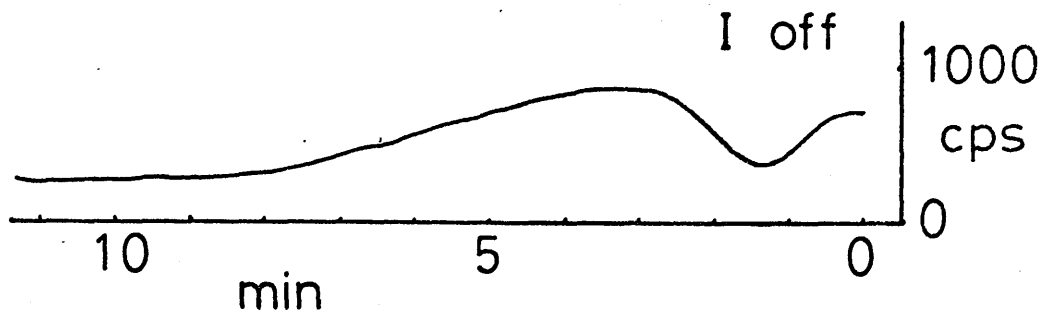

Argon following argon heating.
V = 2kV
I = 3amp

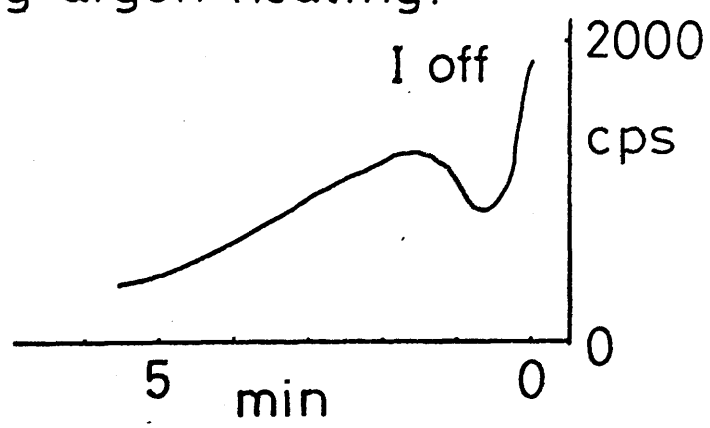

figure 85.

Q gas Cooling curves; Wire 1.
Q gas following Q gas heating.
V=2kV
I=3amp

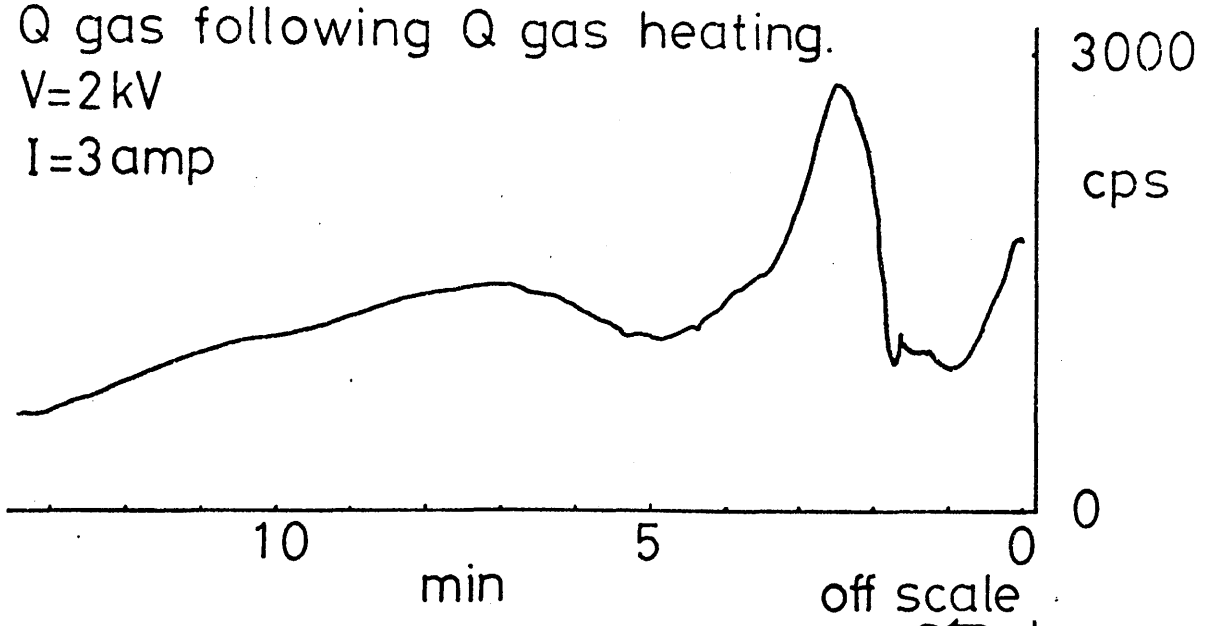

Q gas following oxygen heating.
V=2kV
I=3amp

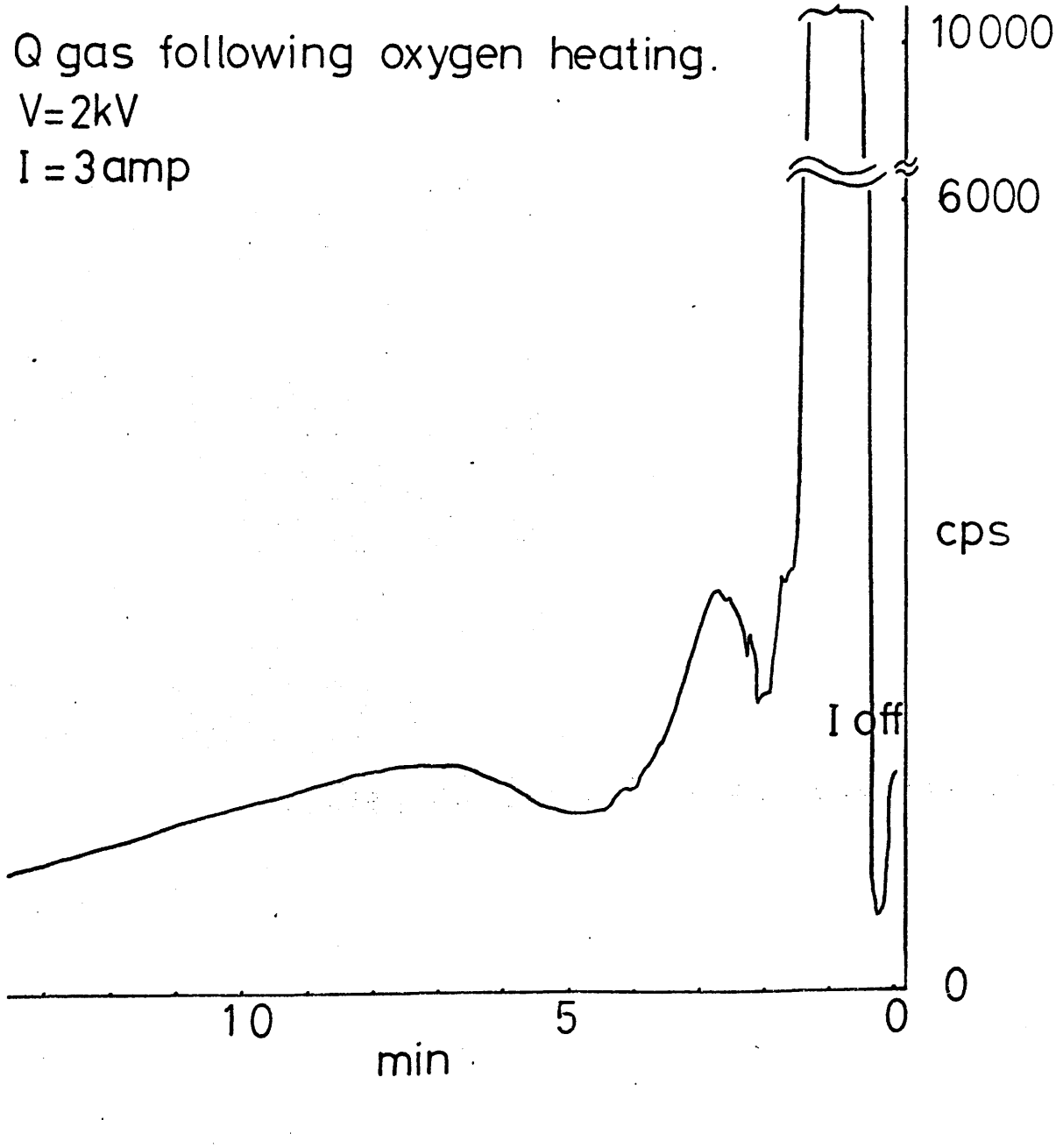

figure 86.

Hydrogen Cooling curve ; Wire 1.
Hydrogen following nitrogen heating.
V= 2 kV
I= 3·8 amp

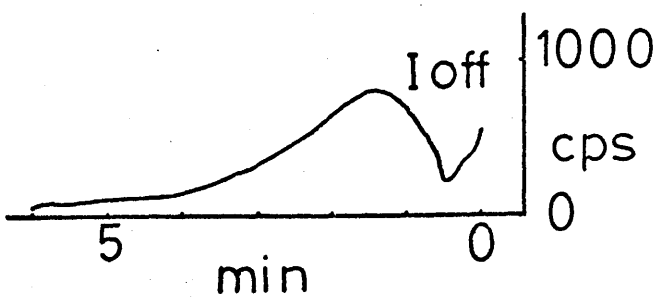

figure 87.

Oxygen Cooling curves; Wire 1.
Oxygen following nitrogen heating.
V=2kV
I=3amp

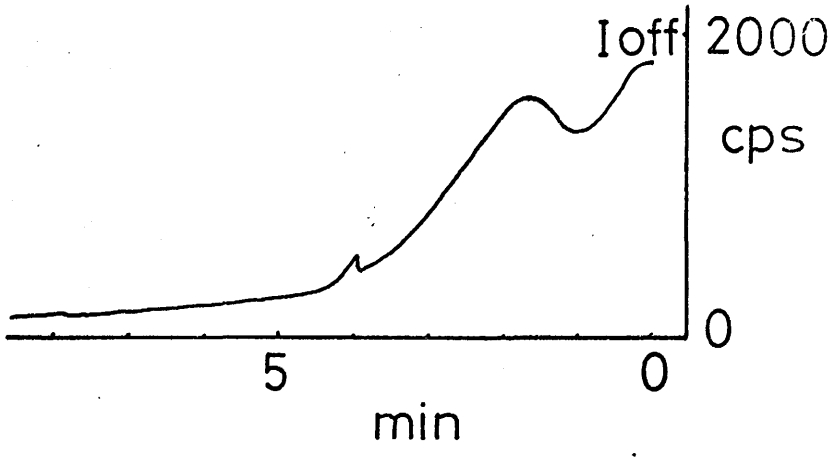

Oxygen cooling following oxygen heating following Q gas cooling.
V=2kV
I=3amp

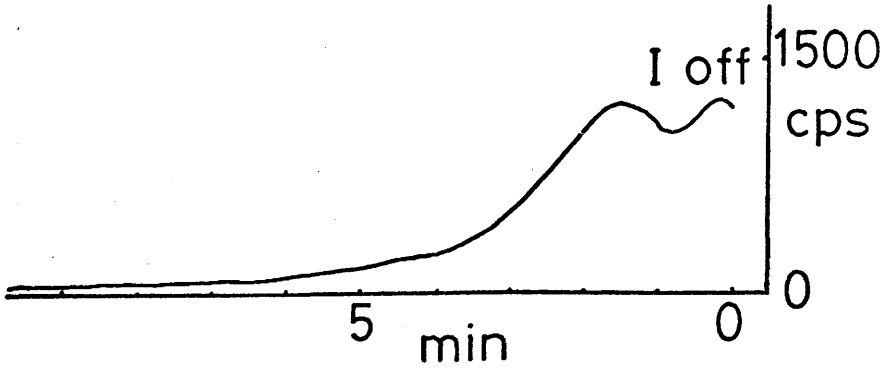

figure 88.

Nitrogen Cooling curves; Wire 1.
Nitrogen following hydrogen heating.
V= 2 kV
I = 3amp

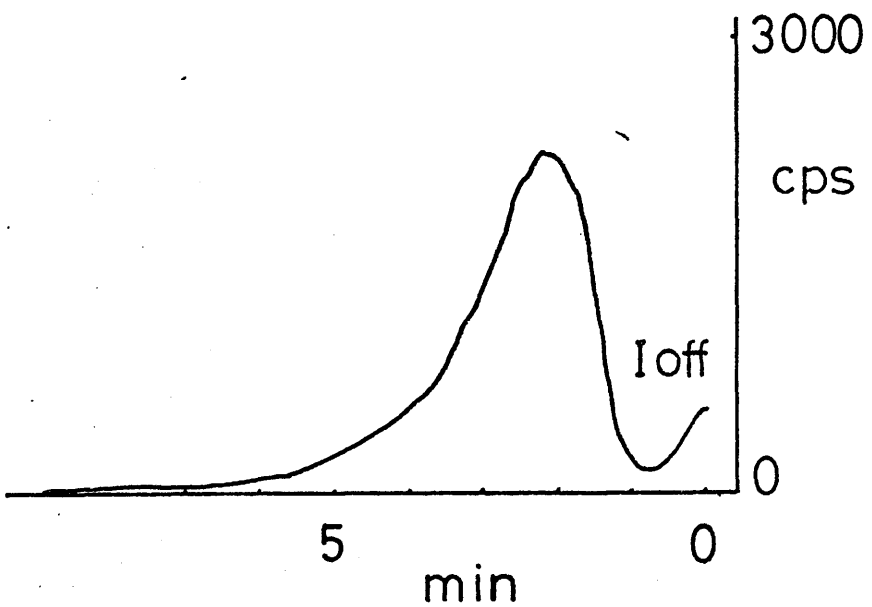

Nitrogen following oxygen heating.
V=2kV
I= 3 amp

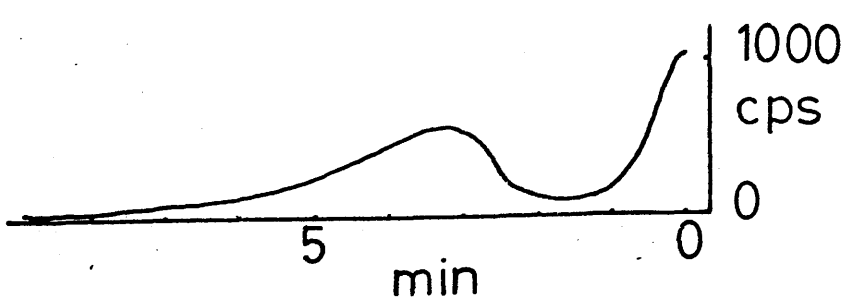

Appendix 13

Discriminator 0·1 x 0·2, 2% window throughout

Gas flow rates 4ml/sec.

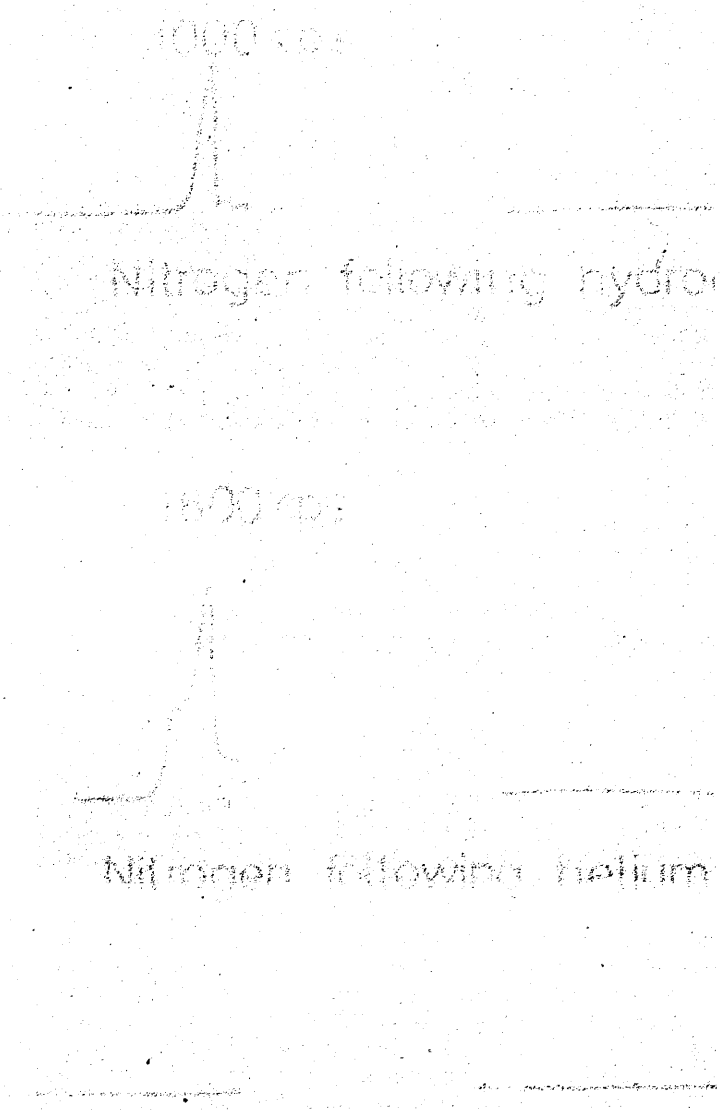

figure 89.

Nitrogen Introduction curves at room temperature.

No platinum

Platinum present

Nitrogen following oxygen

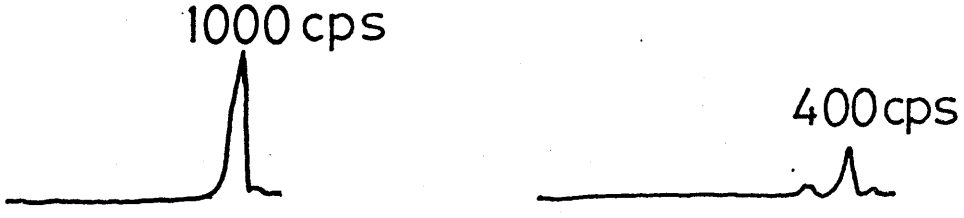

Nitrogen following hydrogen

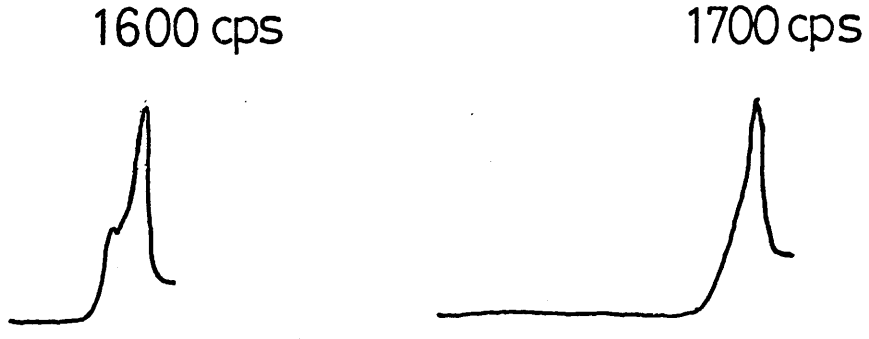

Nitrogen following helium

Nitrogen introduced at time t=0

figure 90.

Hydrogen Introduction curves at room temperature.

Platinum present

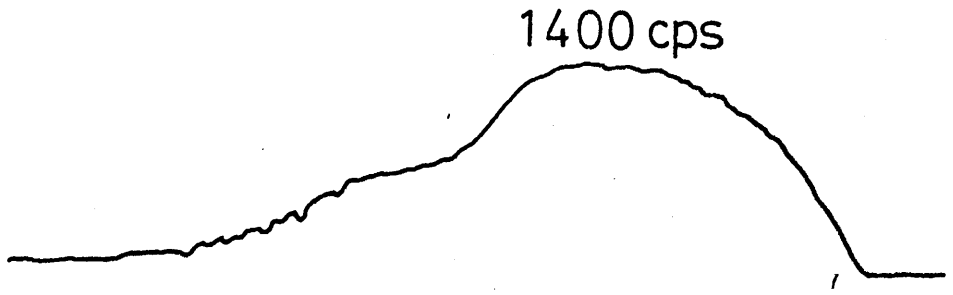

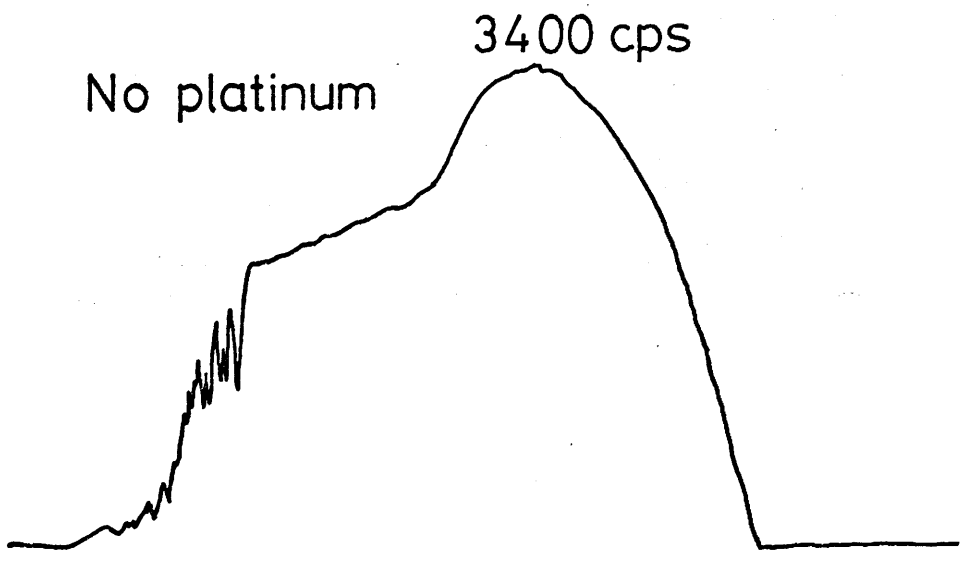

Hydrogen following nitrogen

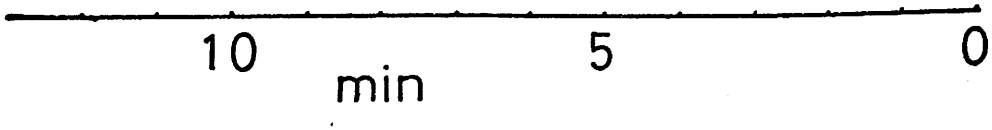

Hydrogen introduced at time t=0

Hydrogen Introduction curves at room temperature continued

No platinum

Platinum present

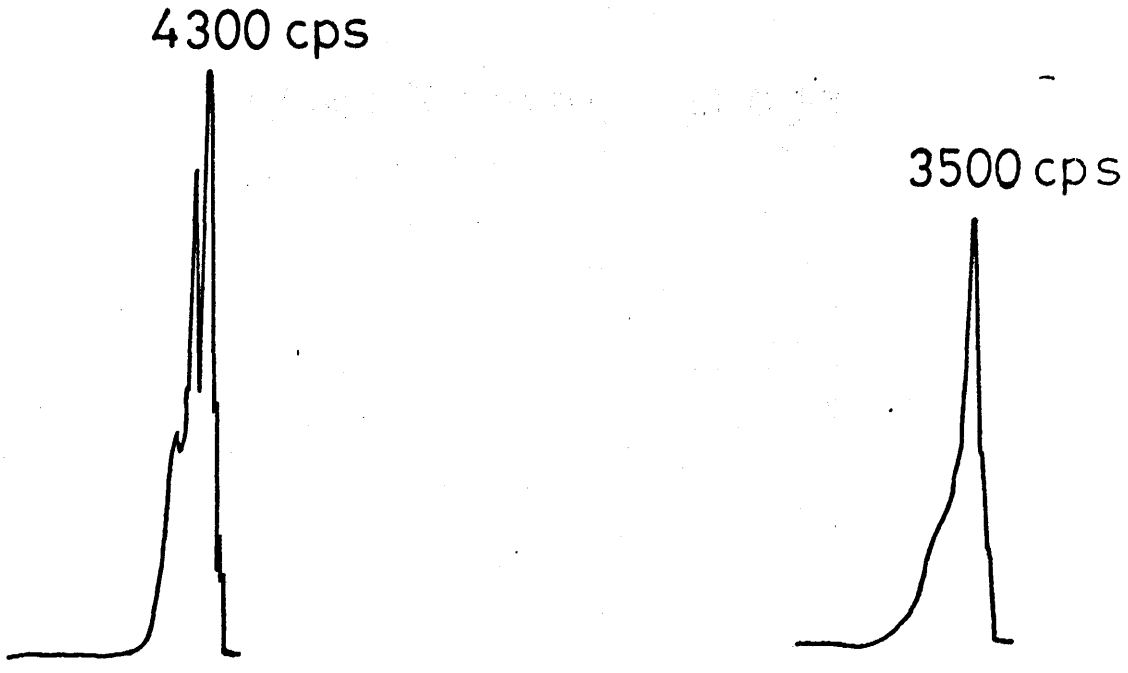

Hydrogen following helium

Hydrogen introduced at time t=0

figure 91.

Oxygen Introduction curves at room temperature.

No platinum Platinum present

Oxygen following nitrogen

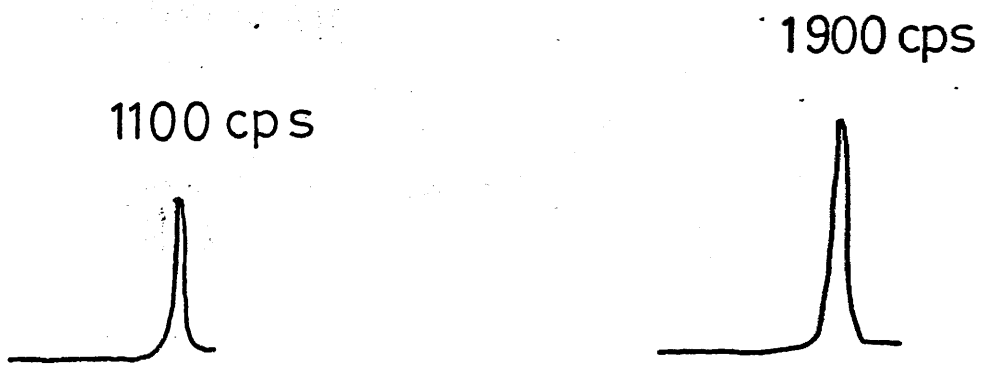

Oxygen following helium

Oxygen introduced at time t=0

figure 92.

Helium Introduction curves at room temperature.

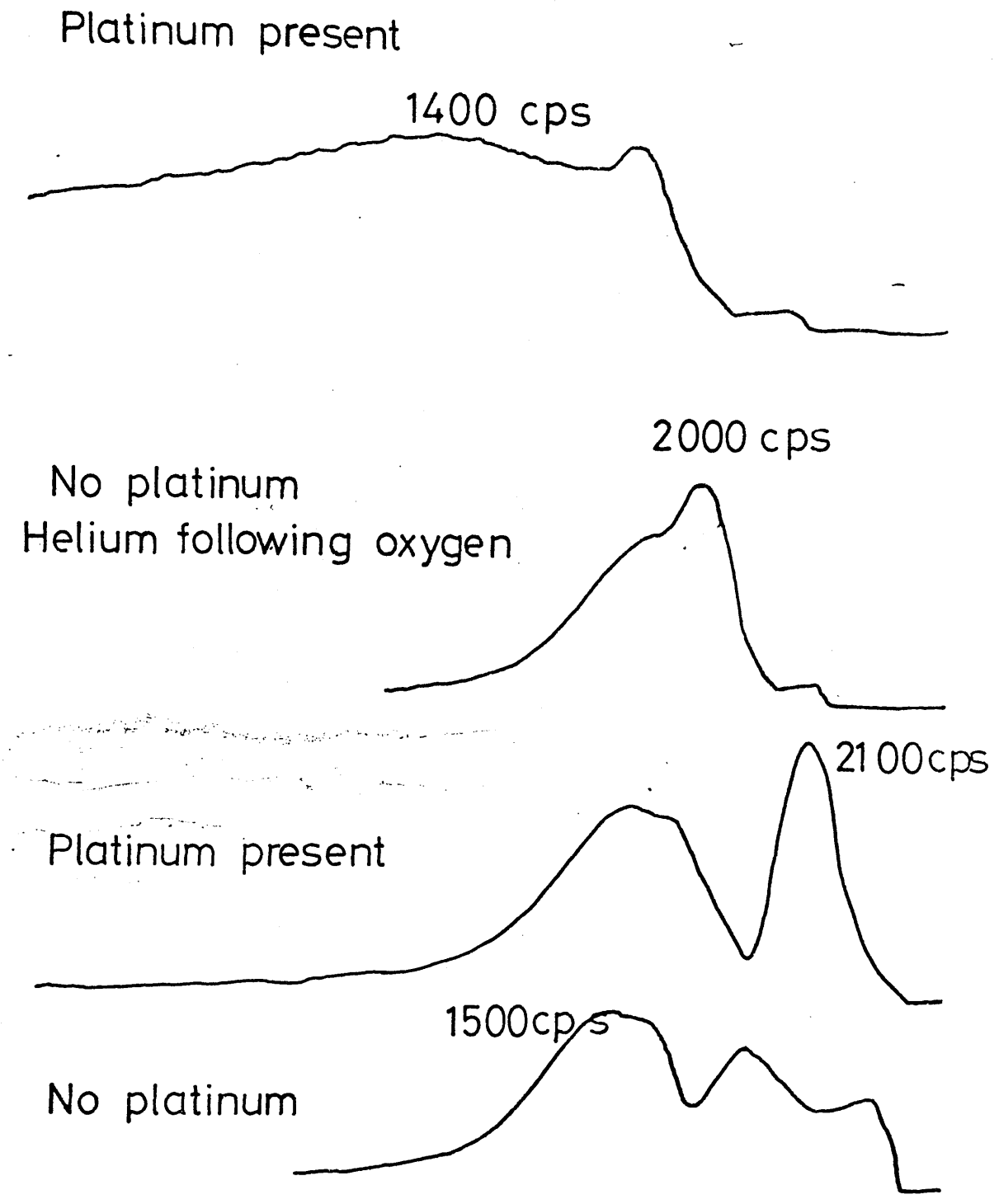

Helium introduction curves at room temperature continued

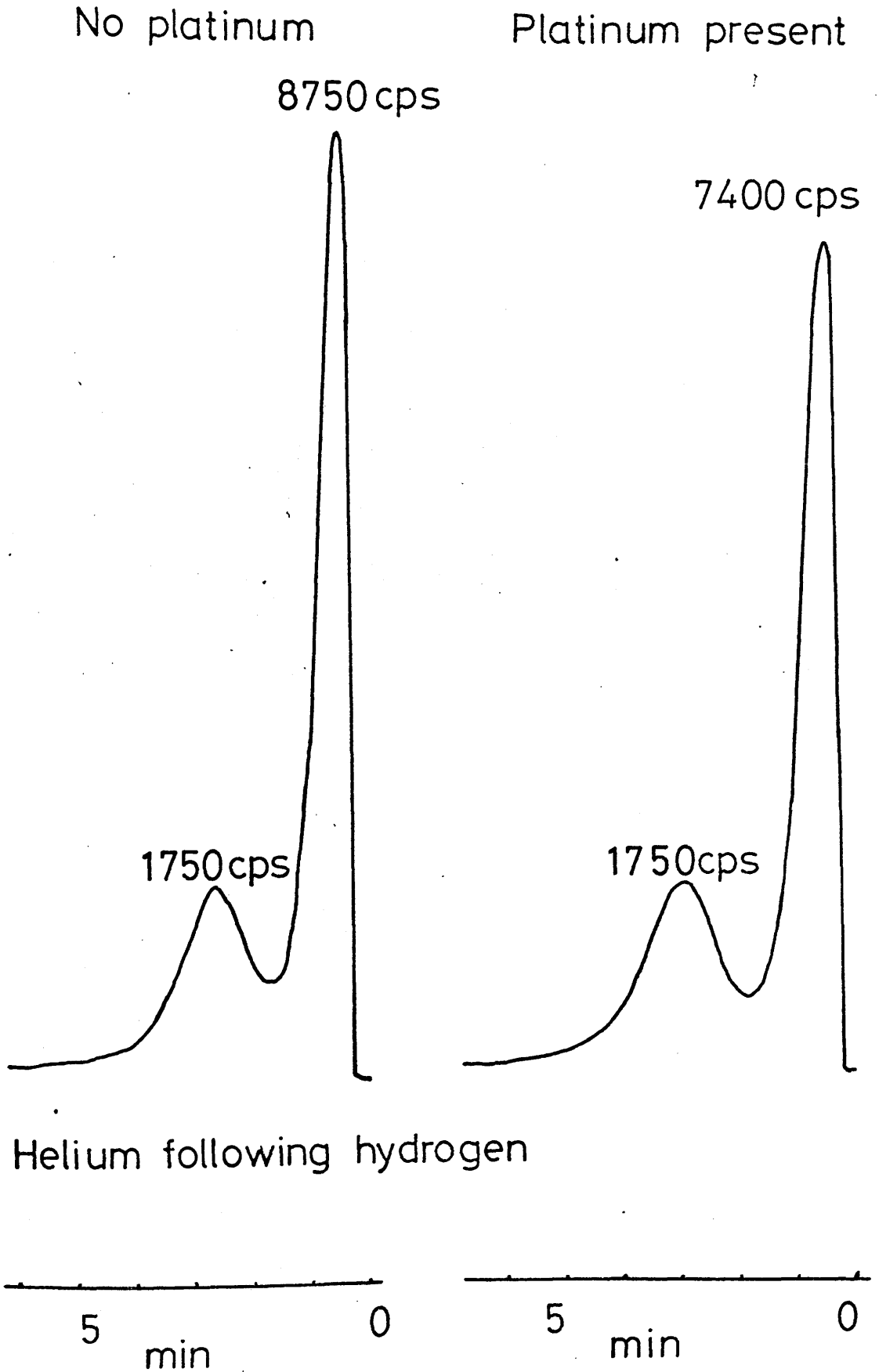

Helium introduced at time t=0. Flow rate 5ml/sec.

Appendix 14

Appendix 14a

Gold

Cooling curves

~1m of 0·16 mm diam gold wire used each time

Wire supplied by Johnson Matthey.

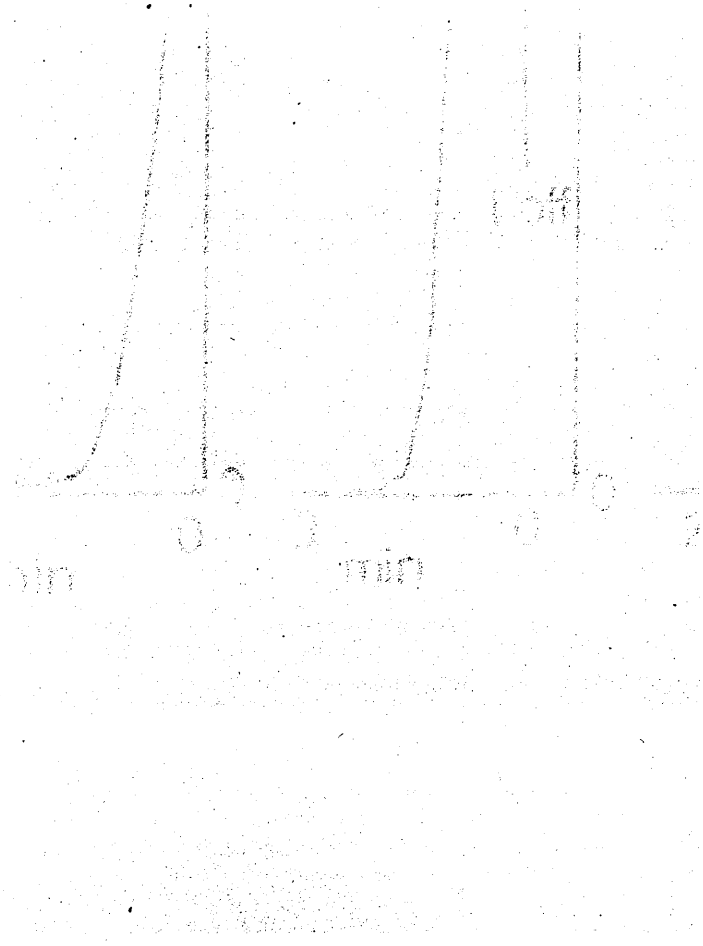

figure 93.

Q gas Cooling curves.
Single thickness of gold wire.

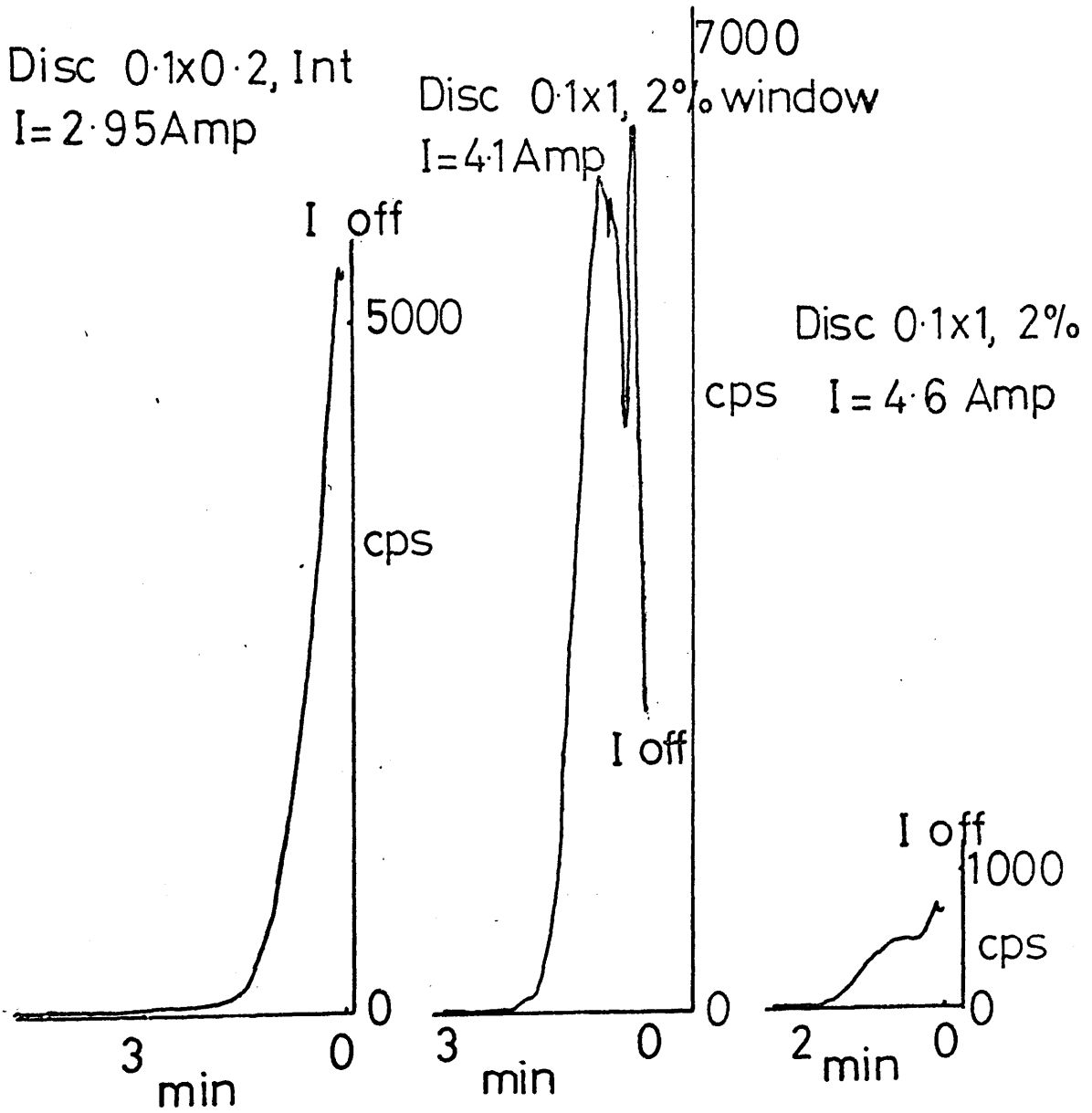

Q gas Cooling curves continued

Double thickness of gold wire

Discriminator 0·1x 1, Integrate

I= 5·3 Amp

Typical Laben spectrum.

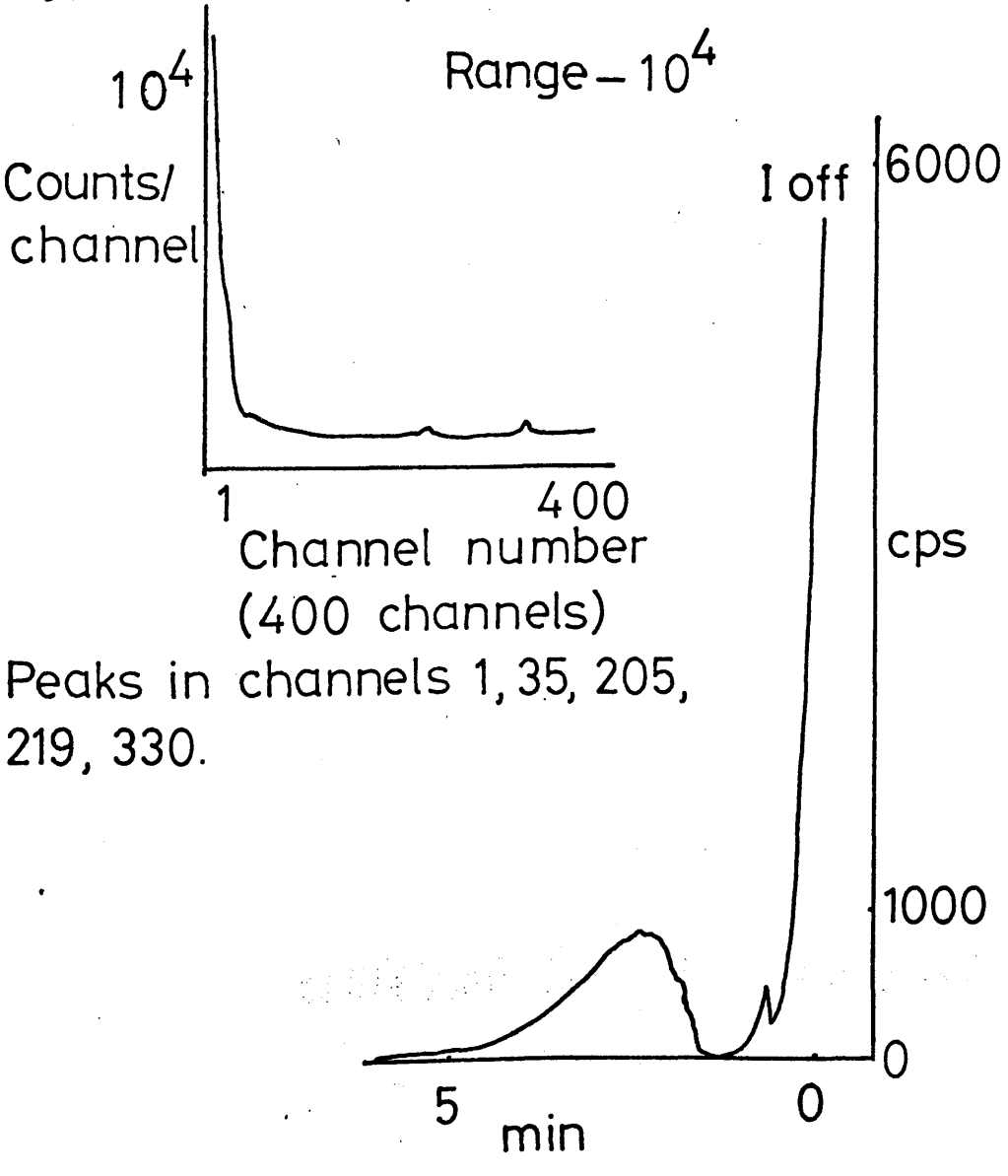

Peaks in channels 1, 35, 205, 219, 330.

figure 94.

Hydrogen Cooling curve

Double thickness of gold wire

Discriminator 0·1x0·2, 2% window.

I=6·05Amp

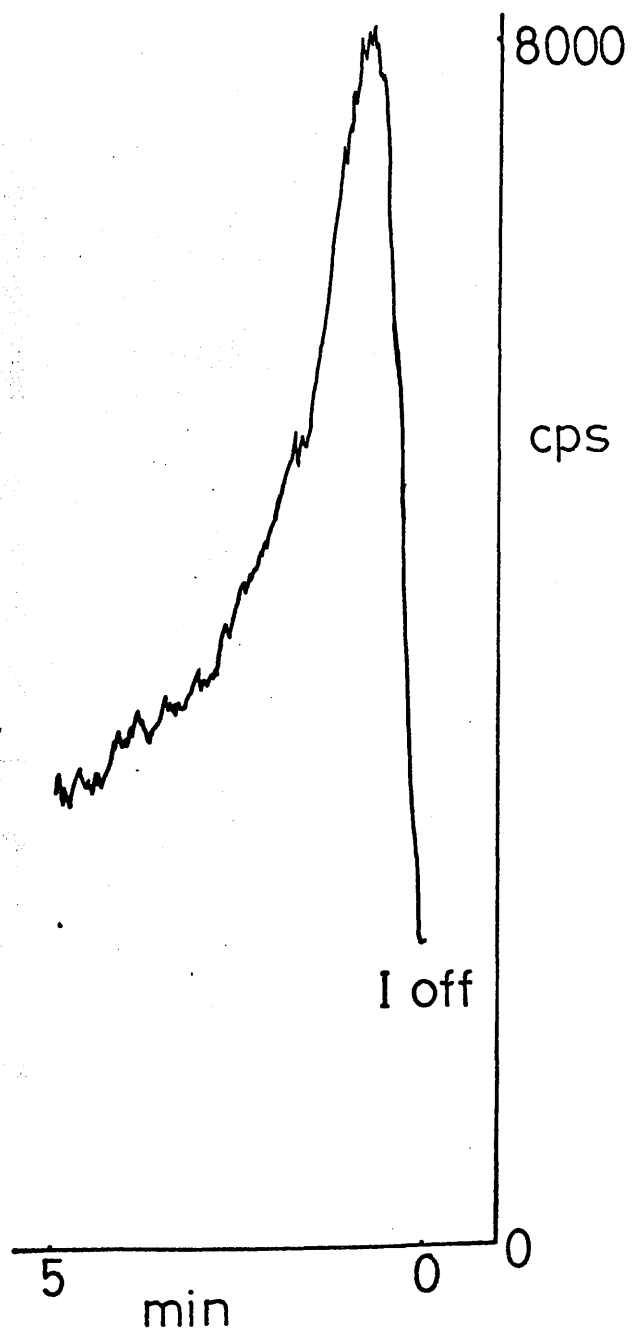

N.B.:- No emission was observed when the wire was allowed to cool in nitrogen.

figure 94 continued

Laben spectrum obtained when the double gold wire was allowed to cool in hydrogen after being heated in nitrogen.

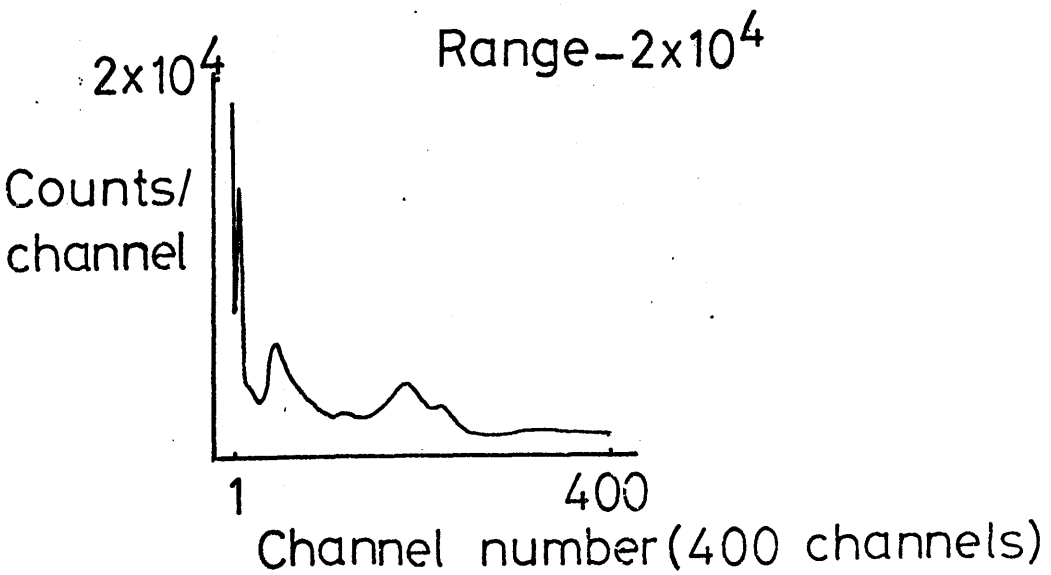

Peaks in channels 1, 4, 44, 117, 167, 217.

Appendix 14b

Gold

Introduction curves

figure 95.

Nitrogen Introduction curve.
Nitrogen following hydrogen.
Discriminator 0·1x1, 2% window
V= 1·9kV

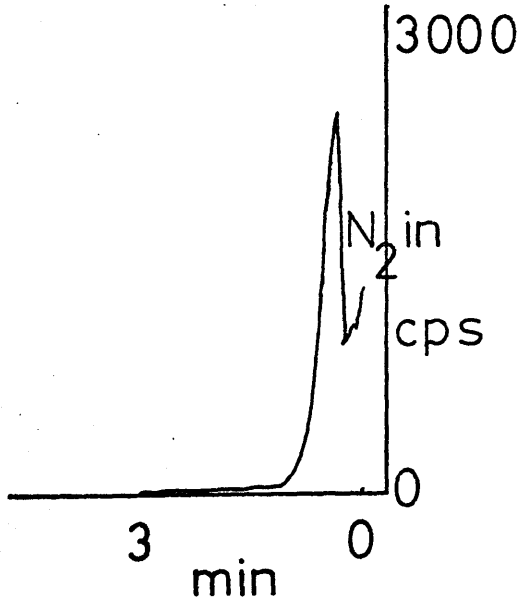

Hydrogen following nitrogen:- no emission.

Appendix 15

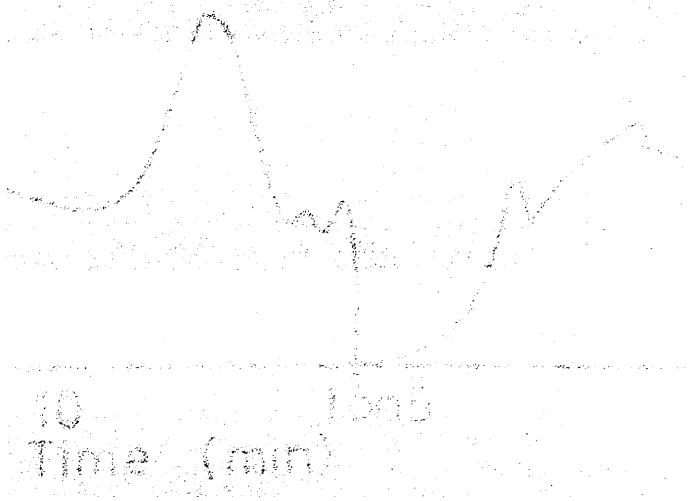

figure 96.

Q gas heating curve.

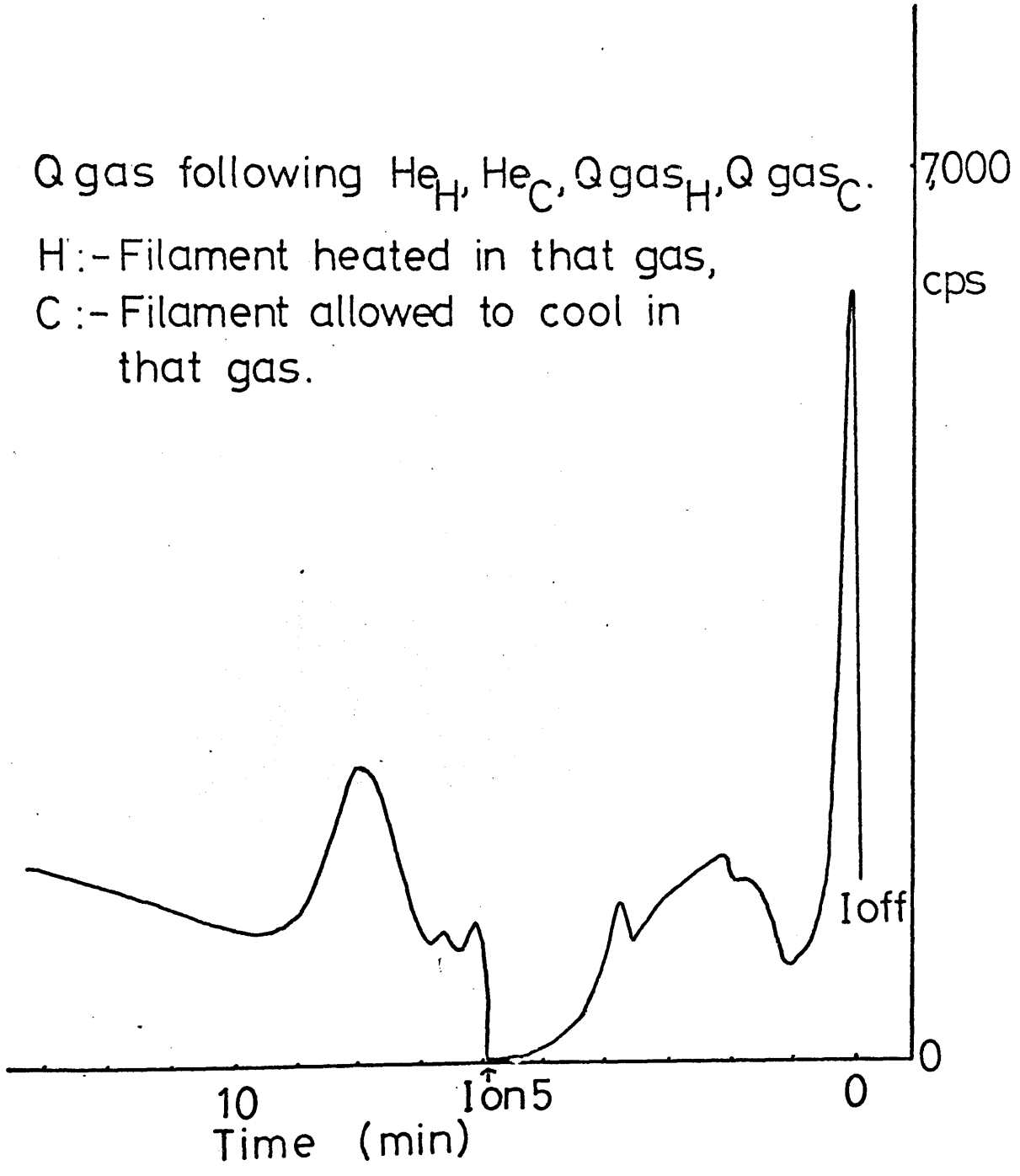

figure 97.

Q gas heating curve.

Q gas following hydrogen.

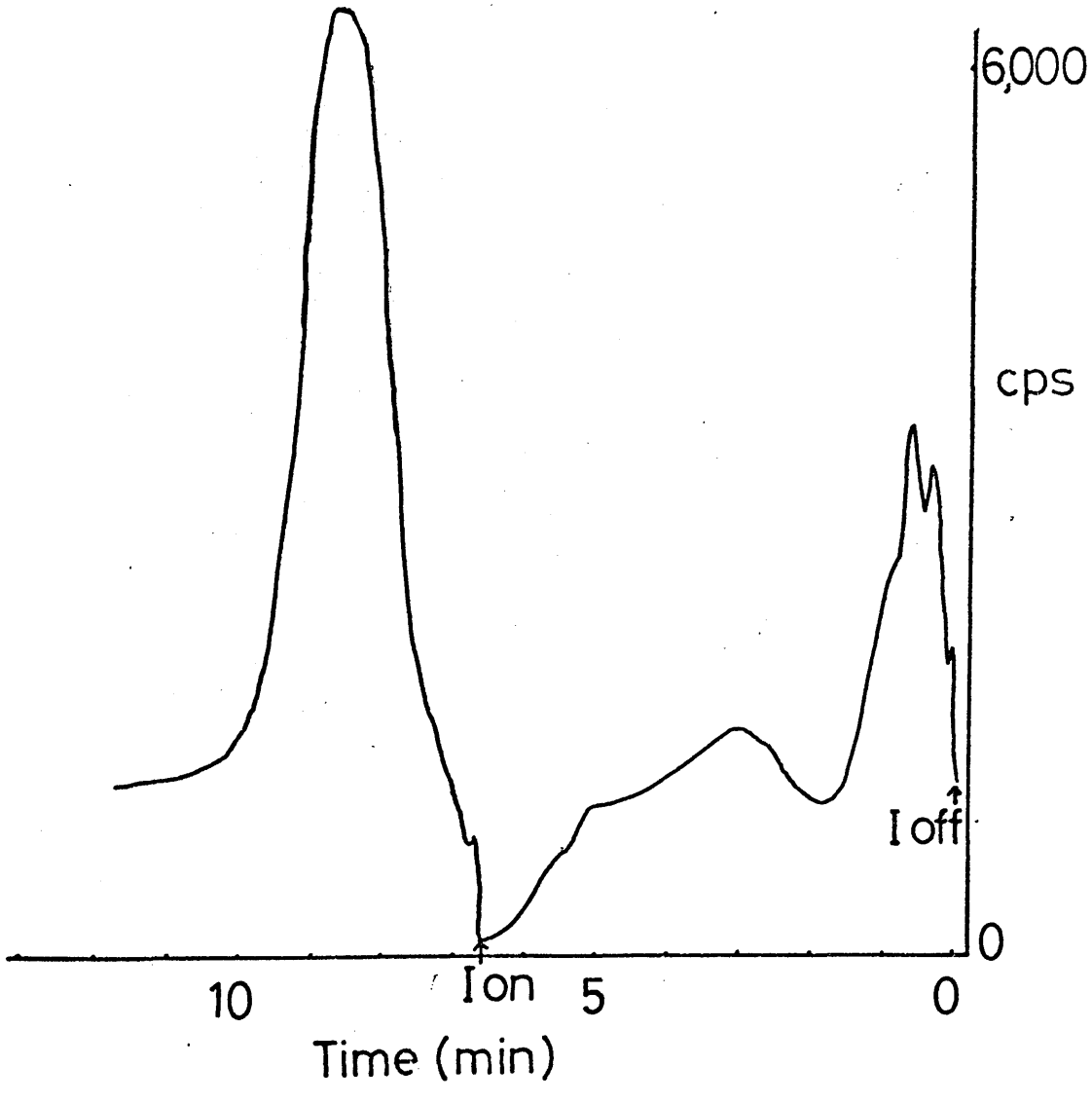

figure 98.

Q gas heating curve.

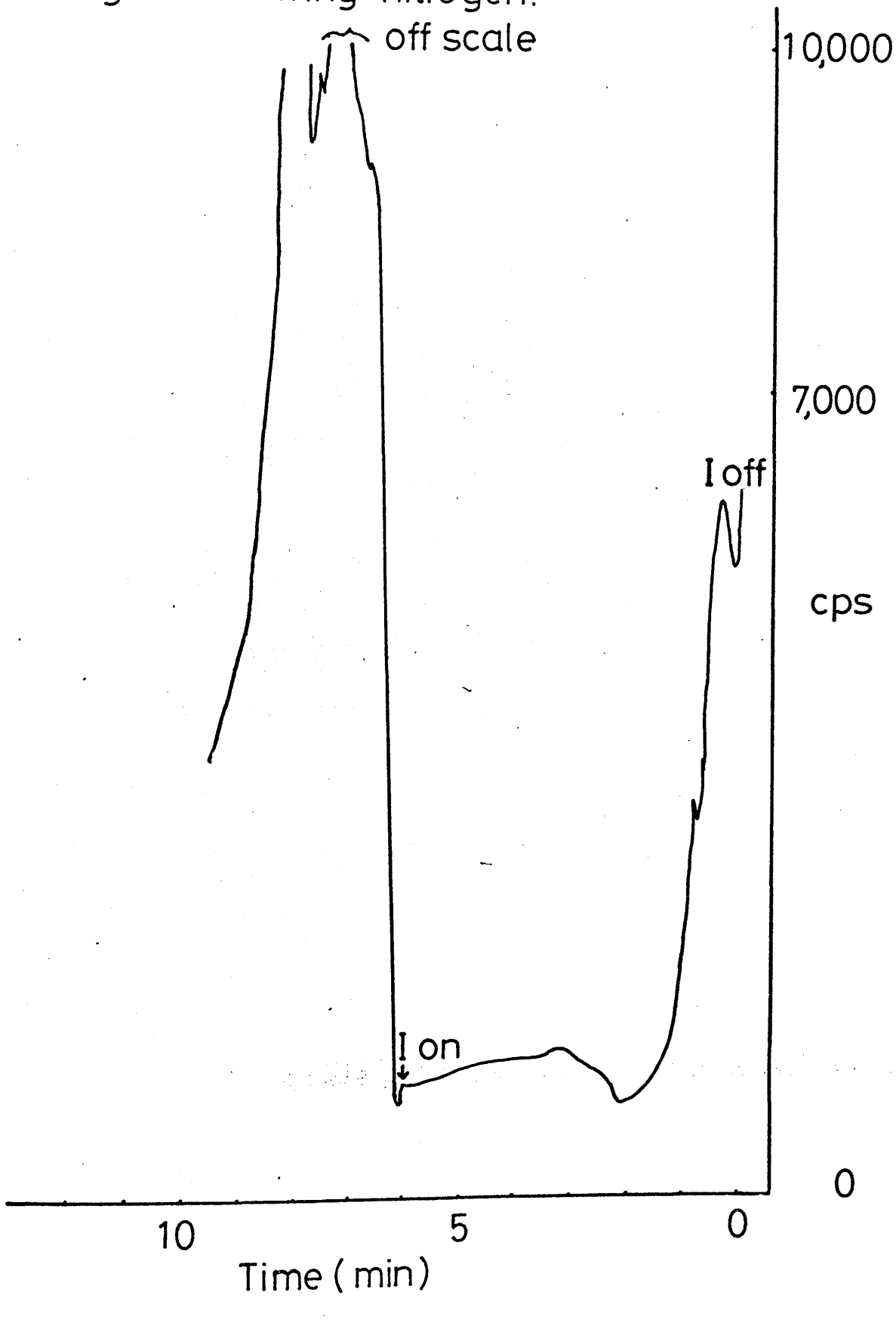

figure 99.

Nitrogen heating curve.

Nitrogen following Q gas.

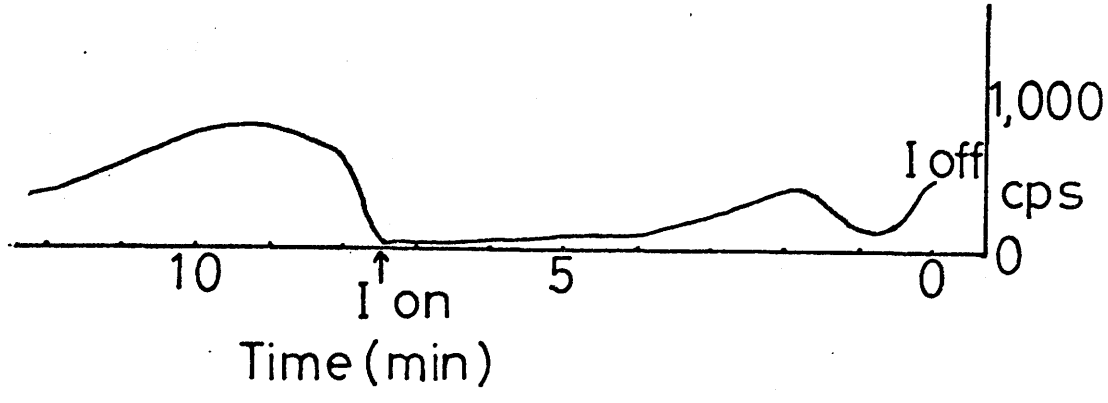

figure 100.

Hydrogen heating curve.

Hydrogen following Q gas.

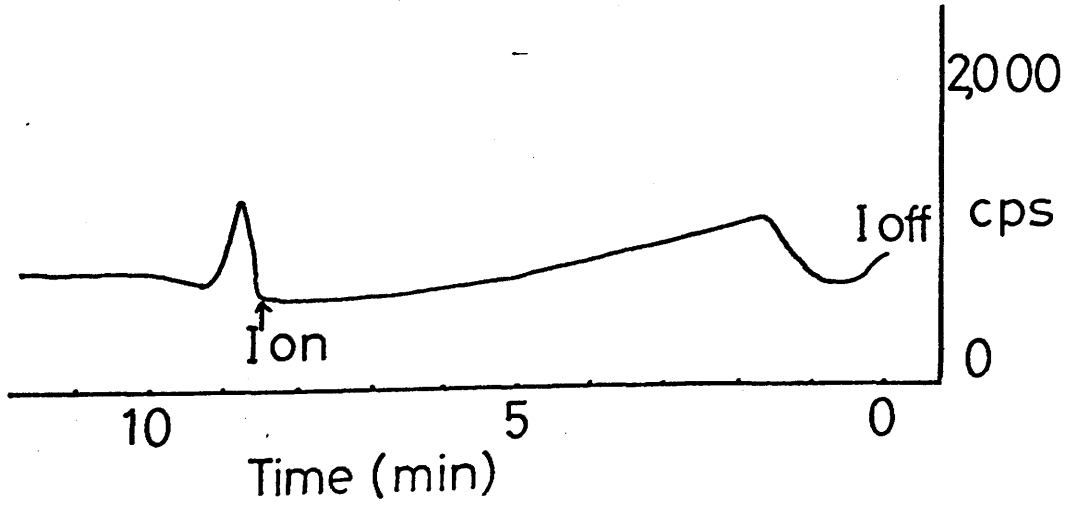

Appendix 16

Appendix 16a

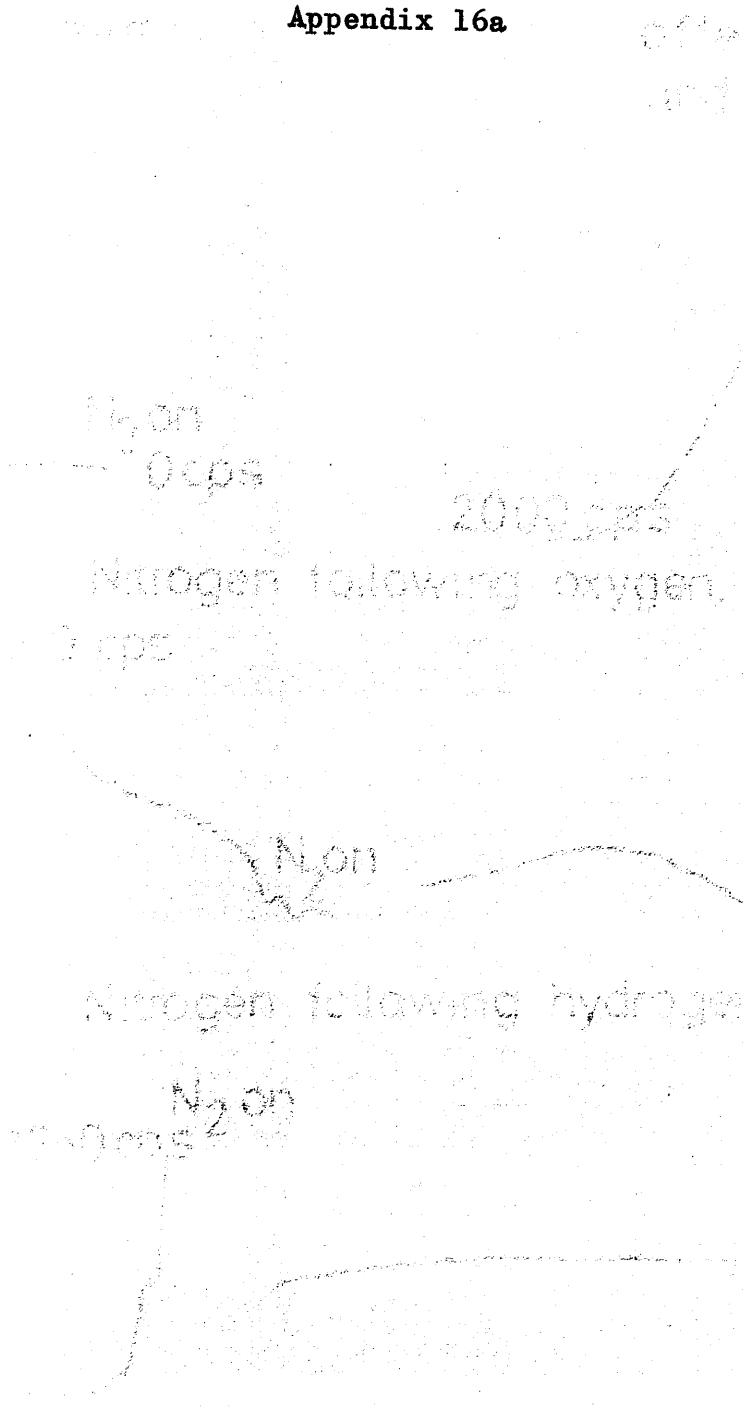

figure 101.

Nitrogen Introduction curves to show the effect of carbiding the platinum filament.

clean wire.

after O gas and air.

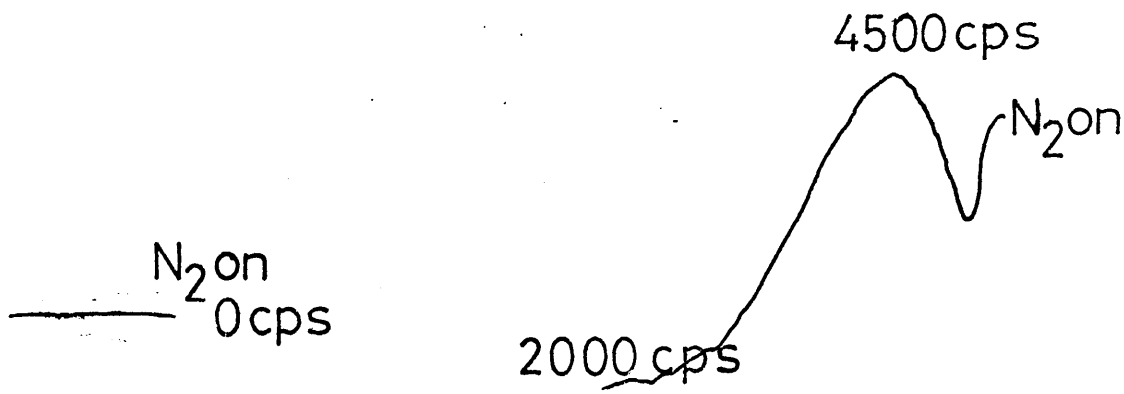

Nitrogen following oxygen.

Nitrogen following hydrogen.

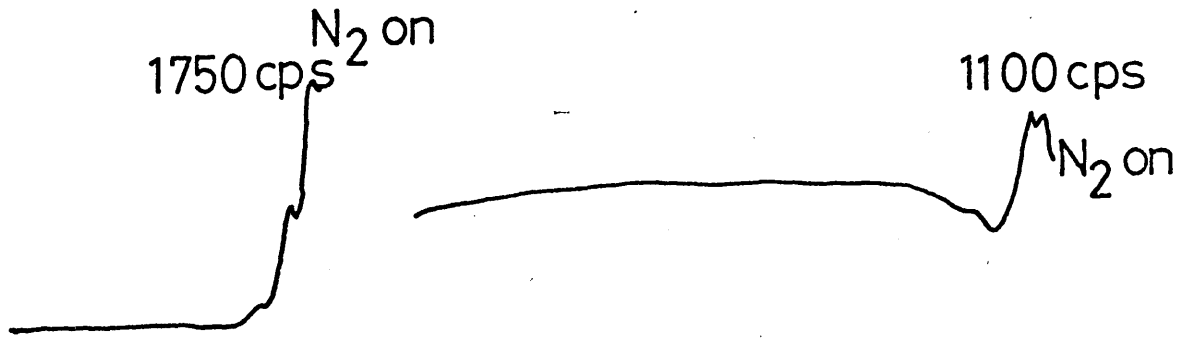

Nitrogen following helium.

Nitrogen Introduction curves continued

clean wire

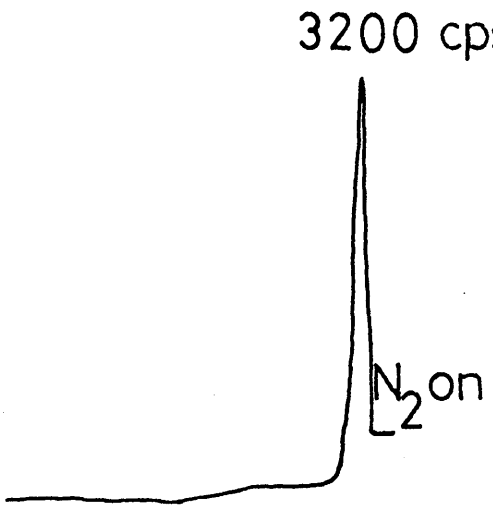

after Q gas and air

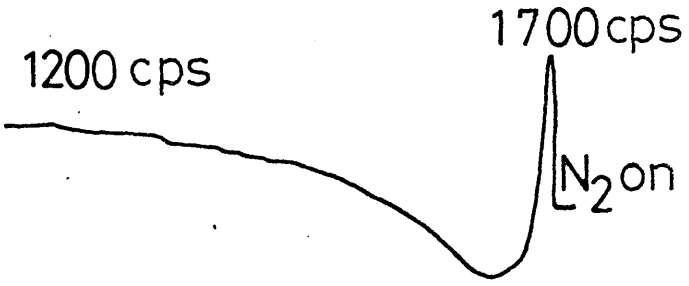

Nitrogen following argon

after Q gas

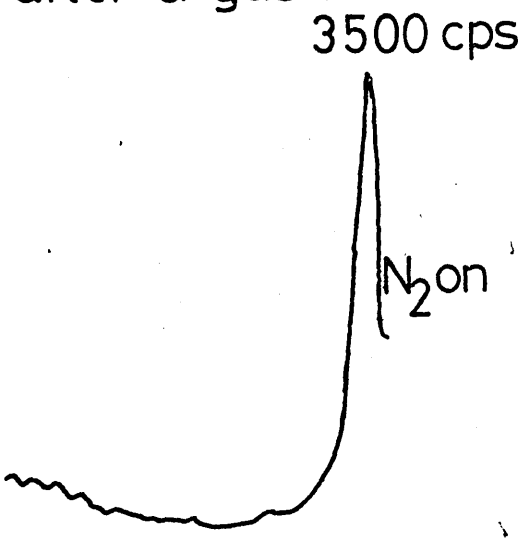

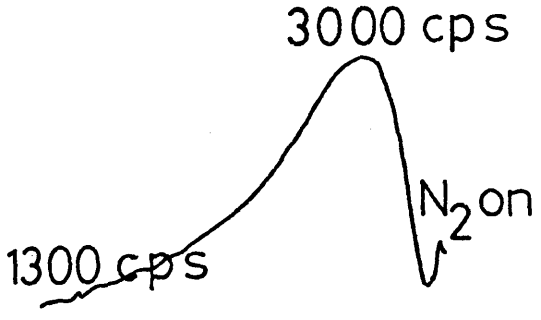

Nitrogen following Q gas

figure 102.

Oxygen Introduction curves to show the effect of carbiding the platinum filament.

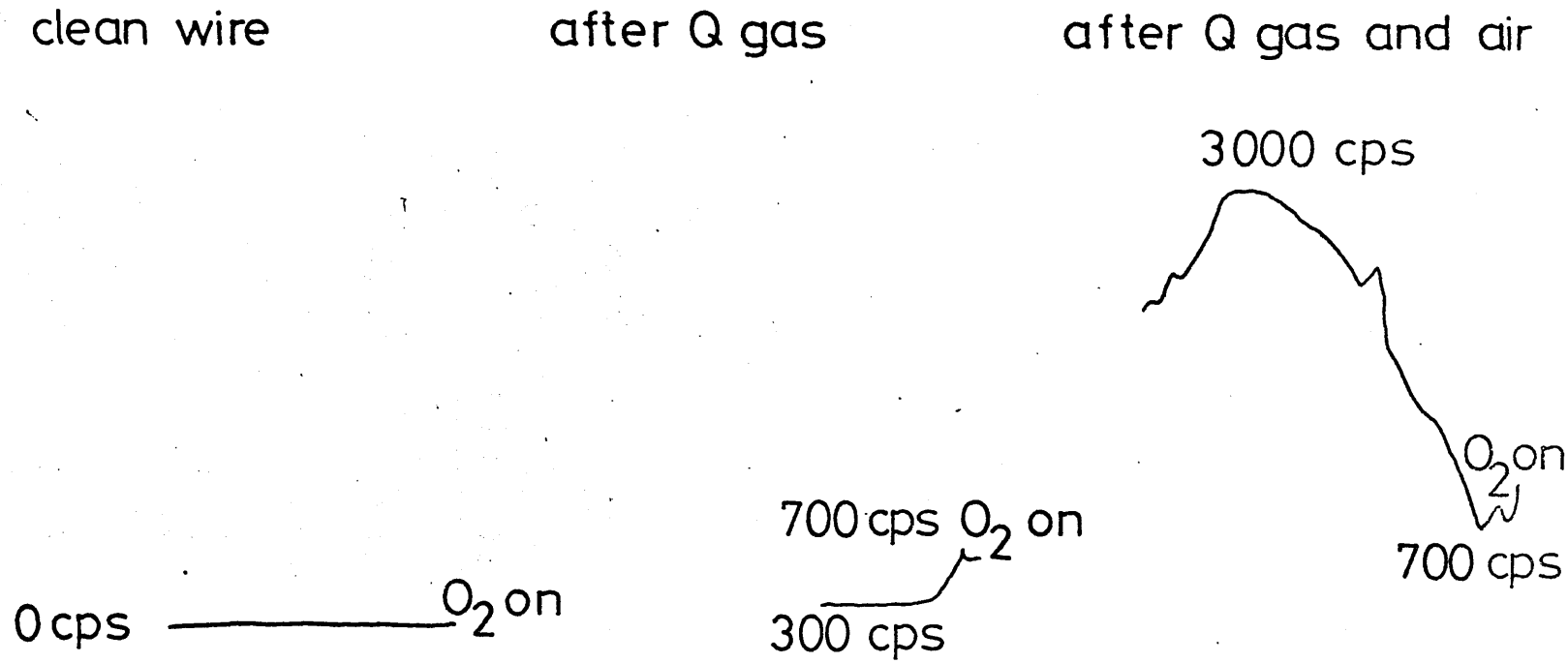

figure 103.

Hydrogen Introduction curves to show the effect of carbiding the platinum filament.

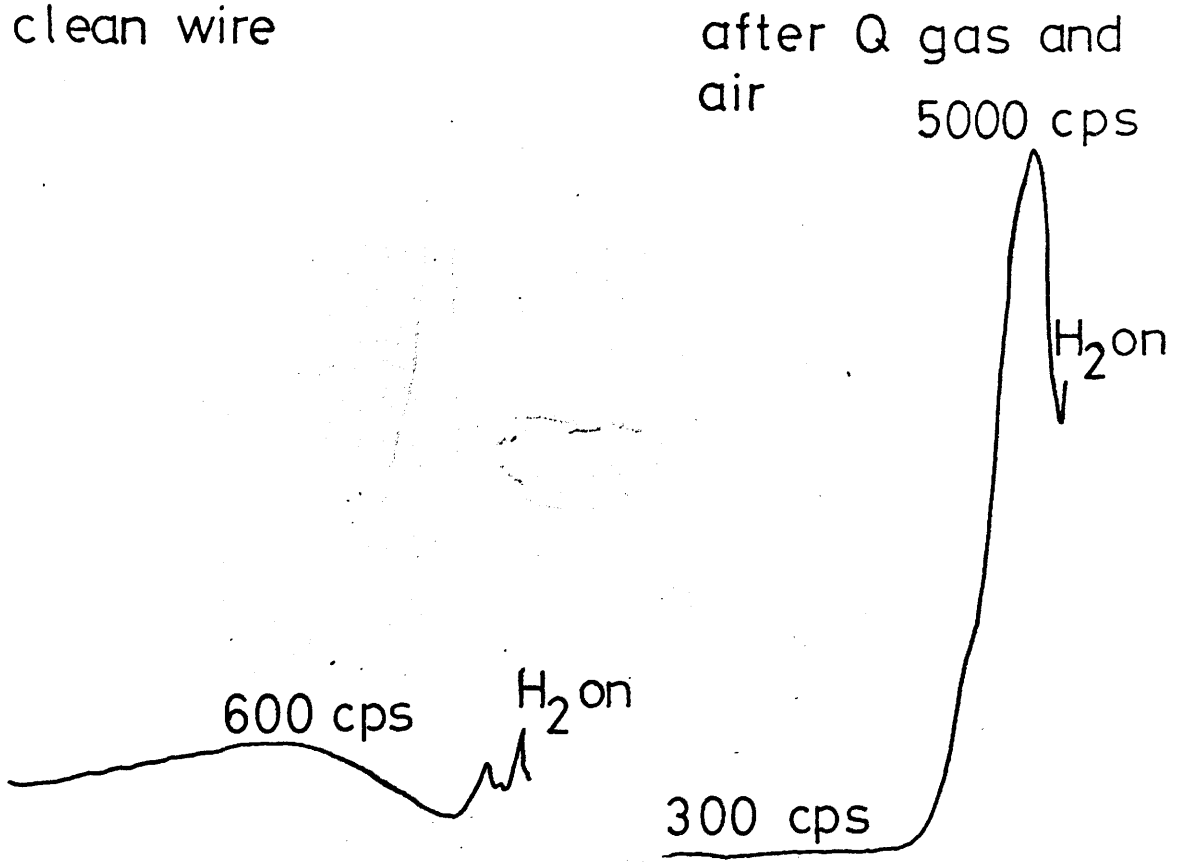

Hydrogen following nitrogen

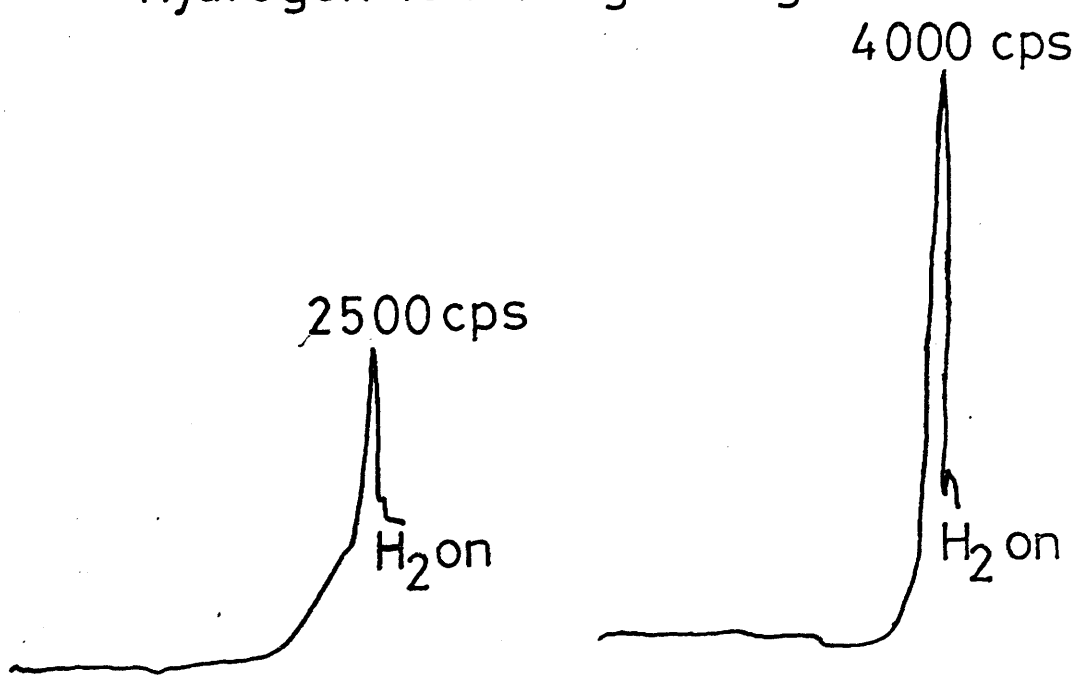

Hydrogen following helium
(following nitrogen)

Hydrogen Introduction curves continued

clean wire

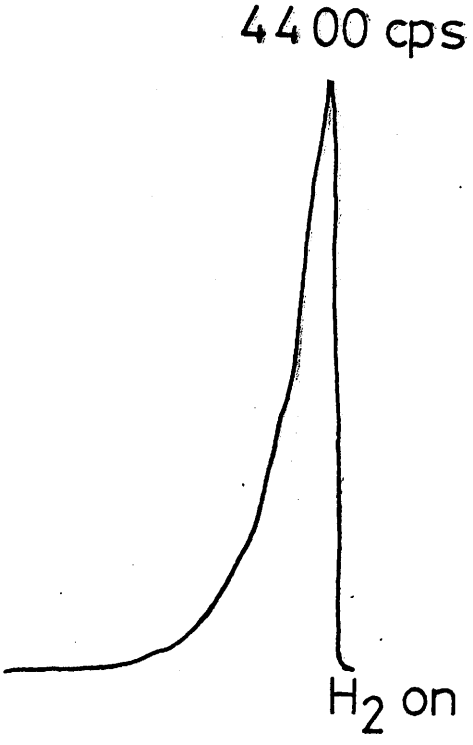

after Q gas and air

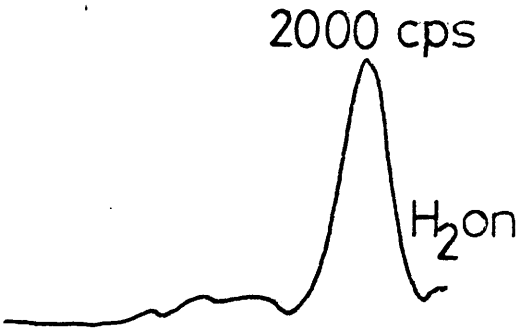

Hydrogen following argon

after Q gas

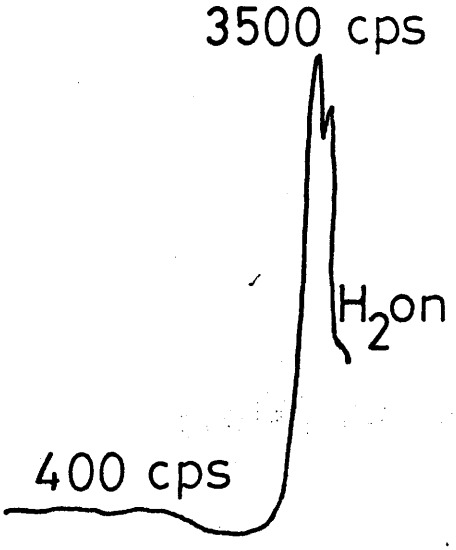

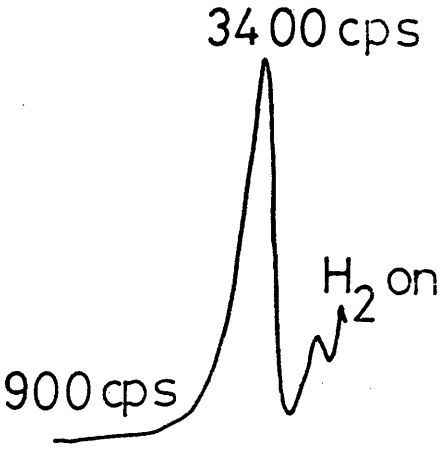

Hydrogen following Q gas

figure 104.

Helium Introduction curves to show the effect of carbiding the platinum filament.

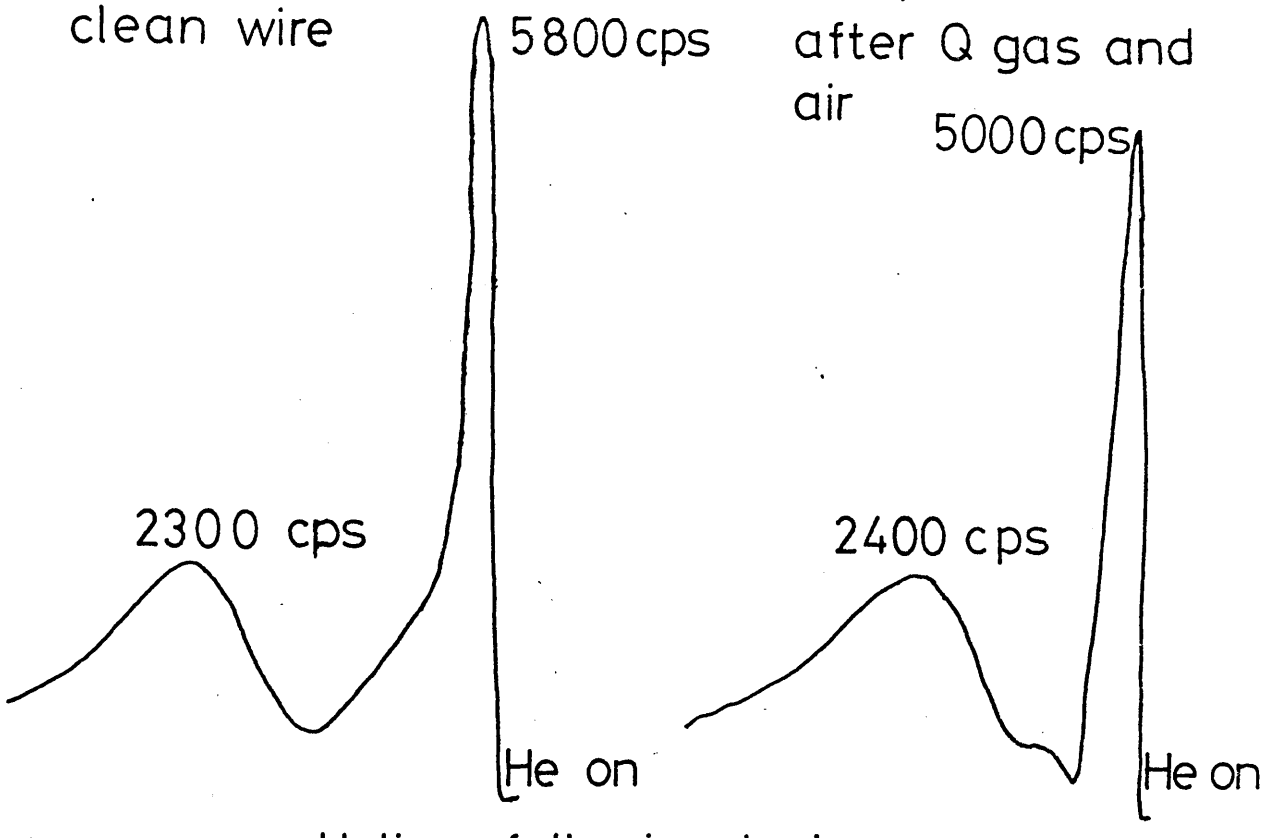

Helium following hydrogen

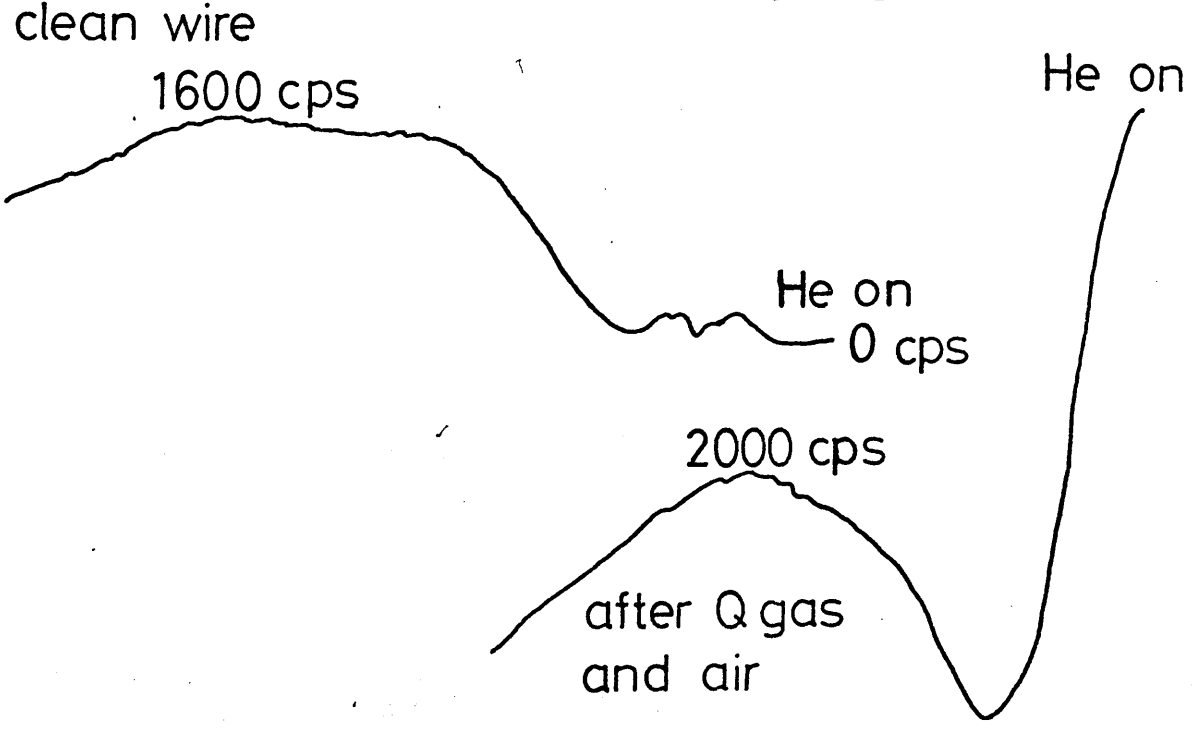

Helium following oxygen

figure 105.

Argon Introduction curves to show the effect of carbiding the platinum filament.

clean wire

after Q gas and air

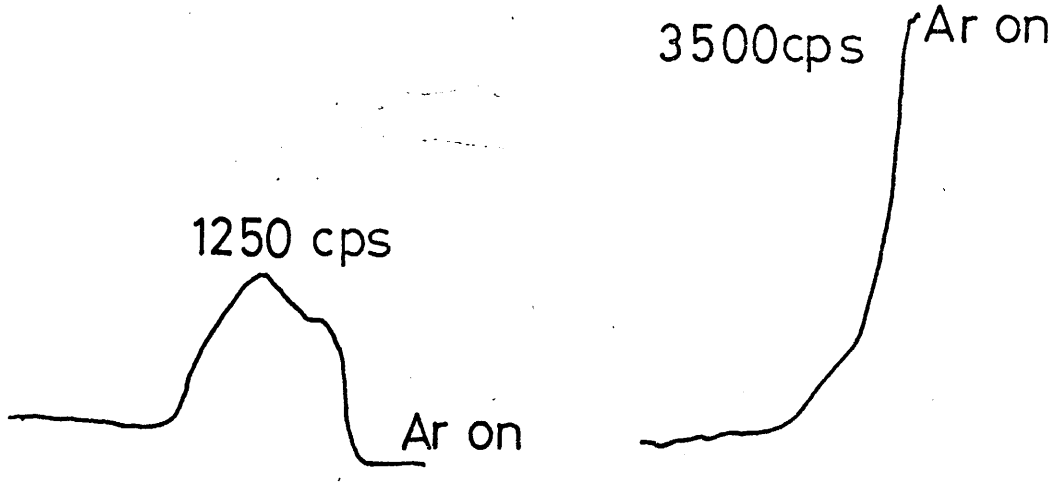

Argon following oxygen

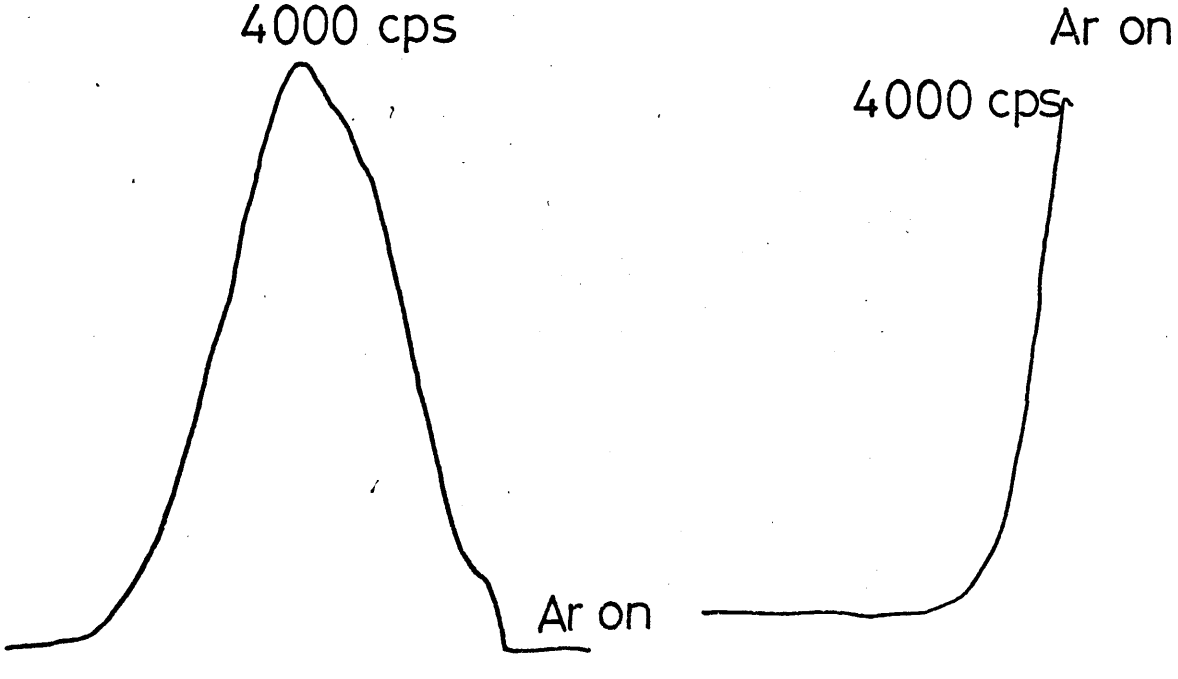

Argon following nitrogen

Argon Introduction curves continued

clean wire

after Q gas and air

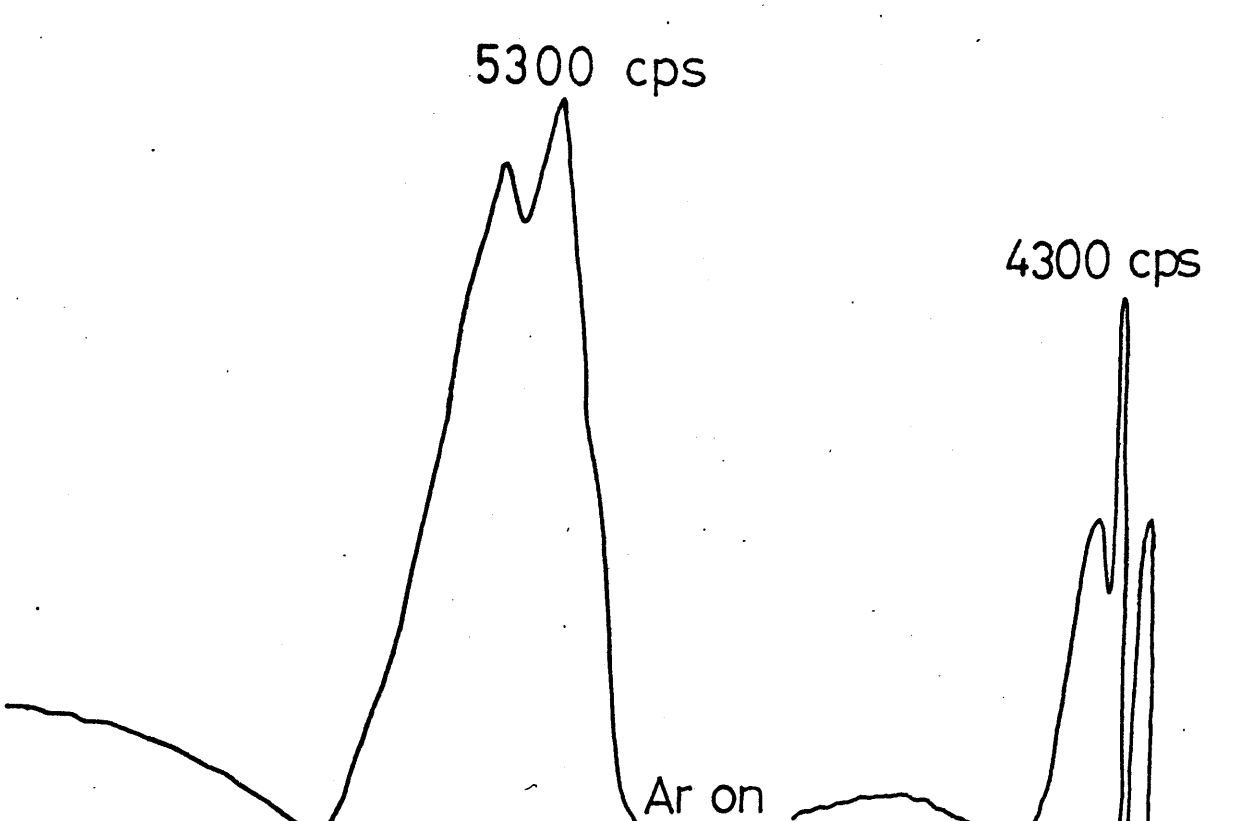

Argon following hydrogen

Appendix 16b

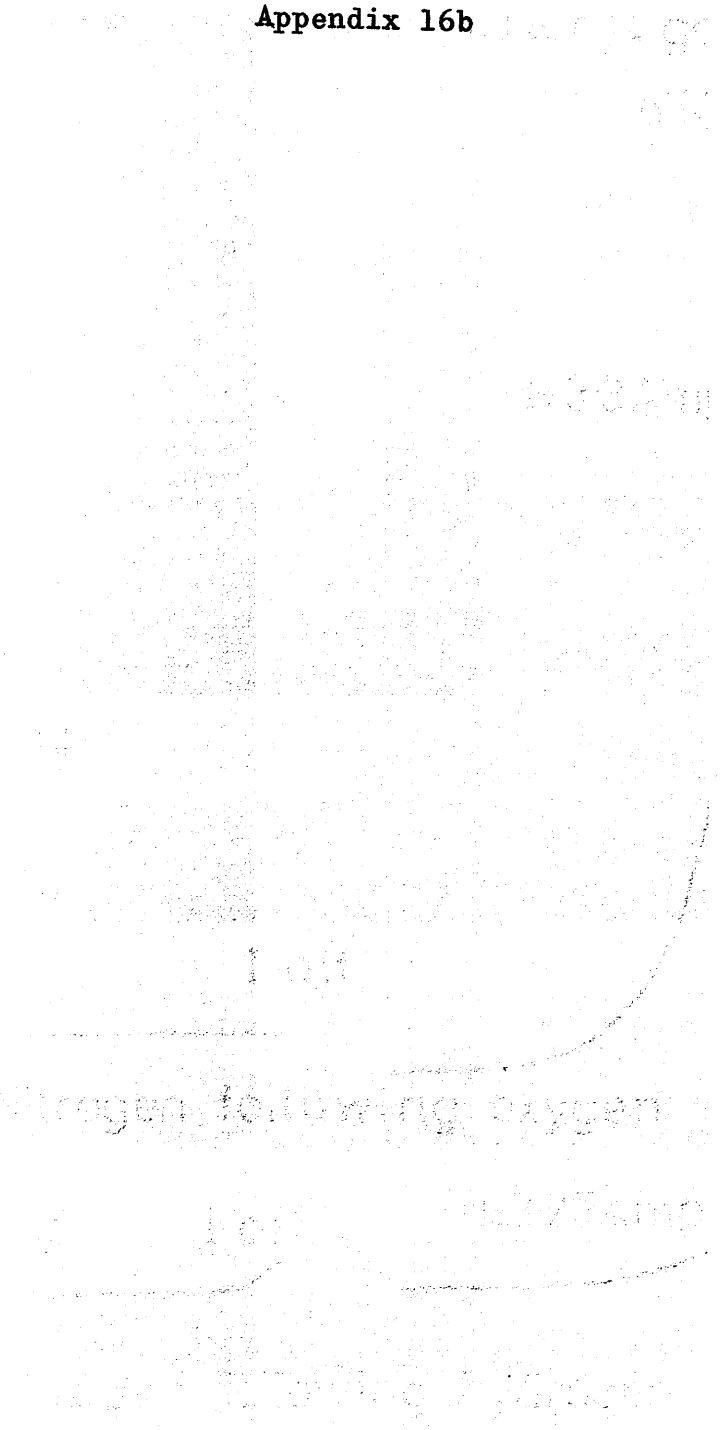

figure 106.

Nitrogen Cooling curves to show the effect of carbiding the platinum filament.

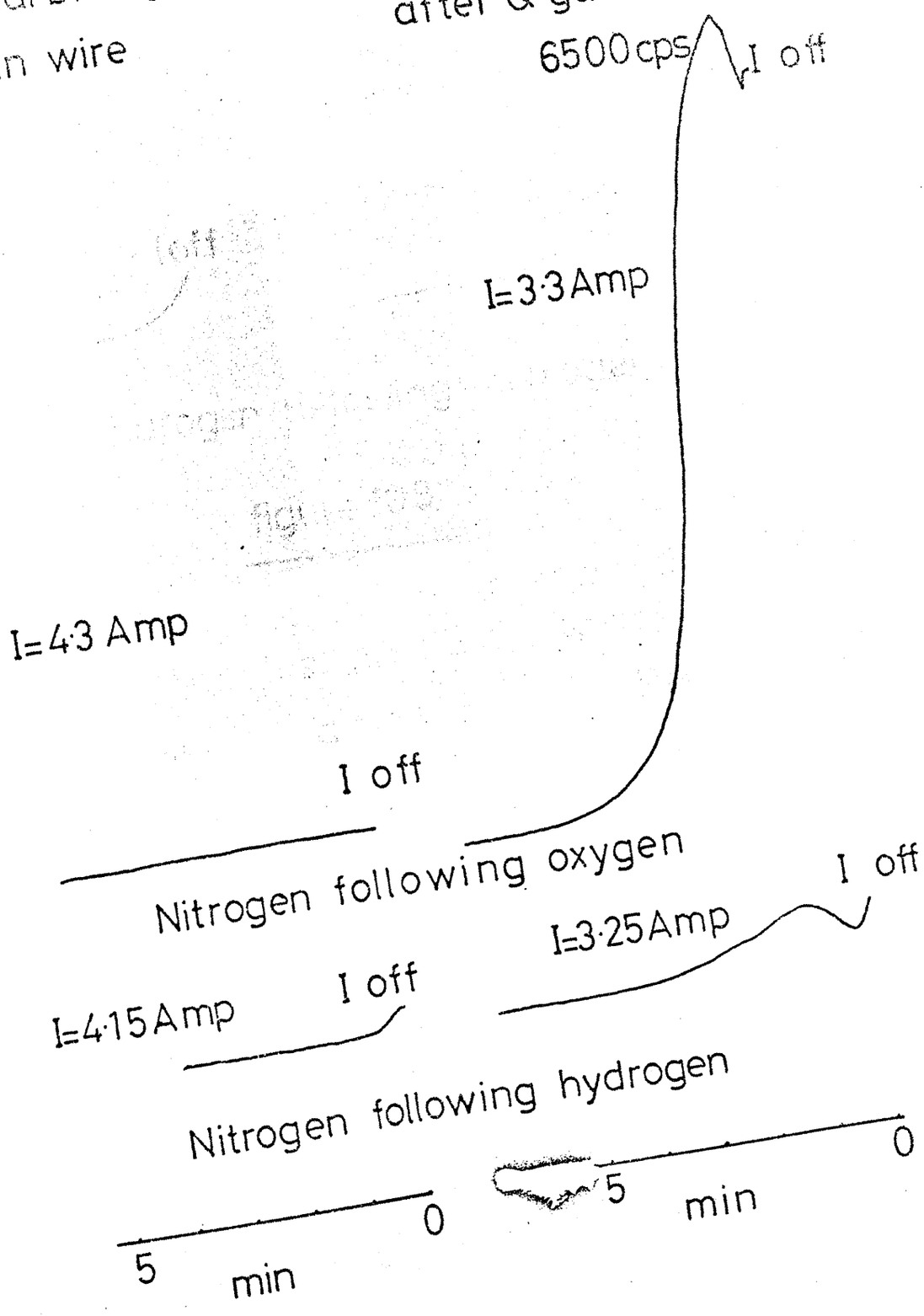

figure 107.

Hydrogen Cooling curves to show the effect of carbiding the platinum filament.

clean wire

I= 3·7 Amp

Ioff

after Q gas and air

I= 4·1 Amp

I off

Hydrogen following nitrogen

figure 108.

Oxygen Cooling curves to show the effect of carbiding the platinum filament.

clean wire

I= 4·25 Amp

I off

after Q gas

I=3·6 Amp

I off

after Q gas and air

3100 cps

I off

I=3·25 Amp

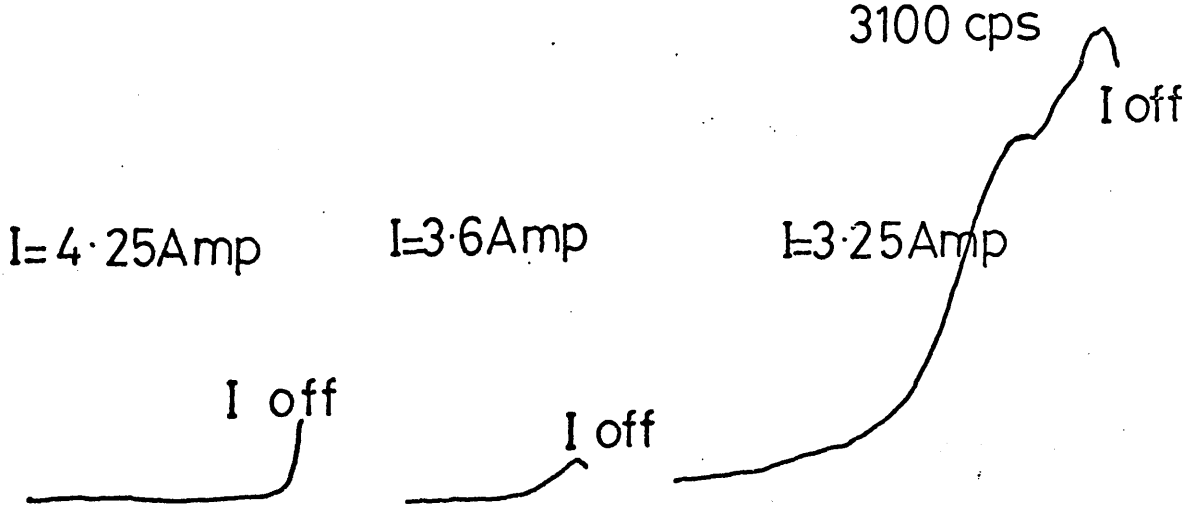

Oxygen following nitrogen

figure 109.

Q gas Cooling curves to show the effect of exposing the platinum filament to air after Q gas.

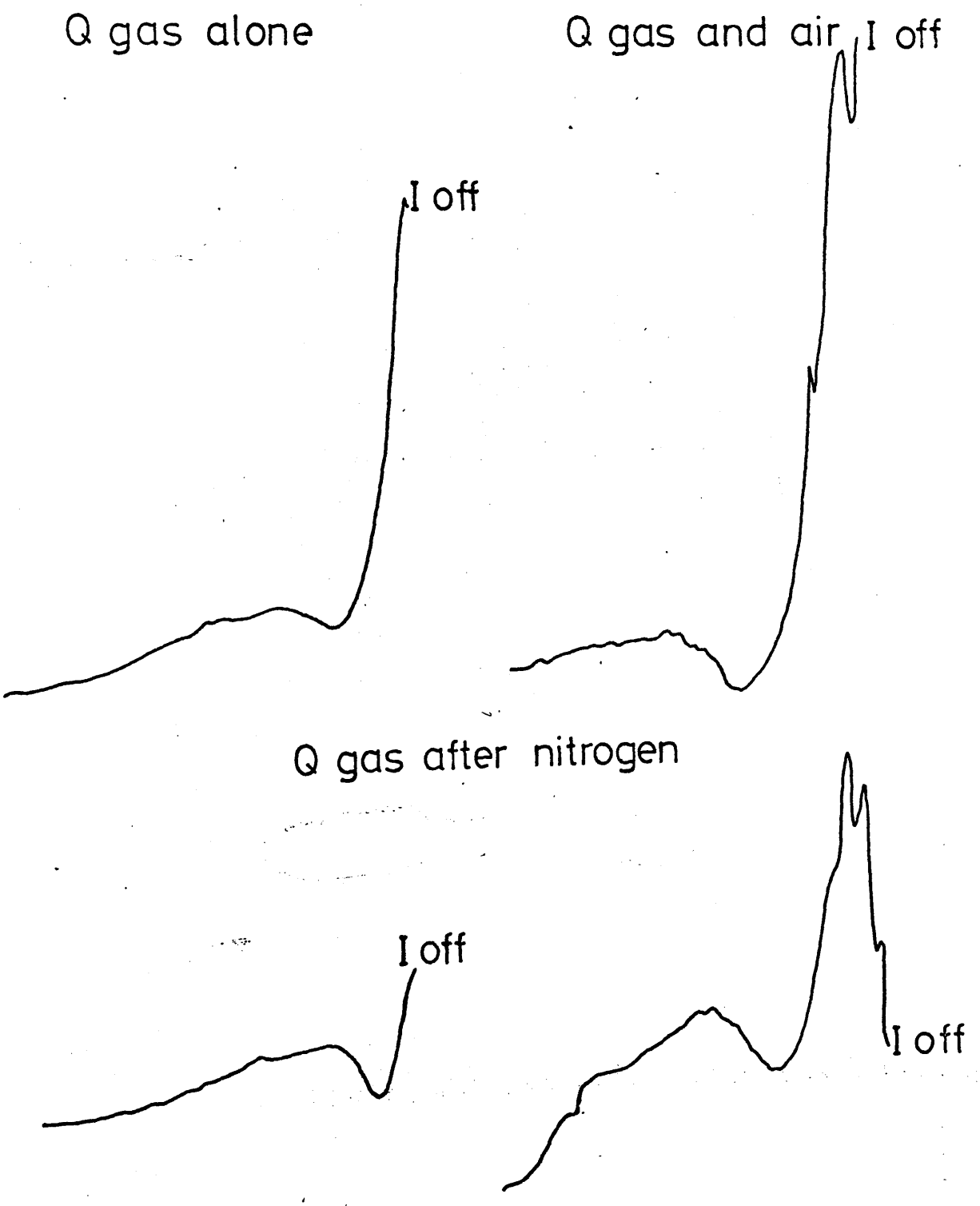

Appendix 17

Appendix 17a

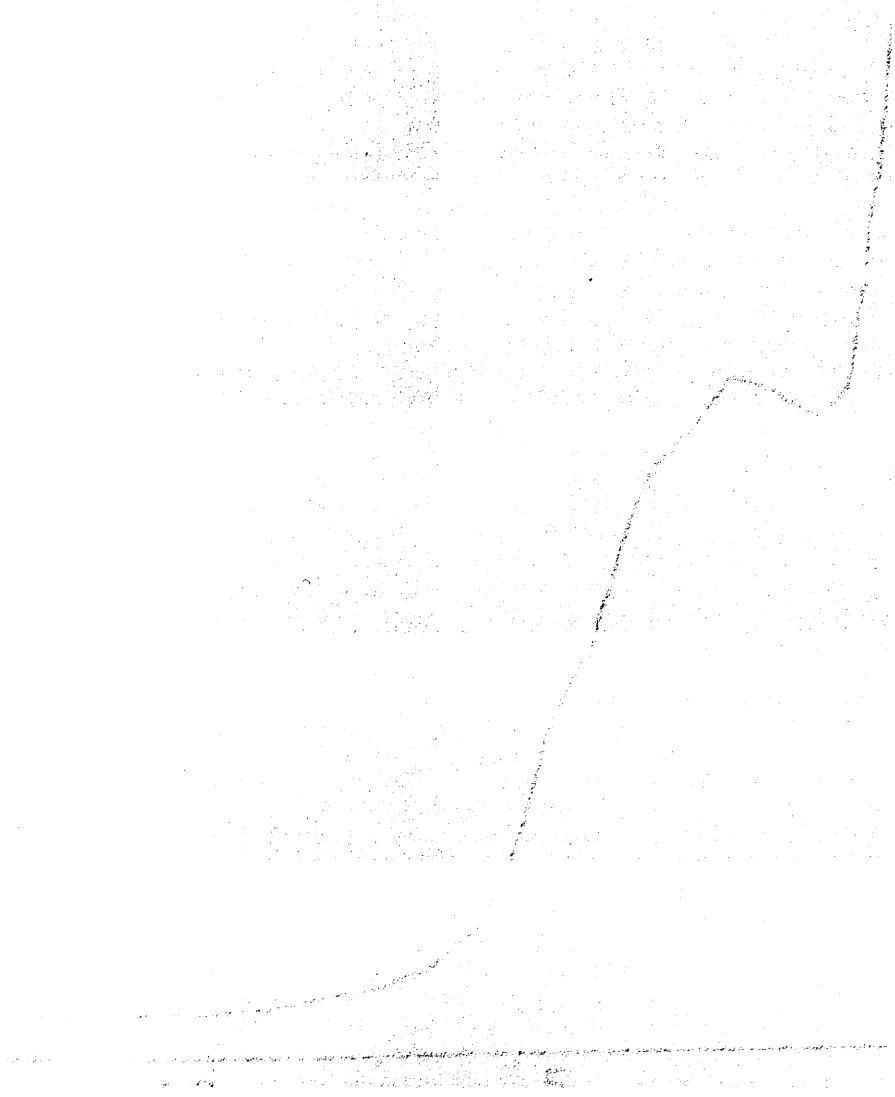

figure 110.

Nitrogen Introduction curve after acetylation of Wire 3.

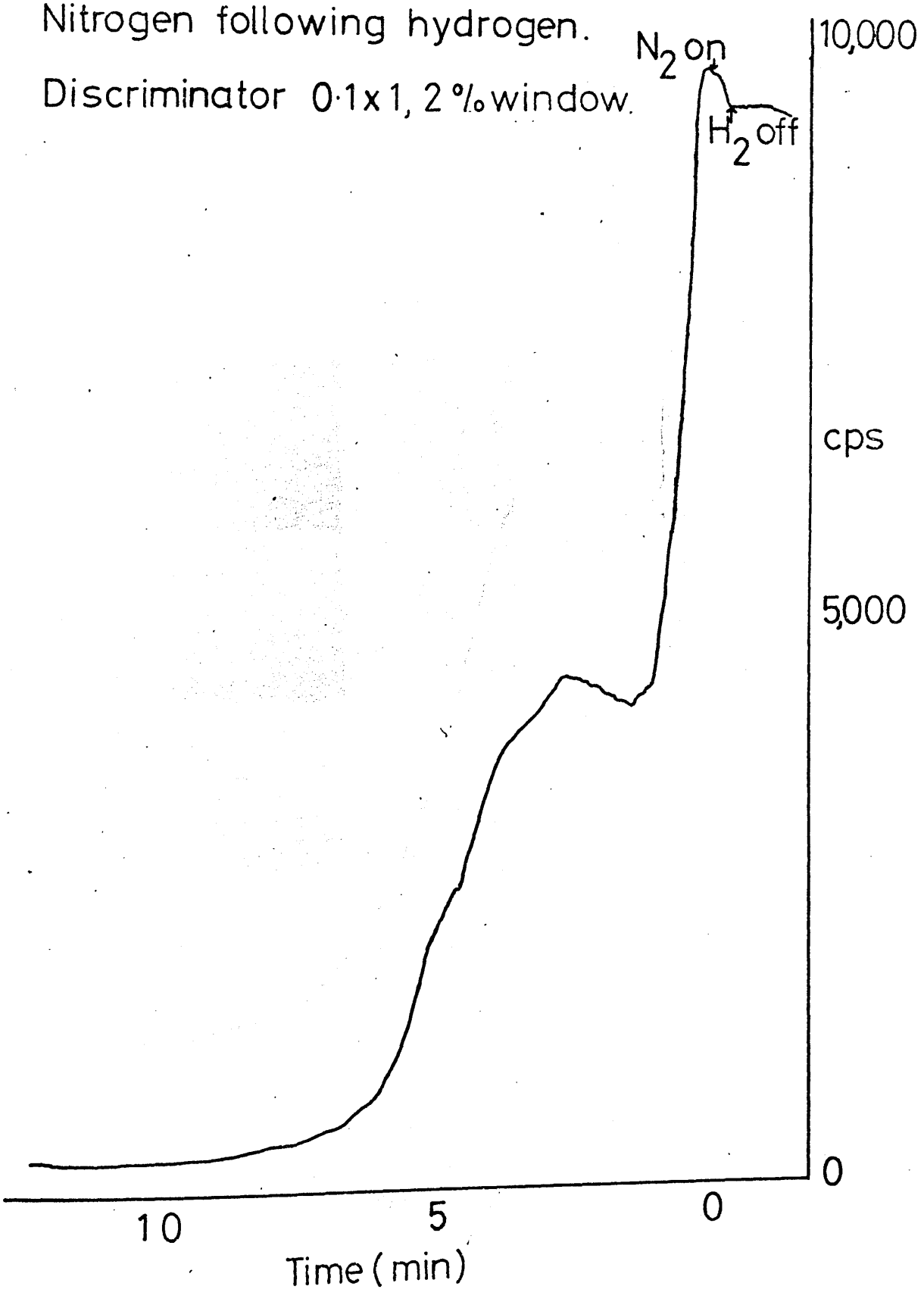

figure 111.

A second example of a nitrogen Introduction curve after acetylation of Wire 3.
Nitrogen following hydrogen.
Discriminator 0·1x1, 2%

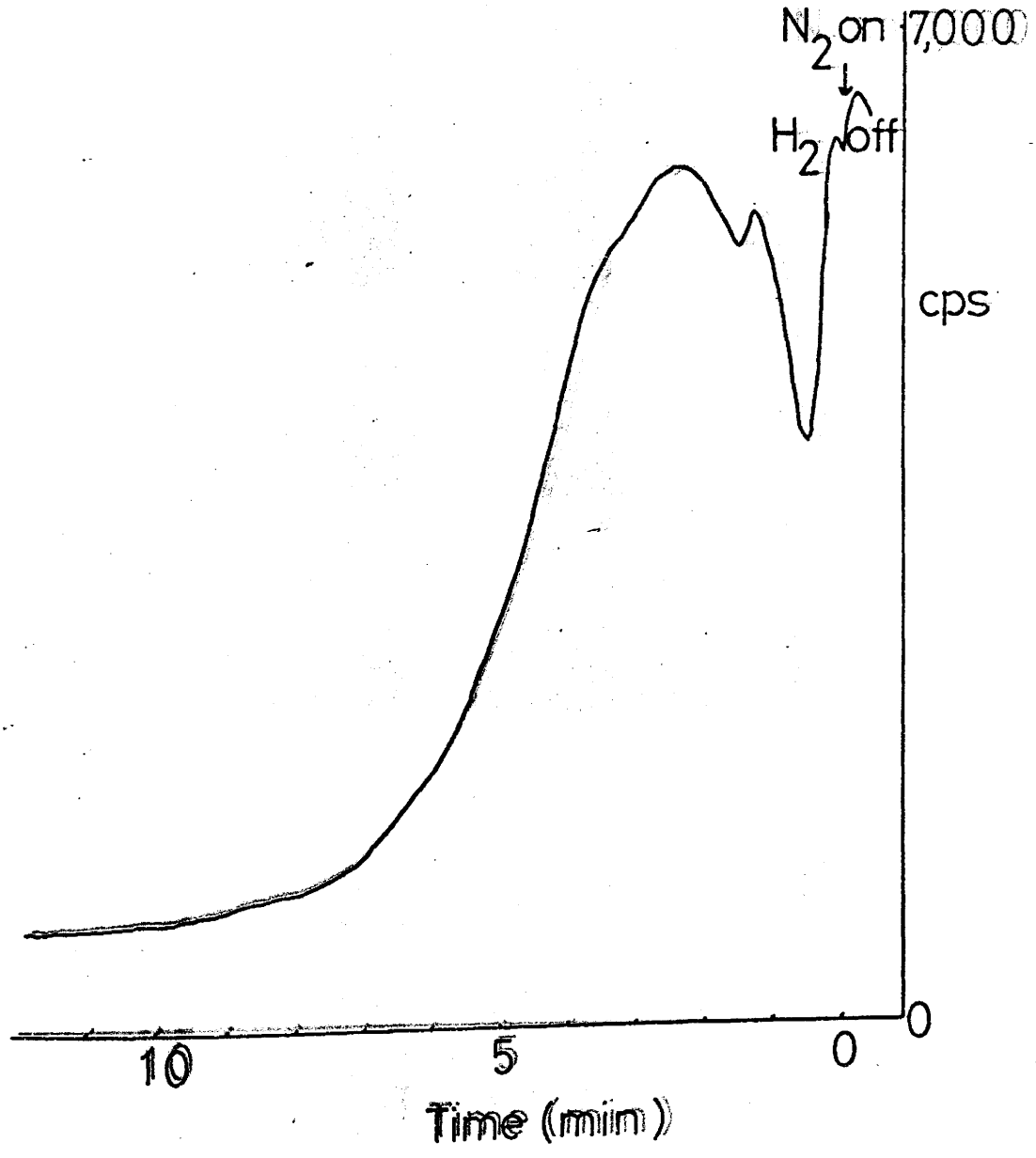

figure 112.

Hydrogen Introduction curve after acetylation of Wire 3.

Hydrogen following nitrogen.

Discriminator 0·1x1, 2%.

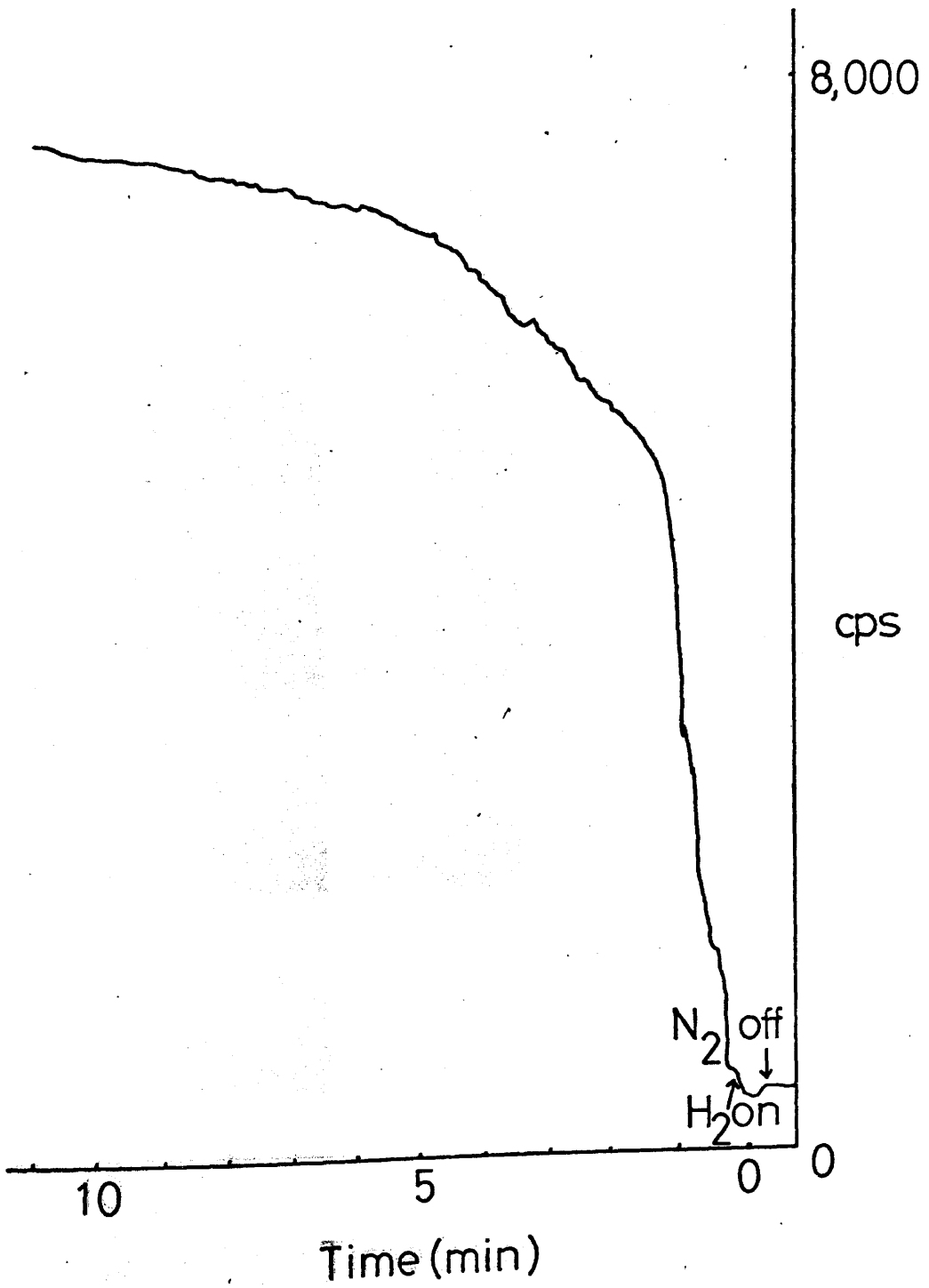

Appendix 17b

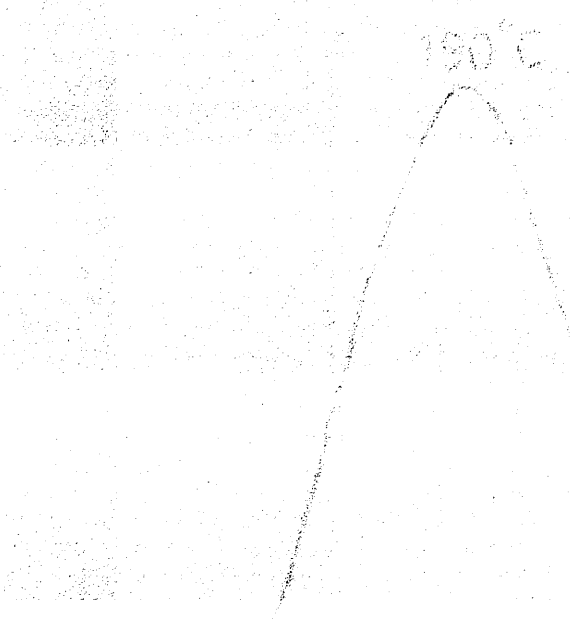

figure 113.

Typical Nitrogen Cooling curve after acetylation of Wire 3.

Nitrogen cooling following hydrogen heating.

Discriminator 0·1x 1, 2%.

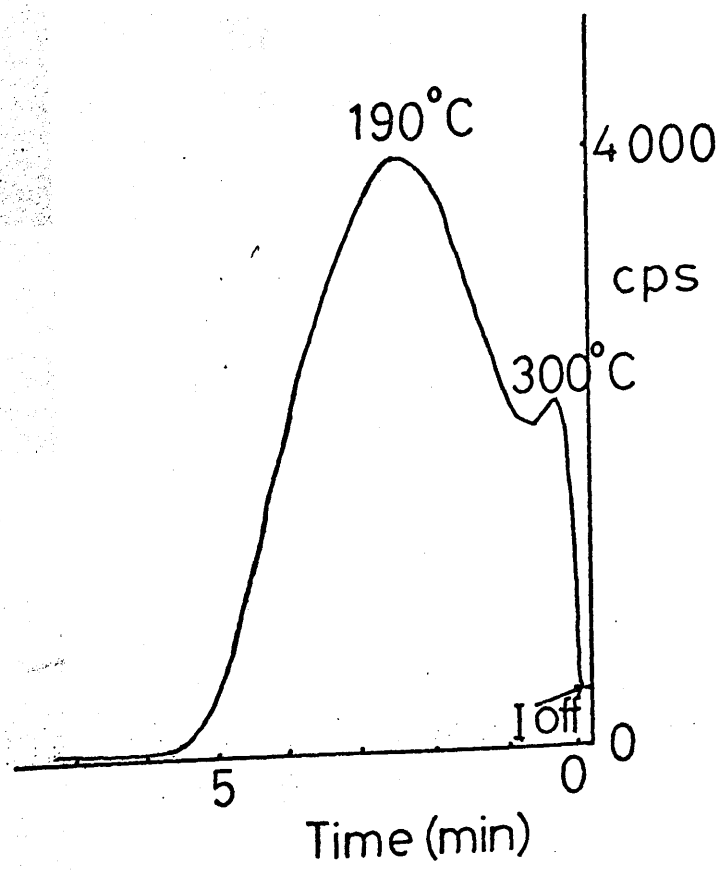

figure 114.

Hydrogen Cooling curves after acetylation of Wire 3.

Hydrogen cooling following nitrogen heating.

Discriminator 0·1x1, 2%window.

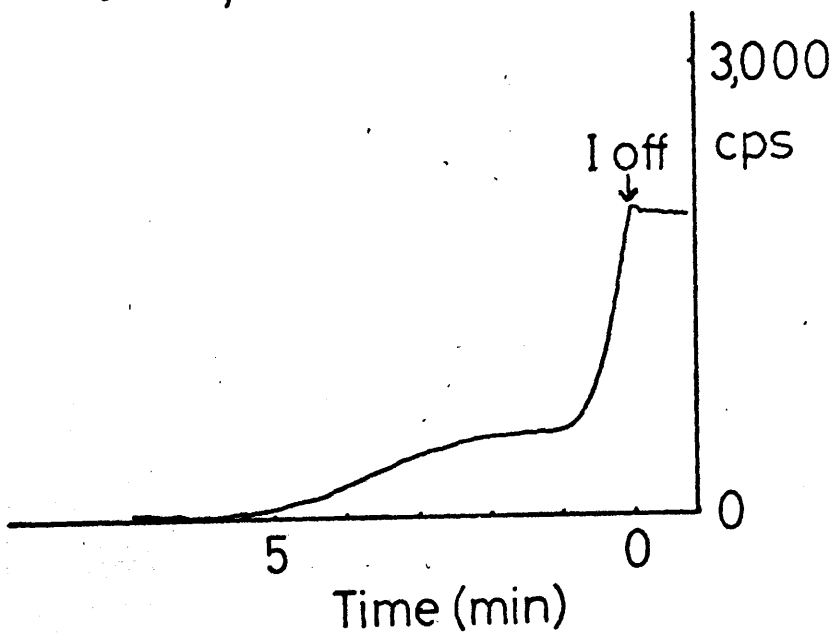

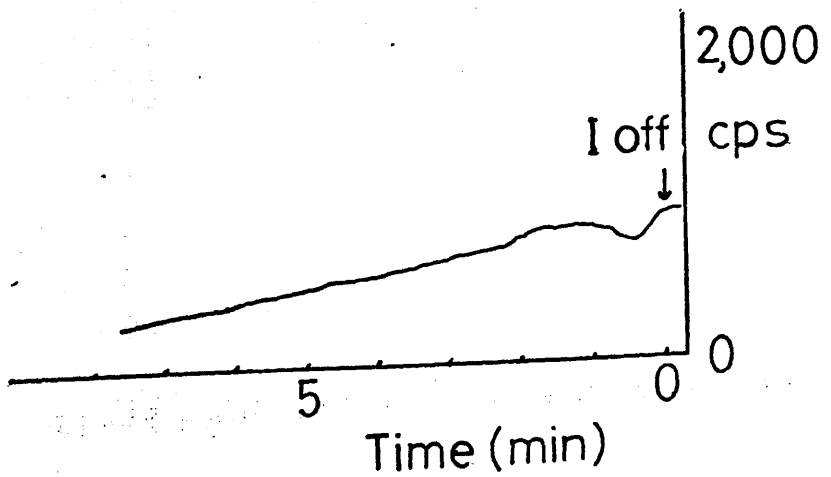

figure 115.

Hydrogen Cooling curve after acetylation of Wire 3.

Hydrogen cooling after prolonged heating in hydrogen.

Discriminator 0·1x 1, 2%.

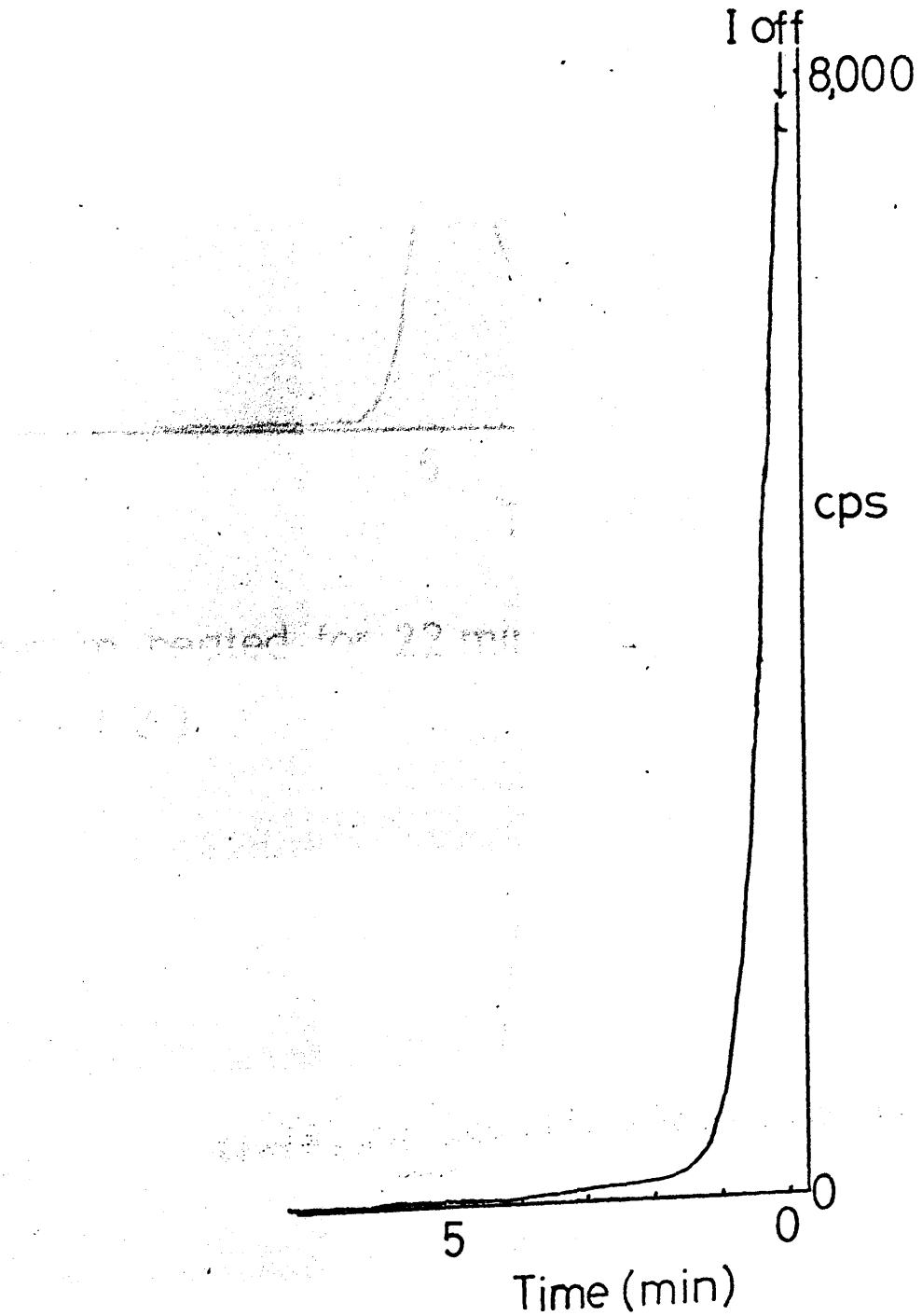

figure 116.

Nitrogen Cooling curves after several cycles of heating in hydrogen and cooling in nitrogen.

Nitrogen cooling following hydrogen heating.

Discriminator 0·1x 1, 2%.

Platinum heated for 67 min

(1)

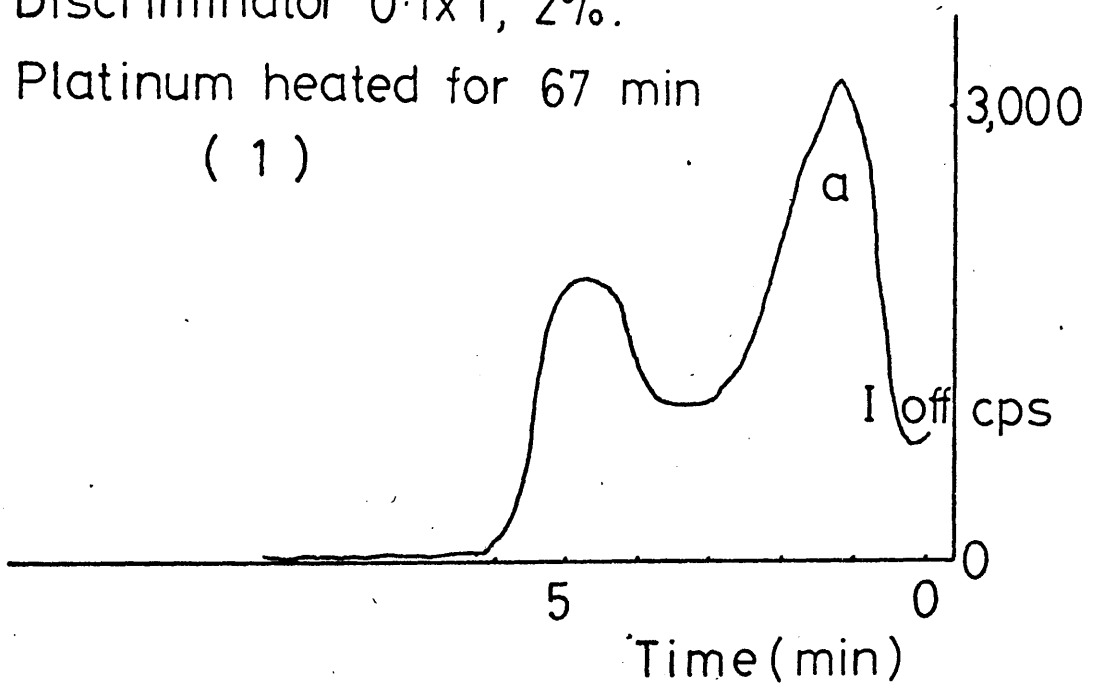

Platinum heated for 22 min

(2)

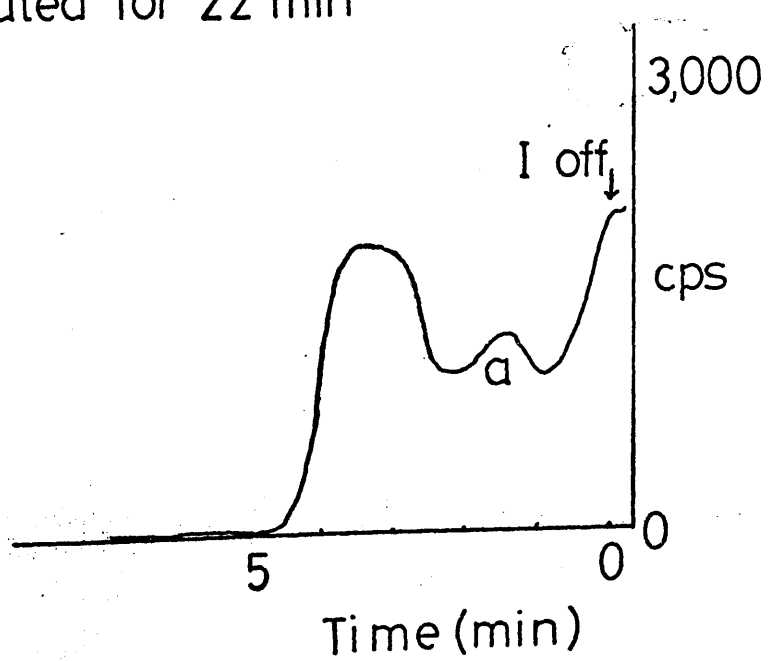

Appendix 18

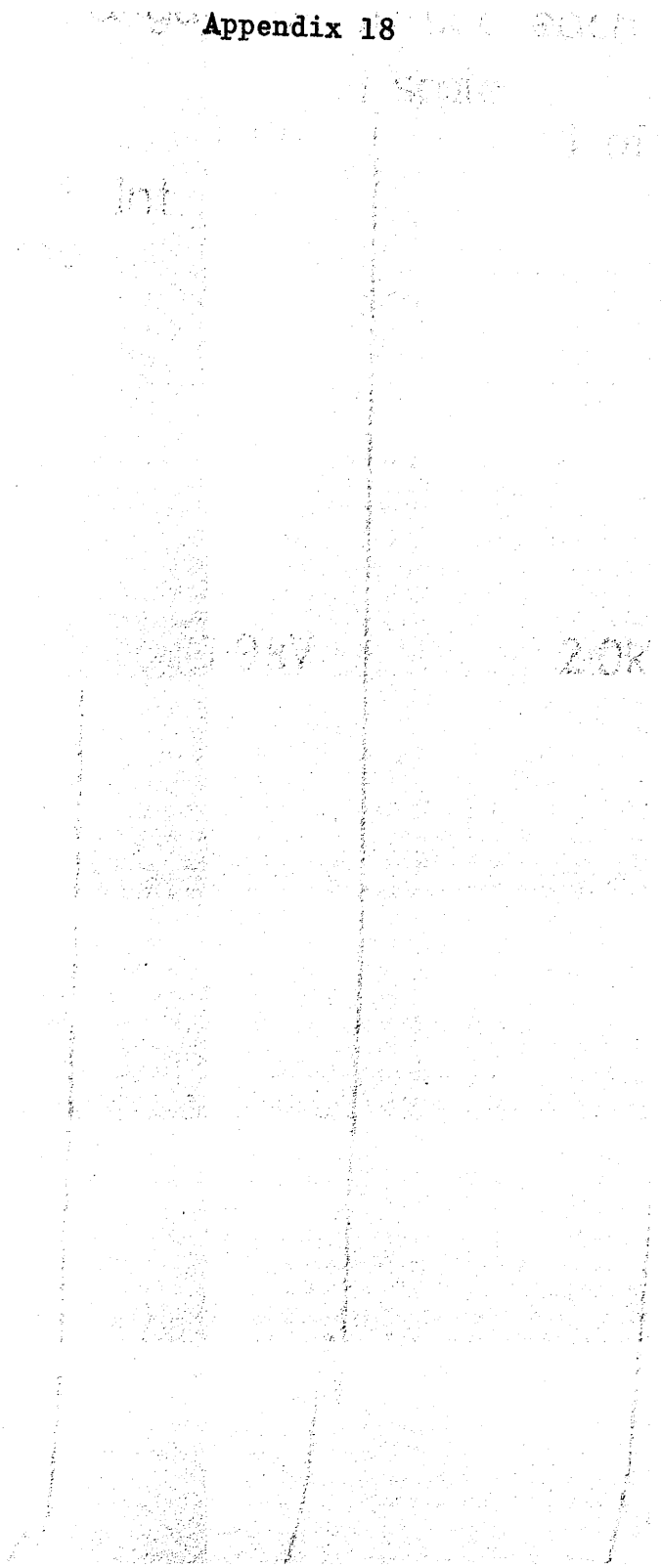

figure 117.

To show the effect of the anode voltage on the cooling curves. The platinum filament was heated in Q gas for 30 sec each time.

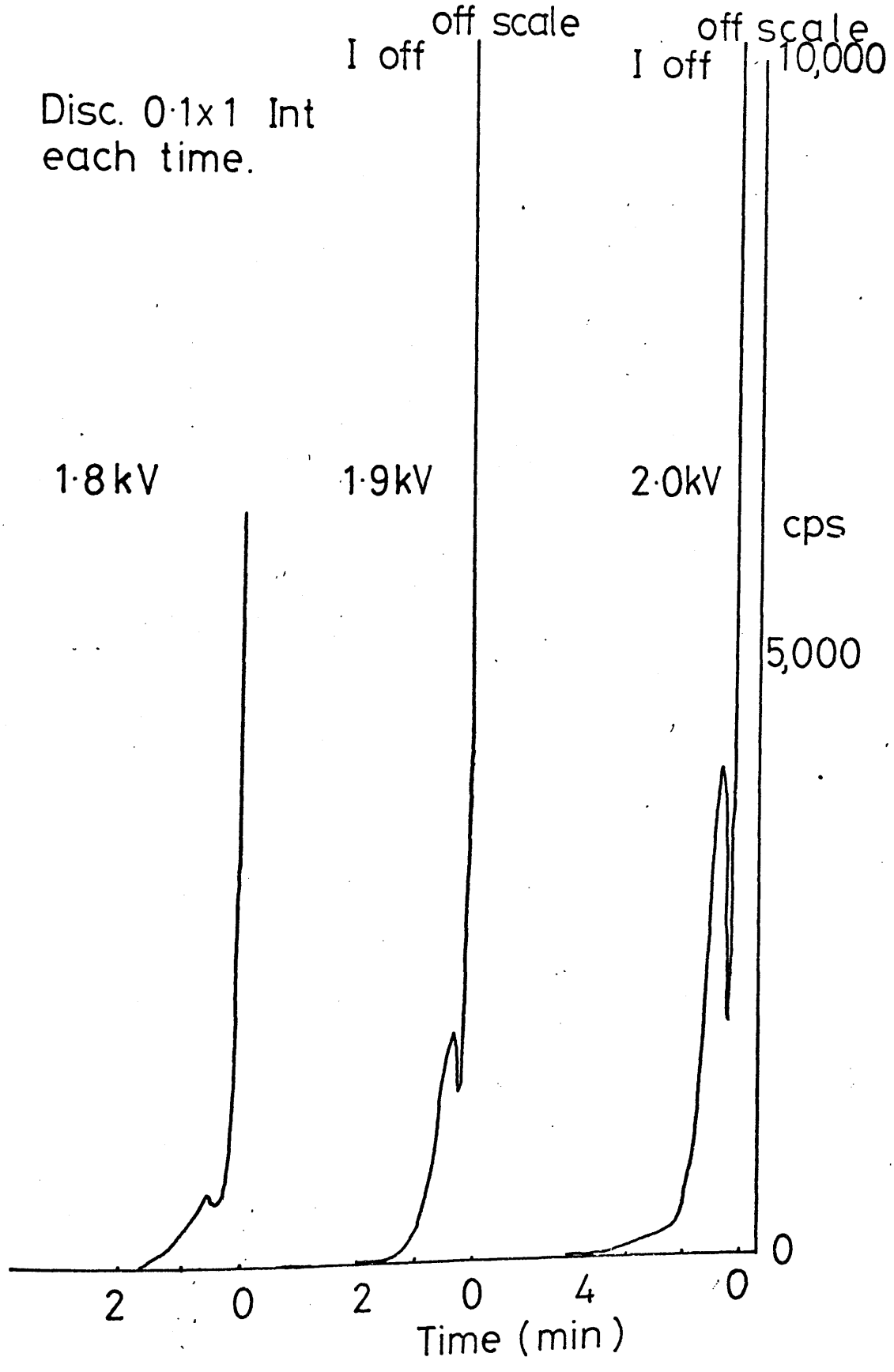

Appendix 19

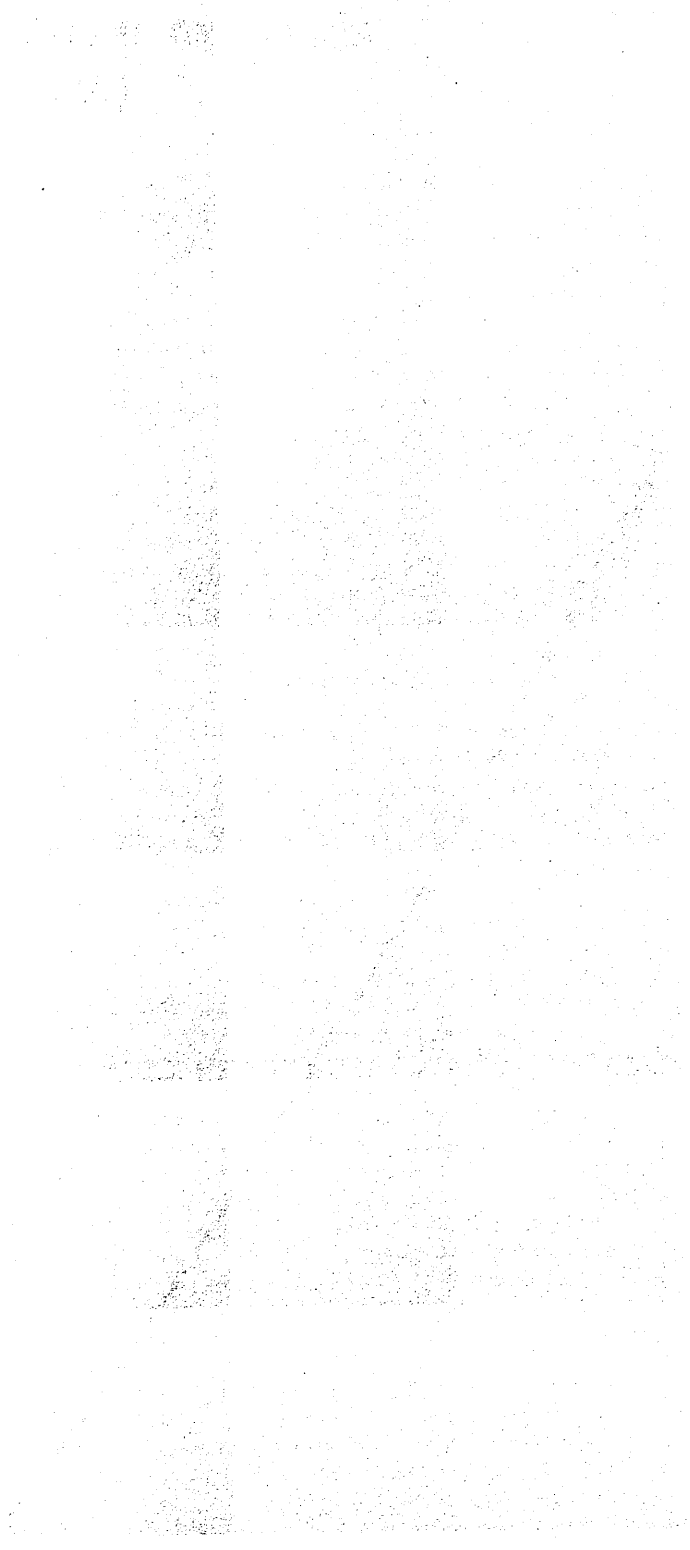

Graph 29.

Calibration curve to convert thermocouple response, measured in mV, to °C (198).

Pt / Pt, 13% Rh.

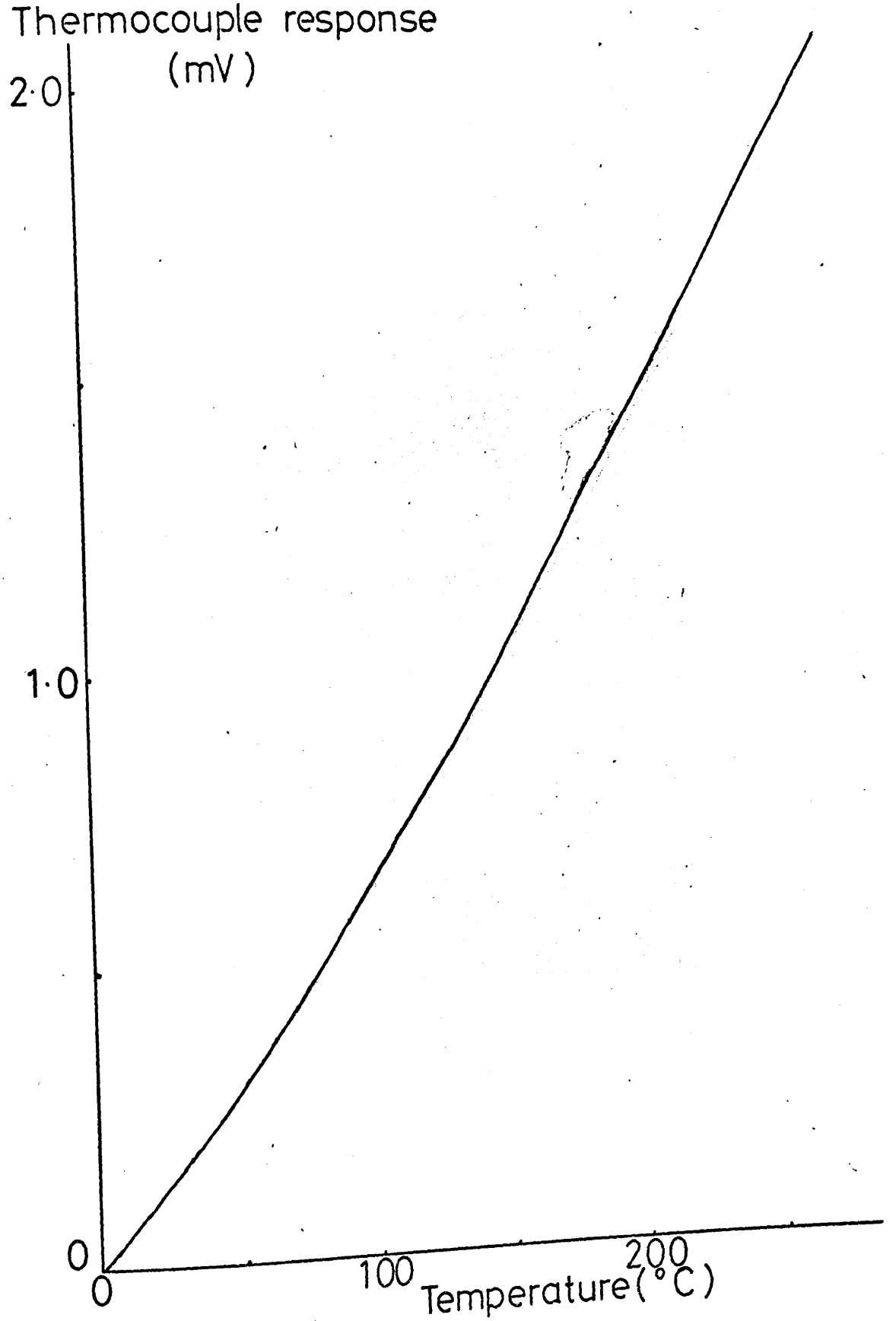

Graph 30.

Calibration curve to convert thermocouple response, measured in mV, to °C (198).

Pt / Pt,10% Rh.

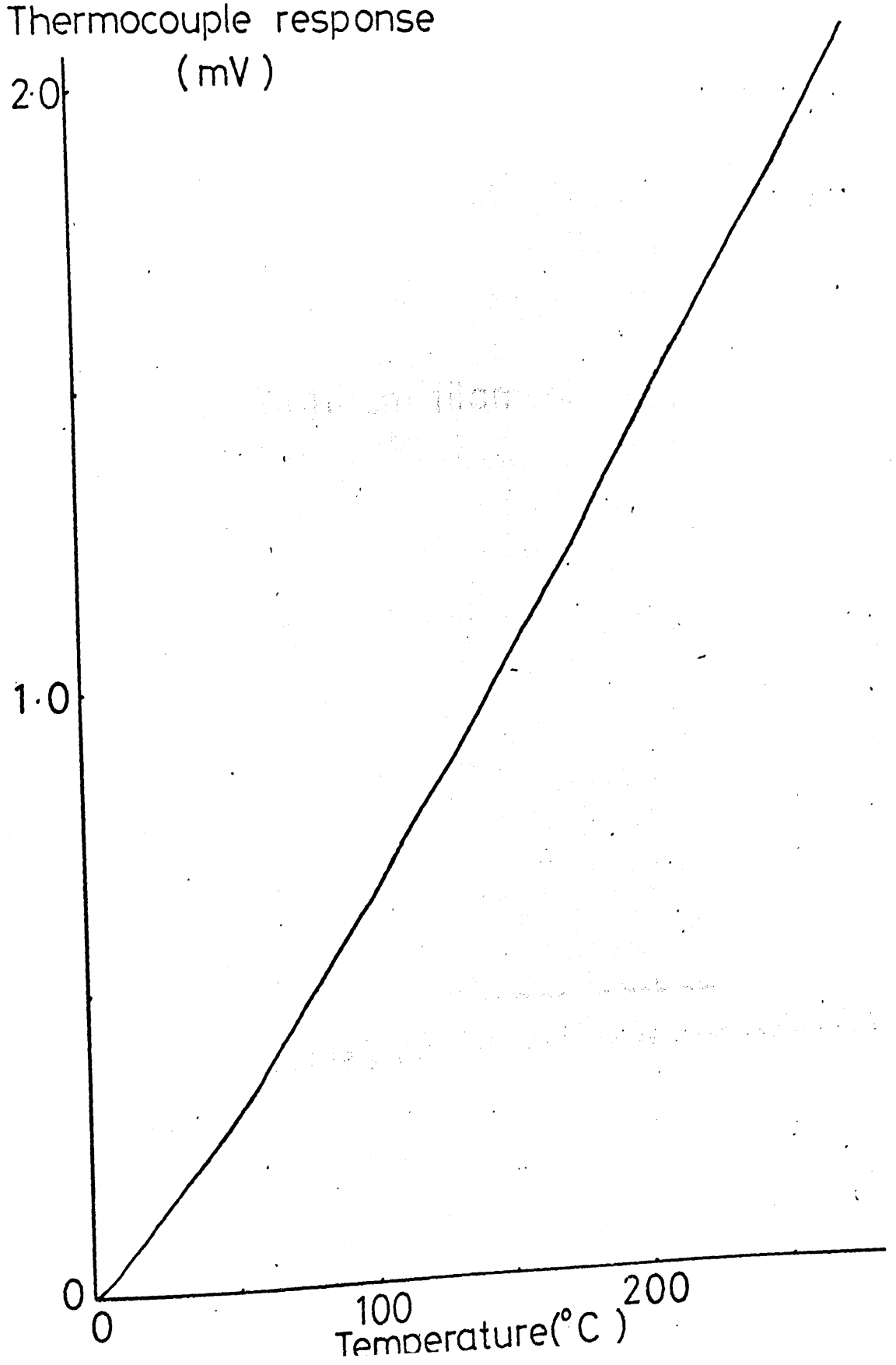

Graph 31.

Plot of temperature versus time to show the difference in cooling rate of the copper cathode and the platinum filament.

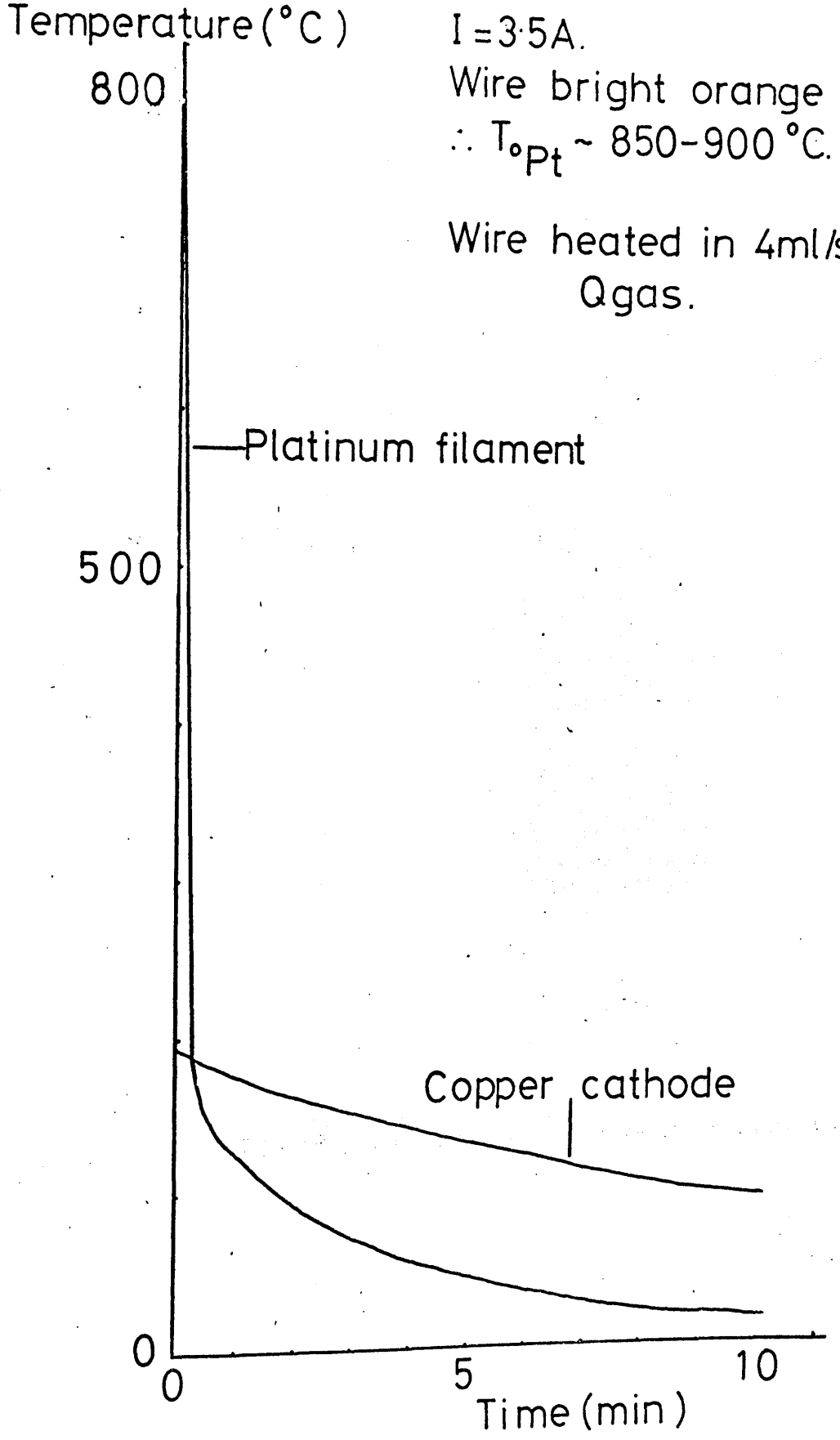

Appendix 20

Table X

Average energy required to produce an Ion Pair for some Gases; see (136).

	eV
Air	35·6
N_2	37·1
H_2	36·0
He	30·0
Ne	29·7
Ar	28·2
Kr	26·2
Xe	23·6

Appendix 21

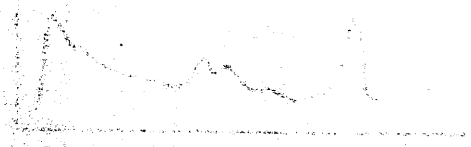

Channel number

Laben Spectrum 7.

Platinum wire heated in nitrogen and allowed to cool in hydrogen. Counts accumulated from 4·0–4·5 min after heating current switched off. Anode voltage 1·8 kV. Range x10^4.

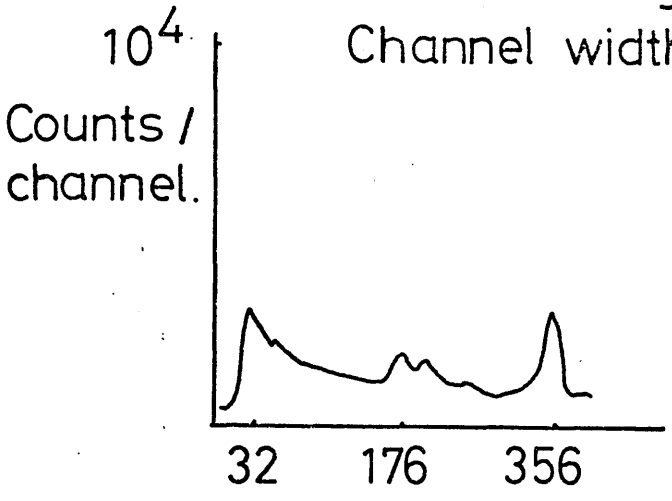

Laben Spectrum 8.

Platinum wire heated in nitrogen and allowed to cool in hydrogen. Counts accumulated from 9·0–9·5 min after heating current switched off. Anode voltage 2·1kV. Range x10^4

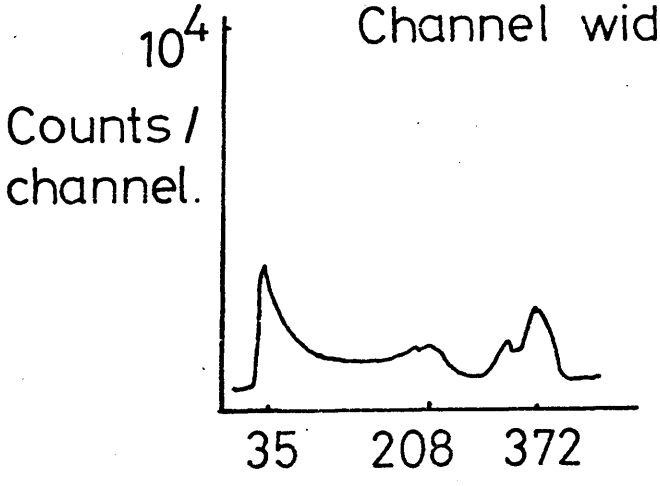

Spectra accumulated during the same cooling cycle.

References

1. Kramer, J.: Der metallische Zustand. (Göttingen: Vandenhoeck & Ruprecht, 1950).
2. Curie, P.: Comptes Rendus, 129 714 (1899).
3. Rutherford, E.: Phil. Mag. 49 161 (1900).
4. Russel, J.W.: Proc. Roy. Soc. 61 424 (1897).
5. Villard, P.: Société de Physique, juillet (1900).
6. McLennan, J.C.: Phil. Mag. 3 195 (1902).
7. Hartley, H.: Proc. Roy. Soc. Ser A. 90 61 (1914).
8. Finch, G.: Proc. Roy. Soc. Ser A. 144 320 (1934).
9. Denisoff, A., Richardson, O.: Proc. Roy. Soc. Ser A. 148 533 (1935) and references therein.
10. Lewis, W.B., Burcham, W.E.: Proc. Camb. Phil. Soc. 32 503 (1936).
11. Tanaka, M.: Proc. Physico-Math Soc. Japan (3rd series) 22 899 (1940)
12. Haxel, O., Houtermans, F.G., Seeger, K.: Z. Phys. 130 109 (1951).
13. Roubinek, F., Seidl, R.: Czech. J. Phys. 2 84 (1953).
14. Kramer, J.: Z. Phys. 133 629 (1952)
15. Grunberg, L., Wright, K.H.R.: Nature (London) 171 890 (1953) see Grunberg, L.: Brit. J. Appl. Phys. 9 85 (1958).
16. Grunberg, L., Wright, K.H.R.: Proc. Roy. Soc. Ser A. 232 403 (1955).
17. Okamoto, Go, Sato, N., Ohashi, H.: J. Electrochem. Soc. Japan. 33 11 (1965)
18. Seidl, R.: Act. phys. Aust. 10 402 (1957).

19. Bohun, A.: Czech. J. Phys. 5 64 (1955).

20. Bohun, A.: J. Phys. Radium 17 783 (1956).

21. Bohun, A., Karpiskova, K., Duskova, A.: Czech. J. Phys. 5 100 (1955).

22. Müller, H., Weinberger, F.: Acta. phys. Aust. 10 409 (1957).

23. Lohff, J.: Z. Phys. ~~145~~ 146 ~~504~~ 436 (1956).

24. Ramsey, J.: Proc. I.R.E.E. Australia 28 139 (1967).

25. Wüstenhagen, J.: Naturwissenschaften 44 228 (1957).

26. Wüstenhagen, J.: Z. Naturf. 14a 634 (1959)

27. Ramsey, J.: J. Appl. Phys. 37 452 (1966).

28. Ramsey, J., Garlick, G.F.J.: Brit. J. Appl. Phys. 15 1353 (1964).

29. Ramsey, J.: J. Aust. Inst. Metals 10 323 (1965).

30. Ramsey, J.: Surface Science 8 313 (1967).

31. Huber, E.E., Kirk, C.T.: Surface Science 5 447 (1966).

32. Doherty, P.E., David, R.S.: J. Appl. Phys. 34 619 (1963).

33. Pimbley, W.T., Francis, E.E.: J. Appl. Phys. 32 1729 (1961).

34. Mueller, R.K., Pontinen, K.: J. Appl. Phys. 35 1500 (1964).

35. Scharmann, A., Seibert, G.: Z. Phys. 183 249 (1965).

36. Gesell, T.F., Arakawa, E.T., Callcott, T.A.: Surface Science 20 174 (1970).

37. Gesell, T.F., Arakawa, E.T., Callcott, T.A.: Surface Science 33 419 (1972).

38. Gel'man, A.G., Roikh, I.L.: Sov. Phys.-Solid State 12 2763 (1971).

39. Gel'man, A.G., Fainshtein, A.I.: Sov. Phys. - Solid State 14 1752 (1973).

40. Krylova, I.V.: Phys. Stat. Sol.(a) 7 359 (1971).

41. Euler, M., Kriegseis, W., Scharmann, A.: Phys. Stat. Sol.(a) 15 431 (1973).

42. Meleka, A.H., Barr, W.: Nature (London) 187 232 (1960).

43. Brotzen, F.R.: Phys. Stat. Sol. 22 9 (1967).

44. Hempel, M., Kochendörfer, A., Tietze, A.: Arch. Eisenhüttenwesen 35 465 (1964).

45. Von Voss, W.D., Brotzen, F.R.: J. Appl. Phys. 30 1639 (1959).

46. Claytor, R.N., Brotzen, F.R.: J. Appl. Phys. 36 3549 (1965).

47. Gieroszynski, A., Mader, J., Sujak, B.: Acta Phys. Pol. 25 3 (1964).

48. Gieroszynski, A., Mader, J., Sujak, B.: Acta Phys. Pol. 26 1033 (1964).

49. Sujak, B., Gieroszynski, A., Mader, J.: Acta Phys. Pol. 28 31 (1965).

50. Sujak, B., Gieroszynski, A., Pega, E.: Acta Phys. Pol. 28 61 (1965).

51. Sujak, B., Gieroszynski, A.: Acta Phys. Pol. 29 523 (1966).

52. Gieroszynski, A., Sujak, B.: Acta Phys. Pol. 29 275 (1966).

53. Sujak, B., Gieroszynski, A., Gajda, R.: Acta Phys. Pol. 28 329 (1965).

54. Gieroszynski, A., Sujak, B.: Acta Phys. Pol. 28 337 (1965).

55. Gieroszynski, A., Sujak, B.: Acta Phys. Pol. 29 533 (1966).

56. Gieroszynski, A., Sujak, B.: Acta Phys. Pol. 28 311 (1965).

57. Arnott, D.R., Ramsey, J.A.: Surface Science 28 1 (1971).

58. Thomas, B.W.: J. Phys. D.: Appl. Phys. 7 L57 (1974).

59. Yoshiro, Y.: J. Appl. Phys. Japan 27 196 (1958).

60. Tanaka, A.: J. Appl. Phys. Japan 29 501 (1960).

61. Mints, R.I., Kortov, V.S., Aleksandrov, V.L., Kryuk, V.I.: U.D.C. 539,433. Translation from Fiz. metal. metalloved. 26 (4) 680 (1968).

62. Baxter, W.J.: Appl. Phys. Letters 21 590 (1972).

63. Baxter, W.J.: J. Appl. Phys. 44 608 (1973).

64. Thompson, N., Wadsworth, N.J.: Adv. Phys. 7 72 (1958).

65. Rabinowicz, E.: Sci. American 236 74 (1977).

66. Futschik, F.: Thesis (Vienna, 1955): see Bruna, O., Lintner, K., Schmid, E.: Z. Phys. 136 605 (1954).

67. Futschik, F., Lintner, K. Schmid, E.: Z. Phys. 145 48 (1956).

68. Bathow, G., Gobrecht, H.: Z. Phys. 146 1 (1956).

69. Kahlert, H., Kralik, G.: Acta phys. Aust. 23 303 (1966).

70. Sujak, B., Gorecki, T., Malkiewicz, M., Stepniowski, I.: Acta Phys. Pol. 30 51 (1966).

71. Biernacki, L., Gorecki, T., Sujak, B.: Acta Phys. Pol. 32 193 (1967).

72. Sujak, B., Biernacki, L., Gorecki, T.: Acta Phys. Pol. 35 679 (1969).

73. Sujak, B., Biernacki, L., Tokarski, M., Gorecki, T.: Acta Phys. Pol. 36 129 (1969).

74. Sujak, B., Biernacki, L., Gorecki, T.: Acta Phys. Pol. 35 475 (1969).

74a. Kedavichus, V. Yuodvirshis, A: Belyatskas R. Sov. Phys. Sol State 11 3032 (1970).

75. Kania, T., Pirog, M., Sujak, B.: Acta Phys. Pol. 37 573 (1965).

76. Hoenig, S.A., Pope, R.A.: Appl. Phys. Letters 14 271 (1969).

77. Hieslmair, H., Müller, H.: Z. Phys. 152 642 (1958).

78. Vogel, A.: Z. Phys. 158 77 (1960).

79. Birgfellner, H.: Act. phys. Aust. 13 293 (1960).

80. Kralik, G.: Acta phys. Aust. 16 137 (1963).

81. Drost, H.: Exper. Tech. Phys. 6 258 (1958).

82. Sinelnikov, M.V.: Radiotekhnika i Electronika 3 1523 (1958).

83. Sinelnikov, M.V.: Dokl. Akad. Nauk SSSR 126 554 (1959).

84. Kramer, J.: Z. Phys. 129 34 (1951).

85. Bohun, A.: Czech. J. Phys. 3 2 (1953).

86. Bohun, A.: Czech. J. Phys. 4 91 (1954).

87. Lepper, J.: Z. Naturforsch 10a 47 (1955).

88. Bohun, A.: Czech. J. Phys. 5 224, 429 (1955).

89. Gourge, G., Hanle, W.: Acta phys. Aust. 10 427 (1957).

90. Kramer, J.: Z. angew. Phys. 15 20 (1963).

91. Becker, K. Cheka, J.S., Gammage, R.B.: P.T.B. Mitteilungen 5 334 (1970).

92. Becker, K., Chantanakom, N.: Nuclear Insts. & Methods 66 353 (1968).

93. Becker, K., Cheka, J.S., Crase, K.W., Gammage, R.B.: Paper SM-143/37, I.A.E.A. Symp. New Radiation Detectors Vienna (1970) (see 94).

94. Gammage, R.B., Crase, K.W., Becker, K.: Health Physics 22 57 (1972).

95. Crase, K.W., Gammage, R.B., Becker, K.: Health Physics 22 402 (1972).

96. Nassenstein, H., Menold, R.: Acta phys. Aust. 10 452 (1957).

97. Lohff, J.: Z. Phys. 146 436 (1956).

98. Menold, R.: Z. Phys. 157 499 (1960).

99. Gibson, E.J.: J. Phys. Chem. Solids 17 220 (1961).

100. Ohashi, H., Kano, H., Sato, N., Okamoto, G.: J. Chem. Soc. Japan Ind. Chem. Section 69 997 (1966).

101. Sato, N., Seo, M.: Nature 216 361 (1967).

102. Sato, N., Seo, M.: J. Cat. 24 224 (1972).

103. Hauffe, K.: Reaktionen in und an festen Stoffen, Springer Verlag, Berlin 1955 (see (105)).

104. Rakhmatullina, I.A., Krylova, I.V.: Russian J. Phys. Chem. 42 1407 (1968).

105. Sujak, B., Gorecki, T., Biernacki, L.: Acta Phys. Pol. A 39 147 (1971).

106. Cabrera, H.: Elementarne procesy wzrostu kryształów PWN, Warsaw (1960)(in Polish).

107. Stone, F.S.: Adv. in Cat. 13 1 (1962).

108. Hoenig, S.A., Lane, J.R.: Surface Science 11 163 (1968).

109. Volkenshtein, F.: Adv. in Cat. 12 189 (1960).

110. Stadnik, P.M., Fentsik, V.P.: Kinet. Katal. 2 562 (1961).

111. Vladov, D., Dyakovitch, Vl., Dinkov, Sh.: J. Cat. 5 412 (1966).

112. Hoenig, S.A., Tamjidi, F.: J. Cat. 28 200 (1973).

113. Momose, Y., Tamai, Y.: J. Inst. Metals 98 110 (1970).

114. Kasemo, B., Walldén, L.: Solid State Communications 15 571 (1974).

115. Sujak, B., Wawrzyniak, J.: Acta Phys. Pol. 20 463 (1961).

116. Sujak, B., Bójko, I.: Acta Phys. Pol. 26 171 (1964).

117. Tamai, Y., Momose, Y.: J. Appl. Phys. 39 5329 (1968).

118. Lewowski, T.: J. Appl. Phys. 33 2393 (1962).

119. Momose, Y.: Z. Phys. 250 198 (1972).

120. Baazov, D.I., Kolbanovskii,Yu A., Polak, L.S.: Izvestiya Vuz. Fiz. 11 150 (1968).

121. Chryssou, E., Holzafel, G.: Phys. Stat. Sol (a) 8 K47 (1971).

122. Baazov, D.I., Kolbanovskii, Yu A., Polak, L.S.: Kinet. Katal. 9 792 (1968).

123. Dolidze, G.M., Kolbanovskii, Yu A., Polak, L.S.: Kinet. Katal. 6 897 (1965).

124. Baazov, D.I., Kolbanovskii, Yu A., Polak, L.S.: Kinet. Katal. 10 228 (1969).

125. Bohun, A.: J. Physique 26 149 (1965).

126. Scharmann, A., Kriegseis, W., Seibert, G.: PTB Mitteilungen 5 329 (1970).

127. Gordan, P., Scharmann, A.: Z. Phys. 217 309 (1968).

128. Kriegseis, W., Scharmann, A.: Z. Naturf. 24a 862 (1969).

129. Holzapfel, G., Nink, R.: Phys. Stat. Sol. A3 K181 (1970).

130. Styrov, V.V., Kharlamov, V.F.: Russ. J. Phys. Chem. 49 571 (1975).

131. McBee, E.T., Haas, H.B., Wiseman, P.A.: Ind. Eng. Chem. 37 432 (1945). See Techniques of Organic Chemistry Vol 11 page 184.

132. Attix, F.H.: Int. J. Appl. Rad^{n} and Isotopes 22 185 (1971).

133. Cairns, J.A., Desborough, C.L., Holloway, D.F.: Nucl. Instrum. Methods 88 239 (1970).

134. Handbuch der Physik 21.ed. S. Flugge, Springer Verlag Berlin (1956) page 183 and 177.

135. Ionization Chambers and Counters, Rossi, B.B., Staub, H.H.: McGraw-Hill Book Company Inc. (1949).

136. The Nuclear Handbook, 14-3, Frisch, O.R. ed.: George Newnes, London (1958).

137. Friedlander, G., Kennedy, J.W., Miller, J.M.: Nuclear and Radiochemistry 2nd ed. Wiley, New York, 1964 page 103.

138. Kasemo, B., Walldén, L.: Surface Science 53 393 (1975).

139. Kramer, J.: Z. Phys. 128 538 (1950).

140. Dienes, G.J., Vineyard, G.H.: Radiation Effects in Solids. Interscience, London (1957).

141. McCabe, R.W., Schmidt, L.D.: Surface Science 60 85 (1976).

142. Wilf, M., Dawson, P.T.: Surface Science 60 561 (1976).

143. Tesner, P.A., Rafal'kes I.S.: Doklady. Akad. Nauk, SSSR 87 821 (1952). See Chem. Abs 47 3671e (1953).

144. Rostrup-Nielsen, J.R.: J. Cat. 27 343 (1972).

145. Baker, R.T.K., Harris, P.S., Thomas, R.B., Waite, R.J.: J. Cat. 30 86 (1973).

146. Fryer, J.R., Paal, Z.: Carbon 11 665 (1973).

147. Somorjai, G.A.: Adv. Cat. 26 1 (1977).

148. Trapnell, B.M.W.: Proc. Roy. Soc. A218 566 (1953).

149. Morgan, A.E., Somorjai, G.A.: Surface Science 12 405 (1968).

150. Weinberg, W.H., Lambert, R.M., Comrie, C.M., Linnet, J.W.: Surface Science 30 299 (1972).

151. Weber, B., Fusy, J., Cassuto,: J. Chim. Phys. 66 708 (1969).

152. Procop, M., Völter, J.: Paper of the IInd Int. Symp. on Adsorption-Desorption Phenomena, Florence, Italy, 1971.

153. Völter, J., Procop, M., Berndt, H.: Surface Science 39 453 (1973).

154. Lang, B., Joyner, R.W., Somorjai, G.A.: Surface Science 30 454 (1972).

155. Heyne, H., Tompkins, F.C.: Proc. Roy. Soc. Ser A 292 460 (1966).

156. Lewis, R., Gomer, R.: Surface Science, 12 157 (1968).

157. Lewis, R., Gomer, R.: Suppl. Nuovo Cimento 5 506 (1967).

158. Presland, A.E.B., Walker, P.L.J.: Carbon 7 1 (1969).

159. Mignolet, J.C.P.: J. Chim. Phys. 54 19 (1957).

160. Lewis, R., Gomer, R.: Surface Science 17 333 (1969).

161. Bernasek, S.L., Somorjai, G.A.: Surface Science 48 204 (1975).

162. Christmann, K., Ertl, G.: Surface Science 60 365 (1976).

163. Lang, B.: Surface Science 53 317 (1975).

164. Kemball, C.: Proc. Roy. Soc. Ser A 216 376 (1953).

165. Bond, G.C.: Catalysis by Metals, Academic Press, New York (1962).

166. Franken, P.E.C., Ponec, V.: Surface Science 53 341 (1975).

167. Baron, K., Blakely, D.W., Somorjai, G.A.: Surface Science 41 45 (1974).

168. Yasumori, I., Shinohara, H., Inoue, Y.: "Catalysis" p771, J.W. Hightower ed. North-Holland Publ. Amsterdam (1972).

169. G. Webb: Private communication.

170. Anderson, J.R., Kemball, C.: Proc. Roy. Soc. Ser A 233 361 (1954).

171. Dowie, R.S., Whan, D.A., Kemball, C.: J. Chem. Soc. Faraday I 68 2150 (1972).

172. Shigeishi, R.A., King, D.A.: Surface Science 62 379 (1977).

173. Van Hardeveld, R., Van Montfoort, A.: Surface Science 4 396 (1966).

174. Egerton, T.A., Sheppard, N.: J. Chem. Soc. Faraday I 7 1357 (1974).

175. Nieuwenhuys, B.E., Sachtler, W.M.H.: Surface Science 34 317 (1974).

176. Mignolet, J.C.P.: Discussions Faraday Soc.: 8 105 (1951).

177. Mignolet, J.C.P.: Chemisorption; Proc. Symposium Keele page 118 (1956)(Garner ed.).

178. Fischer, T.E., Kelemen, S.R.: Surface Science 69 1 (1977).

179. Somorjai, G.A., Kesmodel, L.L.: International Review of Science, Physical Chemistry Series Two Vol 7 pl. Surface Chemistry and Colloids (1975). Butterworths: London & Boston.

180. Bonzel, H.P., Helms, C.R., Kelemen, S.: Phys. Rev. Letters 35 1237 (1975).

181. Reed, P.D., Lambert, R.M.: Surface Science 57 485 (1976).

182. Netzer, F.P.: Surface Science 52 709 (1975).

183. Bridge, M.E., Lambert, R.M.: Surface Science 63 315 (1977).

184. Comrie, C.M., Weinberg, W.H., Lambert, R.M.: Surface Science 57 619 (1976).

185a. Kanski, J., Rhodin, T.N.: Surface Science 65 63 (1977).

186. Collins, D.M., Lee, J.B., Spicer, W.E.: Surface Science 55 389 (1976).

185 Kanski, J., Rhodin, T.N.: Surface Science 60 476 (1976).

187. Ducros, R., Merrill, R.P.: Surface Science 55 227 (1976).

188. Pareja, P., Amariglio, A., Piquard, G., Amariglio, H.: J. Cat. 46 225 (1977).

189. Jech, C.: 2nd Int. Cong. Cat., p2285, Paris 1960 Technip Edition.

190. Lang, B., Joyner, R.W., Somorjai, G.A.: Surface Science 30 440 (1972).

191. McLean, M., Mykura, H.: Surface Science 5 466 (1966).

192. Blakely, D.W., Somorjai, G.A.: Surface Science, 65 419 (1977).

193. Chesters, M.A., Somorjai, G.A.: Surface Science, 52 21 (1975).

194. Ford, R.R., Pritchard, J.: Chem. Commun. 362 (1968).

195. Kortov, V.S., Mints, R.S., Teplov, V.G.: Phys. Stat. Sol. (a) 7 K89 (1971).

196. McCarroll, B.: J. Chem. Phys. 50 4758 (1969).

197. Volkenshtein, F.F.: Russ J. Phys. Chem. 50 456 (1976).

198. Tables of Physical and Chemical Constants 14th edition (1.5,45) Kaye, G.W.C., Laby, T.H.: Longman (1973).